biology

Special Issue Reprint

Nutrition, Environment, and Fish Physiology

Edited by
Quanquan Cao

mdpi.com/journal/biology

MDPI

Nutrition, Environment, and Fish Physiology

Nutrition, Environment, and Fish Physiology

Guest Editor

Quanqan Cao

MDPI

Basel • Beijing • Wuhan • Barcelona • Belgrade • Novi Sad • Cluj • Manchester

Guest Editor
Quanquan Cao
Fisheries College
Sichuan Agricultural
University
Chengdu
China

Editorial Office
MDPI AG
Grosspeteranlage 5
4052 Basel, Switzerland

This is a reprint of the Special Issue, published open access by the journal *Biology* (ISSN 2079-7737), freely accessible at: https://www.mdpi.com/journal/biology/special_issues/4942M2X4OH.

For citation purposes, cite each article independently as indicated on the article page online and as indicated below:

Lastname, A.A.; Lastname, B.B. Article Title. *Journal Name* **Year**, *Volume Number*, Page Range.

ISBN 978-3-7258-9143-6 (Hbk)
ISBN 978-3-7258-9144-3 (PDF)
https://doi.org/10.3390/books978-3-7258-9144-3

© 2026 by the authors. Articles in this reprint are Open Access and distributed under the Creative Commons Attribution (CC BY) license. The reprint as a whole is distributed by MDPI under the terms and conditions of the Creative Commons Attribution-NonCommercial-NoDerivs (CC BY-NC-ND) license (https://creativecommons.org/licenses/by-nc-nd/4.0/).

Contents

About the Editor . . . . . **vii**

Preface . . . . . **ix**

Quanquan Cao
Physiological Adaptations, Nutritional Strategies, and Health Management in Aquatic Organisms
Reprinted from: *Biology* **2026**, *15*, 324, https://doi.org/10.3390/biology15040324 . . . . . **1**

Nguyen Hong Nhat, Mitsuyo Saito, Shin-ichi Onodera, Mayuko Hamada, Fujio Hyodo and Hideaki Nagare
Environmental DNA Reveals the Impact of Submarine Groundwater Discharge on the Spatial Variability of Coastal Fish Diversity
Reprinted from: *Biology* **2024**, *13*, 609, https://doi.org/10.3390/biology13080609 . . . . . **4**

Quanquan Cao, Mohamed S. Kisha, Alkhateib Gaafar, Abdelgayed Metwaly Younes, Haifeng Liu and Jun Jiang
Evaluation of the Dietary Arginine Supplementation on Yellow Catfish: From a Low-Temperature Farming Perspective
Reprinted from: *Biology* **2024**, *13*, 881, https://doi.org/10.3390/biology13110881 . . . . . **17**

Giusy Rusco, Alessandra Roncarati, Michele Di Iorio, Michela Cariglia, Caterina Longo and Nicolaia Iaffaldano
Can IMTA System Improve the Productivity and Quality Traits of Aquatic Organisms Produced at Different Trophic Levels? The Benefits of IMTA—Not Only for the Ecosystem
Reprinted from: *Biology* **2024**, *13*, 946, https://doi.org/10.3390/biology13110946 . . . . . **33**

Pengyu Cai, Zhenhua Wang, Shouyu Zhang and Jintao Yu
Large and Small Yellow Croakers Feeding and Living Together Make Large Yellow Croaker Population Recovery Difficult: A Guild Perspective
Reprinted from: *Biology* **2024**, *13*, 963, https://doi.org/10.3390/biology13120963 . . . . . **56**

Ruoyu Wang, Yutao Li, Yining Zhang, Sihan Wang, Zheng He, Dingchen Cao, et al.
Exploring the Adaptation Process of *Huso dauricus* to High Temperatures Based on Changes in Intestinal Microbiota
Reprinted from: *Biology* **2024**, *13*, 1045, https://doi.org/10.3390/biology13121045 . . . . . **76**

Ju Zhao, Zhongjie Yang, Haifeng Liu, Chao Yang, Yujun Chen, Quanquan Cao and Jun Jiang
Dietary Methionine Hydroxy Analog Regulates Hepatic Lipid Metabolism via SIRT1/AMPK Signaling Pathways in Largemouth Bass *Micropterus salmodies*
Reprinted from: *Biology* **2025**, *14*, 227, https://doi.org/10.3390/biology14030227 . . . . . **88**

Han Zhang, Leyong Yu, Abdur Rahman, Sattanathan Govindharajan, Lingyao Li, Hairui Yu and Muhammad Waqas
Effects of Varying Dietary Concentrations of Menadione Nicotinamide Bisulphite (VK_3) on Growth Performance, Muscle Composition, Liver and Muscle Menaquinone-4 Concentration, and Antioxidant Capacities of Coho Salmon (*Oncorhynchus kisutch*) Alevins
Reprinted from: *Biology* **2025**, *14*, 447, https://doi.org/10.3390/biology14040447 . . . . . **102**

Lang Zhang, Qiuying Qin, Qing Li, Yali Yu, Ziwei Song, Li He, et al.
Molecular Adaptations and Quality Enhancements in a Hybrid (*Erythroculter ilishaeformis* ♀× *Ancherythroculter nigrocauda* ♂) Cultured in Saline–Alkali Water
Reprinted from: *Biology* **2025**, *14*, 718, https://doi.org/10.3390/biology14060718 . . . . . **117**

Quanquan Cao, Ju Zhao, Xuefei Zhang, Laia Ribas, Haifeng Liu and Jun Jiang
Dietary Cottonseed Protein Substituting Fish Meal Induces Hepatic Ferroptosis Through SIRT1-YAP-TRFC Axis in *Micropterus salmoides*: Implications for Inflammatory Regulation and Liver Health
Reprinted from: *Biology* **2025**, *14*, 748, https://doi.org/10.3390/biology14070748 . . . . . **138**

Jie Yan, Faling Zhang, Fenfei Liang, Cheng Zhao, Shaowu Yin and Guosong Zhang
Effects of Hypoxia and Reoxygenation on Hypoxia-Responsive Genes, Physiological and Biochemical Indices in Hybrid Catfish (*Pelteobagrus vachelli* ♀× *Leiocassis longirostris* ♂)
Reprinted from: *Biology* **2025**, *14*, 915, https://doi.org/10.3390/biology14080915 . . . . . **161**

Liuqing Meng, Luoqing Li, Ziyi Ma, Wenyan He, Qin Zhang, Tong Tong, et al.
Effects of Dietary *Rhodotorula mucilaginosa* on Muscle Composition, Serum Biochemical Indicators, Antioxidant Capacity, Lipid Metabolism, and mTOR Signaling Pathway in Red Claw Crayfish (*Cherax quadricanatus*)
Reprinted from: *Biology* **2025**, *14*, 1089, https://doi.org/10.3390/biology14081089 . . . . . **183**

Wei Dao, Jing Long, Yanhui Yin, Anli Wu, Yuanchao Chen, Haitao Gao, et al.
Metabolic Adaptation to Following Temperature Acclimation in Fish on the Yun-Gui Plateau
Reprinted from: *Biology* **2025**, *14*, 1645, https://doi.org/10.3390/biology14121645 . . . . . **206**

Cunhua Zhai, Ziyang Wang, Luye Bai and Bo Ma
Integrated Oxygen Consumption Rate, Energy Metabolism, and Transcriptome Analysis Reveal the Heat Sensitivity of Wild Amur Grayling (*Thymallus grubii*) Under Acute Warming
Reprinted from: *Biology* **2025**, *14*, 1718, https://doi.org/10.3390/biology14121718 . . . . . **224**

About the Editor

Quanquan Cao

Quanquan Cao is an Associate Professor at the College of Fisheries, Sichuan Agricultural University in Chengdu, China. He earned his Ph.D. in Animal Ecophysiology from the University of Montpellier, France. Dr. Cao's research primarily focuses on aquatic animal ecophysiology and molecular breeding of commercial fish. He has led several prestigious national and provincial projects, including the National Overseas Doctoral Talent Program and the Ministry of Science and Technology's "International Young Scientist" Program. His work has resulted in numerous high-impact publications in top-tier journals. Dr. Cao has received notable awards. He acts as a project review expert for the Ministry of Science and Technology and the Department of Agriculture and Rural Affairs of Sichuan Province. Additionally, as a member of the China Democratic League's Sichuan Agricultural University committee, he actively contributes to local fisheries development and policy consultation.

Preface

This Reprint gathers research on the interplay between nutrition, environment, and fish physiology. It explores how dietary components and environmental factors (temperature, salinity, pH, and pollutants) modulate growth, metabolism, immunity, reproduction, and stress responses. The work aims to address challenges in aquaculture and wild fisheries—optimizing practices, improving welfare, mitigating stressors, and supporting sustainable management and biodiversity conservation. Covering molecular to ecological studies, this volume serves a broad audience of physiologists, nutritionists, aquaculturists, ecologists, and conservationists, providing insights for resilient aquatic ecosystems.

Quanquan Cao
Guest Editor

biology

MDPI

Editorial

Physiological Adaptations, Nutritional Strategies, and Health Management in Aquatic Organisms

Quanquan Cao

Fisheries College, College of Animal Science and Technology, Sichuan Agricultural University, Chengdu 611130, China; qq2312159@sicau.edu.cn

Aquatic organisms are continuously challenged by dynamic environmental factors, including temperature, salinity fluctuations, and dissolved oxygen levels [1–8]. In this Special Issue, Zhai et al. [9] delve into thermal sensitivity by integrating oxygen consumption rates and transcriptome analysis to reveal the energy metabolism mechanisms in wild Amur grayling (*Thymallus grubii*) under acute warming. Similarly, Wang et al. [10] explore the adaptation process of *Huso dauricus* to high temperatures through the lens of intestinal microbiota succession, while Dao et al. [11] investigate the metabolic adaptation strategies of fish on the Yun-Gui Plateau following temperature acclimation. Beyond thermal stress, aquatic animals must also cope with hypoxic conditions and salinity variations. Yan et al. [12] focus on the acute effects of hypoxia and reoxygenation on physiological indices in hybrid catfish. Furthermore, building on the broader understanding of osmoregulation in aquatic animals [13], Zhang et al. [14] demonstrate the molecular adaptation mechanisms of the hybrid Erythroculter in saline–alkali water, highlighting the potential for aquaculture expansion in non-conventional waters.

Nutritional regulation is pivotal for optimizing growth and bolstering health, particularly through the modulation of intestinal barrier function and immunity by functional nutrients such as amino acids [15–17] and vitamins [18]. Addressing the industry's need for sustainable protein sources—and the associated challenges regarding intestinal integrity [19]—Cao et al. [20] report that substituting fish meal with cottonseed protein induces hepatic ferroptosis in largemouth bass (*Micropterus salmoides*) via the SIRT1-YAP-TRFC axis. To mitigate metabolic disturbances, functional additives play a crucial role. Contributing to this field, Zhao et al. [21] reveal that dietary methionine hydroxy analog regulates hepatic lipid metabolism via SIRT1/AMPK signaling pathways. Additionally, Meng et al. [22] demonstrate the benefits of dietary *Rhodotorula mucilaginosa* on muscle composition in red claw crayfish, and Zhang et al. [23] evaluate the antioxidant-enhancing effects of vitamin K3 in coho salmon (*Oncorhynchus kisutch*) alevins. Notably, Cao et al. [24] underscore the synergistic power of nutrition and environment by examining the beneficial effects of arginine supplementation on yellow catfish specifically under low-temperature farming conditions.

Finally, sustainable aquaculture requires a holistic perspective that spans from genomic insights for disease resistance [25] to macroscopic ecological management. The current issue expands on this scope through three ecological studies. Cai et al. [26] analyze the guild interactions hindering the population recovery of large yellow croakers. Rusco et al. [27] explore the productivity and quality benefits of Integrated Multi-Trophic Aquaculture (IMTA) systems. On a broader biogeographical scale, Nhat et al. [28] reveal the impact of submarine groundwater discharge on the spatial variability of coastal fish diversity using environmental DNA (eDNA) technology.

Taken together, the studies presented in this Special Issue highlight the complex interconnections between biodiversity, physiological adaptation, nutritional regulation, and environmental variability.

Data Availability Statement: Data available on request from the authors.

Conflicts of Interest: The author declare no conflicts of interest.

References

1. Guan, Q.; Xu, H.; Huang, L.; Zulfahmi, I.; Kisha, M.S.; Masroor, W.; Zhao, C.; Cao, Q. Regulatory mechanisms of temperature on the gonadal development of fish. *Aquaculture* **2025**, *613*, 743382. [CrossRef]
2. Liu, Q.; Wang, H.; Ge, J.; Guo, L.; Tahir, R.; Luo, J.; He, K.; Yan, H.; Zhang, X.; Cao, Q.; et al. Mechanism of acclimation to chronic intermittent hypoxia in the gills of largemouth bass (*Micropterus salmoides*). *Fish Physiol. Biochem.* **2025**, *51*, 22. [CrossRef]
3. Cao, Q.; Liang, F.; Wang, D.; Zhang, X.; Lorin-Nebel, C.; Gu, J.; Yin, S. Dynamic expression of vasotocin and isotocin receptor genes in the marbled eel (*Anguilla marmorata*) following osmotic challenges. *Gene* **2018**, *677*, 49–56. [CrossRef]
4. Wang, D.; Cao, Q.; Zhu, W.; Hu, Y.; Zhang, X.; Yin, S.; Wang, T. Individual and combined effects of salinity and lipopolysaccharides on the immune response of juvenile *Takifugu fasciatus*. *Fish Physiol. Biochem.* **2019**, *45*, 965–976. [CrossRef]
5. Cao, Q.; Chu, P.; Gu, J.; Zhang, H.; Feng, R.; Wen, X.; Wang, D.; Xiong, W.; Wang, T.; Yin, S. The influence of Ca^{2+} concentration on voltage-dependent L-type calcium channels' expression in the marbled eel (*Anguilla marmorata*). *Gene* **2020**, *722*, 144101. [CrossRef]
6. Cao, Q.; Li, J.; Sun, Y.; Geng, D.; Chu, P.; Wang, H.; Yin, S. Time-course studies of osmoregulatory responses in different salinities for the marbled eel (*Anguilla marmorata*). *Aquaculture* **2021**, *540*, 736699. [CrossRef]
7. Cao, Q.; Giffard-Mena, I.; Blondeau-Bidet, E.; Hermet, S.; Hu, Y.C.; Lee, T.H.; Lorin-Nebel, C. Mechanisms of acclimation to hypersalinity in two European sea bass lineages: A focus on the kidney function. *Aquaculture* **2021**, *534*, 736305. [CrossRef]
8. Cao, Q.; Blondeau-Bidet, E.; Lorin-Nebel, C. Intestinal osmoregulatory mechanisms differ in Mediterranean and Atlantic European sea bass: A focus on hypersalinity. *Sci. Total Environ.* **2022**, *804*, 150208. [CrossRef]
9. Zhai, C.; Wang, Z.; Bai, L.; Ma, B. Integrated oxygen consumption rate, energy metabolism, and transcriptome analysis reveal the heat sensitivity of wild Amur grayling (*Thymallus grubii*) under acute warming. *Biology* **2025**, *14*, 1718. [CrossRef]
10. Wang, R.; Li, Y.; Zhang, Y.; Wang, S.; He, Z.; Cao, D.; Sun, Z.; Wang, N.; Zhang, Y.; Ma, B. Exploring the adaptation process of *Huso dauricus* to high temperatures based on changes in intestinal microbiota. *Biology* **2024**, *13*, 1045. [CrossRef]
11. Dao, W.; Long, J.; Yin, Y.; Wu, A.; Chen, Y.; Gao, H.; Pan, X.; Yang, J.; Wang, X.; Zhang, Y. Metabolic adaptation to following temperature acclimation in fish on the Yun-Gui Plateau. *Biology* **2025**, *14*, 1645. [CrossRef] [PubMed]
12. Yan, J.; Zhang, F.; Liang, F.; Zhao, C.; Yin, S.; Zhang, G. Effects of hypoxia and reoxygenation on hypoxia-responsive genes, physiological and biochemical indices in hybrid catfish (*Pelteobagrus vachelli* ♀ × *Leiocassis longirostris* ♂). *Biology* **2025**, *14*, 915. [CrossRef] [PubMed]
13. Cao, Q.; Zhang, Q.; Li, S.; Gaafar, A.; Younes, A.M.; Rind, K.H.; Liu, H.; Jiang, J. Effect of some feed additives on osmoregulation in aquatic animals. *Aquaculture* **2025**, *596*, 741829. [CrossRef]
14. Zhang, L.; Qin, Q.; Li, Q.; Yu, Y.; Song, Z.; He, L.; Sun, Y.; Ye, L.; Wang, G.; Xu, J. Molecular adaptations and quality enhancements in a hybrid (*Erythroculter ilishaeformis* ♀ × *Ancherythroculter nigrocauda* ♂) cultured in saline–alkali water. *Biology* **2025**, *14*, 718. [CrossRef]
15. Zhao, B.; Zhao, J.; Liu, H.; Zhang, H.; Shan, H.; Zong, J.; Cao, Q.; Jiang, J. Impact of dietary glutamate on growth performance and flesh quality of largemouth bass. *Fishes* **2025**, *10*, 151. [CrossRef]
16. Zhao, J.; Li, X.; Zhang, T.; Liu, H.; Cao, Q.; Jiang, J. Dietary valine modulates hepatic immune responses in largemouth bass (*Micropterus salmoides*) against *Aeromonas veronii* infection: Integrated regulation of antioxidant defense, ER stress and autophagy. *Fish Shellfish Immunol.* **2025**, *165*, 110531. [CrossRef]
17. Zhao, J.; Zhao, Y.; Liu, H.; Cao, Q.; Feng, L.; Zhang, Z.; Jiang, W.; Wu, P.; Liu, Y.; Luo, W.; et al. Dietary leucine improves fish intestinal barrier function by increasing humoral immunity, antioxidant capacity, and tight junction. *Int. J. Mol. Sci.* **2023**, *24*, 4716. [CrossRef]
18. Zhao, J.; Cao, Q.; Yan, M.; Ye, Y.; Faggio, C.; Liu, H.; Jiang, J. Dietary vitamin D_3 improves growth performance and hepatic glycolipid metabolism in largemouth bass (*Micropterus salmoides*). *Anim. Feed Sci. Technol.* **2025**, *327*, 116429. [CrossRef]
19. Zhao, J.; Cao, Q.; Jin, M.; Shen, T.; Ribas, L.; Liu, H.; Jiang, J. A comprehensive study of enzyme-treated soy protein on intestinal barrier integrity, inflammatory responses, and liver lipid metabolism in *Micropterus salmoides*. *J. Agric. Food Res.* **2025**, *22*, 102152. [CrossRef]

20. Cao, Q.; Zhao, J.; Zhang, X.; Ribas, L.; Liu, H.; Jiang, J. Dietary cottonseed protein substituting fish meal induces hepatic ferroptosis through SIRT1-YAP-TRFC axis in *Micropterus salmoides*: Implications for inflammatory regulation and liver health. *Biology* **2025**, *14*, 748. [CrossRef]
21. Zhao, J.; Yang, Z.; Liu, H.; Yang, C.; Chen, Y.; Cao, Q.; Jiang, J. Dietary methionine hydroxy analog regulates hepatic lipid metabolism via SIRT1/AMPK signaling pathways in largemouth bass *Micropterus salmodies*. *Biology* **2025**, *14*, 227. [CrossRef] [PubMed]
22. Meng, L.; Li, L.; Ma, Z.; He, W.; Zhang, Q.; Tong, T.; Wang, D.; Wang, R.; Yang, H.; Liu, Y.; et al. Effects of dietary *Rhodotorula mucilaginosa* on muscle composition, serum biochemical indicators, antioxidant capacity, lipid metabolism, and mTOR signaling pathway in red claw crayfish (*Cherax quadricanatus*). *Biology* **2025**, *14*, 1089. [CrossRef] [PubMed]
23. Zhang, H.; Yu, L.; Rahman, A.; Govindharajan, S.; Li, L.; Yu, H.; Waqas, M. Effects of varying dietary concentrations of menadione nicotinamide bisulphite (VK3) on growth performance, muscle composition, liver and muscle menaquinone-4 concentration, and antioxidant capacities of coho salmon (*Oncorhynchus kisutch*) alevins. *Biology* **2025**, *14*, 447. [CrossRef] [PubMed]
24. Cao, Q.; Kisha, M.S.; Gaafar, A.; Younes, A.M.; Liu, H.; Jiang, J. Evaluation of the dietary arginine supplementation on yellow catfish: From a low-temperature farming perspective. *Biology* **2024**, *13*, 881. [CrossRef]
25. Liu, M.; Zhou, K.; Liu, Z.; Wei, S.; Ribas, L.; Cao, Q. Harnessing genomics for identifying disease-resistant eels: Advances, applications, and sustainable aquaculture. *Comp. Biochem. Physiol. Part D Genom. Proteom.* **2026**, *57*, 101695. [CrossRef]
26. Cai, P.; Wang, Z.; Zhang, S.; Yu, J. Large and small yellow croakers feeding and living together make large yellow croaker population recovery difficult: A guild perspective. *Biology* **2024**, *13*, 963. [CrossRef]
27. Rusco, G.; Roncarati, A.; Di Iorio, M.; Cariglia, M.; Longo, C.; Iaffaldano, N. Can IMTA system improve the productivity and quality traits of aquatic organisms produced at different trophic levels? The benefits of IMTA—Not only for the ecosystem. *Biology* **2024**, *13*, 946. [CrossRef]
28. Nhat, N.H.; Saito, M.; Onodera, S.I.; Hamada, M.; Hyodo, F.; Nagare, H. Environmental DNA reveals the impact of submarine groundwater discharge on the spatial variability of coastal fish diversity. *Biology* **2024**, *13*, 609. [CrossRef]

Disclaimer/Publisher's Note: The statements, opinions and data contained in all publications are solely those of the individual author(s) and contributor(s) and not of MDPI and/or the editor(s). MDPI and/or the editor(s) disclaim responsibility for any injury to people or property resulting from any ideas, methods, instructions or products referred to in the content.

biology

MDPI

Article

Environmental DNA Reveals the Impact of Submarine Groundwater Discharge on the Spatial Variability of Coastal Fish Diversity

Nguyen Hong Nhat [1,2], Mitsuyo Saito [3,*], Shin-ichi Onodera [3], Mayuko Hamada [4], Fujio Hyodo [5] and Hideaki Nagare [5]

[1] Graduate School of Environmental and Life Science, Okayama University, Okayama 7008530, Japan; p1qd3i9i@s.okayama-u.ac.jp
[2] Faculty of Technology—Engineering—Environment, An Giang University, Vietnam National University—Ho Chi Minh City, Ho Chi Minh City 880000, Vietnam
[3] Graduate School of Advanced Science and Engineering, Hiroshima University, Higashi Hiroshima 7398521, Japan; sonodera@hiroshima-u.ac.jp
[4] Ushimado Marine Institute (UMI), Graduate School of Environment, Life, Natural Science and Technology, Okayama University, Okayama 7014303, Japan; hamadam@okayama-u.ac.jp
[5] Faculty of Environmental, Life, Natural Science and Technology, Okayama University, Okayama 7008530, Japan; fhyodo@cc.okayama-u.ac.jp (F.H.); nagare-h@okayama-u.ac.jp (H.N.)
* Correspondence: misaito@hiroshima-u.ac.jp; Tel.: +81-82-424-6521

Simple Summary: In environments characterized by small-scale islands, terrestrial inputs, like freshwater discharges, can significantly impact fish communities compared to ocean currents. While the influence of river discharge on marine biodiversity is well documented, the effects of submarine groundwater discharge on nearshore fish communities are less understood. Here, our results provide evidence that submarine groundwater discharge crucially influences coastal fish diversity by altering salinity and nutrient supply. This study also showed that fish community composition varies considerably over a small spatial scale, reflecting habitat partitioning on the target island.

Abstract: Submarine groundwater discharge (SGD) has recently been recognized as an influential factor in coastal ecosystems; however, little research has been conducted on its effects on coastal fish diversity. To investigate the relationship between SGD and fish diversity, we conducted a survey at the coastal island scale using the environmental DNA (eDNA) method. Our findings indicate that fish species richness and functional richness peak at stations with high SGD. Environmental variables, such as salinity, dissolved inorganic nitrogen (DIN) concentration, and SGD, significantly influence fish diversity. Carnivore fish richness was negatively correlated with salinity, while planktivore fish richness was positively correlated. Additionally, SGD and DIN concentrations were found to be crucial in shaping omnivorous and pelagic communities, respectively. This study highlights the role of SGD in enhancing nutrient conditions favorable for diverse fish communities and demonstrates the effectiveness of eDNA metabarcoding for rapid marine biodiversity assessment. These findings provide valuable insights for coastal ecosystem monitoring and management.

Keywords: eDNA; metabarcoding; biodiversity; functional diversity; taxonomic diversity; spatial patterns; environmental variables

1. Introduction

Surface and subsurface water discharge to coastal areas is essential for supporting biodiversity by supplying the necessary nutrients for the growth and reproduction of marine organisms [1] and creating an optimal habitat environment, such as for temperature and salinity [2,3]. Several marine ecological studies have shown how river discharge (RD) affects the biological community structure and supports production in coastal areas [4].

However, few studies have focused on the impacts of submarine groundwater discharge (SGD) on coastal ecosystems [5]. Some studies have revealed that salinity changes caused by SGD influence the macro-benthic community composition [3,6]. Salinity has also been identified as a key variable for fish species distribution; for example, high salinity negatively affects the metabolism and feeding behavior of some fish species [7]. Moreover, SGD usually contains a higher concentration of nutrients than surface water, which can significantly affect phytoplankton growth and species changes in phytoplankton [4–8]. Fujita et al. [8] confirmed a positive relationship between SGD-derived nutrient loading and elevated benthic primary production, affecting the growth of juvenile marbled soles (*Pseudopleuronectes yokohamae*). Lilkendey et al. [9] demonstrated the physiological effects of fresh SGD on the augmented growth of juvenile gray demoiselle (*Chrysiptera glauca*) by providing optimal salinity and low pH conditions. These studies suggest that SGD is important for specific fish species by providing optimal habitats and nutrients to increase primary and secondary production. However, the effects of SGD on coastal fish diversity are poorly understood. A spatial evaluation of the relationship between SGD and fish communities would provide useful information to examine this.

Environmental DNA (eDNA) has emerged as a promising tool for investigating marine biodiversity via rapid and integrative biomonitoring [10]. eDNA is generated when organisms release genetic material into their environment and can be isolated, extracted, and sequenced using metabarcoding techniques [11–14]. This approach has shown superiority in species detection, particularly for cryptic and rare species, while being non-invasive and cost-effective [15–17], offering advantages over traditional surveys [10,18,19]. Recent advancements in eDNA technology and methodology have proven highly accurate in predicting the spatial distribution of species [20]. eDNA can be used to distinguish the taxonomic diversity of various habitats and quickly assess changes in biodiversity at the ecosystem level [17]. However, relying solely on individual taxonomic diversity is insufficient to reveal community variations [21]. Integrating taxonomic and functional diversity offers deeper insight into the intricate relationships between species and their environments [22–24]. Functional diversity, including feeding habits, swimming abilities, and habitat preferences, provides a comprehensive understanding of the responses of fish communities to various environmental conditions [2,25–27]. Hence, using a reliable integrated eDNA-functional biomonitoring method is valuable for fish biodiversity assessment and comprehensive impact evaluation of SGD.

Therefore, in this study, we examined the impact of SGD on the spatial patterns of fish diversity on a coastal island in western Japan where the spatial variability of SGD was confirmed [28]. To investigate the relationship between SGD and the taxonomic and functional diversity of fish, we used eDNA at an island scale.

2. Materials and Methods

2.1. Study Area Information

Ikuchijima Island (34°16′ N, 133°6′ E) is centrally located within the Seto Inland Sea (SIS) of western Japan. This island covers an area of 31.2 km^2, with a perimeter of 33.6 km and a maximum elevation of 472 m. The topographic gradient is steeper in the western, southern, and eastern parts of the island than in the northern areas [28]. Annual average temperature and precipitation are 16 °C and 1100 mm [28,29]. The coastal zone surrounding the island is characterized by a high level of fish diversity of numerous species [29–31]. In November 2022, we surveyed 18 sampling stations (IKR1–18) in the seawater of the island. The numbering and distribution of each sampling station are shown in Figure 1c.

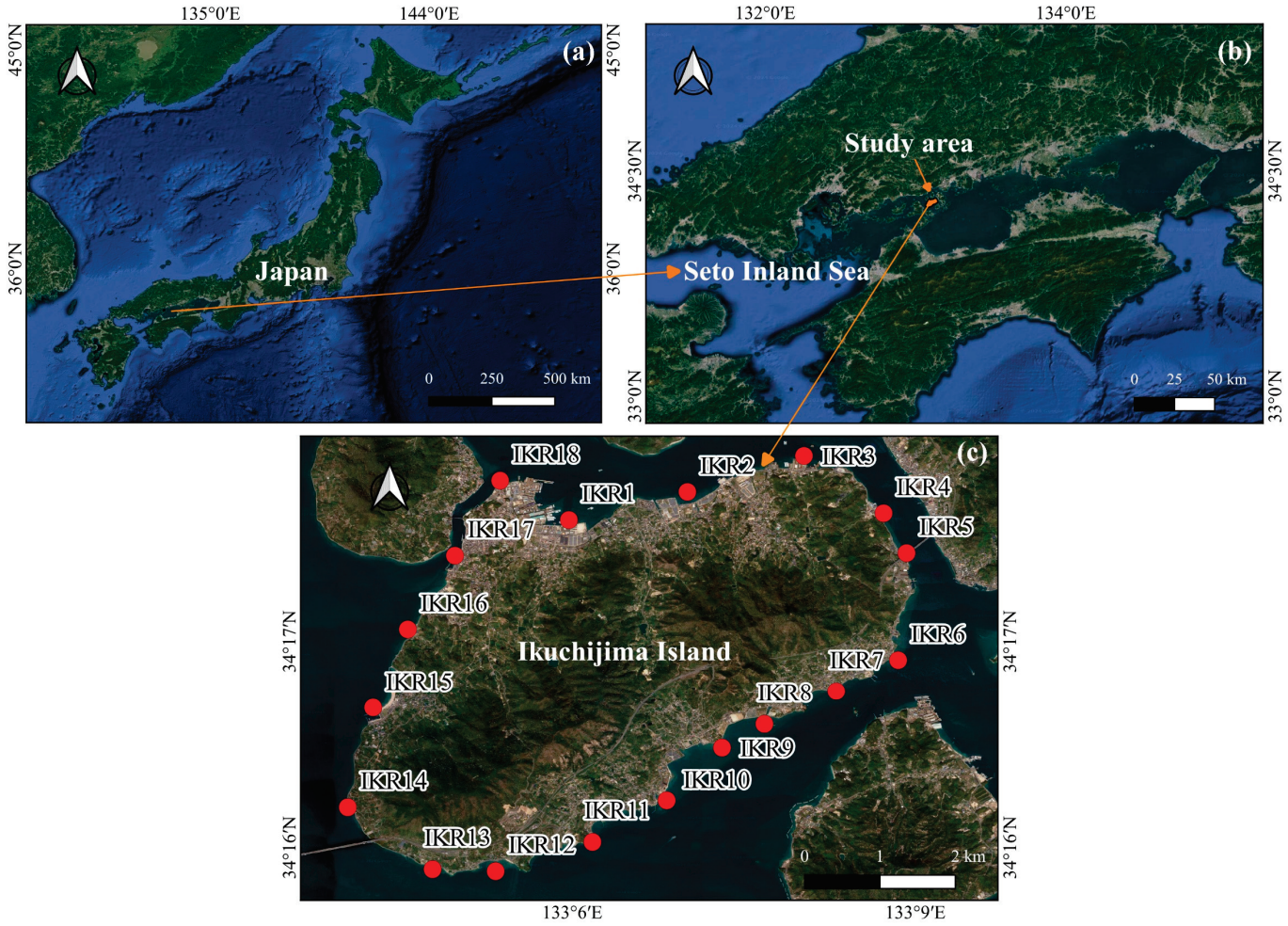


Figure 1. Map showing the study area, with red dots indicating sampling stations. (**a**) Japan; (**b**) Seto Inland Sea and (**c**) Ikuchijima Island.

2.2. Sampling Collection

Seawater samples were collected from a boat by slowly circling around the target island. We used the geo-coordinates of each sampling station, directly measured at the study area with a GPS device for spatial variables. For collecting eDNA, two bottles of 1-L water sample per site (two liters) were collected from the surface using polypropylene bottles in duplicate for each station, immediately adding 1 mL of 10% benzalkonium chloride solution (Osvan 10%, Nihon Pharmaceutical Co., Ltd., Tokyo, Japan) to prevent eDNA degradation by bacteria, following the sampling manual of the eDNA society [32]. Blanks (negative controls) were set up at the study area by sterilized deionized water in the same manner to examine for contamination during the field survey. Field water samples and distilled water were kept on ice during sampling and transportation until filtration. Within 24 h after collection, each 1 L seawater sample was filtered through a Sterivex-HV filter with pore size 0.45 µm (Merck Millipore, Burlington, MA, USA) and was directly immersed in 1.5 mL of RNAlater (Thermo fisher Scientific, Waltham, MA, USA) to avoid degradation of DNA, then filtered samples were transported to the laboratory at −20 °C for further eDNA analysis.

In addition, a further 100 mL of seawater samples for each station were collected with three replicates and transported to the laboratory at 4 °C for nutrients analysis, including ammonium nitrogen (NH_4-N, mg/L), nitrite (NO_2-N, mg/L), nitrate (NO_3-N, mg/L), phosphate (PO_4-P, mg/L) and silicate ($Si(OH)_4$-Si, mg/L). Nutrient analyses were performed using an auto-analyzer (swAAt, BLTEC). We define dissolved inorganic nitrogen (DIN) as the sum of ammonium nitrogen (NH_4-N, mg/L), nitrite (NO_2-N, mg/L), and nitrate

(NO_3-N, mg/L). Phosphate (PO_4-P, mg/L) is reported as dissolved inorganic phosphorus (DIP), while silicate ($Si(OH)_4$-Si, mg/L) is reported as dissolved silica (DSi). We also collected particulate organic matter (POM, an indicator of phytoplankton) of 0.7–125 μm from the surface seawater of each station [33]. Those samples were filtered on pre-combusted glass-fiber filters (Whatman GF/F type, 450 °C, 2 h) after sieving through a 125 μm mesh sieve [33]. While collecting seawater samples, a portable data logger (CTD-Diver, vanEssen Instruments, Delft, The Netherlands) was employed to record seawater temperatures and salinity at each station.

2.3. Environmental DNA Analysis, Taxonomic Verification

eDNA experiments, including extraction of eDNA and polymerase chain reaction (PCR) of technology, were conducted in a dedicated laboratory, PCR-free to avoid any contamination of eDNA samples. Total DNA was extracted by using a DNeasy Blood and Tissue Kit (Qiagen, Hilden, Germany) [34]. After purification, DNA was eluted with 100 μL elution buffer (buffer AE) and stored at −20 °C. The amplicon libraries of the spatial 12S rRNA region were constructed using the universal Mifish primer sets (MiFish-E-F/R-v2:MiFish-U-F/R:MiFish-U2-F/R = 1:2:1) [35]. KAPA HiFi HotStart ReadyMix (KAPA Biosystems, Wilmington, MA, USA) for amplification of eDNA, GeneRead Size Selection Kit (Qiagen, Hilden, Germany) and Agencourt AMPure XP (Beckman Coulter, Tokyo, Japan) for purification of first and second PCR products, respectively, were used according to the manufacturer's protocol. In addition to the field/filtration blanks, PCR-negative controls were made using distilled water instead of eDNA during PCR. Purified PCR products were quantified using a Qubit 2.0 fluorometer and dsDNA HS Assay Kit (Thermo Fisher Scientific, Waltham, MA, USA), and TapeStation 4150 and DNA High Sensitivity D1000 (Agilent, Santa Clara, CA, USA). The obtained sequencing libraries were quantified using a Qubit 2.0 fluorometer and dsDNA HS Assay Kit (Thermo Fisher Scientific) and pooled in equal concentrations. Libraries were sequenced using an Illumina MiSeq system with 600-cycle chemistry (2 × 300 bp paired-end sequencing using the MiSeq Reagent Kit v3) (Illumina, San Diego, CA, USA).

Sequence pairs of all samples were performed following Miya et al. [35] and using the publicly available bioinformatics pipeline, Mifish Pipeline [36,37]. All sequencing data underwent the following processes: quality control, trimming, assembled cleaned, N-base and length filtering (229 ± 25 bp by default), primer removal, clustering and species-level assignment. The zero-radius operation taxonomic units table (ZOTUs) was obtained and queried against the Mitofish database (fish mitochondrial genome database) with threshold of identify 97% and e-value 10^{-5} [37,38]. After this step, a taxonomic database was made and classified based on information obtained from FishBase.

2.4. Functional Traits Verification

Functional traits of the identified fish species, such as feeding habits and depth levels, were compiled from existing literature databases and FishBase (Table 1).

Table 1. Trait groups and modalities were used in the study, with the indication of the category definition and the explanation for trait selection.

Table	Category	Definition	Rationale
Feeding diets	Carnivores	Feeding mainly on smaller fish	Defined based on fish diet and aggregation of fish species that utilize the same food resource [39]
	Herbivore	Feeding mainly on plant material	
	Omnivore	Feeding on food both of plant material and animal origins	
	Planktivore	Feeding mainly on plankton	
Depth habits	Pelagic	Inhabit the upper water column	Reflects the degree of dependence of fish on their position in the water column [40]
	Demersal	Live near the bottom	

2.5. Evaluation of Spatial Variability of SGD

Recently, DSi has become well known as a useful geochemical tracer for estimating SGD [41–43]. SGD typically contains high concentrations of DSi, making DSi a valuable addition to the conventional tracers, such as ^{222}Rn or Ra [44,45]. Here, we applied DSi balance model to estimate the spatial variation in SGD on the island [42,46]. The entire island was divided into 18 boxes based on the locations of DSi sampling stations. The SGD for each box was then calculated by using the DSi balance equation, allowing us to assess the spatial distribution of SGD across the island. At steady state, sources of DSi in a system can be included, such as diffusion from bottom sediments, SGD, RD and mixing with offshore seawater. The mass balance equation for DSi can then be written as follows [41,42,46].

$$F_R^{Si} + F_{Diff}^{Si} + C_{GW}^{Si} \times A_{Bott} \times \varphi_{SGD} + C_{EX}^{Si} \times V_s \times \delta_{Mix} = 0 \quad (1)$$

where F_R^{Si} is the DSi flux by RD (mmol/d), which was estimated from river flow rate (Q_R) and DSi concentrations (C_R^{Si}) of river water ($F_R^{Si} = Q_R \times C_R^{Si}$); $F_{Diff}^{Si} = R_G^{Si} \times A_{Bott}$ is the flux due to diffusion from bottom sediments (mmol/d), R_G^{Si} is the regeneration rate of DSi (mmol/m^{2}d), A_{Bott} is the bottom area of each sections (m^2); $C_{GW}^{Si} \times A_{Bott} \times \varphi_{SGD}$ is the flux of DSi from SGD (F_{SGD}^{Si}), C_{GW}^{Si} is the DSi concentration of groundwater end-member (mmol/m^3), φ_{SGD} is the seepage rate of groundwater (m/d); $C_{EX}^{Si} \times V_s \times \delta_{Mix}$ is the mixing with offshore seawater (F_{Mix}^{Si}), C_{EX}^{Si} is the concentration of DSi in each section (C_{SW}^{Si}) subtracted for the offshore seawater concentration (C_O^{Si}), V_s is the volume of each section (m^3), δ_{Mix} is the rate at which seawater mixed with offshore seawater (d^{-1}).

2.6. Data Analysis and Statistics

In this study, QGis software version 3.16.16 was used to visualize the spatial variation of SGD, alpha diversity, fish species composition and functional traits. The alpha diversity index, including species richness and functional richness, was calculated for characterizing fish diversity by R package vegan and mFD [47]. In a community, functional richness (FRic) indicates the number of ecological niches occupied by species. An increase in FRic indicates a more efficient use of ecological space, which reflects the stability of the community and resistance to invasion [48]. The fish reads were transformed to presence/absence data before undergoing statistical analysis. The Spearman correlation analysis performed using the linkET package (mantel test function) in R to determine the correlations between environmental variables [49], expresses statistical significance as a p-value less than 0.05. Environmental variables that were not normally distributed were transformed by using log transformations and were then standardized depending on the implementation of each analysis process [50]. To identify the major variables explaining the pattern in species richness, functional richness among the target area, we used the generalized linear models (GLMs) with a Poisson distribution and log-link function using the *glm* function [51]. *Ggpairs* function was used to determine the covariation among environmental variables, and the highly correlated variables ($r > 0.5$) were removed to minimize collinearity in the subsequent analyses. For each response variable, we first constructed a full model that comprised of all the environmental variables (i.e., SGD, RD, etc.). Then the *dredge* function in the MuMIn package was used for model selection [51]. The best models were selected using Akaike's information criterion (AIC), and the best models have the lower value of AIC [51]. Distance-based redundancy analysis (dbRDA) was conducted to assess environmental factors affecting fish communities' composition, with ordination biplot explaining the relationships between significant environmental variables and these patterns by R package vegan [52]. To reduce the presence of covariance among the environmental variables, variance inflation factors (VIF) were calculated to assess collinearity among predictors. VIF values were all <2, suggesting non-collinearities [50]. Then some variables with high correlation were removed and only the selected variables were input in the final model. Data underwent a three-step process: first, a community dissimilarity matrix is calculated

using the Jaccard dissimilarity matrix, which derived from presence/absence species level data. Next, we performed dbRDA on dissimilarity matrix by using *capscale* function. Then, the permutation tests were separately performed on the axes of the model and the full model (number of permutations: 999). We analyzed the total fish species community and functional communities separately. All statistical analyses were carried out in R version 4.2.0.

3. Results

3.1. Spatial Variability of Fish Communities

A total of 2,827,847 sequences clustered into 326 ZOTUs were detected by eDNA metabarcoding, which belong to 19 orders, 34 families and 59 species (Table S1). Most of the sequence reads were assigned to *Sparidae* (37%), followed by *Mugilidae* (14%), *Sillaginidae* (9%), *Engraulidae* (8%), *Gobiidae* (6%), and *Siganidae* (5%). Among them, *Sparidae*, *Mugilidae*, *Sillaginidae*, and *Gobiidae* were found frequently in the sampling stations; especially, *Sparidae* and *Mugilidae* had 100% occurrence frequency and were detected across all stations (Figure 2a). By contrast, *Haemulidae*, *Stichaeidae*, *Pristigasteridae*, *Scombridae*, *Sphyraenidae*, *Tripterygiidae*, *Hexagrammidae*, *Atherinidae*, and *Cynoglossidae* were found only once between different sampling stations (Figure S1). Our data showed that 30 fish species (belonging to 12 orders, 23 families) were identified from commercial to highly commercial in terms of fishery (Table S1). The alpha diversity index of fish diversity was found to be different across the sampling stations, suggesting a complex and heterogeneous distribution of fish communities within the island ecosystem (Figure 2b,c). Fish species richness and functional richness were highest in IKR1, 2, 4, 10 and 18, and the lowest in IKR11 and 16.

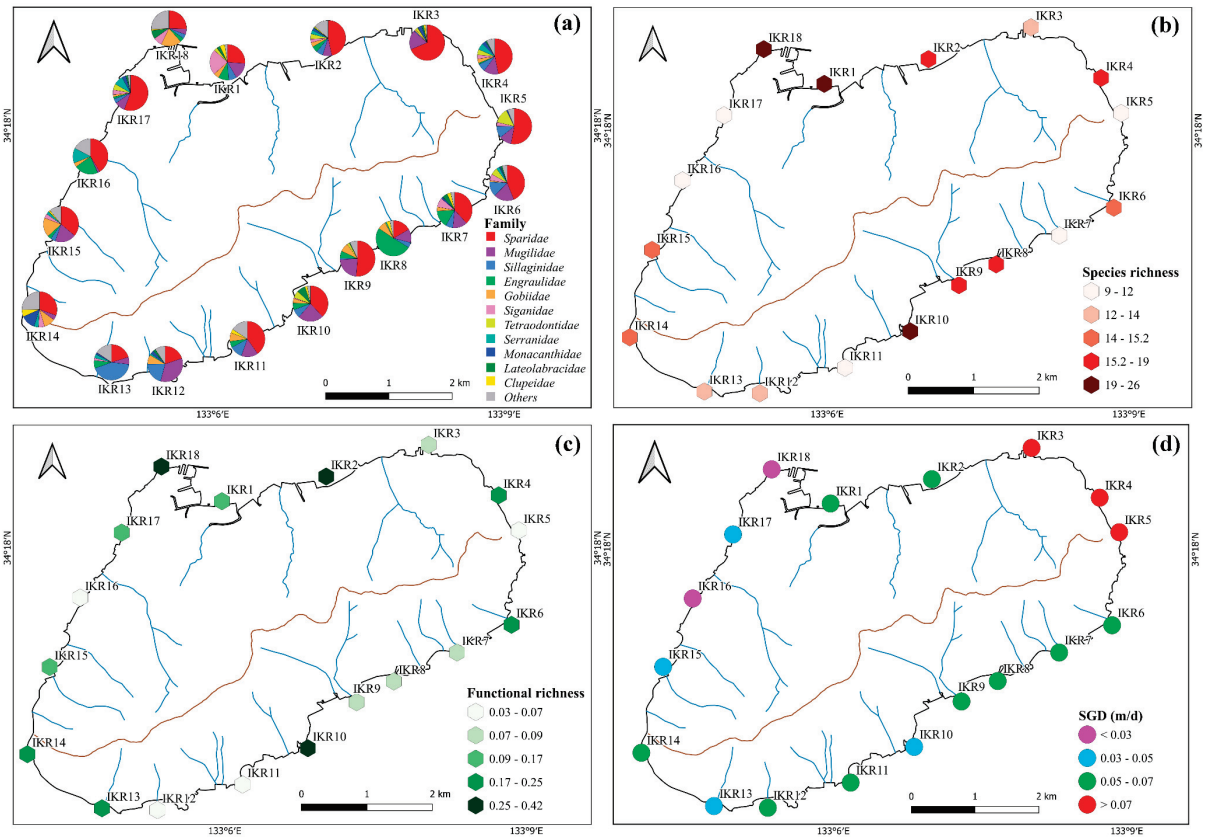


Figure 2. Spatial variation in the percentages of (**a**) fish family, (**b**) species richness, (**c**) functional richness and (**d**) SGD (point color relate to the SGD level of each stations: red for SGD value > 0.07 m/d, green for SGD value range 0.05–0.07 m/d, blue for SGD value range 0.07–0.05 m/d, and purple for SGD value < 0.03).

Based on feeding diet preference, fish were categorized into four groups, the major traits were carnivores (32 species), followed by omnivores (15 species), planktivores (7 species), and herbivores (3 species). Two depth traits were observed based on the trophic distribution of fish, which comprised 42 demersal, and 17 pelagic species. The distribution patterns of a functional fish community were dominated by fish that belonged to carnivores (54%) and with benthic habits (71% of demersal fish) (Figure 3).

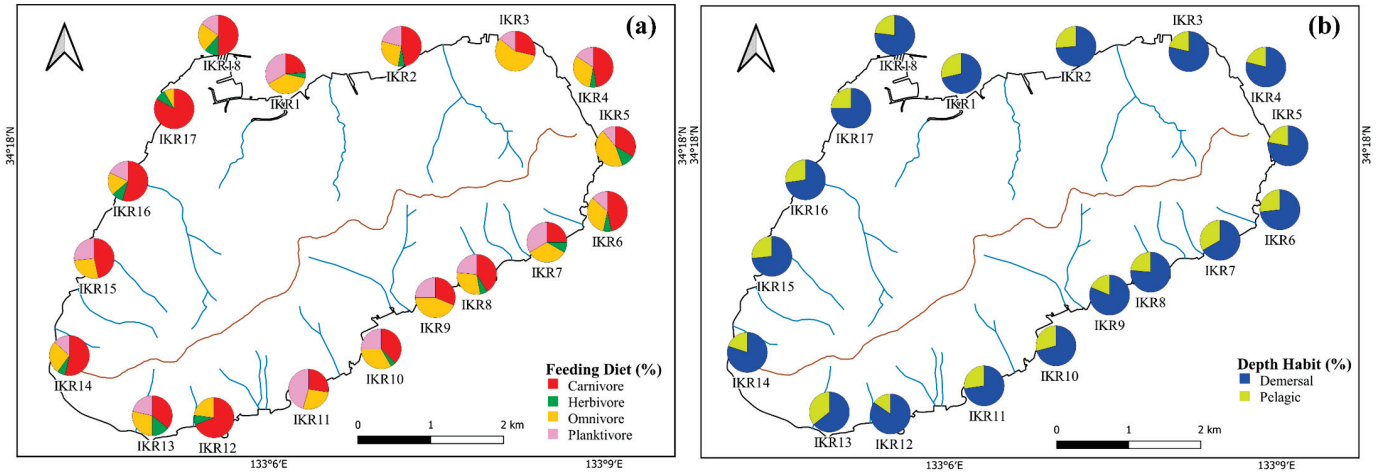


Figure 3. Spatial variation in the percentages of (**a**) feeding diet and (**b**) depth habit.

3.2. Impacts of SGD on Fish Diversities

The temperatures recorded ranged from 19.8 °C to 21.7 °C, with a mean seawater temperature of 20.8 °C ± 0.5 SD (Standard Deviation). The average salinity was 33.5 psu ± 0.5 SD, ranging from 31.85 psu to 34.18 psu. Higher SGD occurred along the northeastern shoreline, and the lowest SGD was found along the northwestern shorelines (Figure 2d). The Spearman correlation analysis showed that SGD had a positive correlation with DSi and DIP concentrations and a negative correlation with water temperature and salinity, while RD had a positive correlation with POM (Figure 4). High positive correlations were observed among DSi and DIP, indicating that their sources were consistent and similar Figure 4).

The Alpha diversity index is an effective tool for characterizing the species diversity of Ikuchijima Island. In this study, higher species richness and functional richness were observed at stations with higher SGD, such as IKR2, 4, 6, and 14, indicating that SGD affects the composition of fish diversity within a small spatial island scale (Figure 2b,c).

Analysis of the effects of environmental variables on the pattern of fish diversity and communities showed that different species and functional traits of fish respond differently to environmental variables. The results of the best models in the GLMs are shown in Table 2. Carnivore richness had significantly negative relationships with salinity ($p < 0.05$), while planktivore richness and salinity had a positive relationship. RD and omnivore richness had a significant positive relationship ($p < 0.05$). These results suggest that the spatial patterns of fish diversity were influenced by different environmental variables.

Table 2. Summary of results of the best models of GLMs used to assess the relationship between the alpha diversity index and environmental variables.

Model	Variable (Intercept)	Salinity	SGD	RD	df	AIC
Carnivore richness	13.76 ***	−0.34 *	−7.5		3	85.4
Omnivore richness	1.62 ***			0.05 *	2	75.2
Planktivore richness	−20.55	0.64 *			0.05	76.2

AIC: Akaike's information criterion. Statistical significance markers: *** $p < 0.001$, * $p < 0.05$ in a Wald test.

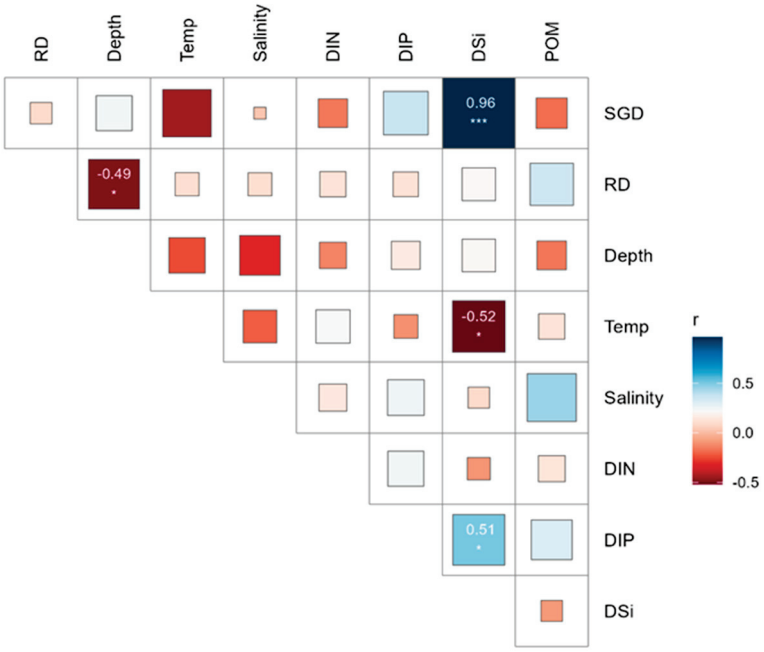


Figure 4. Spearman's correlation matrix illustrates the relationships between environmental variables in the target island. Statistical significance markers: *** $p < 0.001$, * $p < 0.05$.

From the results of dbRDA, SGD and DIN concentration were key factors affecting the spatial composition of omnivore community (full model, F = 1.42, $p < 0.05$) (Figure 5a). SGD showed a strong significant effect on omnivore community composition (SGD, F = 1.46, $p < 0.05$). *Takifugu pardalis* and *Takifugu niphobles* were found to be highly occurring at high SGD sites. DIN concentration also had a strong significant effect on omnivore community (DIN, F = 1.38, $p < 0.05$). *Lateolabrax japonicus* and *Stephanolepis cirrhifer* were highly detected in high DIN sites. For pelagic community composition, RD and SGD were key variables affecting the community composition (full model, F = 1.34, $p < 0.05$) (Figure 5b). RD had a strong significant effect on pelagic community composition (RD, F = 1.56, $p < 0.05$). *Konosirus punctatus* and *Hyporhamphus sajori* were commonly observed in high RD sites.

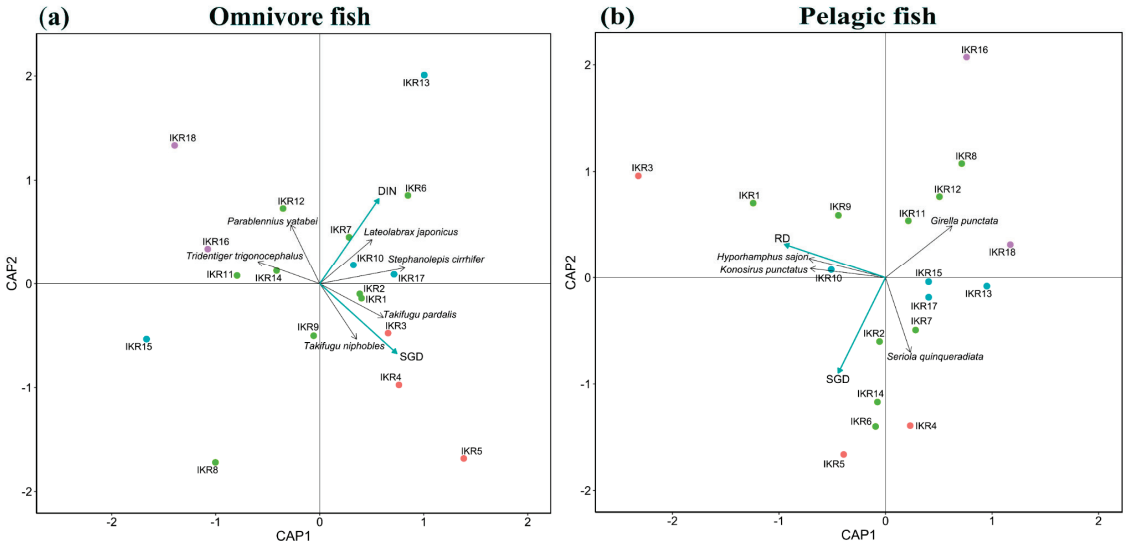


Figure 5. dbRDA results show model residual variables in (**a**) omnivore and (**b**) pelagic fish communities. Point colors relate to the SGD level of each station: red for SGD value > 0.07 m/d, green for SGD value range 0.05–0.07 m/d, blue for SGD value range 0.07–0.05 m/d, and purple for SGD value < 0.03. Blue arrows and black arrows represent environmental variables and fish species, respectively.

4. Discussion

To our knowledge, this is the first study to address questions of spatial patterns of coastal fish communities along with variability of SGD and other environmental factors, using a combination of taxonomic and functional approaches at the coastal-island scale. In this study, we found that the functional group composition of coastal fish is greatly influenced by several variables, such as SGD, RD, salinity, and DIN concentration. Especially, the difference in salinity associated with SGD may affect the spatial distribution of fish through their choice of habitat. The positive correlation between SGD, DSi, and DIP concentrations also provides evidence of the SGD-derived nutrient supply to coastal seawater. Thus, SGD can provide physico-chemical beneficial environmental conditions for the growth and survival of fish communities. For example, the recorded conditions at station IKR2 are characterized by high SGD and RD, coupled with low salinity, as well as elevated levels of nutrients and POM.

Generally, the freshwater SGD can reduce salinity and may act as a buffer against elevated seawater salinity [6,9]. Different fish species prefer different ranges of salinity for growth, survival, feeding, breeding, nursing, etc., throughout their life cycle. We suggest that. at a small spatial scale, varying salinities influenced the spatial distribution of fish diversity within the target study. Additionally, Hata et al. [53] confirmed a high abundance of small crustaceans near the sites with high SGD, which is an important food resource for secondary consumers. Similarly, the high occurrence of omnivore-demersal species, such as panther puffer (*Takifugu pardalis*) and grass puffer (*Takifugu niphobles*), at the high SGD sites in this study suggested a similar causality in a previous study in northern Japan [54]. On the other hand, Kim et al. [55] reveal that RD had an impact on the contribution of the phytoplankton community, which may have influenced higher-trophic consumers, such as planktivore pelagic fish (*Konosirus punctatus*) and omnivore pelagic fish (*Hyporhamphus sajori*) in this study. Besides, the DIN/DIP and DIN/DSi ratios in the seawater of the target area are lower than the Redfield ratio, indicating that primary production is a nitrogen-limited condition [29]. Over recent decades, nutrient concentrations in the SIS have significantly shifted due to comprehensive efforts to reduce anthropogenic nutrient inputs, guided by the Total Pollutant Load Control System initiated in 1979 [56–58]. As a result, the SIS is currently characterized by oligotrophic conditions [59–61]. Several studies have identified nutrient scarcity resulting from oligotrophication as a critical factor in the declining fishery yields in the SIS [30,58,60]. Tanda and Harada [62] have revealed that reductions in nutrient levels are correlated with the fluctuation in the production of small pelagic and demersal fish species.

Besides, this study highlighted the advantages of the eDNA method, which provides a more comprehensive detection of fish species across an entire island than traditional methods, which have limitations in covering large areas [63–65]. According to Nhat et al. [29], eDNA technology can achieve similar or better results in assessing fish diversity than traditional monitoring methods. In this study, we demonstrated the feasibility of rapid marine biodiversity sampling using eDNA combined with functional traits to characterize the composition of coastal island ecosystems. Furthermore, eDNA can be used to capture the spatial distribution of fish communities within a coastal area. Several studies have shown that eDNA signals are localized in marine environments, leading to spatial patterns of fish diversity [20,21]. Here, we observed spatial variations in taxonomic and functional patterns of fish communities based on the localized signals of eDNA in the target area. Therefore, these results suggest that eDNA can provide a solution for rapid application in coastal monitoring of the spatial variability of fish diversity.

However, our study still had a few limitations. While eDNA is a valuable tool for obtaining species information, its current application is constrained in providing insights into the developmental stages of the detected organisms. Moreover, although multiple physico-chemical parameters were analyzed to understand the drivers of fish community composition, this investigation did not encompass the impact of associated communities, such as invertebrates and phytoplankton, which were not monitored during the study

period. Future studies should consider developing a hybrid monitoring approach that integrates frequent eDNA surveys with traditional methods, such as fishing, Underwater Visual Census (UVC), and Baited Remote Underwater Video (BRUV). For example, combining eDNA metabarcoding with visual census methods and food web structure analysis (e.g., model analysis, stable isotope analysis) could offer a comprehensive overview of local fish composition and facilitate the exploration of relationships between fish assemblages and benthic communities. This integrated approach would enable more consistent and holistic monitoring of aquatic ecosystems. Incorporating historical survey data can enhance the precision of eDNA assays and provide a robust framework for interpreting the results. By addressing these limitations and adopting a more integrated monitoring approach, future research can achieve a more detailed and accurate understanding of the diversity and structure of fish communities, thereby improving the effectiveness of conservation and management strategies for coastal ecosystems.

5. Conclusions

In conclusion, this study demonstrated that the spatial patterns of diversity and composition of fish communities were related to the patterns of environmental variables. SGD is well recognized as one of the important factors that shape fish functional communities. This study also confirmed the usefulness of the eDNA method for assessing fish distribution and diversity in coastal ecosystems. By integrating taxonomic and functional diversity, eDNA monitoring provides complementary perspectives on community functions, thereby enhancing the overall assessment of community composition. To achieve a more detailed understanding of fish community diversity and structure, future research should incorporate eDNA methods alongside traditional monitoring techniques and consider a broader range of ecological variables. This integrated approach will offer a more comprehensive understanding of the factors shaping fish communities and improve the effectiveness of coastal ecosystem monitoring.

Supplementary Materials: The following supporting information can be downloaded at: https://www.mdpi.com/article/10.3390/biology13080609/s1, Figure S1: Heatmap of relative abundance (%) of fish family by eDNA metabarcoding at each station. The heatmap colors represent the relative abundances of fish species. Sorting is in proportion to relative abundance, with a decreasing trend from top to bottom; Table S1: Fish information in the target island.

Author Contributions: Conceptualization, M.S. and S.-i.O.; Methodology, M.S., S.-i.O., M.H. and N.H.N.; Validation, S.-i.O.; Formal analysis, N.H.N.; Investigation, M.S., S.-i.O., M.H., F.H. and N.H.N.; Data curation, N.H.N., M.H., M.S., F.H. and H.N.; Writing—original draft preparation, N.H.N.; Writing—review and editing, N.H.N., M.S., M.H., F.H. and H.N.; Visualization, N.H.N.; Supervision, M.S. and S.-i.O.; Project Administration, M.S. All authors have read and agreed to the published version of the manuscript.

Funding: This research was supported by JSPS Grant-in-Aid for Scientific Research (B) (No. 21H03650, PI: Mitsuyo Saito), Fostering Joint International Research (A) (No. 20KK0262, PI: Mitsuyo Saito) and The Asia-Pacific Network for Global Change Research (APN) (No. CRRP2019-09MY-Onodera, PI: Shin-ichi Onodera).

Institutional Review Board Statement: Not applicable.

Informed Consent Statement: Not applicable.

Data Availability Statement: The raw data supporting the conclusions of this article will be made available by the corresponding author on request.

Acknowledgments: We would like to express our gratitude to Tatsuya Sakamoto for support in using the laboratory of Ushimado Marine Institute for eDNA analysis. We would like to thank our laboratory members at Hiroshima University and Okayama University for their support in field campaigns and laboratory analyses.

Conflicts of Interest: The authors declare that they have no known competing financial interests or personal relationships that could have appeared to influence the work reported in this paper. The funders had no role in the design of the study; in the collection, analyses, or interpretation of data; in the writing of the manuscript; or in the decision to publish the results.

References

1. Fabricius, K.E. Effects of Terrestrial Runoff on the Ecology of Corals and Coral Reefs: Review and Synthesis. *Mar. Pollut. Bull.* **2005**, *50*, 125–146. [CrossRef]
2. Kuang, T.; Chen, W.; Huang, S.; Liu, L.; Zhou, L. Environmental Drivers of the Functional Structure of Fish Communities in the Pearl River Estuary. *Estuar. Coast. Shelf Sci.* **2021**, *263*, 107625. [CrossRef]
3. Encarnação, J.; Leitão, F.; Range, P.; Piló, D.; Chícharo, M.A.; Chícharo, L. Local and Temporal Variations in Near-Shore Macrobenthic Communities Associated with Submarine Groundwater Discharges. *Mar. Ecol.* **2015**, *36*, 926–941. [CrossRef]
4. Vinagre, C.; Máguas, C.; Cabral, H.N.; Costa, M.J. Spatial Variation in River Runoff into a Coastal Area—An Ecological Approach. *J. Sea Res.* **2011**, *65*, 362–367. [CrossRef]
5. Moosdorf, N.; Oehler, T. Societal Use of Fresh Submarine Groundwater Discharge: An Overlooked Water Resource. *Earth Sci. Rev.* **2017**, *171*, 338–348. [CrossRef]
6. La Valle, F.F.; Kantar, M.B.; Nelson, C.E. Coral Reef Benthic Community Structure Is Associated with the Spatiotemporal Dynamics of Submarine Groundwater Discharge Chemistry. *Limnol. Oceanogr.* **2021**, *66*, 188–200. [CrossRef]
7. Getz, E.; Eckert, C. Effects of Salinity on Species Richness and Community Composition in a Hypersaline Estuary. *Estuaries Coasts* **2023**, *46*, 2175–2189. [CrossRef]
8. Fujita, K.; Shoji, J.; Sugimoto, R.; Nakajima, T.; Honda, H.; Takeuchi, M.; Tominaga, O.; Taniguchi, M. Increase in Fish Production through Bottom-Up Trophic Linkage in Coastal Waters Induced by Nutrients Supplied via Submarine Groundwater. *Front. Environ. Sci.* **2019**, *7*, 82. [CrossRef]
9. Lilkendey, J.; Pisternick, T.; Neumann, S.I.; Dumur Neelayya, D.; Bröhl, S.; Neehaul, Y.; Moosdorf, N. Fresh Submarine Groundwater Discharge Augments Growth in a Reef Fish. *Front. Mar. Sci.* **2019**, *6*, 613. [CrossRef]
10. Ruppert, K.M.; Kline, R.J.; Rahman, M.S. Past, Present, and Future Perspectives of Environmental DNA (EDNA) Metabarcoding: A Systematic Review in Methods, Monitoring, and Applications of Global EDNA. *Glob. Ecol. Conserv.* **2019**, *17*, e00547. [CrossRef]
11. Nguyen, B.N.; Shen, E.W.; Seemann, J.; Correa, A.M.S.; O'Donnell, J.L.; Altieri, A.H.; Knowlton, N.; Crandall, K.A.; Egan, S.P.; McMillan, W.O.; et al. Environmental DNA Survey Captures Patterns of Fish and Invertebrate Diversity across a Tropical Seascape. *Sci. Rep.* **2020**, *10*, 6729. [CrossRef] [PubMed]
12. Kume, M.; Lavergne, E.; Ahn, H.; Terashima, Y.; Kadowaki, K.; Ye, F.; Kameyama, S.; Kai, Y.; Henmi, Y.; Yamashita, Y.; et al. Factors Structuring Estuarine and Coastal Fish Communities across Japan Using Environmental DNA Metabarcoding. *Ecol. Indic.* **2021**, *121*, 107216. [CrossRef]
13. Bleijswijk, J.D.L.; Engelmann, J.C.; Klunder, L.; Witte, H.J.; Witte, J.I.; Veer, H.W. Analysis of a Coastal North Sea Fish Community: Comparison of Aquatic Environmental DNA Concentrations to Fish Catches. *Environ. DNA* **2020**, *2*, 429–445. [CrossRef]
14. McElroy, M.E.; Dressler, T.L.; Titcomb, G.C.; Wilson, E.A.; Deiner, K.; Dudley, T.L.; Eliason, E.J.; Evans, N.T.; Gaines, S.D.; Lafferty, K.D.; et al. Calibrating Environmental DNA Metabarcoding to Conventional Surveys for Measuring Fish Species Richness. *Front. Ecol. Evol.* **2020**, *8*, 276. [CrossRef]
15. Lee, Y.D.; Lee, G.M.; Park, J.Y.; Gwak, W.S. Comparing Environmental DNA Metabarcoding and Underwater Visual Census to Monitor Korean Coastal Fish Community. *Ocean. Sci. J.* **2022**, *57*, 592–606. [CrossRef]
16. Gösser, F.; Schweinsberg, M.; Mittelbach, P.; Schoenig, E.; Tollrian, R. An Environmental DNA Metabarcoding Approach versus a Visual Survey for Reefs of Koh Pha-ngan in Thailand. *Environ. DNA* **2023**, *5*, 297–311. [CrossRef]
17. Saccò, M.; Guzik, M.T.; van der Heyde, M.; Nevill, P.; Cooper, S.J.B.; Austin, A.D.; Coates, P.J.; Allentoft, M.E.; White, N.E. eDNA in Subterranean Ecosystems: Applications, Technical Aspects, and Future Prospects. *Sci. Total Environ.* **2022**, *820*, 153223. [CrossRef] [PubMed]
18. Xing, Y.; Gao, W.; Shen, Z.; Zhang, Y.; Bai, J.; Cai, X.; Ouyang, J.; Zhao, Y. A Review of Environmental DNA Field and Laboratory Protocols Applied in Fish Ecology and Environmental Health. *Front. Environ. Sci.* **2022**, *10*, 725360. [CrossRef]
19. Blabolil, P.; Harper, L.R.; Říčanová, Š.; Sellers, G.; Di Muri, C.; Růža, T.; Vašek, M.; Sajdlová, Z.; Rychtecký, P.; Znachor, P.; et al. Environmental DNA Metabarcoding Uncovers Environmental Correlates of Fish Communities in Spatially Heterogeneous Freshwater Habitats. *Ecol. Indic.* **2021**, *126*, 107698. [CrossRef]
20. Zhong, W.; Zhang, J.; Wang, Z.; Lin, J.; Huang, X.; Liu, W.; Li, H.; Pellissier, L.; Zhang, X. Holistic Impact Evaluation of Human Activities on the Coastal Fish Biodiversity in the Chinese Coastal Environment. *Environ. Sci. Technol.* **2022**, *56*, 6574–6583. [CrossRef]
21. Czeglédi, I.; Sály, P.; Specziár, A.; Preiszner, B.; Szalóky, Z.; Maroda, Á.; Pont, D.; Meulenbroek, P.; Valentini, A.; Erős, T. Congruency between Two Traditional and EDNA-Based Sampling Methods in Characterising Taxonomic and Trait-Based Structure of Fish Communities and Community-Environment Relationships in Lentic Environment. *Ecol. Indic.* **2021**, *129*, 107952. [CrossRef]

22. Camara, E.M.; de Andrade-Tubino, M.F.; Franco, T.P.; Neves, L.M.; dos Santos, L.N.; dos Santos, A.F.G.N.; Araújo, F.G. Temporal Dimensions of Taxonomic and Functional Fish Beta Diversity: Scaling Environmental Drivers in Tropical Transitional Ecosystems. *Hydrobiologia* **2023**, *850*, 1911–1940. [CrossRef]
23. Li, Y.; Wang, J.; Ju, P.; Zhang, C.; Liu, B.; Wang, Y. Different Responses of Taxonomic and Functional Diversity to Environmental Changes: Case Study of Fish Communities in the Zhoushan Fishing Ground, China. *Aquat. Sci.* **2023**, *85*, 117. [CrossRef]
24. Shah Esmaeili, Y.; Corte, G.N.; Checon, H.H.; Bilatto, C.G.; Lefcheck, J.S.; Zacagnini Amaral, A.C.; Turra, A. Revealing the Drivers of Taxonomic and Functional Diversity of Nearshore Fish Assemblages: Implications for Conservation Priorities. *Divers. Distrib.* **2022**, *28*, 1597–1609. [CrossRef]
25. Aglieri, G.; Baillie, C.; Mariani, S.; Cattano, C.; Calò, A.; Turco, G.; Spatafora, D.; Di Franco, A.; Di Lorenzo, M.; Guidetti, P.; et al. Environmental DNA Effectively Captures Functional Diversity of Coastal Fish Communities. *Mol. Ecol.* **2021**, *30*, 3127–3139. [CrossRef] [PubMed]
26. Henriques, S.; Guilhaumon, F.; Villéger, S.; Amoroso, S.; França, S.; Pasquaud, S.; Cabral, H.N.; Vasconcelos, R.P. Biogeographical Region and Environmental Conditions Drive Functional Traits of Estuarine Fish Assemblages Worldwide. *Fish Fish.* **2017**, *18*, 752–771. [CrossRef]
27. Keck, B.P.; Marion, Z.H.; Martin, D.J.; Kaufman, J.C.; Harden, C.P.; Schwartz, J.S.; Strange, R.J. Fish Functional Traits Correlated with Environmental Variables in a Temperate Biodiversity Hotspot. *PLoS ONE* **2014**, *9*, e93237. [CrossRef] [PubMed]
28. Zhu, A.; Saito, M.; Onodera, S.; Shimizu, Y.; Jin, G.; Ohta, T.; Chen, J. Evaluation of the Spatial Distribution of Submarine Groundwater Discharge in a Small Island Scale Using the 222Rn Tracer Method and Comparative Modeling. *Mar. Chem.* **2019**, *209*, 25–35. [CrossRef]
29. Nhat, N.H.; Saito, M.; Hamada, M.; Onodera, S. Evaluation of the Effects of Environmental Factors on Seasonal Variations in Fish Diversity on a Coastal Island in Western Japan. *Environments* **2024**, *11*, 60. [CrossRef]
30. Yoneda, M.; Fujita, T.; Yamamoto, M.; Tadokoro, K.; Okazaki, Y.; Nakamura, M.; Takahashi, M.; Kono, N.; Matsubara, T.; Abo, K.; et al. Bottom-up Processes Drive Reproductive Success of Japanese Anchovy in an Oligotrophic Sea: A Case Study in the Central Seto Inland Sea, Japan. *Prog. Oceanogr.* **2022**, *206*, 102860. [CrossRef]
31. Fujita, T.; Yamamoto, M.; Kono, N.; Tomiyama, T.; Sugimatsu, K.; Yoneda, M. Temporal Variations in Hatch Date and Early Survival of Japanese Anchovy (*Engraulis japonicus*) in Response to Environmental Factors in the Central Seto Inland Sea, Japan. *Fish. Oceanogr.* **2021**, *30*, 527–541. [CrossRef]
32. *The eDNA Society Environmental DNA Sampling and Experiment Manual*; The eDNA Society: Otsu, Japan, 2019.
33. Takai, N.; Yorozu, A.; Tanimoto, T.; Hoshika, A.; Yoshihara, K. Transport Pathways of Microphytobenthos-Originating Organic Carbon in the Food Web of an Exposed Hard Bottom Shore in the Seto Inland Sea, Japan. *Mar. Ecol. Prog. Ser.* **2004**, *284*, 97–108. [CrossRef]
34. Minamoto, T.; Miya, M.; Sado, T.; Seino, S.; Doi, H.; Kondoh, M.; Nakamura, K.; Takahara, T.; Yamamoto, S.; Yamanaka, H.; et al. An Illustrated Manual for Environmental DNA Research: Water Sampling Guidelines and Experimental Protocols. *Environ. DNA* **2021**, *3*, 8–13. [CrossRef]
35. Miya, M.; Sato, Y.; Fukunaga, T.; Sado, T.; Poulsen, J.Y.; Sato, K.; Minamoto, T.; Yamamoto, S.; Yamanaka, H.; Araki, H.; et al. MiFish, a Set of Universal PCR Primers for Metabarcoding Environmental DNA from Fishes: Detection of More than 230 Subtropical Marine Species. *R. Soc. Open Sci.* **2015**, *2*, 150088. [CrossRef] [PubMed]
36. Zhu, T.; Sato, Y.; Sado, T.; Miya, M.; Iwasaki, W. MitoFish, MitoAnnotator, and MiFish Pipeline: Updates in 10 Years. *Mol. Biol. Evol.* **2023**, *40*, msad035. [CrossRef] [PubMed]
37. Sato, Y.; Miya, M.; Fukunaga, T.; Sado, T.; Iwasaki, W. MitoFish and MiFish Pipeline: A Mitochondrial Genome Database of Fish with an Analysis Pipeline for Environmental DNA Metabarcoding. *Mol. Biol. Evol.* **2018**, *35*, 1553–1555. [CrossRef] [PubMed]
38. Iwasaki, W.; Fukunaga, T.; Isagozawa, R.; Yamada, K.; Maeda, Y.; Satoh, T.P.; Sado, T.; Mabuchi, K.; Takeshima, H.; Miya, M.; et al. Mitofish and Mitoannotator: A Mitochondrial Genome Database of Fish with an Accurate and Automatic Annotation Pipeline. *Mol. Biol. Evol.* **2013**, *30*, 2531–2540. [CrossRef] [PubMed]
39. Elliott, M.; Whitfield, A.K.; Potter, I.C.; Blaber, S.J.M.; Cyrus, D.P.; Nordlie, F.G.; Harrison, T.D. The Guild Approach to Categorizing Estuarine Fish Assemblages: A Global Review. *Fish Fish.* **2007**, *8*, 241–268. [CrossRef]
40. Able, K.W.; Simenstad, C.A.; Strydom, N.A.; Bradley, M.; Sheaves, M. Habitat Use and Connectivity. In *Fish and Fisheries in Estuaries*; Wiley: Hoboken, NJ, USA, 2022; pp. 188–254.
41. Hwang, D.W.; Lee, I.S.; Choi, M.; Kim, T.H. Estimating the Input of Submarine Groundwater Discharge (SGD) and SGD-Derived Nutrients in Geoje Bay, Korea Using222Rn-Si Mass Balance Model. *Mar. Pollut. Bull.* **2016**, *110*, 119–126. [CrossRef] [PubMed]
42. Hwang, D.W.; Lee, Y.W.; Kim, G. Large Submarine Groundwater Discharge and Benthic Eutrophication in Bangdu Bay on Volcanic Jeju Island, Korea. *Limnol. Oceanogr.* **2005**, *50*, 1393–1403. [CrossRef]
43. Street, J.H.; Knee, K.L.; Grossman, E.E.; Paytan, A. Submarine Groundwater Discharge and Nutrient Addition to the Coastal Zone and Coral Reefs of Leeward Hawai'i. *Mar. Chem.* **2008**, *109*, 355–376. [CrossRef]
44. Tamborski, J.J.; Cochran, J.K.; Bokuniewicz, H.J. Submarine Groundwater Discharge Driven Nitrogen Fluxes to Long Island Sound, NY: Terrestrial vs. Marine Sources. *Geochim. Cosmochim. Acta* **2017**, *218*, 40–57. [CrossRef]
45. Oehler, T.; Tamborski, J.; Rahman, S.; Moosdorf, N.; Ahrens, J.; Mori, C.; Neuholz, R.; Schnetger, B.; Beck, M. DSi as a Tracer for Submarine Groundwater Discharge. *Front. Mar. Sci.* **2019**, *6*, 563. [CrossRef]

46. Hwang, D.W.; Kim, G.; Lee, Y.W.; Yang, H.S. Estimating Submarine Inputs of Groundwater and Nutrients to a Coastal Bay Using Radium Isotopes. *Mar. Chem.* **2005**, *96*, 61–71. [CrossRef]
47. Magneville, C.; Loiseau, N.; Albouy, C.; Casajus, N.; Claverie, T.; Escalas, A.; Leprieur, F.; Maire, E.; Mouillot, D.; Villéger, S. MFD: An R Package to Compute and Illustrate the Multiple Facets of Functional Diversity. *Ecography* **2022**, *2022*. [CrossRef]
48. Villéger, S.; Mason, N.W.H.; Mouillot, D. New Multidimensional Functional Diversity Indices for a Multifaceted Framework in Functional Ecology. *Ecology* **2008**, *89*, 2290–2301. [CrossRef] [PubMed]
49. Huang, H. LinkET: Everything Is Linkable. *R Package Version 0.0.3*, Shenzhen, China, 2021; Volume 2.
50. Zuur, A.F.; Ieno, E.N.; Elphick, C.S. A Protocol for Data Exploration to Avoid Common Statistical Problems. *Methods Ecol. Evol.* **2010**, *1*, 3–14. [CrossRef]
51. Bartoń, K. MuMIn: Multi-Model Inference. In *R Package Version 0.12.2*; PAS: Opalenica, Poland, 2023.
52. Oksanen, J.; Simpson, G.L.; Blanchet, F.G.; Kindt, R.; Legendre, P.; McGlinn, D.; Minchin, P.R.; O'Hara, R.B.; Solymos, P. Package "Vegan": Community Ecology Package. *R Package Version 2.6-7*, Helsinki, Finland, 2024.
53. Hata, M.; Sugimoto, R.; Hori, M.; Tomiyama, T.; Shoji, J. Occurrence, Distribution and Prey Items of Juvenile Marbled Sole *Pseudopleuronectes yokohamae* around a Submarine Groundwater Seepage on a Tidal Flat in Southwestern Japan. *J. Sea Res.* **2016**, *111*, 47–53. [CrossRef]
54. Utsunomiya, T.; Hata, M.; Sugimoto, R.; Honda, H.; Kobayashi, S.; Miyata, Y.; Yamada, M.; Tominaga, O.; Shoji, J.; Taniguchi, M. Higher Species Richness and Abundance of Fish and Benthic Invertebrates around Submarine Groundwater Discharge in Obama Bay, Japan. *J. Hydrol. Reg. Stud.* **2017**, *11*, 139–146. [CrossRef]
55. Kim, Y.; Lee, J.H.; Kang, J.J.; Lee, J.H.; Lee, H.W.; Kang, C.K.; Lee, S.H. River Discharge Effects on the Contribution of Small-Sized Phytoplankton to the Total Biochemical Composition of POM in the Gwangyang Bay, Korea. *Estuar. Coast. Shelf Sci.* **2019**, *226*, 106293. [CrossRef]
56. International EMECS Center. *Environmental Conservation of the Seto Inland Sea*; International EMECS Center, Ed.; Kobe International EMECS Center: Kobe, Japan, 2008.
57. Okaichi, T. Environmental Management of the Semi Enclosed Sea and Red Tide Problems in the Seto Inland Sea. *Fish. Sci.* **2002**, *68*, 483–488. [CrossRef] [PubMed]
58. Nishijima, W.; Umehara, A.; Yamamoto, K.; Asaoka, S.; Fujii, N.; Otani, S.; Wang, F.; Okuda, T.; Nakai, S. Temporal Distribution of Primary and Secondary Production Estimated from Water Quality Data in the Seto Inland Sea, Japan. *Ecol. Indic.* **2021**, *124*, 107405. [CrossRef]
59. Abo, K.; Yamamoto, T. Oligotrophication and Its Measures in the Seto Inland Sea, Japan. *Bull. Jpn. Fish. Res. Educ. Agency* **2019**, *49*, 21.
60. Yamamoto, T. The Seto Inland Sea—Eutrophic or Oligotrophic? In *Marine Pollution Bulletin*; Elsevier Ltd.: Amsterdam, The Netherlands, 2003; Volume 47, pp. 37–42.
61. Yanagi, T. Oligotrophication in the Seto Inland Sea. In *Eutrophication and Oligotrophication in Japanese Estuaries*; Yanagi, T., Ed.; Springer: Dordrecht, Germany, 2015; pp. 39–67.
62. Tanda, M.; Harada, K. Nutrient Environment and Fisheries in the Eastern Seto Inland Sea (Harima Nada). *Aquabiology* **2012**, *34*, 132–141.
63. Luo, Z.; Yang, C.; Wang, L.; Liu, Y.; Shan, B.; Liu, M.; Chen, C.; Guo, T.; Sun, D. Relationships between Fish Community Structure and Environmental Factors in the Nearshore Waters of Hainan Island, South China. *Diversity* **2023**, *15*, 901. [CrossRef]
64. Cheng, X.; Wang, Z.; Zhang, S.; Zhao, X.; Lin, J.; Huang, H.; Chen, Y.; Zou, Q. Analysis of Short-Term and Local Scale Variations in Fish Community Structure in Dachen Island Waters. *Front. Mar. Sci.* **2023**, *10*, 1199524. [CrossRef]
65. Snigirov, S.; Goncharov, O.; Sylantyev, S. The Fish Community in Zmiinyi Island Waters: Structure and Determinants. *Mar. Biodivers.* **2012**, *42*, 225–239. [CrossRef]

Disclaimer/Publisher's Note: The statements, opinions and data contained in all publications are solely those of the individual author(s) and contributor(s) and not of MDPI and/or the editor(s). MDPI and/or the editor(s) disclaim responsibility for any injury to people or property resulting from any ideas, methods, instructions or products referred to in the content.

biology

MDPI

Article

Evaluation of the Dietary Arginine Supplementation on Yellow Catfish: From a Low-Temperature Farming Perspective

Quanquan Cao [1]Mohamed S. Kisha [2], Alkhateib Gaafar [3], Abdelgayed Metwaly Younes [3], Haifeng Liu [1,*] and Jun Jiang [1,*]

[1] College of Animal Science and Technology, Sichuan Agricultural University, Chengdu 611130, China
[2] Hormones Department, National Research Centre, Dokki, Cairo 12622, Egypt; kishtamsa@gmail.com
[3] Hydrobiology Department, National Research Centre, Cairo 999060, Egypt; alkhateibyg@yahoo.com (A.G.); tahoon176@yahoo.com (A.M.Y.)
* Correspondence: liuhf@sicau.edu.cn (H.L.); jjun@sicau.edu.cn (J.J.)

Simple Summary: The study focused on the effects of dietary arginine (Arg) supplementation on yellow catfish (*Pelteobagrus fulvidraco*) under low-temperature stress (18 °C). Over eight weeks, 720 fish were divided into six groups and fed diets with varying Arg levels. The results showed that Arg supplementation improved growth, feed efficiency, digestive enzyme activity, and antioxidant responses in the fish. It also enhanced the expression of antioxidant-related genes. Based on the findings, the optimal Arg intake for yellow catfish under these conditions is 26.8 g per kg of diet, equivalent to 37.0 g of dietary protein.

Abstract: The yellow catfish is an economically significant freshwater fish with increasing importance in aquaculture. However, the low temperature environments prevalent in certain regions pose challenges to its growth, development, and overall health. This study aimed to explore the impact of dietary arginine (Arg) addition on the growth, digestive capacity, and intestinal antioxidant response in fish under low temperature acclimation (18 °C). Total 720 fish were randomly distributed into six groups, each containing 120 fish. Over the course of eight weeks, each group was fed with diets about varying Arg concentrations (1.79–3.26 g/kg). The results indicated that Arg supplementation resulted in an increase in specific growth rate (SGR), feed intake (FI), feed efficiency (FE), as well as pancreatic enzyme activities in both pancreas and intestine. Conversely, malondialdehyde (MDA) and protein carbonyl (PC) contents initially decreased but increased with higher Arg concentrations. Glutathione peroxidase 1a (GPX1a) showed a positive correlation with nuclear factor-erythroid 2-related factor-2 (Nrf2), showing its role in antioxidative capacity. Furthermore, this study revealed that Arg significantly enhanced the activities of anti-superoxide anion, anti-hydroxyl radical, and anti-oxidative enzymes, along with the relative mRNA abundance of Copper-Zinc superoxide dismutase (CuZnSOD), catalase, GPX1a, glutamate-cysteine ligase catalytic subunit (GCLC), and Nrf2 in the intestine. It was determined that yellow catfish weighing between 61.0 g and 89.0 g require an intake of 26.8 g of Arg per kilogram of diet based on polynomial regression analysis of specific growth rate (SGR), which is equivalent to 37.0 g of dietary protein, under sub-low temperature conditions of 18 °C.

Keywords: yellow catfish; arginine; growth performance; digestive ability; antioxidant ability; low-temperature

1. Introduction

There is evidence suggesting that environmental stress can disrupt homeostasis and negatively impact the functioning of biological systems [1]. Water temperature is commonly recognized as one of the significant factors influencing aquaculture. Accumulating evidence has demonstrated that low temperatures decrease growth, food intake, and feeding efficiency [2–6]. Previous studies have shown that dietary phosphorus supplementation under

low temperature improves cell viability, antioxidative capacity, energy production, and lipid transportation in puffer fish [7], suggesting that specific nutrients may play a significant part in ameliorating sub-low temperature-induced injury. However, limited research has been conducted on the effects of nutrients on fish exposed to sub-low temperature conditions.

Arginine (Arg), an indispensable amino acid for fish [8,9], plays multiple roles in cell metabolism and regulation. Apart from its requirement for protein synthesis, Arg is also involved in synthesizing important biochemicals such as ornithine, polyamines, proline, creatine, and nitric oxide [10]. Recent studies have increased on the dietary Arg requirements in different fish species. For juvenile yellow groupers (*Epinephelus awoara*) at 27.5 °C, the optimal amount of dietary Arg is estimated to be 2.8% of the dry diet [11], 2.17% for grass carp (*Ctenopharyngodon idellus*) at 28 °C [12], 2.85% for juvenile cobia (Rachycentron canadum) at 30 °C [13], 1.84% for blunt snout bream (*Megalobrama amblycephala*) at 30 °C [14], 2.46% for Indian major carp (*Cirrhinus mrigala*) at 26.5 °C [15], and 1.80% for Jian carp (*Cyprinus carpio*) at 26 °C [16]. It has been reported that a dietary requirement of 2.38% arginine (Arg) in dry diet is necessary for optimal growth of juvenile yellow catfish (*Pelteobagrus fulvidraco*) at 29 °C [17]. Fish have varying Arg requirements at different life stages, growth stages, physiological stages, and environmental conditions, such as water temperature. However, there is limited information available regarding the Arg requirements of yellow catfish at cold temperatures. Fish rely on digestive enzymes and brush border enzymes to digest and absorb nutrients for growth [18]. Several digestive enzymes, including trypsin, chymotrypsin, lipase, and amylase, are produced in the fish exocrine pancreas [19]. Other enzymes, such as γ-glutamyl transpeptidase (γ-GT), alkaline phosphatase (AKP), Na^+/K^+-ATPase (NKA), and creatine kinase (CK), are essential for the final stages of food digestion and assimilation in fish [20]. In a previous study, dietary supplementation of Arg improved the digestive and absorptive abilities of carp (*Cyprinus carpio*) [21]. Similarly, in weaned piglets, the addition of Arg to the diet promoted the development of intestinal mucosa and improved the activity of intestinal sugar digestive enzymes [22]. However, there is currently no research available on the influence of Arg on the digestive abilities and absorptive functions of yellow catfish, particularly under sub-low temperature, which necessitates further investigation.

The intestine plays a crucial role as the primary site for antioxidant capacity in fish [23]. The maintenance of structural integrity and functionality in the fish intestine relies on the capacity of the intestinal antioxidant system [24]. Oxidative damage occurs when the rate of reactive oxygen species (ROS) scavenging by the antioxidant system is lower than the rate of ROS production, as noted by Matés and Sánchez-Jiménez [25]. Li et al. (2014) found that shrimp exhibited increased ROS content when exposed to cold temperatures (17 °C) [26]. Previous research indicates that low water temperatures induce cytomembrane oxidation and antioxidative actions, resulting in increased malondialdehyde (MDA) and protein carbonyl (PC) contents in tail skeletal muscle [27]. Low temperatures have also been found to decrease antioxidant enzyme activities in *Litopenaues vannamei* [4], suggesting that low temperatures reduce antioxidant capacity. Fish intestinal antioxidant capacity improves with enhanced enzyme activities, increased non-enzymatic antioxidant levels, and upregulated antioxidant enzyme gene expression. Nuclear factor-red lineage 2-related factor-2 (Nrf2) is well characterized in sensing oxidants and regulating the expression of antioxidant enzymes-related genes [28]. The addition of Arg to the diet of grass carp increased the intestinal antioxidant enzymes activities and non-enzymatic antioxidant content. However, it remains uncertain whether dietary Arg supplementation can decrease low temperature-induced oxidative damage by enhancing the antioxidant capacity of the intestine.

Yellow catfish has gained popularity in China's freshwater fish farming industry due to its delicious meat quality and high economic value [29]. Being a poikilothermic fish, the water temperature plays a crucial role in its life [30]. The yellow catfish usually grows in freshwater between 20 °C and 32 °C. The optimum growth temperature is 26.8 °C and temperatures below 19 °C leads to reduce food intake and growth performance in yellow

catfish [31]. In China, yellow catfish experience their last growth stage during fall when the water temperature drops to 18 ± 2 °C. However, yellow catfish farming faces challenges in sub-low temperature environments, which can negatively impact fish health and growth. Addressing these challenges is crucial to ensure sustainable aquaculture production. One potential solution lies in optimizing the nutritional composition of fish diets, specifically through dietary supplementation of arginine. The dietary requirements of Arg for yellow catfish under these conditions are not yet clearly understood. This study aims to address the critical need for optimized dietary formulations for yellow catfish, particularly in low-temperature farming conditions where growth rates and feed efficiency can be severely compromised. By evaluating the effects of dietary arginine supplementation, this research seeks to enhance the understanding of amino acid requirements in yellow catfish, ultimately contributing to more sustainable aquaculture practices in challenging environments.

2. Materials and Methods

2.1. Experimental Diets

The L-Arg (>99% purity) used in this study was supplied by Hengyuan Biotech Co., (Shanghai, China). The main protein sources for the test diets included fish meal, rapeseed meal, soybean meal, and maize protein meal, providing a protein content of approximately 37% (Table 1). The diets contained approximately 7% lipid, with soya bean oil being the main lipid source. Six test diets were prepared by adding L-Arg to the diet at concentrations of 1.79 g/kg (control), 2.11 g/kg, 2.36 g/kg, 2.68 g/kg, 2.95 g/kg, and 3.26 g/kg, respectively. All feeds were isonitrogenous and isoenergetic by the addition of glycine. The granular mixture was extruded using a 2 mm diameter screw extruder (SYX62, Xiamen, China), air-dried, and stored in a refrigerator at −20 °C.

Table 1. Composition and nutrients content of diets (g/kg).

Ingredient	Arg 0.179%	Arg 0.211%	Arg 0.236%	Arg 0.268%	Arg 0.295%	Arg 0.326%
Soybean meal	100	100	100	100	100	100
Rapeseed meal	103	103	103	103	103	103
Fishmeal	230	230	230	230	230	230
wheat flour	254	255	256	258	259	260
Corn gluten meal	210	210	210	210	210	210
Soya bean oil	20	20	20	20	20	20
Lysine	9	9	9	9	9	9
Threonine	3	3	3	3	3	3
L-Gly	21	17	13	8	4	0
L-Arg-HCL	0	3	6	9	12	15
CaH_2PO_4	20	20	20	20	20	20
Choline chloride	5	5	5	5	5	5
Vitamin premix/g/kg [1]	10	10	10	10	10	10
Mineral premixg/kg [2]	15	15	15	15	15	15
Nutrients content (%) [3]						
Crude protein	36.8	37.2	36.8	36.8	37.2	36.9
Crude lipid	7.00	6.98	6.97	6.69	6.93	6.60
Ash	7.67	7.75	7.83	7.92	7.54	7.58
Arg	1.79	2.11	2.36	2.68	2.95	3.26

[1] Soybean meal (COFCO Oil Qinzhou Co., Ltd., Qinzhou, China), Rapeseed meal (Chengdu Huatai Grain and Oil Ltd., Chengdu, China), Fish meal (TASA Steam dried fishmeal, Lima, Peru), Corn gluten meal (Changchun Dacheng Industry Group, Changchun, China), Wheat meal (China National Cereals, Oils and Foodstuffs Corporation, Beijing, China), Soy oil (Baker Commodities Inc., Vernon, CA, USA); [2] Vitamin premix (Chengdu NutriMax Animal Health Co., Ltd., Chengdu, China, IU or g/kg premix): retinyl acetate, 2,500,000 IU; cholecalciferol, 500,000 IU; α-tocopherol, 6700 IU; thiamine, 10; riboflavin, 6; pyridoxine hydrochloride, 12; nicotinic acid, 40; d-calcium pantothenate, 15; biotin, 0.25; folic acid, 0.4; inositol, 200; cyanocobalamin 0.02; menadione, 4. All ingredients were diluted with corn starch to 1 kg. [2] Mineral premix (g/kg premix): $FeC_6H_5O_7$, 4.57; $ZnSO_4{\cdot}7H_2O$, 9.43; $MnSO_4{\cdot}H_2O$, 4.14; $CuSO_4{\cdot}5H_2O$, 6.61; $MgSO_4{\cdot}7H_2O$, 238.97; KI, 1.10 g; $NaSeO_3$, 2.50 g; $CoCl_2{\cdot}6H_2O$, 1.36. All ingredients were diluted with $CaCO_3$ to 1 kg. [3] Crude protein, crude fat and ash were measured by using the Association of Official Analytical Chemists (AOAC, 1990) methods. Arg concentrations were measured using high performance liquid chromatography (Agilent Technologies, PaloAlto, CA, USA).

2.2. Fish Trial

Yellow catfish were obtained from Sichuan Rongsen Corporation (Sichuan, China) and acclimatized to the laboratory environment for one month. In the experiment, 720 yellow catfish, averaging 61.2 ± 0.3 g in initial weight, were randomly distributed across 18 tanks (200 cm × 100 cm × 105 cm), with 40 fish per tank. They were fed their respective diets twice daily for 8 weeks to ensure satiety. The water temperature was measured three times a day (08:00, 13:00, and 18:00), and the average water temperature was maintained at 18 ± 2 °C (Automatic control equipment tank, Qingdao Zhongyi Limited Liability Company). Other water quality parameters were measured at 8:00 daily, with a pH of 7.0 ± 0.3 and dissolved oxygen levels maintained above 5 mg/L. A continuous flow rate of 1.2 L/min per water tank was maintained. The photoperiod was natural and all tanks had similar lighting conditions. The study received approval from the Animal Care Advisory Committee of Sichuan Agricultural University under permit No. DKY-S20170512.

2.3. Sample Collection and Analysis

Any uneaten feed was collected 30 min after each feeding session and subsequently dried in an oven at 65 °C to determine the feed intake (FI). Initial body weight (IBW) and Final body weight (FBW) were measured and survival rate (SR), percent weight gain (PWG), specific growth rate (SGR) and feeding efficiency (FE) were calculated. Fish in each tank were weighed at the start and conclusion of the feeding trial. Four fish per tank were randomly selected to assess carcass proximate composition. Twenty-four hours after the final feeding, 12 fish from each group were anesthetized with tricaine methane sulfonate (MS222) at 120 mg/L. Samples were collected to measure the following: visceral index, stomach protein content (SPC), pancreatic protein content (PPC), intestinal protein content (IPC), liver protein content (LPC), hepatosomatic index (HSI) and intestinal enzyme activities [32]. Additionally, twelve additional fish were removed from each tank. Their intestines were quickly extracted, kept in liquid nitrogen, and preserved at −80 °C until gene expression was determined.

2.4. Biochemical Analysis

The dry matter content of the diets and fish were analyzed according to the method 934.01, (AOAC, 1990). The samples were desiccated at a temperature of 104 °C until constant weight for the analysis of dry matter. The total nitrogen (N) was determined according to the method 968.0 (AOAC, 1990) after acid digestion was performed. The crude protein (CP) was obtained by multiplying the total N content by 6.25. The moisture was determined according to the method 935.29 (AOAC, 1990). The crude lipid (EE) was analyzed using the Soxhlet extraction method 983.15 (AOAC, 1990), and the ash contents were examined in the muffle furnace at 550 °C for 4 h according to the method 942.05.

The method used to determine the approximate composition of experimental feeds and entire carcasses was established by the Association of Official Analytical Chemists (AOAC, 1990). Pancreatic, gastric, and intestinal samples were homogenized in a ratio of 1:10 (w/v) in ice-cold saline and then centrifuged at 6000× g at 4 °C for 20 min. Enzyme activity and protein content were determined from the supernatant. The tissue protein contents of each group were measured based on the Bradford method [33]. The activities of pepsin, trypsin, and chymotrypsin were determined according to [34]. Amylase and lipase enzyme activities were measured using the method described by. AKP, NKA, γ-GT, and CK activities were measured as outlined by [35].

The MDA and PC contents were determined using the method described by [36]. CAT activity was measured according to the method [37]. SOD and GPX activities were determined as outlined by [38]. GST activity was measured by monitoring the decrease in GSH concentration, and GR activity was determined by measuring the depletion of NADPH during GSH production according to [39]. The total glutathione (T-GSH) content was measured according to [40], while the anti-superoxide anion (ASA) and anti-hydroxyl radical (AHR) capacity were measured according to [41].

2.5. Real-Time Quantitative PCR

Real-time quantitative PCR was used to detect gene expression. Total RNA was extracted from the intestine using TRIZOL reagent (Invitrogen, Carlsbad, CA, USA) according to the manufacturer's instructions. RNA quantity and quality were assessed by 1% agarose gel electrophoresis and spectrophotometry at 260 and 280 nm. cDNA synthesis was performed with a PrimeScript® Reverse Transcription Kit and gDNA Eraser (TaKaRa, TaKaRa Bio Inc., Shiga, Japan). Specific primers for CuZnSOD, CAT, GPX1a, GCLC, and Nrf2 genes were designed using Primer Premier software (Premier Biosoft International, Palo Alto, CA, USA) based on yellow catfish sequences (GenBank accession nos. KX455916, KX455919, KY312111, KX455918, KX455917) (Table 2). Real-time PCR analysis was conducted with the CFX96 Real-Time PCR Detection System (Bio-Rad, Hercules, CA, USA). The PCR conditions included initial denaturation at 98 °C for 1 min, followed by 40 cycles of denaturation at 95 °C for 5 s and annealing at the temperature specified in Table 2 for 30 s. PCR efficiency was estimated using cDNA sequence dilution analysis, aiming for near 100% efficiency. Relative gene expression was calculated using the $2^{-\Delta\Delta CT}$ method was used to calculate relative gene expression. To normalize the cDNA load, β-actin was utilized as the internal reference gene. The relative expression of the target gene was then normalized to the expression of β-actin in the same sample.

Table 2. Primer sequences, optimal annealing temperatures (OAT), and amplification products (AP) of genes selected for analysis by real-time PCR.

Primes	Sequences	OAT (°C)	AP (bp)	Accession Number
β-actin-RTF	CCTAAAGCCAACAGGGAAAA	59.0	186 bp	EU161066
β-actin-RTR	ATGGGGCAGAGCATAACC			
CuZnSOD-RTF	ATCTGGGTAATGTGACTGCCGA	60.4	152 bp	KX455916
CuZnSOD-RTR	TTCATCATCTCCGCCCTTGC			
CAT-RTF	ACACCGATGAGGGAAACTGG	58	89 bp	KX455919
CAT-RTR	GTGGATGAAGGACGGGAACA			
GPX 1a-RTF	GTGACGACTCTGTGTCCTTG	61.0	139 bp	KY312111
GPX 1a-RTR	AACCTTCTGCTGTATCTCTTGA			
GCLC-RTF	GACAAACGGAGGAAGGAGG	58.2	161 bp	KX455918
GCLC-RTR	TCATCAGGAAAGAAGAGGGACT			
Nrf2-RTF	CGGAACAAGATGGAGAAGCC	64.0	122 bp	KX455917
Nrf2-RTR	ACAGGGAGGAATGGAGGGA			

Copper–zinc superoxide dismutase (CuZnSOD); Catalase (CAT); Glutathione peroxidase-1a (GPx1a); γ-glutamylcysteine ligase catalytic subunit (GCLC); Nuclear factor erythroid 2-related factor 2 (Nrf2).

2.6. Data Analysis

Data were analyzed using the PROC MIXED procedure of SAS 9.3 (SAS Inst. Inc., Cary, NC, USA) with the model: $Y_{ijkl} = \mu + T_i + P_j + S_k + C(_k)_l + T \times S_{ik} + e_{ijkl}$, where Y_{ijkl} refers to the dependent variable; μ, the overall mean; T_i, the fixed treatment effect; P_j, the random period effect; S_k, the random square effect; $C(_k)_l$, the random effect of the lth steer within the kth square; $T \times S_{ik}$, the interaction between the ith treatment and the kth square; and e_{ijkl}, the error residual. The linear and quadratic effects of increasing levels of GA were evaluated using the CONTRAST procedure of SAS 9.3. The Kenward-Roger option was used to calculate the degrees of freedom. Differences among the means of different treatments were tested using Duncan's test. Effects were considered significant at $p \leq 0.05$. All values are presented as least squares means ± standard errors (SE).

3. Results

The mortality rate was low, with only one death occurring among all the groups fed with 2.11% dry feed after one week.

3.1. Growth Performance and Somatic Parameters

The parameters of PWG, SGR, FE, FI, and PER showed a significant increase when the Arg level reached 2.68 g/kg, followed by a significant decrease, as presented in Table 3

($p < 0.05$). The SGR was lowest in the basal diet group ($p < 0.05$). Based on the quadratic regression equation for SGR, the Arg requirement for yellow catfish was evaluated as 2.68 g/kg diet in the fall (water temperature: 18 ± 2 °C), corresponding to a diet protein content of 37 g/kg (Figure 1).

Table 3. Growth performance of yellow catfish fed diets with graded levels of Arg (g/kg) for 8 weeks.

Ingredient	Arg 0.179%	Arg 0.211%	Arg 0.236%	Arg 0.268%	Arg 0.295%	Arg 0.326%	*p*-Value
IBW	61.2 ± 0.17	61.2 ± 0.17	61.2 ± 0.17	61.3 ± 0.17	61.3 ± 0.17	61.3 ± 0.17	0.326
FBW	80.9 ± 0.26 ^{a}	84.4 ± 0.30 ^{ab}	86.9 ± 0.32 ^{bc}	88.9 ± 2.45 ^{c}	86.8 ± 1.74 ^{bc}	85.1 ± 0.32 ^{bc}	0.042
PWG	32.3 ± 0.60 ^{a}	38.0 ± 0.75 ^{b}	42.1 ± 0.49 ^{c}	45.0 ± 0.74 ^{d}	41.5 ± 0.78 ^{c}	38.8 ± 0.15 ^{b}	0.033
SGR	0.50 ± 0.01 ^{a}	0.58 ± 0.01 ^{b}	0.63 ± 0.01 ^{c}	0.66 ± 0.01 ^{d}	0.62 ± 0.02 ^{c}	0.59 ± 0.01 ^{b}	0.031
SR	100 ± 0.00	99.2 ± 0.83	98.3 ± 0.83	100 ± 0.00	97.5 ± 2.5	100 ± 0.00	0.935
FI	40.9 ± 0.89 ^{a}	46.7 ± 2.03 ^{ab}	48.0 ± 2.36 ^{ab}	49.4 ± 2.31 ^{b}	46.9 ± 2.50 ^{b}	46.6 ± 2.43 ^{ab}	0.047
FE	48.4 ± 0.91 ^{a}	50.0 ± 0.09 ^{ab}	53.6 ± 0.42 ^{cd}	55.8 ± 1.22 ^{d}	54.2 ± 1.06 ^{d}	51.4 ± 0.62 ^{bc}	0.024
PER	1.32 ± 0.03 ^{a}	1.33 ± 0.03 ^{ab}	1.33 ± 0.02 ^{ab}	1.51 ± 0.01 ^{d}	1.46 ± 0.03 ^{cd}	1.41 ± 0.03 ^{bc}	0.019
Regression							
$Y_{SGR} = -0.190X^2 + 1.017X - 0.717$					X = 2.68	$R^2 = 0.933$	

Values are means ± S.E. of three replicate groups with 12 fish in each group. Values within the same rows having different superscripts are significantly different ($p < 0.05$). Initial body weight (IBW, g/fish), Final body weight (FBW, g/fish), Survival rate (SR, %), Feed intake (FI, g/fish). Specific growth rate (SGR) = (ln FBW − ln IBW)/days × 100. Feed efficiency (FE) = (weight gain, g/fish)/(feed intake, g/fish) × 100. Percent weight gain (PWG) = (weight gain, g/fish)/(initial weight, g/fish) × 100. Protein efficiency ratio (PER) = weight gain (g)/protein intake (g). A significant quadratic response was observed between SGR and the Arg level, with the regression equation: YSGR = $-0.190X^2 + 1.017X - 0.717$, X = 2.68, $R^2 = 0.933$.

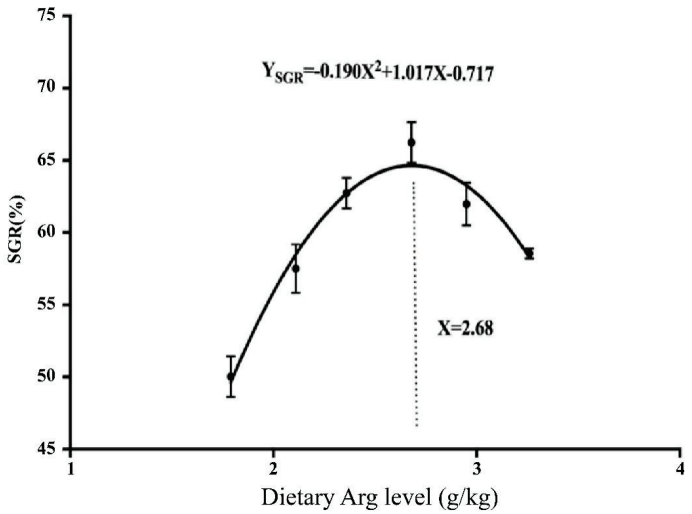


Figure 1. Quadratic regression analysis of specific growth rate (SGR) for yellow catfish (*Pelteobagrus fulvidraco*) fed diets containing graded levels of Arg (g/kg) for 8 weeks.

Table 4 presents the net nutrient deposition and whole fish compositions for yellow catfish. At Arg level 2.68 g/kg, the protein content of the fish increased significantly ($p < 0.05$) and remained relatively constant thereafter ($p > 0.05$). The lipid content gradually increased with the addition of Arg up to 2.68 g/kg, reached a maximum, and then gradually decreased ($p < 0.05$). Similar changes were observed in the levels of PPV and LPV with increasing lipid content. There were no significant changes in water content, ash content, and maximum water content among different groups ($p > 0.05$). In the 2.11 g (Arg/kg) diet, the small intestinal length (RGL) was the largest, while in the control group, the small intestinal length (RGL) was the smallest (Table 5, $p < 0.05$). Pancreatic, intestinal, and liver protein content increased significantly at dietary Arg levels of 2.36 and 2.68 g/kg, respectively, before gradually decreasing (Table 5, $p < 0.05$). The liver body index (HSI),

intestinal body index (ISI), and gastric protein content (SPC) did not show significant differences between dietary groups ($p < 0.05$).

Table 4. Whole body composition (%, wet-basis) of yellow catfish fed diets with graded levels of Arg (g/kg) 8 weeks.

Ingredient	Arg 0.179%	Arg 0.211%	Arg 0.236%	Arg 0.268%	Arg 0.295%	Arg 0.326%	*p*-Value
Moisture	67.9 ± 0.07	68.2 ± 0.42	67.5 ± 0.47	67.6 ± 0.53	68.3 ± 0.14	68.1 ± 0.80	0.658
Protein	15.6 ± 0.10 ^{a}	15.6 ± 0.30 ^{a}	15.6 ± 0.41 ^{a}	16.5 ± 0.35 ^{b}	16.5 ± 0.16 ^{b}	16.0 ± 0.04 ^{b}	0.039
Lipid	11.3 ± 0.26 ^{a}	11.7 ± 0.23 ^{ab}	12.3 ± 0.31 ^{bc}	12.6 ± 0.23 ^{c}	11.7 ± 0.17 ^{ab}	11.4 ± 0.19 ^{a}	0.042
Ash	4.58 ± 0.16	4.51 ± 0.13	4.46 ± 0.15	4.20 ± 0.10	4.43 ± 0.03	4.44 ± 0.07	0.527
PPV	14.2 ± 0.14 ^{a}	15.4 ± 0.57 ^{a}	14.9 ± 0.82 ^{a}	22.8 ± 1.03 ^{c}	19.5 ± 0.66 ^{b}	18.1 ± 0.60 ^{b}	0.016
LPV	96.0 ± 6.02 ^{a}	115 ± 7.92 ^{ab}	131 ± 9.47^{bc}	144 ± 7.43 ^{c}	113 ± 6.03 ^{ab}	112 ± 3.42 ^{ab}	0.021
APV	33.9 ± 1.61	35.6 ± 0.51	33.9 ± 0.80	35.0 ± 0.83	34.5 ± 0.44	33.6 ± 0.93	0.834

Values are means ± S.E. of three replicate groups with 12 fish in each group. Values within the same rows having different superscripts are significantly different ($p < 0.05$). Protein production value (PPV) = fish protein gain (g)/total protein intake (g) × 100. Lipid production value (LPV) = fish lipid gain (g)/total lipid intake (g) × 100. Ash production value (APV) = fish ash gain (g)/total ash intake (g) × 100.

Table 5. Stomach protein content (SPC), pancreas protein content (PPC), intestosomatic index (ISI), relative gut length (RGL), whole intestinal protein content (IPC), hepatosomatic index (HSI), and liver protein content (LPC) of yellow catfish fed diets with graded levels of Arg (g/kg) for 8 weeks.

Ingredient	Arg 0.179%	Arg 0.211%	Arg 0.236%	Arg 0.268%	Arg 0.295%	Arg 0.326%	*p*-Value
			Stomach				
SPC	3.14 ± 0.12	3.32 ± 0.24	3.58 ± 0.22	3.50 ± 0.10	3.19 ± 0.05	3.07 ± 0.05	0.237
			Pancreas				
PPC	3.23 ± 0.09 ^{a}	3.70 ± 0.13 ^{bc}	3.86 ± 0.06 ^{c}	4.26 ± 0.12 ^{d}	3.82 ± 0.16 ^{c}	3.46 ± 0.07 ^{ab}	0.018
			Intestine				
ISI	0.99 ± 0.03	1.05 ± 0.02	1.03 ± 0.03	1.06 ± 0.04	1.07 ± 0.03	1.08 ± 0.04	0.569
RGL	0.60 ± 0.02 ^{a}	0.68 ± 0.01 ^{b}	0.63 ± 0.02 ^{ab}	0.65 ± 0.02 ^{ab}	0.64 ± 0.01 ^{ab}	0.64 ± 0.02 ^{ab}	0.035
IPC	2.85 ± 0.21 ^{a}	2.92 ± 0.12 ^{ab}	3.29 ± 0.10 ^{b}	3.17 ± 0.12 ^{ab}	3.16 ± 0.09 ^{ab}	2.90 ± 0.09 ^{ab}	0.027
			Liver				
HSI	1.37 ± 0.04	1.37 ± 0.05	1.48 ± 0.07	1.42 ± 0.04	1.45 ± 0.03	1.43 ± 0.05	0.663
LPC	9.41 ± 0.21 ^{a}	10.1 ± 0.13 ^{a}	10.7 ± 0.57 ^{ab}	11.1 ± 0.13 ^{b}	9.81 ± 0.12 ^{a}	9.21 ± 0.32 ^{a}	0.047

Values are means ± S.E. of three replicate groups with 12 fish in each group. Values within the same rows having different superscripts are significantly different ($p < 0.05$). HSI = wet liver weight (g)/wet body weight (g) × 100; ISI = wet intestine weight (g)/wet body weight (g) × 100. RGL = whole intestine length (cm)/body length (cm) × 100

3.2. Enzyme Activities

Table 6 displays the digestive enzyme activities of yellow catfish. Trypsin, chymotrypsin, and pancreatic lipase activities significantly increased ($p < 0.05$) with increasing levels of Arg up to 2.68 g/kg in the diet. The highest pancreatic amylase activity was observed at 2.36 g Arg/kg diet. When Arg levels in the diet reached 2.68, 2.36, and 2.95 g/kg, respectively, pancreatic amylase, chymotrypsin, and lipase activities in the intestine increased significantly and then decreased ($p < 0.05$). Intestinal amylase activity did not change significantly. The γ-GT activity of PI and DI increased significantly with increasing Arg levels at 2.36 and 2.68 g/kg diet, respectively, followed by a decreasing trend (Table 7). The group with 2.95 g/kg Arg showed the highest CK activity in PI, while the group with 3.26 g Arg/kg exhibited the lowest CK activity ($p < 0.05$). Creatine kinase activity increased significantly with increasing Arg amount until reaching 2.36 g/kg, after which it decreased rapidly ($p < 0.05$). The addition of 2.68 g Arg/kg to the diet resulted in the highest NKA activity in PI and DI. The highest AKP activity in PI and DI was observed in the group with 2.36 g Arg/kg added to the diet, while the lowest was in the group with 3.26 g Arg/kg ($p < 0.05$). The following equation was obtained for AKP activity in DI: $Y = -23.604X^2 + 117.556X - 120.526$, $R^2 = 0.751$, $p < 0.05$.

Table 6. The digestive enzyme activities (U/g tissue) of yellow catfish fed diets with graded levels of Arg (g/kg) for 8 weeks.

Ingredient	Arg 0.179%	Arg 0.211%	Arg 0.236%	Arg 0.268%	Arg 0.295%	Arg 0.326%	*p*-Value
			Stomach				
Pepsin	967 ± 57.2 ^{a}	1057 ± 26.2 ^{ab}	1519 ± 26.8 ^{c}	1129 ± 22.4 ^{b}	1020 ± 65.5 ^{ab}	1042 ± 29.0 ^{ab}	0.023
			Pancreas				
Trypsin	20.6 ± 0.4 ^{a}	31.8 ± 2.1 ^{bc}	36.3 ± 3.3 ^{bcd}	42.0 ± 1.7 ^{d}	35.5 ± 1.6 ^{bc}	30.0 ± 1.4 ^{b}	<0.001
Chymotrypsin	27.6 ± 1.2 ^{a}	28.8 ± 1.6 ^{a}	33.6 ± 1.2 ^{b}	46.8 ± 3.6 ^{d}	36.0 ± 1.3 ^{c}	26.4 ± 0.6 ^{a}	0.019
Lipase	6.42 ± 0.48 ^{a}	8.80 ± 0.22 ^{ab}	9.59 ± 0.59 ^{b}	13.3 ± 0.86 ^{c}	9.84 ± 0.15 ^{b}	6.80 ± 0.23 ^{a}	<0.001
Amylase	1617 ± 33 ^{a}	2099 ± 84 ^{ab}	2255 ± 75 ^{b}	2121 ± 34 ^{ab}	2016 ± 34 ^{ab}	2028 ± 90 ^{ab}	0.025
			Intestine				
Trypsin	128 ± 3.3 ^{a}	145 ± 2.8 ^{b}	190 ± 6.8 ^{d}	199 ± 8.6 ^{d}	186 ± 2.8 ^{d}	162 ± 3.9 ^{c}	0.033
Chymotrypsin	60.1 ± 2.8 ^{a}	66.1 ± 6.0 ^{a}	118 ± 6.0 ^{c}	90.1 ± 2.1 ^{b}	92.5 ± 3.2 ^{b}	93.7 ± 3.6 ^{b}	<0.001
Lipase	2.10 ± 0.10 ^{a}	2.13 ± 0.11 ^{ab}	2.35 ± 0.09 ^{ab}	2.43 ± 0.09 ^{bc}	2.66 ± 0.12 ^{c}	2.27 ± 0.01 ^{ab}	0.046
Amylase	90.0 ± 9.3	93.7 ± 1.6	107 ± 9.9	105 ± 5.2	105 ± 7.8	90.9 ± 10.1	0.095
Regression							
$Y_{Intestine\ Trypsin} = -89.696X^2 + 483.244X - 457.516$					X = 2.69	R^2 = 0.819	
$Y_{Pancreas\ Trypsin} = -26.725X^2 + 141.121X - 146.711$					X = 2.64	R^2 = 0.823	

Values are means ± S.E. of three replicate groups with 12 fish in each group, while quadratic regressions were run with the triplicate data points. Values within the same rows having different superscripts are significantly different ($p < 0.05$).

Table 7. The activities of alkaline phosphatase (AKP, U/g tissue), Na^+, K^+-ATPase (NKA, U/g tissue), γ-glutamyl transpeptidase (γ-GT, U/g tissue) and creatine kinase (CK, U/g tissue) in proximal intestine (PI) and distal intestine (DI) of yellow catfish fed diets with graded levels of Arg (g/kg) for 8 weeks.

Ingredient	Arg 0.179%	Arg 0.211%	Arg 0.236%	Arg 0.268%	Arg 0.295%	Arg 0.326%	*p*-Value
			PI				
γ-GT	54.9 ± 0.9 ^{a}	54.1 ± 1.5 ^{a}	62.0 ± 0.9 ^{b}	60.3 ± 1.2 ^{b}	53.4 ± 0.5 ^{a}	55.3 ± 0.5 ^{a}	0.046
CK	54.5 ± 2.4 ^{ab}	53.5 ± 0.8 ^{ab}	58.9 ± 2.4 ^{abc}	60.8 ± 2.1 ^{bc}	62.1 ± 2.6 ^{c}	52.9 ± 1.8 ^{a}	0.037
NKA	190 ± 15.8 ^{ab}	198 ± 8.6 ^{ab}	217 ± 8.4 ^{ab}	231 ± 10.7 ^{b}	198 ± 10.8 ^{ab}	173 ± 7.6 ^{a}	0.029
AKP	21.3 ± 2.5 ^{b}	22.8 ± 1.2 ^{b}	30.6 ± 2.5 ^{c}	24.7 ± 3.0 ^{bc}	18.5 ± 0.4 ^{b}	14.7 ± 0.1 ^{a}	<0.001
			DI				
γ-GT	11.1 ± 1.1 ^{a}	15.5 ± 0.8 ^{b}	18.0 ± 1.1 ^{b}	25.4 ± 1.7 ^{c}	18.1 ± 1.4 ^{b}	15.3 ± 1.3 ^{b}	<0.001
CK	51.3 ± 2.1 ^{a}	60.1 ± 3.0 ^{b}	84.5 ± 0.9 ^{c}	61.0 ± 2.8 ^{b}	57.3 ± 1.3 ^{ab}	55.2 ± 2.3 ^{ab}	0.017
NKA	191 ± 5.2 ^{a}	227 ± 15.6 ^{bc}	239 ± 8.1 ^{bc}	256 ± 9.1 ^{c}	236 ± 7.7 ^{bc}	215 ± 3.5 ^{ab}	0.035
AKP	15.2 ± 0.09 ^{ab}	18.9 ± 0.66 ^{b}	29.7 ± 0.61 ^{d}	25.3 ± 1.3 ^{c}	17.9 ± 0.42 ^{b}	13.1 ± 1.0 ^{a}	0.016
Regression							
$Y_{DI\ AKP} = -23.604X^2 + 117.556X - 120.526$					X = 2.49	R^2 = 0.751	

Values are means ± S.E. of three replicate groups with 12 fish in each group, while quadratic regression was run with the triplicate data points. Values within the same rows having different superscripts are significantly different ($p < 0.05$).

3.3. Intestinal Antioxidant Parameters of Yellow Catfish

Table 8 presents the effect of dietary Arg on intestinal antioxidant activity in yellow catfish. At a dietary Arg level of 2.68 g/kg, both MDA and PC levels decreased significantly ($p < 0.05$) as the dietary Arg level increased, but then rose again with further increases in Arg. T-SOD and GPX activity increased significantly ($p < 0.05$) at 2.68 and 2.36 g/kg diets, respectively, and remained stable thereafter ($p > 0.05$). CAT, GST, and GR activities increased significantly with rising Arg levels ($p < 0.05$), up to a maximum at 2.68 g/kg, after which they decreased significantly ($p < 0.05$). T-GSH content was the highest at 2.38 g Arg/kg feed and the lowest at 3.26 g Arg/kg ($p < 0.05$). The ASA exhibited a similar trend to T-SOD. AHR content significantly declined as dietary Arg levels exceeded 2.68 g/kg ($p < 0.05$). Figures 2 and 3 display the relative gene expression of CuZnSOD, CAT, GPX1a, GCLC, and Nrf2 in the intestine of yellow catfish at different Arg levels. As Arg increased to 2.11, 2.36, and 2.68 g/kg in the diets, the expression levels of CuZnSOD, CAT, and GPX1a significantly increased ($p < 0.05$) and then stabilized ($p > 0.05$). In the 2.95 g/kg diet, GCLC mRNA abundance was significantly up-regulated ($p < 0.05$) and subsequently decreased as

Arg levels increased ($p < 0.05$). Dietary Arg significantly up-regulated the expression level of intestinal Nrf2, with the highest expression observed in the 2.68 g/kg Arg diet group ($p < 0.05$).

Table 8. The effect of dietary Arg on intestinal antioxidant activities including malondialdehyde (MDA), protein carbonyl (PC), total Superoxide Dismutase (T-SOD), catalase (CAT), glutathione-S-transferase (GST), glutathione peroxidase (GPx), glutathione reductase (GR), total glutathione (T-GSH), anti-superoxide anion (ASA) and anti-hydroxyl radical (AHR) in yellow catfish fed with graded levels of Arg (g/kg) for 8 weeks.

Ingredient	Arg 0.179%	Arg 0.211%	Arg 0.236%	Arg 0.268%	Arg 0.295%	Arg 0.326%	*p*-Value
MDA	95.1 ± 5.4 ^{e}	86.4 ± 6.9 ^{cd}	77.7 ± 1.2 ^{bc}	59.3 ± 2.4 ^{a}	70.4 ± 2.1 ^{ab}	76.5 ± 2.5 ^{bc}	<0.001
PC	140 ± 3.8 ^{bc}	128 ± 3.8 ^{bc}	121 ± 13.7 ^{b}	83.3 ± 7.6 ^{a}	125 ± 17.4 ^{b}	163 ± 10.0 ^{c}	<0.001
T-SOD	79.2 ± 6.6 ^{a}	92.0 ± 4.7 ^{ab}	101.5 ± 4.9 ^{b}	105.6 ± 2.3 ^{b}	102.3 ± 1.9 ^{b}	96.6 ± 2.5 ^{b}	0.021
CAT	54.0 ± 3.6 ^{a}	69.0 ± 3.9 ^{b}	72.3 ± 4.7 ^{b}	75.5 ± 8.1 ^{b}	54.9 ± 3.0 ^{a}	44.3 ± 2.1 ^{a}	0.006
GST	126 ± 7.1 ^{a}	166 ± 7.9 ^{b}	176 ± 7.8^{b}	213 ± 14.2 ^{c}	187 ± 14.1 ^{bc}	160 ± 7.6 ^{b}	<0.001
GPX	5393 ± 210 ^{a}	6190 ± 261 ^{b}	6270 ± 174 ^{b}	6040 ± 220 ^{b}	6088 ± 174 ^{b}	5997 ± 124 ^{ab}	0.003
GR	41.2 ± 2.4 ^{a}	43.8 ± 3.6 ^{ab}	52.1 ± 5.0 ^{bc}	58.9 ± 2.3 ^{c}	52.6 ± 2.2 ^{bc}	47.8 ± 1.7 ^{ab}	<0.001
T-GSH	0.76 ± 0.04 ^{ab}	0.83 ± 0.02 ^{bc}	0.90 ± 0.04 ^{c}	0.83 ± 0.02 ^{bc}	0.76 ± 0.03 ^{ab}	0.72 ± 0.03 ^{a}	0.029
ASA	261 ± 7.7 ^{a}	277 ± 7.7 ^{ab}	299 ± 11.7 ^{bc}	325 ±11.6 ^{c}	312 ± 6.5 ^{bc}	311 ± 6.1 ^{bc}	0.006
AHR	218 ± 6.6 ^{a}	259 ± 19.7 ^{ab}	252 ± 18.5 ^{ab}	288 ± 8.5 ^{b}	222 ± 7.8 ^{a}	226 ± 12.0 ^{a}	0.027

Values are means ± S.E. of three replicate groups with 12 fish in each group. Values within the same rows having different superscripts are significantly different ($p < 0.05$).

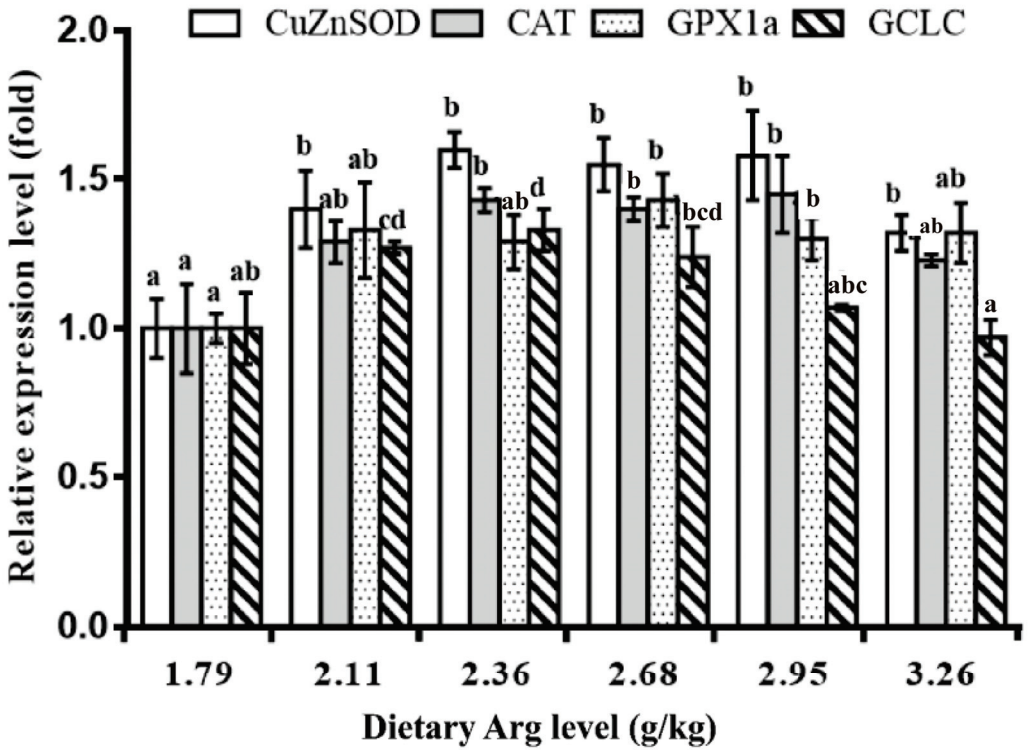


Figure 2. Relative expression of Copper-Zinc superoxide dismutase (CuZnSOD), catalase (CAT) and glutathione peroxidase 1a (GPx1a) and glutamate-cysteine ligase catalytic subunit (GCLC) in the intestine of yellow catfish fed diets containing graded levels of Arg (g/kg). Data represents the means of three replicate groups of yellow catfish with 12 fish per group; error bars indicate standard error. Different letters above a bar denote significant difference ($p < 0.05$).

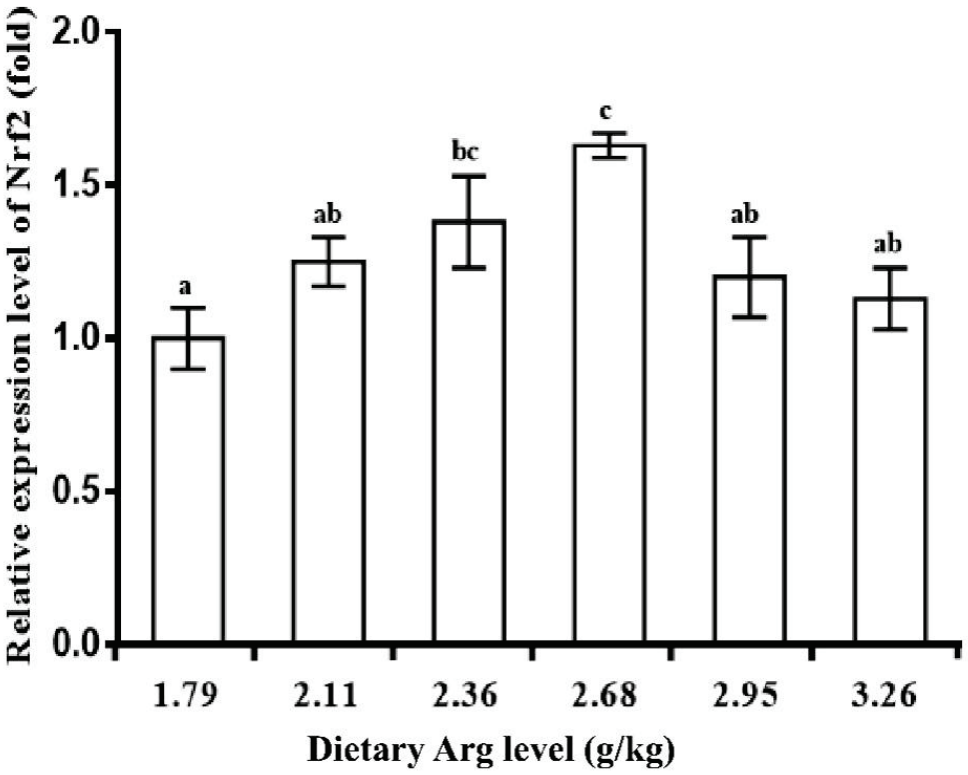


Figure 3. Relative expression of NF-E2-related factor 2 (Nrf2) in the intestine of yellow catfish fed diets containing graded levels of Arg (g/kg). Data represents means of three replicate groups of yellow catfish with 12 fish per group; error bars indicate standard error. Different letters above a bar denote significant difference ($p < 0.05$).

3.4. Principal Component Analysis (PCA)

PCAs were conducted using gene expressions (GCLC, GPX1a, Nrf2, CAT, CuZnSOD) in the intestine (Figure 4). Principal Component 1 (PC1) described 64.5% of the original information, and PC2 described 16.8%, resulting in a cumulative percentage of 81.3% in the gut. A comparison between PC1 and PC2 was performed to understand the contribution of the main components. In the biplot, GCLC, Nrf2, and GPX1a of the intestine formed a positive load on the right side, while CAT and CuZnSOD formed a negative load on the right side. The same variables were used to plot PCA individual factor maps, expressing each factor as the same variable. Both groups of fish were located on the left side of the control area, with 1.79 and 3.26 g/kg Arg as the control. There was a significant population distribution along the PC1 axis in the intestine. In the 2.11, 2.36, and 2.68 g/kg Arg dry diets, fish appeared on the positive side of the biplot along PC2 (Figure 4).

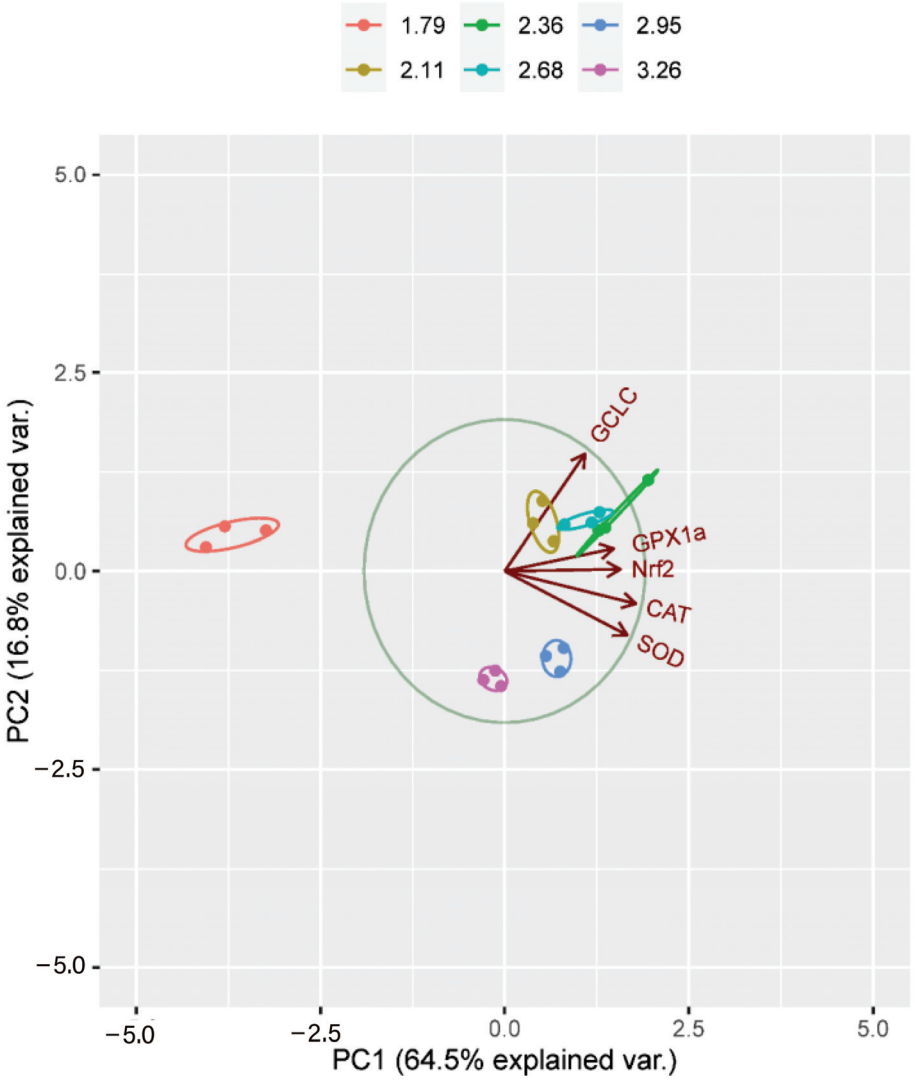


Figure 4. Loading plot of principal component analysis (PCA) in intestine representing measured variables and the individuals based on all the gene expressions of six graded Arg levels (g/kg) in the (PC1 × PC2) coordination plane. Ellipses in group from the six conditions (1.79 g/kg diet in red, 2.11 g/kg in yellow, 2.36 g/kg diet in green, 2.68 g/kg diet in light blue, 2.95 g/kg diet in blue and 3.26 g/kg diets in pink).

4. Discussion

4.1. Effect of Dietary Arg Level on Growth in Sub-Low Temperature Environments

This study investigated the impact of dietary Arg on the growth of yellow catfish under specific temperature conditions. Yellow catfish reared at 18 °C required 2.68 g/kg Arg in the diet to achieve maximum weight gain and a better specific growth rate (SGR). This requirement is higher than the 2.38 g/kg Arg diet observed in yellow catfish juveniles at the optimal water temperature of 29 °C [42]. However, the SGR in this study was lower than that of juvenile yellow catfish in previous studies [42], consistent with findings in juvenile yellow catfish [43], and juvenile common carp [44], where SGR was lower due to water temperature. Water temperature is an important factor influencing the growth process of fish [45]. In nature, fish attempt to adjust themselves to temperature fluctuations, which can impact their overall physiology and result in lower growth rates. This study also demonstrated that SGR increased with the increasing Arg content in the diet, up to an optimum level (2.268 g/kg), which has been observed in Indian major carp [46,47], black sea bream [48], and rainbow trout [30]. The feed intake (FI) and feed efficiency (FE) also improved in response to increasing levels of Arg (Arg), This result shows

that the increase in fish growth is partially attributed to the increase in FI and FE. According to [46], growth is the result of high protein deposition due to the intake of essential amino acids. Our study found a significant increase in the protein retention rate (PRV) when maintaining the optimum concentration of Arg for specific growth rate (SGR). Additionally, Arg has a significant secretory function, which is related to its impact on fish growth and development [49].

4.2. Effect of Dietary Arg Level on Digestive and Absorptive Enzyme Activities

The effect of dietary Arg level on digestive and absorptive enzyme activities is a key factor affecting fish growth and development [50]. It depends on the enzyme activity of the digestive and brush border membrane, responsible for the degradation and absorption of food [51]. Not only can water temperature affect cell membrane structure [52], but it can also have an impact on the digestive process [53,54]. Understanding the enzyme dynamics and digestive processes under seasonal temperature changes is crucial for preparing feeds that optimize growth performance and reduce feed costs for fish. The pancreas of yellow catfish can secrete pancreatic juice containing trypsin, amylase, chymotrypsin, and lipase of the intestine independently of the liver. Many transport systems, such as the entry of amino acids, phosphate, or glucose into cells, utilize the sodium gradient potential energy generated by the sodium-potassium adenosine triphosphatase (NKA) [55]. Alkaline phosphatase (AKP) is involved in the uptake of nutrients like glucose, calcium, lipids, and inorganic phosphates [56]. Gamma-glutamyltransferase (γ-GT) plays an essential role in the active transport of amino acids [57]. Creatine kinase (CK) has a key role in cellular energy metabolism as it catalyzes the transfer of phosphate to creatine in an ATP-dependent manner. When the dietary Arg level increased, there was a significant increase in gastric pepsin activity, as well as hepatopancreatic and intestinal trypsin, chymotrypsin, and amylase activities. Moreover, increasing levels of dietary Arg also led to a significant increase in intestinal NKA, AKP, γ-GT, and CK activities. It is evident that Arg improves digestion and absorption in fish under low-temperature conditions. To the best of our knowledge, this is the first study on the influence of Arg on the digestive and absorption enzyme activities of yellow catfish. Similar results were obtained in Jian carp at the optimum temperature [14]. A study on bull's-eye pufferfish showed a correlation between digestive enzyme activity and the development of the digestive tract [55]. Thus, the addition of appropriate levels of Arg at low temperatures can promote the development of the hepatopancreas and intestinal tract of yellow catfish, thereby increasing digestive enzyme activity. In our research, Arg significantly improved pancreatic protease capacity (PPC), relative gut length (RGL), and intestinal protease capacity (IPC). Furthermore, Arg can be metabolized by nitric oxide synthase (NOS) to form NO, and by arginase and Arg decarboxylase to produce spermine. Previous studies have demonstrated that NO can stimulate pancreatic secretion in pigs [58] and spermine can increase enzyme activity in the pancreas of black bass *Dicentrarchus labrax* [59]. Therefore, it is hypothesized that Arg could improve the secretion of digestive enzymes by stimulating NO and spermine in yellow catfish, which warrants further investigation.

4.3. Effect of Dietary Arg Level on Intestinal Anti-Oxidative Capacity

Reactive oxygen species (ROS) are chemically reactive molecules containing oxygen that are natural by-products of mitochondrial oxygen metabolism and play a vital role in cell signaling and homeostasis [60]. When the generation and accumulation of ROS exceed the body's ability to counteract these reactive substances, several biomolecules, including lipids and proteins, undergo oxidative damage [61]. Li et al. (2014) reported that exposure of shrimp to low temperatures increased the levels of ROS [26]. Similarly, Kake-Guena et al. (2017) reported that temperature changes affect mitochondrial function, leading to an increase in ROS formation [27]. low water temperatures (15 °C and 21 °C) induce stress scenarios that can overwhelm the antioxidant system, resulting in overproduction of ROS. As a result, the addition of Arg to the diet at low temperatures (18 °C) has been shown to reduce malondialdehyde (MDA) and protein carbonyl (PC) levels in the intestine [4]. The similar results have been shown in intestine of grass carp [32]. Therefore, Arg could prevent oxidative stress in the intestine of yellow catfish under seasonal cold stress. Recent studies have found that antioxidant

enzymes are essential for protecting cells from oxidative stress [62]. Superoxide dismutase (SOD) is an enzyme that is the first to respond to O_2 radicals and serves as an essential endogenous antioxidant protecting against oxidative stress. Catalase (CAT) is also essential for defending cells against the toxicity of hydroxyl radicals, while glutathione-S-transferase (GST), glutathione peroxidase (GPx), and glutathione reductase (GR) are GSH-dependent enzymes that counteract peroxidative damage [63]. In a recent study conducted at cold temperatures, the addition of 2.68 g of Arg per kg of diet increased the enzymatic activities of CuZnSOD, CAT, GST, and GPX in the fish intestine. This increase in enzyme activity can be attributed to the enhanced synthesis of enzyme proteins, which is linked to gene transcription and translation [64]. Similarly, previous studies have indicated that dietary addition of Arg enhances tissue antioxidant status and reduces protein and fat oxidation in various animals. The results of the present study indicate that CuZnSOD, CAT, and GPX1a showed similar patterns of change in mRNA levels and enzymatic activity in the intestine. Similar findings have been reported for Arg supplementation in pig [41] and grass carp [65,66]. GSH protects cells from oxidative stress by serving as the major endogenous antioxidant scavenger. GSH/GSSG represents the main cellular redox buffer [67]. Glutamate cysteine ligase (GCL) has been identified as the rate-limiting enzyme for glutamate (Glu) biosynthesis [68], and GSH synthase is coordinately regulated as a subunit of glutamate cysteine ligase. The present study indicated that dietary supplementation of Arg increased intestinal GSH content and the transcriptional level of GCLC. This suggests that Arg supplementation could promote GSH synthesis by upregulating GCLC expression under cold temperatures [68].

Nrf2 is a crucial transcription factor that regulates the expression of antioxidant enzyme genes in fish. Its facilitated translocation into the nucleus plays an essential role in upregulating antioxidant enzyme gene expression [28,46]. The current study indicated that optimal levels of Arg (2.268 g/kg) resulted in the upregulation of intestinal Nrf2 mRNA expression levels in yellow catfish, exhibiting a similar pattern to the expression levels of CuZnSOD, CAT, and GPX mRNA [26]. This suggests that dietary Arg supplementation could enhance the expression of CuZnSOD, CAT, and GPX genes by upregulating Nrf2 mRNA expression. However, further investigation is needed to understand the potential mechanism (Figure 5).

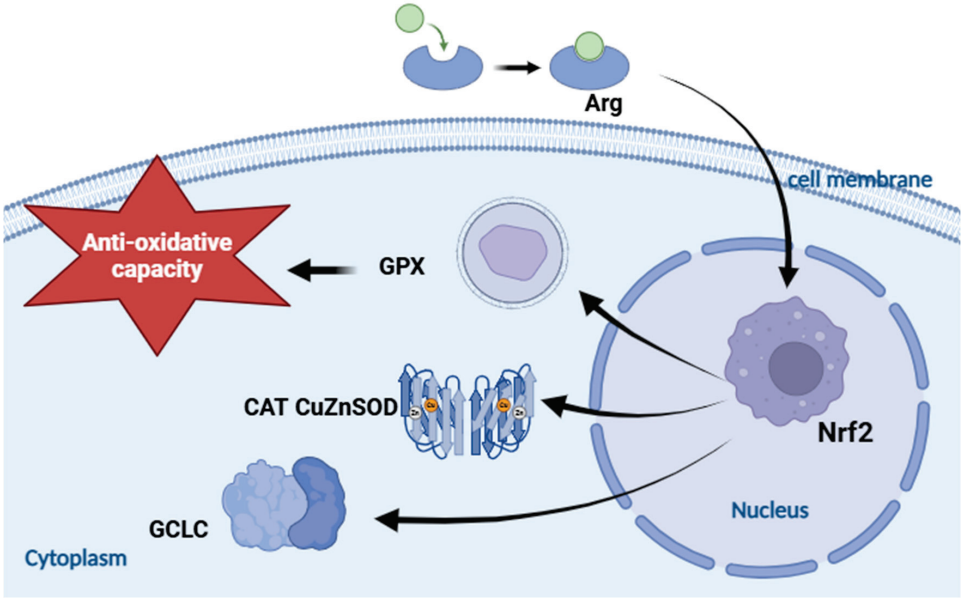


Figure 5. Role of Nrf2 in the regulation of intestinal metabolism in yellow catfish under Arg feed. Nrf2 can induce the downstream pathway genes including GPX, CuZnSOD, CAT, GCLC to increase the anti-oxidative capacity.

5. Conclusions

This study found that dietary supplementation of Arg improved the growth performance, digestion and absorption capacity, and intestinal antioxidant status of yellow catfish in sub-low temperature environments. The optimal Arg level is 2.68 g/kg. It also increased antioxidant capacity by upregulating Nrf2 mRNA expression and the expression of antioxidant-related genes. Quadratic regression analysis was employed to estimate the dietary Arg requirement for yellow catfish at 18 °C, which was determined to be between 61.0 g and 89.0 g, based on a dry feed specific growth rate (SGR) of 2.68 g/kg and a feed protein content of 37.0 g/kg. These findings suggest that optimizing the dietary arginine content in yellow catfish feeds can contribute to better pancreas health, improved intestinal development, and overall fish performance in sub-low temperature aquaculture systems.

Author Contributions: Q.C.: Investigation, Methodology, Writing—original draft, Formal analysis, Visualization. M.S.K.: Investigation, Software, Visualization. A.G. and A.M.Y.: Investigation. H.L. and J.J.: Conceptualization, Methodology, Resources, Writing—review & editing, Visualization, Validation, Supervision. All authors have read and agreed to the published version of the manuscript.

Funding: This research was funded by the Applied Basic Research Programs of the Science and Technology Commission Foundation of Sichuan Province, China (2015JY0067), the National Key R&D Program of China (2019YFD0900200), and Sichuan Agricultural University (031/2222996058).

Institutional Review Board Statement: The animal study protocol was approved by the Ethics Animal Committee of Ya'an, Sichuan Agricultural University, China (Permit No. DKY-S20210416).

Informed Consent Statement: Not available.

Data Availability Statement: Not available.

Acknowledgments: The authors would like to express their gratitude to the anonymous reviewers for their contributions.

Conflicts of Interest: The authors declare no conflict of interest.

References

1. Clarke, W.C.; Shelbourn, J.E. Growth and development of seawater adaptability by juvenile fall chinook salmon (*Oncorhynchus tshawytscha*) in relation to temperature. *Aquaculture* **1985**, *45*, 21–31. [CrossRef]
2. Ahmad, T.; Singh, S.P.; Khangembam, B.K.; Sharma, J.G.; Chakrabarti, R. Food consumption and digestive enzyme activity of Clarias batrachus exposed to various temperatures. *Aquac. Nutr.* **2014**, *20*, 265–272. [CrossRef]
3. Zehra, S.; Khan, M.A. Dietary Arginine Requirement of Fingerling Indian Major Carp, *Catla catla* (Hamilton). *J. World Aquac. Soc.* **2013**, *44*, 363–373. [CrossRef]
4. Souza, D.M.d.; Borges, V.D.; Furtado, P.; Romano, L.A.; Wasielesky, W.; Monserrat, J.M.; Garcia, L.d.O. Antioxidant enzyme activities and immunological system analysis of Litopenaeus vannamei reared in biofloc technology (BFT) at different water temperatures. *Aquaculture* **2016**, *451*, 436–443. [CrossRef]
5. Goolish, E.M.; Adelman, I.R. Effects of ration size and temperature on the growth of juvenile common carp (*Cyprinus carpio* L.). *Aquaculture* **1984**, *36*, 27–35. [CrossRef]
6. Sharma, J.; Singh, S.P.; Chakrabarti, R. Effect of temperature on digestive physiology, immune-modulatory parameters, and expression level of Hsp and LDH genes in *Catla catla* (Hamilton, 1822). *Aquaculture* **2017**, *479*, 134–141. [CrossRef]
7. Yuan, Q.; Wang, Q.; Zhang, T.; Li, Z.; Liu, J. Effects of water temperature on growth, feeding and molting of juvenile Chinese mitten crab Eriocheir sinensis. *Aquaculture* **2017**, *468*, 169–174. [CrossRef]
8. Morteza, H.S.; Mukhtar, A.K.; Morteza, Y.; Benjamin, C. Roles of arginine in fish nutrition and health: Insights for future researches. *Rev. Aquac.* **2020**, *12*, 2091–2108.
9. Wilson, R.P. Protein and amino acid requirements of fishes. *Annu. Rev. Nutr.* **1986**, *6*, 225–244. [CrossRef]
10. Costas, B.; Conceição, L.E.C.; Dias, J.; Novoa, B.; Figueras, A.; Afonso, A. Dietary arginine and repeated handling increase disease resistance and modulate innate immune mechanisms of Senegalese sole (*Solea senegalensis* Kaup, 1858). *Fish Shellfish Immunol.* **2011**, *31*, 838–847. [CrossRef]
11. Zhou, Q.C.; Zeng, W.P.; Wang, H.L.; Xie, F.J.; Wang, T.; Zheng, C.Q. Dietary arginine requirement of juvenile yellow grouper *Epinephelus awoara*. *Aquaculture* **2012**, *350–353*, 175–182. [CrossRef]
12. Gao, Y.-J.; Yang, H.-J.; Guo, D.-Q.; Liu, Y.-J.; Yu, Y.-y.; Chen, S.-J.; Tian, L.-X. Dietary arginine requirement of juvenile grass carp *Ctenopharyngodon idella* (Valenciennes in Cuvier & Valenciennes, 1844). *Aquac. Res.* **2015**, *46*, 3070–3078.

13. Ren, M.; Ai, Q.; Mai, K. Dietary arginine requirement of juvenile cobia (*Rachycentron canadum*). *Aquac. Res.* **2014**, *45*, 225–233. [CrossRef]
14. Ren, M.; Liao, Y.; Xie, J.; Liu, B.; Zhou, Q.; Ge, X.; Cui, H.; Pan, L.; Chen, R. Dietary arginine requirement of juvenile blunt snout bream, Megalobrama amblycephala. *Aquaculture* **2013**, *414–415*, 229–234. [CrossRef]
15. Khan, Y.M.; Khan, M.A. Dietary niacin requirement of fingerling Indian major carp *Catla catla* Hamilton. *Aquac. Nutr.* **2021**, *27*, 1482–1493.
16. Jiang, W.-D.; Feng, L.; Liu, Y.; Jiang, J.; Hu, K.; Li, S.-H.; Zhou, X.Q. Lipid peroxidation, protein oxidant and antioxidant status of muscle, intestine and hepatopancreas for juvenile Jian carp (*Cyprinus carpio* var. Jian) fed graded levels of *myo*-inositol. *Food Chem.* **2009**, *120*, 692–697. [CrossRef]
17. Zhao, Y.; Hu, Y.; Zhou, X.Q.; Zeng, X.Y.; Feng, L.; Liu, Y.; Jiang, W.D.; Li, S.H.; Li, D.B.; Wu, X.Q.; et al. Effects of dietary glutamate supplementation on growth performance, digestive enzyme activities and antioxidant capacity in intestine of grass carp (*Ctenopharyngodon idella*). *Aquac. Nutr.* **2015**, *21*, 935–941. [CrossRef]
18. Hakim, Y.; Harpaz, S.; Uni, Z. Expression of brush border enzymes and transporters in the intestine of European sea bass (*Dicentrarchus labrax*) following food deprivation. *Aquaculture* **2009**, *290*, 110–115. [CrossRef]
19. Cao, X.J.; Wang, W.M. Histology and Mucin Histochemistry of The Digestive Tract of Yellow Catfish, *Pelteobagrus fulvidraco*. *Anat. Histol. Embryol.* **2009**, *38*, 254–261. [CrossRef]
20. Villanueva, J.; Vanacore, R.; Goicoechea, O.; Amthauer, R. Intestinal alkaline phosphatase of the fish *Cyprinus carpio*: Regional distribution and membrane association. *J. Exp. Zool.* **1997**, *279*, 347–355. [CrossRef]
21. Xiao, W.; Feng, L.; Kuang, S.; Liu, Y.; Jiang, J.; Jiang, W.D.; Hu, K.; Li, S.H.; Tang, L.; Zhou, X.Q. Lipid peroxidation, protein oxidant and antioxidant status of muscle and serum for juvenile Jian carp (*Cyprinus carpio var. Jian*) fed grade levels of methionine hydroxy analogue. *Aquac. Nutr.* **2012**, *18*, 90–97.
22. Shan, Y.; Shan, A.; Li, J.; Zhou, C. Dietary supplementation of arginine and glutamine enhances the growth and intestinal mucosa development of weaned piglets. *Livest. Sci.* **2012**, *150*, 369–373. [CrossRef]
23. Geering, K. Subunit assembly and functional maturation of Na, K-ATPase. *J. Membr. Biol.* **1990**, *115*, 109–121. [CrossRef]
24. Jiang, J.; Wu, X.-Y.; Zhou, X.-Q.; Feng, L.; Liu, Y.; Jiang, W.-D.; Wu, P.; Zhao, Y. Effects of dietary curcumin supplementation on growth performance, intestinal digestive enzyme activities and antioxidant capacity of crucian carp *Carassius auratus*. *Aquaculture* **2016**, *463*, 174–180. [CrossRef]
25. Matés, J.M.; Sánchez-Jiménez, F.M. Role of reactive oxygen species in apoptosis: Implications for cancer therapy. *Int. J. Biochem. Cell Biol.* **2000**, *32*, 157–170. [CrossRef]
26. Li, B.; Xian, J.-A.; Guo, H.; Wang, A.-L.; Miao, Y.-T.; Ye, J.-M.; Ye, C.-X.; Liao, S.-A. Effect of temperature decrease on hemocyte apoptosis of the white shrimp *Litopenaeus vannamei*. *Aquac. Int.* **2014**, *22*, 761–774. [CrossRef]
27. Niyogi, S.; Biswas, S.; Sarker, S.; Datta, A. Seasonal variation of antioxidant and biotransformation enzymes in barnacle, Balanus balanoides, and their relation with polyaromatic hydrocarbons. *Mar. Environ. Res.* **2001**, *52*, 13–26. [CrossRef]
28. Qiang, M. Role of nrf2 in oxidative stress and toxicity. *Annu. Rev. Pharmacol. Toxicol.* **2013**, *53*, 401–426.
29. Wu, S.; Gao, T.; Zheng, Y.; Wang, W.; Cheng, Y.; Wang, G. Microbial diversity of intestinal contents and mucus in yellow catfish (*Pelteobagrus fulvidraco*). *Aquaculture* **2010**, *303*, 1–7. [CrossRef]
30. Bush, R.M.; Welch, E.B.; Mar, B.W. Potential effects of thermal discharges on aquatic systems. *Environ. Sci. Technol.* **1974**, *8*, 561–568. [CrossRef]
31. Hu, J.; Zhao, H.; Wang, G.; Sun, Y.; Wang, L. Energy consumption and intestinal microbiome disorders of yellow catfish (*Pelteobagrus fulvidraco*) under cold stress. *Front. Physiol.* **2022**, *13*, 985046. [CrossRef]
32. Fagnon, S.M.; Thorin, C.; Calvez, S. Meta-analysis of dietary supplementation effect of turmeric and curcumin on growth performance in fish. *Rev. Aquac.* **2020**, *12*, 2268–2283. [CrossRef]
33. Bradford, M.M. A rapid and sensitive method for the quantitation of microgram quantities of protein utilizing the principle of protein-dye binding. *Anal. Biochem.* **1976**, *72*, 248–254. [CrossRef]
34. Hummel, B.C. A modified spectrophotometric determination of chymotrypsin, trypsin, and thrombin. *Can. J. Biochem. Physiol.* **1959**, *37*, 1393–1399. [CrossRef]
35. Zhao, Y.; Li, J.Y.; Yin, L.; Feng, L.; Liu, Y.; Jiang, W.D.; Wu, P.; Zhao, J.; Chen, D.F.; Zhou, X.Q.; et al. Effects of dietary glutamate supplementation on flesh quality, antioxidant defense and gene expression related to lipid metabolism and myogenic regulation in Jian carp (*Cyprinus carpio var. Jian*). *Aquaculture* **2019**, *502*, 212–222. [CrossRef]
36. Tokur, B.; Korkmaz, K. The effects of an iron-catalyzed oxidation system on lipids and proteins of dark muscle fish. *Food Chem.* **2007**, *104*, 754–760. [CrossRef]
37. Aebi, H. Catalase in vitro. *Methods Enzymol.* **1984**, *105*, 121–126.
38. Zhang, X.-D.; Zhu, Y.-F.; Cai, L.-S.; Wu, T.-X. Effects of fasting on the meat quality and antioxidant defenses of market-size farmed large yellow croaker (*Pseudosciaena crocea*). *Aquaculture* **2008**, *280*, 136–139. [CrossRef]
39. Lora, J.; Alonso, F.J.; Segura, J.A.; Lobo, C.; Marquez, J.; Matés, J.M. Antisense glutaminase inhibition decreases glutathione antioxidant capacity and increases apoptosis in Ehrlich ascitic tumour cells. *FEBS J.* **2004**, *271*, 4298–4306. [CrossRef]
40. Vardi, N.; Parlakpinar, H.; Ozturk, F.; Ates, B.; Gul, M.; Cetin, A.; Erdogan, A.; Otlu, A. Potent protective effect of apricot and β-carotene on methotrexate-induced intestinal oxidative damage in rats. *Food Chem. Toxicol.* **2008**, *46*, 3015–3022. [CrossRef]

41. Ma, X.; Lin, Y.; Jiang, Z.; Zheng, C.; Zhou, G.; Yu, D.; Cao, T.; Wang, J.; Chen, F. Dietary arginine supplementation enhances antioxidative capacity and improves meat quality of finishing pigs. *Amino Acids* **2010**, *38*, 95–102. [CrossRef]
42. Zhelyazkov, G. Effect of monosodium glutamate dietary supplementation on some productive traits of common carp (Cyprinus carpio L.), cultivated in net cages. *Agric. Sci. Technol.* **2018**, *10*, 204–207. [CrossRef]
43. Williams, K.C.; Barlow, C.G.; Rodgers, L.; Agcopra, C. Dietary composition manipulation to enhance the performance of juvenile barramundi (*Lates calcarifer* Bloch) reared in cool water. *Aquac. Res.* **2006**, *37*, 914–927. [CrossRef]
44. Zeng, L.; Fu, C.; Fu, S. The effects of temperature and food availability on growth, flexibility in metabolic rates and their relationships in juvenile common carp. *Comp. Biochem. Physiol. Part A* **2018**, *217*, 26–34. [CrossRef]
45. Green, B.S.; Fisher, R. Temperature influences swimming speed, growth and larval duration in coral reef fish larvae. *J. Exp. Mar. Biol. Ecol.* **2004**, *299*, 115–132. [CrossRef]
46. Ahmed, I.; Khan, M.A.; Jafri, A.K. Dietary methionine requirement of fingerling Indian major carp, *Cirrhinus mrigala* (Hamilton). *Aquac. Int.* **2003**, *11*, 449–462. [CrossRef]
47. Abidi, S.F.; Khan, M.A. Dietary arginine requirement of fingerling Indian major carp, *Labeo rohita* (Hamilton) based on growth, nutrient retention efficiencies, RNA/DNA ratio and body composition. *J. Appl. Ichthyol.* **2009**, *25*, 707–714. [CrossRef]
48. Zhou, F.; Xiong, W.; Xiao, J.X.; Shao, Q.J.; Bergo, O.N.; Hua, Y.; Chai, X. Optimum arginine requirement of juvenile black sea bream, Sparus macrocephalus. *Aquac. Res.* **2010**, *41*, e418–e430. [CrossRef]
49. Pohlenz, C.; Buentello, A.; Miller, T.; Small, B.C.; MacKenzie, D.S.; Gatlin, D.M. Effects of dietary arginine on endocrine growth factors of channel catfish, Ictalurus punctatus. *Comp. Biochem. Physiol. Part A* **2013**, *166*, 215–221. [CrossRef] [PubMed]
50. Hakim, Y.; Uni, Z.; Hulata, G.; Harpaz, S. Relationship between intestinal brush border enzymatic activity and growth rate in tilapias fed diets containing 30% or 48% protein. *Aquaculture* **2006**, *257*, 420–428. [CrossRef]
51. Perez-Casanova, J.C.; Murray, H.M.; Gallant, J.W.; Ross, N.W.; Douglas, S.E.; Johnson, S.C. Development of the digestive capacity in larvae of haddock (*Melanogrammus aeglefinus*) and Atlantic cod (*Gadus morhua*). *Aquaculture* **2006**, *251*, 377–401. [CrossRef]
52. Hazel, J.R. Effects of temperature on the structure and metabolism of cell membranes in fish. *Am. J. Physiol.—Regul. Integr. Comp. Physiol.* **1984**, *246*, R460. [CrossRef]
53. Brett, J.R.; Higgs, D.A. Effect of temperature on the rate of gastric digestion in finger ling sockeye salmon, *Oncorhynchus nerka*. *J. Fish. Board Can.* **1970**, *27*, 1767–1779. [CrossRef]
54. Klinger, T.S.; Hsieh, H.L.; Pangallo, R.A.; Chen, C.P.; Lawrence, J.M. The effect of temperature on feeding, digestion, and absorption of *Lytechinus variegatus* (Lamarck) (Echinodermata: Echinoidea). *Physiol. Zool.* **1986**, *59*, 332–336. [CrossRef]
55. Geering, K. Functional roles of Na,K-ATPase subunits. *Curr. Opin. Nephrol. Hypertens.* **2008**, *17*, 526–532. [CrossRef]
56. Tengjaroenkul, B.; Smith, B.J.; Caceci, T.; Smith, S.A. Distribution of intestinal enzyme activities along the intestinal tract of cultured Nile tilapia, *Oreochromis niloticus* L. *Aquaculture* **2000**, *182*, 317–327. [CrossRef]
57. Ogawa, M.; Shiozawa, M.; Hiraoka, Y.; Takeuchi, Y.; Aiso, S. Immunohistochemical study of localization of γ-glutamyl transpeptidase in the rat brain. *Tissue Cell* **1998**, *30*, 597–601. [CrossRef]
58. Holst, J.J.; Rasmussen, T.N.; Schmidt, P. Role of nitric oxide in neurally induced pancreatic exocrine secretion in pigs. *Am. J. Physiol.* **1984**, *266*, G206–G213. [CrossRef]
59. Péres, A.; Cahu, C.L.; Infante, J.L.Z. Dietary spermine supplementation induces intestinal maturation in sea bass (*Dicentrarchus labrax*) larvae. *Fish Physiol. Biochem.* **1997**, *16*, 479–485. [CrossRef]
60. Cadenas, E. Biochemistry of oxygen toxicity. *Annu. Rev. Biochem.* **1989**, *58*, 79–110. [CrossRef] [PubMed]
61. Apel, K.; Hirt, H. Reactive Oxygen Species: Metabolism, Oxidative Stress, and Signal Transduction. *Annu. Rev. Plant Biol.* **2004**, *55*, 373–399. [CrossRef]
62. Selvaraj, V.; Yeager Armstead, M.; Murray, E. Protective and antioxidant role of selenium on arsenic trioxide–induced oxidative stress and genotoxicity in the fish hepatoma cell line PLHC-1. *Environ. Toxicol. Chem.* **2012**, *31*, 2861–2869. [CrossRef]
63. David, M.; Munaswamy, V.; Halappa, R.; Marigoudar, S.R. Impact of sodium cyanide on catalase activity in the freshwater exotic carp, *Cyprinus carpio* (Linnaeus). *Pestic. Biochem. Physiol.* **2008**, *92*, 15–18. [CrossRef]
64. Chang, H.R.; Arsenijevic, D.; Vladoianu, I.; Girardier, L.; Dulloo, A.G. Fish oil enhances macrophage tumor necrosis factor-alpha mRNA expression at the transcriptional level. *Metabolism* **1995**, *44*, 800–805. [CrossRef]
65. Wang, B.; Feng, L.; Jiang, W.-D.; Wu, P.; Kuang, S.-Y.; Jiang, J.; Tang, L.; Tang, W.-N.; Zhang, Y.-A.; Liu, Y.; et al. Copper-induced tight junction mRNA expression changes, apoptosis and antioxidant responses via NF-κB, TOR and Nrf2 signaling molecules in the gills of fish: Preventive role of arginine. *Aquat. Toxicol.* **2015**, *158*, 125–137. [CrossRef]
66. Wang, B.; Liu, Y.; Feng, L.; Jiang, W.-D.; Kuang, S.-Y.; Jiang, J.; Li, S.-H.; Tang, L.; Zhou, X.-Q. Effects of dietary arginine supplementation on growth performance, flesh quality, muscle antioxidant capacity and antioxidant-related signalling molecule expression in young grass carp (*Ctenopharyngodon idella*). *Food Chem.* **2015**, *167*, 91–99. [CrossRef]
67. Sies, H. Glutathione and its role in cellular functions. *Free Radic. Biol. Med.* **1997**, *27*, 916–921. [CrossRef] [PubMed]
68. Lu, S.C. Regulation of glutathione synthesis. *Mol. Asp. Med.* **2009**, *30*, 42–59. [CrossRef]

Disclaimer/Publisher's Note: The statements, opinions and data contained in all publications are solely those of the individual author(s) and contributor(s) and not of MDPI and/or the editor(s). MDPI and/or the editor(s) disclaim responsibility for any injury to people or property resulting from any ideas, methods, instructions or products referred to in the content.

biology

MDPI

Review

Can IMTA System Improve the Productivity and Quality Traits of Aquatic Organisms Produced at Different Trophic Levels? The Benefits of IMTA—Not Only for the Ecosystem

Giusy Rusco [1], Alessandra Roncarati [2,*], Michele Di Iorio [1], Michela Cariglia [3,4], Caterina Longo [5] and Nicolaia Iaffaldano [1]

[1] Department of Agricultural, Environmental and Food Sciences, University of Molise, Via De Sanctis snc, 86100 Campobasso, Italy; giusy.rusco@unimol.it (G.R.); michele.diiorio@unimol.it (M.D.I.); nicolaia@unimol.it (N.I.)
[2] School of Biosciences and Veterinary Medicine, University of Camerino, Viale Circonvallazione 93–95, 62024 Matelica, Italy
[3] Gargano Pesca Società Agricola Consortile Arl-Società Benefit, Via Rucher 5, Interno 1/C, 71043 Manfredonia, Italy; cariglia.michela@gmail.com
[4] Gargano Shell Fish Farm Societa' Cooperativa Agricola Arl, Pontile Alti Fondali, SC, 71043 Manfredonia, Italy
[5] Department of Bioscience, Biotechnologies and Environment, University of Bari Aldo Moro, Via Orabona 4, 70125 Bari, Italy; caterina.longo@uniba.it
* Correspondence: alessandra.roncarati@unicam.it

Simple Summary: This review paper aims to summarize, for the first time, the current state of knowledge on the potential value of the Integrated Multi-Trophic Aquaculture (IMTA) system to positively influence the zootechnical performance, animal welfare, and flesh nutritional quality of the co-cultivated species. The crucial role that the characteristic nutritional (i.e., greater availability of food and nutrients) and environmental factors (i.e., better water quality) of the IMTA system play in shaping the physiological responses of aquatic organisms produced at different trophic levels, i.e., growth, survival, stress responses, and welfare, is highlighted. Given the still-limited diffusion of this valuable fish farm system in many European areas, we believe that emphasizing the economic and market value of IMTA products could contribute to improve public perception and interest in the concrete adoption of IMTA on a commercial scale and constitute a basis to encourage further studies in order to explore new IMTA opportunities.

Abstract: IMTA is one of the most innovative and sustainable farming systems, exhibiting the best technique available in rearing aquatic organisms belonging to different positions along the trophic levels. In the literature and in legislation, the environmental benefits of IMTA protocols have been extensively recognized, mainly for its capability to reduce the ecological footprint of intensive aquaculture systems and concretely address the Sustainable Development Goal no. 14 (SDG 14). However, lesser attention is given to the assessments of its role in enhancing the zootechnical performance, animal welfare, and flesh quality of the species involved. To the best of our knowledge, this is the first review that aims to offer a systematic analysis of the existing literature on the main commercial motivations that could draw the attention of stakeholders, including consumers and fish farmers, towards a greater social acceptability and implementation of the IMTA system on a large scale. The findings suggest that, beyond its environmental advantages, IMTA systems can positively influence the productivity, growth, survival, feed efficiency, and animal health and welfare (AH&W), as well as the nutritional quality of the harvested species, thus offering significant economic and market value both in terms of Environmental, Societal and Governance (ESG) parameters and One Health.

Keywords: improve IMTA acceptability; fed species; extractive species; zootechnical performance; animal welfare; flesh nutritional quality; stakeholders; ESG; One Health

1. Introduction

Integrated Multi-Trophic Aquaculture (IMTA) is one of the most innovative and sustainable farming systems for freshwater, brackish, and marine environments, both in land-based and coastal aquaculture systems [1,2]. Unlike monoculture, which involves the rearing of a single species, and polyculture, where species with similar chemical and biological processes are farmed together, IMTA integrates the synergistic culture of aquatic organisms from different trophic levels [2,3]. In this system, waste products such as uneaten feed, feces, and excretory products of fed species (e.g., finfish, shrimp) become the food for the other organisms, such as organic extractive species (e.g., shellfish, herbivorous fish, echinoderm) and inorganic extractive species (e.g., seaweed) [4,5]. IMTA was primarily developed as a mitigation strategy to address the key environmental concerns associated with intensive aquaculture, including sedimentation and the excessive loading of nutrients and chemicals [6].

In this regard, a conspicuous number of articles and reviews have demonstrated the potential IMTA ability to promote the ecological sustainability [7–20] while delivering economic [21] and social benefits [6]. As an example, many bivalves reduce the organic load of the water by feeding on both phytoplankton and particulate organic matter, leading to significantly control eutrophication. This extractive sequestration of nutrients produces water quality and clarity improvements [22,23]. At the same time, large-scale shellfish–macro-algae IMTA plays an important role in the local carbon cycle and contributes to mitigating ocean acidification and hypoxia [24,25]. Despite the multiple positive effects of IMTA on the environment, this system remains underutilized in many European regions, including the Mediterranean, primarily due to various unresolved challenges [10,26]. Among these, a crucial issue concerns its social acceptability by different stakeholders [6,27]. In this regard, several studies agree on the fact that the development of standards for the definition of a certification of products obtained from IMTA system would allow for greater acceptance by consumers and industries [7,10,24,28]. Others studies conducted on the social sustainability of IMTA also stated that consumers would be willing to pay more for IMTA products if labelled as such [6,29,30]. Moreover, another clear consensus by survey participants was that they wanted to see as much information as possible on the labels, including nutritional facts [6]. Overall, these results confirm the increased attention of consumers in animal-welfare-friendly products, with a low environmental impact and associated with properly tracked and certified quality assurance schemes. Scientifically demonstrating that IMTA models can achieve these production goals would help to address stakeholders and fish farmers to move from a monoculture to an approach based on the IMTA system. Nevertheless, these aspects are often overlooked; indeed, until now, few studies were focused on determining the AH&W and nutritional quality traits of fish, bivalves, and the other organisms involved at the different trophic levels. As concerns farmer's acceptability, despite the fact that the potential ability of IMTA to provide financial benefits for aquaculture producers has already been widely reported [21], many of them are still against its use, since they do not foresee fast economic feedback, mostly concerning the commercialization of new products such as invertebrates and seaweeds [7]. In this regard, a promising new market application, such as the use of seaweed and polychaete biomass as alternative protein and lipid sources in fish and livestock feeds, could further increase the profitability of IMTA system and positively affect farmer's acceptance [31–33]. At the same time, studies that highlight a high productivity, improved zootechnical performance, and faster production cycles, could be of paramount importance to encourage stakeholder investment and promote a wider application of IMTA systems [17,21].

In the light of these considerations, the aim of the present review is to summarize the current state of knowledge on the potential value of IMTA in producing high-quality nutritional biomass and enhancing zootechnical performances according to SDG 14, which focuses on the conservation and sustainable use of the oceans, seas, and marine resources. Moreover, the application of IMTA as potential system for the production of alternative ingredients in the feeds of aquatic species is also explored. By highlighting these aspects, we aim to enhance public perception and interest in the concrete adoption of IMTA on a commercial scale.

2. State of the Art of Successful IMTA Practices on the Zootechnical Performance, Nutritional Traits, Animal Welfare, and Sensory Characteristics of Different Aquatic Species

It is generally accepted that to achieve a successful IMTA system it is essential to undertake an interdisciplinary approach. Researchers and stakeholders with different backgrounds, such as biologists, natural and social scientists, aquaculture engineers, economists, and industry investors, have collaborated and will do so again in the future, in order to establish proper IMTA setups to obtain the maximum economic, social, environmental and productive potential from these systems [10,17]. Therefore, the successful results in terms of zootechnical performance and nutritional quality reported in the following sections are the result of experimental IMTA models planned according to an appropriate combination of the co-cultivated species, suitable population sizes, distance within co-cultured species, sites of culture, and farming methods.

Most of the reported studies agree that the better water quality and the greater availability of food and nutrients in IMTA systems were the major reasons behind the improvement of fish performance, the production of final higher quality biomass, and the faster growth of bivalve. The enhanced water quality in IMTA systems is favoured by different mechanisms implemented by the cultivated species themselves. For example, in IMTA systems with filter feeders, bivalves help lower nutrient load by filtering and absorbing particulate waste, as well as any phytoplankton overgrowth that is triggered by the presence of dissolved nutrient waste [34].Through bioturbation, they can release phosphorus, promoting a greater concentration of Cyanobacteria, which release dissolved oxygen into the water above via photosynthesis, improve nitrification (particularly ammonia oxidation), and enhance the system's ability to remove ammonia nitrogen [35]. In earthen ponds, bivalves control the density of the microalgae and particulate matter, contributing to a higher transparency and light penetration of the water column, which in turn increase photosynthetic activity with significantly higher dissolved oxygen and carbon sequestration [36]. Also, deposit feeders such as sea cucumber, cultivated below finfish and shellfish farms, can recycle nutrients, decrease organic carbon loads, and bioturbate sediments, potentially limiting anaerobic bacterial growth and the formation of anoxic zones; at the same time, the inorganic nutrients (P and N) they excrete enhance the benthic habitat [34,37–39]. Seaweeds are also used to maintain water quality as a supplier of oxygen through the process of photosynthesis during the day and to absorb excess inorganic nutrients [40]. Overall, the favourable water quality in these systems plays a crucial role in the growth and physiological functions of different cultured aquatic species, contributes to better animal health, and to a reduction in the energy power uses for water aeration in pond culture, also contributing to greater profitability [36,41] and toward the assessment in terms of ESG for a wider use of IMTA in aquaculture and maritime spatial planning [42]. At the same time, the high nutritional value of biomass production seems mainly due to the ability of particulate organic matter extractive organisms to recover and incorporate nutrients (i.e., fatty acids [FAs]) contained in the uneaten fraction of aquafeeds supplied to farmed species, which would otherwise be wasted. In this context, new predictive models are being developed in order to support the industry to optimize the nutritional value of cultured species and manage the aquatic environmental eutrophication footprint in conditions of IMTA production [43]. These models effectively predict the feed composition effects on growth and ω-3 FA content in cultured spices, as well as the nitrogen and carbon concentrations generated in the farming environment. Therefore, they will allow us to facilitate the development of novel sustainable feeds by the industry and to enhance the management of environmental impacts. In the fish species mostly farmed in the Mediterranean Sea, such as gilthead seabream and European seabass, the use of sustainable feedstuffs from seafood trimming and processing and aquafeed manufacture (extrusion) has already been adopted to improve the feed conversion rate while minimizing the environmental impact [44,45].

In the following, we present currently available evidence on the IMTA potential to improve the quality and growth performance of various kind of organisms involved at different trophic levels. An overview of IMTA studies referenced in the review is reported in Table 1, underlining the IMTA setup and placement and the main results obtained.

Table 1. Overview of the IMTA studies referenced in the review.

Fed Species	Organic Extractive Species	Inorganic Extractive Species	IMTA System Placement	Benefits Drawn from IMTA	References
M. cephalus **(mullet)** ***P. vannamei*** **(shrimp)**	*M. casta* (backwater hard clam)	*A. officinalis* *B. gymnorhiza* (halophyte)	Pond culture	↑ Growth performance (final weight, specific growth rate, feed conversion ratio), survival rate, protein efficiency ratio, total production ↑ Water quality in IMTA = ↑ growth performances	[46]
C. chanos **(milkfish)** ***P. vannamei*** **(shrimp)**	*C. cuttackensis* (oyster)	-	Tank culture	↑ Growth performance (apparent feed conversion ratio), protein, fat and ash contents of whole body composition	[41]
C. chanos **(milkfish)** ***P. vannamei*** **(shrimp)**	-	*E. intestinalis* (seaweed)	Tank culture	↑ Growth and survival rate ↑ Physiological status (blood and haemolymph parameters) ↓ Stress parameters (catalase, superoxide dismutase, and cortisol)	[47]
M. cephalus **(mullet)** ***P. parsia*** **(mullet)** ***P. monodon*** **(shrimp)**	*C. cuttackensis* (oyster)	*Enteromorpha* (seaweed)	Pond culture	↑ Growth performance (final average body weight, apparent feed conversion ratio), total production	[48]
M. cephalus **(mullet)** ***P. tade*** **(mullet)** ***P. monodon*** **(shrimp)**	*C. cuttackensis* (oyster)	*I. aquatic* (water spinach)	Pond culture	↑ Growth performance (final average body weight, apparent feed conversion ratio), total production ↑ Whole body composition	[49]
L. rohita **(Rohu fish)**	*L. marginalis* (mussel)	*W. globosa* (duckweed)	Tank culture	↑ Growth performance, feed utilization ↑ Welfare parameters ↓ Oxidative stress ↑ Water quality in IMTA = ↑ immunity and survival, ↓ oxidative stress	[50]
A. regius **(Meagre)** ***D. sargus*** **(sea bream)** ***M. cephalus*** **(mullet)**	*C. gigas* (oyster)	*Ulva* spp. (seaweed)	Earthen pond culture	↑ Growth performance (fish density, food conversion rate), total final harvested biomass	[36]
P. vannamei **(shrimp)**	-	*E. cottonii* (seaweed)	Sea culture	↑ Growth performance (final weight, specific growth rate, feed conversion ratio), survival rate, total production	[40]
P. vannamei **(shrimp)**	***C. gigas*** **(oyster)**	-	Tank culture	↑ Growth performance (final weight) Variations in digestive bacterial communities ↓ Relative abundance of Vibrionaceae	[51]
E. fuscoguttatus ***E. lanceolatus*** **(groupers)**	*P. vannamei* (shrimp)	*G. bailinae* (seaweed)	Pond culture	↑ Growth performance (final body weight, weight gain, percent weight gain, specific growth rate) ↑ Non-specific immunity ↑ Liver glycolipid metabolism ↑ Beneficial bacterial communities	[52]
S. aurata **(sea bream)**	Shellfish	Algae	Earthen pond culture	↑ Growth performance (final weight), lipid content (PUFAs ω3), sensory quality	[53]
S. aurata (seabream) *D. labrax* (seabass)	***O. edulis*** **(oyster)**	-	Open-sea culture	↑ Condition index, lipid content	[54]
S. aurata (seabream) *D. labrax* (seabass)	***H. roweothuria poli*** **(sea cucumber)**	-	Sea culture	↑ Lipid content (PUFAs ω3)	[55]
S. aurata (seabream)	***H. diversicolor*** *D. neapolitana* *S.* cf. *pavonina* *T. lapidaria* **(polychaetes)**	-	Sand filters, earthen ponds culture	↑ Lipid content (PUFAs ω3)	[56]
P. vannamei (shrimp)	***C. corteziensis*** **(oyster)**	-	Pond culture, channel	↑ Growth performance (wet weight and shell length) exceeded the typical commercial size	[57]
S. salar (atlantic salmon)	***M. edulis*** **(mussel)**	-	Sea culture	↑ Growth performance (final wet meat weight, shell length, condition index)	[58]
S. aurata (seabream) *D. labrax* (seabass)	***M. galloprovincialis*** **(mussel)**	-	Sea culture	↑ Condition index	[59]

Table 1. *Cont.*

Fed Species	Organic Extractive Species	Inorganic Extractive Species	IMTA System Placement	Benefits Drawn from IMTA	References
S. aurata (seabream) *D. labrax* (seabass)	***M. galloprovincialis*** **(mussel)** *S. spallanzanii* (polychaete) *S. spinosulus* *A. aerophoba* *H. perlevis* (sponges)	*C. linum* *G. bursa pastoris* (seaweeds)	Sea culture	↑ Growth performance (shell length, shell dry weight, flesh dry weight, condition index)	[60]
S. aurata (seabream) *D. labrax* (seabass)	***M. galloprovincialis*** **(mussel)** ***P. radiate*** **(pearl oyster)** ***H. pollii*** **(sea cucumber)**	-	Sea culture	↑ Growth performance, survival rate, condition index, meat yield (mussel and oyster) ↑ Survival, ↓ final weight (sea cucumber)	[61]
D. labrax **(seabass)**	***M. galloprovincialis*** **(mussel)** ***O. edulis*** ***C. gigas*** **(oysters)** ***H. sanctori*** **(sea cucumber)**	-	Sea culture	↑ Survival rate, total weight, shell lengths (mussel and oysters) ↑ Survival rate, total weight (sea cucumber) ↑ Feed conversion ratio, feed efficiency (fish)	[34]
S. aurata **(seabream)**	***P. lividus*** **(sea urchin)**	***U. lactuca*** **(seaweed)**	Tank, pond culture	↑ Gonad somatic growth rate, gonad somatic index, protein level in the gonad, bright orange gonads (sea urchin) ↑ Growth rate, protein and lipid levels (seaweed) ↑ Growth rate, food conversion ratio (fish)	[62]
-	***A. californicus*** **(sea cucumbers)** *C. gigas* (oyster)	**-**	Sea culture	↑ Growth rate, survival rate	[63]
A. fimbria (sablefish)	***A. californicus*** **(sea cucumbers)**	**-**	Sea culture	↑ Growth rate, survival rate	[37]
P. major (red seabream)	***A. japonicas*** **(sea cucumber)**	**-**	Sea culture	↑ Growth rate, survival rate	[64]
L. erythopterus (crimson snapper) *E. fario* (blue-spotted grouper) *R. canadum* (cobia)	***A. japonicas*** **(sea cucumber)**	**-**	Sea culture	↑ Growth rate, survival rate	[65]
-	***H. theeli*** **(sea cucumber)** *T. depressus* (sea urchin)	-	Tank culture	↑ Growth rates (length, weight), survival rate	[66]
-	***H. tubulosa*** **(sea cucumber)** ***P. lividus*** **(sea urchin)**	-	Land-based cuture	↑ Growth rates (somatic growth rate, feed conversion ratio), survival rate	[67]
-	***M. galloprovincialis*** **(mussel)** *H. perlevis* (sponge)	-	Sea culture	↓ Bacterial load in the co-cultured *M. galloprovincialis*	[68]
Salmon	-	***G. chilensis*** **(seaweed)**	Sea culture	↑ Biomass production	[69]
S. senegalensis (sole) *S. rhombus* (turbot)	-	***G. vermiculophylla*** **(seaweed)**	Tank, land-based culture	↑ Biomass production ↑ Quality (protein content)	[70]
S. rhombus (turbot) *D. labrax* (seabass)	-	***C. crispus*** ***G. bursa pastoris*** ***P. palmata*** **(seaweeds)**	Tank culture	↑ Biomass yield	[71]
S. aurata (seabream)	*H. discus hannai* (abalone)	***U. lactuca*** ***G. conferta*** **(seaweeds)**	Tank, land-based culture	Biomass yield ↑ *U. lactuca*, ↓ *G. conferta*	[72]

Table 1. *Cont.*

Fed Species	Organic Extractive Species	Inorganic Extractive Species	IMTA System Placement	Benefits Drawn from IMTA	References
S. aurata (seabream)	*H. discus hannai* (abalone) *P. lividus* (sea urchin)	***U. lactuca* (seaweed)**	Tank, pond culture	↑ Biomass production ↑ Quality (protein content)	[73]
-	*S. spallanzanii* (polychaete) *S. spinosulus* (sponge)	***C. linum* *G. bursa pastoris* (seaweed)**	Sea culture	↑ Biomass production, survival rates	[74]

The target species of the studies are reported in bold. The direction of the arrows shows increase (↑) or decrease (↓) of the effect derived from IMTA setup.

2.1. Fed Species

Fish and shellfish are considered among the main fed species in the IMTA [24,75,76] and furnish nutrients to other organisms of the system, in addition to contributing to the economy of the setup [77]. The studies conducted so far, mainly on the zootechnical performance of fed species reared in IMTA systems, have focused on few fish species (current valid name: *Mugil cephalus*, *Argyrosomus regius*, *Chanos chanos*, *Diplodus sargus*, *Epinephelus* spp., *Labeo rohita*, *Planiliza parsia*, *Planiliza tade*, *Sparus aurata*) and two shrimp species (current valid name: *Penaeus vannamei and Peneaus monodon*), with scarce information on the nutritional traits. Some of these articles also include other topics generally few covered in IMTA studies, such as the effect of this innovative aquaculture system on animal welfare, digestive microbiome, and sensory characteristics.

Starting from IMTA systems in brackish water, two recent studies investigated the integration of milkfish *C. chanos* and the white-leg shrimp *P. vannamei* as fed species with oyster [41] or seaweed [47]. Both studies demonstrated positive outcomes in terms of growth and survival rate, using both organic extractive species (*Crassostrea cuttackensis*) and inorganic extractive species (*Enteromorpha intestinalis*). In the first study, Naskar et al. [41] showed that the best growth performance of milkfish (24.66 $\pm$ 0.31 g) and shrimp (15.20 $\pm$ 0.17 g) and the lowest apparent feed conversion ratio (0.92 $\pm$ 0.01) were obtained in the IMTA treatment at the highest oyster density tested (T3—1.8 kg m^{-3}), compared to lower densities (T1—0.6 kg m^{-3} and T2 1.2 kg m^{-3}). Additionally, the proximate composition analysis of *C. chanos*' whole body showed the highest protein and fat contents in T3 (58.04 $\pm$ 0.73% and 18.18 $\pm$ 0.25%, respectively), while in *P. vannamei*, significantly high values were recorded for fat (4.95 $\pm$ 0.19%) and ash (10.08 $\pm$ 0.18%) in T3 and the control. The authors suggest that the probable reason behind these latter results is the better utilization of feed into body nutrients by reared animals in IMTA than in the polyculture. In a subsequent study [47], the same fed species were integrated with the green seaweed *E. intestinalis*. This setup showed a significantly better growth of *C. chanos* (12.52 $\pm$ 0.24 g) and *P. vannamei* (14.77 $\pm$ 0.35 g) at higher seaweed biomass density (T3—1.5 kg m^{-3} and T2—1 kg m^{-3}, respectively), compared to the control (milkfish: 11.01 $\pm$ 0.08 g and shrimp: 11.79 $\pm$ 0.58 g). Notably, shrimp survival rates were significantly higher at all seaweed biomass densities tested (T1—70.0 $\pm$ 2.5%, T2—80.0 $\pm$ 2.1%, T3—85.0 $\pm$ 1.7%) compared to the control (52.6 $\pm$ 4.8%). This improvement was likely due to the reduced cannibalism occurring in the presence of seaweed, covering 10 to 20% of the surface area, thus providing a hiding zone for *P. vannamei* during the daytime. As regards the physiological status, the blood (red blood cells, white blood cells and haemoglobin) and haemolymph (haemocyanin and total haemocyte count) parameters were significantly improved in fish and shrimp, respectively, under IMTA at harvest compared to the control. It is well known that growth of these two categories of aquatic organisms increase when the environment is favourable. The presence of seaweed also provided a reduction in stress parameters (catalase, superoxide dismutase, and cortisol) compared to the polyculture system, as a result of the consumption of seaweed naturally rich in various bioactive molecules, including anxiolytic agents. Another experiment was conducted in brackish-water earthen ponds to investigate the

effect of bivalves (*Meretrix casta*) in halophyte-based IMTA (*Avicennia officinalis* [T1] or *Bruguiera gymnorhiza* [T2]) on the growth performance of the mullet *M. cephalus* and the shrimp *P. vannamei*, used as the fed species [46]. Higher final weight, specific growth rate, protein efficiency ratio, and total productivity were found in shrimp and fish in both halophyte treatments than in the control. The survival rate of *P. vannamei* was significantly higher in IMTA systems (T1—91 ± 1.5%; T2—89 ± 1%) compared to the control (86 ± 1%), while the feed conversion ratio was reduced by 14% and 5% in the presence of *A. officinalis* in *P. vannamei* and *M. cephalus*, respectively. In an IMTA setup similar to that of Kumara et al. [46], the feed conversion ratio was reduced until 22% compared to the polyculture system [48]. In this study, three main fed species, the mullets *M. cephalus*, *P. parsia*, and the tiger shrimp *P. monodon,* were integrated with oyster (*Crassostrea cuttackensis*) and seaweed (*Enteromorpha*) as the extractive species. Here, mullets (*M. cephalus* and *P. parsia*) exhibited a greater growth ($p < 0.05$) compared to that of control ponds, as well as tiger shrimp, although their increase was not significant. At the same time, the total production was 19% higher in IMTA ($p < 0.05$) compared to conventional polyculture. In a subsequent study, Biswas et al. [49] compared polyculture systems (controls) with various IMTA models where three different fed species (*M. cephalus*, *P. tade* and *P. monodon*) were combined with the "water spinach", *Ipomoea aquatica* (T1), and the oyster *C. cuttackensis* (T2), or both these two extractive species (T3). The growth of tiger shrimp, *P. monodon*, was higher ($p < 0.05$) in T3 (22.17 ± 1.29 g), than in T1 (15.15 ± 0.43 g), T2 (15.96 ± 1.25 g) and the control (14.68 ± 1.28 g). The pooled survival of fishes and shrimp was similar among treatments, including control, whereas the total production was significantly higher in T3 (1695.7 kg ha^{-1}), followed by that in T1 (1211.9 kg ha^{-1}), T2 (894.2 kg ha^{-1}) and the control (505.4 kg ha^{-1}). As regards the whole body composition, the crude protein, lipid, and organic matter contents of harvested *M. cephalus* were similar among treatments; crude protein, lipid, ash, and nitrogen-free extract contents of harvested *P. tade* were higher in T1 (60.84 ± 0.16%, 17.22 ± 0.15%, 16.08 ± 0.30%, 9.27 ± 0.21%, respectively), followed by T3, T2, and C; whereas in harvested *P. monodon*, only crude protein content was significantly higher in T1 (56.51 ± 0.10%) and T2 (56.27 ± 0.09%) than that in C (53.83 ± 0.35%) and T3 (54.13 ± 0.20%). Similar results were also observed in a IMTA freshwater system where *L. rohita* was co-cultivated with floating weed, *Wolffia globosa* (T1), freshwater mussel, *Lamellidens marginalis* (T2), or both extractive species (T3) [50]. The total biomass (3641.7 ± 1.33 g), survival (95.38 ± 2.35%), and net fish yield (1.85 ± 0.07 g m^{-2} d^{-1}) were significantly high in the IMTA system when Rohu was cultivated with both organic and inorganic extractive species (T3), compared to other treatments and control. The percentage of protein (T1—64.14 ± 0.57, T2—62.67 ± 0.88, T3—62.33 ± 1.51) and lipid (T1—22.17 ± 0.25, T2—20.49 ± 0.24, T3—22.61 ± 0.17) of the whole body of fish was higher ($p < 0.05$) in the all IMTA treatments than the control (protein: 58.71 ± 0.31 and lipid: 17.59 ± 0.41). As regards welfare parameters, the immunological response (nitroblue tetrazolium activity) was significantly higher in T1 (0.50 ± 0.02) and T3 (0.46 ± 0.03), while superoxide dismutase was highest in T1 (6.85 ± 0.34 units/dl serum). The catalase activity was lowest in T3 (0.16 ± 0.03 units/dl serum) among all the treatment groups. Authors suggested that the optimum water quality maintained in the IMTA system protected fish from oxidative stress, thereby improving their immunity and survival.

The enhanced water quality resulting from the IMTA system was also the main reason for the improved fish performance and higher biomass production in the study conducted by Cunha et al. [36]. In this work, the best results were obtained when three fish species (*A. regius*, *D. sargus* and *M. cephalus*), oyster (*Crassostrea gigas* triploid), phytoplankton, and macroalgae (mainly *Ulva spp*.), were integrated in earthen ponds altogether. In particular, phytoplankton played a crucial role by not only increasing dissolved oxygen levels and absorbing excess nutrients from animal waste but also serving as a food source for oysters. Oysters in turn had an important role in regulating microalgae and particulate matter densities in ponds, which helped to maintain stable dissolved oxygen levels and increase water transparency. This enhanced transparency, along with nutrient input from oyster

excretion, promoted greater phytoplankton growth, with advantages not only for oysters themselves but also for the macroalgae. At the same time, fish benefited from this good ecological balance, recording higher total final harvested biomass (1115 ± 2.4 Kg) and fish density (1.49 ± 0.01) and lower food conversion rate (1.59 ± 0.00) than other IMTA setups tested.

Another interesting study was conducted by Verdian et al. [40], which cultivated white shrimp (*P. vannamei*) in floating net cages (KJA system) at sea as primary commodities integrated with rabbit fish (*Siganus doliatus*) and the rhodophyte seaweed (*Euchema cottonii*). The results indicated that the growth performance in terms of the final weight (9.63 ± 0.03 g), survival rate (71.00 ± 14.53%), specific growth rate (2.72 ± 0.02%), feed conversion ratio (2.84 ± 0.42%), and total production (2.73 ± 0.33 Kg m^{-2}) of white shrimp cultivated in IMTA system were improved compared to shrimp cultivated in a monoculture system. The ability of rabbit fish to eat biofouling attached to the nets' cage system made it cleaner, promoting regular water circulation. This condition prevented the obstruction of cages and the accumulation of feed residue and metabolic waste, positively affecting shrimp growth.

Omont et al. [51] studied the effect of the IMTA system on the digestive microbiome changes in *P. vannamei* and *C. gigas* for the first time. These authors found significant variations in the digestive bacterial communities of both species under co-culture in the IMTA system compared to a monoculture system. The dominant phyla found in shrimp intestine and oyster gut were Proteobacteria, with a relative abundance of 59.2% and 66%, respectively, followed by Bacteroidetes, Actinobacteria, and Firmicutes. Particularly, within Proteobacteria, a significative variation in the abundance of Alphaproteobacteria communities (Sphingomonodales and Rhodobacterales) occurred in the co-cultured oyster gut due to the consumption of shrimp waste. At the same time, the reduction in particulate organic matter in water caused by the co-cultured oysters has been related to the enhancement of shrimp performance. Moreover, the co-culture of *P. vannamei* and *C. gigas* seem to have promoted healthy conditions that reduced the relative abundance of Vibrionaceae in the intestine of both species compared to monoculture treatments.

Zhang et al. [52] explored the application of IMTA to manage nutrient balance, microbial communities, and antibiotic resistance genes (ARGs) in aquaculture systems, focusing on the cultivation of fish, shrimp, and algae. Specifically, IMTA systems were tested using hybrid groupers (*Epinephelus fuscoguttatus* × *E. lanceolatus*), shrimp (*P. vannamei*), and a rhodophyte seaweed (*Gracilaria bailinae*), with different setups. The tested systems included a control with a monoculture of groupers (C), a fish–shrimp IMTA (FS), a fish–algae IMTA (FA), and a fish–shrimp–algae IMTA (FSA). The presence of *G. bailinae* effectively removed inorganic nutrients (nitrogen and phosphorus) accumulated in water, which in turn significantly promoted growth and enhanced non-specific immunity and glycolipid metabolism in the hybrid grouper, boosting overall fish health and resistance to infections. Although the growth performance of hybrid groupers reared in the IMTA systems were all larger than those in the C system, those in the FSA system were significantly higher (final body weight: 82.33 ± 3.57 g; weight gain: 40.89 ± 2.41 g; percent weight gain: 98.22 ± 3.30%; specific growth rate: 2.28 ± 0.05%) than the control (final body weight: 66.45 ± 2.08 g; weight gain: 25.02 ± 1.12 g; percent weight gain: 60.48 ± 2.36%; specific growth rate: 1.57 ± 0.05%). Compared with monoculture, IMTA significantly changed the structure of the bacterial community, fostering the beneficial effect. Regarding AGRs, even though water quality improved in IMTA systems, they remained persistent, indicating that while IMTA mitigates some issues, it does not fully eliminate ARGs.

Finally, to the best of our knowledge, flesh quality differences in terms of sensory properties and the nutritional value of aquaculture products coming from distinct production systems, including the integrated one, were only compared in a study by Valente et al. [53]. These authors compared the flesh quality traits of gilthead sea bream (*S. aurata*) from extensive, integrated, and semi-intensive systems with ones produced intensively. The integrated system consisted of the association of algae, shellfish, and fish in earthen ponds using the enriched water effluent of a seabass hatchery as a fertilizer to enhance

the productivity. Compared to the intensive system, the seabream from IMTA systems developed an intense interorbital yellow band and a shiny orange patch on the gill cover, while the flesh exhibited a darker appearance and more yellowish colour (lower value of L* and higher value of b*, $p < 0.05$), which could be attributed to environmental conditions; the odour of marine/iodine was significantly higher in IMTA, probably due to the ingestion of *Ulvae* that proliferate in those ponds, as suggested by its presence in the sea breams' stomachs. Body weight was greater ($p < 0.05$) in the IMTA system (464.8 ± 0.1 g) than in the intensive (396.6 ± 57.8 g) and semi-intensive (334.0 ± 50.9 g) systems. Regarding nutritional quality, sea bream from the integrated systems displayed significantly higher levels of docosahexaenoic acid (DHA, C22:6ω3 [7.75 ± 0.92%]), docosapentaenoic acid (DPA, C22:5ω3 [4.15 ± 0.92%]), arachidic acid (C20:0 [0.70 ± 0.72%]) and arachidonic acid (C20:4ω6 [1.05 ± 0.64%]), compared to the intensive system (2.85 ± 2.79%, 1.06 ± 1.40%, 0.13 ± 0.30%, 0.08 ± 0.21%, respectively). The highest levels of eicosapentaenoic acid (EPA, C20:5 ω3 [6.75 ± 0.78%]) and the best ω3/ω6 ratio (2.41 ± 0.67) were also observed in the integrated system, although no statistical significance was found over the intensive system (2.80 ± 2.23%, 0.79 ± 0.95%, respectively).

The success of these IMTA models for the production of the main fed species (finfish and shellfish) is the result of the balanced systems which promoted positive effects on the aquatic environments, animal welfare, harvestable yield, and quality traits, contributing to greater profitability for the producers.

2.2. Organic Extractive Species

In IMTA systems, the organic extractive species are used to reduce water nutrient loads acting at different trophic levels according to the type of organic matter generated by fish farms. When it comes to larger organic particles, such as uneaten feed and feces, that settles below the cages, they are eaten by deposit feeders, like polychaetes, sea cucumbers, and sea urchins; while the fine suspended particles are filtered out of the water column by filter-feeding animals like mussels, oysters, scallops, and sponges [5,23]. In a comprehensive book concerning the goods and services of bivalve shellfish [78], bivalves are dealt as filtering nutrients from particulate matter, using the nutrients directly emitted from fish farm in negligible quantities. Thus, when suspended and deposit feeders (for example, bivalves and echinoderms) are combined in IMTA models, the waste removal efficiency of the system tends to increase [17].

Among organic extractive species, bivalves (*Crassostrea corteziensis*, *Ostrea edulis*, *Pinctada radiata*, *Mytilus galloprovincialis*, *Mytilus edulis*), echinoderms (*Apostichopus californicus*, *Apostichopus japonicus*, *Holothuria poli*, *Holothuria sanctori*, *Holothuria theeli*, *Holothuria tubulosa*, *Paracentrotus lividus*, *Tripneustes depressus*), polychaetes (*Capitella* sp., *Diopatra neapolitana*, *Hediste diversicolor*, *Ophryotrocha craigsmithi*, *Sabella* cf. *pavonina*, *Terebella lapidaria*), and sponges (*Hymeniacidon perlevis*) have been the subjects of studies aimed at investigating the effect of IMTA systems on zootechnical performance. The ability of the IMTA systems to modify the nutritional traits of produced biomass were addressed only in few studies.

Aguado-Gimenez et al. [54] proposed an experimental integrated culture of flat oyster (*O. edulis*) in combination with an intensive production of gilthead seabream (*S. aurata*) and seabass (*Dicentrarchus labrax*) in open-sea conditions in the southwestern Mediterranean. In this study, the greater availability of food potentially accessible for oysters around the fish farm induced an enhanced development when compared with oysters reared away from the farm. The IMTA conditions not only led to a significantly higher flesh weight with regard to the total weight (i.e., a larger condition index—CI), but also to a more pronounced fattening state and improved FA profile than that observed in the control, which could be interesting from a commercial point of view. The oysters cultured in the integrated area showed significantly higher levels of FAs of terrestrial origin, such as oleic (C18:1ω9 [4.85 ± 0.14%]) and linoleic (C18:2ω6 [2.95 ± 0.06%]) acids, compared to the reference (3.74 ± 0.29%, 2.18 ± 0.14%, respectively), due to the supplement of vegetable oils in food pellets. At the same time, the levels of essential FA, such as EPA (C20:5ω3 [13.82 ±

0.05%]) and DHA (C22:6ω3 [21.54 ± 0.39%]), mainly of marine origin (since they are both very abundant in phytoplankton), were only slightly lower in integrated than in control oysters (14.28 ± 0.18%, 22.67 ± 0.15%, respectively). These results suggest that integrated oysters used particulate wastes derived from the fish farm, but at a low level, because they preferred to use natural seston when available.

The ability to accumulate FAs from uneaten artificial fish feed in tissue was also demonstrated for sea cucumber (*H. roweothuria poli*) co-cultured in coastal Mediterranean IMTA sites directly below the commercial fish cages (*S. aurata* and *D. labrax*) at 10 m and 25 m away [55]. Compared to sea cucumbers cultivated at the reference sites (over 800 m from the fish farm), a high abundance of individual terrestrial plant FAs, such as oleic (18:1ω-9), linoleic (18:2ω-6), and eicosenoic (20:1ω-9) acids, was revealed in sea cucumber tissue near fish cages. At the reference sites, instead, sea cucumber tissues were characterized by a higher relative abundance of arachidonic acid (20:4ω-6) and marine ω-3 PUFAs (EPA and DPA).

These studies, as well as revealing an important bio-mitigation effect of IMTA systems on eutrophication concerns due to the reduced digestibility of plant-derived ingredients by fish, highlights the nutritional benefits of IMTA for oyster and sea cucumber production, where the natural marine resources are not able to sustain their survival and growth.

Relevant results in terms of nutritional quality were also observed for several polychaete species produced through IMTA systems. Recently, Jerònimo et al. [56] reported the FA profile of four different polychaete species (*H. diversicolor*, *D. neapolitana*, *S.* cf. *pavonina*, *T. lapidaria*) cultured in sand filters supplied with effluent water of earthen ponds stocked with gilthead seabream (*S. aurata*) over 15 weeks. In particular, from the FA profile comparison of cultured and wild *H. diversicolor*, an overall dissimilarity of ≈24.2% was revealed, with cultured biomass showing a higher EPA (cultured: 4.83 ± 0.99 μg mg^{-1}, wild: 3.68 ± 0.13 μg mg^{-1}) and DHA (cultured: 0.99 ± 0.30 μg mg^{-1}, wild: not detect) content. Moreover, *H. diversicolor* and *T. lapidaria* were the species whose FA profiles displayed the highest similarity to that of aquafeed formula. Also, other previous works on *H. diversicolor* [79,80] recorded ω-3 highly unsaturated FAs (HUFA) as a major FA class in IMTA cultured (≈34% and 37.8% of total FA, respectively) when the aquafeeds being supplied to fish displayed a higher proportion of HUFA (24% and 20–28% of total FAs, respectively). Overall, these findings demonstrated that polychaetes can be successfully employed to recover otherwise wasted nutrients present in the particulate organic matter of aquaculture effluents, as well as presenting an essential FA profile suitable to be used as ingredients for fish feed formulation.

A study to evaluate the oyster *C. corteziensis* growth cultured under IMTA concept, using the farm effluents of shrimp *P. vannamei*, was conducted by Mazón-Suástegui et al. [57]. Three different growing sowing cycles (October, November, and December), three stocking densities (low, medium, and high), and three positions of the Nestier®- like tray (top, middle, and bottom), were investigated in the experiment. The best growth performances were obtained from the October grow-out cycle, from oysters at medium stocking density, and at the top position (wet weight: 110.1 ± 3.6 g, shell length: 91.3 ± 1.5 mm, in 9 months), which far exceeded the typical commercial size (>70 g) of *C. corteziensis* cultured under similar conditions (Nestier® trays suspended from long lines). As was mentioned before, in this case, the greater food availability from the shrimp farm, in the form of particulate organic matter and phytoplankton, also helped to explain the higher growth rates obtained for oysters cultivated under IMTA conditions characterized by warm seawater and low salinity.

Lander et al. [58], investigated the effect of two different distances from two separate Atlantic salmon farms (0 m and 200 m) on the growth parameters (shell length, wet meat weight, and condition index) of blue mussels (*M. edulis*) compared to those grown at a reference site outside the aquaculture influence (control). After one year, an overall significant increase in mussels grown directly on the salmon cages (shell length: 57.47 ± 0.41 mm, wet meat weight: 5.76 ± 0.14 g) was observed, compared to mussels 200 m away (shell length: 54.82 ± 0.61 mm, wet meat weight: 4.62 ± 0.14 g) and control (shell length: 49.50 ± 0.90 mm, wet meat weight: 2.76 ± 0.22 g). This result confirmed what was

already observed by the same authors in a previous study, where mussels grew 50% faster in weight when grown in proximity to salmon aquaculture sites [81]. Moreover, mussels held in cages continued to grow in the winter months as well, maintaining a greater meat weight and CI than mussels held 200 m away or at a reference site, which on the contrary recorded a decline in shell growth rate and a decrease in meat weight. This means that mussels at the cage sites gained a more continuous food supply that facilitated early winter growth and enabled overall larger sizes. This phenomenon has also been encountered in the studies by Gvozdenovic et al. [59,82], where higher CI values *of M. galloprovincialis* cultivated close to fish cages (10–100 m distance) were found during a cold period. Overall, the improved growth performance of mussels within and relatively near to fish cages (0 m and 1–100 m distance) under direct organic emission, compared to those grown at larger spatial scales (where there is an increase in particulate dilution), has also been observed in several other papers [60,61,83,84]. In particular, Arduini et al. [60] recently investigated the growth performance of *M. galloprovincialis* under an innovative IMTA system tested in the northern Ionian Sea (Central Mediterranean Sea), that combined fish, mussels and a new group of bio-remediators (sponges, polychaetes and macroalgae), not only in relation to the "horizontal distance" from the cage (1 and 300 m distance), but also to the "vertical distance", namely on the basis of the water depth (1 and 12 m depth). The CI required for marketing (i.e., 0.15) was achieved only in the mussels grown near the fish cages (1 m distance) and at a depth of 12 m (0.15 ± 0.03), recording CI values among the highest measured in the Taranto area in the last twenty years. Mussels grown in these conditions may have benefited to a greater extent from the organic load of fish cages, which tend to settle on the bottom and/or they may have found temporary shelter from potentially harmful "heat waves" which increased the mussel survival rate compared to those grown at the surface (traditional farming method).

Another innovative IMTA setup was proposed by Chatzivasileiou et al. [61], where fish (*S. aurata* and *D. labrax*), bivalves (*M. galloprovincialis* and *P. imbricata radiata*) and sea cucumber (*H. pollii*) were co-cultured in three fish farms in the Aegean Sea with different trophic conditions. The survival, robustness, and growth parameters of the bivalves and sea cucumber recorded in IMTA system were compared to those of their respective wild populations. All the three species showed high survival rates in the IMTA. The values of CI and meat yield (MY) were higher in IMTA Mediterranean mussels (CI: 33–42%, MY: 19–28%) and pearl oysters (CI: 53–56%, MY: 26–33%) compared to those cultivated under natural conditions (mussels: CI 35%, MY 10%; oysters: CI 30–45%, MY 20–31%). With the Mediterranean Sea being mostly oligotrophic, the areas near fish farms may have been an exception for bivalves due to the significant amount of released nutrients from fish cages. Unlike bivalves, sea cucumber did not gain weight under the IMTA regime, with a final weight reduction even being observed (ranged from 8.3 g to 18.3 g) compared to the initial one (ranged from 59.4 g to 70 g), despite the high survival rate (ranged from 40% to 80%). This last result was perhaps related to the fact that sea cucumbers were not placed directly on the sediment, but tied under the fish cages, which may have protected them from hypoxia. However, factors that negatively affected their development are still under question.

The efficiency of a similar IMTA setup to that of Chatzivasileiou et al. [61] was also tested in concrete tanks located at the seacoast with an open-flow seawater system [34]. The system was composed of the European sea bass *D. labrax* and organic extractive species from two trophic levels: suspension filter feeders (the mussel *M. galloprovincialis* and the oysters *O. edulis* and *C. gigas*) and deposit feeders (the sea cucumber *H. sanctori*). All filter and deposit feeders showed a 100% survival; the total weight and shell lengths of bivalves were increased in comparison to their initial state ($p > 0.05$), while the initial and final CI ratios were similar. Sea cucumber, instead, displayed a significant increase in total weight at the end of the experiment (132.55 ± 2.58 g) compared to the initial weight (116.81 ± 2.87 g). It is likely that the different cultivation system or physicochemical characteristics of the water positively affected the growth of the sea cucumber, compared to what was observed

by Chatzivasileiou et al. [61]. Simultaneously, fed fish showed a significantly lower feed conversion ratio (1.47 ± 0.01) and higher feed efficiency (68.10 ± 0.46%) in comparison to the monoculture system (1.66 ± 0.01 and 60.38 ± 0.24%, respectively).

In light of these studies, it emerged that various factors (i.e., water temperature, salinity, etc.) are responsible for the variation in bivalve's growth performance cultivated under IMTA systems; however, among these, food availability seems to be the most influential variable.

Because of the important ecological role and high market value, sea urchins and sea cucumber receive increased attention for their use in IMTA. Shpigel et al. [62] conducted practical investigations on the long-term performance of *P. lividus* as an algivorous in a semi-commercial land-based fish (*S. aurata*), seaweed (*Ulva lactuca*) and urchin IMTA system. The benefits of this co-culture for sea urchins included reducing the growth period (reaching commercial size in 3 years rather than 4–5 years), improving gonadal growth, reaching high protein levels in the gonad (ranged between 49.5 and 53.8%) and the generation of three reproductive cycles in one year (two in the winter and one in the spring) rather than one or two seasonal peaks. Researchers attributed these good results to the ad libitum provision of highly nutritious seaweed and relatively constant water temperature throughout the year, which contributed to generate optimal conditions for sea urchins' growth.

Regarding sea cucumbers, different species were fed several food sources, such as bivalve feces and pseudo-feces, fish bio-deposits, and sea sediment, in open-water and land-based IMTA systems [37,63–65,85].

Thanks to their high protein to lipid ratio, high levels of beneficial polyunsaturated FAs, essential amino acids, collagens, vitamins and minerals, sea cucumbers are considered a premium seafood [86]. Paltzat et al. [63] showed that California sea cucumbers (*A. californicus*) held in experimental trays below the cultured *C. gigas* successfully utilized oyster's bio-deposits (feces and pseudofeces). Sea cucumber showed a mean weight increase of 42.9 g in approximately 12 months compared to the initial weight, and no mortalities in any of the trays deployed during the study were recorded. Positive results were also observed for *A. californicus* of a small size cultivated with sablefish (*Anoplopoma fimbria*) at an IMTA site [37]. Sea cucumbers held below the fish pens grew significantly faster than control animals grown ~250 m away from the farm and recorded a high survival rate (mean 99.5%). High survival (96%) and growth rates were also found for the Japanese common sea cucumber (*A. japonicus*) cultured below a red sea bream cage, compared to the control station [64]. Sea cucumber juveniles reached market size over a culture period of a year and a half (range weight: 142–181 g, mean wet weight: 160 g) and incorporated C3 plant material in fish feed through fish feces. Similar results were also recorded for *A. japonicus* bottom-cultured under a fish farm (main cultivated species: crimson snapper *Lutjanus erythropterus*, blue-spotted grouper *Epinephelus fario*, and cobia *Rachycentron canadum*) in southern China [65]. Debris from the fish cages were efficiently used by sea cucumber, which grew much faster than those at the reference site during winter and early spring.

Overall, these results suggest that co-culture systems among sea cucumber and fish or bivalves would both reduce the amount of organic deposition under farms and produce a valuable secondary cash crop (sea cucumber biomass), promoting the diversification of production.

Combinations of different echinoderm species were also tested in new IMTA setups, where sea urchins are used as primary species and sea cucumbers as the extractive species. An example of this is that reported by Sonnenholzner-Varas et al. [66], based on the co-culture of *T. depressus* (sea urchin) and *H. theeli* (sea cucumber), which was tested to evaluate the use of fresh egested feces of sea urchins that were fed with different natural diets of seaweeds (*Padina durvillaei*, *Sargassum ecuador eanum*, *Kappaphycus alvarezii*, or a mix of these three seaweeds) as food for sea cucumber juveniles. Small (S) and large (L) sea urchins fed with seaweed *P. durvillaei* showed a faster growth (S: 3.0 ± 0.05 cm TD, 7.9 ± 0.2 g; L: 2.1 ± 0.1 cm TD, 5.3 ± 0.1 g, respectively) and lower feed conversion ratio compared to all other

treatments. Moreover, sea urchins produced higher amount of feces per day when fed with *P. durvillaei* (L: 31.1 ± 2.7 g d^{-1}; S: 11.1 ± 1.2 g d^{-1}) and the mixture of seaweeds (L: 28.9 ± 1.9 g d^{-1}; S: 10.9 ± 1.2 g d^{-1}, $p < 0.05$). At the same time, juveniles of sea cucumber assimilated the feces of sea urchins very well from a diet exclusively based on the mix of seaweed, recording the highest growth rates (length: 7.03 ± 0.03 cm, weight: 5.30 ± 0.11 g) and survival. Overall, the mix of three seaweeds as a natural source of food for sea urchin and its feces (as sub-products) for sea cucumber promoted the proper growth of both organisms.

Another successful co-culture between two of the most valuable Mediterranean echinoderms (*P. lividus* and *H. tubulosa*) was reported by Grosso et al. [67]. As in the previous study, the effects of three different diets on sea urchin (*P. lividus*) gonad enhancement and somatic growth were evaluated, integrating various levels of fish meal in a land-based vegetable diet—D-0 (100% vegetables, 0% fish meal); D-20 (80% vegetables, 20% fish meal); D-40 (60% vegetables, 40% fish meal). Subsequently, the survival and somatic growth of sea cucumber (*H. tubulosa*) regarding sea urchin bio-deposits of the different experimental diets used as a sole food source for sea cucumbers were evaluated. Among these experimental diets, D-20 was consumed more efficiently, with a lower feed conversion ratio (sea urchin: 3.64 ± 1.39; sea cucumber: 0.41 ± 0.04) and sustained high somatic growth rates for both co-cultured species (sea urchin: 0.12 ± 0.02%; sea cucumber: 0.28 ± 0.05%). A high final survival rate was also recorded for both sea urchin and sea cucumber, suggesting a synergic consumption of the food source and no side effects of co-existence in a same rearing environment. According to the obtained results, the suitability both of the rearing system and the procedures followed is also evident in this case. However, in this study, the use of small amount of an animal protein integrator, such as fish meal, was necessary to complete the nutritional profile of whole vegetable diets and sustain the growth of both species in IMTA system. Nevertheless, the use of land-based vegetables as the main ingredient of the diet led to a significant reduction in feed costs.

The integration of sponges in IMTA systems fulfils complementary functions to other filter feeders commonly applied, such as shellfish, aiding in maintaining lower bacterial loads, reducing disease pressure, and enhancing production. Recent evidence on the feeding behaviour of sponges indicates that dissolved organic matter (DOM) represents the main food source, while particulate organic matter (POM) represents only a small portion of their total intake [87]. Since DOM is not a bioavailable food source for most other heterotrophic organisms, sponges serve a unique and valuable extractive component in IMTA. Considering the dynamics of fed aquaculture, where DOM is generated and its production significantly increases with the inclusion of seaweeds as IMTA components [88,89], this release of DOM can promote the bacterial growth, including pathogenic bacteria. Sponges can mitigate this microbial load both by consuming DOM [87] or removing them [90]. In addition, in an IMTA system, sponges not only can remove potentially harmful particles (e.g., bacteria, viruses, fecal pellets) but also enhance their productivity by using DOM. Indeed, sponges are able to convert DOM into POM (detritus) through the "sponge loop" [91], returning valuable resources to the benthic food chain. This detritus serves as a food source for detritivores such as the commercially valuable sea cucumbers [92]. On account of the results obtained in the experiment conducted by Longo et al. [68], where the sponge *Hymeniacidon perlevis* and the mussel *M. galloprovincilais* were co-cultured in an integrated rearing system, the efficiency of the proposed mussel–sponge model has been demonstrated. Indeed, the abundances of all the considered microbial parameters (e.g., culturable bacteria at 37 °C, vibrios, coliforms, enterococci) in seawater from the integrated rearing system were lower than the control area. Moreover, due to the higher bacterial accumulation exerted by the sponge compared to the mussel, its presence reduces the bacterial load in the co-cultured *M. galloprovincialis*. This finding has practical implications for aquaculture, as the integrated rearing of the investigated filter–feeders could reduce the contamination of edible mussels by harmful bacteria. This helps prevent infections in humans and lowers the risk of mussel diseases, which can cause significant financial losses, ultimately enhancing the safety of seafood production and farming.

2.3. Inorganic Extractive Species

In the IMTA cultivation system, seaweed serves as the primary producer at the base of the food chain. They play a crucial role by supplying oxygen through photosynthesis during the day, lowering CO_2 levels, removing ammonia, and absorbing excess nutrients from the aquatic environment [40]. At the same time the seaweeds are converted into potentially valuable biomass and considered as an important secondary cash crop.

Ulva and *Gracilaria* are the most widespread genera due to good large-scale seaweed biomass production and significant revenues for the fish aquaculture when adopting the IMTA approach [93]. An example of the high productivity of *Gracilaria chilensis* species cultivated in a long line near salmon farms in an open-water IMTA system was reported by Abreu et al. [69]. High growth performance (average 1.7 kg m^{-2} fresh weight) was recorded up to 1 km from a 1 ha salmon farm with a production capacity of 1500 tonnes, compared to the control (7 km away from the salmon farm) and the traditional bottom culture. The same authors [70] tested the performance of another species of *Gracilaria* (*G. vermiculophylla*) in a land-based aquaculture pilot scale system for sole (*Solea senegalensis*) and turbot (*Scophthalmus rhombus*). The best results were achieved at the lowest stocking density tested of 3 kg m^{-2}, where the seaweed system produced 0.7 ± 0.05 kg (dw) m^{-2} $month^{-1}$ of biomass. The present study recorded higher yields than the one reported by Matos et al. [71] in a similar experiment for *Gracilaria bursa pastoris* cultivated at a stocking density of 5 kg m^{-2} (27.0 ± 15.70 g dw m^{-2} day^{-1}). Moreover, the *Gracilaria vermiculophylla* biomass reported a high protein mean value of 37.5% (with highest values of 50%).

The seaweed *G. bursa pastoris*, coupled with *Chaetomorpha linum*, was also co-cultivated for the first time with a new set of filter–feeder bioremediator organisms, such as the polychaete *Sabella spallanzanii* and the sponge *Sarcotragus spinosulus*, in an IMTA system realized at a preindustrial level in the Gulf of Taranto (southern Italy) [74]. This innovative setup showed interesting growth performances (a mean of specific growth rates of 11%, in short time intervals of 11 and 7 days for *C. linum* and *G. bursa pastoris,* respectively), with high survival rates and a significant amount of biomass produced.

A more complex system involving the integrated culture of three organisms, abalone (*Haliotis discus hannai*) fish (*S. aurata*), and seaweed (*U. lactuca* or *G. conferta*), in a land-based system, was proposed by Neori et al. [72]. The nutrients excreted by the fish supported high yields of *U. lactuca* (78 kg m^{-2} $year^{-1}$), while *Gracilaria* functioned poorly (only 14 kg annually). In turn, *Ulva* supported an abalone growth rate of 0.9% day^{-1} and a length increase of 40–66 μm day^{-1} in juveniles, and 0.34% day^{-1} and 59 μm day^{-1} in young adults. The total abalone yield was 9.4 kg $year^{-1}$.

Another system, consisting of abalone (*H. discus hannai*) and sea urchin (*P. lividus*) tanks, an intensive fishpond (*S. aurata*), and a three-stage *U. lactuca* biofilter, was proposed by Schuenhoff et al. [73]. During the two experimental periods without (from November to January) and with greenhouse cover (from February to March), *U. lactuca* yield totalled 310 kg (fresh weight) and the protein content averaged above 34% of dry weight. The three-stage biofilter design improved the protein level of the seaweed along with maintaining high nutrient uptake efficiency. The authors suggested that the conversion of nutrient pollution into useful, high-quality seaweed biomass can at the same time offset the costs of biofiltration.

3. IMTA as Potential System for the Production of Alternative Ingredients in the Feeds of Aquatic Species

In aquaculture, fish feeding represents a range between 30 and 70% of the total operating costs of the aquaculture production system. It is known that fish meal and fish oil, mainly from small pelagic fish, are the main sources of protein and essential FAs of the ω-3 series, respectively, as well as the most expensive ingredients for the formulation of commercial feeds [94]. Moreover, the overfishing of wild fish stocks for the production of fishmeal and fish oil is one of the major issues in aquaculture sustainability [95]. Therefore, in order to sustain the expected global growth of aquaculture, the search for new protein

and lipid sources is of utmost importance. In addition, according to the last FAO Sofia report [96], the aquaculture production has surpassed fishing for the first time; therefore, it becomes increasingly necessary to address the global aquaculture system toward more sustainable models, like IMTA, considering the key role of aquatic foods in climate change. In this regard, the reduction or elimination of dependence on fish-to-feed is also included among the advantages of IMTA [9]. Several studies reported that it is a valid approach for the production of alternative protein and lipid sources for the formulation of aquafeeds. In particular, it has been proven that IMTA systems have been successfully employed to improve the nutritional quality of seaweed [31,97–100] and polychaete biomass [56] compared to those of wild species, making them more suitable to be used as fish-feed ingredients. Specifically, it has been demonstrated that seaweeds co-cultivated under a high nutrient flux, in addition to promoting higher productivity levels, can increase the protein content over 40% [70,73] and present a high-quality protein profile characterized by a complete essential amino acid profile [100]. Likewise, it seems that polychaetes can be successfully employed to recover and retain protein and valuable HUFA (i.e., EPA and DHA) from uneaten fish feeds that would otherwise be lost to the environment, negatively impacting adjacent aquatic ecosystems [56,79,80,101–103].

The production of high-nutritional-value biomass to use as ingredient in feeds represents an important economic incentive for promoting a wider and faster implementation of IMTA systems at a commercial scale. Indeed, the integration of SDG 14 with the parameters related to the circular economy by the exploitation of by-products from IMTA allows us to save costs and environmental benefits [104], and encourages the sector toward the adoption of more sustainable practices and assessment aligned with the ESG parameters, both in a horizontal cross-cut and vertically along seafood production. The cost increase and availability of feeds with proper nutritional composition is on the agenda of FAO, and it is necessary to adopt models like IMTA and enhance technology use throughout the process.

The successful results of the partial replacement of fish meals with seaweed meals that have emerged from the literature seem to be dose- and species-dependent. For the Nile tilapia, several studies investigated the effect of increasing levels of IMTA-produced *Ulva* spp. meal (from 5 up to 30%) in diets at different fish life stages and on various parameters [31,32,98,105]. In particular, the results obtained by Marinho et al. [32], Valente et al. [98], and Silva et al. [105] agree on the fact that the inclusion of *Ulva* spp. meal in diets for Nile tilapia seems to be possible up to 10% without compromising growth performance, body composition, flesh organoleptic properties, and protein utilization and retention. The good capacity of Nile tilapia juveniles to digest and absorb *Ulva* nutrients was suggested from the results obtained by Silva et al. [105], where no significant alterations of gut morphology were observed compared to the control diet. In the same way, with an *Ulva* inclusion level of 30%, Pereira et al. [31] reported the values of protein and energy apparent digestibility coefficients (ADC) most similar to the reference diet, as well as those higher than other tested seaweeds. Moreover, *Ulva* spp. enhanced the innate immune response of Nile tilapia by increasing complement activity (ACH50), promoting the health status of the fish [98]. Overall, these finding suggests that *Ulva* meal could be a suitable partial replacement for fish meal in Nile tilapia diets.

In California Yellowtail (*Seriola lalandi* syn. *S. dorsalis*) juveniles, the effects of different levels (0.5, 1, and 2%) of dietary supplementation with IMTA-cultivated *Ulva fasciata* on growth performance, haematology, and FA profiles were evaluated [106]. According to the obtained results, *U. fasciata* supplementation up to 2% did not affect fish growth and health. Regarding the haematological parameters, the percentage of haematocrit increased significantly with the higher inclusion of *U. fasciata* meal (46.83 ± 0.76) compared to the control (39.50 ± 3.77), followed also by an increasing trend for red blood cell count ($3.19 \pm 0.34 \times 10^6$ cel mm^3) and the mean corpuscular volume (150.59 ± 17.32 fL). These results are most likely be associated with the antioxidant compounds contained in seaweed, such as carotenoids and antimicrobial compound ulvan. Also, the total PUFA ω-3 was significantly higher, with a seaweed inclusion level of 1% and 2% in comparison with 0.5% and control,

in particular for the value of DHA in the muscle, which increased by approximately 49%. However, considering that this FA was not detected in the *U. fasciata* meal used in this study, the authors assumed that the antioxidants contained in the seaweed meal (e.g., carotenoids) could have prevented lipid peroxidation, preserving the long-chain PUFAs contained in fish feed.

Another interesting result was reported by Shpigel et al. [107], which showed that high-protein *Ulva lactuca* produced in an IMTA system was proven to be suitable to replace 100% of fishmeal, adding up to 14.6% seaweed in diets for juvenile of *S. aurata*. This percentage of replacements with alga biomass allowed us to obtain a similar performance in terms of SGR (1.44 ± 0.03%) survival (100%) and FCR (1.7 ± 0.05), to those of fish fed the commercial control feed (1.98 ± 0.02%, 100%, 1.5 ± 0.03, respectively), saving almost 10% on the cost of the feed.

The use of *U. lactuca* harvested from a land-based IMTA system was also tested as a partial replacement (25 and 50%) or a supplement (25%) to a commercial shrimp diet for *P. vannamei* juveniles [99]. It was observed that *U. lactuca* can be substituted for up to 25% of a commercial shrimp feed without significantly compromising production performance in terms of growth (2.7 ± 0.26%), survival (81 ± 13.6%), and FCR (2.06 ± 0.49), compared to the control (3.0 ± 0.2%, 81 ± 11.8%, 2.47 ± 0.84, respectively). Moreover, from the nutritional profile comparison between a pelleted diet and *U. lactuca*, it emerged that seaweed contained high levels of protein and an amino acid profile comparable to commercial shrimp feed. This suggests that freshly harvested *U. lactuca* can partially replace a high-protein pelleted diet for shrimp.

A couple of studies on rainbow trout (*Oncorhynchus mykiss*) instead highlight the preference of this species towards *Gracilaria vermiculophylla* seaweed. According to the results by Pereira et al. [31], rainbow trout seems to better digest *G. vermiculophylla* compared to IMTA-cultivated *Ulva spp.* and *Porphyra dioica*, recording an ADC of protein (89.5 ± 0.5%) and lipid (97.5 ± 0.5%) similar to the reference diet (90.3 ± 0.5% and 97.8 ± 0.2, respectively) and significantly higher than other tested diets. In the same way, Araujo et al. [97] observed that the inclusion of *G. vermiculophylla* meal in diets for rainbow trout was possible up to 5%, without impairing gut morphology (intestine diameter and villi height) and thus growth performance. This diet also enhanced the innate immune response of rainbow trout, inducing the highest peroxidase activity (6.86 ± 0.60 U mL^{-1}), lysozyme activities (1077.47 ± 161.74 U mL^{-1}) and ACH50 alternative complement pathway activity (55.30 ± 6.36 U mL^{-1}), compared to the control (4.05 ± 0.37 U mL^{-1}, 667.90 ± 54.85 U mL^{-1}, 35.85 ± 4.94 U mL^{-1}, respectively).

Recently, an innovative mixture of dietary ingredients, that has seen the addition to fishmeal of 10% of polychaete meal (*S. spallanzanii*) and 5% of algal meal (*C. linum*) cultivated by an IMTA system, was tested for farmed juveniles of seabass *D. labrax* [103]. This new formulation, rich in lipids, especially ω-3 PUFAs, showed a survival rate higher than 80% and did not produce negative effects on the fish growth; in fact, no statistical differences were evidenced in biomass gain and specific growth rate between fishes nourished with the control (2.87 ± 0.15 g, 2.96 ± 0.16%, respectively) and the innovative meal (2.1 ± 0.12 g, 2.4 ± 0.11%, respectively). However, as this is a preliminary study, further investigations are needed in order to test higher percentages of *C. linum* and *S. spallanzanii*, aiming to provide fish with additional beneficial compounds and also partially replacing fishmeal.

The potential inclusion of seaweed biomass harvested from the IMTA system in feed is also being considered for livestock, especially rabbits. In fact, a market for algae in the main rabbit-producing countries used in animal feed as alternative to antibiotics already exists. Therefore, the introduction of marine macroalgae coming from IMTA system could be used as a marketing strategy for consumers who are increasingly concerned about issues of environmental sustainability and who are looking for different, high-quality foods [33].

4. Considerations and Future Prospects

A very important point emerging from this review was the identification of IMTA system not only as a valuable approach to environmental bioremediation, but also as a method to improve the growth performances and the quality traits of the products and by-products generated in terms of sustainability toward the climate mitigation. In this regard, it emerged that a large body of research literature has been produced in the last two decades, aiming to scientifically prove the potential of various IMTA setups, especially to increase the productivity, and to a lesser extent, the welfare and quality of cultivated species, while reducing waste loadings and environmental impacts. It is known that animal stress and welfare are crucial concerns for producers, as they directly affect the whole-animal's performance, like survival, growth, reproductive performance, health, susceptibility to diseases [108], and meat quality [109]. Hence, the low presence of studies that support the improvement of animal welfare and sea food nutritional and sensory quality produced by IMTA systems leads us to suggest the development of further joint applied research and projects between universities and industries, aiming to reinforce the results achieved to date. In this regard, proteomics integrated with another "omics" approach has emerged in aquaculture welfare studies as an extremely valuable tool to try to better understand fish welfare, improve welfare status assessment, optimize the fish's capacity to cope with unavoidable challenges/stress, and find candidate stress biomarkers [110].

According to what was expressed by the EU fisheries policy on aquaculture since 2002 [111], in order to improve the competitive position of the sector and to promote environmental, economic, and social sustainability, it is necessary to find a system able to increase the production and the diversification of species, as well as the product quality. Although the IMTA concept fully meets these requirements, for its wider application, it is imperative that the results of researchers move forward from pilot-scale to commercial-scale development, also taking into account the biosafety of the species involved, as potential risks of contaminant bioaccumulation by extractive species could emerge [76]. In this regard, to enhance their quality and their safety even more, moving forward from open systems to innovative integrated multi-trophic recirculating aquaculture systems (IMTRAS), composed of IMTA and RAS in pairs, is a good strategy [112]. Moreover, it is pivotal to understand that the move to commercial-scale IMTA systems has to also pass through the social acceptability of different kinds of stakeholders. To this aim, the development of a set of production standards and certifications could both increase the consumer confidence in this system and protect producers' investments. Indeed, precision aquaculture farming could be a possible solution, especially for offshore and open-water IMTA systems, toward the achievement of standardized production methods through the autonomous and continuous monitoring of environmental (i.e., water temperature and tilt, salinity, dissolved oxygen, blue-green algae, chlorophyll, turbidity) and animal variables (parameters related to the behavioural or physiological state of the fish). In particular, this approach applies various technologies and adaptive tools (i.e., wireless sensors, computer vision, AI, underwater video monitoring, hydroacoustic technology, drone, cloud) to monitor, analyze, interpret, predict, and provide more reliable decision support which allows for more effective, precise, accurate, and repeatable farm management [113]. On the basis of these considerations, future studies could be focused on evaluating the possible combination of these two cutting-edge aquaculture practices, precision farming and IMTA, in order to optimize and standardize the productivity, the overall quality of products, and aquatic environmental sustainability, insofar a life below water is considered linked to climate change mitigation.

In addition, the studies here reported underline the IMTA application as a protocol multivariable, which allows us to increase the market value of by-products obtained along the seafood supply chain by using them as sustainable ingredients to reduce or eliminate aquaculture's dependence on fish meal and oil. From an economical point of view, the potential inclusion of seaweeds and polychaetes with high quantitative–qualitative proteins and lipids in the feed industrial processing for aquaculture and land-side species can be

a promising parallel activity to increase the IMTA system profitability and encourage the companies and policymakers to implement it.

5. Conclusions

IMTA showed the potentiality to increase the efficiency and productivity of monoculture systems, adding the possibility of generating products and by-products with improved nutritional profiles and characterized by a high market value, while reducing environmental impact. This productive approach could indeed contribute to achieve SDG 14 and the blue revolution in terms of ESG application in sustainable aquaculture development, which further allows us to apply the recent, viable EU Nature Restoration Law (17.6.2024) [114] that introduces the obligation to restore marine-degraded ecosystems by cross-cutting technologies and bioremediation regarding edible and inedible species. The potential benefits of the IMTA system captured in this review could constitute a basis to encourage further studies in order to explore new IMTA opportunities to improve the public perception of this system and to better understand the commercial motivation to promote the scaling up of experimental IMTA systems towards commercial operations. In this regard, further investigations could be useful to deepen the knowledge of fish farming managed with cutting-edge technological supports in order to provide standardized methods for a high-quality product and environmental protection from the perspective of "precision aquaculture farming" adoption.

Author Contributions: Conceptualization, N.I. and A.R.; Methodology, G.R., N.I. and A.R.; Formal Analysis, G.R., N.I. and A.R.; Writing—Original Draft Preparation, G.R., N.I. and A.R.; Writing—Review and Editing, G.R., N.I., A.R., M.D.I., M.C. and C.L.; Visualization, N.I. and A.R.; Supervision, N.I. and A.R.; Project Administration, N.I.; Funding Acquisition, N.I., A.R. and M.C. All authors have read and agreed to the published version of the manuscript.

Funding: The study was partially supported by PNRR—NEXTGENERATIONEU, Agritech [CN00000022], Spoke 5, linea C, sottotematica 2, UNIVERSITÀ DEGLI STUDI DELLA TUSCIA, FishVision Project (CUP J83C22000830005).



Conflicts of Interest: The authors declare no conflicts of interest.

References

1. Chopin, T. Integrated Multi-Trophic Aquaculture Ancient, Adaptable Concept Focuses on Ecological Integration. *Glob. Aquac. Advocate* **2013**, *16*, 16–19.
2. Shpigel, M. Mariculture Systems, Integrated Land-Based. In *Sustainable Food Production*; Christou, P., Savin, R., Costa-Pierce, B.A., Misztal, I., Whitelaw, C.B.A., Eds.; Springer: New York, NY, USA, 2013; pp. 1111–1120. [CrossRef]
3. Chopin, T.; Troell, M.; Reid, G.K.; Knowler, D.; Robinson, S.M.C.; Neori, A.; Buschmann, A.H.; Pang, S.J. Integrated Multi-Trophic Aquaculture. In *Advancing the Aquaculture Agenda*; OECD Publishing: Paris, France, 2010; pp. 195–217.
4. Hughes, A.; Black, K. Going beyond the Search for Solutions: Understanding Trade-Offs in European Integrated Multi-Trophic Aquaculture Development. *Aquac. Environ. Interact.* **2016**, *8*, 191–199. [CrossRef]
5. Nissar, S.; Bakhtiyar, Y.; Arafat, M.Y.; Andrabi, S.; Mir, Z.A.; Khan, N.A.; Langer, S. The Evolution of Integrated Multi-Trophic Aquaculture in Context of Its Design and Components Paving Way to Valorization via Optimization and Diversification. *Aquaculture* **2023**, *565*, 739074. [CrossRef]
6. Barrington, K.; Ridler, N.; Chopin, T.; Robinson, S.; Robinson, B. Social Aspects of the Sustainability of Integrated Multi-Trophic Aquaculture. *Aquac. Int.* **2010**, *18*, 201–211. [CrossRef]
7. Giangrande, A.; Gravina, M.F.; Rossi, S.; Longo, C.; Pierri, C. Aquaculture and Restoration: Perspectives from Mediterranean Sea Experiences. *Water* **2021**, *13*, 991. [CrossRef]
8. Moffitt, C.M.; Cajas-Cano, L. Blue Growth: The 2014 FAO State of World Fisheries and Aquaculture. *Fisheries* **2014**, *39*, 552–553. [CrossRef]
9. Granada, L.; Sousa, N.; Lopes, S.; Lemos, M.F.L. Is Integrated Multitrophic Aquaculture the Solution to the Sectors' Major Challenges?—A Review. *Rev. Aquac.* **2015**, *8*, 283–300. [CrossRef]

10. Kleitou, P.; Kletou, D.; David, J. Is Europe Ready for Integrated Multi-Trophic Aquaculture? A Survey on the Perspectives of European Farmers and Scientists with IMTA Experience. *Aquaculture* **2018**, *490*, 136–148. [CrossRef]
11. Troell, M.; Halling, C.; Neori, A.; Chopin, T.; Buschmann, A.H.; Kautsky, N.; Yarish, C. Integrated Mariculture: Asking the Right Questions. *Aquaculture* **2003**, *226*, 69–90. [CrossRef]
12. Troell, M.; Joyce, A.; Chopin, T.; Neori, A.; Buschmann, A.H.; Fang, J.-G. Ecological Engineering in Aquaculture—Potential for Integrated Multi-Trophic Aquaculture (IMTA) in Marine Offshore Systems. *Aquaculture* **2009**, *297*, 1–9. [CrossRef]
13. Buck, B.H.; Troell, M.F.; Krause, G.; Angel, D.L.; Grote, B.; Chopin, T. State of the Art and Challenges for Offshore Integrated Multi-Trophic Aquaculture (IMTA). *Front. Mar. Sci.* **2018**, *5*, 165. [CrossRef]
14. Fang, J.; Zhang, J.; Xiao, T.; Huang, D.; Liu, S. Integrated Multi-Trophic Aquaculture (IMTA) in Sanggou Bay, China. *Aquac. Environ. Interact.* **2016**, *8*, 201–205. [CrossRef]
15. Ridler, N.; Wowchuk, M.; Robinson, B.; Barrington, K.; Chopin, T.; Robinson, S.; Page, F.; Reid, G.; Szemerda, M.; Sewuster, J.; et al. Integrated multi-trophic aquaculture (IMTA): A potential strategic choice for farmers. *Aquac. Econ. Manag.* **2007**, *11*, 99–110. [CrossRef]
16. Carras, M.A.; Knowler, D.; Pearce, C.M.; Hamer, A.; Chopin, T.; Weaire, T. A Discounted Cash-Flow Analysis of Salmon Monoculture and Integrated Multi-Trophic Aquaculture in Eastern Canada. *Aquac. Econ. Manag.* **2019**, *24*, 43–63. [CrossRef]
17. Khanjani, M.H.; Zahedi, S.; Mohammadi, A. Integrated Multitrophic Aquaculture (IMTA) as an Environmentally Friendly System for Sustainable Aquaculture: Functionality, Species, and Application of Biofloc Technology (BFT). *Environ. Sci. Pollut. Res.* **2022**, *29*, 67513–67531. [CrossRef]
18. Hossain, A.; Senff, P.; Glaser, M. Lessons for Coastal Applications of IMTA as a Way towards Sustainable Development: A Review. *Appl. Sci.* **2022**, *12*, 11920. [CrossRef]
19. Arduini, D.; Borghese, J.; Gravina, M.F.; Trani, R.; Longo, C.; Pierri, C.; Giangrande, A. Biofouling role in mariculture environment restoration: An example in the Mar Grande of Taranto (Mediterranean Sea). *Front. Mar. Sci.* **2022**, *9*, 842616. [CrossRef]
20. Stabili, L.; Giangrande, A.; Arduini, D.; Borghese, J.; Petrocelli, A.; Alabiso, G.; Ricci, P.; Cavallo, R.A.; Acquaviva, M.I.; Narracci, M.; et al. Environmental quality improvement of a mariculture plant after its conversion into a multi-trophic system. *Sci. Total Environ.* **2023**, *884*, 163846. [CrossRef]
21. Knowler, D.; Chopin, T.; Martínez-Espiñeira, R.; Neori, A.; Nobre, A.; Noce, A.; Reid, G. The Economics of Integrated Multi-Trophic Aquaculture: Where Are We Now and Where Do We Need to Go? *Rev. Aquac.* **2020**, *12*, 1579–1594. [CrossRef]
22. Viji, C.S.; Chadha, N.K.; Kripa, V.; Prema, D.; Prakash, C.; Sharma, R.; Jenni, B.; Mohamed, K.S. Can Oysters Control Eutrophication in an Integrated Fish-Oyster Aquaculture System? *J. Mar. Biol. Assoc. India* **2014**, *56*, 67–73. [CrossRef]
23. Viji, C.S. Studies on Integrated Multitrophic Aquaculture in a Tropical Estuarine System in Kerala, India. Ph.D. Thesis, Central Institute of Fisheries Education, Mumbai, India, 2015.
24. Chopin, T. Marine Aquaculture in Canada: Well-Established Monocultures of Finfish and Shellfish and an Emerging Integrated Multi-Trophic Aquaculture (IMTA) Approach Including Seaweeds, Other Invertebrates, and Microbial Communities. *Fisheries* **2015**, *40*, 28–31. [CrossRef]
25. Liu, Y.; Zhang, J.; Wu, W.; Zhong, Y.; Li, H.; Wang, X.; Yang, J.; Zhang, Y. Effects of Shellfish and Macro-Algae IMTA in North China on the Environment, Inorganic Carbon System, Organic Carbon System, and Sea–Air CO_2 Fluxes. *Front. Mar. Sci.* **2022**, *9*, 864306. [CrossRef]
26. Lane, A.; Hough, C.; Bostock, J. The Long-Term Economic and Ecologic Impact of Larger Sustainable Aquaculture. In *Study for the European Parliament, Directorate General for Internal Policies, Policy Department B, Structural and Cohesion Policies—Fisheries*; European Union: Brussels, Belgium, 2014; Available online: http://www.europarl.europa.eu/RegData/etudes/STUD/2014/529084/IPOL_STU(2014)529084_EN.pdf (accessed on 15 July 2024).
27. Alexander, K.A.; Angel, D.; Freeman, S.; Israel, D.; Johansen, J.; Kletou, D.; Meland, M.; Pecorino, D.; Rebours, C.; Rousou, M.; et al. Improving Sustainability of Aquaculture in Europe: Stakeholder Dialogues on Integrated Multi-Trophic Aquaculture (IMTA). *Environ. Sci. Policy* **2016**, *55*, 96–106. [CrossRef]
28. Chopin, T.; Cooper, J.A.; Reid, G.; Cross, S.; Moore, C. Open-water Integrated Multi-trophic Aquaculture: Environmental Biomitigation and Economic Diversification of Fed Aquaculture by Extractive Aquaculture. *Rev. Aquac.* **2012**, *4*, 209–220. [CrossRef]
29. Van Osch, S.; Hynes, S.; O'Higgins, T.; Hanley, N.; Campbell, D.; Freeman, S. Estimating the Irish Public's Willingness to Pay for More Sustainable Salmon Produced by Integrated Multi-Trophic Aquaculture. *Mar. Policy* **2017**, *84*, 220–227. [CrossRef]
30. Piper, L.; de Cosmo, L.M.; Sestino, A.; Giangrande, A.; Stabili, L.; Longo, C.; Guido, G. Perceived social welfare as a driver of green products consumption: Evidences from an integrated multi-trophic aquaculture production. *Curr. Res. Environ. Sustain.* **2021**, *3*, 10008. [CrossRef]
31. Pereira, R.; Valente, L.M.P.; Sousa-Pinto, I.; Rema, P. Apparent Nutrient Digestibility of Seaweeds by Rainbow Trout (*Oncorhynchus mykiss*) and Nile Tilapia (*Oreochromis niloticus*). *Algal Res.* **2012**, *1*, 77–82. [CrossRef]
32. Marinho, G.; Nunes, C.; Sousa-Pinto, I.; Pereira, R.; Rema, P.; Valente, L.M.P. The IMTA-Cultivated Chlorophyta *Ulva* spp. as a Sustainable Ingredient in Nile Tilapia (*Oreochromis niloticus*) Diets. *J. Appl. Phycol.* **2013**, *25*, 1359–1367. [CrossRef]
33. Al-Soufi, S.; García, J.; Muíños, A.; López-Alonso, M. Marine Macroalgae in Rabbit Nutrition—A Valuable Feed in Sustainable Farming. *Animals* **2022**, *12*, 2346. [CrossRef]

34. Cotou, E.; Miliou, H.; Chatzoglou, E.; Schoina, E.; Politakis, N.; Kogiannou, D.; Fountoulaki, E.; Androni, A.; Konstantinopoulou, A.; Assimakopoulou, G.; et al. Growth Performance and Environmental Quality Indices and Biomarkers in a Co-Culture of the European Sea Bass with Filter and Deposit Feeders: A Case Study of an IMTA System. *Fishes* **2024**, *9*, 69. [CrossRef]
35. Kong, S.; Chen, Z.; Zhao, F.; Liu, Q.; Li, J. Cultivation of *Ulva lactuca* Changes Bacterial Community Structure and Abundances of Nitrogen Cycling Functional Genes in an IMTA System. *Res. Sq.* **2023**. [CrossRef]
36. Cunha, M.E.; Quental-Ferreira, H.; Parejo, A.; Gamito, S.; Ribeiro, L.; Moreira, M.; Monteiro, I.; Soares, F.; Pousão-Ferreira, P. Understanding the Individual Role of Fish, Oyster, Phytoplankton and Macroalgae in the Ecology of Integrated Production in Earthen Ponds. *Aquaculture* **2019**, *512*, 734297. [CrossRef]
37. Hannah, L.; Pearce, C.M.; Cross, S.F. Growth and Survival of California Sea Cucumbers (*Parastichopus californicus*) Cultivated with Sablefish (*Anoplopoma fimbria*) at an Integrated Multi-Trophic Aquaculture Site. *Aquaculture* **2013**, *406–407*, 34–42. [CrossRef]
38. Cubillo, A.M.; Ferreira, J.G.; Robinson, S.M.C.; Pearce, C.M.; Corner, R.A.; Johansen, J. Role of Deposit Feeders in Integrated Multi-Trophic Aquaculture—A Model Analysis. *Aquaculture* **2016**, *453*, 54–66. [CrossRef]
39. Tolon, M.T.; Emiroglu, D.; Gunay, D.; Ozgul, A. Sea Cucumber (*Holothuria tubulosa gmelin*, 1790) Culture under Marine Fish Net Cages for Potential Use in Integrated Multi-Trophic Aquaculture (IMTA). *Indian J. Mar. Sci.* **2017**, *46*, 749–756.
40. Verdian, A.H.; Effendi, I.; Budidardi, T.; Diatin, I. Production Performance Improvement of White Shrimp (*Litopenaeus vannamei*) Culture with Integrated Multi Trophic Aquaculture System in Seribu Islands, Jakarta, Indonesia. *Iran. J. Fish. Sci.* **2020**, *19*, 1415–1427.
41. Naskar, S.; Biswas, G.; Kumar, P.; De, D.; Sawant, P.B.; Das, S.; Roy, U. Effects of Estuarine Oyster, *Crassostrea cuttackensis* as the Extractive Species at Varied Densities on Productivity and Culture Environment in Brackishwater Integrated Multi-Trophic Aquaculture (BIMTA) System. *Aquaculture* **2022**, *554*, 738128. [CrossRef]
42. Wale, C.; Nagabhatla, N.; Yeojin, K.; Cottier-Cook, E.J. Trends and Patterns of the Seaweed Industry and Its Links with SDGs. In *Life Below Water*; Leal Filho, W., Azul, A.M., Brandli, L., Lange Salvia, A., Wall, T., Eds.; Encyclopedia of the UN Sustainable Development Goals; Springer: Cham, Switzerland, 2022; pp. 1–17. [CrossRef]
43. MacDonald, A.; Serpetti, N.; Franco, S.C. Optimising Seafood Nutritional Value and Environmental Sustainability in Aquaculture through a Novel Integrated Modelling Tool Applicable to IMTA and Monoculture. *Aquaculture* **2024**, *590*, 741046. [CrossRef]
44. Welker, T.L.; Overturf, K.; Snyder, S.; Liu, K.; Abernathy, J.; Frost, J.; Barrows, F.T. Effects of Feed Processing Method (Extrusion and Expansion-Compression Pelleting) on Water Quality and Growth of Rainbow Trout in a Commercial Setting. *J. Appl. Aquac.* **2018**, *30*, 97–124. [CrossRef]
45. Fiordelmondo, E.; Magi, G.E.; Mariotti, F.; Bakiu, R.; Roncarati, A. Improvement of the Water Quality in Rainbow Trout Farming by Means of the Feeding Type and Management over 10 Years (2009–2019). *Animals* **2020**, *10*, 1541. [CrossRef]
46. Kumara, R.; Syamala, K.; Anand, P.S.S.; Chadha, N.K.; Sawant, P.B.; Prasad; Doddamani, P.L.; Muralidhar, A.P. Effect of Bivalves on Water Quality, Microbial Load and Growth Performance of *P. vannamei* and *M. cephalus* in Halophyte-Based Integrated Multi-Trophic Aquaculture Reared under Pond Conditions. *Indian J. Anim. Res.* **2023**, *57*, 988–994. [CrossRef]
47. Naskar, S.; Biswas, G.; Kumar, P.; De, D.; Das, S.; Sawant, P.B.; Chadha, N.K.; Behera, P. The Green Seaweed, Enteromorpha Intestinalis: An Efficient Inorganic Extractive Species for Environmental Remediation and Improved Performances of Fed Species in Brackishwater Integrated Multi-Trophic Aquaculture (BIMTA) System. *Aquaculture* **2023**, *569*, 739359. [CrossRef]
48. Biswas, G.; Kumar, P.; Kailasam, M.; Ghoshal, T.K.; Bera, A.; Vijayan, K.K. Application of Integrated Multi Trophic Aquaculture (IMTA) Concept in Brackishwater Ecosystem: The First Exploratory Trial in the Sundarban, India. *J. Coast. Res.* **2019**, *86*, 49. [CrossRef]
49. Biswas, G.; Kumar, P.; Ghoshal, T.K.; Kailasam, M.; De, D.; Bera, A.; Mandal, B.; Sukumaran, K.; Vijayan, K.K. Integrated Multi-Trophic Aquaculture (IMTA) Outperforms Conventional Polyculture with Respect to Environmental Remediation, Productivity and Economic Return in Brackishwater Ponds. *Aquaculture* **2020**, *516*, 734626. [CrossRef]
50. Nath, K.; Munilkumar, S.; Patel, A.B.; Kamilya, D.; Pandey, P.K.; Sawant, P.B. *Lamellidens* and *Wolffia canopy* Improves Growth, Feed Utilization and Welfare of *Labeo rohita* (Hamilton,1822) in Integrated Multi-Trophic Freshwater Aquaculture System. *Aquaculture* **2021**, *534*, 736207. [CrossRef]
51. Omont, A.; Elizondo-González, R.; Quiroz-Guzmán, E.; Escobedo-Fregoso, C.; Hernández-Herrera, R.; Peña-Rodríguez, A. Digestive Microbiota of Shrimp Penaeus Vannamei and Oyster *Crassostrea gigas* Co-Cultured in Integrated Multi-Trophic Aquaculture System. *Aquaculture* **2020**, *521*, 735059. [CrossRef]
52. Zhang, M.-Q.; Yang, J.-L.; Lai, X.-X.; Li, W.; Zhan, M.-J.; Zhang, C.-P.; Jiang, J.-Z.; Shu, H. Effects of Integrated Multi-Trophic Aquaculture on Microbial Communities, Antibiotic Resistance Genes, and Cultured Species: A Case Study of Four Mariculture Systems. *Aquaculture* **2022**, *557*, 738322. [CrossRef]
53. Valente, L.M.P.; Cornet, J.; Donnay-Moreno, C.; Gouygou, J.P.; Bergé, J.P.; Bacelar, M.; Escórcio, C.; Rocha, E.; Malhão, F.; Cardinal, M. Quality Differences of Gilthead Sea Bream from Distinct Production Systems in Southern Europe: Intensive, Integrated, Semi-Intensive or Extensive Systems. *Food Control* **2011**, *22*, 708–717. [CrossRef]
54. Aguado-Giménez, F.; Hernández, M.D.; Cerezo-Valverde, J.; Piedecausa, M.A.; García-García, B. Does Flat Oyster (*Ostrea edulis*) Rearing Improve under Open-Sea Integrated Multi-Trophic Conditions? *Aquac. Int.* **2014**, *22*, 447–467. [CrossRef]

55. Cutajar, K.; Falconer, L.; Massa-Gallucci, A.; Cox, R.E.; Schenke, L.; Bardócz, T.; Andolina, C.; Signa, G.; Vizzini, S.; Sprague, M.; et al. Stable Isotope and Fatty Acid Analysis Reveal the Ability of Sea Cucumbers to Use Fish Farm Waste in Integrated Multi-Trophic Aquaculture. *J. Environ. Manag.* **2022**, *318*, 115511. [CrossRef]
56. Jerónimo, D.; Lillebø, A.I.; Maciel, E.; Domingues, M.R.M.; Cremades, J.; Calado, R. Unravelling the Fatty Acid Profiles of Different Polychaete Species Cultured under Integrated Multi-Trophic Aquaculture (IMTA). *Sci. Rep.* **2021**, *11*, 10812. [CrossRef] [PubMed]
57. Mazón-Suástegui, J.M.; Arcos-Ortega, G.F.; Contreras-Mendoza, C.N.; Medina-Sánchez, J.R.; Chávez-Villalba, J.; Lodeiros, C.; Cruz-Flores, R.; López-Carvallo, J.A. Enhanced Growth of the Pleasure Oyster *Crassostrea corteziensis* Cultured under Integrated Multi-trophic Aquaculture (IMTA) Concept, Using Farm Effluents of Shrimp *Penaeus Vannamei*. *Aquac. Res.* **2022**, *53*, 5214–5226. [CrossRef]
58. Lander, T.R.; Robinson, S.M.C.; MacDonald, B.A.; Martin, J.D. Enhanced Growth Rates and Condition Index of Blue Mussels (*Mytilus edulis*) Held at Integrated Multitrophic Aquaculture Sites in the Bay of Fundy. *J. Shellfish Res.* **2012**, *31*, 997–1007. [CrossRef]
59. Gvozdenovic, S.; Mandic, M.; Peras, I. Morphometry and Condition Index in Mediterranean Mussels (*Mytilus galloprovincialis* Lamarck, 1819) from Boka Kotorska Bay (Montenegro, Southeast Adriatic Sea). *Stud. Mar.* **2020**, *33*, 15–26.
60. Arduini, D.; Portacci, G.; Giangrande, A.; Acquaviva, M.I.; Borghese, J.; Calabrese, C.; Giandomenico, S.; Quarta, E.; Stabili, L. Growth Performance of *Mytilus galloprovincialis* Lamarck, 1819 under an Innovative Integrated Multi-Trophic Aquaculture System (IMTA) in the Mar Grande of Taranto (Mediterranean Sea, Italy). *Water* **2023**, *15*, 1922. [CrossRef]
61. Chatzivasileiou, D.; Dimitriou, P.D.; Theodorou, J.; Kalantzi, I.; Magiopoulos, I.; Papageorgiou, N.; Pitta, P.; Tsapakis, M.; Karakassis, I. An IMTA in Greece: Co-Culture of Fish, Bivalves, and Holothurians. *J. Mar. Sci. Eng.* **2022**, *10*, 776. [CrossRef]
62. Shpigel, M.; Shauli, L.; Odintsov, V.; Ben-Ezra, D.; Neori, A.; Guttman, L. The Sea Urchin, *Paracentrotus lividus*, in an Integrated Multi-Trophic Aquaculture (IMTA) System with Fish (*Sparus aurata*) and Seaweed (*Ulva lactuca*): Nitrogen Partitioning and Proportional Configurations. *Aquaculture* **2018**, *490*, 260–269. [CrossRef]
63. Paltzat, D.L.; Pearce, C.M.; Barnes, P.A.; McKinley, R.S. Growth and Production of California Sea Cucumbers (*Parastichopus californicus stimpson*) Co-Cultured with Suspended Pacific Oysters (*Crassostrea gigas* Thunberg). *Aquaculture* **2008**, *275*, 124–137. [CrossRef]
64. Yokoyama, H. Growth and Food Source of the Sea Cucumber *Apostichopus japonicus* Cultured below Fish Cages—Potential for Integrated Multi-Trophic Aquaculture. *Aquaculture* **2013**, *372–375*, 28–38. [CrossRef]
65. Yu, Z.; Zhou, Y.; Yang, H.; Ma, Y.; Hu, C. Survival, Growth, Food Availability and Assimilation Efficiency of the Sea Cucumber *Apostichopus japonicus* Bottom-Cultured under a Fish Farm in Southern China. *Aquaculture* **2014**, *426–427*, 238–248. [CrossRef]
66. Sonnenholzner-Varas, J.I.; Moreira, J.A.; Orrala, M.M.P. Growth Performance and Survival of *Holothuria theeli* (Holothurian) Fed with Feces of *Tripneustes depressus* (Echinoid): A Multi-Trophic Aquaculture Approach. *Aquaculture* **2019**, *512*, 734345. [CrossRef]
67. Grosso, L.; Rakaj, A.; Fianchini, A.; Morroni, L.; Cataudella, S.; Scardi, M. Integrated Multi-Trophic Aquaculture (IMTA) System Combining the Sea Urchin *Paracentrotus lividus*, as Primary Species, and the Sea Cucumber *Holothuria tubulosa* as Extractive Species. *Aquaculture* **2021**, *534*, 736268. [CrossRef]
68. Longo, C.; Cardone, F.; Corriero, G.; Licciano, M.; Pierri, C.; Stabili, L. The Co-Occurrence of the Demosponge *Hymeniacidon perlevis* and the Edible Mussel *Mytilus galloprovincialis* as a New Tool for Bacterial Load Mitigation in Aquaculture. *Environ. Sci. Pollut. Res.* **2016**, *23*, 3736–3746. [CrossRef] [PubMed]
69. Abreu, M.H.; Varela, D.A.; Henríquez, L.; Villarroel, A.; Yarish, C.; Sousa-Pinto, I.; Buschmann, A.H. Traditional vs. Integrated Multi-Trophic Aquaculture of *Gracilaria chilensis* C. J. Bird, J. McLachlan & E. C. Oliveira: Productivity and Physiological Performance. *Aquaculture* **2009**, *293*, 211–220. [CrossRef]
70. Abreu, M.H.; Pereira, R.; Yarish, C.; Buschmann, A.H.; Sousa-Pinto, I. IMTA with *Gracilaria vermiculophylla*: Productivity and Nutrient Removal Performance of the Seaweed in a Land-Based Pilot Scale System. *Aquaculture* **2011**, *312*, 77–87. [CrossRef]
71. Matos, J.; Costa, S.; Rodrigues, A.; Pereira, R.; Pinto, I.S. Experimental Integrated Aquaculture of Fish and Red Seaweeds in Northern Portugal. *Aquaculture* **2006**, *252*, 31–42. [CrossRef]
72. Neori, A.; Shpigel, M.; Ben-Ezra, D. A Sustainable Integrated System for Culture of Fish, Seaweed and Abalone. *Aquaculture* **2000**, *186*, 279–291. [CrossRef]
73. Schuenhoff, A.; Shpigel, M.; Lupatsch, I.; Ashkenazi, A.; Msuya, F.E.; Neori, A. A Semi-Recirculating, Integrated System for the Culture of Fish and Seaweed. *Aquaculture* **2003**, *221*, 167–181. [CrossRef]
74. Giangrande, A.; Pierri, C.; Arduini, D.; Borghese, J.; Licciano, M.; Trani, R.; Corriero, G.; Basile, G.; Cecere, E.; Petrocelli, A.; et al. An Innovative IMTA System: Polychaetes, Sponges and Macroalgae Co-Cultured in a Southern Italian In-Shore Mariculture Plant (Ionian Sea). *J. Mar. Sci. Eng.* **2020**, *8*, 733. [CrossRef]
75. Zhang, J.; Zhang, S.; Kitazawa, D.; Zhou, J.; Park, S.; Gao, S.; Shen, Y. Bio Mitigation Based on Integrated Multi Trophic Aquaculture in Temperate Coastal Waters: Practice, Assessment, and Challenges. *Lat. Am. J. Aquat. Res.* **2019**, *47*, 212–223. [CrossRef]
76. Rosa, J.; Lemos, M.F.L.; Crespo, D.; Nunes, M.; Freitas, A.; Ramos, F.; Pardal, M.Â.; Leston, S. Integrated Multitrophic Aquaculture Systems—Potential Risks for Food Safety. *Trends Food Sci. Technol.* **2020**, *96*, 79–90. [CrossRef]
77. Sasikumar, G.; Viji, C.S. *Integrated Multitrophic Aquaculture Systems (IMTA)*; Winter School on Technological Advances in Mariculture for Production Enhancement and Sustainability; ICAR: Kochi, India, 2015; pp. 47–55.

78. Petersen, J.K.; Holmer, M.; Termansen, M.; Hasle, B. *Goods and Services of Marine Bivalves*; Smaal, A.C., Ferreira, J.G., Grant, J., Petersen, J.K., Strand, Ø., Eds.; Springer Open: Cham, Switzerland, 2019; Chapter 10; pp. 179–208.
79. Bischoff, A.A.; Fink, P.; Waller, U. The Fatty Acid Composition of Nereis Diversicolor Cultured in an Integrated Recirculated System: Possible Implications for Aquaculture. *Aquaculture* **2009**, *296*, 271–276. [CrossRef]
80. Marques, B.; Lillebø, A.; Ricardo, F.; Nunes, C.; Coimbra, M.; Calado, R. Adding Value to Ragworms (*Hediste diversicolor*) through the Bioremediation of a Super-Intensive Marine Fish Farm. *Aquac. Environ. Interact.* **2018**, *10*, 79–88. [CrossRef]
81. Lander, T.; Barrington, K.; Robinson, S.; MacDonald, B.; Martin, J. Dynamics of the Blue Mussel as an Extractive Organism in an Integrated Multi-Trophic Aquaculture System. *Bull. Aquac. Assoc. Can.* **2004**, *104*, 19–28.
82. Gvozdenović, S.; Ikica, Z.; Pešić, A.; Nikolić, M.; Pešić, V.; Mandić, M. Comparison between IMTA and Monoculture Farming of Mussels (*Mytilus galloprovincialis* L.) in the Boka Kotorska Bay. *Acta Adriat.* **2017**, *58*, 271–284. [CrossRef]
83. Sarà, G.; Zenone, A.; Tomasello, A. Growth of Mytilus Galloprovincialis (Mollusca, Bivalvia) Close to Fish Farms: A Case of Integrated Multi-Trophic Aquaculture within the Tyrrhenian Sea. *Hydrobiologia* **2009**, *636*, 129–136. [CrossRef]
84. Kerrigan, D.; Suckling, C.C. A Meta-analysis of Integrated Multitrophic Aquaculture: Extractive Species Growth Is Most Successful within Close Proximity to Open-water Fish Farms. *Rev. Aquac.* **2016**, *10*, 560–572. [CrossRef]
85. Zamora, L.N.; Jeffs, A.G. Feeding, Selection, Digestion and Absorption of the Organic Matter from Mussel Waste by Juveniles of the Deposit-Feeding Sea Cucumber, *Australostichopus mollis*. *Aquaculture* **2011**, *317*, 223–228. [CrossRef]
86. Zamora, L.N.; Yuan, X.; Carton, A.G.; Slater, M.J. Role of Deposit-feeding Sea Cucumbers in Integrated Multitrophic Aquaculture: Progress, Problems, Potential and Future Challenges. *Rev. Aquac.* **2016**, *10*, 57–74. [CrossRef]
87. De Goeij, J.M.; Lesser, M.P.; Pawlik, J.R. Nutrient Fluxes and Ecological Functions of Coral Reef Sponges in a Changing Ocean. In *Climate Change, Ocean Acidification and Sponges*; Carballo, J.L., Bell, J.J., Eds.; Springer International: Cham, Switzerland, 2017; pp. 373–410.
88. Wang, X.; Andresen, K.; Handå, A.; Jensen, B.; Reitan, K.; Olsen, Y. Chemical Composition and Release Rate of Waste Discharge from an Atlantic Salmon Farm with an Evaluation of IMTA Feasibility. *Aquac. Environ. Int.* **2013**, *4*, 147–162. [CrossRef]
89. Khailov, K.M.; Burlakova, Z.P. Release of dissolved organic matter by marine seaweeds and distribution of their total organic production to inshore communities. *Limnol. Oceanogr.* **1969**, *14*, 521–527. [CrossRef]
90. Zhang, X.; Zhang, W.; Xue, L.; Zhang, B.; Jin, M.; Fu, W. Bioremediation of Bacteria Pollution Using the Marine Sponge *Hymeniacidon perlevis* in the Intensive Mariculture Water System of Turbot Scophthalmus Maximus. *Biotechnol. Bioeng.* **2010**, *105*, 59–68. [CrossRef] [PubMed]
91. De Goeij, J.M.; Van Oevelen, D.; Vermeij, M.J.A.; Osinga, R.; Middelburg, J.J.; De Goeij, A.F.P.M.; Admiraal, W. Surviving in a Marine Desert: The Sponge Loop Retains Resources Within Coral Reefs. *Science* **2013**, *342*, 108–110. [CrossRef] [PubMed]
92. Maxwell, K.H.; Gardner, J.P.A.; Heath, P.L. The Effect of Diet on the Energy Budget of the Brown Sea Cucumber, *Stichopus mollis* (Hutton). *J. World Aquac. Soc.* **2009**, *40*, 157–170. [CrossRef]
93. Bolton, J.J.; Robertson-Andersson, D.V.; Shuuluka, D.; Kandjengo, L. Growing Ulva (Chlorophyta) in Integrated Systems as a Commercial Crop for Abalone Feed in South Africa: A SWOT Analysis. *J. Appl. Phycol.* **2009**, *21*, 575–583. [CrossRef]
94. Hodar, A.R.; Vasava, R.J.; Mahavadiya, D.R.; Joshi, N.H. Fish Meal and Fish Oil Replacement for Aqua Feed Formulation by Using Alternative Sources: A Review. *J. Exp. Zool. India* **2020**, *23*, 13–21.
95. Grigorakis, K.; Rigos, G. Aquaculture Effects on Environmental and Public Welfare—The Case of Mediterranean Mariculture. *Chemosphere* **2011**, *85*, 899–919. [CrossRef]
96. FAO. *FAO Report: Global Fisheries and Aquaculture Production Reaches a New Record High*; The State of World Fisheries and Aquaculture (SOFIA): Rome, Italy, 2024.
97. Araújo, M.; Rema, P.; Sousa-Pinto, I.; Cunha, L.M.; Peixoto, M.J.; Pires, M.A.; Seixas, F.; Brotas, V.; Beltrán, C.; Valente, L.M.P. Dietary Inclusion of IMTA-Cultivated *Gracilaria vermiculophylla* in Rainbow Trout (*Oncorhynchus mykiss*) Diets: Effects on Growth, Intestinal Morphology, Tissue Pigmentation, and Immunological Response. *J. Appl. Phycol.* **2016**, *28*, 679–689. [CrossRef]
98. Valente, L.M.P.; Araújo, M.; Batista, S.; Peixoto, M.J.; Sousa-Pinto, I.; Brotas, V.; Cunha, L.M.; Rema, P. Carotenoid Deposition, Flesh Quality and Immunological Response of Nile Tilapia Fed Increasing Levels of IMTA-Cultivated *Ulva* spp. *J. Appl. Phycol.* **2016**, *28*, 691–701. [CrossRef]
99. Laramore, S.; Baptiste, R.; Wills, P.S.; Hanisak, M.D. Utilization of IMTA-Produced *Ulva lactuca* to Supplement or Partially Replace Pelleted Diets in Shrimp (*Litopenaeus vannamei*) Reared in a Clear Water Production System. *J. Appl. Phycol.* **2018**, *30*, 3603–3610. [CrossRef]
100. Machado, M.; Machado, S.; Pimentel, F.B.; Freitas, V.; Alves, R.C.; Oliveira, M.B.P.P. Amino Acid Profile and Protein Quality Assessment of Macroalgae Produced in an Integrated Multi-Trophic Aquaculture System. *Foods* **2020**, *9*, 1382. [CrossRef] [PubMed]
101. Stabili, L.; Schirosi, R.; Licciano, M.; Mola, E.; Giangrande, A. Bioremediation of Bacteria in Aquaculture Waste Using the Polychaete *Sabella spallanzanii*. *New Biotechnol.* **2010**, *27*, 774–781. [CrossRef] [PubMed]
102. Giangrande, A.; Cavallo, A.; Licciano, M.; Mola, E.; Pierri, C.; Trianni, L. Utilization of the Filter Feeder Polychaete *Sabella spallanzanii* Gmelin (Sabellidae) as Bioremediator in Aquaculture. *Aquac. Int.* **2005**, *13*, 129–136. [CrossRef]
103. Stabili, L.; Cecere, E.; Licciano, M.; Petrocelli, A.; Sicuro, B.; Giangrande, A. Integrated Multitrophic Aquaculture By-Products with Added Value: The Polychaete *Sabella spallanzanii* and the Seaweed *Chaetomorpha linum* as Potential Dietary Ingredients. *Mar. Drugs* **2019**, *17*, 677. [CrossRef] [PubMed]

104. Sachs, J.D.; Agarwal, U.; Espinosa, G.; Mardirossian, N.; Marrero, A.; O'Dwyer, E.; Plekenpol, R.; Rincón, R.; Marcela, D.; Sachs, L.; et al. Fixing the Business of Food: Aligning Food Company Practices with the SDGs. *SSRN Electron. J.* **2021**. [CrossRef]
105. Silva, D.M.; Valente, L.M.P.; Sousa-Pinto, I.; Pereira, R.; Pires, M.A.; Seixas, F.; Rema, P. Evaluation of IMTA-Produced Seaweeds (*Gracilaria*, *Porphyra*, and *Ulva*) as Dietary Ingredients in Nile Tilapia, *Oreochromis niloticus* L., Juveniles. Effects on Growth Performance and Gut Histology. *J. Appl. Phycol.* **2015**, *27*, 1671–1680. [CrossRef]
106. Legarda, E.C.; Viana, M.T.; Del Rio Zaragoza, O.B.; Skrzynska, A.K.; Braga, A.; De Lorenzo, M.A.; Vieira, F.D.N. Effects on Fatty Acids Profile of *Seriola dorsalis* Muscle Tissue Fed Diets Supplemented with Different Levels of *Ulva fasciata* from an Integration Multi-Trophic Aquaculture System. *Aquaculture* **2021**, *535*, 736414. [CrossRef]
107. Shpigel, M.; Guttman, L.; Shauli, L.; Odintsov, V.; Ben-Ezra, D.; Harpaz, S. *Ulva lactuca* from an Integrated Multi-Trophic Aquaculture (IMTA) Biofilter System as a Protein Supplement in Gilthead Seabream (*Sparus aurata*) Diet. *Aquaculture* **2017**, *481*, 112–118. [CrossRef]
108. Conte, F.S. Stress and welfare of cultured fish. *Appl. Anim. Behav. Sci.* **2004**, *86*, 205–223. [CrossRef]
109. Daskalova, A. Farmed fish welfare: Stress, post-mortem muscle metabolism, and stress-related meat quality changes. *Int. Aquat. Res.* **2019**, *11*, 113–124. [CrossRef]
110. De Magalhães, C.S.F.R.; Cerqueira, M.A.C.; Schrama, D.; Moreira, M.J.V.; Boonanuntanasarn, S.; Rodrigues, P.M.L. A Proteomics and Other Omics Approach in the Context of Farmed Fish Welfare and Biomarker Discovery. *Rev. Aquac.* **2018**, *12*, 122–144. [CrossRef]
111. CEC. *COM 511—Communication from the Commission to the Council and the European Parliament: A Strategy for the Sustainable Development of European Aquaculture*; Commission of the European Communities (CEC): Brussels, Belgium, 2002; Available online: https://eur-lex.europa.eu/LexUriServ/LexUriServ.do?uri=COM:2002:0511:FIN:EN:PDF (accessed on 11 September 2024).
112. Huo, Y.; Stuart, K.; Rotman, F.; Ernst, D.; Drawbridge, M. The culture of fish, mussels, sea cucumbers and macroalgae in a modular integrated multi-tropic recirculating aquaculture system (IMTRAS): Performance and waste removal efficiencies. *Aquaculture* **2024**, *585*, 740720. [CrossRef]
113. O'Donncha, F.; Grant, J. Precision Aquaculture. *IEEE Internet Things Mag.* **2019**, *2*, 26–30. [CrossRef]
114. European Union. Nature Restoration Law. 17 June 2024. Available online: https://environment.ec.europa.eu/topics/nature-and-biodiversity/nature-restoration-law_en (accessed on 30 September 2024).

Disclaimer/Publisher's Note: The statements, opinions and data contained in all publications are solely those of the individual author(s) and contributor(s) and not of MDPI and/or the editor(s). MDPI and/or the editor(s) disclaim responsibility for any injury to people or property resulting from any ideas, methods, instructions or products referred to in the content.

biology

MDPI

Article

Large and Small Yellow Croakers Feeding and Living Together Make Large Yellow Croaker Population Recovery Difficult: A Guild Perspective

Pengyu Cai [1], Zhenhua Wang [1,2,*], Shouyu Zhang [1,2,*] and Jintao Yu [1]

[1] College of Oceanography and Ecological Science, Shanghai Ocean University, Shanghai 201306, China; bruinboar@gmail.com (P.C.); yujintao185061039@163.com (J.Y.)
[2] Engineering Technology Research Center of Marine Ranching, Shanghai Ocean University, Shanghai 201306, China
* Correspondence: zh_wang@shou.edu.cn (Z.W.); syzhang@shou.edu.cn (S.Z.)

Simple Summary: Due to unrestrained and excessive fishing, the migratory fishing season and spawning groups of the large yellow croaker (*Larimichthys crocea*) in the East China Sea have been hard to detect since the 1980s. Since the 1990s, the Chinese government has initiated large-scale stock enhancement programs to restore the endangered wild large yellow croaker population. However, after several decades, the stock enhancement has not achieved its desired effects. The reasons for this remain poorly understood. Our results provide evidence that in the early-growth stage of the large yellow croaker, when its body length and body mass are similar to those of the small yellow croaker (*Larimichthys polyactis*), it may have a life history strategy of cohabitation and forming a guild with the small yellow croaker. Since the fishery resources of the small yellow croaker are far higher than those of the large yellow croaker, fishing targeting the small yellow croaker will indirectly lead to the large-scale capture of the cohabitate large yellow croaker, dealing a heavy blow to the slightly recovering fishery resources of the large yellow croaker. Therefore, optimizations and adjustments are necessary in order for the fishing ban policy and stock enhancement strategy to effectively restore the resources of the large yellow croaker.

Abstract: In recent decades, China's large-scale stock enhancement programs to restore the collapsing large yellow croaker (*Larimichthys crocea*) fishery resources have not yielded the desired results, and a comprehensive analysis of the underlying reasons for this problem is required. Based on small yellow croaker (*Larimichthys polyactis*) catch survey data obtained from 15 fishing ports along the coast of the East China Sea, we examined the proportion of large yellow croakers mixed in the small yellow croaker catch and their biological parameters. In addition, we analyzed the differences in the intestinal microbiota and feeding ecology between these two species to explore the reason why the stock enhancement program failed to achieve the desired outcome. The results show that there is a high likelihood of the two species appearing in each other's ecological niches, and there is a significant overlap in their dietary ecology. They may cohabitate and form a guild. The fishing season targeting the small yellow croaker indirectly catches the large yellow croaker population, which puts huge fishing pressure on large yellow croaker resource and shows obvious overfishing. Therefore, it is necessary to optimize and adjust the fishing ban policy and stock enhancement strategies, appropriately reducing the fishing intensity after the fishing ban to facilitate the effective accumulation of resource replenishment effects during the fishing ban period, thus effectively restoring wild large yellow croaker resources.

Keywords: *Larimichthys crocea*; *Larimichthys polyactis*; guild; stock enhancement; overfishing; ecological niche overlap; cohabitation

1. Introduction

The excessive exploitation of marine resources combined with the intensive discharge of wastewater significantly impairs the capacity of the primary elements in the aquatic ecosystem to be transformed and utilized by higher trophic-level organisms [1,2]. Due to the scarcity of adequate predators, significant energy accumulates in small or juvenile organisms, thereby resulting in a higher local abundance of prey organisms [3]. In this context, some already highly differentiated biological populations will inevitably exhibit cohabitation due to insufficient competitive conditions, which ultimately leads to abundant guilds in the early stages or specific phases of their life history [4,5].

In ecology, a guild is a collective of species that utilize similar types of resources in analogous ways. These groups frequently consist of closely related species with a shared ancestor; thus, they exploit resources in comparable ways due to their common lineage. Consequently, various species within a particular genus may form a guild within a community [6,7]. One advantage of guild studies is the simplification of community analysis by providing an operational unit that bridges the gap between individual species and the entire community. This aids the streamlining of data collection under constraints on funding or personnel [6] and allows for the inference of dynamic changes in other guild members based on monitoring a single member within the guild and tracking fluctuations in its abundance [8]. Therefore, research into guilds can contribute to conservation efforts for severely threatened biological populations. The concept of a guild was originally proposed for analyzing avian communities but has since been further applied to studies of fish communities [9,10]. Previous studies of guilds primarily focused on habitat utilization [11,12], guild structure [13,14], and co-occurrence guild food web dynamics [15,16]. However, comprehensive systematic studies of the impacts of economic marine fish guilds on resource utilization and conservation are still relatively scarce.

The large yellow croaker (*Larimichthys crocea* (Richardson, 1846)) and the small yellow croaker (*Larimichthys polyactis* (Bleeker, 1877)) both belong to the family Sciaenidae. They are important economic demersal species in the East China Sea. During the overwintering grounds, large yellow croakers and small yellow croakers inhabit different water layers in the offshore regions, but as they migrate towards the coastal areas, they share the same feeding and spawning grounds, leading to habitat overlap [17,18]. The appearance and coloration during the early-life stages, not yet having reached initial sexual maturity, are similar for the large yellow croaker and small yellow croaker, so it is difficult for fishermen to distinguish them based on naked-eye observations [19]. Previous regional fisheries resource surveys in the fishing boats moored at the same fishing port by our team observed that fishermen often mistakenly identified young large yellow croakers as small yellow croakers or labeled them as "small-scaled small yellow croaker" for sale [20]. Consequently, significant proportions of large yellow croaker were mixed with the small yellow croaker catch on the market. A limited number of previous studies also reported similar findings, albeit without thoroughly elucidating the underlying scientific issues [21]. The large yellow croaker is one of the four traditional major economic marine fish species in China, alongside the *Larimichthys polyactis*, *Trichiurus japonicus*, and *Sepiella japonica*. It has a pivotal position in the marine fish fauna structure of China and has become intertwined with the folk culture of the coastal areas of the East China Sea. After the 1950s, the fishing pressure on wild large yellow croakers steadily increased. Following a peak of around 200,000 tons in the mid-1970s, the catch plummeted by over 90% within a mere 20 years. Subsequently, wild large yellow croaker resources declined sharply, leading to its classification as critically endangered (CR) by the International Union for Conservation of Nature (IUCN 2016 ver. 3.1) [22]. Since a breakthrough in the breeding technology for large yellow croakers in the 1980s, the provinces of Fujian, Zhejiang, and Jiangsu initiated stock enhancement with juvenile breeding large yellow croakers in coastal waters to supplement the natural population and improve the aquatic ecosystem [21]. Subsequently, the scale and frequency of stock enhancement for large yellow croakers gradually increased in the hope of restoring wild large yellow croaker resources. According to the data, from 1987 to 2018, Fujian

Province released a total of 115 million large yellow croakers [23]. During the 5 years from 2017 to 2021, Zhejiang Province released a total of 303,198,000 large yellow croakers, with an average release size of 6.5 cm and a total investment of 64.049 million yuan [24]. Overall, the enhancement of the large yellow croaker stocks in China is now conducted on a massive scale, and the stock enhancement activities are mainly conducted during the fishing ban period with the aim of achieving better outcomes.

Despite the massive scale and frequency of release, only a limited number of studies have indicated that supplementation of the natural large yellow croaker population by stock enhancement has been effective [25]. However, the reported catch of wild large yellow croakers in the main release regions in China (Zhejiang, Fujian, and Jiangsu) has not to show significant growth [26]. The important spawning grounds in the East China Sea still fail to generate a fishing season, and there are no clear signs of recovery in the wild large yellow croaker fishery resources [23]. Some studies even suggest that China's large yellow croaker stock enhancement programs over the past few decades have not to be successful [22]. However, these studies only provided limited insights into the role of stock enhancement in the recovery of wild resources of the large yellow croakers, and they failed to elucidate the reasons behind the prolonged lack of recovery in large yellow croaker fishery resources and fishing seasons. We speculate that against the backdrop of large-scale stock enhancement, large yellow croakers in the early-life stages may have a profound cohabitation with small yellow croaker populations and form a typical guild. The small yellow croaker is one of China's traditional four major economic marine fish species, and production is relatively high in China. Furthermore, based on the China Fishery Statistical Yearbook, the data indicate that the output of the small yellow croaker along the coast of the East China Sea in 2022 was 268,730 tons, while that of the large yellow croaker was merely 37,098 tons, with the former being seven times that of the latter. If a large-scale cohabitation phenomenon exists between the large yellow croaker and the small yellow croaker, it is likely that the reasonable fishing of the small yellow croaker may, unintentionally, deal a heavy blow to the fishery resources of the large yellow croaker. Therefore, understanding the mechanisms and intensity of this cohabitation between the two species is of great importance for the conservation of the large yellow croaker. Moreover, in the future, taking the guild as the unit will enable more scientific and rational promotion of the assessment and protection of the fishery resources of the large yellow croaker, as well as the management of its stock enhancement. Therefore, in this study, we conducted a field investigation based on the catches of fishing boats at fishing ports in three provinces of China's nearshore waters to obtain insights into the actual scale of fishing for large yellow croakers to infer the reasons for the lack of success in stock enhancement efforts in China over the years. We also compared the intestinal microbial structures and feeding ecology of the large yellow croaker and the small yellow croaker and aimed to verify whether the large yellow croaker and the small yellow croaker are in cohabitation and whether they form a guild. By better understanding the resource structure during the transition from young to adults of the large yellow croaker, the results obtained in this study can inform the management of large yellow croaker fishery resources and subsequent stock enhancement efforts.

2. Materials and Methods

2.1. Sample Collection and Morphological Identification Methods

During our team's past investigations of fishery resources in local sea areas off the coast of Zhejiang and the catches of fishing boats at Luchao Port in Shanghai, it was observed that from 2018 to 2022, during the autumn months following the fishing ban period from May to September, large and small yellow croakers smaller than 20 cm were frequently captured together, while a similar phenomenon rarely occurred in the following spring [20]. To verify whether this phenomenon exists universally in the East China Sea and to eliminate the intense interference of fishing activities and obtain the catch information that best represents the actual situation, this study was carried out during the first large-scale trading cycle after the closed fishing period in the autumn of 2023. The sampling period was from

late September to early October. Considering the distribution characteristics of coastal fishing port cities and the four major sea areas from south to north in China, a total of 15 sampling sites were designated across three provinces (Figure 1). At each station, the catches of yellow croakers from three different fishing boats were randomly collected and identified. To ensure the reliability of sample sources, information on the fishing area should be obtained from fishermen before the identification of the catch to make sure the samples are from the local sea area and inquire about the approximate fishing area range. Then, morphological identification is carried out on the fish catch to distinguish large yellow croakers and small yellow croakers, and the number and proportion of the two different catches at different stations are recorded. In this study, a total of 8330 yellow croaker samples were classified and identified. For each sampling site, the total length (TL) and body mass of both the large yellow croaker and the small yellow croaker were measured on the spot, with a total of 883 individual measurements taken for each species. Body length was measured using a standard ruler (to the nearest 1 mm), and body mass was measured using an electronic balance (to the nearest 0.01 g). Additionally, 30 large yellow croakers were randomly sampled from the catch of every sampling site, and when the number of the large yellow croakers caught was less than 30, all were sampled, along with an equal number of the small yellow croakers. A total of 402 samples of both the large yellow croaker and the small yellow croaker were collected, respectively. All samples were transported back to the laboratory under low-temperature preservation conditions for subsequent experiments. The catches were primarily obtained from trawl nets and gill nets. We obtained the fishing boat number and obtained the AIS data through the Hifleet website (https://www.hifleet.com (accessed on 27 December 2023)) to receive its fishing trajectory and draw the contour of the working area of different boats.

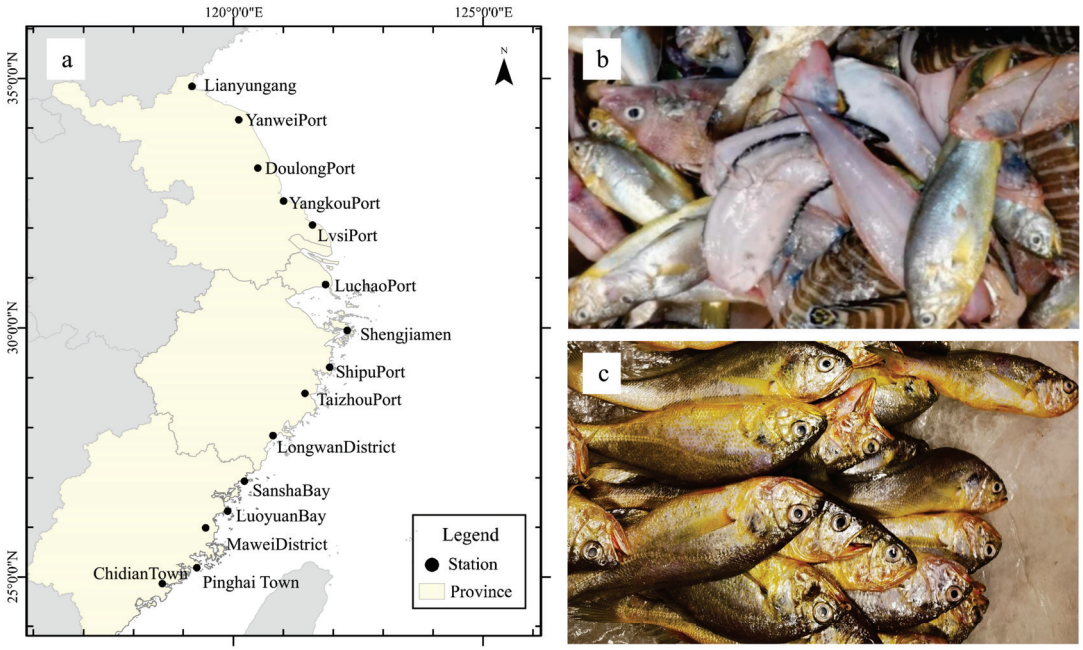


Figure 1. (**a**) Distribution map of coastal survey sampling sites. (**b**) One of the catches from the trawler boat. (**c**) Fishermen will mix the large yellow croaker and the small yellow croaker for sale after preliminarily sorting their catch.

The differentiation between large yellow croakers and small yellow croakers primarily relies on morphological identification methods. Small yellow croakers exhibit 5–6 rows of sparse scales from the dorsal fin origin to the lateral line, whereas large yellow croakers display 8–9 rows of densely packed scales (Figure 2b). In terms of lateral line characteristics, small yellow croakers have a thick midline pattern with a gentle mid-body concavity, while large yellow croakers feature a fine midline pattern with a sudden mid-body concavity

(Figure 2a). The collected samples were further species-confirmed in the laboratory through the examination of the swim bladder lateral branches. In small yellow croakers, the two small branches at the margin of the branch of the swim bladder lateral branch are of unequal length, whereas in large yellow croakers, these two small branches are of equal length (Figure 2c).



Figure 2. The morphological distinctions between large and small yellow croakers [19], (**a**,**b**) depict the varying quantities of scales in two fish species, while (**c**) illustrates the differences in the swim bladder lateral branchs of the two fish species.

2.2. Stable Isotope Analysis Methodology

Following the conclusion of biological indicator measurements, a total of 40 specimens of large and small yellow croakers, 10 from each, were selected randomly from the regions of Zhoushan and Taizhou. The fish were meticulously cleansed of impurities using ultrapure water. Subsequently, rectangular muscle tissue measuring 2 cm^2 from below the dorsal fin was carefully excised and subjected to a 24 h drying process in the freeze dryer (Alpha 1-2LDplus, Martin Christ, Osterode, Germany) before being ground into powder for further analysis. A sample weighing 1.5 mg was meticulously encapsulated in tin foil and subjected to analysis for carbon and nitrogen stable isotope ratios using the DELTA V Advantage Isotope Ratio Mass Spectrometer in conjunction with Thermo Fisher Scientific's EA-HT Elemental Analyzer (Waltham, MA, USA). The stable carbon and nitrogen isotope values were determined relative to the internationally recognized standards: Pee Dee Belemnite (PDB) for carbon and atmospheric nitrogen for nitrogen. The results are expressed in the form of a carbon stable isotope ratio ($\delta\ ^{13}C$) and a nitrogen stable isotope ratio ($\delta\ ^{15}N$). The calculations for $\delta\ ^{13}C$ and $\delta\ ^{15}N$ were performed using the following formula:

$$\delta\ X = [R_{sa}/R_{st} - 1] \times 1000.$$

In the formula provided: X represents either ^{13}C or ^{15}N; and R denotes the ratio of $^{13}C/^{12}C$ or $^{15}N/^{14}N$ between the sample under analysis (R_{sa}) and the standard reference (R_{st}). The analytical precision achieved is 0.1‰ for $\delta\ ^{13}C$ and 0.06‰ for $\delta\ ^{15}N$.

Under the assumptions of normal distribution and homogeneity of variance in the data, a one-way analysis of variance (ANOVA) was conducted to test for significant differences

in $\delta\ ^{13}C$ and $\delta\ ^{15}N$ values between the two fish species at a significance level of $\alpha = 0.05$. Nutritional levels were calculated based on the formula as described by Vander [27].

$$TL = \left[\left(\delta^{15}N_c - \delta^{15}N_b\right)/TEF + \lambda\right]$$

In the formula provided: TL represents the trophic level estimated for the organism; $\delta\ ^{15}N_c$ denotes the $\delta\ ^{15}N$ ratio of the consumer; while $\delta\ ^{15}N_b$ represents the $\delta\ ^{15}N$ ratio of the baseline organism. For this study, the baseline organism selected was the thick-shelled mussel (with a $\delta\ ^{15}N$ ratio of 3.9‰), a year-round presence in the Zhoushan Sea area with a simple diet. *TEF* stands for the trophic enrichment factor for a nutritional level, set at 3.4‰ in this context. λ represents the trophic level of the chosen reference organism, which is 2 in this case.

2.3. High-Throughput Sequencing of Genetic Material in Gastric Contents

Ten large yellow croakers collected randomly from the Zhoushan Sea area were dissected using ethanol-disinfected dissecting scissors. The stomach pouches were opened along the gastric wall, and all gastric contents were scraped off. Gastric contents of the same species were grouped, crushed, and quantified. Subsequently, DNA extraction was performed using the QIAamp Power Fecal Pro DNA Extraction Kit (Tianlin Biotechnology Co., Ltd., Shanghai, China)) according to the manufacturer's instructions. The obtained DNA was subjected to 1% agarose gel electrophoresis for detection, quantified, and then stored. Universal primers mlCOIintF (5′-GGWACWGGWTGAACWGTWTAYCCYCC-3′) and jgHCO2198 (5′-TAIACYTCIGGRTGICCRAARAAYCA-3′) were utilized for amplification [28]. The mitochondrial cytochrome c oxidase subunit I (COI) gene was amplified via PCR, yielding a gene fragment of approximately 313 bp in length. The PCR reaction mixture, totaling 25 uL, consisted of 12.5 uL Taq PCR Master Mix, 9.5 uL ddH2O, 1 uL each of forward and reverse primers, and 1 uL of DNA template. The reaction program was set as follows: initial denaturation at 94 °C for 4 min, denaturation at 94 °C for 30 s, annealing at 55 °C for 30 s, extension at 72 °C for 45 s, followed by a final extension at 72 °C for 10 min, with a total of 30 cycles. After amplification, the products were subjected to 2% agarose gel electrophoresis for verification and then underwent paired-end sequencing on the Illumina Miseq platform (Shanghai Paisenno Biotechnology Co., Ltd., Shanghai, China).

In Excel (Microsoft Excel 2023), the relative abundance of OTUs at the phylum level was statistically analyzed. Simultaneously, the OTU species with the highest relative abundance were selected for Blast alignment to explore information on closely related species. Following the removal of sequences related to large and small yellow croaker, OTU sequences with a minimum of 90% sequence similarity were identified based on the analysis of their gastric contents and the aquatic biota catalog of the East China Sea. Subsequently, using MEGA11 (Tamura, Stecher, and Kumar 2021), the neighbor-joining algorithm and maximum likelihood estimation were employed to construct a phylogenetic tree of the bait organisms, with a bootstrap value set to 1000 iterations. Additionally, based on the relative abundance of OTUs from the bait organisms, a heatmap analysis was conducted in Excel to investigate feeding differences between the two fish species.

2.4. Sample Grouping and Extraction of Intestinal DNA for High-Throughput Sequencing Analysis

Sixteen yellow croakers were randomly selected, including four large yellow croakers (LZS) and four small yellow croakers (SZS) from Zhoushan, as well as four large yellow croakers (LTZ) and four small yellow croakers (STZ) from Taizhou. The large and small yellow croakers were delicately wiped with 75% alcohol and underwent aseptic dissection to extract the digestive tract, and the contents of the rectums from each fish were meticulously collected, blended, and preserved by flash freezing them in liquid nitrogen. The extraction of intestinal microbial DNA was conducted using the E.Z.N.A™ Mag-Bind Soil DNA Kit

(Guangzhou, China), following a detailed procedure as outlined in the product manual. Post extraction, the DNA underwent assessment for concentration and purity before being subjected to PCR amplification targeting the V3-V4 hypervariable region of the 16S rDNA sequence. The primers used for amplification were 338F (5′-ACTCCTACGGGAGGCAGCA-3′) and 806R (5′-GGACTACHVGGGTWTCTAAT-3′). Upon successful validation of the amplification products through agarose gel electrophoresis, a library was constructed, and high-throughput sequencing was carried out on the Illumina MiSeq PE300 platform. The specific operational steps followed the methodology outlined by Zhang [29].

The paired-end reads obtained from intestinal microbiota sequencing were concatenated, filtered, and dechimerized to generate the final clean data in fastq format. The Qiime 1.9.1 standardized pipeline was employed, utilizing the open reference algorithm to cluster OUTs at 97% similarity, followed by alignment with the GreenGene database to create a Biom dataset containing sample names, taxonomic annotations, and abundance information. Alpha diversity indices (OTU, Chao1, PD whole tree, Shannon, and Simpson indices) of the samples were analyzed using Mothur 1.30 software, while Beta diversity (Bray Curtis PCoA and Weighted Unifrac PCoA) analysis was conducted using QIIME software (version 1.8.0). The species abundance of the samples was then examined at the phylum and genus levels to analyze the composition of the microbial community.

3. Results

3.1. Proportions of Large Yellow Croaker Catches to Small Yellow Croaker Catches at Different Sampling Sites

The proportions of the large yellow croakers were determined at different sampling sites (Table 1), and the results showed that the proportion of the large yellow croakers at the 15 sampling sites ranged from 5.45% to 34.08%, with the lowest proportion at Yanwei Port (5.45%) and the highest at Taizhou Port (34.08%). The proportion of the large yellow croaker in the small yellow croaker samples was highest in Zhejiang (25.91 ± 7.53%), followed by Fujian (24.69 ± 8.78%), and lowest in Jiangsu (15.77 ± 9.15%). The average proportion of the large yellow croaker in the small yellow croaker catch in China's nearshore waters was 21.44 ± 9.35%.

Table 1. Proportions of large and small yellow croakers caught in different sites in the East China Sea.

Province and City	Sampling Site	*N.* of Samples	*N.* of *L. crocea*	*N.* of *L. polyactis*	Proportion of *L. crocea* (%)	Proportion of *L. crocea* in Different Province (%)	Total Percentage
Jiangsu	Lvsiport	326	37	299	11.35%	15.77 ± 9.15%	21.44 ± 9.35%
	Yangkou port	232	59	173	25.43%		
	Doulong port	550	128	422	23.27%		
	Yanwei port	220	12	208	5.45%		
	Lianyungang	356	22	334	6.18%		
Shanghai	Luchao port	340	78	262	22.94%		
	Longwan	696	199	497	28.59%		
Zhejiang	Taizhou port	986	336	650	34.08%	25.91 ± 7.53%	
	Shipu port	1408	349	1059	24.79%		
	Shengjiameng	1460	236	1224	16.16%		
Fujian	Chidian town	240	65	175	27.08%	24.69 ± 8.78%	
	Pinhai town	50	8	42	16.00%		
	Mawei district	862	128	734	14.85%		
	Luoyuan bay	164	53	111	32.32%		
	Sansha bay	440	146	294	33.18%		

The different fishing areas and historical large yellow croaker migration routes are shown in Figure 3a. The main catches of the large yellow croaker fisheries come from Lvsi Fishing Ground, Zhoushan Fishing Ground, Changjiangkou Fishing Ground, Zhouwai Fishing Ground, and Minzhong and Mindong Fishing Ground. As shown in Figure 3b, the current large yellow croaker fishing area overlaps with part of the historical spawning ground, nursing ground, overwintering ground, and migration route of the large yellow croaker in the East China Sea.

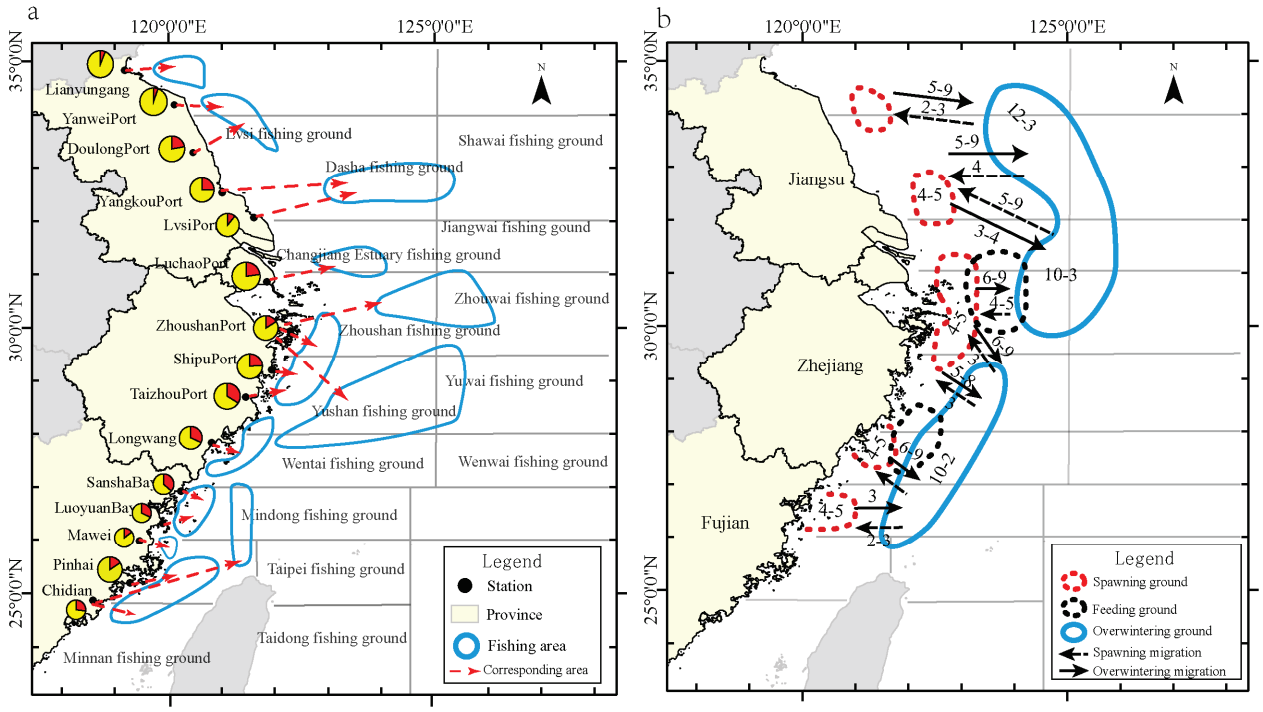


Figure 3. Proportions of large and small yellow croakers in fish catches at different survey stations and fishing areas: red color represents the large yellow croaker; yellow color represents the small yellow croaker (**a**). Historical spawning ground, nursing ground, overwintering ground, and migration route for the large yellow croaker. The numbers on (**b**) indicate the months when large yellow croakers migrate [30].

3.2. Body Length and Body Mass Composition of the Large Yellow Croaker

The body length range in the large yellow croaker samples obtained from the coastal survey was 99 to 187 mm, with an average body length of 141.73 ± 14.61 mm, and the dominant body length group was 125 to 160 mm, accounting for 87.6% of the total. The average body length of the large yellow croaker collected in Jiangsu was the largest, followed by Fujian and Zhejiang. The body mass ranged from 12.7 to 135.08 g, with an average body mass of 49.45 ± 17.77 g, and the dominant body mass group was 30 to 75 g, accounting for 82.2% of the total (Table 2) (Figure 4). It can be determined from Table 2 that there is no significant difference in body length and body mass between the large yellow croaker and the small yellow croaker as collected in this study ($p > 0.05$). Accordingly, we can infer that in the early-life stage of the large yellow croaker, when its body length and body mass are similar to those of the small yellow croaker, it may be more likely to have a life history strategy of cohabiting with small yellow croaker.

3.3. Sex Ratio and Gonadal Maturity of the Large Yellow Croaker

As shown in Figure 5, the gonadal maturity of the large yellow croaker caught in China's nearshore waters was mainly at stage II, accounting for 63.43%, with 20.39% at stage III, 1.4% at stage IV, 0.4% in the spawning state (stage V), and 0% at stage VI. Thus, gonad development was premature in some large yellow croakers, which was related to the ecological adaptation of the large yellow croaker under the background of transition fishing.

Table 2. Regional variations in body length and body mass composition for the large yellow croaker in the East China Sea.

Province	Specie	Body Length/mm			Body Mass/g		
		Range	Dominant Group	Mean ± SD	Range	Dominant Group	Mean ± SD
Jiangsu	*L. crocea*	118–187	130–160	143.17 ± 14.04	12.7–116.2	30–60	46.65 ± 15.33
	L. polyactis	125–176	120–150	140.91 ± 10.17	33.54–89.22	30–60	47.73 ± 10.46
Zhejiang	*L. crocea*	104–166	130–160	140.5 ± 13.451	16.78–75.3	30–60	41.17 ± 11.82
	L. polyactis	98–160	100–130	136.31 ± 14.24	15.32–55.82	20–50	37.44 ± 10.69
Fujian	*L. crocea*	99–183	130–160	141.79 ± 16.57	22.06–135.08	40–80	61.91 ± 18.89
	L. polyactis	111–169	140–170	138.14 ± 16.93	24.58–80.1	20–70	54.76 ± 11.54

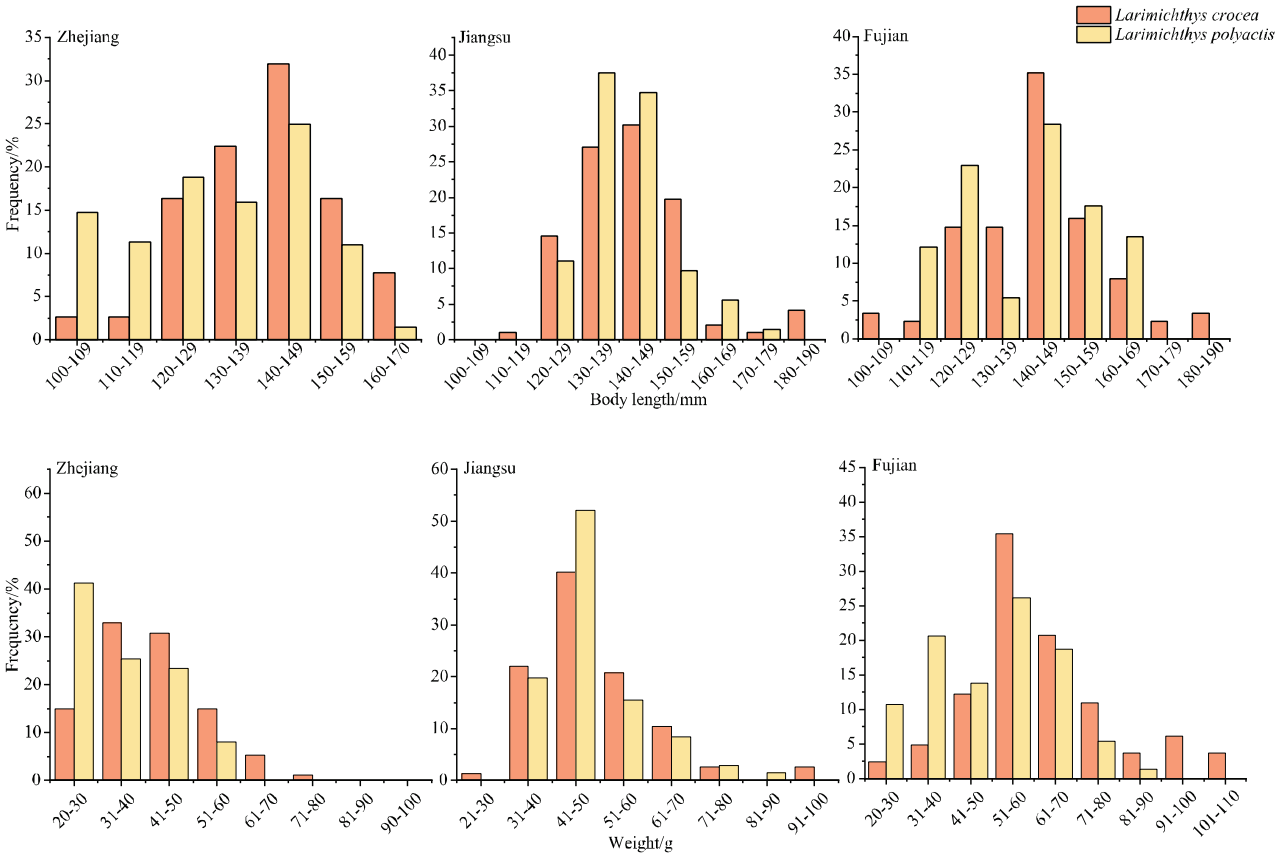


Figure 4. Frequency distribution of body length and body mass for large and small yellow croakers in different regions.

3.4. Stable Isotope Characteristics and Interspecific Nutritional Hierarchy Differences

The δ ^{13}C and δ ^{15}N values for the large yellow croaker and the small yellow croaker are shown in Table 3. The total δ ^{13}C values for the small yellow croaker ranged from −18.64‰ to −15.30‰, with a maximum difference of 3.34‰. The δ ^{13}C values for the large yellow croaker ranged from −17.22‰ to −15.88‰, with a maximum difference of 1.34‰. The mean value was −19.62 ± 1.11‰, and the small yellow croaker had a higher mean δ ^{13}C value than the large yellow croaker. The total δ ^{15}N ratios for the small yellow croaker ranged from 9.95‰ to 12.04‰, with a maximum difference of 2.09‰ and a mean value of 10.71 ± 0.50‰. Small yellow croakers had a higher mean value compared with large yellow croakers. Univariate analysis of variance indicated no significant differences in the carbon and nitrogen stable isotope ratios between large and small yellow croakers ($p > 0.05$).

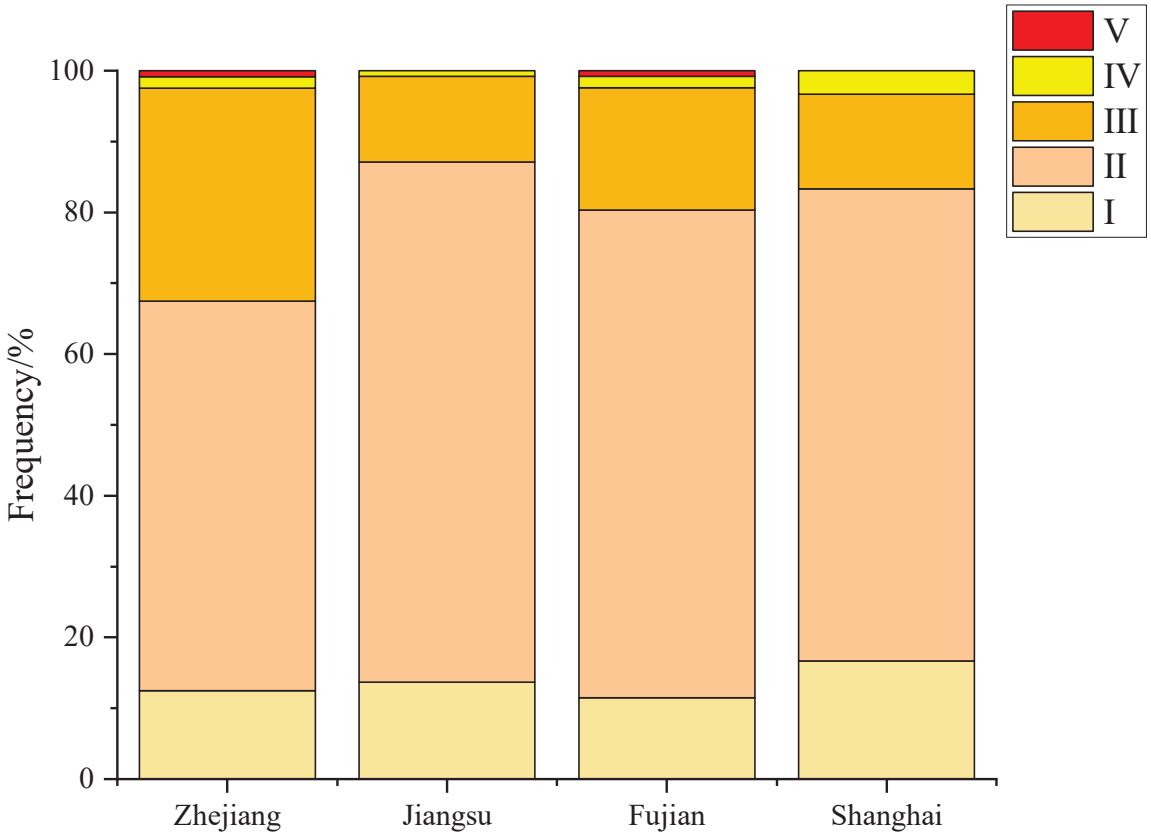


Figure 5. Proportions of large yellow croakers in different gonadal maturity stages.

Table 3. The $\delta^{13}C$ (‰) and $\delta^{15}N$ (‰) values for the two fish species in the Zhejiang sea area.

Region	Species	Number	$\delta^{13}C$		$\delta^{15}N$		Trophic Level
			Range	Mean ± SD	Range	Mean ± SD	
Zhoushan	*L. crocea*	10	−16.80~−15.88	−16.22 ± 0.51	10.52~11.94	10.84 ± 0.17	4.16 ± 0.05
	L. polyactis	10	−17.32~−15.30	−16.31 ± 1.01	10.69~11.56	10.79 ± 0.11	4.15 ± 0.03
Taizhou	*L. crocea*	10	−17.22~−16.95	−17.11 ± 0.14	10.27~10.56	10.39 ± 0.15	4.03 ± 0.04
	L. polyactis	10	−18.64~−16.35	−18.06 ± 1.5	9.95~12.04	10.84 ± 1.07	4.16 ± 0.32

By using *Mytilus coruscus* ($\delta^{15}N$ value of 3.9 ‰) as the reference organism, the average trophic levels of large and small yellow croakers in Zhoushan and Taizhou waters were calculated based on the stable isotope ratio analysis results as 4.16 ± 0.05 and 4.15 ± 0.03, respectively. One-way analysis of variance showed that there were no significant differences in the trophic levels between large and small yellow croakers in different regions ($p > 0.05$).

Using the nicheROVER niche model, the degree of niche overlap between the two species was calculated. The results showed that the nutrient niches of the two species overlapped. Figure 6 shows the posterior distribution of the niche overlap measure. nicheROVER analysis indicates the probability that a species is found in the niche region of another species. In the Taizhou and Zhoushan regions, the probabilities that the stable isotope niche of the large yellow croaker overlapped with the niche region of the small yellow croaker were 65% and 94%, respectively.

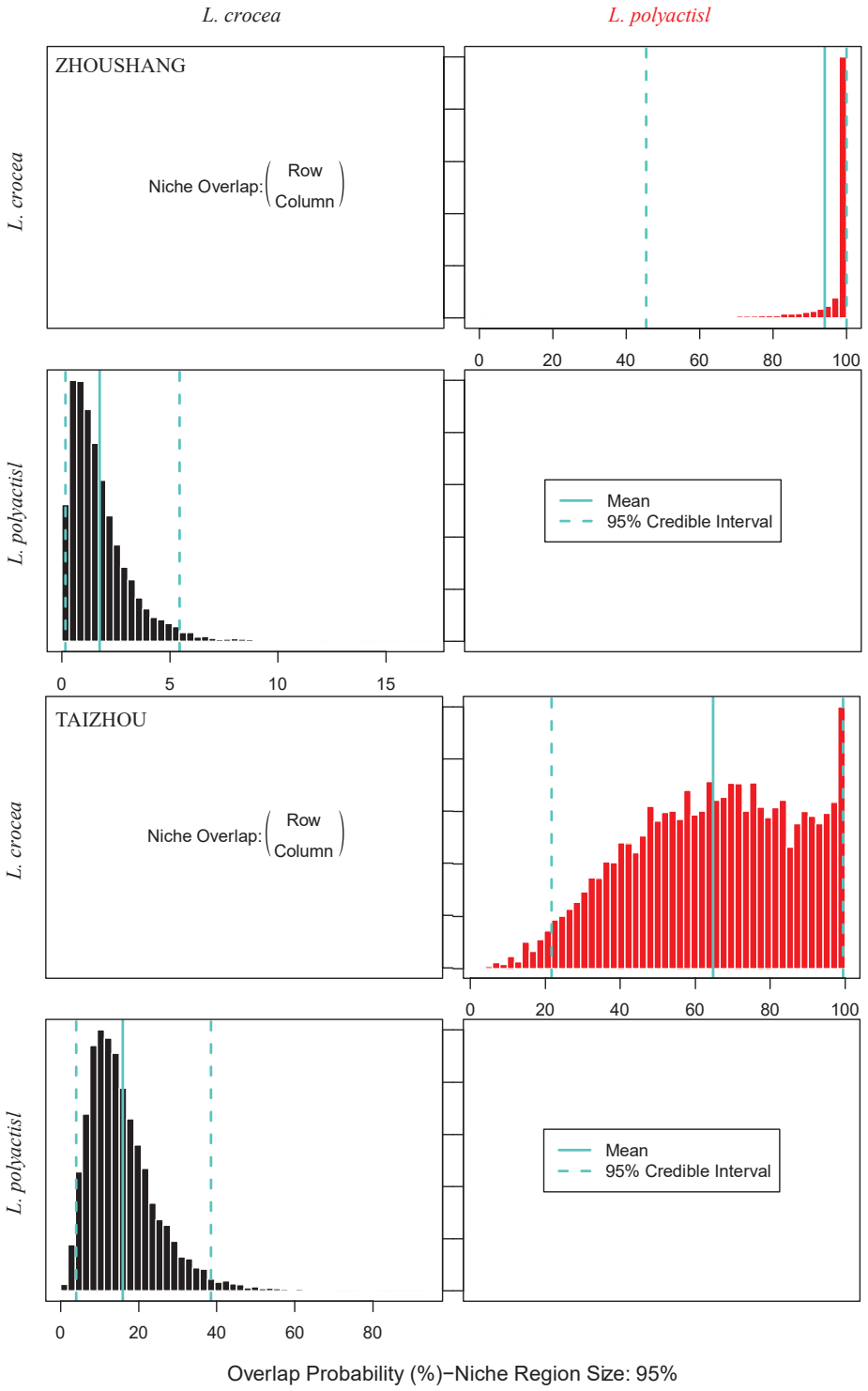


Figure 6. Bayesian plot of the posterior probability distributions of species niche regionalization measures (%) obtained using nicheROVER, with the posterior mean and 95% credible interval displayed in blue.

3.5. Comparison of Gastric Contents of the Two Fish Species

Analysis of the gastric contents of the two fish species is shown in Figure 7. We find that in the large yellow croaker, the dominant operational taxonomic unit (OTU) in its food was OTU1 (relative abundance of 56.96%), which was similar to *Benthosema pterotum*, and the second was OTU2 (relative abundance of 22.32%), which was similar to *Jaydia lineata*. The relative abundance of OTU5 was also relatively high (there was a relative abundance of

12.22%), and it was similar to *Mierspenaeopsis hardwickii*. The dominant OTUs in the diet of the small yellow croaker were similar to those for the large yellow croaker, where the main food items were *Benthosema pterotum* and *Jaydia lineata*, with a relative abundance of 38.81% and 34.32%. The relative abundance of OTU4 was also relatively high (there was a relative abundance of 12.25%), and it was similar to *Harpadon nehereus*. The relative abundance values for all other OTUs in the stomach contents were less than 3.0%.

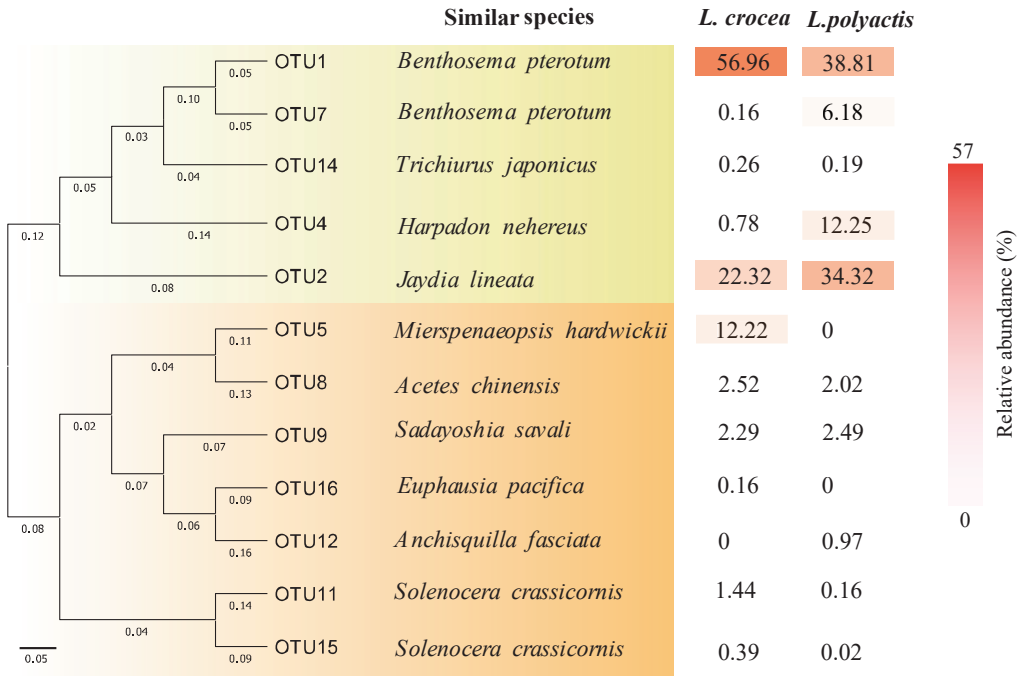


Figure 7. High-throughput sequencing analysis of COI gene to assess the dietary compositions for the large yellow croaker and the small yellow croaker.

3.6. Analysis of Intestinal Microbial Diversity

Figure 8 presents a Venn diagram illustrating the OTU feature sequences for large yellow croakers (LZS) and small yellow croakers (SZS) collected in Zhoushan, as well as those for large yellow croakers (LTZ) and small yellow croakers (STZ) collected in Taizhou. The total number of OTUs shared between the two marine regions for both species was 535, representing 25.9% of the overall total. The large and small yellow croakers in the Zhoushan region had 357 and 317 unique OTUs, respectively, with a combined total of 675 OTUs, constituting 50.03% of the total for both species. In the Taizhou region, the large and small yellow croakers together had 1147 OTUs, representing 59.4% of the total for both species. Clearly, the intestinal microbiota compositions were similar for large and small yellow croakers in the two marine regions.

The α-diversity indices obtained for intestinal microbiota can directly reflect the species diversity within a group. To investigate differences in the richness and diversity of bacterial communities in intestinal samples, α-diversity analysis was conducted based on sequencing data. The results indicated that there were no significant differences in the Shannon, Simpson, Chao1, and Ace indices between large and small yellow croakers from the same region (Table 4) ($p > 0.05$).

Principal coordinates analysis (PCoA) was performed based on weighted Unifrac distances to assess the β-diversity of different groupings. The PCoA plot (Figure 9) showed that there were no significant differences between large and small yellow croakers in the Taizhou marine area (PerMANOVA) ($p = 0.77$), and no significant difference between the two species in the Zhoushan marine area ($p = 0.82$). These results indicate that large and small yellow croakers had similar characteristic intestinal microbiota communities in both marine areas.

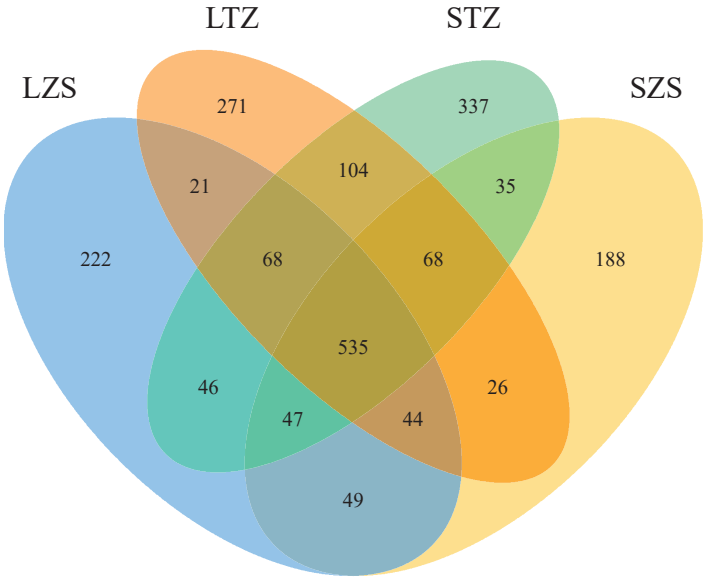


Figure 8. Venn diagram showing the intestinal microbiota in large yellow croaker and small yellow croaker in different regions.

Table 4. Analysis of alpha diversity indices obtained for intestinal microbiota in the two species in different sea areas.

Groups	Numbers of Sequences	ACE	Chao1	Shannon	Simpson
LZS	91,217	500.19 ± 347.17	473.91 ± 320.92	2.4 ± 0.45	0.19 ± 0.04
SZS	94,712	549.4 ± 363.46	523.16 ± 329.18	2.34 ± 0.32	0.21 ± 0.01
LTZ	83,392	656.37 ± 332.40	615.2 ± 298.06	2.38 ± 0.45	0.2 ± 0.03
STZ	70,322	810.32 ± 16.19	763.01 ± 16.53	2.5 ± 0.05	0.21 ± 0.01

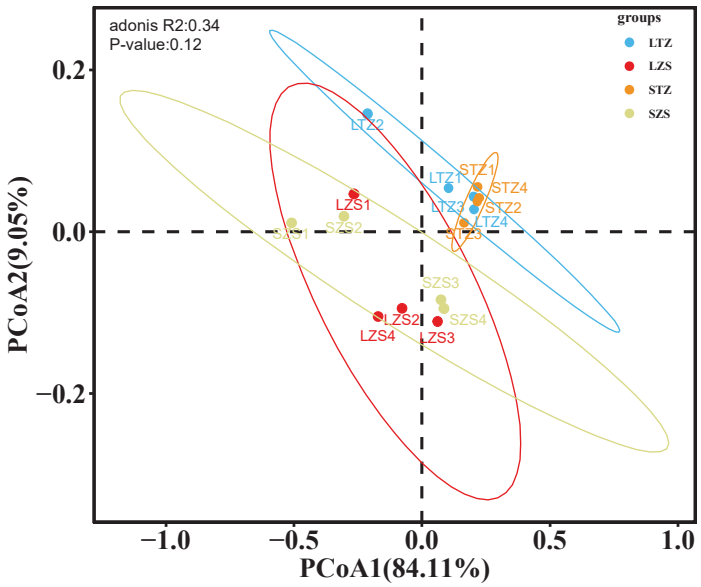


Figure 9. Principal coordinates analysis (PCoA) results based on weighted Unifrac distances. Note: Each point in the figure represents one sample, samples from the same group are depicted in the same color, and the color regions indicate confidence intervals. LZS 1–4 represent the four samples from the large yellow croaker group in Zhoushan; SZS 1–4 represent the four samples from the small yellow croaker group in Zhoushan; LTZ 1–4 represent the four samples from the large yellow croaker group in Taizhou; STZ 1–4 represent the four samples from the small yellow croaker group in Taizhou. The same applies to Figure 10.

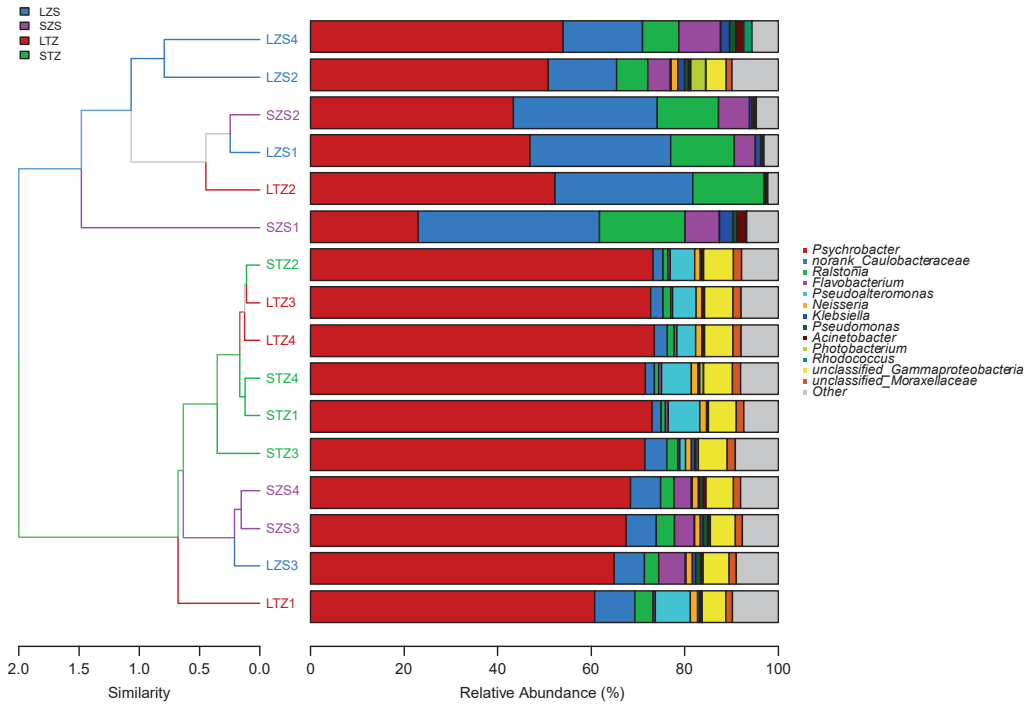


Figure 10. Sample cluster tree and histogram combined analysis diagram.

3.7. Comparison of Intestinal Microbiota Structure

The left-hand side of Figure 10 shows a dendrogram representing the similarity between samples, where samples with minor differences are clustered together on the same branch and distinguished by color based on group information. The right-hand side shows a bar graph illustrating the species distribution within each sample. In the dendrogram, the large yellow croaker group and small yellow croaker group are situated on the same branch, thereby indicating a lack of significant differences between the two sample sets. The relative abundance plot (Figure 10) shows that *Psychrobacter* was the dominant genus for both large yellow croaker and small yellow croaker samples. In total, 530 genera were identified in the large yellow croaker and small yellow croaker samples, and the compositions of the dominant genera were similar in each sample, where they consisted of *Psychrobacter*, *Caulobacteraceae*, *Ralstonia*, and *Flavobacterium*. Overall, except for *Pseudoalteromonas* and *Neisseria*, the compositions of the other dominant bacterial genera were similar, and the similarity of the intestinal microbial composition was high at the genus level in large yellow croaker and small yellow croaker.

4. Discussion

4.1. Stock Enhancement During the Fishing Ban Significantly Affected the Catch Ratios of Two Sciaenidae Species

Under the background that the fishery resources of the large yellow croaker in the East China Sea of China remain depressed at present, and the migratory fishing seasons and spawning groups are still hard to find, we consider that the vast majority of the large yellow croakers which were caught and marketed as small yellow croakers are mostly from stock enhancement during the fishing ban. Our results showed that as a result of large-scale stocking activities in the coastal areas of three provinces in the East China Sea after the fishing ban period, the average catch proportion of the large yellow croaker in the three provinces accounted for 21.44 ± 9.35% of the total yellow croaker catch. Compared with the average release size of 65 mm, the average length of these catches was 147.3 mm. Based on the Von Bertalanffy growth model ($L_t = 481 \times \left(1 - e^{-0.5 \times (t+0.25)}\right)$) obtained from previous studies on the expected growth pattern of the large yellow croaker in the East China Sea [31], it can be calculated that the theoretical body length of the large yellow

croaker released for stock enhancement at the beginning of the fishing ban in May of the current year would be 142.05 mm after five and a half months of growth, which is consistent with the aforesaid results. This result indicates that large yellow croaker juveniles released in the year could feed and grow under natural conditions. Meanwhile, studies have indicated that there is no significant difference in body length and body mass between the large yellow croaker and the small yellow croaker, which, together, constitute the guild. Accordingly, we can speculate that in the early-life stage of the large yellow croaker, when its body length and body mass are similar to those of the small yellow croaker, it is more likely to have a life history strategy of cohabitating with them. According to the fishing production data reported in the China Fishery Statistical Yearbook (2023) [26], China's catch volume of the small yellow croaker in 2022 was 268,000 tons, whereas the catch volume of the large yellow croaker was only 37,000 tons. Based on the results, we can infer that the actual catch volume of the large yellow croaker in that year was significantly higher than the reported figure, thereby highlighting the positive impact of stocking on resource recovery. However, during a repeated survey of the landing catches at LuChao Port in Shanghai from March to April in the following year, that is, half a year after the end of the stock enhancement, it was discovered that the proportion of large yellow croaker catches decreased to less than 3%; thus, there was a sharp decline in the recently recovering large yellow croaker resource abundance. In addition, the fishing production data reported in the China Fishery Statistical Yearbook (2023) indicate that the catch volume of the large yellow croaker in 2022 decreased by 10,600 tons compared with 2021, i.e., a decrease of 2.8%. In particular, the catch volume of the large yellow croaker of Guangdong and Hainan provinces in the South China Sea reached 29,000 tons, accounting for 79.4% of the national catch volume. Thus, the enhancement of the large yellow croaker stocks in the coastal provinces of eastern China did not increase its fishable resource abundance, which our results suggest was due to the large yellow croaker released for stocking during the closed fishing period being caught along with the small yellow croaker after the fishing ban was lifted, and this led to underestimation of the yield of the large yellow croaker and had a detrimental effect on the initially successful stocking programs. However, there have been occasional news reports in recent years of large-sized large yellow croakers weighing over 1 kg being caught in the East China Sea [32,33]. Moreover, large yellow croaker populations have even been discovered in the Ma'an Islands, thereby highlighting the ability of the released but uncaught large yellow croaker to thrive in habitats such as island reefs and to contribute to the restoration of wild populations. Meanwhile, through historical fisheries statistics and estimations from other researchers on the East China Sea large yellow croaker fishery resources [30], we have found that compared to the near-extinct population of the large yellow croakers in the 1990s, the current population has recovered. This recovery can be attributed to the working of the restocking program. Therefore, we consider that enhancing large yellow croaker stocks is important for resource recovery.

4.2. Guild of Large and Small Yellow Croakers Influences the Conservation of the Large Yellow Croaker Species

Our investigations of intestinal microbiota, stable isotopes in muscle tissues, and stomach content compositions showed that the early-life stages of the large yellow croaker released in the sea areas of Zhejiang formed a typical guild with small yellow croakers, with cohabitation in the same habitat and utilization of similar resources. Previous studies have shown that the current environmental conditions in the East China Sea can provide sufficient and rich food resources for both large yellow croaker and small yellow croaker fish species, and there is no intense interspecies competition. For example, Xu [3] found that the current summer fishing ban system has promoted structural improvement of the East China Sea ecosystem and the recovery of food resources. Li [34] found that the food source diversity level and nutritional trophic level span were relatively high and stable in the feeding ground of the East China Sea southwestern waters. The current habitat provides sufficient food and good ecosystem structure, which alleviates resource competition and

promotes the formation of the guild. We believe that in the policy context of the long-term implementation of the summer fishing ban, the absence of intense competition will be sustainable in the long term. However, it should be noted that the current summer fishing ban system has only achieved short-term effects on the utilization of resources, with an increase in resources for a short period of time. After the end of the fishing ban period, massive amounts of the guild of large and small yellow croakers were caught. This strong fishing effort for the small yellow croaker in a short period negated the restoration effects of the fishing ban system, indirectly hindering the recovery of large yellow croaker resources and preventing the sustainable effects of stock enhancement. In studying the impact of the fishing ban on fishery resources, Barnes et al. [35] established a closed-area model to determine the impact of the fishing ban on fisheries production. Their research revealed that the recovery time of fish resources is correlated with the fishing ban, highlighting the importance of avoiding overfishing to ensure sustainable fisheries production. Therefore, it is believed that extending the fishing ban or adjusting fishing cessation regulations in the presence of guilds can facilitate the sustainable recovery of large yellow croaker resources in the East China Sea, as well as other fishery resources.

Previous reports indicate that the minimum body length and weight for the sexual maturation of female large yellow croakers are 220–240 mm and 200 g, respectively, and those for males are 200–220 mm and 150 g [36]. In the present study, the average body length of the sampled large yellow croaker was 141.73 mm, with an average weight of 48.32 g. Therefore, the caught large yellow croakers were smaller than the minimum body length and weight required for reaching sexual maturity. This uncontrolled fishing of immature large yellow croakers hinders the replenishment of mature individuals in the crucial spawning grounds of the East China Sea, thereby making it challenging for spawning seasons to regenerate the population. Thus, even under the background of large-scale stock enhancement, the recovery of large yellow croaker resources is still quite difficult. We also discovered that the gonadal development of some small-sized individuals reached the V-stage of sexual maturity prematurely. This indicates that the large yellow croaker has a tendency to reach sexual maturity earlier and transform into an R-strategy selector. In the study by Zhou et al. [30], utilizing the yield per recruit model, the authors calculated the $F_{0.1}$ and F_{max}. Their findings revealed that $F_{0.1} < F_{max} < F_{cur}$, indicating that regardless of whether the $F_{0.1}$ or F_{max} is used as the reference point for fisheries management, the nearshore large yellow croaker population in the East China Sea is in a state of overexploitation. Uncontrolled fishing is actually destroying the large yellow croaker fishery resources, which have just begun to recover. Therefore, the failure to recover the large yellow croaker fishery resources has further promoted the implementation of stock enhancement, and the impact of stock enhancement on the genetic diversity of wild fishery resources and the associated genetic risk has also attracted attention. Some previous studies on stock enhancement for other species have shown that stock enhancement could have potential genetic impacts on wild populations of the released species. For instance, the large-scale release of red sea bream in Kagoshima Bay, Japan, has resulted in genetic impacts on wild populations, ultimately leading to the loss of rare alleles through genetic drift in wild individuals [37], and potential negative genetic impacts could lead to the collapse of the wild resource and possibly make stock enhancement efforts counterproductive. There have been no previous studies on the genetic diversity of large yellow croaker individuals released for stock enhancement; thus, the impact of stock enhancement releases on the genetic diversity of the wild population of the large yellow croaker is unclear. It is necessary to control the fishing intensity and to pay special attention to the long-term genetic effects of stock enhancement to better maintain the wild population of the large yellow croaker.

4.3. Suggestions Regarding the Management of the Large Yellow Croaker Fisheries

The large yellow croaker stock enhancement program aimed at restoring the population involves releasing hatchery juvenile fishes into the wild to restore the seriously depleted spawning population and allow it to provide regular, substantial yields again [25].

Overfishing is widely recognized as one of the main causes of fishery resource degradation worldwide, and it can lead to a direct reduction in the resource through removing the target species from the water. Therefore, the recovery and sustainable utilization of resources can only be achieved by maintaining a dynamic balance between fishing and releasing.

For the past two decades, the implementation of the fishing ban policy by the Chinese government has garnered widespread support from fishermen and has yielded positive ecological, economic, and social benefits. However, there are still numerous issues that need to be addressed [3]. In the present study, we showed that due to the lack of timely, effective, or adequate management, heavy fishing pressure, especially transition fishing for the early-life-stage large yellow croaker in spawning and wintering grounds, is the main factor that has contributed to the decline of its resources and its inability to recover. During the fishery production process after the fishing ban period, the guild composed of large and small yellow croakers was the focus of indiscriminate intensive fishing, and many young large yellow croakers were caught, which readily causes the size cut-off effect, thereby affecting the reproduction, growth, and ecological role of the population [38]. Due to the migratory and feeding habits of the large yellow croaker, which cover vast geographical areas, the protection and management processes of the fishery resources of this species are complex and require strong management and enforcement. If fishing activities are not scientifically and adequately regulated, it will be difficult to achieve ideal results when releasing migratory fish such as the large yellow croaker back into the wild.

The concept of a guild can be used to answer important fisheries management questions, such as how community composition varies with habitat [16], how fishing development affects food web stability [39], and how fishing induces changes in ecosystem processes [40]. We consider that given the formation of the guild of large and small yellow croakers, resource protection for the large yellow croaker must be coordinated with the protection of small yellow croaker resources. An important example is the establishment of the National Aquatic Germplasm Resource Protection Area for Ribbon Fish in the East China Sea by Zhejiang Province in 2008. Since 2013, fishing has been prohibited in the core area of the protection area, with a fishing ban lasting approximately 1 month longer than the East China Sea fishing ban period. These conservation measures have led to increases in the biomasses of both the large yellow croaker and ribbon fish (*Trichiurus lepturus*) [41]. Currently, the existing single protection measures for the large yellow croaker are not sufficient. Instead, we advocate for the development of a collaborative conservation strategy for the marine region known as the "spawning ground, nursing ground, overwintering ground, and migration route", where the guild consisting of the large yellow croaker and the small yellow croaker can thrive.

Given the aforementioned issues and the need to ensure the recovery of wild large yellow croaker resources and the effectiveness of the fishing ban in the spawning season, we provide the following recommendations: (1) The fisheries authorities should regulate the number and total power of fishing boats, adjust the marine fisheries structure, allocate a portion of the funds for large yellow croaker stock enhancement toward labor transition and placement, and gradually reduce the intensity of marine fishing each year. (2) By treating a guild as a management unit, the catch of the small yellow croaker can be used to estimate the utilization level of the large yellow croaker fishery resources. (3) Gradually extend the fishing ban period for the "spawning ground, nursing ground, overwintering ground, and migration route" used by the guild, transition the ban on trawl, sail-style net, and gillnet fishing to year-round prohibition, and only allow hook-and-line fishing; accelerate the implementation of the total allowable catch system (TAC) for major economic fish species; and establish net mesh size specifications to gradually restore the large yellow croaker stock resource. (4) Develop recreational fishing and support the construction of marine farms. Develop offshore marine aquaculture and strengthen research into scientific utilization to promote ecological restoration while ensuring economic development.

5. Conclusions

In conclusion, this study demonstrated that when the released and enhanced large yellow croaker grew to an average body length of 141.73 ± 14.61 mm and an average body weight of 49.45 ± 17.77 g in the wild, large yellow croaker individuals of this size exhibited a life history strategy of cohabitation with the small yellow croaker, and the two formed a guild. Based on this phenomenon, fishing targeting the small yellow croaker after the end of the fishing ban would impose significant fishing pressure on the large yellow croaker population, ultimately leading to the failure of China's long-standing large yellow croaker stock enhancement activities to achieve their desired effects.

Author Contributions: Designed and planned the study, P.C. and Z.W.; drafted the manuscript, P.C. and Z.W.; analyzed the data, P.C.; field work, P.C. and J.Y.; funding, S.Z. and Z.W.; acquisition and supervision, S.Z. and Z.W. All authors have read and agreed to the published version of the manuscript.

Funding: This study was supported by the National Key R&D Program of China (2023YFD2401903, 2019YFD0901303).

Institutional Review Board Statement: The experiments comply with current laws in China. All the samples in this study were obtained from legal commercial fisheries, and the samples were dead when they were obtained.

Informed Consent Statement: Not applicable.

Data Availability Statement: The data presented in this study are available on request from the corresponding author.

Acknowledgments: We would like to thank our laboratory members at Shanghai Ocean University for their support in field campaigns and laboratory analyses.

Conflicts of Interest: The authors declare no conflicts of interest.

References

1. Niles, L.J.; Dey, A.D.; Maslo, B. *Overexploitation of Marine Species and Its Consequences for Terrestrial Biodiversity Along Coasts. Coastal Conservation*; Cambridge University Press: Cambridge, UK, 2014; pp. 347–367. [CrossRef]
2. Merino, G.; Barange, M.; Blanchard, J.L.; Harle, J.; Holmes, R.; Allen, I.; Rodwell, L.D. Can marine fisheries and aquaculture meet fish demand from a growing human population in a changing climate? *Global. Environ. Change* **2012**, *22*, 795–806. [CrossRef]
3. Xu, L.; Song, P.; Wang, Y.; Xie, B.; Huang, L.; Li, Y.; Lin, L. Estimating the impact of a seasonal fishing ban on the East China Sea ecosystem from 1997 to 2018. *Front. Mar. Sci.* **2022**, *9*, 865645. [CrossRef]
4. Welcomme, R.L.; Winemiller, K.O.; Cowx, I.G. Fish environmental guilds as a tool for assessment of ecological condition of rivers. *River Res. Appl.* **2006**, *22*, 377–396. [CrossRef]
5. Benoit, D.M.; Jackson, D.A.; Chu, C. Partitioning fish communities into guilds for ecological analyses: An overview of current approaches and future directions. *Can. J. Fish. Aquat. Sci.* **2021**, *78*, 984–993. [CrossRef]
6. Root, R.B. The niche exploitation pattern of the blue-gray gnatcatcher. *Ecol. Monogr.* **1967**, *37*, 317–350. [CrossRef]
7. Simberloff, D.; Dayan, T. The guild concept and the structural organization of ecological communities. *Annu. Rev. Ecol. Evol. Syst.* **1991**, *22*, 115–143. [CrossRef]
8. Severinghaus, W.D. Guild theory development as a mechanism for assessing environmental impact. *Environ. Manag.* **1981**, *5*, 187–190. [CrossRef]
9. Austen, D.J.; Bayley, P.B.; Menzel, B.W. Importance of the Guild Concept to Fisheries Research and Management. *Fisheries* **1994**, *19*, 12–20. [CrossRef]
10. Auster, P.J.; Link, J.S. Compensation and recovery of feeding guilds in a northwest Atlantic shelf fish community. *Mar. Ecol. Prog. Ser.* **2009**, *382*, 163–172. [CrossRef]
11. Noble, R.A.A.; Cowx, I.G.; Goffaux, D.; Kestemont, P. Assessing the health of European rivers using functional ecological guilds of fish communities: Standardising species classification and approaches to metric selection. *Fish. Manag. Ecol.* **2007**, *14*, 381–392. [CrossRef]
12. Patterson, L.; Phelan, J.; Goudreau, C.; Dykes, R. Flow-biology relationships based on fish habitat guilds in North Carolina. *J. Am. Water Resour. Assoc.* **2017**, *53*, 56–66. [CrossRef]
13. Goldstein, R.M.; Simon, T.P. Toward a united definition of guild structure for feeding ecology of North American freshwater fishes. In *Assessing the Sustainability and Biological Integrity of Water Resources Using Fish Communities*; CRC Press: Boca Raton, FL, USA, 2020; pp. 123–202.

14. Reum, J.C.P.; Essington, T.E. Seasonal variation in guild structure of the Puget Sound Demersal Fish Community. *Estuar. Coasts* **2008**, *31*, 790–801. [CrossRef]
15. Villéger, S.; Brosse, S.; Mouchet, M.; Mouillot, D.; Vanni, M.J. Functional ecology of fish: Current approaches and future challenges. *Aquat. Sci.* **2017**, *79*, 783–801. [CrossRef]
16. Osuka, K.; Kochzius, M.; Vanreusel, A.; Obura, D.; Samoilys, M. Linkage between fish functional groups and coral reef benthic habitat composition in the Western Indian Ocean. *J. Mar. Biol. Assoc. UK* **2016**, *98*, 387–400. [CrossRef]
17. Wang, X.; Lu, G.; Zhao, L.; Yang, Q.; Gao, T. Assessmentof fishery resources using environmental DNA: Small yellow croaker (*Larimichthys polyactis*) in East China Sea. *PLoS ONE* **2020**, *15*, e0244495. [CrossRef]
18. Wang, X.; Lu, G.; Zhao, L.; Du, X.; Gao, T. Assessment of fishery resources using environmental DNA: The large yellow croaker (*Larimichthys crocea*) in the East China Sea. *Fish. Res.* **2021**, *235*, 105813. [CrossRef]
19. Han, Z. Studies of Morphological Characteristics and Genetic Diversity on Populations of SmallYellow Croaker (*Larimichthys polyactis*) and the Difference between Small Yellow Croaker and Large Yellow Croaker (*Larimichthys crocea*). Master's Thesis, Ocean University of China, Qingdao, China, 2012. (In Chinese).
20. Lin, Y.; Li, J.; Wang, Z.; Zhang, S.; Wang, K.; Li, X. A Comparison of Fish Diversity in Rocky Reef Habitats by Multi-Mesh Gillnets and Environmental DNA Metabarcoding. *Front. Ecol. Evol.* **2022**, *10*, 874558. [CrossRef]
21. Lü, H.; Xu, J.; Haegen, G.V. Supplementing Marine Capture Fisheries in the East China Sea: Sea Ranching of Prawn *Penaeus orientalis*, Restocking of Large Yellow Croaker *Pseudosciaena crocea*, and Cage Culture. *Rev. Fish. Sci.* **2008**, *6*, 366–376. [CrossRef]
22. Liu, M.; Mitcheson, Y.S. Profile of a fishery collapse: Why mariculture failed to save the large yellow croaker. *Fish. Fish.* **2008**, *9*, 219–242. [CrossRef]
23. Yuan, J.; Lin, H.; Wu, L.; Zhuang, X.; Ma, J.; Kang, B.; Ding, S. Resource status and effect of long-term stock enhancement of large yellow croaker in China. *Front. Mar. Sci.* **2021**, *8*, 743836. [CrossRef]
24. Chen, X.; Xu, K.; Li, P.; Wang, H.; Zhou, Y.; Wang, M. Analysis of the Status of Marine Fish Proliferation and Release in Zhejiang Offshore. *Marine. Dev. Manag.* **2023**, *40*, 128–135. [CrossRef]
25. Ye, G.; Lin, Y.; Feng, C.; Chou, L.M.; Jiang, Q.; Ma, P.; Sanders, C. Could the wild population of Large Yellow Croaker *Larimichthys crocea* (Richardson) in China be restored? A case study in Guanjingyang, Fujian, China. *Aquat. Living. Resour.* **2020**, *33*, 24. [CrossRef]
26. Ministry of Agriculture and Rural Affairs of the People's Republic of China. *National Fisheries Technology Extension Center, The China Society of Fisheries China Fishery Statistical Yearbook*; Agriculture Press: Beijing, China, 2023; pp. 38–40.
27. Zanden, M.J.V.; Fetzer, W.W. Global patterns of aquatic food chain length. *Oikos* **2007**, *116*, 1378–1388. [CrossRef]
28. Leray, M.; Yang, J.Y.; Meyer, C.P. A new versatile primer set targeting a short fragment of the mitochondrial COI region for metabarcoding metazoan diversity: Application for characterizing coral reef fish gut contents. *Front. Zool.* **2013**, *10*, 34. [CrossRef]
29. Zhang, J.; Wang, Y.; Liu, J.; Xu, W.; Yin, Z.; Liu, Y.; Ai, Q. Effects of fecal bacteria on growth, digestive capacity, antioxidant capacity, intestinal health of large yellow croaker (*Larimichthys crocea*) larvae. *Aquaculture* **2023**, *562*, 738796. [CrossRef]
30. Zhou, Y.; Li, S. *Atlas of "Spawning Ground, Feeding Ground, Overwintering Ground, and Migration Routes and Protect Areas" of Main Economic Fisheries in East China Sea*; Marine Press: Beijing, China, 2018; pp. 1–105.
31. Zhang, Q.; Sun, H.; Zhou, Y.; Jiang, R.; Xu, K.; Xu, G.; Zhao, P. Population Resource of Larimichthys crocea in Inshore Waters of Northern East China Sea Under the Background of Releasing Stock Enhancement. *J. Zhejiang Ocean Univ. Nat. Sci. Edit.* **2024**, *02*, 127–136. (In Chinese)
32. Tang, X.F. Dazzling Display! Fishing Vessel from Ningbo Nets 36 Crates of Wild Large Yellow Croakers, Worth Millions! *Qianjiang Evening News*. 20201130. Available online: https://zjnews.zjol.com.cn/zjnews/nbnews/202011/t20201130_12450149.shtml (accessed on 30 November 2020).
33. Tang, X.F. Net Sales of Nearly 10 Million? Is the King of Wild Yellow Croaker in the East China Sea Back? You Want to Go Fishing, Too? No, No, No. *Qianjiang Evening News*. 20220119. Available online: https://zjnews.zjol.com.cn/202201/t20220119_23664586.shtml (accessed on 19 January 2022).
34. Li, Y.; Chen, Y.; Olson, D.; Yu, N.; Chen, L. Evaluating ecosystem structure and functioning of the East China Sea Shelf ecosystem, China. *Hydrobiologia* **2009**, *636*, 331–351. [CrossRef]
35. Barnes, B.; Sidhu, H. The impact of marine closed areas on fishing yield under a variety of management strategies and stock depletion levels. *Ecol. Model.* **2013**, *269*, 113–125. [CrossRef]
36. Yu, C.; Yan, X.; Jiang, Q.; Zang, Y. Cause Analysis of Resources Change and Reconstruction Strategy of *Larimichthys crocea* Daiqu Group in the East China Sea. *J. Fish. Ch.* **2022**, *46*, 616–625. [CrossRef]
37. Hamasaki, K.; Toriya, S.; Shishidou, H. Genetic effects of hatchery fish on wild populations in red sea bream Pagrus major (*Perciformes, Sparidae*) inferred from a partial sequence of mitochondrial DNA. *J. Fish. Biol.* **2010**, *77*, 2123–2136. [CrossRef]
38. Su, S.; Tang, Y.; Chang, B.; Zhu, W.; Chen, Y. Evolution of marine fisheries management in China from 1949 to 2019: How did China get here and where does China go next? *Fish. Fish.* **2020**, *21*, 435–452. [CrossRef]
39. Houk, P.; Cuetos-Bueno, J.; Kerr, A.M.; McCann, K. Linking fishing pressure with ecosystem thresholds and food web stability on coral reefs. *Ecol. Monogr.* **2018**, *88*, 109–119. [CrossRef]

40. Garrison, L.P.; Link, J.S. Fishing effects on spatial distribution and trophic guild structure of the fish community in the Georges Bank region. *ICES J. Mar. Sci.* **2000**, *57*, 723–730. [CrossRef]
41. Zhang, Q.Y.; Hong, W.S.; Cheng, S.X. Stock changes and resource protection of the large yellow croaker (*Larimichthys crocea*) and ribbon fish (*Trichiurus japonicus*) in coastal waters of China. *J. Appl. Ocean* **2017**, *36*, 438–445. (In Chinese)

Disclaimer/Publisher's Note: The statements, opinions and data contained in all publications are solely those of the individual author(s) and contributor(s) and not of MDPI and/or the editor(s). MDPI and/or the editor(s) disclaim responsibility for any injury to people or property resulting from any ideas, methods, instructions or products referred to in the content.

biology

MDPI

Article

Exploring the Adaptation Process of *Huso dauricus* to High Temperatures Based on Changes in Intestinal Microbiota

Ruoyu Wang [1,2], Yutao Li [1], Yining Zhang [1,3], Sihan Wang [1,2], Zheng He [1,2], Dingchen Cao [1], Zhipeng Sun [1], Nianmin Wang [1], Ying Zhang [1,2,3,*] and Bo Ma [1,2,3,*]

[1] Key Open Laboratory of Cold Water Fish Germplasm Resources and Breeding of Heilongjiang Province, Heilongjiang River Fisheries Research Institute, Chinese Academy of Fishery Sciences, Harbin 150076, China; wangruoyu@hrfri.ac.cn (R.W.)
[2] College of Fisheries and Life Science, Dalian Ocean University, Dalian 116023, China
[3] College of Fisheries and Life Science, Shanghai Ocean University, Shanghai 201306, China
* Correspondence: zhangying@hrfri.ac.cn (Y.Z.); mabo@hrfri.ac.cn (B.M.)

Simple Summary: As global temperatures rise due to climate change, the survival of fish is increasingly at risk. This study aimed to understand how *Huso dauricus* adapts to high temperatures, focusing on the crucial role of its intestinal microbiota in helping the fish cope with temperature changes. When the fish were exposed to different water temperatures, noticeable changes were observed in the types and proportions of bacteria in their intestines. Over time, the fish adapted to the high temperatures, with one particular type of intestinal bacteria becoming dominant. These findings suggest that the intestinal microbiota of the fish help them adjust to high temperatures. The results of this study are important for understanding how fish can survive in a warming world and may lead to more effective strategies for managing fish populations in the face of climate change.

Abstract: Global warming has led to rising water temperatures, posing a significant threat to fish survival. Understanding the mechanisms by which fish respond to and adapt to temperature variations is thus of considerable importance. This study employed high-throughput 16S rRNA gene sequencing and bioinformatics to investigate changes in the intestinal microbiota of the kaluga sturgeon (*Huso dauricus*) under four temperature conditions (19 °C, 25 °C, 28 °C, and 31 °C) and its relationship with adaptation to high-temperature stress. The results indicated that temperature variations caused significant changes in the intestinal microbiota. Over time, differences in the microbiota structure became more pronounced under different temperature conditions, and within-group variability gradually decreased. At higher temperatures, the relative abundance of *Sphingomonas* significantly decreased, while that of *Clostridium sensu stricto 1*, *Cetobacterium*, and *Plesiomonas* exhibited a significant increase in relative abundance. Upon the cessation of rapid mortality under various high-temperature conditions, the intestinal microbiota structure and composition became highly similar, with *Clostridium sensu stricto 1* dominating both in terms of composition and relative abundance, suggesting a central role in adaptation to high-temperature stress. This study preliminarily confirms that the high-temperature adaptability of *Huso dauricus* is closely related to the structure and composition of its intestinal microbiota, with bacteria such as *Clostridium sensu stricto 1* playing an important role. These findings provide new scientific insights into enhancing fish adaptability to high-temperature stress.

Keywords: high-temperature stress; *Huso dauricus*; intestinal microbiota; high-temperature adaptability

1. Introduction

Global climate warming, accompanied by seasonal increases in water temperature and frequent extreme heatwave events, has resulted in severe, widespread, and irreversible

consequences for the survival of aquatic organisms [1]. As ectothermic animals, fish are particularly sensitive to temperature fluctuations. Moreover, intensive aquaculture practices prevent fish from escaping high temperatures through vertical migration, leaving them continuously exposed to high-temperature stress. Prolonged stress can impair fish health and even lead to mortality, severely affecting the economic benefits of aquaculture [1–4]. Therefore, understanding the mechanisms by which fish respond to and adapt to temperature changes is crucial for developing scientifically sound and effective countermeasures.

Intestinal microbiota, regarded as a "special organ" in fish, are involved in regulating physiological processes such as growth, development, digestion, metabolism, and immune responses. The composition and function of the intestinal microbiota are critical for maintaining fish health and environmental adaptability [5–7]. Understanding the changes in intestinal microbiota under high-temperature stress is of significant importance for improving our understanding of fish adaptation to climate warming. Research has shown that temperature fluctuations can reshape the intestinal microbiota in fish. Zhao et al. [8] reported that under high-temperature stress, the diversity of the intestinal microbiota in *Oncorhynchus mykiss* was altered, with significant changes in the relative abundance of Proteobacteria, Firmicutes, and Fusobacteriota. In a study by Kim et al. [9], it was found that elevated water temperature increased the proportion of Firmicutes in the intestinal microbiota of *Chromis notata*, reduced α-diversity, and induced changes in β-diversity. Environmental stress-induced changes in intestinal microbiota can positively affect the physiological functions of the host, thereby enhancing its environmental adaptability [10–13]. However, under certain conditions, such changes may exacerbate the negative effects of environmental stress [3,4]. Although several studies have observed a correlation between temperature-induced changes in intestinal microbiota and host adaptability [14,15], the underlying mechanisms remain poorly understood.

The kaluga sturgeon (*Huso dauricus*), belonging to the family Acipenseridae, is an economically significant cold-water fish species. Its optimal growth temperature range is between 15 °C and 22 °C, with mortality observed above 25 °C. As one of the oldest fish species on Earth, it has a history of over 200 million years, and its long evolutionary process has endowed it with remarkable environmental adaptability. Therefore, *Huso dauricus* serves as an ideal model for studying the mechanisms of fish adaptation to high-temperature stress. In this study, high-throughput 16S rRNA gene sequencing and bioinformatics were employed to investigate the dynamic changes in the intestinal microbiota under different temperatures (19 °C, 25 °C, 28 °C, and 31 °C). The cessation of rapid mortality in fish is used as an indicator of their adaptation to high-temperature stress. A Venn diagram and heatmap were used to identify the core microbial taxa during this period. Furthermore, co-occurrence network analysis was used to pinpoint keystone species within the core taxa, revealing potential microbial candidates that could enhance fish adaptation to high temperatures. This study preliminarily explores the microbial ecological mechanisms underlying the adaptation of *Huso dauricus* to high-temperature stress. The findings of this study provide a theoretical foundation for the application of microbiome regulation technology to improve the high-temperature adaptability of fish in the future.

2. Materials and Methods

2.1. Experimental Design and Sample Collection

The experimental F2 generation 5-month-old *Huso dauricus* were sourced from the Hulan Experimental Station of Heilongjiang Fisheries Research Institute, Chinese Academy of Fishery Sciences. A total of 288 healthy fish, exhibiting no visible external injuries and similar body sizes, with an average body weight of (24.76 $\pm$ 2.48) g, were evenly distributed into 16 indoor temperature-controlled recirculating aquaculture tanks (60 cm $\times$ 40 cm $\times$ 50 cm) for temporary rearing. During this period, the light–dark cycle was set at 12 h:12 h, with a water temperature of 19.0 °C, a pH of ~6.9, and a dissolved oxygen concentration of 7.44–7.68 mg/L. Feeding was conducted twice daily at 7:00 and 19:00, with a daily feeding

rate equivalent to 3% of the initial body weight for the young fish (Shandong Shengsuo brand sturgeon commercial pellet feed: crude protein $\geq$ 40%, crude fat $\geq$ 10%, crude fiber $\leq$ 6%, crude ash $\leq$ 18%, moisture $\leq$ 12%). Daily sludge suction and water exchange were performed before morning feeding, with a water exchange volume of 50% using pre-heated water at the same temperature. After acclimatization for one week, formal experiments were initiated with four groups: a control group maintained at 19 °C and three high-temperature stress groups at 25 °C, 28 °C, and 31 °C, each with four replicates at a stocking density of 18 individuals per tank. The water temperature was gradually adjusted to reach the experimental temperatures at a rate of 1 °C per hour. The management procedures during the experiment were consistent with those during the acclimatization period.

Daily inspections of the tanks were carried out 3 times a day (morning, noon, and evening) to monitor the survival status of *Huso dauricus*. Dead fish were promptly removed and recorded for constructing the survival curve. Sampling was conducted after the rapid mortality phase had ended at each temperature, specifically on day 0 (start of the experiment), day 11 (after rapid mortality ceased at 31 °C), day 26 (after rapid mortality ceased at 28 °C), and day 53 (after rapid mortality ceased at 25 °C). At each sampling point, one fish was randomly selected from each tank in each group, 4 h after feeding, totaling four fish per group. The fish were anesthetized with 40 mg/L MS-222 (Sigma-Aldrich, Beijing, China) and then dissected on a clean ice surface for sampling. Intestinal contents were carefully extruded from the foregut to the hindgut using sterile forceps, thoroughly mixed in sterile culture dishes, and transferred into a 1.5 mL sterile centrifuge tube, with each fish serving as an independent sample. The samples were flash-frozen in liquid nitrogen and then stored at −80 °C for microbiome analysis.

2.2. DNA Extraction and Bacterial 16S rRNA Gene Sequencing

The total bacterial DNA from the intestinal content samples was isolated with the HiPure Stool DNA Kit (Magen Biotech Inc., Guangzhou, China) following the provided protocol. The DNA concentration and quality were assessed using a NanoDrop™ 2000 spectrophotometer (NanoDrop Technologies, LLC, Wilmington, DE, USA). All DNA samples met the required standards for PCR amplification. The amplification of the V3-V4 region of the 16S rRNA gene was conducted using the primers 338F (5′-ACTCCTACGGGAGGCAG CA-3′) and 806R (5′-GGACTACHVGGGTWTCTAAT-3′). PCR was performed with a 30 μL reaction mixture comprising 15 μL of 2× Gflex Buffer, 2 μL of dNTPs (2.5 mM), 1 μL each of the forward and reverse primers (5 μM), 0.6 μL of Tks Gflex™ DNA Polymerase (1.25 U/μL), and 50 ng of the DNA template. The amplification was executed on an ABI GeneAmp® 9700 (ABI, Carlsbad, CA, USA) with the following thermal profile: initial denaturation at 94 °C for 5 min, followed by 26 cycles of denaturation at 94 °C for 30 s, annealing at 56 °C for 30 s, and extension at 72 °C for 20 s, ending with a final extension at 72 °C for 5 min. Three independent PCR reactions were conducted for each sample. The quality of the PCR products was evaluated using agarose gel electrophoresis. PCR products that were successful were purified with magnetic beads. The purified PCR products served as templates for a second round of amplification. The second PCR round employed the same reaction mix and conditions as the first, but with only seven cycles. After the second round of PCR, the products were re-evaluated using agarose gel electrophoresis and purified again with magnetic beads. The concentration of the purified products was measured with a Qubit 2.0 fluorometer (Life Technologies, Carlsbad, CA, USA). The samples were combined in equimolar amounts according to the quantified concentrations of the PCR products. The combined samples were subsequently sequenced using the NovaSeq 6000 platform (Illumina, Inc., San Diego, CA, USA).

2.3. Processing of Illumina Sequencing Data

Raw 16S rRNA amplicon sequences were analyzed using QIIME2 (2020.11) [16]. The DADA2 pipeline was employed for denoising, which produced a table of amplicon sequence variants (ASVs) [17]. Representative sequences for each ASV were chosen using the

default settings and taxonomically assigned via the SILVA 138 database [18]. For consistency across samples, the ASV abundance table was rarefied to the lowest sequence depth of 65,708.

2.4. Statistical Analyses

The survival curve was plotted using GraphPad Prism 8 (GraphPad Software Inc., San Diego, CA, USA) software. Taxonomic compositions of microbiota were determined using the QIIME command "*summarize_taxa_through_plots.py*". Alpha diversity was assessed using the species richness index (observed species), which was calculated with "*alpha_diversity.py*" and "*collate_alpha.py*". Beta diversity was assessed using Bray–Curtis distance metrics, which were calculated with the command "*beta_diversity.py*". Principal Coordinates Analysis (PCoA) based on the Bray–Curtis distance was used to visualize differences in the microbiota composition among groups. Clustering analysis of the microbiota composition among groups based on the Bray–Curtis distance was performed using the unweighted pair-group method with the arithmetic mean (UPGMA) from the R package "phangorn". Microbiota structure differences were assessed using ADONIS (Permutational Multivariate Analysis of Variance, PERMANOVA) from the R package "vegan". One-way Analysis of Variance (ANOVA) was performed using the R function "aov", followed by Tukey's post hoc test from the "multcomp" package. Relative abundance differences were analyzed using Linear Discriminant Analysis (LDA) Effect Size (LEfSe) (LDA score > 3.0) on the Galaxy tool (Galaxy server 2.0; http://galaxy.biobakery.org/; accessed: 22 August 2024) [19]. ASVs with a relative abundance greater than 1% in at least one sample were selected, and the Spearman correlation coefficients between all ASV pairs were calculated. Pairs with $R > 0.6$ and $p < 0.05$ were retained to construct a co-occurrence network. Spearman correlations were calculated using the R package "Hmisc". The co-occurrence network was visualized by Gephi 0.10 [20]. Based on the network analysis results, ASVs that rank in the top five for all of the following metrics—relative abundance, degree, closeness centrality, harmonic closeness centrality, betweenness centrality, authority, hub, pagerank, and eigencentrality—are defined as the "keystone" of the network. Data visualizations were created using the R package "ggplot2".

3. Results

3.1. Survival Status Under Different Temperatures

High-temperature stress caused a large number of deaths in *Huso dauricus*, with the mortality rate increasing as the temperature rose (Figure 1A). The cumulative mortality over 53 days at 19 °C, 25 °C, 28 °C, and 31 °C was 0.42%, 41.6%, 45.8%, and 62.5%, respectively. Notably, all the deaths occurred during the early stages of high-temperature stress and became more rapid as the temperature increased. Rapid mortality at 25 °C, 28 °C, and 31 °C was concentrated within the first 43 days, 25 days, and 10 days, respectively.

3.2. Diversity of Intestinal Microbiota Under Different Temperatures

The diversity of intestinal microbiota in *Huso dauricus* showed significant differences under different temperatures (Figure 1B–D). On day 11, the species richness index at 31 °C was significantly higher than that at 19 °C and 25 °C ($p < 0.05$). However, after day 26, no significant differences in the species richness index were found across temperatures ($p > 0.05$). The species richness index of intestinal microbiota decreased over time at 28 °C and 31 °C, while it remained stable at 19 °C and 25 °C (Figure 1B). UPGMA clustering analysis, PCoA, and ADONIS results all showed that on day 11, there were no significant differences in the intestinal microbiota structure among the different temperatures ($p > 0.05$). However, starting on day 26, the differences in the intestinal microbiota structure among the temperatures gradually increased, reaching a significant level by day 53 ($p < 0.05$). At 19 °C, the intestinal microbiota structure did not change significantly over time, whereas at 25 °C, 28 °C, and 31 °C, the intestinal microbiota structure changed significantly after day 26 ($p < 0.05$, Figure 1C,D, Table S1). Additionally, the within-group similarity of the

intestinal microbiota structure under high-temperature stress showed a trend of initially decreasing (0–11 days) and then increasing (11–53 days) (Figure 1D,E).

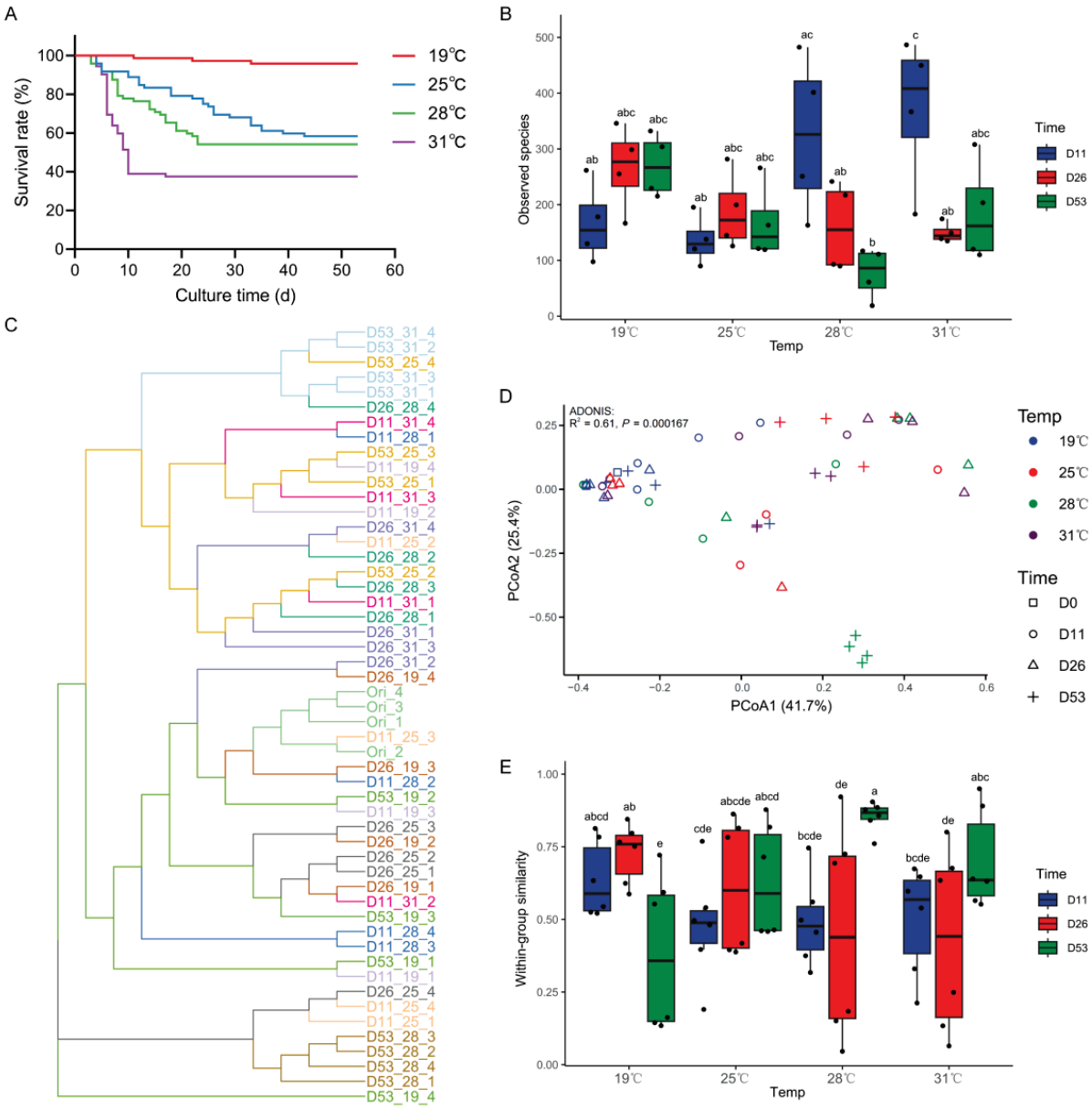


Figure 1. (**A**) Survival curve, (**B**) species richness index (observed species) of intestinal microbiota, (**C**) UPGMA clustering of intestinal microbiota based on the Bray–Curtis distance, (**D**) PCoA of intestinal microbiota based on the Bray–Curtis distance, (**E**) within-group similarities of intestinal microbiota based on the Bray–Curtis distance under different temperatures and times in *Huso dauricus*. Different letters indicate significant difference ($p < 0.05$). Dx_y_z represents the z-th fish on day x under temperature y.

3.3. Dominant Bacterial Composition of Intestinal Microbiota Under Different Temperatures

The composition of the intestinal microbiota in *Huso dauricus* showed significant differences under different temperatures (Figure 2). At the phylum level, the dominant bacterial phyla in the intestines across the different temperatures were similar: on day 11, Proteobacteria and Firmicutes were the dominant phyla at both 19 °C and 31 °C, while Proteobacteria, Firmicutes, and Fusobacteriota were dominant at 25 °C and 28 °C. On day 26, Proteobacteria was the dominant phylum in the intestines at both 19 °C and 25 °C, while at 28 °C and 31 °C, Proteobacteria and Firmicutes were dominant. On day 53, the

dominant phyla at 19 °C, 25 °C, and 31 °C were Proteobacteria and Firmicutes, whereas Fusobacteriota was dominant at 28 °C. At the genus level, the differences in the dominant bacterial genera across temperatures were more pronounced: on day 11, the dominant genera at 19 °C and 31 °C were *Sphingomonas* and *Clostridium sensu stricto 1*, while at 25 °C, *Sphingomonas*, *Clostridium sensu stricto 1*, and *Cetobacterium* were dominant, and at 28 °C, *Sphingomonas* was dominant. On day 26, *Sphingomonas* was the dominant genus at both 19 °C and 25 °C, while at 28 °C and 31 °C, *Sphingomonas* and *Clostridium sensu stricto 1* were dominant. On day 53, the dominant genera showed distinct differences across temperatures: *Sphingomonas* was dominant at 19 °C, *Sphingomonas* and *Clostridium sensu stricto 1* were dominant at 25° C, *Cetobacterium* was dominant at 28 °C, and *Sphingomonas* and *Plesiomonas* were dominant at 31 °C.

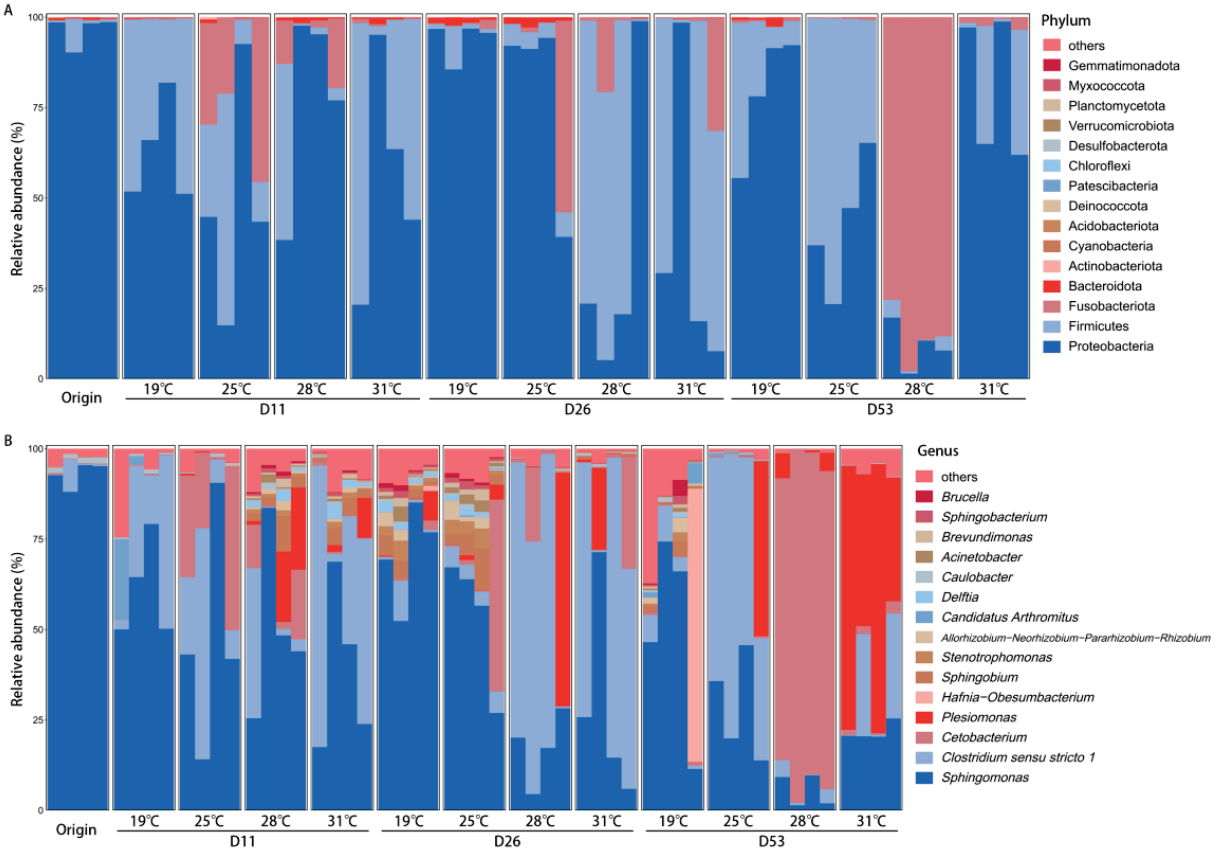


Figure 2. Dominant bacterial composition of intestinal microbiota under different temperatures and times in *Huso dauricus* (top 15 relative abundances): (**A**) phylum level; (**B**) genus level. Dx represents day x.

3.4. Differential Bacterial Composition of Intestinal Microbiota Under Different Temperatures

The differential intestinal bacteria on day 53 under different temperatures were selected based on LefSE (Figures 3 and S1). A total of 30 bacterial genera showed significant differences ($p < 0.05$). Among them, the largest number of differential genera were observed at 19 °C, with 26 genera, primarily belonging to Proteobacteria, Firmicutes, and Bacteroidota. At 25 °C, *Clostridium sensu stricto 1* was the dominant genus (relative abundance 33.8–78.6%). At 28 °C, the dominant genus was *Cetobacterium* (78.0–97.9%). At 31 °C, two dominant genera were identified: *Plesiomonas* (34.3–74.4%) and *Serratia* (0.3–0.5%).

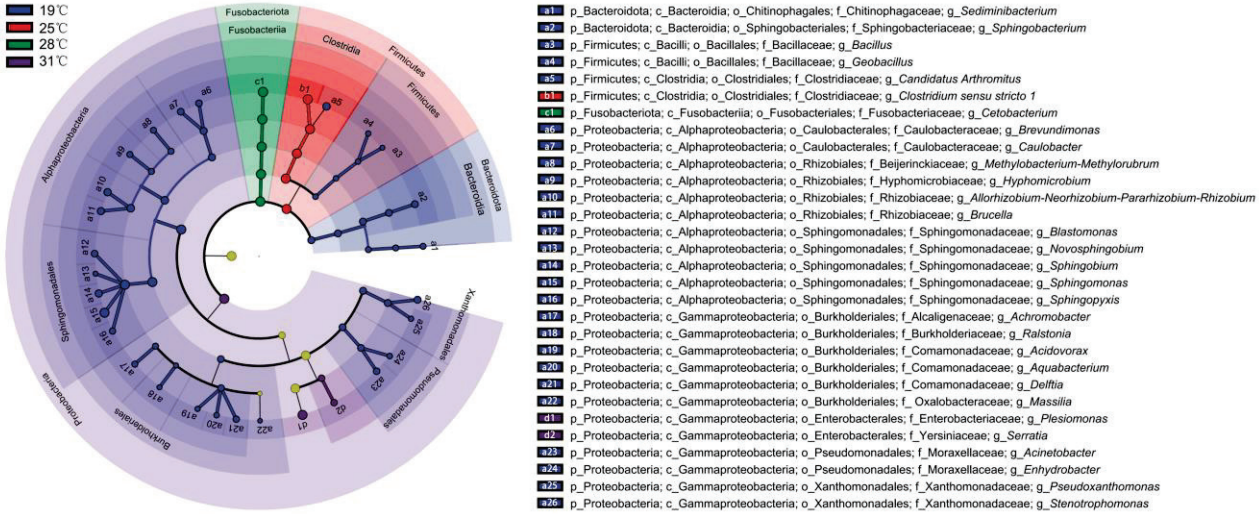


Figure 3. LefSE of the intestinal microbiota in *Huso dauricus* on day 53 under different temperatures at the genus level with an LDA score > 3.

3.5. Relationship Between Intestinal Microbiota and High-Temperature Adaptability

Huso dauricus showed adaptation to high-temperature stress, as no further mortality occurred after a period of time (Figure 1A). Meanwhile, the intestinal microbiota at the time when rapid mortality ceased (D11_31, D26_28, D53_25) under different high temperatures showed a highly similar structure and composition (Figure 1C,D, Figure 2). A Venn diagram was used to identify the shared bacteria, revealing 28 shared ASVs and 136 non-shared ASVs (Figure S2). These shared ASVs primarily belong to *Clostridium sensu stricto 1*, *Cetobacterium*, *Sphingomonas*, and *Plesiomonas* (Figure 4). Among them, ASV2 of *Clostridium sensu stricto 1* exhibited a higher relative abundance during days 11–53 at 31 °C, days 26–53 at 28 °C, and day 53 at 25 °C, which corresponds to the period when *Huso dauricus* adapted to high temperatures.

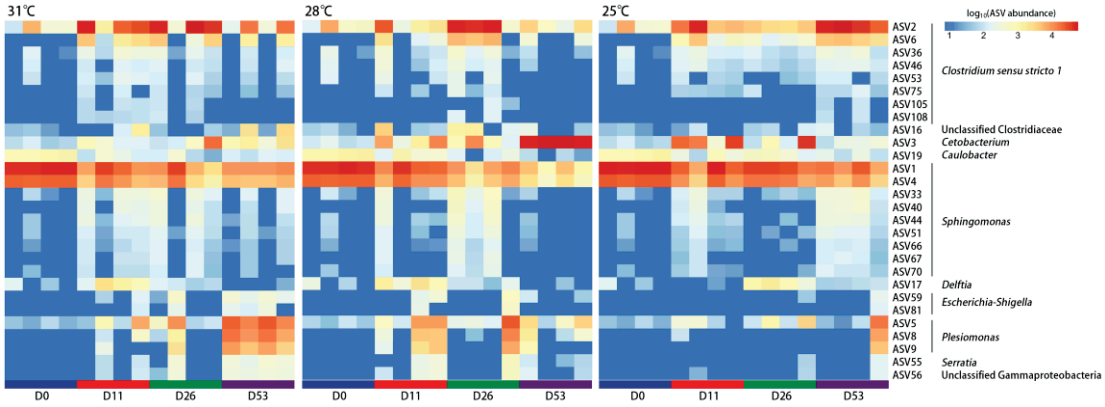


Figure 4. Heatmap of shared ASVs (D11_31, D26_28, D53_25) in the intestinal microbiota of *Huso dauricus* under different temperatures and times.

The interactions among intestinal bacteria were inferred based on co-occurrence network analysis (Figure 5). The results showed that the shared ASVs were primarily clustered in the same module (Module 4), with close interactions observed among them. Additionally, network topological parameters such as the degree, closeness centrality, harmonic closeness centrality, and betweenness centrality all indicated that ASV2 is a crucial central node, serving as the "keystone" of the co-occurrence network (Figure 5, Table S2).

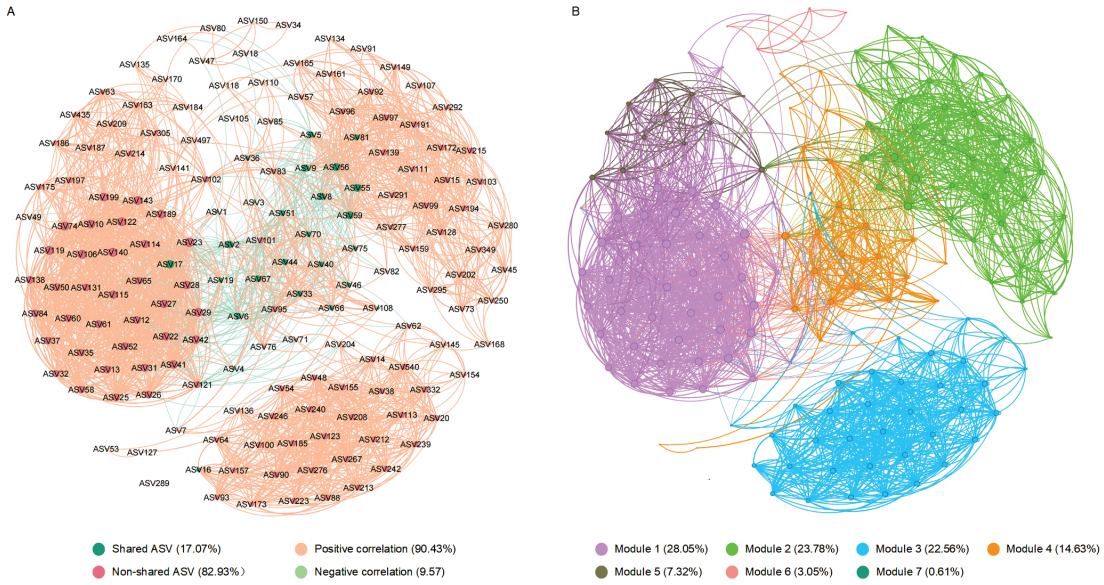


Figure 5. Co-occurrence networks of the intestinal microbiota in *Huso dauricus* (D11_31, D26_28, D53_25, relative abundance > 0.1% at least in one sample). The nodes are colored based on whether they are shared ASVs (**A**) and modules (**B**), respectively. The size of each node is proportional to the degree.

4. Discussion

4.1. Different Temperatures Shape Intestinal Microbiota with Distinct Characteristics

The plasticity of the intestinal microbiota is an important factor determining the phenotypic plasticity of vertebrates, playing a significant role in their adaptation to and response to rapid environmental changes [10,21]. This study investigated the dynamics of the intestinal microbiota in *Huso dauricus* under different temperatures over time. The results showed that different temperatures shaped intestinal microbiota with distinct characteristics. Under high-temperature stress, the species richness index of the intestinal microbiota significantly increased, first rising and then decreasing over time. This may be due to the disruption of the microbiota balance caused by temperature changes, leading to a transient increase in certain bacteria, thereby increasing the species richness index. As time progressed, the intestinal microbiota gradually adapted and became stable, leading to a decrease in the species richness index and a return to normal levels [22]. This may also explain why variations in α-diversity have been observed in different studies, with some showing an increase [3] while others report a decrease [4,9]. Such discrepancies are likely due to differences in sampling time points, as different periods may reflect distinct stages in the response of the intestinal microbiota to high-temperature stress. It was also observed that the structure of the intestinal microbiota remained relatively stable over time under normal temperature conditions, whereas significant changes were noted under high-temperature stress. Additionally, the differences in the microbiota structure over time became increasingly significant under different temperature conditions, with a gradual reduction in intra-group variation. These results suggest that high temperatures induce changes in the intestinal microbiota and that different temperatures shape distinct microbiota structures. These findings are consistent with those of Zhang et al. [21] on *Cyprinus carpio* and Hassenrück et al. [23] on *Chanos chanos*. In addition, the same pattern has also been observed in studies of other species, such as *Xenopus tropicalis* [24] and *Anas platyrhynchos* [25].

In this study, notable differences were found in the dominant bacterial compositions under different temperature conditions, and these differences became more pronounced over time. Under high temperatures, the relative abundance of *Sphingomonas* decreased significantly, while the relative abundance of *Clostridium sensu stricto 1*, *Cetobacterium*,

and *Plesiomonas* increased significantly. *Sphingomonas* is one of the core microbiota in the intestine of sturgeon [26], playing a crucial role in maintaining fish health [27]. High-temperature stress disrupts the original microbial balance, leading to a decrease in the abundance of certain indigenous bacteria [28]. *Clostridium sensu stricto 1* is also a core microbiota of sturgeon [29], involved in the breakdown of carbohydrates and proteins and exhibiting probiotic functions that promote host digestion [30]. Under high-temperature stress, fish experience increased energy expenditure [31], and the high relative abundance of *Clostridium sensu stricto 1* may be key to maintaining the energy metabolism balance in fish. *Cetobacterium* is known to play an important role in carbohydrate degradation and is commonly found in the intestines of herbivorous and omnivorous fish species [32,33]. It has been shown to effectively improve intestinal health and enhance disease resistance in fish [34,35]. The high relative abundance of *Cetobacterium* may be a crucial factor in maintaining fish survival under high-temperature stress. *Plesiomonas* is also one of the core microbiota of sturgeon [36] and is typically considered an opportunistic pathogen [37], which may partially explain why the mortality rate of sturgeon is highest at 31 °C. In summary, through the study of dynamic changes in the intestinal microbiota under different temperature conditions, it has been demonstrated that the intestinal microbiota of *Huso dauricus* is highly plastic, and this plasticity likely plays a vital role in adapting to environmental changes.

4.2. Specific Intestinal Bacterial Taxa Are Associated with the Development of High-Temperature Adaptation

The intestinal microbiota is closely related to the environmental adaptability of its host, with the presence of specific bacteria playing a critical role [22]. Studies on *Penaeus vannamei* [38] and *Drosophila melanogaster* [39] have demonstrated that specific intestinal bacteria can influence environmental adaptability in the host. In this study, the intestinal microbiota structure and composition of *Huso dauricus* under different high-temperature stresses showed striking similarity when rapid mortality ceased, with *Clostridium sensu stricto 1* dominating both in terms of composition and relative abundance. *Clostridium sensu stricto 1* is known to possess digestive-promoting functions [30], and its increased abundance may help *Huso dauricus* compensate for energy deficits under high-temperature stress, ensuring survival under conditions of increased energy demand. A study on mice also confirmed that *Clostridium* can enhance energy absorption and promote fat generation in the host [40]. Co-occurrence network analysis provides a comprehensive perspective for studying the interactions among intestinal bacteria in aquatic animals [41,42]. In this study, the microbial co-occurrence network of *Huso dauricus* under high-temperature stress was divided into seven modules, with shared ASVs primarily clustering in the same module. Bacteria within the same module are often more closely related in terms of survival or function [43], suggesting that the shared ASVs may jointly contribute to the adaptation process of high temperatures. Furthermore, both the heatmap and network topological parameters indicated that ASV2 of *Clostridium sensu stricto 1* is the "keystone" of the intestinal microbiota under high-temperature stress, and changes in its abundance may directly influence the high-temperature adaptability. This finding was also confirmed in two studies on pigs, where hosts with a higher abundance of *Clostridium sensu stricto 1* in the intestine exhibited better high-temperature adaptability [44,45]. In summary, this study preliminarily confirms that the high-temperature adaptability of *Huso dauricus* is closely related to the structure and composition of its intestinal microbiota, with bacteria such as *Clostridium sensu stricto 1* playing an important role. In the future, the abundance of *Clostridium sensu stricto 1* in the intestine could be increased through microbiota modulation techniques, thereby enhancing the adaptability of the fish to high-temperature stress. This approach could ultimately lead to more sustainable and efficient aquaculture practices, ensuring fish welfare and optimizing production in the face of climate change challenges.

5. Conclusions

This study demonstrates that temperature variation can reshape the structure and composition of the intestinal microbiota in *Huso dauricus*, with distinct characteristics of the microbiota formed under different temperature conditions. The intestinal microbiota is closely associated with the development of high-temperature adaptation in *Huso dauricus*, with intestinal bacteria, primarily *Clostridium sensu stricto 1*, playing a key role. These findings provide new insights into the mechanisms underlying the development of high-temperature adaptation in *Huso dauricus* and offer a theoretical basis for the use of microbiota-based intervention strategies to enhance high-temperature adaptability in fish.

Supplementary Materials: The following supporting information can be downloaded at: https://www.mdpi.com/article/10.3390/biology13121045/s1, Figure S1: LDA scores distribution of the intestinal microbiota in *Huso dauricus* on day 53 under different temperatures at the genus level with an LDA score > 3; Figure S2: Venn diagram at the ASV level of intestinal microbiota in *Huso dauricus* for D11_31, D26_28, and D53_25; Table S1: ADONIS of intestinal microbiota in *Huso dauricus* under different temperatures and times based on Bray–Curtis distance; Table S2: Co-occurrence network topological parameters of shared ASVs (D11_31, D26_28, D53_25).

Author Contributions: Conceptualization, Y.Z. (Ying Zhang) and B.M.; Methodology, Y.L. and N.W.; Validation, Y.L. and S.W.; Formal analysis, R.W. and Z.H.; Investigation, Y.L., Y.Z. (Yining Zhang) and S.W.; Resources, D.C. and Z.S.; Data curation, Y.Z. (Yining Zhang); Writing—original draft, R.W.; Writing—review and editing, Y.Z. (Ying Zhang) and B.M.; Visualization, R.W. and Y.Z. (Yining Zhang); Funding acquisition, R.W., Y.Z. (Ying Zhang) and B.M. All authors have read and agreed to the published version of the manuscript.

Funding: This research was funded by the earmarked fund for CARS-46, the Central Public-interest Scientific Institution Basal Research Fund, HRFRI (HSY202302YB), the Central Public-interest Scientific Institution Basal Research Fund, CAFS (2023TD59 and 2023TD07), and the Agricultural Finance Special Project of the Ministry of Agriculture and Rural Affairs, "Regularized monitoring of Fisheries Resources and Environment in Key Waters in Northeast China".

Institutional Review Board Statement: The animal experiment was performed according to the Guidelines for the Feeding and Application of Laboratory Animals of Heilongjiang Fisheries Research Institute, Chinese Academy of Fishery Sciences and was approved by the Committee on the Ethics of Animal Experiments of Heilongjiang Fisheries Research Institute, Chinese Academy Fishery Sciences (20230728-003). The study was conducted in accordance with the local legislation and institutional requirements.

Informed Consent Statement: Not applicable.

Data Availability Statement: All raw sequencing data have been deposited in the Genome Sequence Archive at the National Genomics Data Center (https://bigd.big.ac.cn/gsa; accessed: 28 August 2024), Beijing Institute of Genomics (China National Center for Bioinformation), Chinese Academy of Sciences, with the accession number CRA020801.

Conflicts of Interest: The authors declare that there are no conflicts of interest associated with this article.

References

1. Alfonso, S.; Gesto, M.; Sadoul, B. Temperature increase and its effects on fish stress physiology in the context of global warming. *J. Fish Biol.* **2021**, *98*, 1496–1508. [CrossRef]
2. Chen, Y.; Wu, X.; Lai, J.; Liu, Y.; Song, M.; Li, F.; Gong, Q. Integrated biochemical, transcriptomic and metabolomic analyses provide insight into heat stress response in Yangtze sturgeon (*Acipenser dabryanus*). *Ecotoxicol. Environ. Saf.* **2022**, *249*, 114366. [CrossRef] [PubMed]
3. Yang, S.; Zhang, C.; Xu, W.; Li, D.; Feng, Y.; Wu, J.; Luo, W.; Du, X.; Du, Z.; Huang, X. Heat stress decreases intestinal physiological function and facilitates the proliferation of harmful intestinal microbiota in sturgeons. *Front. Microbiol.* **2022**, *13*, 755369. [CrossRef] [PubMed]
4. Zhou, C.; Yang, S.; Ka, W.; Gao, P.; Li, Y.; Long, R.; Wang, J. Association of gut microbiota with metabolism in rainbow trout under acute heat stress. *Front. Microbiol.* **2022**, *13*, 846336. [CrossRef] [PubMed]

5. Visconti, A.; Le Roy, C.I.; Rosa, F.; Rossi, N.; Martin, T.C.; Mohney, R.P.; Li, W.; de Rinaldis, E.; Bell, J.T.; Venter, J.C. Interplay between the human gut microbiome and host metabolism. *Nat. Commun.* **2019**, *10*, 4505. [CrossRef]
6. Luan, Y.; Li, M.; Zhou, W.; Yao, Y.; Yang, Y.; Zhang, Z.; Ringø, E.; Olsen, R.E.; Clarke, J.L.; Xie, S. The fish microbiota: Research progress and potential applications. *Engineering* **2023**, *29*, 137–146. [CrossRef]
7. Ou, W.; Yu, G.; Zhang, Y.; Mai, K. Recent progress in the understanding of the gut microbiota of marine fishes. *Mar. Life Sci. Technol.* **2021**, *3*, 434–448. [CrossRef] [PubMed]
8. Zhao, C.; Wang, J.; Ren, W.; Zheng, S.; Ren, Y. Histological, immune, and intestine microbiota responses of the intestine of rainbow trout (*Oncorhynchus mykiss*) to high temperature stress. *Aquaculture* **2024**, *582*, 740465. [CrossRef]
9. Kim, J.A.; Park, Y.; Kim, J.; Choi, C.Y. Impact of water temperature on oxidative stress and intestinal microbiota in pearl-spot chromis, *Chromis notata* (Temminck & Schlegel, 1843). *Comp. Biochem. Physiol. Part B Biochem. Mol. Biol.* **2025**, *275*, 111029.
10. Alberdi, A.; Aizpurua, O.; Bohmann, K.; Zepeda-Mendoza, M.L.; Gilbert, M.T.P. Do vertebrate gut metagenomes confer rapid ecological adaptation? *Trends Ecol. Evol.* **2016**, *31*, 689–699. [CrossRef] [PubMed]
11. Macke, E.; Tasiemski, A.; Massol, F.; Callens, M.; Decaestecker, E. Life history and eco-evolutionary dynamics in light of the gut microbiota. *Oikos* **2017**, *126*, 508–531. [CrossRef]
12. Khakisahneh, S.; Zhang, X.; Nouri, Z.; Wang, D. Gut microbiota and host thermoregulation in response to ambient temperature fluctuations. *Msystems* **2020**, *5*, 10–1128. [CrossRef] [PubMed]
13. Freitas, C.; Villegas-Ríos, D.; Moland, E.; Olsen, E.M. Sea temperature effects on depth use and habitat selection in a marine fish community. *J. Anim. Ecol.* **2021**, *90*, 1787–1800. [CrossRef] [PubMed]
14. Zhu, T.; Li, X.; Wu, X.; Yang, D. Temperature acclimation alters the thermal tolerance and intestinal heat stress response in a Tibetan fish *Oxygymnocypris Stewarti*. *Front. Microbiol.* **2022**, *13*, 898145. [CrossRef]
15. Moeller, A.H.; Ivey, K.; Cornwall, M.B.; Herr, K.; Rede, J.; Taylor, E.N.; Gunderson, A.R. The lizard gut microbiome changes with temperature and is associated with heat tolerance. *Appl. Environ. Microbiol.* **2020**, *86*, e01181-20. [CrossRef] [PubMed]
16. Bolyen, E.; Rideout, J.R.; Dillon, M.R.; Bokulich, N.A.; Abnet, C.C.; Al-Ghalith, G.A.; Alexander, H.; Alm, E.J.; Arumugam, M.; Asnicar, F. Reproducible, interactive, scalable and extensible microbiome data science using QIIME 2. *Nat. Biotechnol.* **2019**, *37*, 852–857. [CrossRef]
17. Callahan, B.J.; McMurdie, P.J.; Rosen, M.J.; Han, A.W.; Johnson, A.J.A.; Holmes, S.P. DADA2: High-resolution sample inference from Illumina amplicon data. *Nat. Methods* **2016**, *13*, 581–583. [CrossRef]
18. Quast, C.; Pruesse, E.; Yilmaz, P.; Gerken, J.; Schweer, T.; Yarza, P.; Peplies, J.; Glöckner, F.O. The SILVA ribosomal RNA gene database project: Improved data processing and web-based tools. *Nucleic Acids Res.* **2012**, *41*, D590–D596. [CrossRef]
19. Segata, N.; Izard, J.; Waldron, L.; Gevers, D.; Miropolsky, L.; Garrett, W.S.; Huttenhower, C. Metagenomic biomarker discovery and explanation. *Genome Biol.* **2011**, *12*, R60. [CrossRef] [PubMed]
20. Bastian, M.; Heymann, S.; Jacomy, M. Gephi: An open source software for exploring and manipulating networks. In Proceedings of the International Aaai Conference on Web and Social Media, San Jose, CA, USA, 17–20 May 2009; pp. 361–362.
21. Zhang, L.; Yang, Z.; Yang, F.; Wang, G.; Zeng, M.; Zhang, Z.; Yang, M.; Wang, Z.; Li, Z. Gut microbiota of two invasive fishes respond differently to temperature. *Front. Microbiol.* **2023**, *14*, 1087777. [CrossRef]
22. Sepulveda, J.; Moeller, A.H. The effects of temperature on animal gut microbiomes. *Front. Microbiol.* **2020**, *11*, 384. [CrossRef] [PubMed]
23. Hassenrück, C.; Reinwald, H.; Kunzmann, A.; Tiedemann, I.; Gärdes, A. Effects of thermal stress on the gut microbiome of juvenile milkfish (*Chanos chanos*). *Microorganisms* **2020**, *9*, 5. [CrossRef] [PubMed]
24. Tian, Y.; Li, G.; Chen, L.; Bu, X.; Shen, J.; Tao, Z.; Zeng, T.; Du, X.; Lu, L. High-temperature exposure alters the community structure and functional features of the intestinal microbiota in Shaoxing ducks (*Anas platyrhynchos*). *Poult. Sci.* **2020**, *99*, 2662–2674. [CrossRef]
25. Li, J.; Rui, J.; Li, Y.; Tang, N.; Zhan, S.; Jiang, J.; Li, X. Ambient temperature alters body size and gut microbiota of *Xenopus tropicalis*. *Sci. China Life Sci.* **2020**, *63*, 915–925. [CrossRef] [PubMed]
26. Yang, S.; Xu, W.; Feng, L.; Zhang, C.; Yan, C.; Zhang, J.; Lai, J.; Yan, T.; He, Z.; Du, X. Resveratrol improves the digestive ability and the intestinal health of Siberian sturgeon. *Int. J. Mol. Sci.* **2022**, *23*, 11977. [CrossRef] [PubMed]
27. Legrand, T.P.; Wynne, J.W.; Weyrich, L.S.; Oxley, A.P. A microbial sea of possibilities: Current knowledge and prospects for an improved understanding of the fish microbiome. *Rev. Aquac.* **2020**, *12*, 1101–1134. [CrossRef]
28. Yu, J.; Zhong, D.; Li, S.; Zhang, Z.; Mo, H.; Wang, L. Acute temperature stresses trigger liver transcriptome and microbial community remodeling in largemouth bass (*Micropterus salmoides*). *Aquaculture* **2023**, *573*, 739573. [CrossRef]
29. Abdul Razak, S.; Bauman, J.M.; Marsh, T.L.; Scribner, K.T. Changes in lake sturgeon gut microbiomes relative to founding origin and in response to chemotherapeutant treatments. *Microorganisms* **2022**, *10*, 1005. [CrossRef] [PubMed]
30. Wüst, P.K.; Horn, M.A.; Drake, H.L. Clostridiaceae and Enterobacteriaceae as active fermenters in earthworm gut content. *Isme J.* **2011**, *5*, 92–106. [CrossRef]
31. Ma, S.; Lv, Y.; Hou, L.; Jia, Z.; Lin, S.; Wang, S.; He, X.; Hou, J. Effect of acute temperature stress on energy metabolism, immune performance and gut microbiome of largemouth bass (*Micropterus salmoides*). *Aquac. Fish.* 2023; *in press*. [CrossRef]
32. Di Maiuta, N.; Schwarzentruber, P.; Schenker, M.; Schoelkopf, J. Microbial population dynamics in the faeces of wood-eating loricariid catfishes. *Lett. Appl. Microbiol.* **2013**, *56*, 401–407. [CrossRef]

33. van Kessel, M.A.; Dutilh, B.E.; Neveling, K.; Kwint, M.P.; Veltman, J.A.; Flik, G.; Jetten, M.S.; Klaren, P.H.; Op den Camp, H.J. Pyrosequencing of 16S rRNA gene amplicons to study the microbiota in the gastrointestinal tract of carp (*Cyprinus carpio* L.). *Amb Express* **2011**, *1*, 41. [CrossRef]
34. Xie, M.; Xie, Y.; Li, Y.; Zhou, W.; Zhang, Z.; Yang, Y.; Olsen, R.E.; Ringø, E.; Ran, C.; Zhou, Z. Stabilized fermentation product of *Cetobacterium somerae* improves gut and liver health and antiviral immunity of zebrafish. *Fish Shellfish Immunol.* **2022**, *120*, 56–66. [CrossRef] [PubMed]
35. Tran, N.T.; Li, Z.; Wang, S.; Zheng, H.; Aweya, J.J.; Wen, X.; Li, S. Progress and perspectives of short-chain fatty acids in aquaculture. *Rev. Aquac.* **2020**, *12*, 283–298. [CrossRef]
36. Pérez, T.; Alba, C.; Aparicio, M.; de Andrés, J.; Santa Quiteria, J.A.R.; Rodríguez, J.M.; Gibello, A. Abundant bacteria in the proximal and distal intestine of healthy Siberian sturgeons (*Acipenser baerii*). *Aquaculture* **2019**, *506*, 325–336. [CrossRef]
37. Deng, D.; Mu, Z.; Lv, X.; Jiang, X.; Zhou, J.; Guo, H.; Zhang, W.; Wang, B.; Lu, Y.; Wu, J. Pathogenicity of *Plesiomonas shigelloides* and *Citrobacter freundii* isolated from the endangered Chinese sturgeon (*Acipenser sinensis*). *Microb. Pathog.* **2022**, *173*, 105818. [CrossRef]
38. Guo, H.; Fu, X.; He, J.; Wang, R.; Yan, M.; Wang, J.; Dong, P.; Huang, L.; Zhang, D. Gut bacterial consortium enriched in a biofloc system protects shrimp against *Vibrio parahaemolyticus* infection. *Microbiome* **2023**, *11*, 230. [CrossRef] [PubMed]
39. Gould, A.L.; Zhang, V.; Lamberti, L.; Jones, E.W.; Obadia, B.; Korasidis, N.; Gavryushkin, A.; Carlson, J.M.; Beerenwinkel, N.; Ludington, W.B. Microbiome interactions shape host fitness. *Proc. Natl. Acad. Sci. USA* **2018**, *115*, E11951–E11960. [CrossRef] [PubMed]
40. Du, L.; Wang, J.; Qiu, X.; Wang, Q.; Peng, H.; Huang, J.; Yang, F.; Liu, Z.; Qi, R. *Clostridium sporogenes* increases fat accumulation in mice by enhancing energy absorption and adipogenesis. *Microbiol. Spectr.* **2024**, *12*, e04116-23. [CrossRef] [PubMed]
41. Wang, R.; Chen, H.; Zhu, Y.; Al-Masqari, Z.A.; Yan, M.; Wang, G.; Dong, P.; Gao, F.; Lu, T.; Zhang, D. Survival status of *Penaeus vannamei* is associated with the homeostasis and assembly process of the intestinal bacterial community. *Aquaculture* **2022**, *558*, 738398. [CrossRef]
42. Liu, G.; Verdegem, M.; Ye, Z.; Liu, Y.; Zhao, J.; Zhu, S. Co-occurrence patterns in biofloc microbial communities revealed by network analysis and their impact on the host. *Aquaculture* **2023**, *577*, 739964. [CrossRef]
43. Borthagaray, A.I.; Arim, M.; Marquet, P.A. Inferring species roles in metacommunity structure from species co-occurrence networks. *Proc. R. Soc. B Biol. Sci.* **2014**, *281*, 20141425. [CrossRef] [PubMed]
44. Le Sciellour, M.; Zemb, O.; Hochu, I.; Riquet, J.; Gilbert, H.; Giorgi, M.; Billon, Y.; Gourdine, J.; Renaudeau, D. Effect of chronic and acute heat challenges on fecal microbiota composition, production, and thermoregulation traits in growing pigs. *J. Anim. Sci.* **2019**, *97*, 3845–3858. [CrossRef] [PubMed]
45. Labussière, E.; Achard, C.; Dubois, S.; Combes, S.; Castex, M.; Renaudeau, D. *Saccharomyces cerevisiae boulardii* CNCM I-1079 supplementation in finishing male pigs helps to cope with heat stress through feeding behaviour and gut microbiota modulation. *Br. J. Nutr.* **2022**, *127*, 353–368. [CrossRef] [PubMed]

Disclaimer/Publisher's Note: The statements, opinions and data contained in all publications are solely those of the individual author(s) and contributor(s) and not of MDPI and/or the editor(s). MDPI and/or the editor(s) disclaim responsibility for any injury to people or property resulting from any ideas, methods, instructions or products referred to in the content.

biology

MDPI

Article

Dietary Methionine Hydroxy Analog Regulates Hepatic Lipid Metabolism via SIRT1/AMPK Signaling Pathways in Largemouth Bass *Micropterus salmodies*

Ju Zhao [1,†], Zhongjie Yang [1,†], Haifeng Liu [1], Chao Yang [1], Yujun Chen [1], Quanquan Cao [1,*] and Jun Jiang [1,2,*]

[1] College of Animal Science and Technology, Sichuan Agricultural University, Chengdu 611130, China; 2024102020@stu.sicau.edu.cn (J.Z.); 2024302171@stu.sicau.edu.cn (Z.Y.); liuhf@sicau.edu.cn (H.L.); 2018302040@stu.sicau.edu.cn (C.Y.); 2024202073@stu.sicau.edu.cn (Y.C.)

[2] Fish Nutrition and Safety Production University Key Laboratory of Sichuan Province, Sichuan Agricultural University, Ya'an 625014, China

* Correspondence: qq2312159@sicau.edu.cn (Q.C.); jjun@sicau.edu.cn (J.J.); Tel.: +86-28-86291010 (J.J.)

† These authors contributed equally to this work.

Simple Summary: MHA serves as a functional and economical Met source. Prior studies show that dietary Met affects fish liver lipid metabolism, but MHA's impact on largemouth bass liver lipid metabolism remains unstudied. Therefore, we investigated whether dietary MHA increased hepatic lipid vacuoles and content. A total of 9.0 g/kg MHA in a diet boosted ACC, FAS, and SCD-1 activities and lipid synthesis gene expressions. It reduced lipid oxidation enzyme activities and related gene expressions, and decreased SIRT1 and AMPK levels. We concluded that MHA promotes lipid accumulation via SIRT1/AMPK in largemouth bass livers.

Abstract: This experiment was arranged to explore the impacts of dietary MHA on liver lipid metabolism in largemouth bass. A total of 480 fish (14.49 ± 0.13 g) were randomly allocated into four groups, each with three replicates. They were then given four different diets containing graded levels of MHA (0.0, 3.0, 6.0, and 9.0 g/kg) for 84 days. The results showed that dietary MHA increased hepatic lipid vacuoles and lipid content ($p < 0.05$). Dietary supplementation with MHA 9.0 g/kg diets increased the activities of acetyl-coA carboxylase (ACC), fatty acid synthase (FAS), and stearoyl-coA desaturase 1 (SCD-1). Dietary MHA up-regulated the mRNA expressions of liver lipid synthesis (ACC, FAS, SCD-1 and SREBP-1c) ($p < 0.05$). Furthermore, compared with the 0.0 g/kg diet group, the group supplemented with 9.0 g/kg MHA in the diet exhibited a significant decrease in the activities of liver lipid-oxidation-related enzymes (acetyl-CoA carboxylase (ACC), fatty acid synthase (FAS), and stearoyl-CoA desaturase 1 (SCD-1), as well as HSL and CPT1) and the gene expressions of ATGL, HSLa, HSLb, CPT1a, and PPARα ($p < 0.05$). Additionally, the mRNA expressions and protein levels of SIRT1 and AMPK in the 9.0 g/kg MHA-supplemented group were significantly lower than those in the 0.0 g/kg diet group ($p < 0.05$). Overall, the present results suggested that dietary MHA could increase lipid accumulation through regulating SIRT1/AMPK signaling pathways in the livers of largemouth bass.

Keywords: methionine hydroxy analog; lipid metabolism; liver; largemouth bass

1. Introduction

2-Hydroxy-4-(methylthio)butanoic acid, a methionine hydroxy analog (MHA), has been utilized more and more frequently in aquaculture feeds as a functional and cost-

effective source of methionine (Met). Previous research conducted in our laboratory has demonstrated that dietary supplementation with MHA can potentially confer benefits in terms of growth, intestinal antioxidant capacity, and the intestinal microbiota of largemouth bass (*Micropterus salmoides*) [1]. The liver is an important organ involved in digestion, metabolism, and detoxification in fish [2–4]. In fish, excessive lipid accumulation in the liver can lead to hepatic damage [5]. A study has shown that a partial restriction of dietary methionine reduces lipid deposition in the livers of mice [6]. Conversely, dietary supplementation with Met has been shown to promote liver lipid accumulation in tiger puffer (*Takifugu rubripes*) and cobia (*Rachycentron canadum*) [5,7]. Nevertheless, the understanding of whether MHA can regulate lipid metabolism in fish remains limited.

Lipid accumulation in the liver is mainly related to lipid synthesis and degradation [8,9]. Sterol regulatory element-binding protein-1c (SREBP-1c) is a membrane-bound transcription factor, which regulates the expression of target genes involved in lipid anabolism, including acetyl-coA carboxylase (ACC), fatty acid synthase (FAS), and stearoyl-coA desaturase 1 (SCD-1) [7,10]. Adipose triglyceride lipase (ATGL) and hormone-sensitive lipase (HSL) play a decisive role in lipid mobilization and are the key enzymes of triglyceride hydrolysis [11]. Peroxisome proliferator activated receptor α (PPARα) is a critical transcriptional regulator, which stimulates the genes involved in mitochondrial fatty acid oxidation, such as aconitase, and carnitine palmitoyl acyl-coA transferase-1 (CPT-1) [12]. Aissa et al. (2014) reported that dietary Met supplementation improved the mRNA expression of SREBP-1 and decreased the mRNA expression of PPARα, which resulted in abnormalities in the lipid metabolism in mice [13]. A study on rainbow trout (*Oncorhynchus mykiss*) demonstrated that a partial Met restriction down-regulated the mRNA expression of FAS and SREBP-1, while up-regulating the PPARα expression [14]. Similarly, in cobia, a dietary Met deficiency suppressed the expression of genes associated with hepatic de novo lipogenesis (FAS, SCD-1, ACC1, SREBP-1) and up-regulated the PPARα expression [7]. The Met up-regulated the mRNA expression of ATGL in both yellow catfish (*Pelteobagrus fulvidraco*) and the HepG2 cells line [15]. In juvenile tiger puffers, high dietary methionine levels significantly enhanced the hepatic mRNA expression of HSL [5]. Furthermore, a Met supplementation markedly increased the hepatic mRNA expression of PPARα in blunt snout bream (*Megalobrama amblycephala*) [16]. These results suggested that Met has a regulatory effect on lipid metabolism. Nevertheless, so far, there is no information available regarding the effect of dietary MHA on lipid metabolism in fish.

Silent information regulator T1 (SIRT1) is a member of the NAD-dependent family of protein deacetylases and plays a crucial role in regulating hepatocyte lipid metabolism by activating AMP-activated protein kinase (AMPK) [17–19]. It has been reported that a partial restriction of dietary Met up-regulated the expression of SIRT1 in the kidneys of mice [20,21]. Related research also reported that when mice were fed with Met dissolved in water, the expression of SIRT1 in the aortic endothelium was repressed [20]. In rainbow trout, a dietary Met deficiency inhibits lipogenesis, probably due to the activation of AMPK [14,22,23]. Met deficiency significantly increases AMPK phosphorylation in the muscle cells of turbot (*Scophthalmus maximus*). However, the knowledge about the effect of MHA on the SIRT1/AMPK signaling pathway remains scarce. Whether the MHA can modulate lipid metabolism through the SIRT1/AMPK signaling pathway in fish remains to be investigated.

Largemouth bass is a freshwater carnivorous fish that is widely farmed in China, with the production of 619,519 tons in 2020 [24]. Our previous study demonstrated that dietary MHA, as a source of Met, promoted growth and modified intestinal microbiota diversity and composition [1]. Based on these findings, we hypothesized that MHA could also influence hepatic lipid metabolism in fish. To test this hypothesis, this study investigated

the impact of MHA on lipid metabolism in the liver of largemouth bass. These results may provide a theoretical foundation for understanding the potential regulatory mechanisms by which MHA affects hepatic lipid metabolism.

2. Materials and Methods

2.1. Experimental Diets, Feeding Trial and Sampling

All experimental procedures used were conducted with the approval of the Animal Care Advisory Committee of Sichuan Agricultural University (Permit NO. DKY-2018202027). This experiment followed the same feeding trial setup and feed formulation as our previous study [1] (Table 1). MHA was added to the experimental diets at levels of 0.0 (control), 3.0, 6.0, and 9.0 g/kg. The Met content measured in the four experimental diets was 8.3, 11.0, 13.6 and 16.3 g/kg of dry diet (Table 2). A total of 480 juvenile largemouth bass of similar sizes (14.49 $\pm$ 0.13 g) were randomly assigned to 12 concrete tanks (2 m $\times$ 1 m $\times$ 1.05 m), with each replicate containing 40 fish. Throughout the feeding trial, the fish were hand-fed daily until they showed signs of apparent satiation at 08:00 and 18:00, following the natural photoperiod. Forty minutes after each feeding session, any uneaten feed was collected, dried, and weighed. These data were then used to calculate the feed intake. The feeding period was 12 weeks. At the end of the growth experiment, fish were starved for 24 h. Afterward, fish were anesthetized with benzocaine solution (50 mg/L). Livers from nine largemouth bass per tank were sampled and quickly frozen in liquid nitrogen, then transferred to -80 °C for the subsequent biochemical analysis, lipid extraction, real-time quantitative PCR, and Western blot assays. Livers from three fish per tank were preserved in 4% paraformaldehyde for histological examination.

Table 1. Composition and nutrient content of diets (g/kg).

Ingredients	Dietary MHA Level			
	0.0	**3.0**	**6.0**	**9.0**
Fish meal	250.0	250.0	250.0	250
Soybean meal	220.0	220.0	220.0	220.0
Corn protein meal	100.0	100.0	100.0	100.0
Gelatin	60.0	60.0	60.0	60.0
Soybean oil	100.0	100.0	100.0	100.0
Wheat flour	165.0	162.0	159.0	156.0
CaH_2PO_4	40.0	40.0	40.0	40.0
Methionine hydroxy analog	0.0	3.0	6.0	9.0
Vitamin premix [1]	10.0	10.0	10.0	10.0
Mineral premix [2]	20.0	20.0	20.0	20.0
Amino acid premix [3]	11.8	11.8	11.8	11.8
Choline chloride (50%)	10.0	10.0	10.0	10.0
Ethoxyquin (30%)	0.5	0.5	0.5	0.5
Microcrystalline cellulose	12.7	12.7	12.7	12.7
Nutrients content [4]				
Crude protein	419.6	417.8	417.7	416.7
Crude lipid	124.6	126.8	127.0	125.2
Crude ash	105.8	106.2	105.7	106.4
Moisture	96.2	94.1	93.7	94.9

[1] Vitamin premix (IU or mg/kg diet): biosterol, 18,000 IU; vitamin D_3 9000 IU, 0.001; vitamin K_3, 16.56; thiamine, 20.03; riboflavin, 54; vitamin B_6, 33.21; cyanocobalamin, 0.27; α-tocopherol, 28.00; ascorbic acid, 150.00; niacinamide, 26.00; calcium pantothenate, 25.00; folic acid, 1.00; biotin, 0.06; inositol, 400.00. [2] Mineral premix (mg/kg diet): Cu, 5.00; Zn, 37.00; Mn, 7.00; Fe, 30.00; I, 1.10; Se, 0.25; Co, 0.20; Mg, 600.00. [3] Amino acid premix (g/kg diet): histidine, 0.95; isoleucine, 1.97; lysine, 1.67; valine, 1.69; cystine, 2.08; tyrosine, 2.88; threonine, 2.69. [4] Crude protein, crude fat and ash was measured using the Association of Official Analytical Chemists Methods.

Table 2. Amino acid composition of experimental diets (on DM-basis, g/kg).

MHA Levels	0.0	3.0	6.0	9.0
Thr	16.6	16.4	17.1	16.8
Val	18.5	18.7	17.9	19.2
Met	8.3	11.0	13.6	16.3
Cys	6.5	6.2	6.7	6.4
Ile	15.5	16.4	16.0	16.7
Leu	31.0	30.5	31.3	31.6
Phe	15.7	16.2	15.8	16.4
Tyr	12.9	12.7	12.1	12.5
His	10.6	10.2	10.8	10.3
Lys	20.1	20.6	20.8	19.9
Arg	22.5	22.7	22.2	22.6
Trp	3.4	3.6	3.3	3.1

Thr: Threonine; Val: Valine; Met: Methionine; Cys: Cysteine; Ile: Isoleucine; Leu: Leucine; Phe: Phenylalanine; Tyr: Tyrosine; His: Histidine; Lys: Lysine; Arg: Arginine; Trp: Tryptophan.

2.2. Biochemical Analysis

The proximate composition of the diets was analyzed following the previously established methods [25]. Hepatic lipids were extracted using a 2:1 chloroform-methanol method [26]. Liver samples were homogenized in ice-cold physiological saline solution (10 volumes, *w*/*v*) and then centrifuged at 3000 rpm and 4 °C for 20 min. The supernatant was collected for enzyme activity analysis. Protein content was determined by the Bradford method [27]. The activities of ACC (H232-1-1), FAS (H231-1-1), SCD-1 (H648-1-1), HSL (H238-1-1), and CPT-1 (H230-1-1) were measured by an enzyme-linked immunosorbent assay (ELISA) using commercial detection kits (Nanjing Jiancheng Bioengineering Institute, Nanjing, China).

2.3. Hepatic Histological Analysis

The processes of dehydration, dyeing, and image collection were performed [28]. After the fixation, the livers were dehydrated by the standard procedures, embedded in paraffin, and cut to 5 μm sections. A total of 9 fish per treatment (3 fish per tank) were stained with Hematoxylin eosin (H&E), to evaluate the liver morphology, and observed in light microscopy. The areas of lipid vacuoles in the H&E sections were evaluated using Image J software (version 1.42, National Institutes of Health, USA), as described by [29].

2.4. Real-Time Quantitative PCR

The total RNA from liver tissue was isolated using the TRIzol reagent (TaKaRa, Liaoning, Dalian, China) and reverse-transcribed into cDNA using the PrimeScript® RT reagent Kit (TaKaRa). The Nano Drop® 2000 spectrophotometer (Shanghai Musen Biotechnology Co., Ltd., Shanghai, China) and agarose gel (1.5%) electrophoresis were used to test the RNA quantity and quality, respectively. RT-qPCR was conducted using the SYBR green method and the CFX96 Real-Time PCR Detection System (Bio-Rad, Hercules, CA, USA). The gene-specific primers and optimal annealing temperatures used in this study are shown in Table 3. The β-actin and 18S rRNA were used as the internal control. The mRNA abundances of target genes were calculated according to the $2^{-\Delta\Delta CT}$ method [30].

Table 3. Primer sequences and optimal annealing temperatures (OAT, °C) of genes selected for analysis by real-time PCR.

Name	Sequences	OAT	Accession Number
ACC1-QF	GGCTCAGTGATGGAGGTCTAT	62.3	MW465382
ACC1-QR	GGTGATCGTAGCAGTGAAGGA		
ACC2-QF	TGGAAAGGGTATCCGTAAAGT	61.8	MW435454
ACC2-QR	AGCAGTCTCGTCCGAACAG		
FAS-QF	CAGGTCTGTACGGTCTTCCA	62.2	MW465391
FAS-QR	CGGGTTCACTCCTCCATCTA		
SCD1-QF	TATCTTTGAATGGGCTCGTGA	60.1	MW465401
SCD1-QR	AACTTTGTCGGCGTACAGGTC		
ATGL-QF	GGAATCTCAGACAACCTGCCTC	62.7	XM_038705351
ATGL-QR	GGTGGAGTGAACTGGATGCTT		
HSLa-QF	TGAACGCATTACCCAGAACC	61.8	MW465409
HSLa-QR	GTGTAGAGTCACAGGAGGCAAA		
HSLb-QF	TCGTCTCCCTGCCTCCTAAT	62.3	MW465407
HSLb-QR	GGCGTAGAAACACTCCTCCAG		
CPT1-QF	TTCCCCTTTATTGAC	60.0	XM_038705335.1
CPT1-QR	AGAACTTCCCTTTGTC		
PPARα-QF	TGGAGCTGGATGACACTGACC	59.0	MK388672.1
PPARα-QR	GAGCCGTAGTGCCTGAACAAT		
SREBP-1c-QF	CCTCCCAGTCCTTTGCTATTG	57.9	MW465403
SREBP-1c-QR	TCCTTGGAGCCAGTTGATGA		
AMPKα1-QF	CCTGAAGGAGGTATGTGACAAG	60.7	MW465410
AMPKα1-QR	CAATGATGAGATGGTAGGCAAC		
AMPKα2-QF	GAGGCGTCTTCTACATCCCA	58.7	MW465405
AMPKα2-QR	GGTCCTGCTTAAACCATTCAT		
LKB1-QF	CTACCAGCCACGGAGGAAG	62.7	MW465396
LKB1-QR	TGCGGCATAGTGTCTCTGAGT		
SIRT1-QF	TACCAGAACAGCCACCAAGT	58.7	MW465402
SIRT1-QR	CATTATTACCAGCAGTCTCCGT		
β-actin-QF	CCCCATCCACCATGAAGA	55.7	AF253319.1
β-actin-QR	CCTGCTTGCTGATCCACAT		
18S-QF	TGAATACCGCAGCTAGGAATAATG	59.0	MH018569.1
18S-QR	CCTCCGACTTTCGTTCTTGATT		

2.5. Protein Extraction and Western Blot Analysis

The liver tissues were lysed with RIPA buffer (Beyotime, Shanghai, China). The protein concentration was determined by a BCA protein assay kit (Beyotime, Shanghai, China). Protein extracts (20 μg) were separated by 12% SDS-PAGE electrophoresis and then transferred onto polyvinyl difluoride (PVDF) membrane. After being blocked with 5% bovine serum albumin (BSA) in PBS, the PVDF membranes were dipped in the diluted primary antibody overnight at 4 °C. The anti-SIRT1 (1:1000, A11267, anti-rabbit), anti-AMPK (1:1000, A1229, anti-rabbit) were purchased from ABclonal Biotechnology Co., Ltd. (Wuhan, Hubei, China) The P-AMPK (1:1000; Thr172, AF3423, anti-rabbit) was purchased from Affinity Biosciences. The β-actin (1:1000; R23613, anti-rabbit, Zen Biotechnology, Chengdu, Sichuan, China) was used as the control protein. After primary antibody incubation, the membranes were washed by TBS/T and then incubated with second antibodies (1:2000; Zen Biotechnology, Chengdu, Sichuan, China). Finally, the protein was visualized by enhanced chemi-luminescence, then quantified by the Gel-Pro Analyzer (Media Cybernetics, Bethesda, MD, USA).

2.6. Statistical Analysis

The normality and homogeneity of the data were verified using the D'Agostino-Pearson and Bartlett tests. Data were analyzed using one-way analysis of variance (ANOVA), using SPSS 25.0 statistical software (IBM, Michigan Avenue, Chicago, IL, USA). The difference among treatments was examined using the Duncan's multiple-range test. Orthogonal polynomial contrasts were used to determine the linear and quadratic effects of dietary MHA inclusion levels. The results were presented as the mean and the standard error of the mean (SEM). Statistical significance was set as $p < 0.05$.

3. Results

3.1. Hepatic Steatosis and Lipid Content

The hepatic microanatomy is illustrated in Figure 1A. Compared with the control group and the group fed with 3.0 g MHA kg/diet, the groups fed with 6.0 and 9.0 g MHA/kg diets showed a dramatic increase in the size and number of lipid droplets, characterized by hepatocytes filled with lipid vacuoles and a modified nucleus position. The orthogonal polynomial contrasts indicated that the increasing MHA levels linearly increased the relative areas of hepatic lipid vacuoles and hepatic lipid content (Figure 1B,C, $p < 0.05$).

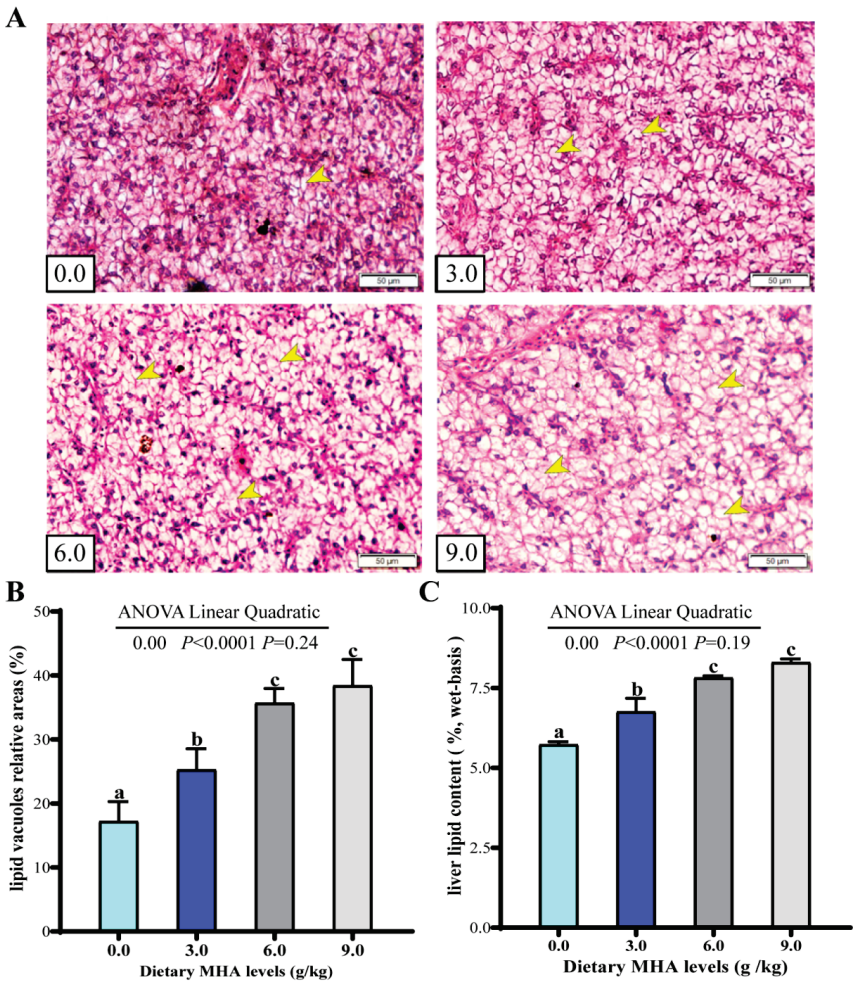


Figure 1. Effects of dietary MHA on lipid accumulation in liver largemouth bass fed diets with graded levels of MHA (g/kg) for 84 days. (**A**) Representative photomicrographs of histological alterations in the liver, stained with H&E staining at 200× magnification. The yellow arrow indicated the lipid vacuoles; (**B**) Relative areas for lipid vacuoles in H&E staining section ($n = 9$); (**C**) Lipid content of the liver ($n = 9$); Different letters denote significant differences ($p < 0.05$).

3.2. Lipid Synthesis-Related Parameters in Liver

As shown in Table 4, the activities of ACC and SCD-1 increased linearly with the increasing dietary MHA levels ($p < 0.05$). The FAS activity increased significantly in both the linear and the quadratic manner ($p < 0.05$). The expressions of genes involved in hepatic lipid synthesis are presented in Figure 2. There was a linear and quadratic effect of dietary MHA level on mRNA expressions of ACC1 and FAS ($p < 0.05$). As dietary MHA levels increased, the mRNA expressions of ACC2, SCD1, and SREBP-1c increased linearly ($p < 0.05$).

Table 4. The activities (U/mg protein) of ACC, FAS, SCD-1, HSL, and CPT-1 in livers of largemouth bass fed diets with graded levels of MHA (g/kg) for 84 days [1].

Items [2]	Dietary MHA Levels, g/kg				*Pr* > *F*[2]		
	0.0	3.0	6.0	9.0	ANOVA	Linear	Quadratic
ACC	65.86 ± 4.70 [a]	77.54 ± 4.73 [b]	80.88 ± 5.05 [b]	86.96 ± 2.54 [c]	0.00	<0.0001	0.06
FAS	48.86 ± 5.44 [a]	61.36 ± 2.72 [b]	73.29 ± 3.25 [c]	75.25 ± 2.25 [c]	0.00	<0.0001	0.00
SCD-1	52.93 ± 3.03 [a]	64.24 ± 3.10 [b]	84.37 ± 9.13 [c]	89.49 ± 7.11 [c]	0.00	<0.0001	0.14
HSL	205.04 ± 14.56 [c]	164.07 ± 6.40 [b]	155.73 ± 6.52 [b]	133.59 ± 13.79 [a]	0.00	<0.0001	0.06
CPT-1	243.67 ± 4.24 [c]	212.75 ± 4.36 [b]	179.42 ± 10.19 [a]	168.79 ± 7.20 [a]	0.00	<0.0001	0.15

[1] With nine fish in each group. Values within the same rows having different superscripts are significantly different ($p < 0.05$). [2] Acetyl-CoA carboxylase (ACC), fatty acid synthetase (FAS), stearoyl-coenzyme A desaturase-1 (SCD-1), hormone sensitive lipase (HSL), and carnitine palmitoyl transferase-1 (CPT-1).

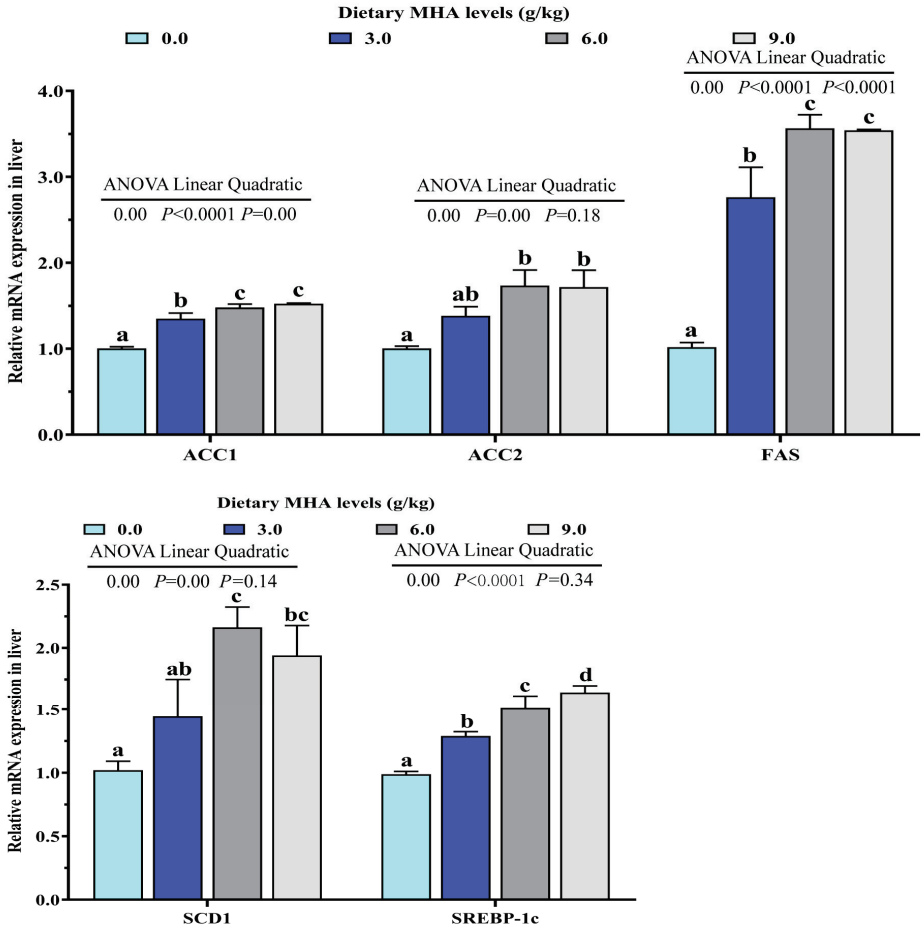


Figure 2. Effects of dietary MHA on lipid synthesis related gene expressions of ACC1, ACC2, FAS, SCD1 and SREBP-1c in livers of largemouth bass fed diets containing graded levels of MHA (g/kg) for 84 days. Means within columns with different superscript letters show significant differences at $p < 0.05$.

3.3. Lipid Oxidation-Related Parameters in Liver

With an increasing dietary MHA level, the HSL and CPT-1 activities decreased linearly ($p < 0.05$). The mRNA expressions of ATGL, CPT-1a and HSLb were linearly and quadratically decreased with increasing dietary MHA levels ($p < 0.05$). The mRNA expressions of HSLa and PPARα decreased linearly ($p < 0.05$, Figure 3).

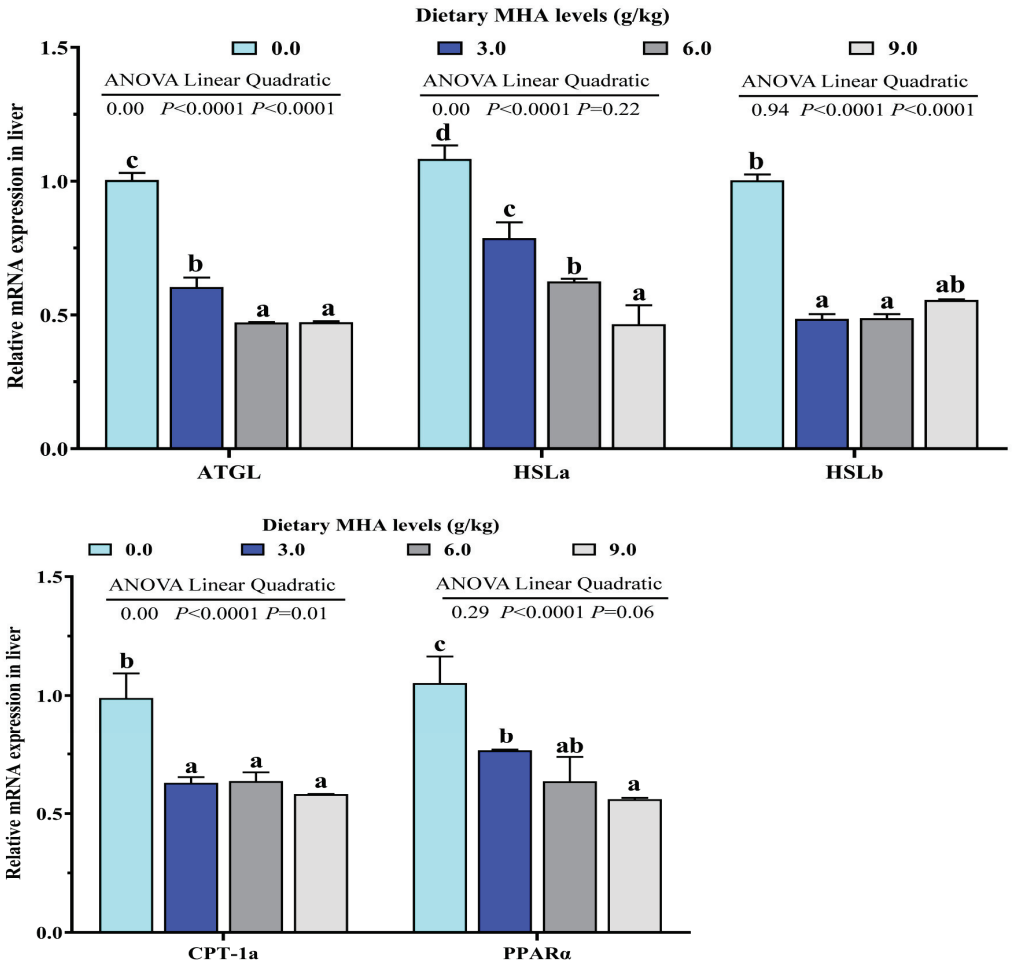


Figure 3. Effects of dietary MHA on lipid oxidation-related gene expressions ATGL, HSLa, HSLb, CPT-1a and PPARα in livers of largemouth bass fed diets containing graded levels of MHA (g/kg) for 84 days. Different letters denote significant differences at $p < 0.05$ ($n = 9$).

3.4. Dietary MHA Down-Regulated Hepatic SIRT1/AMPK Signaling Pathway

As presented in Figure 4A, the orthogonal polynomial contrasts showed that the increasing MHA levels linearly and quadratically decreased the mRNA expression of liver AMPKα2 ($p < 0.05$). The mRNA expressions of SIRT1 and AMPKα1 decreased linearly ($p < 0.05$). The ratio of SIRT1/β-actin, P-AMPK/β-actin, and T-AMPK/β-actin linearly decreased with increasing dietary MHA levels (Figure 4B–F, $p < 0.05$).

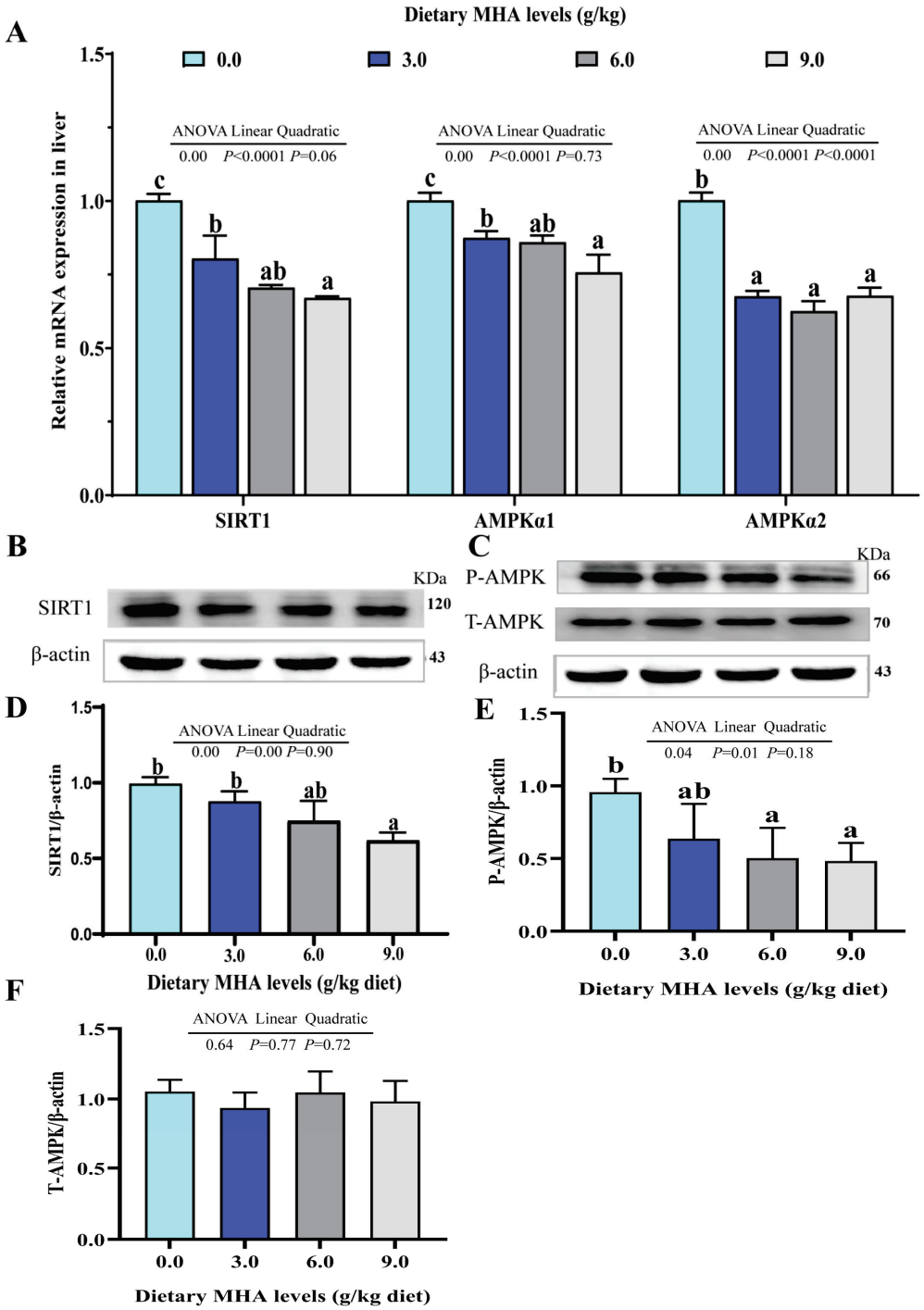


Figure 4. Effect of dietary MHA on the SIRT1/AMPK signaling pathway in the livers of largemouth bass fed diets with graded levels of MHA (g/kg) for 84 days. (**A**) The mRNA expressions of SIRT1, AMPKα1, and AMPKα2; (**B**–**D**) Protein abundances of SIRT1, β-actin, and ratio of SIRT1 and β-actin; (**C**,**E**,**F**) Protein abundances of P-AMPK, T-AMPK, and β-actin, and ratio of P-AMPK and T-AMPK. Different letters denote significant differences at $p < 0.05$ ($n = 9$).

4. Discussion

The digestive and metabolic functions of fish are largely dependent on the structural integrity of the liver, which is responsible for fat synthesis and storage [31,32]. Excessive lipid accumulation in the liver can be detrimental to liver health and, consequently, affect the growth performance of fish [5,33,34]. In the current study, as the dietary levels of MHA increased, the lipid content in the livers of fish also increased. In this research, this

was further corroborated by a histological examination of the liver H&E-stained sections. Higher dietary MHA levels led to an increase in the number of lipid vacuoles within hepatocytes. Collectively, these results indicated that dietary MHA could promote lipid accumulation in the liver. Previous studies on tiger puffers and cobia demonstrated that dietary Met increased hepatic lipid deposition [5,7]. Similarly, Craig et al. (2013) reported that a dietary Met restriction decreased lipid content in liver of rainbow trout [14]. A study conducted on mice also found that a dietary Met restriction limited lipid deposition in liver [6]. Nevertheless, the detailed reasons require further investigation.

Lipid accumulation in the liver is primarily influenced by lipid synthesis and degradation [8,9]. ACC and FAS are the key rate-limiting enzymes in long-chain fatty acid biosynthesis [35,36]. SCD1 is required for biosynthesis of the long-chain monounsaturated fatty acids [37]. On the other hand, HSL and CPT1 are involved in lipolysis and fatty acid β-oxidation, respectively [15,38]. In the present experiment, the activities of ACC, FAS, and SCD1 significantly increased linearly and/or quadratically. With increasing dietary MHA level, the activities of HSL and CPT-1 decreased linearly. Consistently, the expression levels of lipid synthesis-related genes (including ACC1, ACC2, FAS, and SCD1) were up-regulated in largemouth bass fed the 6.0 and 9.0 g MHA/kg diets, and the transcriptional levels of lipid degradation-related genes (ATGL, HSLa, HSLb, and CPT1) were down-regulated in largemouth bass fed the 6.0 and 9.0 g MHA/kg diets. These results suggested that dietary MHA promoted lipid deposition in the liver by regulating lipid metabolism. A correlation analysis showed that the expressions of ACC1, FAS, SCD1, HSLa, and CPT1 were positively correlated with their corresponding enzyme activities (r_{ACC1} = +0.956, p = 0.044; r_{FAS} = +0.976, p = 0.024; r_{SCD1} = +0.953, p = 0.047; r_{HSLa} = +0.988, p = 0.012; r_{CPT1} = +0.0.818, p = 0.091, Table 5). These results also indicated that dietary MHA increased the activities of lipogenic enzymes and decreased the activities of lipolytic enzymes by regulating their gene expressions. As far as we know, no information is available regarding the impact of MHA on the activities of lipid-metabolism-related enzymes in the liver. It has been reported that L-carnitine, a metabolite of MHA, reduced the activities of FAS and enhanced the activities of CPT1 in the livers of fish [24]. The reason for the different effects of MHA and its metabolite carnitine on the activities of lipid metabolism enzymes needs further study. Previous studies in cobia, rainbow trout, and tiger puffers found that a high Met supplemental level increased hepatic lipid accumulation. Dietary Met led to an increase in lipolytic gene expression and a decrease in lipogenetic gene expression [4,5,7].

Table 5. Correlation coefficients of some parameters.

Independent Parameters	Dependent Parameters	Correlation Coefficients	*p*
ACC	ACC1 mRNA	0.956	0.044
FAS	FAS mRNA	0.976	0.024
SCD1	SCD1 mRNA	0.953	0.047
HSL	HSLa mRNA	0.988	0.012
CPT-1	CPT-1 mRNA	0.818	0.091
SREBP-1c mRNA	ACC1 mRNA	0.977	0.023
	ACC2 mRNA	0.981	0.019
	FAS mRNA	0.963	0.037
	SCD1 mRNA	0.932	0.068
PPARα mRNA	ATGL mRNA	0.984	0.016
	HSLa mRNA	0.988	0.012
	CPT-1 mRNA	0.942	0.058
AMPKα1 mRNA	SREBP-1c mRNA	−0.964	0.036
	PPARα mRNA	0.962	0.038
	SIRT1 mRNA	0.947	0.053

SREBP-1c is the main transcription factor that mediates the expression of lipogenesis genes, such as ACC, FAS, and SCD in liver of fish [7,10]. Conversely, PPARα plays a crucial role in fatty acid oxidation by upregulating genes involved in mitochondrial and peroxisomal β-oxidation, including CPT1 [39]. In this study, with the increasing dietary MHA levels, the mRNA expressions of SREBP-1c increased linearly and the mRNA expressions of PPARα decreased linearly. These results are consistent with the observations in cobia [7] and rainbow trout [14]. Correlation analysis showed that the expression of SREBP-1c was positively correlated with lipogenesis genes (r_{ACC1} = +0.977, p = 0.023; r_{ACC2} = +0.981, p = 0.019; r_{FAS} = +0.963, p = 0.037; r_{SCD1} = +0.932, p = 0.068), while the expression of PPARα was positively correlated with CPT1 expression (r_{CPT1} = +0.942, p = 0.058, Table 5). These results suggested that dietary MHA increased the expression of lipogenic genes, and decreased that of lipolysis genes partly by regulating the expression of SREBP-1c and PPARα, respectively.

The AMPK is an important integrator of signals that control the energy balance [40]. Previous studies demonstrated that AMPK activation suppressed the activities of SREBP-1c, and promoted PPARα and downstream fatty acids β-oxidation-related gene expression [41–44]. In the present study, the liver mRNA expressions of AMPKα1 and AMPKα2 linearly and quadratically decreased, respectively. The ratio of P-AMPK/T-AMPK/β-actin linearly decreased with increasing dietary MHA levels. Similar results were also found in rainbow trout [14]. Correlation analysis found that the expression of AMPKα was positively correlated with PPARα ($r_{PPAR\alpha}$ = +0.962, p = 0.038), and negatively correlated with SREBP-1c ($r_{SREBP\text{-}1c}$ = −0.964, p = 0.036). These results suggested that dietary MHA up-regulated the mRNA expressions of SREBP-1c and down-regulated the mRNA expressions of PPARα partly via AMPK. In terrestrial animals, the SIRT1/AMPK signaling pathway plays a crucial role in hepatic lipid metabolism. Activation of this pathway exerts inhibitory effects on fatty acid uptake and synthesis while promoting fatty acid β-oxidation [45,46]. In this study, we identified that the mRNA expression of SIRT1 and the ratio of SIRT1/β-actin linearly decreased with increasing dietary MHA levels. A correlation analysis showed that the expression of SIRT1 was positively correlated with AMPKα1 ($r_{AMPK\alpha1}$ = +0.947, p = 0.053), suggesting that dietary MHA promotes lipid accumulation in the liver, partly via repressing the SIRT1/AMPK signaling pathway. Grant et al. (2016) reported that a Met restriction up-regulated the mRNA expression of SIRT1 in the kidneys of mice [21]. Chan et al. (2018) also found that Met repressed the mRNA expression and protein level of SIRT1 in mouse aortic endothelium [20]. These results suggest that MHA might have a similar function to Met in regulating the SIRT1 gene expression of fish. However, the detailed mechanism by which MHA regulates lipid synthesis and lipid oxidation via the SIRT1/AMPK pathway in fish requires further investigation.

5. Conclusions

In summary, the present study demonstrated that dietary MHA increased hepatic lipid vacuoles and lipid content. Furthermore, supplying dietary MHA could enhance enzyme activity parameters and gene expression related to lipid synthesis, which reduce enzyme activity parameters and gene expression related to lipid oxidation. Dietary MHA-induced lipid accumulation was mediated, at least in part, through the regulation of the SIRT1/AMPK signaling pathway. These findings provide new insights into the impact of MHA on hepatic lipid metabolism in fish, helping to fill the existing knowledge gaps in this area.

Author Contributions: J.Z. and Z.Y.: investigation, methodology, data curation, writing—original draft. H.L.: investigation, methodology, data curation. C.Y.: investigation, methodology, data curation. Y.C.: investigation, methodology, data curation. Q.C.: conceptualization, supervision,

funding acquisition. J.J.: conceptualization, supervision, funding acquisition, writing—review and editing. All authors have read and agreed to the published version of the manuscript.

Funding: This research was funded by National Natural Science Foundation of China grant number 32172987.

Institutional Review Board Statement: All experimental procedures used were conducted with the approval of the Animal Care Advisory Committee of Sichuan Agricultural University, license number DKY-2018202027.

Informed Consent Statement: Not applicable.

Data Availability Statement: The data presented in this study are available in this manuscript.

Conflicts of Interest: The authors declare that no conflicts of interest exist.

References

1. Zhao, Y.; Yang, C.; Zhu, X.; Feng, L.; Liu, Y.; Jiang, W.; Wu, P.; Huang, X.; Chen, D.; Yang, S.; et al. Dietary methionine hydroxy analogue supplementation benefits on growth, intestinal antioxidant status and microbiota in juvenile largemouth bass *Micropterus salmoides*. *Aquaculture* **2022**, *556*, 738279. [CrossRef]
2. Rajeev Raghavan, P.Z.X.L. Low levels of aflatoxin b1 could cause mortalities in juvenile hybrid sturgeon, *Acipenser ruthenus* ♂ × *A. Baeri*♀. *Aquacult. Nutr.* **2011**, *17*, e39–e47. [CrossRef]
3. Moraes, G.; de Almeida, L.C. Nutrition and functional aspects of digestion in fish. In *Biology and Physiology of Freshwater Neotropical Fish*; Baldisserotto, B., Urbinati, E.C., Cyrino, J.E.P., Eds.; Academic Press: Cambridge, MA, USA, 2020; pp. 251–271.
4. Skiba-Cassy, S.; Geurden, I.; Panserat, S.; Seiliez, I. Dietary methionine imbalance alters the transcriptional regulation of genes involved in glucose, lipid and amino acid metabolism in the liver of rainbow trout (*Oncorhynchus mykiss*). *Aquaculture* **2016**, *454*, 56–65. [CrossRef]
5. Xu, H.; Zhang, Q.; Wei, Y.; Liao, Z.; Liang, M. Dietary methionine increased the lipid accumulation in juvenile tiger puffer Takifugu rubripes. *Comp. Biochem. Physiol. B Biochem. Mol. Biol.* **2019**, *230*, 19–28. [CrossRef] [PubMed]
6. Malloy, V.L.; Perrone, C.E.; Mattocks, D.A.; Ables, G.P.; Caliendo, N.S.; Orentreich, D.S.; Orentreich, N. Methionine restriction prevents the progression of hepatic steatosis in leptin-deficient obese mice. *Metabolism* **2013**, *62*, 1651–1661. [CrossRef]
7. Wang, Z.; Mai, K.; Xu, W.; Zhang, Y.; Liu, Y.; Ai, Q. Dietary methionine level influences growth and lipid metabolism via GCN2 pathway in cobia (*Rachycentron canadum*). *Aquaculture* **2016**, *454*, 148–156. [CrossRef]
8. Nguyen, P.; Leray, V.; Diez, M.; Serisier, S.; Le Bloc'H, J.; Siliart, B.; Dumon, H. Liver lipid metabolism. *J. Anim. Physiol. Anim. Nutr.* **2008**, *92*, 272–283. [CrossRef]
9. Peng, M.; Xu, W.; Mai, K.; Zhou, H.; Zhang, Y.; Liufu, Z.; Zhang, K.; Ai, Q. Growth performance, lipid deposition and hepatic lipid metabolism related gene expression in juvenile turbot (*Scophthalmus maximus* L.) fed diets with various fish oil substitution levels by soybean oil. *Aquaculture* **2014**, *433*, 442–449. [CrossRef]
10. Moon, Y.A. The SCAP/SREBP pathway: A mediator of hepatic steatosis. *Endocrinol. Metab.* **2017**, *32*, 6–10. [CrossRef]
11. Morak, M.; Schmidinger, H.; Riesenhuber, G.; Rechberger, G.N.; Kollroser, M.; Haemmerle, G.; Zechner, R.; Kronenberg, F.; Hermetter, A. Adipose triglyceride lipase (ATGL) and hormone-sensitive lipase (HSL) deficiencies affect expression of lipolytic activities in mouse adipose tissues. *Mol. Cell. Proteom.* **2012**, *11*, 1777–1789. [CrossRef]
12. Chen, H.; Zhang, L.; Li, X.; Li, X.; Sun, G.; Yuan, X.; Lei, L.; Liu, J.; Yin, L.; Deng, Q.; et al. Adiponectin activates the AMPK signaling pathway to regulate lipid metabolism in bovine hepatocytes. *J. Steroid Biochem. Mol. Biol.* **2013**, *138*, 445–454. [CrossRef] [PubMed]
13. Aissa, A.F.; Tryndyak, V.; de Conti, A.; Melnyk, S.; Gomes, T.D.; Bianchi, M.L.; James, S.J.; Beland, F.A.; Antunes, L.M.; Pogribny, I.P. Effect of methionine-deficient and methionine-supplemented diets on the hepatic one-carbon and lipid metabolism in mice. *Mol. Nutr. Food Res.* **2014**, *58*, 1502–1512. [CrossRef] [PubMed]
14. Craig, P.M.; Moon, T.W. Methionine restriction affects the phenotypic and transcriptional response of rainbow trout (*Oncorhynchus mykiss*) to carbohydrate-enriched diets. *Br. J. Nutr.* **2013**, *109*, 402–412. [CrossRef] [PubMed]
15. Song, Y.; Gao, Y.; Hogstrand, C.; Li, D.; Pan, Y.; Luo, Z. Upstream regulators of apoptosis mediates methionine-induced changes of lipid metabolism. *Cell Signal.* **2018**, *51*, 176–190. [CrossRef]
16. Ji, K.; Liang, H.; Ren, M.; Ge, X.; Pan, L.; Yu, H. Nutrient metabolism in the liver and muscle of juvenile blunt snout bream (*Megalobrama amblycephala*) in response to dietary methionine levels. *Sci. Rep.-Uk* **2021**, *11*, 23843. [CrossRef]
17. Hou, X.; Xu, S.; Maitland-Toolan, K.A.; Sato, K.; Jiang, B.; Ido, Y.; Lan, F.; Walsh, K.; Wierzbicki, M.; Verbeuren, T.J.; et al. SIRT1 regulates hepatocyte lipid metabolism through activating AMP-activated protein kinase. *J. Biol. Chem.* **2008**, *283*, 20015–20026. [CrossRef]

18. Li, J.; Liu, M.; Yu, H.; Wang, W.; Han, L.; Chen, Q.; Ruan, J.; Wen, S.; Zhang, Y.; Wang, T. Mangiferin Improves Hepatic Lipid Metabolism Mainly Through Its Metabolite-Norathyriol by Modulating SIRT-1/AMPK/SREBP-1c Signaling. *Front. Pharmacol.* **2018**, *9*, 201. [CrossRef]
19. Zhang, Y.; Geng, C.; Liu, X.; Li, M.; Gao, M.; Liu, X.; Fang, F.; Chang, Y. Celastrol ameliorates liver metabolic damage caused by a high-fat diet through Sirt1. *Mol. Metab.* **2017**, *6*, 138–147. [CrossRef]
20. Chan, S.H.; Hung, C.H.; Shih, J.Y.; Chu, P.M.; Cheng, Y.H.; Lin, H.C.; Hsieh, P.L.; Tsai, K.L. Exercise intervention attenuates hyperhomocysteinemia-induced aortic endothelial oxidative injury by regulating SIRT1 through mitigating NADPH oxidase/LOX-1 signaling. *Redox Biol.* **2018**, *14*, 116–125. [CrossRef]
21. Grant, L.; Lees, E.K.; Forney, L.A.; Mody, N.; Gettys, T.; Brown, P.A.; Wilson, H.M.; Delibegovic, M. Methionine restriction improves renal insulin signalling in aged kidneys. *Mech. Ageing Dev.* **2016**, *157*, 35–43. [CrossRef]
22. Hasek, B.E.; Stewart, L.K.; Henagan, T.M.; Boudreau, A.; Lenard, N.R.; Black, C.; Shin, J.; Huypens, P.; Malloy, V.L.; Plaisance, E.P.; et al. Dietary methionine restriction enhances metabolic flexibility and increases uncoupled respiration in both fed and fasted states. *Am. J. Physiol. Regul. Integr. Comp. Physiol.* **2010**, *299*, R728–R739. [CrossRef] [PubMed]
23. Jiang, H.; Bian, F.; Zhou, H.; Wang, X.; Wang, K.; Mai, K.; He, G. Nutrient sensing and metabolic changes after methionine deprivation in primary muscle cells of turbot (*Scophthalmus maximus* L.). *J. Nutr. Biochem.* **2017**, *50*, 74–82. [CrossRef] [PubMed]
24. Chen, Y.S.Z.L. Addition of l-carnitine to formulated feed improved growth performance, antioxidant status and lipid metabolism of juvenile largemouth bass, *Micropterus salmoides*. *Aquaculture* **2020**, *518*, 734434. [CrossRef]
25. Jiang, J.; Wu, X.Y.; Zhou, X.Q.; Feng, L.; Liu, Y.; Jiang, W.D.; Wu, P.; Zhao, Y. Glutamate ameliorates copper-induced oxidative injury by regulating antioxidant defences in fish intestine. *Br. J. Nutr.* **2016**, *116*, 70–79. [CrossRef]
26. Folch, J.; Lees, M.; Sloane, S.G. A simple method for the isolation and purification of total lipides from animal tissues. *J. Biol. Chem.* **1957**, *226*, 497–509. [CrossRef]
27. Hultmann, L.; Phu, T.M.; Tobiassen, T.; Aas-Hansen, Ø.; Rustad, T. Effects of pre-slaughter stress on proteolytic enzyme activities and muscle quality of farmed Atlantic cod (*Gadus morhua*). *Food Chem.* **2012**, *134*, 1399–1408. [CrossRef]
28. Yu, L.L.; Yu, H.H.; Liang, X.F.; Li, N.; Wang, X.; Li, F.H.; Wu, X.F.; Zheng, Y.H.; Xue, M.; Liang, X.F. Dietary butylated hydroxytoluene improves lipid metabolism, antioxidant and anti-apoptotic response of largemouth bass (*Micropterus salmoides*). *Fish. Shellfish. Immunol.* **2018**, *72*, 220–229. [CrossRef]
29. Ye, H.; Xu, M.; Chen, L.; Tan, X.; Chen, S.; Zou, C.; Sun, Z.; Liu, Q.; Ye, C.; Wang, A. Effects of dietary plant protein sources influencing hepatic lipid metabolism and hepatocyte apoptosis in hybrid grouper (*Epinephelus lanceolatus*♂ × *Epinephelus fuscoguttatus*♀). *Aquaculture* **2019**, *506*, 437–444. [CrossRef]
30. Livak, K.J.; Schmittgen, T.D. Analysis of relative gene expression data using real-time quantitative PCR and the $2^{-\Delta\Delta CT}$ method. *Methods* **2001**, *25*, 402–408. [CrossRef]
31. Wu, P.; Tang, L.; Jiang, W.; Hu, K.; Liu, Y.; Jiang, J.; Kuang, S.; Tang, L.; Tang, W.; Zhang, Y.; et al. The relationship between dietary methionine and growth, digestion, absorption, and antioxidant status in intestinal and hepatopancreatic tissues of sub-adult grass carp (Ctenopharyngodon idella). *J. Anim. Sci. Biotechnol.* **2017**, *8*, 63. [CrossRef]
32. Tocher, D.R. Metabolism and functions of lipids and fatty acids in teleost fish. *Rev. Fish. Sci.* **2003**, *11*, 107–184. [CrossRef]
33. Greene, D.H.; Selivonchick, D.P. Lipid metabolism in fish. *Prog. Lipid Res.* **1987**, *26*, 53–85. [CrossRef] [PubMed]
34. Qiang, J.; Tao, Y.F.; Bao, J.W.; Chen, D.J.; Li, H.X.; He, J.; Xu, P. High fat diet-induced miR-122 regulates lipid metabolism and fat deposition in genetically improved farmed tilapia (GIFT, *Oreochromis niloticus*) liver. *Front. Physiol.* **2018**, *9*, 1422. [CrossRef] [PubMed]
35. Kim, K.H. Regulation of mammalian acetyl-coenzyme A carboxylase. *Annu. Rev. Nutr.* **1997**, *17*, 77–99. [CrossRef]
36. Smith, S.; Witkowski, A.; Joshi, A.K. Structural and functional organization of the animal fatty acid synthase. *Prog. Lipid Res.* **2003**, *42*, 289–317. [CrossRef]
37. Forney, L.A.; Stone, K.P.; Wanders, D.; Ntambi, J.M.; Gettys, T.W. The role of suppression of hepatic SCD1 expression in the metabolic effects of dietary methionine restriction. *Appl. Physiol. Nutr. Metab.* **2018**, *43*, 123–130. [CrossRef]
38. Schlaepfer, I.R.; Joshi, M. CPT1a-mediated fat oxidation, mechanisms, and therapeutic potential. *Endocrinology* **2020**, *161*, bqz046. [CrossRef]
39. Canbay, A.; Bechmann, L.; Gerken, G. Lipid metabolism in the liver. *Z. Für Gastroenterol.* **2007**, *45*, 35. [CrossRef]
40. Steinberg, G.R.; Kemp, B.E. AMPK in health and disease. *Physiol. Rev.* **2009**, *89*, 1025–1078. [CrossRef]
41. Barroso, E.; Rodriguez-Calvo, R.; Serrano-Marco, L.; Astudillo, A.M.; Balsinde, J.; Palomer, X.; Vazquez-Carrera, M. The PPARβ/δ activator GW501516 prevents the down-regulation of AMPK caused by a high-fat diet in liver and amplifies the PGC-1α-Lipin 1-PPARα pathway leading to increased fatty acid oxidation. *Endocrinology* **2011**, *152*, 1848–1859. [CrossRef]
42. Jung, E.J.; Kwon, S.W.; Jung, B.H.; Oh, S.H.; Lee, B.H. Role of the AMPK/SREBP-1 pathway in the development of orotic acid-induced fatty liver. *J. Lipid Res.* **2011**, *52*, 1617–1625. [CrossRef] [PubMed]

43. Li, Y.; Xu, S.; Mihaylova, M.M.; Zheng, B.; Hou, X.; Jiang, B.; Park, O.; Luo, Z.; Lefai, E.; Shyy, J.Y.; et al. AMPK phosphorylates and inhibits SREBP activity to attenuate hepatic steatosis and atherosclerosis in diet-induced insulin-resistant mice. *Cell Metab.* **2011**, *13*, 376–388. [CrossRef] [PubMed]
44. Shen, J.; Sun, B.; Yu, C.; Cao, Y.; Cai, C.; Yao, J. Choline and methionine regulate lipid metabolism via the AMPK signaling pathway in hepatocytes exposed to high concentrations of nonesterified fatty acids. *J. Cell Biochem.* **2020**, *121*, 3667–3678. [CrossRef] [PubMed]
45. Liou, C.J.; Dai, Y.W.; Wang, C.L.; Fang, L.W.; Huang, W.C. Maslinic acid protects against obesity-induced nonalcoholic fatty liver disease in mice through regulation of the Sirt1/AMPK signaling pathway. *Faseb J.* **2019**, *33*, 11791–11803. [CrossRef]
46. Zhang, D.; Yan, Y.; Tian, H.; Jiang, G.; Li, X.; Liu, W. Resveratrol supplementation improves lipid and glucose metabolism in high-fat diet-fed blunt snout bream. *Fish. Physiol. Biochem.* **2018**, *44*, 163–173. [CrossRef]

Disclaimer/Publisher's Note: The statements, opinions and data contained in all publications are solely those of the individual author(s) and contributor(s) and not of MDPI and/or the editor(s). MDPI and/or the editor(s) disclaim responsibility for any injury to people or property resulting from any ideas, methods, instructions or products referred to in the content.

biology

MDPI

Article

Effects of Varying Dietary Concentrations of Menadione Nicotinamide Bisulphite (VK_3) on Growth Performance, Muscle Composition, Liver and Muscle Menaquinone-4 Concentration, and Antioxidant Capacities of Coho Salmon (*Oncorhynchus kisutch*) Alevins

Han Zhang [1,2,3], Leyong Yu [2,4], Abdur Rahman [2,5,6,*], Sattanathan Govindharajan [2,5], Lingyao Li [2,7], Hairui Yu [1,2,3,*] and Muhammad Waqas [8]

1 College of Fisheries and Life Science, Shanghai Ocean University, Shanghai 201306, China; a787382102@gmail.com
2 Key Laboratory of Biochemistry and Molecular Biology in Universities of Shandong, Weifang Key Laboratory of Coho Salmon Culturing Facility Engineering, Institute of Modern Facility Fisheries, College of Biology and Oceanography, Weifang University, Weifang 261061, China; leyong618@gmail.com (L.Y.); sattanathanphd@gmail.com (S.G.); 980714742@163.com (L.L.)
3 Shandong Freshwater Fisheries Research Institute, Jinan 250013, China
4 College of Fisheries, Huazhong Agricultural University, Wuhan 430070, China
5 Weifang Key Laboratory of Salmon and Trout Health Culture, Conqueren Leading Fresh Science & Technology Inc., Ltd., Weifang 261205, China
6 Department of Animal Sciences, University of Veterinary and Animal Sciences, Lahore 54000, Pakistan
7 Shandong Collaborative Innovation Center of Coho Salmon Health Culture Engineering Technology, Shandong Conqueren Marine Technology Co., Ltd., Weifang 261108, China
8 Department of Animal Nutrition and Nutritional Diseases, Faculty of Veterinary Medicine, Ondokuz Mayıs University, Samsun 55139, Türkiye; m.waqas@uvas.edu.pk
* Correspondence: abdurrehman@uvas.edu.pk (A.R.); yhr6003@hotmail.com (H.Y.)

Simple Summary: Coho salmon farming has experienced rapid expansion in China, driven by the species' fast growth, exceptional nutritional value, and highly desirable fillet quality. Rich in high-quality protein, omega-3 fatty acids, and carotenoids such as astaxanthin, coho salmon is widely recognized for its health benefits, making it a valuable commodity in both domestic and international markets. However, the intensification of large-scale farming has created a pressing need for optimized feed formulations to ensure sustainable production and maintain fish health. Despite its economic significance, the specific nutritional requirements of coho salmon remain insufficiently explored, particularly regarding vitamin K_3 (menadione), an essential micronutrient that plays a pivotal role in blood coagulation, bone metabolism, antioxidant activity, and overall growth. To bridge this critical knowledge gap, optimizing the dietary dosage of VK_3 for coho salmon alevins is imperative. This study focuses on the optimization of the dosage of vitamin K_3 and its beneficial effects on growth performance, muscle composition, and antioxidant capacity during freshwater rearing.

Abstract: Vitamin K_3 (VK_3) is an essential micronutrient for fish growth and metabolism. To determine the optimal required dietary concentration of VK, a 12-week-long trial was planned to investigate the impact of VK_3 on growth performance, muscle composition, liver menaquinone-4 (MK-4), whole-body MK-4 concentration, and antioxidant capacity (T-AOC) in coho salmon alevins. A total of 2100 coho salmon alevins were divided into twenty-one tanks, with 100 alevins in each tank, and three tanks represented one group. Each of the seven groups were randomly assigned to one of the experimental diets formulated with varying levels of menadione nicotinamide bisulphite (VK_3), i.e., 0.16 (control), 5.25, 10.22,

14.93, 20.51, 40.09, and 59.87 mg/kg, respectively. The results revealed that the inclusion of VK_3 from 5.25 to 40.09 mg/kg improved ($p < 0.05$) the survival rate (SR), weight gain (WG), specific growth rate (SGR), and feed conversion ratio (FCR), while no effect ($p > 0.05$) was observed on the hepatosomatic index (HSI), viscerosomatic index (VSI), Fulton's condition factor (K), and muscle composition. The whole-body MK-4, liver MK-4, liver T-AOC, total superoxide dismutase (T-SOD), and catalase (CAT) enzymes were also increased ($p < 0.05$). Malondialdehyde (MDA) contents were reduced ($p < 0.05$) in all supplemented groups with a decreasing trend. The predicted optimal required dietary concentrations of VK_3 were found to be 34.0, 43.5, 38.54, and 31.97 mg/kg based on WG, SGR, liver MK-4 concentration, and T-AOC, respectively, by quadratic regression analysis. It is concluded that the dietary VK_3 has improved the growth performance and antioxidant status in alevins during early development in the range of 31.97 to 43.5 mg/kg diet.

Keywords: antioxidant; aquaculture; menadione; menaquinones; vitamin; growth

1. Introduction

Fish is a vital part of the human diet and is well known for its health benefits. Its global consumption has nearly doubled over the last four decades [1,2]. In fish farming, the provision of complete balanced feed, including macronutrients along with micronutrients, is the fundamental nutritional strategy to obtain the maximum yield by avoiding health-related issues [3] and skeletal anomalies during the developmental phase [4–6]. Although the micronutrients are equally and synergistically involved in imparting the real-time effects of all nutrients into the final yield, the majority of the research has been focused on exploring the requirements of macronutrients in fish farming, while the assessment of micronutrients for growth and allied parameters has remained neglected [7]. Especially with the new trends of intensive freshwater fish farming, it is becoming imperative to optimize and fulfill the need for all nutrients for cost-effective and efficient production of fish during early growth stages [8]. The early growth stage is critical for nutritionists to provide varying levels of required nutrients. The requirements of the early development stage are usually different than the subsequent life periods and proper care during this phase determines the future life span success [9–11]. Among the various micronutrients, vitamin K3 (VK3), a fat-soluble compound, has received particular attention in fish feed, especially in the current context of freshwater aquaculture [12]. Based on its origin, vitamin K has different forms: phylloquinone (VK1) is derived from plants, menaquinone (VK_2) is derived from microbes, and menadione (VK_3) is the synthetic provitamin form of vitamin K_3 [13,14]. The naturally occurring VK in the feeds is sometimes not sufficiently available, and synthetic derivatives of VK_3, especially menadione (VK_3), are supplemented in the feeds [15,16], which is converted into menaquinone-4 (MK-4) to be available in tissue metabolism [17]. Vitamin K is a micronutrient and is needed in minute quantities for various vital biochemical and physiological functions in the body. It promotes growth and blood coagulation in case of injury by producing thrombin [18]; it is also helpful in bone formation and mineralization by osteoblast cells through the production of osteocalcin, a calcium-binding protein for mineralization of the bone matrix; and it regulates the homeostasis of calcium and bone, as well [18,19]. The mechanism of involvement of VK_3 in this process is through the protein carboxylation with the help of MK-4 as a cofactor along with γ-glutamyl carboxylase to convert glutamyl residues to produce clotting factors, osteocalcin, and Gla matrix for bone mineralization [19–21]. The presence of VK_3 in an optimal concentration in the fish diet is highly essential to maintain growth, homeostasis, and bone strength [8], and deficiency of

VK_3 will lead to skeletal disorders, anemia, prolonged clotting time, and may ultimately lead to poor growth [22–26].

Despite the known fact that the optimal dietary concentration of VK_3 in feed is an essential nutrient to achieve normal growth, bone development, and overall health status during early life, no or little literature is available on the dose optimization of VK_3 in coho salmon alevins in their early stages of development. However, in some research studies, it is evident that VK_3 addition to the diet has improved the growth performance, nutrient digestion, and antioxidant status in Jian juvenile carp fish (*Cyprinus carpio)* [26] with a dose rate of 3.13 mg/kg of diet, and in Senegalese sole (*Solea senegalesis*) larva up to 250 mg/kg [8]. Some other studies demonstrated that vitamin K supplementation in the diet has improved feed efficiency and protein efficiency ratio in fleshy prawn (*Penaeus chinensis*) shrimp [27]; antioxidant parameters were improved in *Haliotis discus hannai* (abalone) [28]; improved weight and feed efficiency were observed in gilthead seabream (*Sparus aurata*) fingerlings [16]; 5 mg/kg dietary vitamin K has resulted in better growth and bone development in gilthead seabream larva [29]; and dietary vitamin K_3 does not affect growth but improves antioxidant status and immunity in whiteleg shrimp (*Litopenaeus vannamei)* [30]. On the other hand, some studies claimed that there is no need for dietary supplementation of VK_3 and naturally occurring VK_3 in basal feed is sufficient for growth, but an optimal dietary concentration of 2–4 mg/kg is required for other body functions in Nile Tilapia (*Oreochromis niloticus*) juveniles [31]. Dai et al. [30] reported that dietary VK_3 had no effect on growth, but 39.06 mg/kg improved antioxidant status and immunity in whiteleg shrimp. The nutrient requirement for VK varies with age. The VK requirements for juvenile and adult fish in some species including grass carp (*Ctenopharyngodon Idella*), lake trout (*Salvelinus namaychus*), Mummichog (*Fundulus heteroclitus), Pseudosciaena crocea* large yellow croaker (*Larimichtys crocea* juveniles, Jian carp juveniles, largemouth bass (*Micropterus salmoides*), and gilthead seabream fingerlings [15,16,24,32–34] have been quantified, but no quantifications of dietary vitamin K_3 requirements for the larval stage of coho salmon (*Oncorhynchus kisutch)* has been conducted [8]. This literature gap urges us to investigate the need, importance, and dose optimization of VK_3 in coho salmon alevins.

Coho salmon, a species of significant commercial importance, is anadromous, meaning it migrates between freshwater and marine environments throughout its life cycle, from hatching to spawning. [35,36]. Coho salmon is highly regarded for its exceptional nutritional profile, fast growth, delicious meat, high-quality protein and polyunsaturated fatty acids (PUFAs), including significant levels of omega-3 fatty acids. Additionally, it contains astaxanthin and phospholipids, which are well known for their health benefits, including antioxidant, anti-inflammatory, anti-thrombotic, and cardio-protective properties [37–39]. Due to its high nutritional value and economic potential, coho salmon farming has expanded rapidly worldwide, particularly in China [40]. This expansion of large-scale farming of coho salmon has increased the demand for optimized feed formulations to support sustainable production. However, research on the nutritional requirements of coho salmon remains limited, particularly regarding dietary vitamin K, which plays a crucial role in physiological processes such as blood coagulation, bone metabolism, antioxidant activity, and overall growth [41]. Addressing this gap in the literature, it was hypothesized that optimizing the dietary vitamin K3 (menadione) dosage for coho salmon alevins is crucial to enhance growth performance, improve muscle composition, and support antioxidant capacity during freshwater rearing.

Therefore, the present study was designed to evaluate the effects of different dietary vitamin K_3 inclusion levels on growth performance, body muscle composition, MK-4 concentration, and antioxidant capacity in coho salmon alevins. The findings of this study will contribute to a better understanding of coho salmon nutrition and provide valuable insights for optimizing feed formulation in aquaculture.

2. Materials and Methods

2.1. Ethical Statement

The present study was carried out according to the recommendations (animal handling, care, and housing) in the "Guide for the Ethical Use of Experimental Animals" of the Weifang University, Weifang, Shandong, China (No. 20200601) and it was approved by the Institutional Animal Care and Use Committee of the Institute of Modern Facility Fisheries, Weifang University, China (IACUC NO. 20220516003).

2.2. Experimental Diets

Menadione nicotinamide bisulphite (VK_3) was procured from Shanghai Yuanye Bio-Technology Co., Ltd., Shanghai, China. Seven isocaloric and isonitrogenous diets were formulated with supplemented levels of VK_3: 0.00; 5.00, 10.00, 15.00, 20.00, 40.00, and 60.00_3mg/kg VK_3, producing analyzed dietary VK_3 contents of 0.16, 5.25, 10.22, 14.93, 20.51, 40.09, and 59.87 mg/kg, respectively. The ingredients and chemical composition of diets are given in Table 1.

Table 1. Formulation and proximate composition of the experimental diets for coho salmon alevins (% dry matter).

Ingredients	Dietary Vitamin K_3 Levels (mg/kg)						
	0.16	**5.25**	**10.22**	**14.93**	**20.51**	**40.09**	**59.87**
Casein [1]	38.00	38.00	38.00	38.00	38.00	38.00	38.00
Gelatin [1]	12.00	12.00	12.00	12.00	12.00	12.00	12.00
Dextrin [1]	28.00	28.00	28.00	28.00	28.00	28.00	28.00
Corn oil [1]	6.00	6.00	6.00	6.00	6.00	6.00	6.00
Fish oil [1]	3.00	3.00	3.00	3.00	3.00	3.00	3.00
α-cellulose [1]	8.00	8.00	8.00	8.00	8.00	8.00	8.00
Mono-calcium phosphate [1]	1.50	1.50	1.50	1.50	1.50	1.50	1.50
Mineral premix [2]	2.50	2.50	2.50	2.50	2.50	2.50	2.50
Vitamin premix (vitamin K_3 free) [3]	1.00	1.00	1.00	1.00	1.00	1.00	1.00
Vitamin K_3 (mg/kg)	0.00	5.00	10.00	15.00	20.00	40.00	60.00
Proximate nutrient composition							
Moisture	10.37	10.28	10.49	10.22	9.91	10.44	10.31
Crude protein	45.12	45.15	44.90	44.97	45.02	44.87	45.23
Crude lipid	10.32	10.17	10.45	10.27	10.51	10.39	10.25
Ash	5.53	5.67	5.60	5.59	5.66	5.62	5.71
Gross energy (MJ/kg)	20.86	21.01	21.11	21.23	20.97	21.20	21.15
Vitamin K_3 (mg/kg)	0.16	5.25	10.22	14.93	20.51	40.09	59.87

[1] Provided by Shandong Conqueren Marine Technology Co., Ltd., Weifang, China; [2] composition (g/kg mineral premix): $AlK(SO_4)_2 \cdot 12H_2O$, 123.7; $CuSO_4.5H_2O$, 32.0; $CoCl_2 \cdot 6H_2O$, 49.0; $FeSO_4.7H_2O$, 707.0; $MgSO_4.7H_2O$, 4317.0; $MnSO_4.4H_2O$, 31.0; KI, 5.3; NaCl, 4934.0; $Na_2SeO_3.H_2O$, 3.4; $ZnSO_4.7H_2O$, 177.0; [3] vitamin premix supplied the diets with (mg/kg dry diet): retinal palmitate, 0.75; cholecalciferol, 0.04; α-tocopherol, 50.0; thiamine-HCl, 12.0; riboflavin, 30.0; D-calcium pantothenate, 20.0; pyridoxine-HCl, 15.0; choline chloride, 500.0; meso-inositol, 200.0; D-biotin, 0.5; folic acid, 1.5; ascorbic acid, 100.0; niacin, 75.0; cyanocobalamin, 0.01.

2.3. Animals and Feeding Management

The coho salmon alevins were procured from the hatchery of the National Aquatic Product Introduction and Breeding Centre (Beijing, China). The coho salmon alevins were cultured and reared at one of the experimental base sites of the Coho Salmon Health Culture Engineering Technology Center of Shandong Collaborative Innovation Center (Weifang, China). A total of 2100 alevins were divided into 21 tanks, with 100 coho salmon alvenis in each tank, and 3 tanks represented one group. The fish were fed in 21 white plastic tanks (0.8 × 0.6 × 0.6 m, L × W × H, and water volume 240 L/tank) with 100 fish per tank in triplicate per dietary treatment. There were seven treatment groups. Fish were fed four times daily (7:00, 10:30, 14:00, and 17:30) for a trial period of 12 weeks. The feeding rate

was 3% of the body weight. The alevins were reared in filtered underground spring water and natural light during the feeding period. The temperature, dissolved oxygen, and pH were in the range of 15.7 ± 0.5 °C, 9.3 ± 0.5 mg/L, and 7.1 ± 0.2, respectively.

2.4. Euthanasia Methods for Coho Salmon Alevins

At the end of the feeding trial, the fish were withheld from feed for 24 h, anesthetized with tricaine methanesulfonate (MS-222; Wuhan Biocar Pharmaceutical Co., Ltd., Wuhan, China) at a concentration of 30 mg/L, and then quickly frozen using liquid nitrogen to −80 °C just after finishing the samples at tank sites and immediately transferred to the laboratory and then stored at −20 °C in the refrigerator for the subsequent analyses.

2.5. Sampling Procedures and Analytical Methods

2.5.1. Growth Performance

Body weight and number of fish counts were recorded for all fish in each replicate at the start and end of the trial. Then, at the end of the trial, three fish from each replicate were randomly caught, and their final weight and body length were recorded. These fish were then immediately dissected to collect the whole-body muscle, liver, and viscera samples. The whole body, liver, and viscera of the fish were weighed and stored at −20 °C for further analysis. Fish muscle samples were used for muscle composition analysis and whole-body MK-4 concentrations. Liver samples were used to assess the MK-4 concentrations and total antioxidant capacity (T-AOC). The above-recorded values about growth performance were then used to calculate the survival rate (SR), weight gain (WG), specific growth rate (SGR), feed conversion ratio (FCR), Fulton condition factor (K), hepatosomatic index (HSI), and viscerosomatic index (VSI) by using the equations below [42].

$$\text{SR (\%)} = (\text{final fish number}/\text{initial fish number}) \times 100$$

$$\text{WG (g)} = \text{final weight (g)} - \text{initial weight (g)}$$

$$\text{SGR (\%/d)} = 100 \times ((\ln\text{final body weight}) - (\ln\text{initial body weight}))/\text{days}$$

$$\text{FCR} = \text{total feed intake (g)}/(\text{final body weight (g)-initial body weight (g)})$$

$$\text{Protein intake (g)} = \text{total feed intake (g)} \times \text{protein percent in feed}$$

$$\text{K (\%)} = (W/l^3) \times 100; [(W = \text{weight (g)}; Tl = \text{total length (cm}^3)]$$

$$\text{HSI (\%)} = (\text{liver weight}/\text{final weight}) \times 100$$

$$\text{VSI (\%)} = (\text{visceral weight}/\text{final weight}) \times 100$$

2.5.2. Analysis of Feed Samples and Chemical Composition of Muscles

The feed samples and stored muscle and liver samples from the dissected fish were analyzed by the methods prescribed in AOAC [43] for nutrient composition analysis; crude protein was determined by Kjeldhal apparatus (Automatic Apparatus Kjeltec 8400, FOSS, Hillerød, Denmark) by calculating nitrogen (N × 6.25); crude fat was determined by Soxhlet apparatus (ST 243, FOSS, Hillerød, Denmark); moisture was determined at 105 °C for four h in a hot air oven to constant weight; and samples were burnt in a muffle furnace at 550 °C for 12 h for crude ash analysis.

2.5.3. MK-4 Concentration Determination in Whole-Body Muscles and Liver Tissue, and Liver Anti-Oxidative Enzyme Activity Analysis

The whole-body muscle (1.0 g) and liver (0.2 g) samples were separately homogenized. The homogenate of the muscle sample and liver were then analyzed by following the

technique prescribed by Ostermeyer and Schmidt [44] for whole-body muscle and liver menaquinone-4 (MK-4) concentration analysis.

The liver samples were homogenized and placed in 0.1 M pH 7.4 Tris-HCl buffer (Qingdao Miruida Trade Co., Ltd., Qingdao, China) at 4 °C, and then used for analysis. The liver anti-oxidative enzyme activity, including total antioxidant capacity (T-AOC), total superoxide dismutase (T-SOD) activity, catalase (CAT), and liver malondialdehyde (MDA) content were determined by the commercial reagent kit (Nanjing Jiancheng Bioengineering Institute, Nanjing, China) with the help of an automatic analyzer.

2.5.4. Statistical Analysis

The data obtained from the experiment were statistically analyzed by one-way ANOVA in SPSS software (IBM SPSS 21.0) and the mean value was tested by the Duncan test. The values in the table are presented as mean ± SE and the level of significant difference was $p \leq 0.05$. The polynomial quadratic regression was used (Microsoft Excel 97-2003 Worksheet and Chart Design) on the data of WG, SGR, liver vitamin K (MK-4), and T-AOC to predict the optimal required dietary concentration of VK_3 for these parameters in coho salmon alevins.

3. Results

3.1. Growth Performance

Growth performance parameters have been presented in Table 2. The survival rate of the coho salmon alevins was recorded significantly higher in all dietary treatments as compared to the control basal diet (0.16 mg/kg). Among the treatments, the highest survival rate ($p < 0.05$) was in diet groups supplemented with 59.87 and 20.51 mg/kg of VK_3 followed by 40.09, 14.93, 10.22, and 5.25 mg/kg diet groups, while the control (0.16 mg/kg) group was observed with the lowest survival rate. Weight gain and SGR were observed to be higher ($p < 0.05$) in all VK_3-supplemented groups as compared to the control group. The highest weight gain was observed in groups with 14.93 and 20.51 mg/kg VK_3, and the highest SGR was in the diet group of 14.93 mg/kg VK exclusively. The FCR was also found to be better ($p < 0.05$) in all VK_3-supplemented groups as compared to the control group, with pronounced better effects in the diet group with 14.93 mg/kg and 20.51 mg/kg of VK_3, followed by the 40.09 and 59.87 mg/kg dose groups. The other parameters, including K, HSI, and VSI, remained unaffected ($p > 0.05$) in all of the treatment groups (Table 2). The predicted optimal required concentration of VK_3 for maximum WG and SGR was found to be 34 mg/kg and 43.50 mg/kg, respectively, by polynomial quadratic regression analysis in the coho salmon alevin diet (Figures 1 and 2).

Table 2. Growth performance and feed utilization of coho salmon alevins fed diets with graded levels of VK_3 for 12 weeks.

Diet Groups	Dietary Vitamin K_3 Levels (mg/kg)							*p*-Value
	0.16	5.25	10.22	14.93	20.51	40.09	59.87	
SR (%)	95.33 ^{c} ± 0.88	96.00 ^{bc} ± 0.58	96.67 ^{abc} ± 0.88	97.33 ^{abc} ± 0.88	98.33 ^{a} ± 0.33	97.67 ^{ab} ± 0.67	98.33 ^{a} ± 0.33	0.05
IBW (g)	0.32 ± 0.03	0.33 ± 0.04	0.32 ± 0.02	0.32 ± 0.04	0.33 ± 0.03	0.33 ± 0.02	0.33 ± 0.03	0.53
FBW (g)	4.32 ^{e} ± 0.03	4.44 ^{d} ± 0.04	4.59 ^{c} ± 0.02	4.90 ^{a} ± 0.04	4.87 ^{a} ± 0.03	4.83 ^{ab} ± 0.02	4.76 ^{b} ± 0.03	<0.001
WG (g)	4.00 ^{e} ±0.03	4.12 ^{d} ±0.04	4.27 ^{c} ±0.02	4.58 ^{a} ± 0.04	4.55 ^{a} ±0.03	4.51 ^{ab} ±0.02	4.44 ^{b} ± 0.03	<0.001
SGR (%/d)	3.09 ^{f} ± 0.01	3.11 ^{e} ± 0.01	3.16 ^{d} ± 0.01	3.24 ^{a} ± 0.01	3.22 ^{ab} ± 0.01	3.21 ^{bc} ± 0.01	3.19 ^{c} ± 0.01	<0.001
FCR (%)	1.27 ^{a} ± 0.02	1.22 ^{b} ± 0.01	1.17 ^{c} ± 0.01	1.08 ^{d} ± 0.01	1.08 ^{d} ± 0.01	1.10 ^{d} ± 0.01	1.11 ^{d} ± 0.01	<0.001
K (%)	1.66 ± 0.05	1.71 ± 0.03	1.62 ± 0.04	1.60 ± 0.04	1.61 ± 0.05	1.65 ± 0.04	1.73 ± 0.03	0.28
HSI (%)	1.16 ± 0.03	1.10 ± 0.04	1.14 ± 0.03	1.08 ± 0.04	1.15 ± 0.07	1.16 ± 0.04	1.11 ± 0.05	0.79
VSI (%)	7.68 ± 0.07	7.86 ± 0.06	7.69 ± 0.09	7.74 ± 0.04	7.78 ± 0.07	7.49 ± 0.11	7.63 ± 0.09	0.09

$^{a–f}$ Within the same row, mean values with different superscripts differ significantly ($p < 0.05$) with mean ± SE. Abbreviations: SR: survival rate; IBW: initial body weight; FBW: final body weight; SGR: specific growth rate; FCR: feed conversion ratio; CF: condition factor; HSI: hepatosomatic index; VSI: viscerosomatic index.

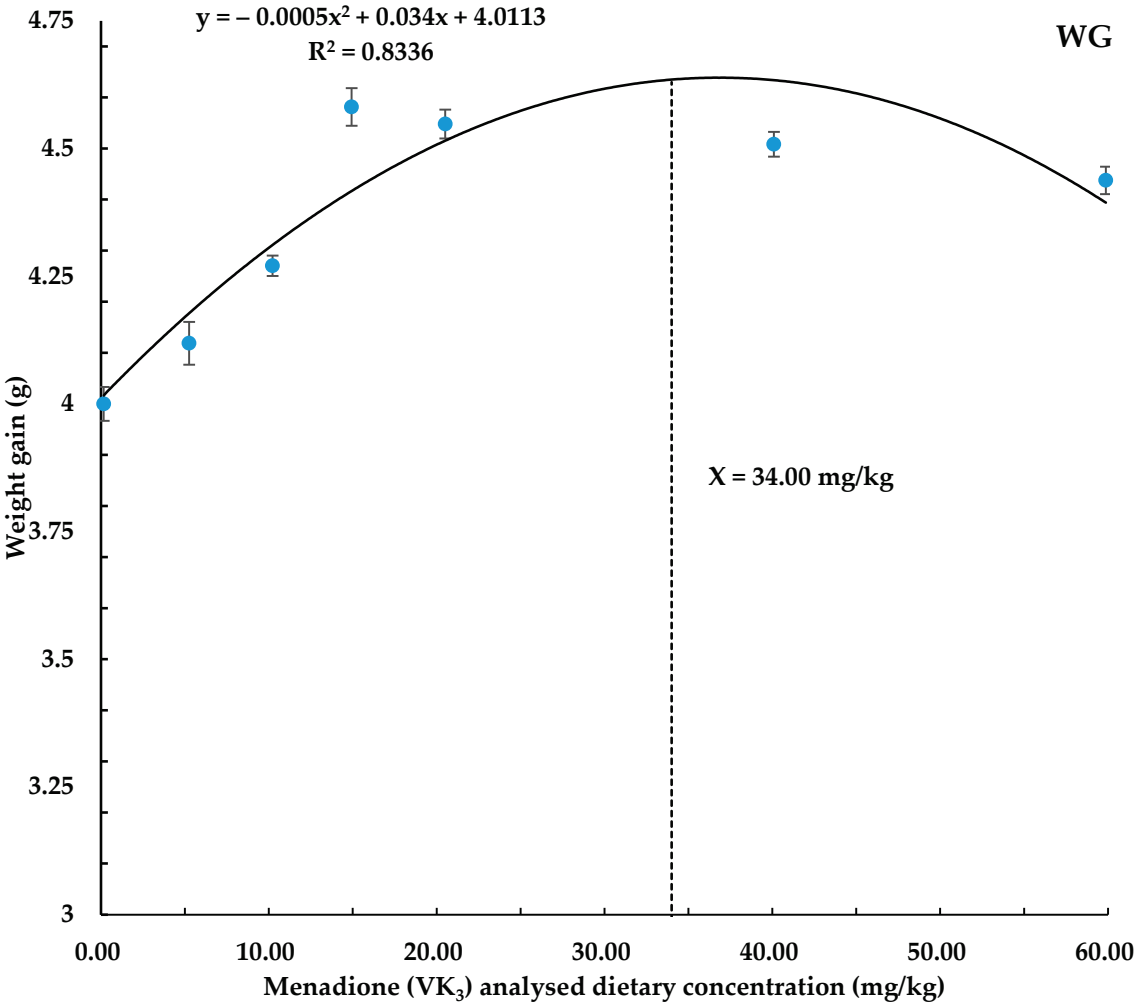


Figure 1. Polynomial quadratic regression analysis of WG with graded levels of vitamin K_3 in coho salmon alevins predicted that the optimum vitamin K_3 requirement for WG was 34 mg/kg. Abbreviation: WG, weight gain; dotted line shows X value and complete curve line shows trend.

3.2. Muscle Chemical Composition

Muscle chemical composition analysis revealed no effect ($p > 0.05$) on muscle composition, including moisture percentage, crude protein, crude lipid, and/or ash content with any level of VK_3 supplementation (Table 3).

Table 3. Body muscle proximate composition (%) of coho salmon alevins fed diets with graded levels of VK_3 for 12 weeks (on a dry matter basis).

Dietary Vitamin K_3 Levels (mg/kg)	Moisture	Crude Protein	Crude Lipid	Ash
0.16	73.13 ± 0.26	19.65 ± 0.12	3.66 ± 0.12	3.28 ± 0.10
5.25	72.93 ± 0.34	19.72 ± 0.18	3.61 ± 0.15	3.36 ± 0.09
10.22	73.03 ± 0.42	19.74 ± 0.14	3.55 ± 0.15	3.39 ± 0.12
14.93	72.74 ± 0.57	19.55 ± 0.19	3.63 ± 0.10	3.48 ± 0.07
20.51	73.01 ± 0.50	19.39 ± 0.26	3.54 ± 0.11	3.51 ± 0.07
40.09	73.23 ± 0.53	19.58 ± 0.21	3.75 ± 0.09	3.56 ± 0.10
59.87	72.88 ± 0.32	19.53 ± 0.17	3.71 ± 0.11	3.54 ± 0.08
p-Value	0.99	0.86	0.86	0.33

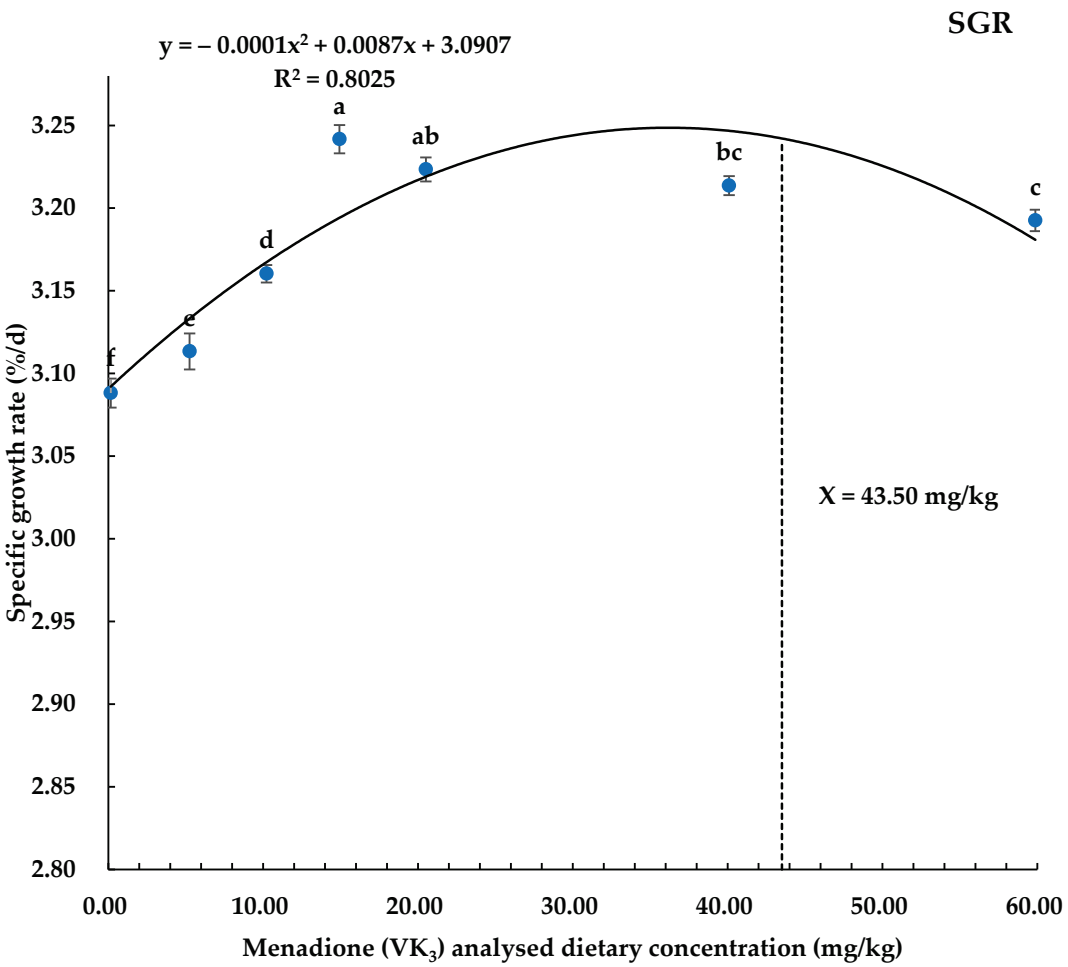


Figure 2. Polynomial quadratic regression analysis of SGR with graded levels of vitamin K_3 in coho salmon alevins predicted that the optimum vitamin K_3 requirement for SGR was 43.50 mg/kg. Abbreviation: SGR, specific growth rate; dotted line shows X value and complete curve line shows trend.

3.3. MK-4 Concentrations in Whole-Body and Liver Tissue and Liver Anti-Oxidative Enzyme Activity

Whole-body MK-4 and whole-liver MK-4 concentrations were recorded to be higher ($p < 0.05$) in all diets with high VK_3 dietary levels as compared to the control (0.16 mg/kg of VK_3). The highest value of whole-body MK-4 was noticed in the 59.87 mg/kg VK_3 dietary group, and the highest liver MK-4 values were recorded in the 59.87, 40.09, and 20.51 mg/kg of VK_3 dietary groups (Table 4). Quadratic regression analysis predicted that 38.54 mg/kg was a suitable required dietary concentration of VK_3 to achieve maximum liver vitamin K (MK-4) concentration in coho salmon alevins (Figure 3).

Table 4. Whole-body and liver vitamin K (MK-4) concentrations of coho salmon alevins fed diets with graded levels of VK_3 for 12 weeks.

Dietary Vitamin K_3 Levels (mg/kg)	Whole-Body MK-4 Concentration (ng/g)	Liver MK-4 Concentration (ng/g)
0.16	5.14 ^{g} ± 0.17	33.76 ^{d} ± 0.73
5.25	21.97 ^{f} ± 0.39	257.65 ^{c} ± 4.29
10.22	33.58 ^{e} ± 0.74	362.58 ^{b} ± 6.41
14.93	42.99 ^{d} ± 0.70	423.88 ^{a} ± 3.22
20.51	47.65 ^{c} ± 0.41	433.07 ^{a} ± 4.82
40.09	64.12 ^{b} ± 0.73	437.05 ^{a} ± 3.72
59.87	75.24 ^{a} ± 0.95	435.85 ^{a} ± 7.33
p-Value	<0.001	<0.001

$^{a–g}$ Within the same column, mean values with different superscripts differ significantly ($p < 0.05$) with mean ± SE.

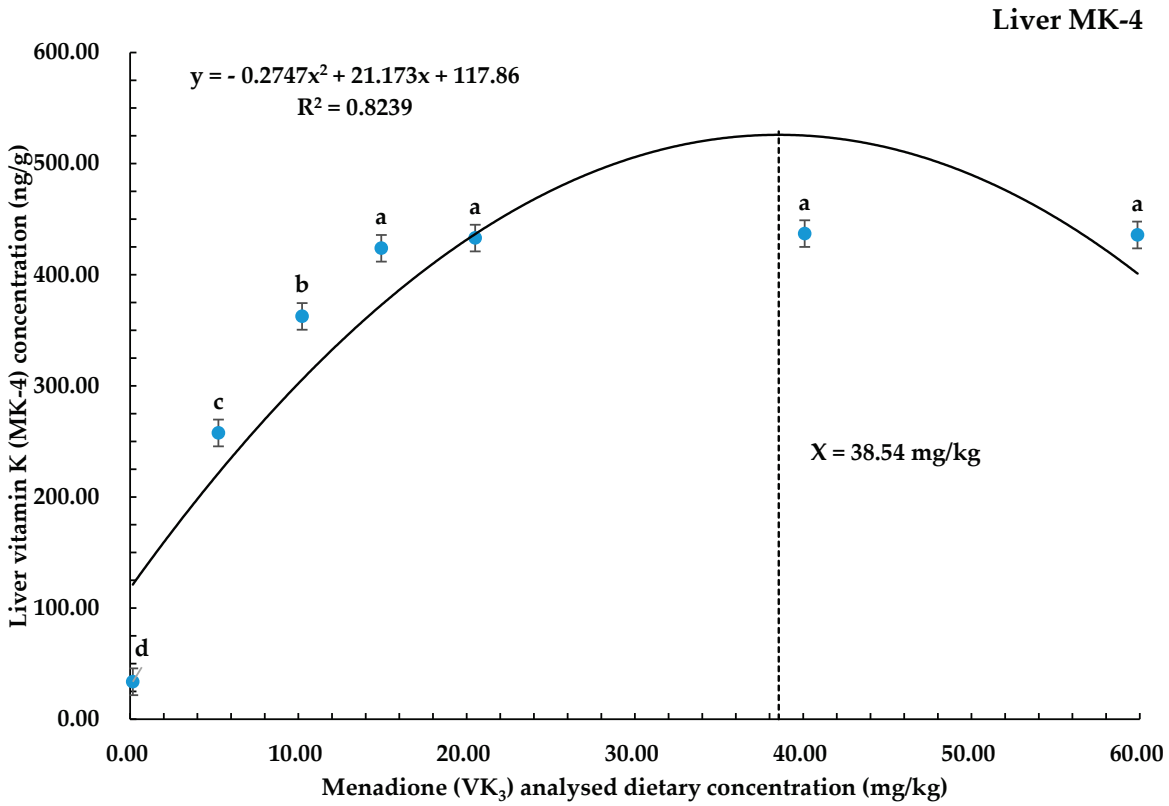


Figure 3. Polynomial quadratic regression analysis of liver vitamin K (MK-4) with graded dietary vitamin K_3 levels for coho salmon alevins predicted that the optimum vitamin K_3 requirement for liver MK-4 was 38.54 mg/kg. Abbreviations: MK-4, menaquinone-4; dotted line shows X value and complete curve line shows trend.

Whole-liver T-AOC, T-SOD, and CAT were significantly higher ($p < 0.05$) in all groups receiving higher dietary treatment levels compared to the control group. The highest values of T-AOC were in diet groups 10.22, 14.93, 20.51, and 40.09 mg/kg of VK_3, while in the case of T-SOD and CAT, the highest values were found in the dietary group 14.93 mg/kg VK_3. The predicted required concentration of dietary VK_3 for liver T-AOC was found to ebb to 31.97 mg/kg in coho salmon alevins (Figure 4). In the case of MDA contents, the results revealed significantly lower values ($p < 0.05$) in all dietary levels as compared to the control. The significantly lowest ($p < 0.05$) values of MDA contents were found in the dietary group with 14.93 and 20.51 mg/kg VK_3 (Table 5).

Table 5. Liver anti-oxidative enzyme activities of coho salmon (*Oncorhynchus kisutch*) alevins fed diets with graded levels of VK_3 for 12 weeks.

Dietary Vitamin K_3 Levels (mg/kg)	T-AOC (U/mg prot.)	T-SOD (U/mg prot.)	CAT (U/mg prot.)	MDA (nmol/mg prot.)
0.16	20.02 ^{c} ± 0.80	118.90 ^{d} ± 5.01	7.38 ^{f} ± 0.10	11.52 ^{a} ± 0.17
5.25	23.34 ^{b} ± 0.54	143.86 ^{c} ± 7.34	9.50 ^{e} ± 0.16	9.46 ^{b} ± 0.14
10.22	26.27 ^{a} ± 0.39	173.77 ^{ab} ± 5.44	12.07 ^{b} ± 0.15	7.71 ^{d} ± 0.15
14.93	28.19 ^{a} ± 0.54	182.22 ^{a} ± 5.95	13.33 ^{a} ± 0.18	6.65 ^{e} ± 0.09
20.51	27.80 ^{a} ± 0.74	176.70 ^{ab} ± 6.05	11.23 ^{c}± 0.29	6.80 ^{e} ± 0.10
40.09	26.57 ^{a} ± 0.66	168.30 ^{ab} ± 6.37	10.50 ^{d} ± 0.16	7.35 ^{d} ± 0.12
59.87	23.49 ^{b} ± 0.71	156.68 ^{bc} ± 6.97	10.23 ^{d} ± 0.23	8.63 ^{c} ± 0.11
p-Value	<0.001	<0.001	<0.001	<0.001

$^{a–f}$ Within the same column, mean values with different superscripts differ significantly ($p < 0.05$) with mean ± SE. Abbreviations: CAT: catalase; MDA: malondialdehyde; T-AOC: total antioxidant capacity; T-SOD: total superoxide dismutase.

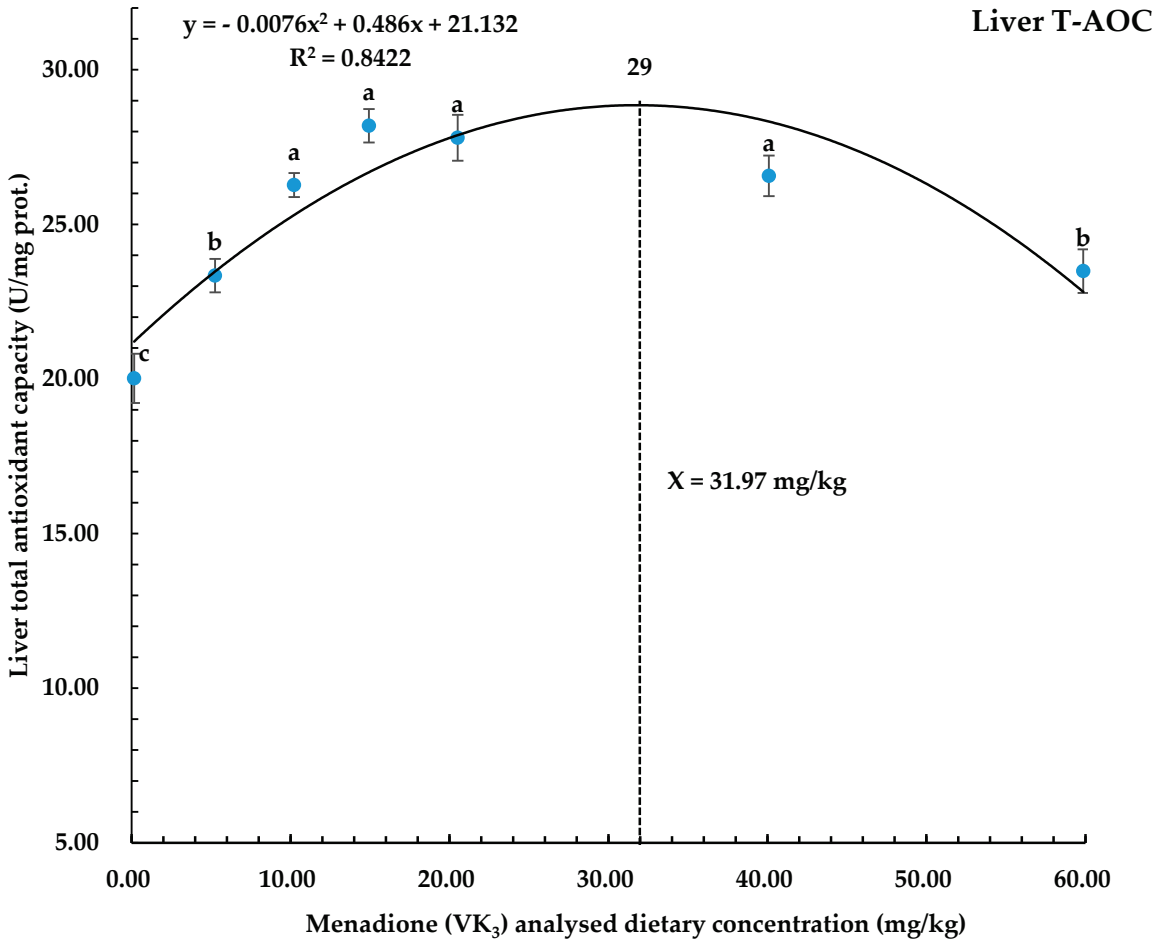


Figure 4. Polynomial quadratic regression analysis of T-AOC with graded levels of vitamin K_3 in coho salmon alevins predicted that the optimum vitamin K_3 requirement for T-AOC was 31.97 mg/kg. Abbreviations: T-AOC, total antioxidant capacity; dotted line shows X value and complete curve line shows trend.

4. Discussion

It is well documented that Vitamin K is essential in attaining and maintaining optimal growth during early growing and developmental stages [8,34]. The deficiency and excessive intake of VK_3 have also been reported to reduce growth performance [27,45,46].

In the current study, results showed that VK_3 addition to the diet has improved the SR, WG, SGR, and FCR in all VK_3-supplemented groups. Different researchers have studied different doses for growth parameters. In line with the present study, an increase in body weight gain was reported at 6.5 to 9.8 mg/kg menadione in cod, while suggesting a decrease in body weight on excess or low dietary inclusion of VK_3 (43). Wei et al. [34] recommended adding 15.08 mg/kg menadione sodium bisulfite to the diet of largemouth bass, but negative WG and SGR were observed with 20.85 mg/kg, pointing out toxicity effects at higher doses. Similarly, Sivagurunathan et al. [29] have found that the addition of VK_3 up to 70 mg/kg has shown improvement in growth and survival rate in gilthead seabream larvae. Additionally, Dominguez et al. [16] recommended the use of an optimal level of 12 mg/kg of VK_3 in gilthead seabream fingerlings for improvement in growth, while similar recommendations for growth with increasing levels of VK_3 were suggested by Richard et al. [8] in Senegalese sole larvae. In contrast to the present study, some researchers found no effect of VK_3 addition in the diet on growth-related parameters. For example, Abdelhamid et al. [31] found no effect in juvenile Nile tilapia on the addition of

2–12 mg/kg VK_3, and Dai et al. [30] found that 9.97–156.09 mg/kg of VK_3 had no effect in shrimps, while Grisdale-Helland et al. [47] suggested avoiding the use of menadione sodium bisulfite (MSB), noting that vitamin K_1 was more effective in reducing mortality in Atlantic salmon (*Salmo salar*). They suggested that MSB may increase the fish's susceptibility to environmental and pathogenic stressors, possibly due to its lower stability and higher toxicity, as well as its tendency to undergo redox reactions that generate reactive oxygen species, leading to oxidative stress and cytotoxicity. The variation in VK_3 requirements observed across studies may be attributed to different fish species, growth stages, rearing conditions, and feeding nature. Based on the findings of our research regarding growth parameters, we concluded that the predicted required dietary concentration of VK_3 for WG and SGR was 34.0 and 43.50 mg/kg, respectively, for coho salmon alevins during early growth.

The dietary ingredients have a direct impact on the muscle composition [48]. The different concentrations of VK_3 in the diet have revealed no effect on the whole-body chemical composition during the present study. Likewise, Wei et al. [34] found no effect of VK_3 dietary supplementation on body muscle composition, including crude protein, crude fat, ash, and moisture contents up to 20.85 mg/kg VK_3 in largemouth bass. Dominguez et al. [16] also stated that whole-muscle composition was not altered with dietary VK_3 addition in the diet of gilthead seabream fingerlings. Graff et al. [49] also supported this claim in Atlantic salmon. This indicates that the presence of VK_3 in the diet has no adverse effects on the muscle composition.

The VK_3 acts as a pro-vitamin K and is converted to menaquinone-4 (MK-4) in body tissues [45] and stored mainly in the liver [23]. This study's results showed that during whole-body muscle and liver sample analyses for MK-4, the concentrations of MK-4 were increased with a gradual increase in dietary VK_3 supplementation. Similar findings were noticed by Grahl-Madsen and Lie [45] in Atlantic cod (*Gadus morhua*) with a dietary concentration of up to 9.93 to 15.22 mg/kg VK_3 in the diet. Wei et al. [34] also endorsed that the addition of VK_3 in the diet may increase the MK-4 in the liver of largemouth bass with the optimal dietary concentration of 11.20 mg/kg VK_3. Vera et al. [50] added that increasing the level of dietary VK_3 has an increasing effect on the whole-body MK-4 concentration in adult Atlantic salmon, and this was also supported by Graff et al. [49] in Atlantic salmon parr. However, no supporting literature was available for adding and quantifying the dietary concentration level of VK_3 in coho salmon alevins. However, contrary to the findings of this study, previous research [34] suggests that higher doses (20.85 mg/kg) of MNB may lead to a decline in MK-4 concentration in largemouth bass due to potential toxicity effects. In the present study, dietary VK_3 was efficiently converted into menaquinone-4 (MK-4) without any adverse effects on liver metabolism, and MK-4 was distributed throughout the body as dietary VK_3 levels increased. The optimal dietary requirement of VK_3 for achieving adequate MK-4 levels in the liver was estimated to be 38.54 mg/kg. The higher MK-4 concentrations observed in both the liver and the whole body suggest that increasing VK_3 doses may provide more substrate for conversion to MK-4, as lower VK_3 may degrade during the conversion process or feed manufacturing, leading to a reduced bioavailable amount of VK_3 for conversion into MK-4 in the tissues [17]. Therefore, the increase in dietary VK_3 likely resulted in higher availability of MK-4 in both the liver and body. Regardless of the other physiological effects of VK_3 in fish, it protects the body by reducing the production of peroxides, as these peroxides are mainly involved in lipid peroxidation by producing free radicals [31,51,52]. The liver enzymes are present in the liver and are released into the blood when damage to cells occurs. The high concentration of these liver enzymes will represent higher values in the blood too. Antioxidant enzymes, such as superoxide dismutase (SOD) and catalase (CAT), act as

natural scavengers of free radicals. They protect cells from oxidative stress and prevent lipid peroxidation caused by reactive oxygen species (ROS), thereby enhancing the overall antioxidant status [31,32,53]. Total antioxidant capacity (T-AOC) serves as a comprehensive indicator of the body's antioxidant defense system. It plays a crucial role in protecting the body against oxidative damage induced by free radicals [54].

Certain natural bioactive compounds, including VK_3, have the capacity to increase the production of SOD and CAT, which ultimately help to capture the free radicals, thus improving the antioxidant capacity in the fish at 39.06 mg/kg VK_3 in the diet [30], and up to 2–4 mg/kg was reported by Abdelhamid et al. [31]. Similarly, MDA is the product of lipid peroxidation, which increases with more free radical reactions and is considered a potent indicator of tissue damage in the liver [55]. Some nutraceuticals have shown the potential to reduce lipid peroxidation by various mechanisms, including the increase in the concentration of liver SOD and CAT. In the current study, the increasing concentration of dietary VK_3 has increased the T-AOC, T-SOD, and CAT while it has decreased the concentration of MDA in liver samples, indicating the positive effects of VK_3 on liver health [32]. In line with the present study, Dai et al. [30] reported that the addition of 39.06 mg/kg VK_3 in the diet has increased the T-AOC and catalase enzyme concentration in serum while it has reduced the MDA contents in whiteleg shrimp. Similarly, Wei et al. [34] also reported that the optimal dose of up to 9.93 to 15.22 mg/kg VK_3 in the diet of largemouth bass was found to be effective to improve SOD and T-AOC contents and to lower MDA contents in the liverQuadratic regression analysis in the present study has predicted the optimal required dietary VK_3 level of 31.97 mg/kg for better T-AOC in coho salmon alevins.

5. Conclusions

In conclusion, this study demonstrates that the inclusion of synthetic vitamin K_3 has significantly improved the growth performance, whole-body MK-4, and liver MK-4 concentrations and liver total antioxidant capacity in coho salmon alevins at a dietary concentration of above 0.16 mg/kg in all treatments. Quadratic regression analysis based on the WG, SGR, liver MK-4, and liver T-AOC predicted the optimal dietary vitamin K_3 levels to be 34.00, 43.50, 38.54, and 31.97 mg/kg, respectively, in coho salmon alevins.

Author Contributions: H.Y.: Project Administration, Conceptualization, Validation, Review and Editing, S.G. and L.L.: Software, Review and Editing, A.R. and M.W.: Original draft writing, Software Analysis, Review and Editing, H.Z. and L.Y.: Methodology, Formal Analyses, Review and Editing. All authors have read and agreed to the published version of the manuscript.

Funding: Funding for this research was provided by Shandong Provincial Key Research and Development Programs (Major Scientific and Technological Innovation Projects, MSTIP), Grant/Award Numbers: 2018CXGC0102 and 2019JZZY020710; Scientific and Technologic Development Program of Weifang, Grant/Award Number: 2019ZJ1046; Shandong Provincial Natural Science Foundation, Grant/Award Number: ZR2020MC174; Technical Development (Entrustment) Project between University and Enterprise (Grant/Award Number: 20240701CLFWFU01).

Institutional Review Board Statement: The present study was carried out according to the recommendations in the "Guide for the Ethical Use of Experimental Animals" of the Weifang University, Weifang, Shandong, China (No. 20200601) and it was approved by the Institutional Animal Care and Use Committee of the Institute of Modern Facility Fisheries, Weifang University, China (IACUC NO. 20220516003). The funder was not involved in the study design, collection, analysis, interpretation of data, the writing of this article, or the decision to submit it for publication.

Informed Consent Statement: Not applicable.

Data Availability Statement: All the data in the article are available from the corresponding author upon reasonable request.

Conflicts of Interest: Authors Abdur Rahman, Sattanathan Govindharajan, and Lingyao Li were employed by the company "Conqueren Leading Fresh Science & Technology Inc., Ltd.; Shandong Conqueren Marine Technology Co., Ltd." The remaining all authors declare that the research was conducted in the absence of any commercial or financial relationships that could be construed as a potential conflict of interest. So, all authors certify that they have no conflicts to declare. The funder was not involved in the study design, collection, analysis, interpretation of data, the writing of this article, or the decision to submit it for publication.

References

1. Caires, R.; Sierra-Valdez, F.J.; Millet, J.R.; Herwig, J.D.; Roan, E.; Vásquez, V.; Cordero-Morales, J.F. Omega-3 Fatty Acids Modulate TRPV4 Function through Plasma Membrane Re-modeling. *Cell Rep.* **2017**, *21*, 246–258. [CrossRef] [PubMed]
2. Ullah, M.; Rasool, F.; Khan, N.; Ali, S.; Sheikh, A.A. Antibiotic resistance and its gene profile in Escherichia coli isolated from diseased farm-raised carps in Punjab, Pakistan. *Pak. Vet. J.* **2023**, *43*, saa 470–476. [CrossRef]
3. Alsulami, M.N.; El-Saadony, M.T. The Enhancing Effect of Bacterial Zinc Nanoparticles on Performance, Immune Response, and Microbial Load of Nile Tilapia (*Oreochromis niloticus*) by Reducing the Infection by *Trichodina heterodentata*. *Pak. Vet. J.* **2024**, *44*, 599–610. [CrossRef]
4. Andrades, J.A.; Becerra, J.; Fernández-Llebrez, P. Skeletal deformities in larval, juvenile, and adult stages of cultured gilthead seabream (*Sparus aurata* L.). *Aquaculture* **1996**, *141*, 1–11. [CrossRef]
5. Afonso, J.M.; Montero, D.; Robaina, L.; Astorga, N.; Izquierdo, M.S.; Ginés, R. Association of a lordosis-scoliosis-kyphosis deformity in gilthead seabream (*Sparus aurata*) with family structure. *Fish Physiol. Biochem.* **2000**, *22*, 159–163. [CrossRef]
6. Boglione, C.; Gagliardi, F.; Scardi, M.; Cataudella, S. Skeletal descriptors and quality assessment in larvae and post-larvae of wild-caught and hatchery-reared gilthead seabream (*Sparus aurata* L. 1758). *Aquaculture* **2001**, *192*, 1–22. [CrossRef]
7. Berillis, P. Skeletal deformities in seabreams: Understanding the genetic origin can improve production? *J. Fish Sci.* **2017**, *11*, 57–59. [CrossRef]
8. Richard, N.; Fernández, I.; Wulff, T.; Hamre, K.; Cancela, L.; Conceição, L.E.C.; Gavaia, P.J. Dietary supplementation with vitamin K affects transcriptome and proteome of Senegalese sole, improving larval performance and quality. *Mar. Biotechnol.* **2014**, *16*, 522–537. [CrossRef]
9. Izquierdo, M.; Domínguez, D.; Jiménez, J.I.; Saleh, R.; Hernández-Cruz, C.M.; Zamorano, M.J.; Hamre, K. Interaction between taurine, vitamin E, and vitamin C in microdiets for gilthead seabream (*Sparus aurata*) larvae. *Aquaculture* **2019**, *498*, 246–253. [CrossRef]
10. Izquierdo, M.; Fernandez-Palacios, H. Nutritional requirements of marine fish larvae and broodstock. *Cah. Options Méditerranéennes* **1997**, *22*, 243–264.
11. Izquierdo, M.S.; Socorro, J.; Arantzamendi, L.; Hernández-Cruz, C.M. Recent advances in lipid nutrition in fish larvae. *Fish Physiol. Biochem.* **2000**, *22*, 97–107. [CrossRef]
12. National Research Council (NARC). *Nutrient Requirements of Fish and Shrimp*; National Academies Press: Washington, DC, USA, 2011.
13. Graff, I.E.; Øyen, J.; Kjellevold, M.; Frøyland, L.; Gjesdal, C.G.; Almås, B.; Rosenlund, G.; Lie, Ø. Reduced bone resorption by intake of dietary vitamin D and K from tailor-made Atlantic salmon: A randomized intervention trial. *Oncotarget* **2016**, *7*, 69200–69215. [CrossRef]
14. Furukawa, N.; Chen, X.; Asano, S.; Matsumoto, M.; Wu, Y.; Murata, K.; Takeuchi, A.; Tode, C.; Homma, T.; Koharazawa, R.; et al. Synthesis of New Vitamin K Derivatives with a Ketone Group at the C-1′ Position of the Side Chain and Their Conversion to Menaquinone-4. *J. Mol. Struct.* **2023**, *1276*, 134614. [CrossRef]
15. Krossøy, C.; Waagbø, R.; Ørnsrud, R. Vitamin K in fish nutrition. *Aquac. Nutr.* **2011**, *17*, 585–594. [CrossRef]
16. Dominguez, D.; Castro, P.; Lall, S.; Montero, D.; Zamorano, M.J.; Fontanillas, R.; Izquierdo, M. Effects of menadione sodium bisulphite (vitamin K3) supplementation of diets based on plant feed ingredients on growth and bone health of gilthead seabream (*Sparus aurata*) fingerlings. *Aquac. Nutr.* **2022**, 1613030. [CrossRef]
17. Graff, I.E.; Krossøy, C.; Gjerdevik, K.; Julshamn, K. Influence of dietary menadione nicotinamide bisulphite (vitamin K3) and phylloquinone (vitamin K1) on Atlantic salmon (*Salmo salar* L.) tissue levels. *Aquac. Nutr.* **2010**, *16*, 637–647. [CrossRef]
18. Lall, S.P.; Lewis-McCrea, L.M. Role of nutrients in skeletal metabolism and pathology in fish—An overview. *Aquaculture* **2007**, *267*, 3–19. [CrossRef]
19. Neacsu, C.D.; Grosch, M.; Tejada, M.; Winterpacht, A.; Paulsson, M.; Wagener, R.; Tagariello, A. Ucmaa (Grp-2) is required for zebrafish skeletal development: Evidence for a functional role of its glutamate γ-carboxylation. *Matrix Biol.* **2011**, *30*, 369–378. [CrossRef] [PubMed]

20. Oldenburg, J.; Marivona, M.; Müller-Reible, C.; Waltzka, M. The vitamin K cycle. *Vitam. Horm.* **2008**, *78*, 35–62. [CrossRef]
21. Rishavy, M.A.; Berkner, K.L. Vitamin K oxygenation, glutamate carboxylation, and processivity: Defining the three critical facets of catalysis by the vitamin K-dependent carboxylase. *Adv. Nutr.* **2012**, *3*, 135–148. [CrossRef]
22. Poston, H.A. Relative effect of two dietary water-soluble analogues of menaquinone on coagulation and packed cell volume of blood of lake trout (*Salvelinus namaycush*). *J. Fish Res. Board Can.* **1976**, *33*, 1791–1793. [CrossRef]
23. Taveekijakarn, P.; Miyazaki, T.; Matsumoto, M.; Arai, S. Studies on vitamin K deficiency in Amago salmon, *Oncorhynchus rhodurus* (Jordan & McGregor). *J. Fish Dis.* **1996**, *19*, 209–214.
24. Udagawa, M. The Effect of Dietary Vitamin K (Phylloquinone and Menadione) Levels on the Vertebral Formation in Mummichog Fundulus heteroclitus. *Fish Sci.* **2001**, *67*, 104–109. [CrossRef]
25. Halver, J.E.; Hardy, R.W. The Vitamins. In *Fish Nutrition*, 3rd ed.; Academic Press: San Diego, CA, USA, 2002; pp. 62–141.
26. Roy, P.K.; Lall, S.P. Vitamin K Deficiency Inhibits Mineralization and Enhances Deformity in Vertebrae of Haddock (*Melanogrammus aeglefinus* L.). *Comp. Biochem. Physiol. B Biochem. Mol. Biol.* **2007**, *148*, 174–183. [CrossRef]
27. Shiau, S.-Y.; Liu, J.-S. Estimation of the Dietary Vitamin K Requirement of Juvenile (*Penaeus chinensis*) Using Menadione. *Aquaculture* **1994**, *126*, 129–135. [CrossRef]
28. Fu, J.-H.; Xu, W.; Mai, K.; Zhang, W.-B.; Feng, X.-N.; Liufu, Z.-G. Effects of Dietary Menadione on the Activity of Antioxidant Enzymes in Abalone (*Haliotis discus hannai Ino*). *Chin. J. Oceanol. Limnol.* **2012**, *30*, 118–123. [CrossRef]
29. Sivagurunathan, U.; Dominguez, D.; Tseng, Y.; Zamorano, M.J.; Prabhu, A.J.; Izquierdo, M. Deficiency and Excess in Dietary Vitamin K3 Negatively Affect Gilthead Seabream (*Sparus aurata*) Larvae Performance and Bone Health. *Aquaculture* **2023**, *574*, 739646. [CrossRef]
30. Dai, T.; Zhang, X.; Li, M.; Tao, X.; Jin, M.; Sun, P.; Jiao, L. Dietary Vitamin K3 Activates Mitophagy, Improves Antioxidant Capacity, Immunity, and Affects Glucose Metabolism in L. vannamei. *Food Funct.* **2022**, *13*, 6362–6372. [CrossRef]
31. Abdelhamid, A.F.; Gewida, A.G.A.; El-Sayed, A.F.M.; Badran, M.F. Impacts of Different Levels of Vitamin K on the Growth Performance, Hematological Parameters, and Immunological Response of Juvenile Nile Tilapia (*Oreochromis niloticus*). *Aquac. Int.* **2024**, *32*, 477–488. [CrossRef]
32. Yuan, J.; Feng, L.; Jiang, W.D.; Liu, Y.; Jiang, J.; Li, S.H.; Zhou, X.Q. Effects of Dietary Vitamin K Levels on Growth Performance, Enzyme Activities and Antioxidant Status in the Hepatopancreas and Intestine of Juvenile Jian Carp (*Cyprinus carpio* var. Jian). *Aquac. Nutr.* **2016**, *22*, 352–366. [CrossRef]
33. Cheng, L.; Zhang, W.; Lin, S.; Xu, W.; Mai, K. Effects of Dietary Vitamin K on Growth Performances, Blood Coagulation Time, and Menaquinone-4 (MK-4) Concentration in Tissues of Juvenile Large Yellow Croaker (*Pseudosciaena crocea*). *Aquac. Res.* **2015**, *46*, 1269–1275. [CrossRef]
34. Wei, X.; Hang, Y.; Li, X.; Hua, X.; Cong, X.; Yi, W.; Guo, X. Effects of Dietary Vitamin K3 Levels on Growth, Coagulation, Calcium Content, and Antioxidant Capacity in Largemouth Bass(*Micropterus salmoides*). *Aquac. Fish.* **2023**, *8*, 159–165. [CrossRef]
35. Hart, J.L. Pacific Fishes of Canada. *Bull. Fish. Res. Board Can.* **1973**, *180*, 1–740, reprinted in **1975**, *1980*, 1988.
36. FAO. *Brief to The State of World Fisheries and Aquaculture 2024*; Blue Transformation in Action; FAO: Rome, Italy, 2024. [CrossRef]
37. Swanson, D.; Block, R.; Mousa, S.A. Omega-3 Fatty Acids EPA and DHA: Health Benefits throughout Life. *Adv. Nutr.* **2012**, *3*, 1–7. [CrossRef]
38. Tsoupras, A.; Brummell, C.; Kealy, C.; Vitkaitis, K.; Redfern, S.; Zabetakis, I. Cardio-Protective Properties and Health Benefits of Fish Lipid Bioactives; The Effects of Thermal Processing. *Mar. Drugs* **2022**, *20*, 187. [CrossRef]
39. Kiranpreet, K.; Trond, M.K.; Tibiabin, B.S.; Lena, B. Effects of Antarctic Krill Products on Feed Intake, Growth Performance, Fillet Quality, and Health in Salmonids. *Aquac. Nutr.* **2022**, *2022*, 3170854. [CrossRef]
40. Yu, H.-R.; Guo, M.-J.; Yu, L.-Y.; Li, L.-Y.; Wang, Q.-H.; Li, F.-H.; Zhang, Y.-Z.; Zhang, J.-Y.; Hou, J.-Y. Effects of Dietary Riboflavin Supplementation on the Growth Performance, Muscle composition and Anti-Oxidative Capacity of Coho Salmon (*Oncorhynchus kisutch*) Post-Smolts. *Animals* **2022**, *12*, 3218. [CrossRef] [PubMed]
41. Paulus, M.C.; Drent, M.; Kouw, I.W.K.; Balvers, M.G.J.; Bast, A.; van Zanten, A.R.H. Vitamin K: A Potential Missing Link in Critical Illness—A Scoping Review. *Crit. Care* **2024**, *28*, 212. [CrossRef]
42. Yu, H.; Sattanathan, G.; Yu, L.; Li, L.; Xiao, Y. Impact of Nutritional Tea Polyphenols on Growth, Feed Efficiency, Biochemical Traits, Antioxidant Capacity, Haematological Parameters and Immunity in Coho Salmon (*Oncorhynchus kisutch*). *Animals* **2024**, *14*, 2104. [CrossRef]
43. AOAC (Association of Official Analytical Chemists). *Official Methods of Analysis*, 15th ed.; AOAC: Arlington, VA, USA, 1990.
44. Ostermeyer, U.; Schmidt, T. Determination of vitamin K in edible part of fish by high-performance liquid chromatography. *Eur. Food Res. Technol.* **2001**, *212*, 518–528. [CrossRef]
45. Grahl-Madsen, E.; Lie, Ø. Effects of different levels of vitamin K in diets for cod (*Gadus morhua*). *Aquaculture* **1997**, *151*, 269–274. [CrossRef]
46. Duan, Y.H.; Zhu, X.M.; Han, D.; Yang, Y.X.; Jin, J.Y.; Xie, S.Q. Dietary vitamin K requirement of juvenile gibel carp (*Carassius auratus gibelio*). *Acta Hydrobiol. Sin.* **2013**, *37*, 8–15.

47. Grisdale-Helland, B.; Helland, S.J.; Åsgård, T. Problems associated with the present use of menadione sodium bisulfite and vitamin A in diets for Atlantic salmon. *Aquaculture* **1991**, *92*, 351–358. [CrossRef]
48. Krossøy, C.; Waagbø, R.; Fjelldal, P.-G.; Wargelius, A.; Lock, E.-J.; Graff, I.E.; Ørnsrud, R. Dietary menadione nicotinamide bisulphite (vitamin K3) does not affect growth or bone health in first-feeding fry of Atlantic salmon (*Salmo salar* L.). *Aquac. Nutr.* **2009**, *15*, 532–540. [CrossRef]
49. Graff, I.E.; Waagbø, R.; Fivelstad, S.; Vermeer, C.; Lie, Ø.; Lundebye, A.K. A multivariate study on the effects of dietary vitamin K, vitamin D3, and calcium, and dissolved carbon dioxide on growth, bone minerals, vitamin status, and health performance in smolting Atlantic salmon (*Salmo salar* L.). *J. Fish Dis.* **2002**, *25*, 93–106. [CrossRef]
50. Vera, L.M.; Hamre, K.; Espe, M.; Hemre, G.I.; Skjærven, K.; Lock, E.J.; Prabhu, A.J.; Leeming, D.; Migaud, H.; Tocher, D.R.; et al. Higher dietary micronutrients are required to maintain optimal performance of Atlantic salmon (*Salmo salar*) fed a high plant material diet during the full production cycle. *Aquaculture* **2020**, *528*, 735551. [CrossRef]
51. Tampo, Y.; Yonaha, M. Enzymatic and molecular aspects of the antioxidant effect of menadione in hepatic microsomes. *Arch. Biochem. Biophys.* **1996**, *334*, 163–174. [CrossRef]
52. Kohen, R.; Nyska, A. Oxidation of biological systems: Oxidative stress phenomena, antioxidants, redox reactions, and methods for their quantification. *Toxicol. Pathol.* **2002**, *30*, 620–650. [CrossRef]
53. Fang, Y.Z.; Yang, S.; Wu, G. Free radicals, antioxidants, and nutrition. *Nutrition* **2002**, *18*, 872–879. [CrossRef]
54. Mukai, K.; Morimoto, H.; Okauchi, Y.; Nagaoka, S.-I. Kinetic study of reactions between tocopheroxyl radicals and fatty acids. *Lipids* **1993**, *28*, 753–756. [CrossRef]
55. Sahin, M.A.; Yucel, O.; Guler, A.; Doganci, S.; Jahollari, A.; Cingoz, F.; Arslan, S.; Gamsizkan, M.; Yaman, H.; Demirkilic, U. Is there any cardioprotective role of taurine during cold ischemic period following global myocardial ischemia? *J. Cardiothorac. Surg.* **2011**, *6*, 31. [CrossRef] [PubMed]

Disclaimer/Publisher's Note: The statements, opinions and data contained in all publications are solely those of the individual author(s) and contributor(s) and not of MDPI and/or the editor(s). MDPI and/or the editor(s) disclaim responsibility for any injury to people or property resulting from any ideas, methods, instructions or products referred to in the content.

biology

MDPI

Article

Molecular Adaptations and Quality Enhancements in a Hybrid (*Erythroculter ilishaeformis* ♀× *Ancherythroculter nigrocauda* ♂) Cultured in Saline–Alkali Water

Lang Zhang [1,†], Qiuying Qin [2,†], Qing Li [3,4], Yali Yu [1], Ziwei Song [1], Li He [1], Yanhong Sun [3,4], Liting Ye [1], Guiying Wang [3,4,*] and Jing Xu [2,*]

[1] Yangtze River Fisheries Research Institute, Chinese Academy of Fishery Sciences, Wuhan 430223, China; zhanglang@yfi.ac.cn (L.Z.); ylyu8811@yfi.ac.cn (Y.Y.); 2021203010012@whu.edu.cn (Z.S.); heli@yfi.ac.cn (L.H.); 2024308120018@webmail.hzau.edu.cn (L.Y.)
[2] College of Pharmacy, South Central University for Nationalities, Wuhan 430074, China; 2022120658@mail.scuec.edu.cn
[3] Fisheries Research Institute, Wuhan Academy of Agricultural Sciences, Wuhan 430207, China; liqing@wuhanagri.com (Q.L.); sunyanhong@wuhanagri.com (Y.S.)
[4] Wuhan Xianfeng Aquaculture Technology Co., Ltd., Wuhan 430207, China
* Correspondence: wangguiying@wuhanagri.com (G.W.); xuj@mail.scuec.edu.cn (J.X.)
† These authors contributed equally to this work.

Simple Summary: Global freshwater shortages are pushing farmers to explore fish farming in "saline–alkali" water, but how fish adapt to these conditions and whether their meat quality changes remains unclear. To investigate this phenomenon, we conducted a study on a hybrid fish reared in saline–alkali water for a duration of two months, employing enzyme activity assays and multi-omics analysis. The findings revealed that the fish developed stress defense mechanisms conferring protection against adverse environmental conditions. This suggests the potential for employing saline–alkali water in sustainable aquaculture practices, especially in regions where freshwater resources are limited.

Abstract: Declining freshwater resources have spurred interest in saline–alkali (SA) water aquaculture, with species like tilapia and rainbow trout demonstrating ecological plasticity in such environments. However, the molecular mechanisms underlying fish adaptation and quality impacts remain unclear. This study investigated the hybrid fish "Xianfeng No. 1" (*Erythroculter ilishaeformis* × *Ancherythroculter nigrocauda*), a key aquaculture species in China, under 60-day SA exposure. The results showed increased levels of oxidative stress markers (MDA) and antioxidant enzymes (SOD, CAT, GSH-Px), alongside improved quality traits. Transcriptomics revealed differentially expressed genes (DEGs) in muscle tissue associated with oxidative stress (*UQCRFS1*, *UQCR10*, *CYC1*), ion transport (*COX5A*, *COX7C*, *COX7B*), and the immune response (*ATG9A*, *ATG2B*, *ATG2A*, *ULK1*, *ULK2*, *CFI*, *CFH*). Metabolomics identified increased non-volatile flavors (e.g., glycine, proline) and collagen-related compounds. Integrated analysis highlighted the upregulation of *GSR* and *GGT*, and the downregulation of *CHDH* and *GBSA*, potentially driving glycine accumulation. These findings suggest that SA stress enhances antioxidant capacity, activates immune pathways, and modulates ion transport, enabling adaptation while improving meat quality. This study elucidates molecular mechanisms of fish acclimation to SA environments, providing insights for sustainable aquaculture development and breeding of stress-tolerant species in SA regions.

Keywords: saline–alkali stress; antioxidant defense; immune response; environment; nutrition

1. Introduction

Saline–alkali (SA) water is a widespread phenomenon globally, typically forming in regions experiencing prolonged dry spells, inadequate rainfall, or intense evaporation [1]. In China alone, approximately 46 million hectares of such water exist [2]. The consequences of excessive concentrations of SA are severe, disrupting the growth, survival, and reproduction of aquatic life in water bodies such as rivers and lakes. This disruption leads to reduced biomass and significant shifts in ecological diversity [3,4]. Moreover, contemporary research suggests that climate change exacerbates the salinization and alkalization of water ecosystems, posing a threat to the already limited habitat available for freshwater aquaculture [5]. This trend has heightened concerns regarding the increasing salinity and alkalinity of water environments, prompting efforts to enhance aquaculture in such challenging conditions. Moreover, there is evidence indicating negative impacts on physiological functions such as immune modulation and oxidative stress [6]. For instance, alkaline stress triggers reactive oxygen species (ROS)-mediated activation of the mitogen-activated protein kinase (MAPK) pathway and mammalian target of rapamycin (mTOR) inhibition, leading to autophagy in *Eriocheir sinensis* [7]. Additionally, alkaline conditions can induce physiological disorders in fish, such as hypocapnia and respiratory alkalosis [8]. Furthermore, under low-salinity conditions, fish must allocate more energy to osmotic pressure regulation and less energy to growth, disrupting biochemical homeostasis and causing growth retardation [9]. Thus, understanding the intricate molecular processes governing fish responses to SA stress could significantly mitigate these impacts and enhance the efficient utilization of SA waters for fish farming.

Saline waters not only influence the adaptation and survival of fish but also have an impact on their essential nutritional components and quality attributes [10]. For instance, research has shown that low-salt conditions significantly alter the metabolic pathways of amino acids and fatty acids in fish, resulting in noticeable changes in flavor and meat quality [11,12]. SA stress can modify the biochemical composition of fish muscle, thereby affecting its nutritional and sensory properties, which are critical factors for consumer preference and market value [13]. These alterations may manifest as fluctuations in the levels of free amino acids, contributing to taste, and modifications in fatty acid profiles, influencing both the health benefits and taste of fish [11]. While existing studies have addressed the impact of SA stress on amino acids, fatty acids, and traditional nutritional components of fish, there is still a gap in understanding its effects on the muscle quality characteristics of fish.

The ongoing progression of omics techniques has significantly advanced the field of systems biology and provided indispensable tools for investigating aquatic organisms [14–16]. The recent research focus has shifted towards utilizing transcriptomics to unravel the adaptive mechanisms employed by fish in SA environments [9,17]. Previously, we conducted transcriptomic studies on Xiangfeng No. 1, investigating its transcriptomic expression under various experimental conditions [18]. Transcriptomics reveals gene expression patterns but lacks resolution for metabolite-driven pathway analysis [19,20]. In contrast, metabolomics has emerged as a critical technique for elucidating the intricate association between metabolite fluxes and the internal or external stimuli encountered by organisms, offering new avenues for in-depth research in this domain [21]. The use of a single omics technology often poses challenges in comprehensively deciphering the underlying molecular mechanisms of environmental stress responses. In comparison, multi-omics approaches are valuable tools for comprehensively and precisely evaluating mechanisms in the field [22,23]. Therefore, the synergistic integration of transcriptomics and metabolomics analyses holds promise for providing a nuanced understanding of the interplay between metabolic pathways and gene expression networks, revealing the intricate coordination involved.

The top-mouth culter (*Erythroculter ilishaeformis*) is a highly consumed commercial fish in China [24]. However, artificial breeding of this species can be challenging and costly due to its substantial size. In contrast, *Ancherythroculter nigrocauda*, a member of the Cyprinidae family, is smaller in size and of lower economic significance due to its slower rate of development [25]. In recent years, scientists have successfully utilized distant hybridization techniques to create a hybrid F1 known as "Xianfeng No. 1" for aquaculture purposes [26]. Offspring resulting from the cross between *A. nigrocauda* (♂) and *E. ilishaeformis* (♀) exhibit superior traits, including increased stress tolerance, compared to their parental species, along with enhanced disease resistance [27]. Moreover, these hybrid fish are easier to catch and transport and are well-suited to aquaculture in ponds. To advance the expansion of hybrid aquaculture into SA environments, it is critical to investigate the mechanistic basis of its adaptability in SA stress and systematically characterize the physiological and genetic traits that enable its survival in such conditions. Regrettably, there exists a dearth of research regarding the tolerance of the species to SA waters and the potential methods for enhancing the nutritional value of its fish fillets [28].

In this research, we conducted a thorough study using multi-omics techniques to analyze gene expression and metabolic changes in the hybrid fish "Xianfeng No. 1" exposed to SA conditions. Our goal was to identify the molecular mechanisms involved in the fish's response and adaptation to this stress. Furthermore, our study evaluated alterations in the quality traits of hybrids in SA water through non-targeted metabolomics analysis. The findings of this investigation have the potential to enhance our knowledge of stress responses in fish, contribute to the advancement of aquaculture practices, and aid in the development of breeding strategies for species with increased tolerance to SA conditions.

2. Materials and Methods

2.1. Ethics Statement

The culter hybrids are widely cultivated in mainland China and are not subject to protection. All experiments conducted adhered to the guidelines of the Yangtze River Fisheries Research Institute, Chinese Academy of Fishery Sciences (Permit No. 2022zhanglang002).

2.2. Chemical Reagents

The chemical reagents $NaHCO_3$ (Cat No. 10018960) and NaCl (Cat No. 10019318) were purchased from the National Medicines Corporation Ltd., Beijing, China.

2.3. Experimental Animals and Design

The hybrid fish were acclimatized in an indoor recirculating water system with predefined water parameters for a duration of two weeks before the initiation of the experiment. Following the acclimation period, 120 hybrid fish with an average weight of 162.21 ± 32.41 g and a body length of 25.6 ± 2.3 cm were randomly selected and divided into two groups ($n = 60$). Subsequently, each group was allocated to six separate circular flumes with specific dimensions (height = 80 cm; diameter = 140 cm); each flume contained 10 hybrid fish. One group was designated as the control group and provided with fresh water, while the other group was subjected to SA stress, achieved by adding $NaHCO_3$ (12 mmol/L) and NaCl (86 mmol/L) to the water. The concentrations of SA were determined based on data from previous studies [29]. After an additional three-day acclimation period without feeding, the formal experiment was initiated.

The fish were provided with commercial pellets (Haida Co., Ltd., Nantong City, Jiangsu Province, China) that were formulated in accordance with the Chinese national standard for fish feed (GB/T 22919.5-2008) [30]. The feed composition included 32% crude protein, 6% lipid, 4% crude fiber, 12% ash, and 40% carbohydrate, supplemented with

trace amounts of vitamins and minerals to fulfill nutritional requirements. Feeding was conducted twice daily until the fish exhibited visible satisfaction. Every three days, one-third of the water in the circular flumes was replaced. Over the course of 60 days, water quality parameters were monitored daily (pH 8.5 ± 0.5; dissolved oxygen > 6.8 mg/L; NH3 0–0.4 mg/L; nitrite 0–0.2 mg/L). Notably, no fish mortality occurred throughout the duration of the experiment.

2.4. Measurement of Enzyme Activities

The activities of the enzymes malondialdehyde (MDA), superoxide dismutase (SOD), catalase (CAT), and glutathione peroxidase (GSH-Px) were assessed utilizing specific assay kits provided by Jiancheng Bioengineering (MDA: Cat. No. A003-1-2, SOD: Cat. No. A001-3, CAT: Cat. No. A007-1, GSH-Px: Cat. No. A005-1-2). Muscle tissue samples were homogenized in ice-cold physiological saline at a 1:9 weight-to-volume ratio, followed by centrifugation at 2500× *g* at 4 °C for 10 min to obtain the supernatant for subsequent analysis. Protein concentrations in the supernatant were quantified using the bicinchoninic acid (BCA) assay, as per the manufacturer's protocol (Jiancheng Bioengineering Testing Kit, Nanjing, China, Cat. No. A045-4-2). Absorbance was measured at 562 nm using a Shimadzu UV-1800 spectrophotometer, Kyoto, Japan, and protein concentrations were calculated based on a standard curve generated from bovine serum albumin (BSA). The assays for enzymatic activities and subsequent calculations for MDA, SOD, CAT, and GSH-Px were performed in accordance with the manufacturer's guidelines and established literature [31,32], with results normalized to protein concentration.

2.5. Sample Collection

On the 60th day of the experiment, before sampling, all 120 fish were anesthetized using MS-222 (100 mg/L, Sigma, St. Louis, MO, USA). Their muscle tissues were then dissected on ice. The tissues were then immediately frozen in liquid nitrogen and stored at stored at −80 °C to ensure experimental stability for the quantitative polymerase chain reaction (qRT-PCR) and RNA sequencing (RNA-seq). All sampling procedures were conducted within an ultra-clean workstation. Sixty muscle samples were collected from each group. For transcriptomics analysis, every five muscles were combined to create one sample, with three randomly selected samples per group. For ultra-high-pressure liquid chromatography–mass spectrometry (UHPLC-MS) metabolomics analysis, every five remaining muscles were combined to create one sample, resulting in six samples per group.

2.6. Metabolomics Analysis

The samples were thawed at 4 °C and then divided into aliquots, which were added to a cold solution containing methanol, acetonitrile, and water in a 2:2:1 (*v*/*v*) ratio. The mixture was vortexed, sonicated for 30 min, and centrifuged at 14,000× *g* for 20 min at 4 °C. The resulting supernatant was collected, dried under vacuum conditions, and reconstituted using a solution of acetonitrile and water in a 1:1 volume ratio. Then, the samples were analyzed using mass spectrometry.

The raw mass spectrometry data contained within wiff.scan files were converted into MzXML files using ProteoWizard MSConvert (Version 3.0.20069) and imported into XCMS software (Version 3.14.0) for analysis. CAMERA was used for the annotation of isotopes and adducts. Ion features were retained when at least one group exhibited more than 50% non-zero measurements. Metabolite identification was accomplished using known accurate *m*/*z* values (<10 ppm) and MS/MS with an in-house database that includes readily accessible authentic standards (Personal Bio, Shanghai, China).

For data analysis, the R package ropls was utilized (v4.1.2; R Core Team, Vienna, Austria, 2021), and multivariate data analysis was conducted using Pareto-scaled principal component analysis (PCA) and orthogonal partial least squares discriminant analysis (OPLS-DA) to visualize metabolic differences between the control and experimental groups. Variables with a Variable Importance in Projection (VIP) > 1 and p-value < 0.05 were considered statistically significant. Metabolite-based pathway analysis was performed using MetaboAnalyst 5.0 (http://www.metaboanalyst.ca (accessed on 1 December 2023)) with the Kyoto Encyclopedia of Genes and Genomes (KEGG) pathway database (http://www.genome.jp/kegg/ (accessed on 1 December 2023)).

2.7. Transcriptomics Analysis

2.7.1. RNA Extraction and Sequencing

RNA extraction from control and treated samples was conducted using TRIzol reagent (Invitrogen, Waltham, MA, USA), following the manufacturer's protocol with phase separation by chloroform. RNA precipitation was achieved through isopropanol incubation and subsequent centrifugation at 12,000× g for 15 min at 4 °C, followed by two ethanol (75%) washes. The concentration and purity of RNA were assessed based on the ratios of A260/A280 and 28S/18S. Only samples with RNA integrity numbers (RINs) exceeding 7.0 were included in subsequent analyses. RNA-seq was performed by Shanghai Paisennuo Biotechnology Co., Ltd., Shanghai, China, and the sequencing of the cDNA libraries was performed using the Illumina HiSeqTM 4000 platform, which yielded 150 bp paired-end reads. Adapter trimming and quality filtering were performed using Trimmomatic v0.39.

2.7.2. Transcriptome Annotation

Trinity software version 2.4.0 was used to conduct de novo transcriptome assembly with clean reads, as previously described [33]. Gene function annotation was performed using several databases, including NCBI non-redundant protein sequences (NR), Kyoto Encyclopedia of Genes and Genomes (KEGG), Gene Ontology (GO), evolutionary genealogy of genes Non-supervised Orthologous Groups (eggNOG), protein family (Pfam), and Swissprot databases; details are given in Table S1.

2.7.3. Transcriptome Assembly

The RNA-seq data was analyzed as previously described [18]. Quality control measures were implemented using the Trimgalore v0.4.3 software to remove adapter sequences (https://github.com/FelixKrueger/TrimGalore (accessed on 12 December 2023)). The fastq files were assessed with FASTQC v0.11.5 (http://www.bioinformatics.babraham.ac.uk/projects/fastqc/ (accessed on 12 December 2023)), and a perl script was utilized to clean the raw fastq data by removing low-quality sequences, adaptor sequences, and poly-N sequences, resulting in clean reads. Next, an analysis was conducted to determine the Q20, Q30, and GC content, as well as sequence duplication levels, before submission to the National Center for Biotechnology Information (NCBI) with the ID PRJNA1097380 (https://dataview.ncbi.nlm.nih.gov/object/PRJNA1097380 (accessed on 8 April 2024)).

In accordance with previous studies [34], differentially expressed genes (DEGs) were identified using stringent criteria (adjusted p-value < 0.05 and $|\log2\ (\text{Fold Change})| \geq 1$). R software (v4.1.2; R Core Team, 2021) was used for data analysis and construct volcano plots and heatmaps. KOBAS software (version 2.1.1) was utilized to assess the statistical significance of DEG enrichment based on KEGG pathway enrichment and Gene Ontology (GO) analysis using a false discovery rate (FDR) threshold of <0.05 to determine statistically significant enrichments.

2.8. Quantitative Real-Time PCR Analysis

Table S2 presents primer sequences for genes related to the oxidation–reduction process, which were utilized to validate the RNA-seq data. In line with prior research, *β-actin* was selected as the internal reference gene for the hybrid species under investigation [27]. Furthermore, the stability of β-actin expression was confirmed under the experimental conditions, justifying its continued use as an internal control gene. Prior to total RNA extraction, DNase I was employed to eliminate DNA, following procedures described in a previous study [18]. RT-qPCR was conducted using SYBR Green. The relative gene expression was determined utilizing the $2^{-\triangle\triangle Ct}$ method [35].

2.9. Construction of PPI Network

Protein–protein interaction (PPI) networks were constructed using STRING v12.0 to analyze functional associations among genes linked to specific Gene Ontology (GO) terms, focusing on oxidative stress, ion transport, the complement system, and autophagy in the hybrid under SA stress. Hub genes were identified within each GO category based on maximal interaction connectivity. Network visualization was performed using Cytoscape (Version 3.10.1) to elucidate interaction patterns and key molecular pathways.

2.10. Statistical Analysis

Data analysis was performed using the Statistical Package for the Social Sciences (SPSS) version 15.0. Independent Student's *t*-tests were used to compare differences between the control and saline–alkali groups, with significance levels set at *p*-values less than 0.05. The results are presented as the mean ± standard deviation (S.D.), with asterisks (*) denoting statistically significant differences between the experimental and control groups (* $p < 0.05$, ** $p < 0.01$, and *** $p < 0.001$).

3. Results

3.1. Effect of SA Exposure on Biochemical Indicators

After 60 days of exposure to SA water, the activities of MDA (Figure 1A), SOD (Figure 1B), CAT (Figure 1C), and GSH-Px (Figure 1D) in the SA stress group were significantly elevated compared to those in the control group.

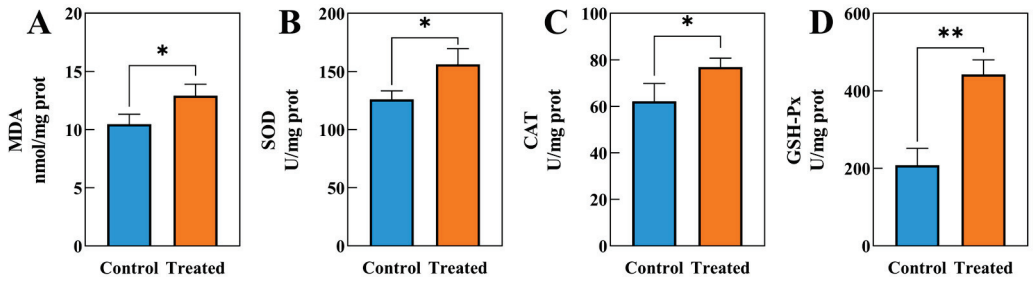


Figure 1. The biochemical indicators changes in muscle tissue in hybrids under SA exposure ($n = 3$). (**A**) MDA, (**B**) SOD, (**C**) CAT, (**D**) GSH-Px, * indicates $p < 0.05$, ** indicates $p < 0.01$.

3.2. Metabolome Quality Analysis

Multivariate statistical analyses, including PCA and OPLS-DA, were conducted to assess the differences in metabolites in the muscles of experimental fish. PCA was utilized to assess the inter- and intra-experimental group variability in a general sense. In both positive mode (Figure 2A) and negative mode (Figure 2B), the CT and SA groups were distinctly separated in the unsupervised principal component analysis model, suggesting that the instrument exhibited high stability and reproducibility, as evidenced by the tight clustering of quality control (QC) samples. OPLS-DA was performed to filter out noise

unrelated to categorical information, thereby enhancing the model's parsing ability and effectiveness. As shown in Figure 2C,D, the distinct separation between the CT and SA groups indicates SA's significant impact on the metabolic profiles of the experimental fish's muscle tissue. Furthermore, statistical graphics were produced using R software version 4.1.2 (R Core Team, 2021). It was observed that the R^2Y and Q^2 values in both positive and negative modes, obtained through random permutations, exceeded those of the original OPLS-DA model (Figure 2E,F). Thus, the OPLS-DA model demonstrated an excellent fit and high predictability, rendering it suitable for further analysis.

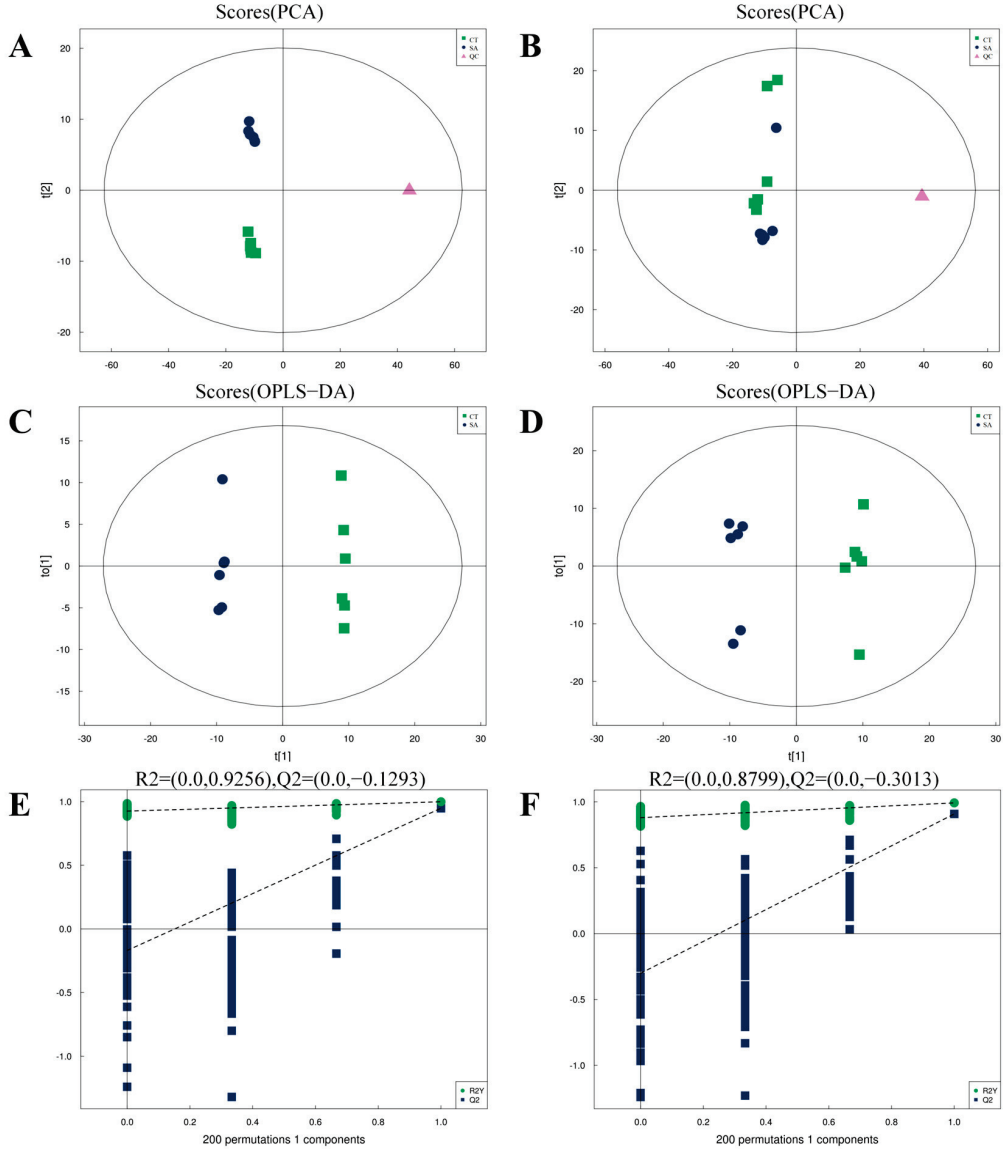


Figure 2. Quality analysis of metabolomics data (n = 6). (**A**) PCA scores plot for positive mode samples. (**B**) PCA scores plot for negative mode samples. (**C**) OPLS-DA score plot for positive mode. (**D**) OPLS-DA score plot for negative mode. (**E**) OPLS-DA permutation test for positive mode. (**F**) OPLS-DA permutation test for negative mode.

3.3. Differential Metabolite Identification

Next, differential metabolites (DMs) between the SA and CT groups were identified using criteria of VIP > 1 and p-value < 0.05. Two volcano plots were generated: Figure 3A displays a total of 813 DMs in positive mode (513 upregulated, 300 downregulated), and Figure 3B shows 623 DMs in negative mode (371 upregulated, 252 downregulated). The results of cluster analysis heatmaps, in both positive and negative modes, demonstrated

that SA significantly influenced the metabolism of muscle tissues in the experimental fish (Figure 3C). Among these metabolites, the top three categories were lipids and lipid-like molecules, organic acids and derivatives, and organic oxygen compounds. Notably, lipid metabolites comprised the largest proportion (Figure 3D).

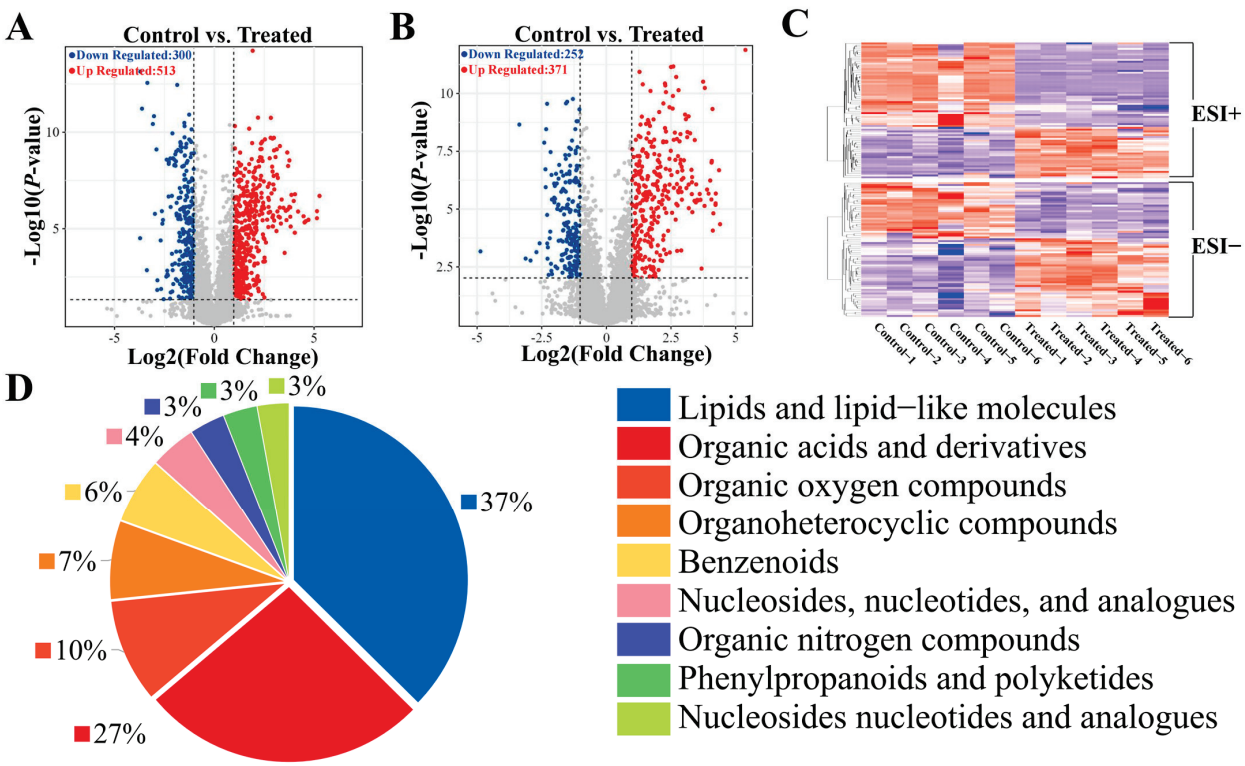


Figure 3. Hierarchical clustering analysis and classification of DMs. (**A**) Volcano plots comparing DMs in positive mode between CT and SA groups. The horizontal black dotted line represents the threshold of $p = 0.05$, while the vertical black dotted lines represent the threshold of $|\log2 \text{ (Fold Change)}| = 1$. (**B**) Volcano plots comparing DMs in negative mode between CT and SA groups. (**C**) Hierarchical clustering analysis of DMs in positive and negative mode, with red indicating upregulation and blue indicating downregulation. (**D**) Classification pie chart of DMs.

3.4. Pathway Enrichment and Categorization of DMs

To further explore the composition and interconnections of DMs and elucidate the metabolic mechanisms underlying the impact of SA on muscle tissues in experimental fish between CT and SA, a cluster analysis was performed. Figure 4A and Table S3 illustrate the most significant metabolites in the top 30 positive and negative ion patterns, revealing notable differences in substances such as amino acids and fatty acids between the SA and CT groups.

Using KEGG enrichment analysis, we determined the significance of metabolite enrichment in each pathway (Figure 4B). The results showed that the enriched pathways included mineral absorption, protein digestion and absorption, aminoacyl-tRNA biosynthesis, ABC transporters, and biosynthesis of amino acids. These results point to enhanced adaptations in nutrient uptake, protein synthesis and metabolism, and the transport of substances across membranes in experimental fish in response to environmental changes.

Next, we generated heatmaps to categorize DMs with significant differences. The differences between CT and SA groups for amino acids, peptides, and analogs are shown in Figure 5A, while the differences for fatty acids and derivatives are shown in Figure 5B. Among these DMs, certain amino acids and flavor substances such as glycine, proline, valine, leucine, alanine, and glutamine demonstrated increased levels in the SA group

(Figure 5C–H). Overall, these findings suggest that SA may impact the metabolism of flavor and collagen-related substances. In addition, amino acids, peptides, and their analogous metabolites, as well as fatty acids and their derivative metabolites, are presented in Tables S4 and S5, respectively.

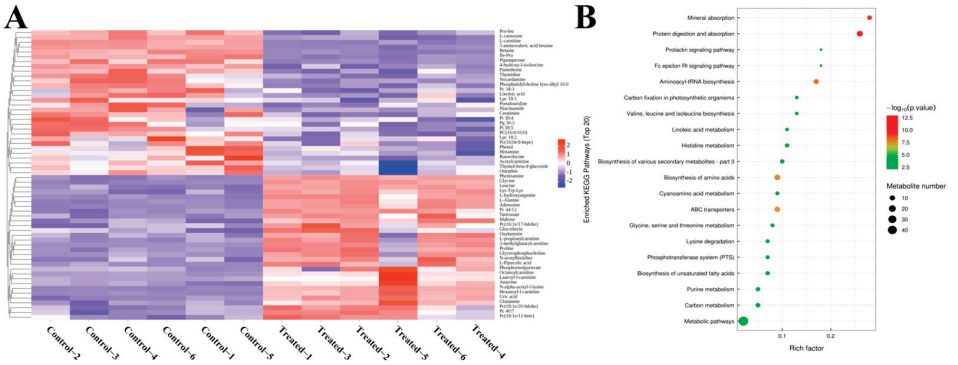


Figure 4. Heat map of DMs and KEGG bubble plots. (**A**) Heatmap of cluster analysis displaying the most significant DMs. (**B**) Bubble plot illustrating KEGG pathway enrichment.

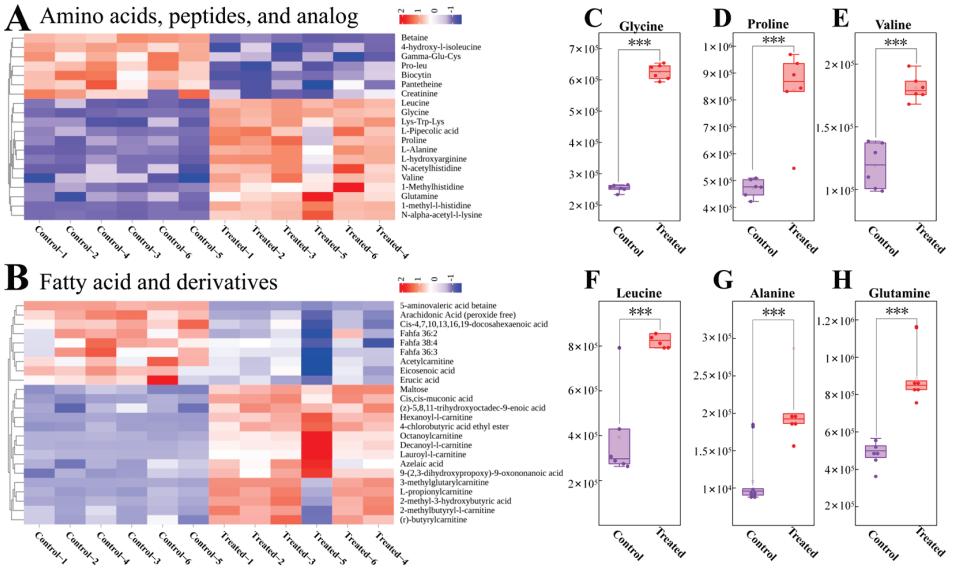


Figure 5. Heatmap of cluster analysis of different classes of DMs and boxplots of special DMs. (**A**) Heatmap displaying cluster analysis results for amino acids, peptides, and analogs. (**B**) Heatmap illustrating cluster analysis results for fatty acids and derivatives. (**C–H**) Box plots depicting specific DMs. The purple box represents the control group, while the red box represents the treated group. Each data point represents to the peak area of an individual sample. *** indicates $p < 0.001$.

3.5. Overview of Transcriptomics Sequencing Results

Using the Illumina HiSeq sequencing platform, we excluded sequences with junctions at the 3′ end and removed reads with average quality scores below Q20, following which we obtained high-quality sequence data comprising 41.93 million and 46.86 million reads for the CT and SA groups, respectively. Quality analysis of the obtained data revealed that the average Q20 values for the CT and SA groups were 98.16% and 97.98%, respectively, while the average Q30 values were 94.52% and 94.16% (Table S6). Additionally, the average GC content of clean reads for the CT and SA groups was 45.04% and 44.82%, respectively (Table S7). Figures S1–S5 presented the de novo assembly unigenes' information, including their GO, KEGG, EggNOG, and NR annotations for the hybrid species. These results confirm the high quality of our transcriptome sequencing data, ensuring the credibility

of subsequent analyses. The functional annotations and classification information were detailed in the Supplementary Materials, Sections S1.1 and S1.2.

3.6. Identification of DEGs

Further analysis led to the identification of a total of 2384 DEGs meeting the criteria of p-value < 0.05 or $|\log2\ (\text{Fold Change})| \geq 1$. The overall distribution of these DEGs, with 1087 upregulated and 1297 downregulated genes is shown in Figure 6A. The heatmap of the cluster analysis of DEGs showed a significant difference in the expression of the CT versus the SA group (Figure 6B), which suggests that SA has a significant impact on cellular transcription in the muscle tissues of the experimental fish.

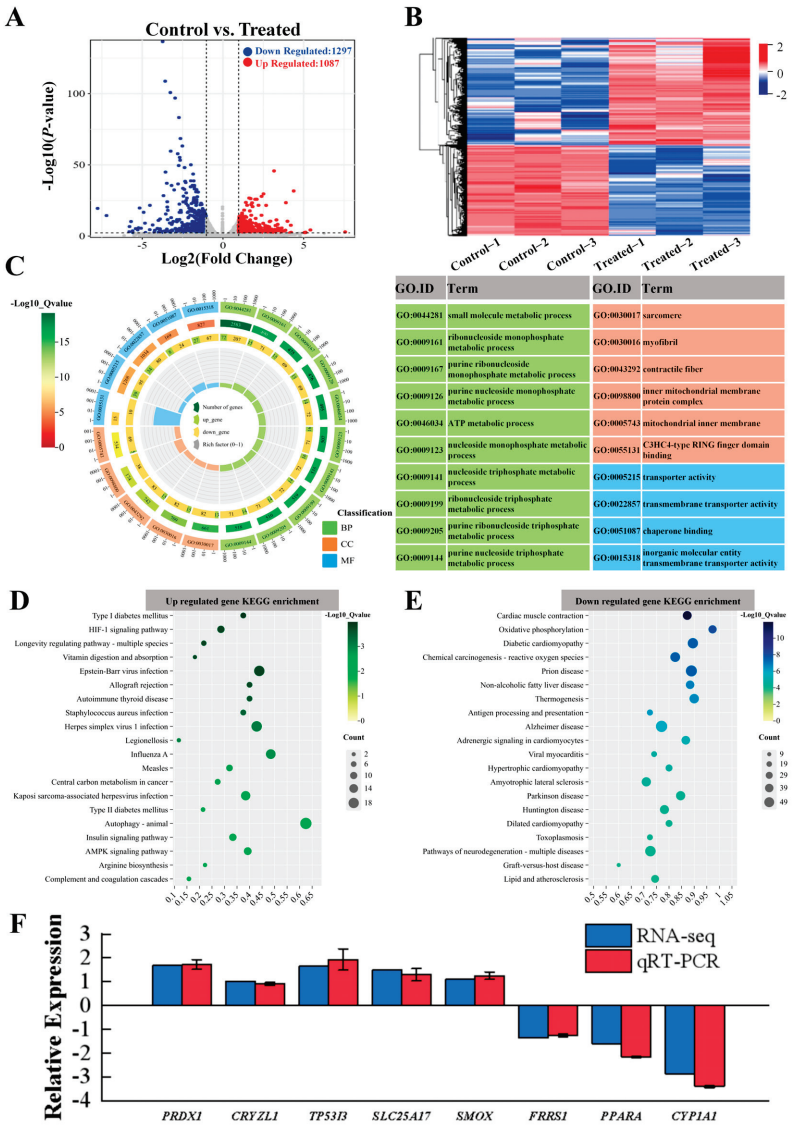


Figure 6. Transcriptome analysis graphs depicting differentially expressed genes (DEGs) in the muscles of hybrids under SA stress. (**A**) Volcano plots comparing DEGs between CT and SA groups. (**B**) Heatmap displaying clustering analysis results of differentially expressed genes. (**C**) Gene Ontology (GO) term enrichment analysis of significantly altered DEGs. Green corresponds to biological processes (BP), red corresponds to cellular components (CC), and blue corresponds to molecular functions (MF). A higher −log10 (Qvalue) indicates a more significant enrichment of genes. (**D**,**E**) Enrichment bubble plots illustrating up- and downregulated genes in the KEGG pathway. (**F**) Comparison of gene expression data between RNA-Seq and qRT-PCR.

3.7. Pathway Enrichment and Verification of DEGs

Considering that DEGs have a certain biological significance, this prompted us to explore their expression patterns. Through GO enrichment analysis (Figure 6C), we found that the top biological process categories included small molecule metabolic process, ribonucleoside monophosphate metabolic process, and purine ribonucleoside monophosphate metabolic process. To further investigate the relationship between metabolic pathways and DEGs, we conducted KEGG enrichment analysis, following which we observed the upregulation of DEGs in pathways such as vitamin digestion and absorption, autophagy—animal, and Epstein–Barr virus infection (Figure 6D) and the downregulation of DEGs in pathways like cardiac muscle contraction, oxidative phosphorylation, and diabetic cardiomyopathy, suggesting potential effects of SA on immune pathways, inflammatory responses, and energy metabolism in experimental fish (Figure 6E). In addition, Tables S8–S11 presented representative DEGs associated with various biological processes: oxidation-reduction (Table S8), ion transport (Table S9), complement and coagulation cascades (Table S10), and autophagy-animals differentiation (Table S11), respectively.

To validate the results of the transcriptomics analysis and to test whether SA has an effect on redox DEGs, we performed qRT-PCR on eight DEGs from the oxidation–reduction pathway. Among these, five genes were found to be upregulated (*PRDX1*, *CRYZL1*, *TP53I3*, *SLC25A17*, *SMOX*), while three genes were downregulated (*FRRS1*, *PPARA*, *CYP1A1*). The results obtained from qRT-PCR were consistent with those from RNA-Seq, indicating a similar trend in gene expression levels and reinforcing the reliability of our data (Figure 6F). As shown in Figure 7A–D, several genes associated with the oxidation–reduction, ion transport, complement system, and autophagy were identified, the PPI network diagram shows the association between some special genes (Figure 7E–H). These findings suggest that SA influences both the oxidation–reduction process and ion transport in experimental fish.

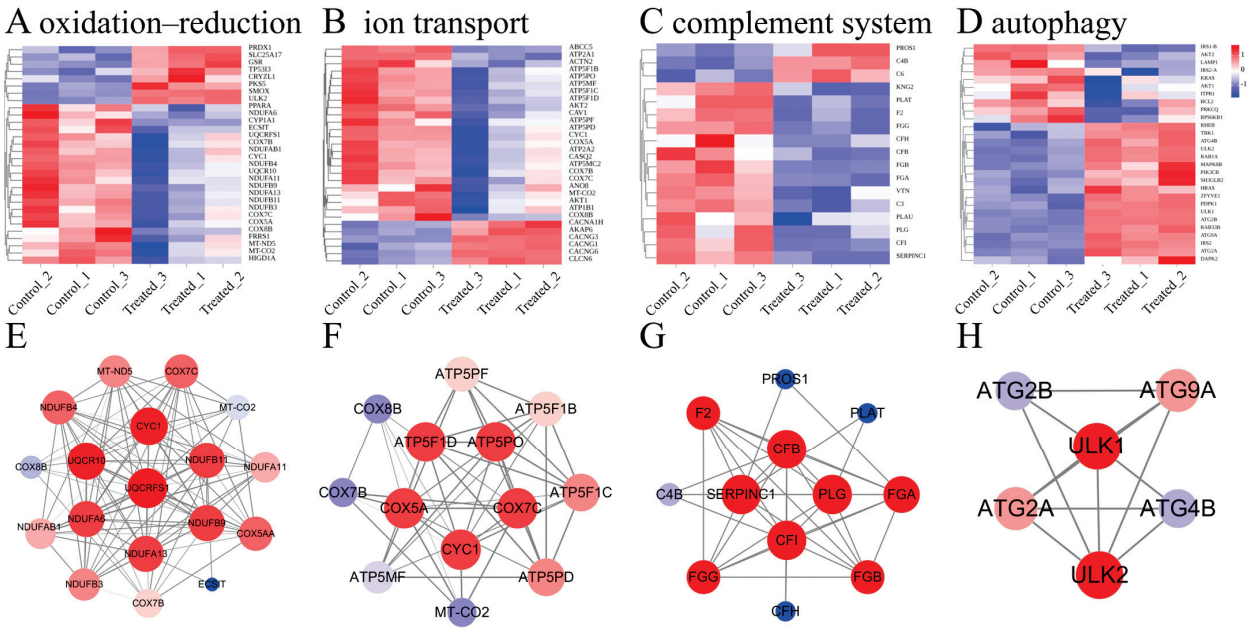


Figure 7. Transcriptome analysis map of differentially expressed genes (DEGs) enriched for some pathways in muscle of hybrids under SA stress. (**A**–**D**) Heatmap of some DEGs enriched for specific pathways. (**E**–**H**) PPI network diagram of some DEGs enriched for specific pathways, the redder color of the circle means that the gene is more important in that PPI network, and the thicker line means that two-by-two genes are more strongly correlated.

3.8. Metabolomics and Transcriptomics Integrated Analysis

Using Pearson correlation analysis, we conducted correlation analyses between metabolomics and transcriptomics data and observed strong correlations between each transcript and metabolite in the CT and SA groups (Figure 8). For instance, a strong positive correlation (R = 0.999) was observed between the DEG symbolized as TRINITY_DN5002_c0_g1 and betaine. Conversely, choline exhibited a statistically significant inverse relationship (R = −0.984) with DEG TRINITY_DN1018_c0_g1. Both betaine and choline are involved in the synthesis of numerous amino acids, highlighting specific metabolites associated with each transcript.

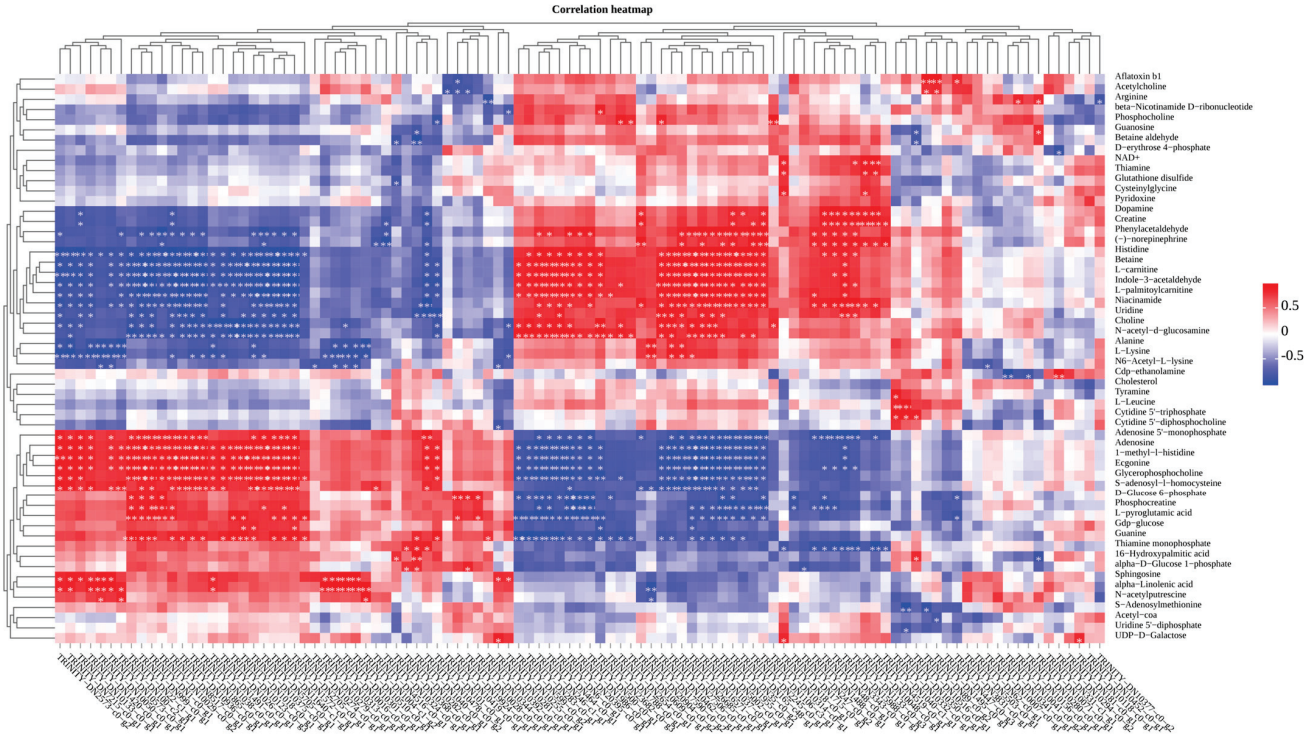


Figure 8. Correlation heatmap of metabolomics and transcriptomics. The heatmap illustrates the correlation between metabolomics and transcriptomics, with genes arranged in columns and metabolites quantified in behavioral units. Positive correlations are denoted in red, while negative correlations are denoted in blue. * indicates $p < 0.05$, ** indicates $p < 0.01$.

Figure 9A summarizes the relationship between DMs and DEGs in glycerophospholipid and glycine metabolism. In this context, lysophospholipase 1 (LYPLA1) was found to be upregulated, while choline dehydrogenase (CHDH) and betaine-aldehyde dehydrogenase (GBSA) were downregulated, and glycine, a DM, was upregulated. Figure 9B highlights glutathione metabolism, where glutathione-disulfide reductase (GSR) and gamma-glutamyltransferase 1 (GGT) were upregulated among the DEGs, while glutathione oxidized (GSSG) and glycine, among the DMs, were upregulated as well. These findings suggest that SA influences the expression of gene-to-metabolite networks in experimental fish muscle tissue.

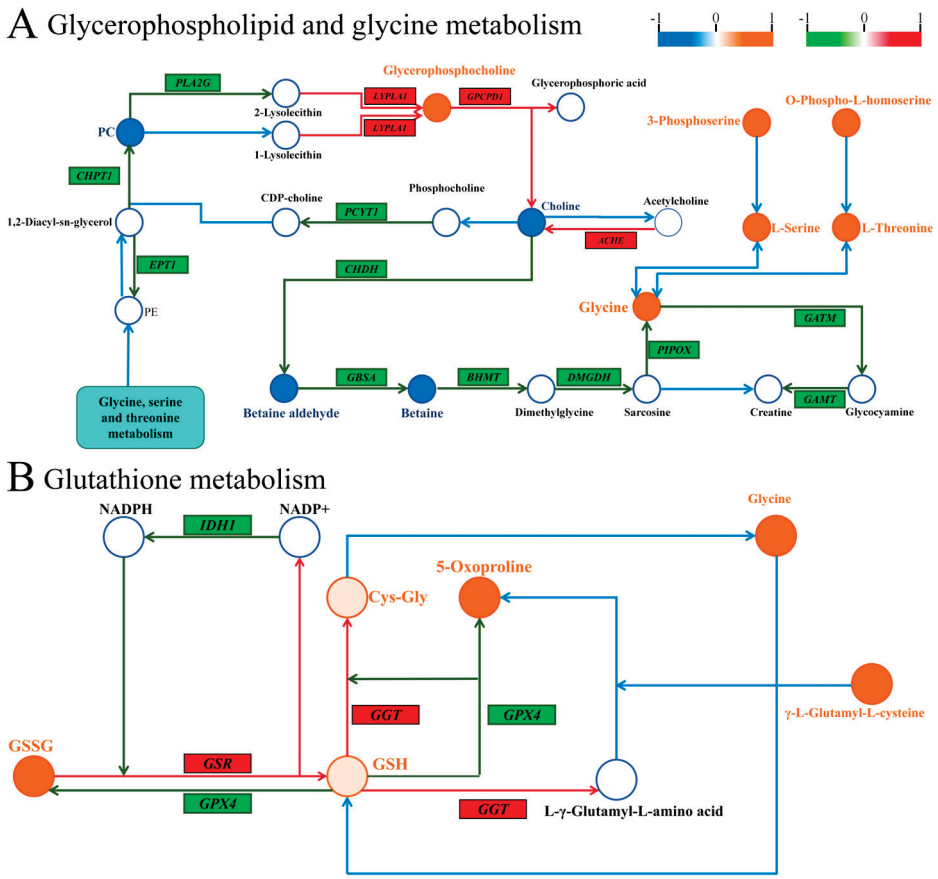


Figure 9. Combined metabolomics and transcriptomic citation of uncovered molecular mechanisms. (**A**) Correlation plot of genes and metabolites regulating glycerophospholipid and glycine metabolism. (**B**) Correlation plot of genes and metabolites regulating glutathione metabolism. Similarly, significant metabolite changes are depicted in orange (upregulated) or blue (downregulated), and differential genes are indicated in red (upregulated) or green (downregulated). Genes are shown in italics for clarity.

4. Discussion

Saline–alkali (SA) water, a widespread global occurrence, remains underutilized due to its inhospitable nature for aquatic life. With freshwater sources diminishing due to climate change and overexploitation, there is increasing interest in leveraging SA water for aquaculture. This study uses a comprehensive approach, integrating metabonomics and transcriptomics, to compare data on SA stress. Our research suggests that exposure to SA water alters biochemical indicators associated with oxidative stress in fish. Furthermore, changes in gene expression related to oxidative stress, the immune response, and ion transport were detected, as well as improvements in fish quality characteristics being identified. This suggests that SA stress may boost antioxidant defense, activate immune responses, affect ion transport balance, and enhance the quality characteristics of this hybrid.

4.1. Influence of SA Water on Redox Metabolism

Redox homeostasis is essential for maintaining metabolism and supporting growth as it helps to eliminate excess ROS and restores cellular redox balance. However, the specific mechanism involved in redox metabolism under SA stress remains largely unknown.

Prior research has revealed that SA stress can lead to the production of ROS in aquatic animals, causing oxidative stress [7,36]. This can result in an increase in MDA concentration, which is a key factor in organism damage [37]. The accumulation of ROS in animals can

lead to lipid oxidation and the formation of MDA, causing severe cell damage [38]. MDA content is a key indicator of tissue peroxidative damage. This study found higher MDA levels in the SA stress group compared to the control group, showing that long-term stress led to oxidative damage in the muscle cells of this hybrid (Figure 1A).

SOD and CAT are indispensable antioxidant enzymes in organisms [39]. The SOD-CAT system is commonly recognized as the main defense mechanism against reactive oxygen species (ROS) generation during periods of oxidative stress, playing a crucial role in scavenging reactive oxygen species and protecting cells [39]. SOD helps to convert excess O^{2-} into H_2O_2, which is then broken down by CAT to reduce oxidative stress [40,41]. In the current investigation, elevated levels of SOD and CAT activities were observed in the muscles of the hybrid species following 60 days of exposure to SA water (Figure 1B,C). This finding aligns with a study [42], which noted heightened SOD activity in the serum of Nile tilapia (*Oreochromis niloticus*) when subjected to elevated salinity levels. The enhanced SOD and CAT activity in the muscles of the hybrid species may be attributed to a response to SA stress, potentially serving a protective role in mitigating oxidative damage to cells. Furthermore, in addition to CAT, GSH-Px has the capability to inhibit reactive ROS production by counteracting hydrogen peroxide (H_2O_2) [43]. The current investigation revealed a significantly higher GSH-Px activity in the SA group compared to the CT group (Figure 1D), aligning with a recent study on the impact of SA exposure on Luciobarbus capito gills [44]. Under SA stress conditions, fish accumulate H_2O_2, ROS that cause oxidative damage [44]. The observed increase in GSH-Px activity likely represents a compensatory response to SA stress. Therefore, the upregulation of GSH-Px activity in this study may be linked to the removal of hydrogen peroxide buildup during SA stress.

Ubiquitin–cytochrome c oxidoreductase is a key enzyme complex on the inner mitochondrial membrane that is closely associated with oxidative phosphorylation processes [45]. As the first component of the respiratory chain, enabling the electron transfer from NADH to ubiquinone (CoQ10), the proper functioning of the electron transport chain is essential for maintaining redox balance within the cell and preventing the leakage of electrons into oxygen, which could otherwise result in the formation of ROS [46]. Proteins associated with ubiquinol–cytochrome c reductase, such as UQCRFS1, UQCR10, and CYC1, constitute integral components of the ubiquinol–cytochrome c oxidoreductase complex [47–49]. Significant enrichment of oxidatively phosphorylated DEGs was also detected when Nile tilapia were exposed to salt water [50]. In this study, *UQCRFS1*, *UQCR10*, and *CYC1* were significantly downregulated, suggesting that the process of oxidative phosphorylation may be inhibited under saline and alkaline stress, leading to the production of ROS (Figure 7E).

4.2. Influence of SA Water on Ion Transport

Ion transport plays a crucial role in regulating essential physiological parameters, including ion balance and membrane potential, which are vital for various biological functions [51]. The cytochrome c oxidase complex catalyzes the pumping of protons from the mitochondrial matrix across the inner membrane into the membrane gap along with electron transfer, a process known as proton pumping: this is the driver of oxidative phosphorylation [52]. *COX5A*, *COX7C*, and *COX7B* are subunits of the cytochrome c oxidase (COX) complex. The genes encoding ubiquitin–cytochrome c oxidoreductases are primarily associated with the redox pathway. Similarly, the genes encoding cytochrome c oxidases, discussed in the current chapter, are predominantly involved in the ion transport pathway. Ubiquitin–cytochrome c oxidoreductase and cytochrome c oxidase are critical constituents of the electron transport chain [52,53]. In high-salt environments, Na^+ can damage mitochondria in two ways. First, excessive Na^+ disrupts the calcium balance within mito-

chondria, leading to calcium buildup and the production of ROS, which directly damages the mitochondria's energy production system [54]. Second, Na^+ alters the mitochondrial inner membrane, hindering the free movement of essential substances like ubiquinone, which is crucial for energy production [55]. Our study demonstrated that the expression of the COX5A, COX7C, and COX7B genes was downregulated in response to saline–alkali stress. This downregulation may be mediated through two distinct mechanisms. Firstly, elevated Na^+ concentrations compromise the structural integrity of the mitochondrial inner membrane, leading to a compensatory transcriptional downregulation aimed at mitigating the energy metabolic burden. Secondly, stress-induced excessive accumulation of reactive oxygen species (ROS) exerts feedback inhibition on gene expression through pathways such as ROS-p53 signaling, thereby effectively interrupting the self-perpetuating cycle of ROS generation.

4.3. Influence of SA Water on Immune Response

Autophagy is a conserved cellular recycling process critical for maintaining homeostasis, eliminating damaged components, and adapting to nutrient stress [56]. Emerging evidence underscores its interplay with immune regulation [56,57]. Central to autophagosome formation are the autophagy-related proteins *ATG2A*, *ATG2B*, and *ATG9A*. *ATG2A* collaborates with *ATG9A* to initiate autophagosome assembly [58], while *ATG2B* mediates the lipid transfer essential for autophagosome expansion and lipid droplet dynamics [59]. *ATG9A* further supports vesicle maturation through lipid remodeling [60]. Unc-51 Like Autophagy Activating Kinase 1 (*ULK1*) and Unc-51 Like Autophagy Activating Kinase 2 are two key proteins in the autophagy signaling pathway [61,62]. They regulate the formation of autophagophores by acting upstream of phosphatidylinositol 3-kinase [62,63]. In our study, we observed significant upregulation of *ATG9A*, *ATG2B*, *ATG2A*, *ULK1*, and *ULK2* (Figure 7G); this is consistent with previous studies suggesting that alkali exposure induces autophagy in fish, which was detrimental to them [7]. In the SA group, SA induces cellular autophagy, thereby impacting the immune system further.

The complement system, comprising over 35 plasma and membrane proteins, plays an important role in host defense against pathogenic microorganisms by facilitating the innate immune response and connecting innate and adaptive immunity [64]. Complement factor I (*CFI*) gene mediates the innate immune response in the yellow catfish Pelteobagrus fulvidraco [65]. Moreover, Complement Factor H (*CFH*) also contributes to maintaining a balanced immune response by regulating complement activation as a soluble inhibitor of complement. In our study [66], *CFI* and *CFH* were significantly downregulated in the SA group, suggesting that SA may impact the immune system (Figure 7H).

4.4. Effect of SA Water on Muscle Quality Characteristics

The chemical composition of fish meat is routinely assessed for protein, fat, moisture, amino acids, and sugar content. Collagen, the primary protein in animals, maintains the structural integrity of connective tissues like bones, skin, and cartilage, with elevated levels indicating increased muscle tone and strength [26,67]. Glycine, proline, and hydroxyproline constitute a significant portion of collagen's amino acid composition and protein content in animals [68,69]. Valine supports amino acid transport and synthesis, promoting protein synthesis in fish [70].

Additionally, leucine and glutamine help in skeletal muscle protein synthesis, contributing to fish elasticity and tenderness [71–73]. In this study, glycine, proline, valine, leucine, and glutamine were found to be significantly higher in the SA group compared to the CT group, suggesting increased collagen and skeletal muscle protein levels in fish muscle tissue, which may enhance fish elasticity and palatability (Figure 5A). Sweet-

tasting amino acids in fish, such as glycine, serine, and alanine, contribute to flavor perception [3,74]. Moreover, we observed that the glycine and alanine levels were higher in the SA group compared to the CT group (Figure 5A), indicating potentially sweeter-flavored fish under low-SA aquaculture conditions.

During glycerophospholipid and glycine metabolism, lysophospholipase 1 (*LYPLA1*) catalyzes the hydrolysis of lysophosphatidylcholine, yielding glycerophosphocholine (GPC) [75]. GPC is a key phospholipid constituent of cell membranes, essential for membrane stability and neurotransmitter expression [76]. Our multi-omics analysis revealed an upregulation of the *LYPLA1* gene and GPC metabolites, suggesting that saline exposure may induce *LYPLA1* gene expression, facilitating GPC synthesis and potentially enhancing cellular membrane integrity (Figure 9A). Additionally, choline undergoes oxidation by choline dehydrogenase (*CHDH*) and betaine aldehyde dehydrogenase (*GBSA*) to produce betaine, with downstream production of glycine from betaine [77–79]. Furthermore, we observed that the downregulation of *CHDH* and *GBSA* gene expression under SA conditions led to decreased betaine aldehyde and betaine levels and a consequent increase in glycine content downstream, suggesting that reduced upstream products may enhance downstream glycine production (Figure 9A). Meanwhile, serine is also an important source of glycine [79], which is significantly increased as shown in Figure 9A, suggesting that the increase in glycine under SA stress conditions may also result from serine conversion.

In glutathione metabolism, glutathione reductase (GSR) catalyzes the reduction of glutathione disulfide (GSSG) to glutathione (GSH), while gamma-glutamyltransferase (*GGT*) converts GSH to cysteinylglycine (Cys-Gly), a precursor substance for glycine [80]. Through the integration of transcriptomics and metabolomics, we observed a significant increase in GSSG content and elevated *GSR* expression in glutathione metabolism. Additionally, there was a notable upregulation of *GGT* expression (Figure 9B). These findings suggest that SA exposure may disrupt the balance between GSSG and glycine transformation, leading to increased glycine levels. This disturbance could affect protein metabolism and amino acid transport, potentially resulting in glycine accumulation.

In summary, our findings suggest that SA exposure could potentially increase collagen levels and enhance the content of sweet substances in fish, which may contribute to enhancing the characteristic qualities of fish, potentially influencing their taste and texture.

5. Conclusions

This study investigated how "Xianfeng NO.1" muscle tissues respond to prolonged saline–alkali exposure using untargeted metabolomics and transcriptomics. Saline–alkali stress significantly affected the antioxidant system, increasing levels of MDA, SOD, CAT, and GSH-Px. Genes linked to oxidative stress resistance (*UQCRFS1*, *UQCR10*, *CYC1*) and ion transport (*COX5A*, *COX7C*, *COX7B*) were upregulated, enhancing antioxidant defenses and affecting sodium and amino acid transport. Furthermore, the upregulation of immune-related genes, such as *ATG9A*, *ULK1*, *CFI*, and *CFH*, may be essential for enhancing the immune system's efficacy. Our metabolomic analysis showed a notable rise in non-volatile flavor substances like glycine and proline under saline–alkali stress. Gene regulation in glycerophospholipids, glycine, and glutathione metabolism suggested the increased glycine production, possibly due to serine conversion. This multi-omics study offered insights into fish adaptation and muscle quality to saline–alkali environments, aiding in breeding high-quality, stress-tolerant species.

Supplementary Materials: The following supporting information can be downloaded at https://www.mdpi.com/article/10.3390/biology14060718/s1, Figure S1: The information of de novo assembly unigenes. Figure S2: GO annotations of the assembled unigenes of hybrid species. Figure S3: KEGG annotations of the assembled unigenes of hybrid species. Figure S4: EggNOG

annotations of the assembled unigenes of hybrid species. Figure S5: NR annotations of the assembled unigenes of hybrid species. (**A**) Distribution of species. (**B**) E-value distribution of comparisons. (**C**) Sequence similarity distribution. Table S1. Summary of annotation results. Table S2. Primers used in the quantitative PCR analysis. Table S3. Significantly different metabolites. Table S4. Amino acids, peptides, and analogue metabolites. Table S5. Fatty acid and derivatives metabolites. Table S6. Statistical assessment of sequencing data. Table S7. Overall sequence statistics. Table S8. Representative oxidation-reduction-related DEGs. Table S9. Representative ion transport-related DEGs. Table S10. Representative complement and coagulation cascades-related DEGs. Table S11. Representative autophagy-animals differentiatio-related DEGs.

Author Contributions: Conceptualization, L.Z., Q.Q., L.H., G.W. and J.X.; Data curation, L.Z., Q.Q., Q.L., Y.Y., Z.S., L.H., Y.S. and L.Y.; Formal analysis, L.Z. and Q.Q.; Funding acquisition, L.Z., G.W. and J.X.; Investigation, L.Z., Q.Q., Q.L., Y.Y., Z.S., Y.S. and L.Y.; Methodology, L.Z., Q.Q. and Q.L.; Software, L.Z., Q.Q., Q.L., Y.Y., Z.S. and L.H.; Supervision, G.W. and J.X.; Writing—original draft, L.Z. and Q.Q.; Writing—review and editing, G.W. and J.X. All authors have read and agreed to the published version of the manuscript.

Funding: This work was supported by the Key Research and Development Program of Hubei Province (No. 2023BBB051); National Key Research and Development Program of China (NO. 2022YFF0608202, and No. 2023ZD04054); the Hubei Scientific and Technological Program (2018ABA105); the key project of "Science and Technology for Economy 2020"; the National Natural Science Foundation of China (No. 32302982); the Central Public interest Scientific Institution Basal Research Fund, CAFS (No. YFI202409, No. YFI202213, No. 2020TD74, and No. Y2024JC07); and the Earmarked Fund for China Agriculture Research System of MOF and MARA (No. CARS-45-22).

Institutional Review Board Statement: The Animal Care and Use Committee of Yangtze River Fisheries Research Institute permitted this study on 3 May 2022 (Permit No. 2022zhanglang002).

Informed Consent Statement: Not applicable.

Data Availability Statement: Data are contained within the article and Supplementary Materials.

Conflicts of Interest: The authors Qing Li, Yanhong Sun, and Guiying Wang are employed by Wuhan Xianfeng Aquaculture Technology Co. Ltd. The remaining authors declare no conflicts of interest. The funders had no role in the design of the study; in the collection, analyses, or interpretation of data; in the writing of the manuscript; or in the decision to publish the results.

References

1. Brauner, C.J.; Gonzalez, R.J.; Wilson, J.M. 9—Extreme Environments: Hypersaline, Alkaline, and Ion-Poor Waters. In *Fish Physiology*; McCormick, S.D., Farrell, A.P., Brauner, C.J., Eds.; Academic Press: Cambridge, MA, USA, 2012; Volume 32, pp. 435–476.
2. Zhang, R.; Zhao, Z.G.; Li, M.S.; Luo, L.; Wang, S.H.; Guo, K.; Xu, W. Effects of saline-alkali stress on the tissue structure, antioxidation, immunocompetence and metabolomics of *Eriocheir sinensis*. *Sci. Total Environ.* **2023**, *871*, 162109. [CrossRef] [PubMed]
3. Chen, Y.; Qin, K.; Liang, G.; Li, X.; Niu, M.; Wang, H.; Wang, C.; Mu, C.; Zhu, R. Comparative study on non-volatile flavor substances of *Scylla paramamosain* cultured in inland low saline-alkaline water. *J. Food Compos. Anal.* **2023**, *118*, 105157. [CrossRef]
4. Kültz, D. Physiological mechanisms used by fish to cope with salinity stress. *J. Exp. Biol.* **2015**, *218*, 1907–1914. [CrossRef] [PubMed]
5. Ondrasek, G.; Rengel, Z. Environmental salinization processes: Detection, implications & solutions. *Sci. Total Environ.* **2021**, *754*, 142432. [CrossRef]
6. Tavares-Dias, M. Toxicity, physiological, histopathological, handling, growth and antiparasitic effects of the sodium chloride (salt) in the freshwater fish aquaculture. *Aquac. Res.* **2022**, *53*, 715–734. [CrossRef]
7. Wang, J.; Sun, L.; Li, X.; Tao, S.; Wang, F.; Shi, Y.; Guan, H.; Yang, Y.; Zhao, Z. Alkali exposure induces autophagy through activation of the MAPKpathway by ROS and inhibition of mTOR in *Eriocheir sinensis*. *Aquat. Toxicol.* **2023**, *258*, 106481. [CrossRef]
8. Yao, Z.; Guo, W.; Lai, Q.; Shi, J.; Zhou, K.; Qi, H.; Lin, T.; Li, Z.; Wang, H. *Gymnocypris przewalskii* decreases cytosolic carbonic anhydrase expression to compensate for respiratory alkalosis and osmoregulation in the saline-alkaline lake Qinghai. *J. Comp. Physiol.* **2016**, *186*, 83–95. [CrossRef]

9. Lu, Z.; Huang, W.; Wang, S.; Shan, X.; Ji, C.; Wu, H. Liver transcriptome analysis reveals the molecular responses to low-salinity in large yellow croaker *Larimichthys crocea*. *Aquaculture* **2020**, *517*, 734827. [CrossRef]
10. Yang, L.; Yu, Y.; Wang, C.; Hu, L.; Ma, Y.; Zi, F.; Ma, R.; Huo, Q.; Song, Y.; Sun, Z.; et al. Analysis and evaluation of the muscle quality of high-salinity aquaculture fish in Xinjiang, China. *J. Food Compos. Anal.* **2025**, *144*, 107750. [CrossRef]
11. Li, Y.-Y.; Hu, C.-B.; Zheng, Y.-J.; Xia, X.-A.; Xu, W.-J.; Wang, S.-Q.; Chen, W.-Z.; Sun, Z.-W.; Huang, J.-H. The effects of dietary fatty acids on liver fatty acid composition and Δ6-desaturase expression differ with ambient salinities in *Siganus canaliculatus*. *Comp. Biochem. Physiol. Part B Biochem. Mol. Biol.* **2008**, *151*, 183–190. [CrossRef]
12. Bradshaw, D.J.; Uribe, V.; King, L.E.; Perricone, C.S.; Illán, G.; Allmon, E.; Sepulveda, M.; Riche, M.; Wills, P.S.; Mejri, S. Effects of low salinities on growth, fatty acid composition, and transcriptome in Florida pompano (*Trachinotus carolinus*) at early developmental stages. *Aquaculture* **2023**, *563*, 738964. [CrossRef]
13. Jiang, X.; Niu, M.; Qin, K.; Hu, Y.; Li, Y.; Che, C.; Wang, C.; Mu, C.; Wang, H. Enhancement of Nutrient Composition and Non-Volatile Flavor Substances in Muscle Tissue of Red Drum (*Sciaenops ocellatus*) Through Inland Low Salinity Saline-Alkaline Water Culture. *J. Agric. Food Chem.* **2024**, *20*, 7326–7335. [CrossRef] [PubMed]
14. Mora, L.; Gallego, M.; Toldrá, F. New approaches based on comparative proteomics for the assessment of food quality. *Curr. Opin. Food Sci.* **2018**, *22*, 22–27. [CrossRef]
15. Nissa, M.U.; Pinto, N.; Parkar, H.; Goswami, M.; Srivastava, S. Proteomics in fisheries and aquaculture: An approach for food security. *Food Control.* **2021**, *127*, 108125. [CrossRef]
16. Kim, C.-H.; Park, C.J.; Kim, E.J.; Nam, Y.K. Transcriptional modulation patterns of abalone Haliotis discus hannai hypoxia inducible factor-1α (HIF-1α) in interdependent crosstalk between hypoxia, infection, and environmental stresses. *Aquac. Rep.* **2021**, *19*, 100566. [CrossRef]
17. Cui, Q.; Qiu, L.; Yang, X.; Shang, S.; Yang, B.; Chen, M.; Liu, X.; Chen, B.; Fu, X.; Wang, W.; et al. Transcriptome profiling of the low-salinity stress responses in the gills of the juvenile *Pseudopleuronectes yokohamae*. *Comp. Biochem. Physiol. Part D Genom. Proteom.* **2019**, *32*, 100612. [CrossRef]
18. Zhang, L.; Wei, H.; Yu, Y.; Li, Q.; Song, Z.; Sun, Y.; Li, P.; Chen, J.; Gan, J.; Zhang, H.; et al. Insights into the molecular mechanism of muscle textural quality improvement treated by exercise using comparative transcriptome analysis on the hybrid (*Erythroculter ilishaeformis* ♀× *Anchorythroculter nigrocauda* ♂). *Aquac. Rep.* **2023**, *31*, 101672. [CrossRef]
19. Qiao, F.; Lei, K.; Li, Z.; Wei, Z.; Liu, Q.; Yang, L.; He, J.; An, L.; Qi, H.; Cui, S. Transcriptomic responses of the freshwater snail (*Parafossarulus striatulus*) following dietary exposure to cyanobacteria. *Sci. Total Environ.* **2018**, *624*, 153–161. [CrossRef]
20. Hao, R.; Du, X.; Yang, C.; Deng, Y.; Zheng, Z.; Wang, Q. Integrated application of transcriptomics and metabolomics provides insights into unsynchronized growth in pearl oyster *Pinctada fucata martensii*. *Sci. Total Environ.* **2019**, *666*, 46–56. [CrossRef]
21. Liu, X.; Zhou, L.; Shi, X.; Xu, G. New advances in analytical methods for mass spectrometry-based large-scale metabolomics study. *TrAC Trends Anal. Chem.* **2019**, *121*, 115665. [CrossRef]
22. Li, X.W.; Hu, X.C.; Lv, A.J.; Guan, Z.G. Skin immune response to Aeromonas hydrophila infection in crucian carp *Carassius auratus* revealed by multi-omics analysis. *Fish Shellfish Immunol.* **2022**, *127*, 866–875. [CrossRef] [PubMed]
23. Gika, H.G.; Theodoridis, G.A.; Plumb, R.S.; Wilson, I.D. Current practice of liquid chromatography–mass spectrometry in metabolomics and metabonomics. *J. Pharm. Biomed. Anal.* **2014**, *87*, 12–25. [CrossRef] [PubMed]
24. Lu, X.; Wei, H.J.; Yang, C.G.; Li, Q.; Li, P.; Chen, J.; Sun, Y.H.; Wen, H.; Jiang, M.; Wang, G.Y. Effects of dietary protein levels on growth performance and liver transcriptome changes in juvenile top-mouth culter *Erythroculter ilishaeformis*. *Aquac. Rep.* **2021**, *21*, 100964. [CrossRef]
25. Zhai, D.D.; Li, W.J.; Liu, H.Z.; Cao, W.X.; Gao, X. Genetic diversity and temporal changes of an endemic cyprinid fish species, *Anchorythroculter nigrocauda*, from the upper reaches of Yangtze River. *Zool. Res.* **2019**, *40*, 427–438. [CrossRef]
26. Liu, X.; Zheng, C.; Luo, X.; Wang, X.; Jiang, H. Recent advances of collagen-based biomaterials: Multi-hierarchical structure, modification and biomedical applications. *Mater. Sci. Eng. Mater. Biol. Appl.* **2019**, *99*, 1509–1522. [CrossRef]
27. Tian, J.; Peng, D.; Wen, H.; Wang, G.Y.; Li, P.; Chen, J.; Sun, Y.H.; Lu, X.; Wu, F.; Li, Q. A comparative study on protein-sparing effects among juvenile *Erythroculter ilishaeformis* line, *Anchorythroculter nigrocauda* line and their hybrid F1 fed diets with different protein to carbohydrate ratios. *Aquac. Nutr.* **2020**, *26*, 993–1006. [CrossRef]
28. Liu, T.; Zu, X.; Yang, B.; Liu, Y.; Yi, W.; Li, L.; Mao, R. An analysis of hybrid bleak pond seedling culture in cold regions (*Erythroculter ilishaeformis* × *Anchorythroculter nigrocauda*). *Sci. Fish Farming* **2023**, *4*, 26–27. [CrossRef]
29. Zhao, L.; Jia, J.; Zhang, Y.; Ren, B.; Wang, F.; Liang, C.; Zhuang, Q.; Yan, B.; Zhao, J. Comparison of the growth of three strains of Nile tilapia larvae in net-pen culture under different salinity and alkalinity levels. *South China Fish. Sci.* **2013**, *9*, 1–7. [CrossRef]
30. *GB/T 22919.5-2008*; Fish Compound Feed. China Standards Press: Beijing, China, 2008.
31. Zheng, P.; Song, Y.; Tian, Y.; Zhang, H.; Yu, B.; He, J.; Mao, X.; Yu, J.; Luo, Y.; Luo, J.; et al. Dietary Arginine Supplementation Affects Intestinal Function by Enhancing Antioxidant Capacity of a Nitric Oxide-Independent Pathway in Low-Birth-Weight Piglets. *J. Nutr.* **2018**, *148*, 1751–1759. [CrossRef]

32. Zhang, L.; Song, Z.; He, L.; Zhong, S.; Ju, X.; Sha, H.; Xu, J.; Qin, Q.; Peng, J.; Liang, H. Unveiling the toxicological effects and risks of prometryn on red swamp crayfish (*Procambarus clarkii*): Health assessments, ecological, and molecular insights. *Sci. Total Environ.* **2024**, *951*, 175512. [CrossRef]
33. Grabherr, M.G.; Haas, B.J.; Yassour, M.; Levin, J.Z.; Thompson, D.A.; Amit, I.; Adiconis, X.; Fan, L.; Raychowdhury, R.; Zeng, Q.; et al. Full-length transcriptome assembly from RNA-Seq data without a reference genome. *Nat. Biotechnol.* **2011**, *29*, 644–652. [CrossRef] [PubMed]
34. Benjamini, Y.; Yekutieli, D. The control of the false discovery rate in multiple testing under dependency. *Ann. Stat.* **2001**, *29*, 1165–1188. [CrossRef]
35. Livak, K.J.; Schmittgen, T.D. Analysis of Relative Gene Expression Data Using Real-Time Quantitative PCR and the $2^{-\Delta\Delta CT}$ Method. *Methods* **2001**, *25*, 402–408. [CrossRef] [PubMed]
36. Tian, L.; Tan, P.; Yang, L.; Zhu, W.; Xu, D. Effects of salinity on the growth, plasma ion concentrations, osmoregulation, non-specific immunity, and intestinal microbiota of the yellow drum (*Nibea albiflora*). *Aquaculture* **2020**, *528*, 735470. [CrossRef]
37. Tsikas, D. Assessment of lipid peroxidation by measuring malondialdehyde (MDA) and relatives in biological samples: Analytical and biological challenges. *Anal. Biochem.* **2017**, *524*, 13–30. [CrossRef]
38. Katikaneni, A.; Jelcic, M.; Gerlach, G.F.; Ma, Y.; Overholtzer, M.; Niethammer, P. Lipid peroxidation regulates long-range wound detection through 5-lipoxygenase in zebrafish. *Nat. Cell Biol.* **2020**, *22*, 1049–1055. [CrossRef]
39. Ighodaro, O.M.; Akinloye, O.A. First line defence antioxidants-superoxide dismutase (SOD), catalase (CAT) and glutathione peroxidase (GPX): Their fundamental role in the entire antioxidant defence grid. *Alex. J. Med.* **2018**, *54*, 287–293. [CrossRef]
40. Marrocco, I.; Altieri, F.; Peluso, I. Measurement and Clinical Significance of Biomarkers of Oxidative Stress in Humans. *Oxid. Med. Cell. Longev.* **2017**, *2017*, 6501046. [CrossRef]
41. Regoli, F.; Giuliani, M.E. Oxidative pathways of chemical toxicity and oxidative stress biomarkers in marine organisms. *Mar. Environ. Res.* **2014**, *93*, 106–117. [CrossRef]
42. Song, L.; Zhao, Y.; Song, Y.; Zhao, L.; Ma, C.; Zhao, J. Effects of saline-alkaline water on growth performance, nutritional processing, and immunity in Nile tilapia (*Oreochromis niloticus*). *Aquaculture* **2021**, *544*, 737036. [CrossRef]
43. Brigelius-Flohé, R.; Flohé, L. Regulatory Phenomena in the Glutathione Peroxidase Superfamily. *Antioxid. Redox Signal.* **2020**, *33*, 498–516. [CrossRef] [PubMed]
44. Shang, X.; Geng, L.; Yang, J.; Zhang, Y.; Xu, W. Transcriptome analysis reveals the mechanism of alkalinity exposure on spleen oxidative stress, inflammation and immune function of *Luciobarbus capito*. *Ecotoxicol. Environ. Saf.* **2021**, *225*, 112748. [CrossRef] [PubMed]
45. Nolfi-Donegan, D.; Braganza, A.; Shiva, S. Mitochondrial electron transport chain: Oxidative phosphorylation, oxidant production, and methods of measurement. *Redox Biol.* **2020**, *37*, 101674. [CrossRef] [PubMed]
46. Bleier, L.; Dröse, S. Superoxide generation by complex III: From mechanistic rationales to functional consequences. *Biochim. Biophys. Acta Bioenerg.* **2013**, *1827*, 1320–1331. [CrossRef]
47. Sun, Q.; Li, J.; Dong, H.; Zhan, J.; Xiong, X.; Ding, J.; Li, Y.; He, L.; Wang, J. UQCRFS1 serves as a prognostic biomarker and promotes the progression of ovarian cancer. *Sci. Rep.* **2023**, *13*, 8335. [CrossRef]
48. Burska, D.; Stiburek, L.; Krizova, J.; Vanisova, M.; Martinek, V.; Sladkova, J.; Zamecnik, J.; Honzik, T.; Zeman, J.; Hansikova, H.; et al. Homozygous missense mutation in UQCRC2 associated with severe encephalomyopathy, mitochondrial complex III assembly defect and activation of mitochondrial protein quality control. *Biochim. Biophys. Acta Mol. Basis. Dis.* **2021**, *1867*, 166147. [CrossRef]
49. Chishiki, M.; Takagi, K.; Sato, A.; Miki, Y.; Yamamoto, Y.; Ebata, A.; Shibahara, Y.; Watanabe, M.; Ishida, T.; Sasano, H.; et al. Cytochrome c1 in ductal carcinoma in situ of breast associated with proliferation and comedo necrosis. *Cancer Sci* **2017**, *108*, 1510–1519. [CrossRef]
50. Xu, Z.; Gan, L.; Li, T.; Xu, C.; Chen, K.; Wang, X.; Qin, J.G.; Chen, L.; Li, E. Transcriptome Profiling and Molecular Pathway Analysis of Genes in Association with Salinity Adaptation in Nile Tilapia *Oreochromis niloticus*. *PLoS ONE* **2015**, *10*, e0136506. [CrossRef]
51. McCauley, H.A.; Matthis, A.L.; Enriquez, J.R.; Nichol, J.T.; Sanchez, J.G.; Stone, W.J.; Sundaram, N.; Helmrath, M.A.; Montrose, M.H.; Aihara, E.; et al. Enteroendocrine cells couple nutrient sensing to nutrient absorption by regulating ion transport. *Nat. Commun.* **2020**, *11*, 4791. [CrossRef]
52. Watson, S.A.; McStay, G.P. Functions of Cytochrome c oxidase Assembly Factors. *Int. J. Mol. Sci.* **2020**, *21*, 7254. [CrossRef]
53. Hunte, C.; Palsdottir, H.; Trumpower, B.L. Protonmotive pathways and mechanisms in the cytochrome bc1 complex. *FEBS Lett.* **2003**, *545*, 39–46. [CrossRef] [PubMed]
54. Hong, Q.; Qi, K.; Feng, Z.; Huang, Z.; Cui, S.; Wang, L.; Fu, B.; Ding, R.; Yang, J.; Chen, X.; et al. Hyperuricemia induces endothelial dysfunction via mitochondrial Na^+/Ca^{2+} exchanger-mediated mitochondrial calcium overload. *Cell Calcium* **2012**, *51*, 402–410. [CrossRef] [PubMed]

55. Hernansanz-Agustín, P.; Choya-Foces, C.; Carregal-Romero, S.; Ramos, E.; Oliva, T.; Villa-Piña, T.; Moreno, L.; Izquierdo-Álvarez, A.; Cabrera-García, J.D.; Cortés, A.; et al. Na^+ controls hypoxic signalling by the mitochondrial respiratory chain. *Nature* **2020**, *586*, 287–291. [CrossRef] [PubMed]
56. Huang, M.; Zhang, W.; Yang, Y.; Shao, W.; Wang, J.; Cao, W.; Zhu, Z.; Yang, F.; Zheng, H. From homeostasis to defense: Exploring the role of selective autophagy in innate immunity and viral infections. *Clin. Immunol.* **2024**, *262*, 110169. [CrossRef]
57. Xie, Y.; Zhou, Y.; Wang, J.; Du, L.; Ren, Y.; Liu, F. Ferroptosis, autophagy, tumor and immunity. *Heliyon* **2023**, *9*, e19799. [CrossRef]
58. van Vliet, A.R.; Chiduza, G.N.; Maslen, S.L.; Pye, V.E.; Joshi, D.; De Tito, S.; Jefferies, H.B.J.; Christodoulou, E.; Roustan, C.; Punch, E.; et al. ATG9A and ATG2A form a heteromeric complex essential for autophagosome formation. *Mol. Cell* **2022**, *82*, 4324–4339.E8. [CrossRef]
59. Velikkakath, A.K.; Nishimura, T.; Oita, E.; Ishihara, N.; Mizushima, N. Mammalian Atg2 proteins are essential for autophagosome formation and important for regulation of size and distribution of lipid droplets. *Mol. Biol. Cell* **2012**, *23*, 896–909. [CrossRef]
60. Maeda, S.; Yamamoto, H.; Kinch, L.N.; Garza, C.M.; Takahashi, S.; Otomo, C.; Grishin, N.V.; Forli, S.; Mizushima, N.; Otomo, T. Structure, lipid scrambling activity and role in autophagosome formation of ATG9A. *Nat. Struct. Mol. Biol.* **2020**, *27*, 1194–1201. [CrossRef]
61. Rong, Z.; Zheng, K.F.; Chen, J.; Jin, X.F. Function and regulation of ULK1: From physiology to pathology. *Gene* **2022**, *840*, 146772. [CrossRef]
62. Lee, E.J.; Tournier, C. The requirement of uncoordinated 51-like kinase 1 (ULK1) and ULK2 in the regulation of autophagy. *Autophagy* **2011**, *7*, 689–695. [CrossRef]
63. Ro, S.H.; Semple, I.A.; Park, H.; Park, H.; Park, H.W.; Kim, M.; Kim, J.S.; Lee, J.H. Sestrin2 promotes Unc-51-like kinase 1 mediated phosphorylation of p62/sequestosome-1. *FEBS J.* **2014**, *281*, 3816–3827. [CrossRef] [PubMed]
64. Lv, W.; Ma, A.; Chi, X.; Li, Q.; Pang, Y.; Su, P. A novel complement factor I involving in the complement system immune response from *Lampetra morii*. *Fish Shellfish Immunol.* **2020**, *98*, 988–994. [CrossRef]
65. Tang, Y.Y.; Li, Y.T.; Zha, X.H.; Zhang, D.Z.; Tang, B.P.; Liu, Q.N.; Jiang, S.H.; Dai, L.S. A complement factor I (CFI) gene mediates innate immune responses in yellow catfish *Pelteobagrus fulvidraco*. *Genomics* **2021**, *113*, 1257–1264. [CrossRef] [PubMed]
66. Kajander, T.; Lehtinen, M.J.; Hyvärinen, S.; Bhattacharjee, A.; Leung, E.; Isenman, D.E.; Meri, S.; Goldman, A.; Jokiranta, T.S. Dual interaction of factor H with C3d and glycosaminoglycans in host-nonhost discrimination by complement. *Proc. Natl. Acad. Sci. USA* **2011**, *108*, 2897–2902. [CrossRef] [PubMed]
67. Cappello, T.; Brandao, F.; Guilherme, S.; Santos, M.A.; Maisano, M.; Mauceri, A.; Canário, J.; Pacheco, M.; Pereira, P. Insights into the mechanisms underlying mercury-induced oxidative stress in gills of wild fish (*Liza aurata*) combining ^{1}H NMR metabolomics and conventional biochemical assays. *Sci. Total Environ.* **2016**, *548*, 13–24. [CrossRef]
68. Li, P.; Wu, G.Y. Roles of dietary glycine, proline, and hydroxyproline in collagen synthesis and animal growth. *Amino Acids* **2018**, *50*, 29–38. [CrossRef]
69. Li, X.Y.; Zheng, S.X.; Wu, G.Y. Nutrition and Functions of Amino Acids in Fish. In *Amino Acids in Nutrition and Health: Amino Acids in the Nutrition of Companion, Zoo and Farm Animals*; Wu, G., Ed.; Springer International Publishing: Cham, Switzerland, 2021; Volume 1285, pp. 133–168.
70. Ahmad, I.; Ahmed, I.; Fatma, S.; Peres, H. Role of branched-chain amino acids on growth, physiology and metabolism of different fish species: A review. *Aquac. Nutr.* **2021**, *27*, 1270–1289. [CrossRef]
71. Lefaucheur, L. A second look into fibre typing—Relation to meat quality. *Meat Sci.* **2010**, *84*, 257–270. [CrossRef]
72. Zhao, J.; Zhao, Y.; Liu, H.F.; Cao, Q.Q.; Feng, L.; Zhang, Z.H.; Jiang, W.D.; Wu, P.; Liu, Y.; Luo, W.; et al. Dietary Leucine Improves Fish Intestinal Barrier Function by Increasing Humoral Immunity, Antioxidant Capacity, and Tight Junction. *Int. J. Mol. Sci.* **2023**, *24*, 4716. [CrossRef]
73. Li, X.; Zheng, S.; Wu, G. Nutrition and metabolism of glutamate and glutamine in fish. *Amino Acids* **2020**, *52*, 671–691. [CrossRef]
74. Wang, H.; Tang, L.; Wei, H.; Mu, C.; Wang, C. "Butter Crab": An environment-induced phenotypic variation of *Scylla paramamosain* with special nutrition and flavour. *Aquac. Res.* **2019**, *50*, 541–549. [CrossRef]
75. Wepy, J.A.; Galligan, J.J.; Kingsley, P.J.; Xu, S.; Goodman, M.C.; Tallman, K.A.; Rouzer, C.A.; Marnett, L.J. Lysophospholipases cooperate to mediate lipid homeostasis and lysophospholipid signaling. *J. Lipid. Res.* **2019**, *60*, 360–374. [CrossRef] [PubMed]
76. Anaokar, S.; Kodali, R.; Jonik, B.; Renne, M.F.; Brouwers, J.; Lager, I.; de Kroon, A.; Patton-Vogt, J. The glycerophosphocholine acyltransferase Gpc1 is part of a phosphatidylcholine (PC)-remodeling pathway that alters PC species in yeast. *J. Biol. Chem.* **2019**, *294*, 1189–1201. [CrossRef] [PubMed]
77. Roci, I.; Watrous, J.D.; Lagerborg, K.A.; Jain, M.; Nilsson, R. Mapping choline metabolites in normal and transformed cells. *Metabolomics* **2020**, *16*, 125. [CrossRef]
78. Li, G.; Wu, H.; Sun, Y.; Zhang, S. Betaine Aldehyde Dehydrogenase (BADH) Expression and Betaine Production in Sugarbeet Cultivars with Different Tolerances to Drought Stress. *Sugar Tech* **2016**, *18*, 420–423. [CrossRef]

79. Wang, W.; Wu, Z.; Dai, Z.; Yang, Y.; Wang, J.; Wu, G. Glycine metabolism in animals and humans: Implications for nutrition and health. *Amino Acids* **2013**, *45*, 463–477. [CrossRef]
80. Lu, S.C. Glutathione synthesis. *Biochim. Biophys. Acta Gen. Subj.* **2013**, *1830*, 3143–3153. [CrossRef]

Disclaimer/Publisher's Note: The statements, opinions and data contained in all publications are solely those of the individual author(s) and contributor(s) and not of MDPI and/or the editor(s). MDPI and/or the editor(s) disclaim responsibility for any injury to people or property resulting from any ideas, methods, instructions or products referred to in the content.

biology

MDPI

Article

Dietary Cottonseed Protein Substituting Fish Meal Induces Hepatic Ferroptosis Through SIRT1-YAP-TRFC Axis in *Micropterus salmoides*: Implications for Inflammatory Regulation and Liver Health

Quanqun Cao [1,†], Ju Zhao [1,†], Xuefei Zhang [1], Laia Ribas [2], Haifeng Liu [1,*] and Jun Jiang [1,*]

[1] College of Animal Science and Technology, Sichuan Agricultural University, Chengdu 611130, China; qq2312159@sicau.edu.cn (Q.C.); 2024102020@stu.sicau.edu.cn (J.Z.); 2020302169@stu.sicau.edu.cn (X.Z.)
[2] Institut de Ciències del Mar, Consejo Superior de Investigaciones Científicas (ICM-CSIC), 08003 Barcelona, Spain; lribas@icm.csic.es
* Correspondence: liuhf@sicau.edu.cn (H.L.); jjun@sicau.edu.cn (J.J.); Tel./Fax: +86-28-86291010 (J.J.)
† These authors contributed equally to this manuscript.

Simple Summary: This study investigated the effects of high-level cottonseed protein (CP) inclusion in diets on largemouth bass (*M. salmoides*). Replacing fish meal with CP beyond 24% impaired growth and liver health, elevating inflammation and ferroptosis markers. Excessive CP (60%) disrupted mitochondrial integrity, triggered oxidative stress, and activated ferroptosis via SIRT1-YAP-TRFC signaling, highlighting the need for balanced CP substitution in aquafeeds.

Abstract: Cottonseed protein (CP), a plant-derived protein with high crude protein content (65%), has emerged as a sustainable alternative to fish meal (FM) in aquafeeds. However, excessive substitution of FM with CP may trigger hepatic dysfunction in aquatic species, though the underlying mechanisms remain unclear. This study evaluated the effects of high CP inclusion on growth, liver inflammation, and ferroptosis in largemouth bass (*M. salmoides*). A controlled experiment employed 720 juvenile specimens (39.36 ± 0.10 g) randomly allocated across six dietary groups in triplicate tanks (40 fish/tank). Nutritionally balanced isonitrogenous/isocaloric diets (51% protein, 8% lipid) were formulated with progressive CP inclusion levels (0%, 12%, 24%, 36%, 48%, 60%) over an 8-week trial period. We found that specific growth rate (SGR), percent weight gain (PWG), viscerosomatic index (VSI), and hepatosomatic index (HSI) significantly declined when CP replacement exceeded 24%. Hepatic dysfunction manifested as elevated serum biomarkers of aspartate aminotransferase (AST) and alanine aminotransferase (ALT) activities and collagen deposition in CP60 group. Pro-inflammatory cytokine (IL-1β and TNF-α) upregulation and anti-inflammatory cytokines suppression (IL-10 and TGF-β) accompanied dysregulated immune homeostasis. Mechanistically, CP60 diet induced mitochondrial ultrastructural damage and ferroptosis activation through ROS accumulation, lipid peroxidation, and iron overload. Molecular analysis demonstrated SIRT1/GPX4 downregulation with concurrent upregulation of TRFC, ACSL4, PTGS2, and nuclear YAP. Our findings establish that excessive CP (60%) substitution triggers hepatic ferroptosis via SIRT1-YAP-TRFC signaling, exacerbates inflammatory imbalance, and compromises growth performance in *M. salmoides*, providing critical insights for sustainable feed formulation.

Keywords: cottonseed protein; inflammatory regulation; ferroptosis; liver fibrosis; *M. salmoides*

1. Introduction

Fish meal (FM) is a crucial high-quality protein source in aquafeeds, prized for its excellent palatability, high digestibility, and rich protein content [1]. However, the ecological and economic sustainability of FM-dependent aquaculture systems faces dual challenges: volatile market prices linked to fluctuating marine harvests and mounting environmental concerns over wild fishery depletion [2]. These constraints have intensified global efforts to identify sustainable plant-based protein alternatives that can partially or fully replace FM without compromising aquatic animal health [3].

Cottonseed protein (CP), a byproduct of cotton oil extraction, has emerged as a promising candidate for aquafeed formulation. Through advanced processing techniques that reduce crude fiber and free gossypol [4,5], CP now achieves protein content exceeding 60% (dry weight basis) with essential amino acid profiles comparable to soybean meal [6]. Successful FM substitution trials using CP have been documented across phylogenetically diverse species, including rainbow trout (*Oncorhynchus mykiss*) [7], juvenile large yellow croaker (*Larimichthys crocea*) [8], juvenile southern flounder (*Paralichthys lethostigma*) [9], pearl gentian grouper (*Epinephelus fuscoguttatus* ♀× *E. lanceolatu* ♂) [10], black tiger shrimp (*Penaeus monodon*) [11], and common carp (*Cyprinus carpio*) [12,13]. Nevertheless, emerging evidence reveals threshold-dependent hepatotoxicity: 18% CP substitution induced hepatic lipid vacuolation in largemouth bass (*M. salmoides*) [14], while combined plant protein blends reduced antioxidant capacity (e.g., T-AOC and GSH-Px) in Japanese sea bass [15]. These findings underscore the critical need to delineate the molecular mechanisms underlying CP-induced hepatic pathology.

Mounting evidence implicates ferroptosis—an iron-dependent cell death pathway driven by lipid peroxidation—in chemical-induced liver injury [16]. This process is characterized by glutathione (GSH) depletion, mitochondrial cristae fragmentation, and transferrin receptor (TFRC)-mediated iron overload [17]. Notably, CP components exhibit dual pro-ferroptotic effects: gossypol directly depletes GSH through thiol conjugation [18], while CP hydrolysates downregulate sirtuin 1 (SIRT1) expression [19]. SIRT1, an NAD^+-dependent deacetylase, modulates both ferroptosis and the Hippo/YAP signaling pathway [20]. The SIRT1-YAP axis further amplifies iron uptake through TFRC transactivation [21], creating a pathogenic cascade potentially central to CP hepatotoxicity.

Available evidence indicates that CP is a promising plant-based protein source for aquafeeds. However, excessive substitution of FM with CP has been associated with adverse effects, including hepatic structural damage, elevated ROS production, and oxidative stress. Given the economic and ecological significance of *M. salmoides* in Chinese freshwater aquaculture, evaluating the feasibility and potential risks of CP as an FM alternative is crucial. This study aimed to assess the effects of graded FM replacement with CP on growth performance and hepatic ferroptosis in *M. salmoides*.

2. Materials and Methods

2.1. Animal Ethics Statement

The present study followed the recommendations of Care and Use of Laboratory Animals in China, Animal Ethical and Welfare Committee of China Experimental Animal Society. All experimental procedures conducted in this study received approval from the Animal Care Advisory Committee of Sichuan Agricultural University, under permit number DKY-2018202027.

2.2. Experimental Diets and Feeding Management

In this study, CP was procured from Chenguang Biotechnology Group Kashgar Co., Ltd. (Kashgar, China). Diets were formulated with CP inclusion levels ranging from

7% to 35%, replacing FM protein at rates of 12%, 24%, 36%, 48%, and 60% (designated as CP12, CP24, CP36, CP48, and CP60, respectively). Specific lysine and methionine levels were adjusted according to established standards [22]. All ingredients were finely ground, pelletized into 4.0 mm floating pellets using a double-screw extruder, and stored at −20 °C until use. The formulation, nutrient composition, and chemical analysis of four isonitrogenous and isolipidic diets (crude protein, 52.0%; crude lipid, 8.0%) and nutrient levels are presented in Table 1.

Table 1. Composition and nutrients content of basal diet (g/kg).

Ingredients	FM	CP12	CP24	CP36	CP48	CP60
Soya bean oil [1]	40.2	44.0	47.8	51.6	55.4	59.2
Bentonite	84.8	69.0	52.6	34.4	17.2	0.0
Fish meal	520.0	458.8	397.6	336.4	275.2	214.0
Chicken meal	160.0	160.0	160.0	160.0	160.0	160.0
Wheat gluten	70.0	70.0	70.0	70.0	70.0	70.0
Cottonseed protein	0.0	70.0	140.0	210.0	280.0	350.0
Wheat flour	50.0	50.0	50.0	50.0	50.0	50.0
Tapioca	34.0	34.0	34.0	34.0	34.0	34.0
Lysine	0.0	0.5	1.6	4.3	6.2	8.2
DL-methionine	2.0	2.7	3.4	4.3	5.0	5.6
CaH_2PO_4	10.0	12.0	14.0	16.0	18.0	20.0
Choline chloride	4.0	4.0	4.0	4.0	4.0	4.0
Mineral element premix [2]	10.0	10.0	10.0	10.0	10.0	10.0
Vitamin premix [3]	15.0	15.0	15.0	15.0	15.0	15.0
Total	1000	1000	1000	1000	1000	1000
			Nutrients content [4]			
Crude protein	518.5	521.2	521.0	522.3	521.2	520.3
Crude lipid	78.8	80.8	81.2	80.3	80.7	79.4
Moisture	49.8	48.8	49.7	50.0	50.2	48.5

[1] Soya bean oil (Dongguan Yihai Jiali Cerui Starch Co., Ltd. Dongwan, China), Fish meal (contains 68% protein and 13.75% lipid) (Tianbao Grain and Feed Trading Co., Ltd. Lima, Peru), Chicken meal (Sichuan Xinrui Feed Technology Co., Ltd. Meishan, China), Wheat gluten (Qionglai Sonaker Biotechnology Co., Ltd. Qionglai, China), Cottonseed protein (contains 63.89% protein and 1.23% lipid.) (Chenguang Biotechnology Group Kashgar Co., Ltd. Kashgar, China), Tapioca (Xiong Hebei Light Co., Ltd. Baoding, China), DL-methionine (Chuanheng Ecological Technology Co., Ltd. Deyang, China). [2] The premix provides minerals for a kilogram of diet: $FeSO_4 \cdot H_2O$ (300 g/kg Fe), 10.00 g; $MgSO_4 \cdot H_2O$ (160 g/kg Mg), 62.50 g; $CuSO_4 \cdot 5H_2O$ (250 g/kg Cu), 2.00 g; $ZnSO_4 \cdot H_2O$ (340 g/kg Zn), 11.59 g; $MnSO_4 \cdot H_2O$ (310 g/kg Mn), 3.77 g; $CoCl_2 \cdot 6H_2O$ (10 g/kg Co), 8.2 g; Ca $(IO3)_2$ (30 g/kg I), 6.14 g; Na_2SeO_3 (10 g/kg Se), 20 g; KH_2PO_4 (520 g/kg K), 9.50 g; NaCl (390 g/kg Na), 7.63 g. All ingredients were diluted with $CaCO_3$ to 1 kg. [3] The premix provides vitamins for kilogram of diet: retinyl acetate (500,000 IU/g), 8.89 g; thiamine (1000 g/kg), 1.40 g; riboflavine (800 g/kg), 2.92 g; pyridoxine (1000 g/kg), 1.47 g; folic acid (1000 g/kg), 0.13 g; cobalamine (10 g/kg), 6.67 g; Ascorbic acid (950 g/kg), 10.53 g; cholecalaiferol (500,000 IU/g), 0.16 g; DL-α-tocopherol acetate (500 g/kg), 14.67 g; menadione (1000 g/kg), 1.55 g; pantothenic acid (910 g/kg), 2.56 g; nicotinic acid (1000 g/kg), 2.51 g; biotin (20 g/kg), 3.33 g; inositol (980 g/kg), 27.21 g. All ingredients were diluted with corn starch to 1 kg. [4] Crude protein, lipid, ash, and moisture are expressed on a dry matter basis and given as means.

The *M. salmoides* were sourced from a local aquafarm in Sichuan, China. Before the start of the experiments, the fish were fed a basal diet for two weeks to acclimate them to the experimental conditions. A total of 720 fish, with an average initial weight of 39.36 ± 0.10 g, were carefully selected and randomly distributed into 18 tanks (200 × 100 × 105 cm^3). There were three replicates (tanks) for each treatment, with 40 fish per tank. The fish were fed ad libitum with experimental diets until they appeared satiated twice a day (at 7:00 AM and 7:00 PM) for a duration of 8 weeks. Fish were held under natural photoperiod condition throughout the feeding trial. Each tank received freshwater at a flow rate of 1.2 L per minute. The water temperature ranged from 26 ± 3 °C, and the dissolved oxygen level

was maintained above 5 mg per liter. The pH was kept within the range of 7.1–7.3 and total ammonia nitrogen was <0.04 mg/L.

2.3. Sample Collection and Indicator Measurements

Prior to the feeding trial, samples from 40 fish in each treatment group were stored at −20 °C for proximate composition analysis to calculate nutrient retention. At the trial's conclusion, the fish were fasted for 24 h, and individual tanks were counted and weighed to calculate performance indices. Following anesthesia with 0.01% MS-222, blood samples were collected from the tail veins of nine fish per group and centrifuged at 1000 g for 10 min at 4 °C to isolate serum for analysis. The fish were immediately dissected, and the visceral mass was removed and weighed. Tissues such as the liver, intestine, and stomach were then separated for further analysis. The following parameters were measured as previously described [23]: survival rate (SR), initial body weight (IBW), final body weight (FBW), percent weight gain (PWG), specific growth rate (SGR), feed intake (FI), feed efficiency (FE), relative gut length (RGL), intestosomatic index (ISI), viscerosomatic index (VSI), and hepatosomatic index (HSI). Additionally, a 1 cm^3 central portion of the liver was fixed in a 4% paraformaldehyde solution for histological analysis. The remaining liver tissue was frozen in liquid nitrogen for subsequent RNA and protein extraction experiments.

2.4. Proximate Composition Analysis

The proximate composition of diets, as well as whole-body and dorsal muscle fish samples, was analyzed according to the procedures outlined by the Association of Official Analytical Chemists [24]. For moisture determination, diet samples were dried at 105 °C until reaching a constant weight, while fish samples underwent vacuum freeze-drying. A semi-automatic nitrogen analyzer (KDN-08A, Shanghai Xinjia Electron Co., Ltd. Shanghai, China) was employed to measure crude protein content via the Kjeldahl method. The Soxhlet extraction technique was utilized to quantify the crude lipid content of diets, and ash content was determined by incinerating diet samples in a muffle furnace at 550 °C.

2.5. Liver Haematological and Homogenate Parameters

Triglyceride (TG, A110-1-1), total cholesterol (TC, A111-1-1), alanine aminotransferase (ALT, C009-2-1), aspartate aminotransferase (AST, C010-2-1), alkaline phosphatase (AKP, A059-2-2), L-Hydroxyproline (HYP, A030-2-1), Glutathione S-transferase (GST, A004-1-1), Malondialdehyde (MDA, A003-1-2), Adenosine triphosphate (ATP, A095-1-1), and total protein (TP, A045-2-2) levels in serum and liver homogenate were determined using assay kits (Catalog No.A002-045, Nanjing Jiancheng Co., Nanjing, China) following the manufacturer's protocols.

2.6. Hematoxylin and Eosin Staining

Liver tissues were fixed in 4% paraformaldehyde (Catalog No. P6148, Sigma-Aldrich, Saint Louis, MI, USA), embedded in paraffin (Leica, Wetzlar, Germany, Catalog No. 39601006), and cut into 4 μm thick sections. After dewaxing using different concentrations of xylene (Fisher Chemical, Pittsburgh, PA, USA, Catalog No. X5S-1) and ethanol, the nuclei were stained with hematoxylin solution (Sigma-Aldrich, Catalog No. HHS32), and the cytoplasm was stained with eosin solution (Sigma-Aldrich, Catalog No. HT110232). The sections were then dehydrated and made transparent with alcohol and xylene. Subsequently, the sections were sealed with neutral gel, and pathological changes were observed under a microscope (Olympus CX43, Olympus Corp. Tokyo, Japan).

2.7. Fe^{2+} Content Detection

The Fe^{2+} content in liver tissue was determined using a colorimetric method according to the instructions provided (E-BC-K773-M, Wuhan Elabscience Biotechnology Co., Ltd., Wuhan, China). Liver tissues were added to the ferrous kit buffer, homogenized thoroughly on ice using a homogenizer, then centrifuged at 10,000× *g* for 10 min and the supernatant was collected for subsequent assays. Finally, 300 μL of the reagent mixture was incubated with 150 μL of supernatant in a 1.5 mL EP tube for 10 min at 37 °C, and the optical density (OD) value was measured at 593 nm.

2.8. Molecular Docking

The small molecular structure of gossypol was downloaded from the PubChem database (https://pubchem.ncbi.nlm.nih.gov/, 6 June 2022). Hydrogenation and energy minimization were carried out using Chem3D, v19.0.0.22. The crystal structure of SIRT1 was obtained from the SIRT1 protein database (PDB code: 4L7B). Molecular docking of gossypol and SIRT1 was performed using AutoDock Vina v1.2.0 to determine the binding energy. Three-dimensional binding patterns of protein–small molecule complexes were analyzed and mapped using PyMOL v2.6.1, while Discovery Studio 2020 client was employed for further analysis and mapping of two-dimensional interaction patterns of protein–small molecule complexes.

2.9. Transmission Electron Microscope

Fresh liver tissues were sampled at a volume of 1 mm × 1 mm × 2 mm and were fixed in fixative (2.5% glutaraldehyde in pH 7.4 cacodylate buffer) for 2 h at room temperature. The liver tissues were washed three times in PBS and post-fixed in 1% osmium tetroxide. The samples were dehydrated through ascending concentrations of alcohol and post-embedded in Araldite. Ultra-thin sections were stained with uranyl acetate and lead citrate, and images were captured with a HITACHI HT7700 transmission electron microscope (Tokyo, Japan).

2.10. Mitochondrial Membrane Potential (MMP)

Fresh liver tissues (100 mg each) were obtained from fish in all CP groups following deep anesthesia and then cut into pieces using scissors before mitochondrial isolation using a commercial kit (Beyotime, Catalog No. C3606, Beyotime Biotechnology, Shanghai, China). The MMP assay was conducted using the JC-1 fluorescent probe method (Beyotime, Catalog No. C2006) for rapid visualization in the dark using green and red fluorescence (Ex = 490 nm and Em = 530 nm for JC-1 monomers; Ex = 525 nm and Em = 590 nm for J-aggregates).

2.11. Reactive Oxygen Species (ROS) Detection

The fish were anesthetized with 0.01% MS-222. The liver tissue was quickly removed and cleaned with PBS for 3 times. Liver tissue samples were dissected into 1 cm × 1 cm × 1 cm pieces using surgical scissors, digested with 0.25% trypsin, and incubated on an orbital shaker for 10 min. Single-cell suspension was prepared, the fluorescent probe was added, and the precipitation was suspended with diluted DCFH-DA (Beyotime Biotechnology, Shanghai, China). Cell precipitation was incubated at 27 °C for 40–60 min, centrifuged at 7000× *g* for 10 min, and the supernatant was collected and deposited with PBS. Photographs of the precipitate were taken using a confocal fluorescence microscope (Eclipse-Ti-S, Niko, Tokyo, Japan) after it had been suspended and mixed. The absorbance was detected at 525 nm by a fluorescence microplate to calculate the ROS content. Measure-

ment of fluorescence signal intensity of larvae by Image J software (Version 1.53k, National Institutes of Health, Bethesda, MD, USA).

2.12. Real-Time Quantitative PCR

Total RNA was extracted from the liver using Trizol reagent (Invitrogen, Carlsbad, CA, USA) following standard procedures and quantified using a NanoDrop 2000 (Thermo, Waltham, MA, USA). cDNA was synthesized from 2 μL of total RNA using the PrimeScript® Reverse Transcription Kit and gDNA Eraser (TaKaRa, Dalian, China). Real-time PCR was performed in the CFX96 Real-Time PCR Detection System (Bio-Rad, Hercules, CA, USA). The sequences of all primers used in this study are listed in Table 2. The Real-time PCR reaction (10 μL) included 5 μL of ChamQ Universal SYBR qPCR Master Mix (Vazyme, Nanjing, China), 3 μL of ddH_2O, 0.5 μL of each primer, and 1 μL of cDNA. The qRT-PCR protocol in this study was conducted as follows: 95 °C for 2 min, followed by 40 cycles of denaturation 95 °C for 5 s, annealing at the melting temperature (Tm) for 30 s, then 95 °C for 5 s, extension at 65 °C for 5 s, and a final extension at 95 °C for 15 s. The qRT-PCR was performed using a CFX96 Real-Time PCR Detection System (Bio-Rad, Hercules, CA, USA). β-actin and 18S rRNA were chosen as internal reference genes for normalization. The results were calculated using the $2^{-\Delta\Delta CT}$ method.

Table 2. The primers used for qRT-PCR.

Item [1]	Sequence	Tm (°C) [2]	GenBank ID
IL-1β-QF	CATGTTGGATCGTTACGGCAT	61	XM_038733429.1
IL-1β-QR	CCCATCTTCACGTTTTAGGCAC		
TNF-α-QF	AGCAAGGAAGCAGACAACGG	59	XM_038723994.1
TNF-α-QR	ATTTGCCTCAATGTGTGACGAT		
IL-10-QF	AGCCAGCAGCATCATTACCA	59	XM_038696252.1
IL-10-QR	AGAACCAGGACGGACAGGAG		
TGF-β2-QF	ACACTTTGCTGAAACTGGGGA	64	XM_038710299.1
TGF-β2-QR	GAACACGGACGACACACAGGT		
Sirt1-QF	TACCAGAACAGCCACCAAGT	64.0	XM 038736812
Sirt1-QR	CATTATTACCAGCAGTCTCCGT		
Yap-QF	GCTTGTAAGGCCAACCTCCT	61.4	XM_038693048.1
Yap-QR	GATTTGGGGACCCTTGCGTA		
Trf-QF	GGGCAACAATCCCCAAACT	61.4	XM 038718037
Trf-QR	TCATCCACCAGACACTGAAAGG		
Trfc-QF	CTTCCTGTCGCCCTATGAGTC	64.5	XM 038718573
Trfc-QR	GTCTGCCTTAGGGTTGTTGGT		
Gpx4-QF	GTTTACGCATCCTTGCCTTCC	59.0	XM 038716292
Gpx4-QR	GCTCTTTCAGCCACTTCCACAA		
Acsl4-QF	GATCTGCACTCACCCCGACA	61.4	XM 038699899
Acsl4-QR	GCTCTGGACTCAAATGCACCT		
Lpcat3-QF	CAGCCCTTCTGGTATCGTTG	63.3	XM 038711111
Lpcat3-QR	ATACACCCTCCGCTATAACCC		
Ptgs2-QF	GCCTCGTCTGTAATAATGTCCG	64.5	XM 038715374
Ptgs2-QR	CTGAATGGGATGTGCTTGAGTT		
β-actin-QF	CCCCATCCACCATGAAGA	55.7	AF 253319.1
β-actin-QR	CCTGCTTGCTGATCCACAT		
18S-QF	TGAATACCGCAGCTAGGAATAATG	59.0	MH 018569.1
18S-QR	CCTCCGACTTTCGTTCTTGATT		

[1] *Acsl4*: acyl-CoA Synthetase long chain family member 4; *β-actin:* beta actin; *Gpx4*: glutathione peroxidase 4; *Lpcat3*: lysophosphatidylcholine acyltransferase 3; *Ptgs2*: prostaglandin endoperoxide synthase 2; *Sirt1*: sirtuin 1; *18S:* 18S ribosomal RNA; *Trf*: transferrin; *Trfc:* transferrin receptor; *Yap*: yes associated protein; [2] Tm: melting temperature.

2.13. Western Blotting

Proteins were separated from cells using a Cold Lysis Buffer (Beyotime, Shanghai, China) containing a mixture of protease and phosphatase inhibitors. Protein content in

the cell supernatant was measured using a BCA protein quantification kit (Beyotime, Shanghai, China). Samples containing equal amounts of protein (20 μg) were separated by 10% SDS-polyacrylamide gel electrophoresis and then transferred to polyvinyl alcohol difluoride membranes (Bio-Rad Co., USA). Membranes were blocked and incubated with primary antibodies overnight at 4 °C (SIRT1, 1:2000, ZenBio (Chengdu, China), R25721; Yap, 1:1000, ABclonal (Wuhan, China), A1001; phospho-Yap (p-Yap), 1:1500, ZenBio, 381297; Trfc, 1:2000, ABclonal, A21622; Trf, 1:2000, ABclonal, A1448; Gpx4, 1:1500, ZenBio, 381958; β-actin, 1:3000, ZenBio, 380624; Lamin B, 1:1000, Abclonal, A1910). After washing four times with TBST (5 min each), proteins were visualized by incubating the membranes with the corresponding HRP-labeled secondary antibodies for 2 h at 25 °C. The membranes were washed four times for 5 min each with TBST using the ECL chemiluminescence kit. Finally, protein density analysis was performed using the Gel-Pro Analyzer (Rockville, MD, USA). All proteins were normalized for relative expression to β-actin or LaminB1 (Figure S1).

2.14. Immunohistochemistry

The paraffin-embedded liver sections were prepared for immunohistochemical analysis. De-paraffinization was performed with ethanol, while xylene was used for hydration. Samples were incubated with three percent hydrogen peroxide to block endogenous peroxidases. Primary antibody (Gpx4, 1:1000; ZenBio) incubation occurred overnight at 4 °C, followed by washing with PBS every 5 min. PBS washing was followed by continuous incubation with secondary antibody (1:5000; Affinity, Nanjing, China) and color development with DAB. A neutral resin adhesive sealed the nuclei, which were then dehydrated, cleared, and counterstained with hematoxylin. Stained sections were examined with an Olympus microscope (Olympus corporation, Tokyo, Japan).

2.15. Immunofluorescence Staining

Paraffin-embedded liver sections 5 μm thick were fixed and washed twice with PBS. Sections were blocked with bovine serum albumin and then incubated with anti-TRFC and YAP antibodies. Subsequently, the sections were incubated with FITC- or Cy3-coupled secondary antibodies for 2 h at room temperature (Ex = 525 nm and Em = 488 nm for FITC; Ex = 570 nm and Em = 550 nm for Cy3). Cell nuclei were counterstained with DAPI. Images of the cells were captured using a fluorescent microscope (IX70, Olympus, Tokyo, Japan).

2.16. Statistical Analysis

Data normality and homogeneity were assessed using D'Agostino–Pearson and Bartlett tests, respectively. If the data met these criteria, a one-way ANOVA with Duncan's multiple comparison test was performed to compare main factors. The data were analyzed using the PROC MIXED procedure of SAS 9.3 (SAS Inst. Inc., Cary, NC, USA) with the following model:

$$Y_{ijkl} = \mu + T_i + P_i + S_k + C(_K)_l + T \times S_{ik} + e_{ijkl},$$

where Y_{ijkl} refers to the dependent variable; μ, the overall mean; T_i, the fixed treatment effect; P_j, the random period effect; S_k, the random square effect; $C(_k)_l$, the random effect of the lth steer in the kth square; $T \times S_{ik}$, the interaction between the *i*th treatment and the *k*th square; and *eijkl*, the error residual. The linear and quadratic effects of increasing CP levels were analyzed using the CONTRAST procedure in SAS 9.3 (SAS Institute Inc., Cary, NC, USA). The Kenward–Roger option was used to calculate the degrees of freedom. Differences among the means of different treatments were tested using Duncan's test. Effects were considered significant at $p < 0.05$. All values are presented as least squares means ± standard errors (SEs).

3. Results

3.1. Growth Performance and Whole-Body Composition

Table 3 present the effects of CP levels on the growth performance of *M. salmoides* observed in this study. Compared to the FM group, the CP36 group exhibited notable reductions in FBW ($p < 0.001$), PWG ($p < 0.001$), SGR ($p < 0.001$), HSI ($p < 0.001$), VSI ($p < 0.001$), and ISI ($p = 0.001$). FI ($p = 0.119$) and FE ($p = 0.061$) were lower in the CP48 and CP60 groups compared to the FM group. Whole-body composition, including crude protein ($p = 0.432$), crude lipid ($p = 0.448$), and ash content ($p = 0.446$), showed no significant differences among the groups (Table 4). However, the CP24 group had significantly lower moisture content compared to the other groups ($p = 0.039$). No significant effects of dietary crude protein level were observed for protein production value (PPV) ($p = 0.340$) and lipid production value (LPV) ($p = 0.273$). The broken-line regression model, using SGR as the response variable, identified 23% as the optimum replacement ratio of FM by CP in the feed formulation (Figure 1).

Table 3. Growth performance of *M. salmoides* fed diets with different levels of CP for eight weeks.

Parameter [1]	Diets						SEM	*p*-Value		
	FM	CP12	CP24	CP36	CP48	CP60		ANOVA	Linear	Quadratic
Initial body weight (g/fish)	39.40	39.37	39.27	39.47	39.40	39.27	0.093	0.609	0.476	0.509
Final body weight (g/fish)	99.77 ^{a}	97.97 ^{a}	99.37 ^{a}	94.03 ^{b}	92.21 ^{bc}	89.79 ^{c}	1.462	<0.001	0.000	0.193
Percent weight gain (%)	153.21 ^{a}	148.87 ^{a}	153.07 ^{a}	138.25 ^{b}	134.04 ^{bc}	128.68 ^{c}	4.732	<0.001	0.000	0.251
Specific growth rate (%)	1.47 ^{a}	1.45 ^{a}	1.47 ^{a}	1.38 ^{b}	1.35 ^{bc}	1.31 ^{c}	0.023	<0.001	0.000	0.224
Feed intake (g/fish)	63.51 ^{a}	63.72 ^{a}	61.28 ^{ab}	60.94 ^{ab}	58.37 ^{b}	58.81 ^{ab}	1.932	0.119	0.001	0.831
Feed efficiency (%)	95.03 ^{ab}	92.11 ^{ab}	98.25 ^{a}	89.65 ^{bc}	90.46 ^{bc}	86.00 ^{c}	3.287	0.061	0.027	0.383
Relative gut length (%)	78.03	77.56	78.42	77.69	77.67	76.32	1.673	0.738	0.256	0.342
Intestosomatic index (%)	0.84 ^{a}	0.81 ^{ab}	0.81 ^{ab}	0.76 ^{bc}	0.74 ^{cd}	0.69 ^{d}	0.037	0.001	<0.001	0.263
Viscerosomatic index (%)	8.48 ^{a}	8.31 ^{ab}	8.53 ^{a}	7.94 ^{b}	7.93 ^{b}	7.46 ^{c}	0.182	<0.001	<0.001	0.027
Hepatosomatic index (%)	2.33 ^{a}	2.21 ^{ab}	2.41 ^{a}	2.08 ^{bc}	1.95 ^{c}	1.89 ^{c}	0.126	<0.001	<0.001	0.104

[1] Initial body weight (IBW, g/fish), final body weight (FBW, g/fish). Survival rate (SR, %) = 100 × final amount of fish/initial amount of fish; Percent weight gain (PWG, %) = 100 × (final body weight − initial body weight)/Initial body weight; Specific growth rate (SGR, %/d) = 100 × [ln (final body weight) − ln (initial body weight)]/days; Feed intake (FI, g/fish) = (feed offered in dry basis − uneaten feed in dry basis)/amount of fish; Feed efficiency (FE, %) = 100 × (final body weight − initial body weight)/Feed intake; Relative gut length (RGL, %) = 100 × intestine length/body length. Intestosomatic index (ISI, %) = 100 × wet intestine weight / wet body weight. Viscerosomatic index (VSI, %) = 100 × wet viscera weight/wet body weight; and Hepatosomatic index (HSI, %) = 100 × wet liver weight/wet body weight. *p*-value: significant probability associated with the F-statistic. Data presented as mean of three replicates. Different superscript letters ($^{a, b, c, d}$) within a row indicate significant differences ($p < 0.05$). Without letter or bars shared the same letter represents no significant difference by Duncan's test ($p < 0.05$, $n = 12$).

Table 4. Effects of FM replacement by CP on flesh composition of *M. salmoides* (%, wet-basis).

Parameters [1]	Diets						SEM	*p*-Value		
	FM	CP12	CP24	CP36	CP48	CP60		AVOVA	Linear	Quadratic
Moisture	70.95 ^{c}	70.73 ^{bc}	69.83 ^{a}	70.01 ^{a}	70.92 ^{c}	70.50 ^{ab}	0.015	0.039	0.596	0.025
Crude protein	18.50	18.67	19.00	19.00	18.83	19.00	<0.001	0.432	0.587	0.016
Crude lipid	7.09	7.17	7.25	7.15	7.00	7.06	<0.001	0.448	0.805	0.298
Ash	3.76	3.71	3.81	3.78	3.72	3.84	0.010	0.446	0.801	0.322
Protein production value	0.73	0.83	0.81	0.81	0.77	0.81	0.050	0.340	0.213	0.547
Lipid production value	2.30	2.50	2.45	2.44	2.23	2.48	0.110	0.273	0.306	0.926

[1] PPV: protein production value; LPV: lipid production value. p-value: significant probability associated with the F-statistic. Data presented as mean of three replicates. Different superscript letters ($^{a, b, c}$) within a row indicate significant differences ($p < 0.05$). Without letter or bars shared the same letter represents no significant difference by Duncan's test ($p < 0.05$, $n = 9$).

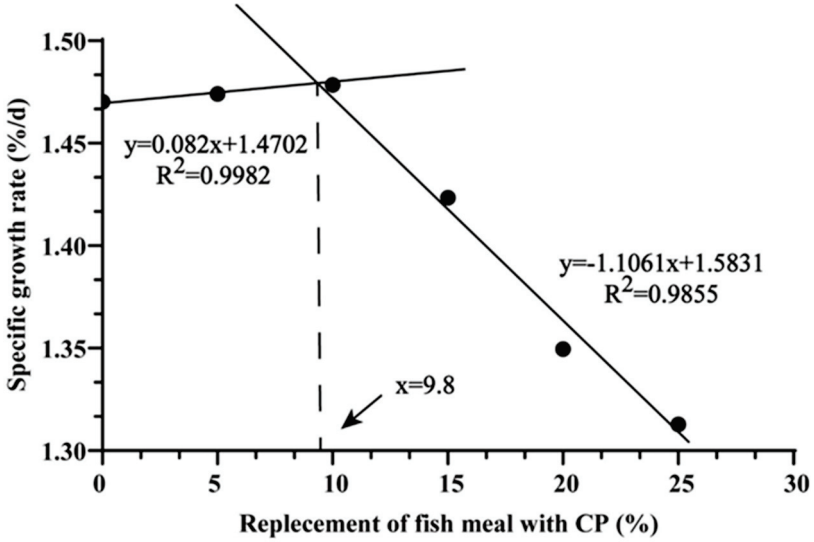


Figure 1. The relationship between SGR and dietary CP replacement level in *M. salmoides*.

3.2. Serum and Liver Biochemical Parameters

Table 5 summarizes the serum and liver biochemical parameters. Serum TG and TC levels gradually increased in the CP24 and CP36 groups ($p < 0.001$). The CP48 group exhibited significantly higher HYP levels than the other groups ($p < 0.001$). Serum AKP activities initially increased and then decreased as CP replacement levels rose ($p < 0.001$). AKP activities peaked in the CP36 group compared to the FM group ($p < 0.001$). Liver ALT and AST activities were significantly higher in the CP60 group than in all other groups ($p < 0.001$).

Table 5. Effects of FM replacement by CP on serum and liver biochemical indices of *M. salmoides*.

Parameters [1]	Diets						SEM	*p*-Value		
	FM	CP12	CP24	CP36	CP48	CP60		ANOVA	Linear	Quadratic
Serum										
Triglyceride (mmol/L)	9.19 ^{a}	8.46 ^{a}	14.99 ^{c}	17.75 ^{d}	17.78 ^{d}	12.30 ^{b}	3.462	<0.001	0.000	0.000
Total cholesterol (mmol/L)	11.41 ^{ab}	10.78 ^{a}	12.03 ^{b}	13.07 ^{c}	13.19 ^{c}	12.82 ^{c}	0.353	<0.001	0.000	0.092
Alkalinephosphatase (King /g prot)	7.70 ^{b}	7.74 ^{b}	7.66 ^{b}	9.52 ^{c}	7.36 ^{ab}	6.39 ^{a}	0.493	<0.001	0.067	0.001
L-Hydroxyproline (ug/mL)	5.90 ^{a}	9.12 ^{b}	8.88 ^{b}	9.37 ^{bc}	13.32 ^{d}	11.26 ^{c}	0.996	<0.001	0.000	0.133
Liver										
Aspartate aminotransferase (U/g prot)	39.05 ^{b}	36.43 ^{b}	35.87 ^{ab}	32.41 ^{a}	39.65 ^{b}	53.19 ^{c}	1.983	<0.001	0.000	0.000
Alanine aminotransferase (U/g prot)	160.04 ^{b}	163.35 ^{b}	161.71 ^{b}	141.58 ^{a}	168.07 ^{b}	195.69 ^{c}	8.372	<0.001	0.000	0.000

[1] TG: triglyceride; TC: total cholesterol; AST: aspartate aminotransferase; ALT: alanine aminotransferase; AKP: alkalinephosphatase; HYP: L-Hydroxyproline. *p*-value: significant probability associated with the F-statistic. Data presented as mean of three replicates. Different superscript letters ($^{a, b, c, d}$) within a row indicate significant differences (p <0.05). Without letter or bars shared the same letter represents no significant difference by Duncan's test ($p < 0.05$, $n = 9$).

3.3. Liver Morphology and Inflammation-Related Genes

Histological examination of liver morphology (Figure 2) demonstrated that the FM group exhibited bright red coloration and smooth hepatic architecture, with intact, well-organized lobules and centrally located, round hepatocyte nuclei. In contrast, the CP36, CP48, and CP60 groups displayed yellowish, blunted livers. The CP36 and CP48 groups showed inflammatory cell infiltration and vascular wall thickening. Hepatocyte outlines were indistinct in the CP48 and CP60 groups, with nuclei dissolving and disappearing.

Masson staining indicated collagen fiber deposition in the CP36, CP48, and CP60 groups. In each CP group, there was an obvious increase in IL-1β and TNF-α expression as compared to the control group ($p < 0.05$). After feeding CP60, there was a downregulation of the anti-inflammatory cytokine IL-10 and TGF-β2 ($p < 0.05$, Figure 3).

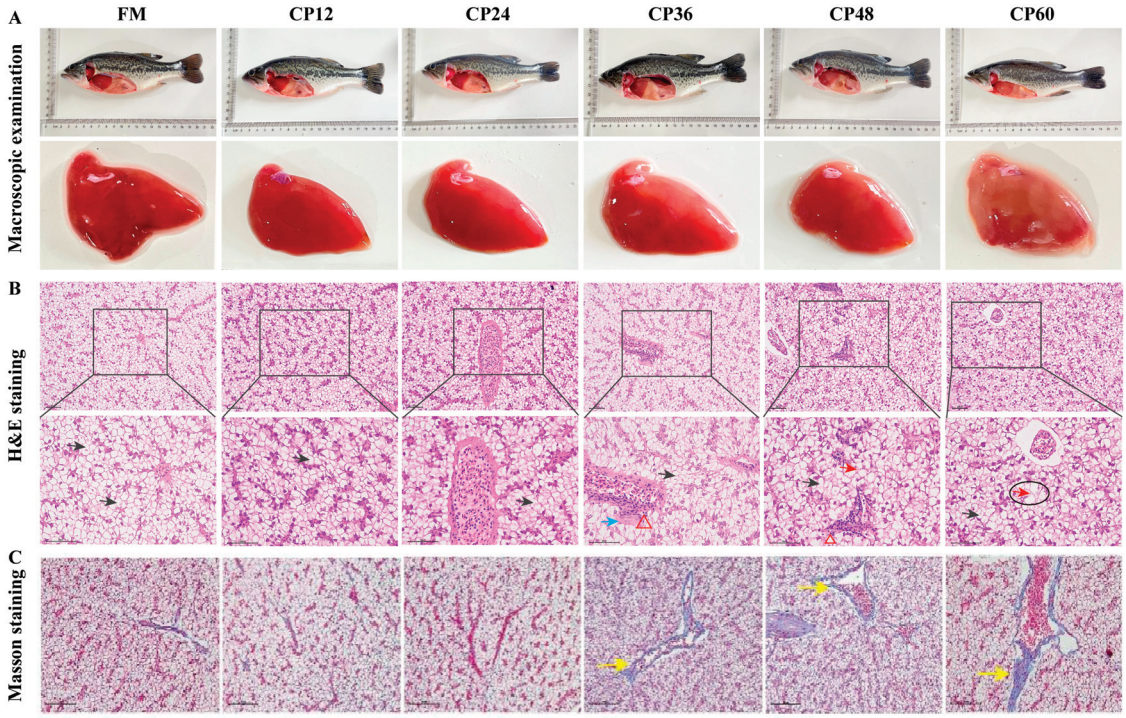


Figure 2. Histology of liver in juvenile *M. salmoides* fed diets containing different levels of CP.: (**A**) Fish body and liver images; (**B**) Hematoxylin and eosin (H&E); (**C**) Masson's trichrome staining. H&E: 100 μm and 20 μm, Masson: 20 μm. Black arrow: hepatocytes; Blue arrow: vascular wall hyperplasia; Red arrow: hepatic nucleolysis; Red triangle: inflammatory cell infiltration; Black circle: local necrosis of hepatocytes; Yellow arrow: collagen fiber deposition.

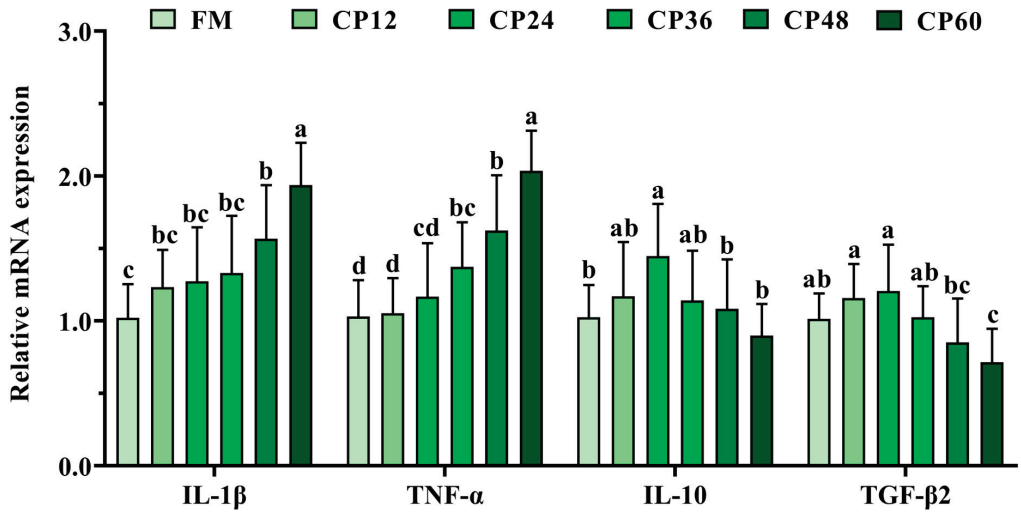


Figure 3. Effects of CP on the expression of pro-inflammatory cytokines (IL-1β and TNF-α), anti-inflammatory cytokines (IL-10 and TGF-β2) in the liver of *M. salmoides*. All data represent means ± SEM of three replicates. Bars with different letters indicate significant differences by Duncan's test ($p < 0.05$, $n = 9$).

3.4. Oxidation Indicators and Fe^{2+} Content

Mitochondrial function was assessed using transmission electron microscopy (TEM), JC-1 membrane potential staining, and ATP content measurement. Most liver mitochondria in the FM and CP24 groups appeared normal, with oval shapes, intact membranes, and well-distributed cristae (Figure 4A). However, in the CP60 group, the outer mitochondrial membrane was ruptured, and mitochondrial cristae were absent, indicating characteristics of ferroptotic mitochondria. Correspondingly, liver MMP and ATP content decreased in the CP60 group compared to the FM and CP24 groups ($p < 0.05$) (Figure 4B,C).

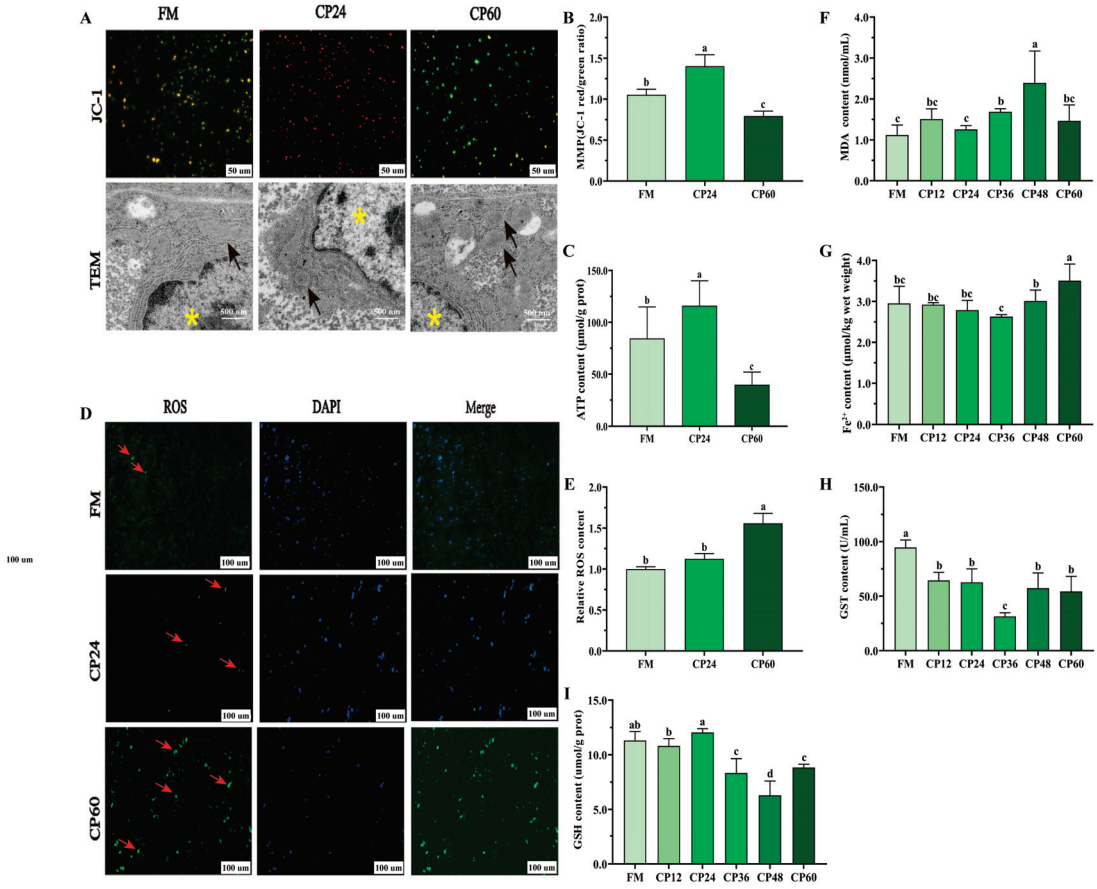


Figure 4. Excess CP caused liver damage and was associated with ferroptosis in the *M. salmoides*. (**A**): Liver mitochondria were collected for JC-1 staining (Scale: 50 um) and Transmission Electron Microscope (TEM) examination (Scale: 500 nm, $n = 9$); black arrows: mitochondrion; yellow asterisk: hepatic nucleus; (**B**): The ratio of red and green fluorescence of JC-1; (**C**): ATP contents; (**D**): fluorescence probe reactive oxygen species (ROS) staining, red arrows represent ROS ($n = 9$); (**E**): relative ROS fluorescence value statistics; (**F**–**H**): glutathione (GSH), glutathione S-transferase (GST), and malondialdehyde (MDA), respectively; (**I**): Liver Fe^{2+} level. All data represent means ± SEM of three replicates. Bars with different letters indicate significant differences by Duncan's test ($p < 0.05$, $n = 12$).

ROS accumulation, a marker of ferroptosis, was significantly higher in the CP60 group compared to FM and CP24 ($p < 0.05$) (Figure 4D,E). Furthermore, the levels of the antioxidant factor GSH and GST activities in liver tissues were reduced with higher CP substitution levels (Figure 4F,G). Liver GSH levels in the CP48 group exhibited the lowest GSH levels ($p < 0.05$), while GST activity was lowest in the CP36 group ($p < 0.05$) (Figure 4H). MDA levels were highest in the CP48 group and the CP24 group also showed higher levels than the FM group ($p > 0.05$). MDA levels progressively increased in the CP36 group and reached a peak in the CP48 group ($p < 0.05$).

Iron overload, a hallmark of ferroptosis, was assessed via liver Fe^{2+} content in the different CP replacement FM groups using an iron assay kit. The results showed that the Fe^{2+} content of CP48 and CP60 groups was significantly increased compared with other groups (Figure 4I).

3.5. Hepatic Ferroptosis-Related Genes

CP levels altered the expression of ferroptosis-related genes (Figure 5). The mRNA expression of *Trf* increased in the CP12, CP24, and CP36 groups but decreased in the CP48 and CP60 groups. The *Trf* mRNA expression did not significantly differ between the FM, CP12, CP24, and CP36 groups, whereas levels were significantly reduced in CP48 and CP60 ($p < 0.05$). *Lpcat3* mRNA expression remained unaffected in the CP12, CP24, and CP36 groups ($p > 0.05$) but was higher in the CP24 and CP36 groups ($p < 0.05$) (Figure 5A–C). *Acsl4* and *Ptgs2* mRNA expression levels increased with increasing CP levels ($p < 0.05$) (Figure 5D,E). Similar to *Trf* mRNA expression, TRF protein levels did not significantly differ among the CP12, CP24, CP36, and CP48 groups but showed significant differences in the CP60 group compared to the FM group ($p < 0.05$) (Figure 5F,H). Notably, the CP48 and CP60 groups exhibited higher TRF protein levels ($p < 0.05$).

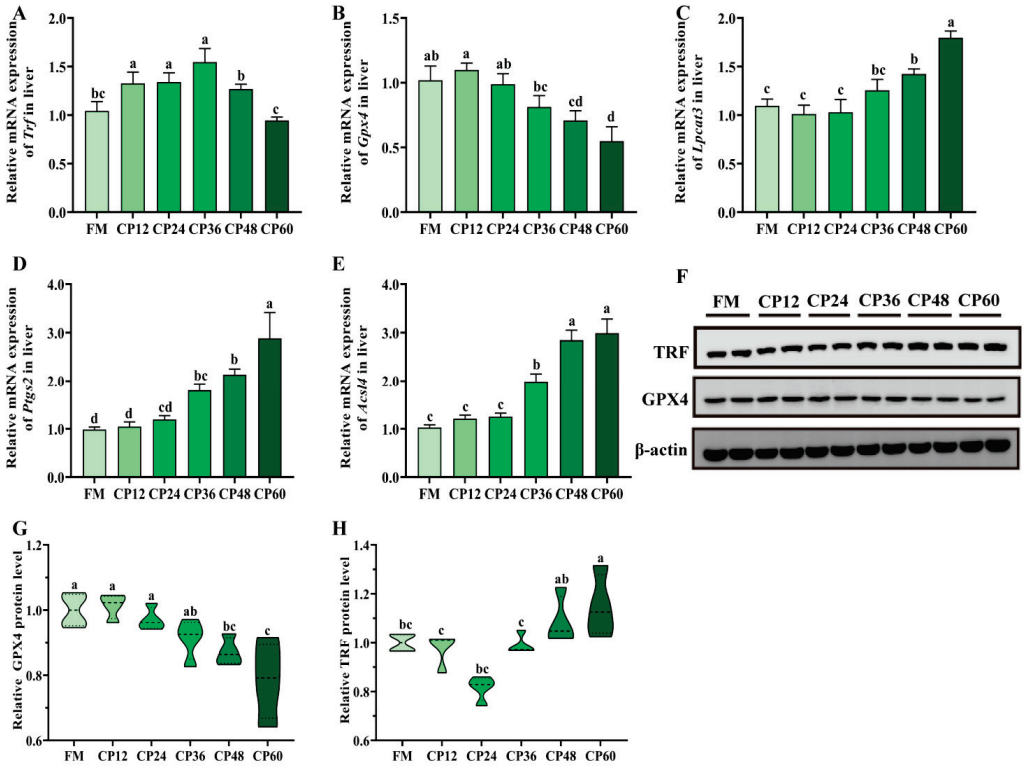


Figure 5. Effect of excess cotton protein (CP) on ferroptosis-related genes in the liver of juvenile *M. salmoides*. (**A**–**E**): Effect of dietary CP on mRNA expression of TRF, GPX4, LPCAT3, PTGS2, and ACSL4 in the liver of juvenile *M. salmoides*; (**F**): Representative western blot of TRF, and GPX4 in the liver; (**G**,**H**): Protein levels of GPX4 and TRF. Data represent means ± SEM of three replicates. Bars with different letters indicate significant differences by Duncan's test ($p < 0.05$, $n = 12$).

3.6. SIRT1-YAP-TRFC Pathway

The expression levels of *Sirt1* and *Yap* mRNA decreased as CP replacement increased. *Sirt1* mRNA expression levels were significantly lower in the CP48 and CP60 groups compared to the control FM group ($p < 0.05$) (Figure 6A). In the CP36 group, the expression level of *Yap* mRNA began to decrease, and it was significantly lower in the CP60 group than in the control group ($p < 0.05$) (Figure 6B). *Trfc* mRNA expression levels increased

with the increase in CP substitution levels, and in the CP60 group, the expression level was significantly higher than that in the FM, CP12, CP24, and CP36 groups ($p < 0.05$) (Figure 6C). The SIRT1 protein level correlated with mRNA expression and decreased to the lowest level in the CP48 and CP60 groups ($p < 0.05$) (Figure 6D,E). YAP protein level gradually decreased with the increase in CP replacement rate, although no significant differences were observed among the CP36, CP48, and CP60 groups ($p > 0.05$). However, these levels were higher than those in the other three groups ($p < 0.05$) (Figure 6D,F). Nuclear TRFC and YAP protein levels increased with higher CP substitution, with the CP48 and CP60 groups showing significantly higher levels than the FM group ($p < 0.05$) (Figure 6D,G,H). IHC of GPX4 protein in the liver of juvenile *M. salmoides* revealed a gradual decrease in the brownish-yellow positive signal compared to the FM group (Figure 6I). This indicated reduced GPX4 protein accumulation in the cytoplasm with the increase in CP content. The subcellular localization of YAP and TRFC, assessed via immunofluorescence assays (Figure 7), demonstrated increased TRFC expression and nuclear enrichment of YAP protein in hepatocytes in the CP48 and CP60 groups. YAP, a transcriptional cofactor, was shown to translocate from the cytoplasm to the nucleus under these conditions.

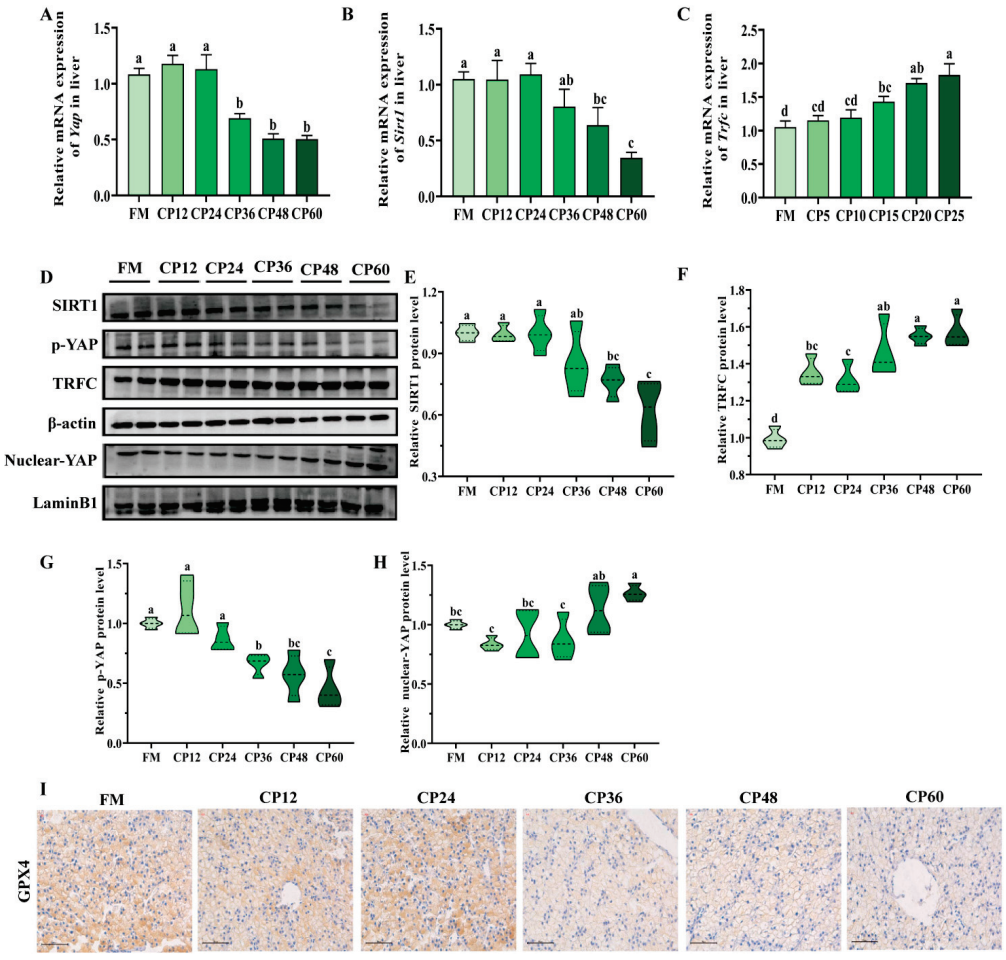


Figure 6. Effect of dietary CP on *SIRT1-YAP-TRFC* pathway in the liver of juvenile *M. salmoides*. (**A**–**C**): mRNA expression of SIRT1, YAP, and TRFC. (**D**): Representative Western blot images of nuclear YAP, SIRT1, p-YAP, and TRFC; Protein levels of (**E**) SIRT1; (**F**) p-YAP (Ser 127); (**G**) TRFC; (**H**) nuclear YAP; (**I**): liver sections immunohistochemically stained for GPX4 (Scale = 50 μm), the brown signal represents positive expression. Data represent means ± SEM of three replicates. Bars with different letters indicate significant differences by Duncan's test ($p < 0.05$, $n = 12$).

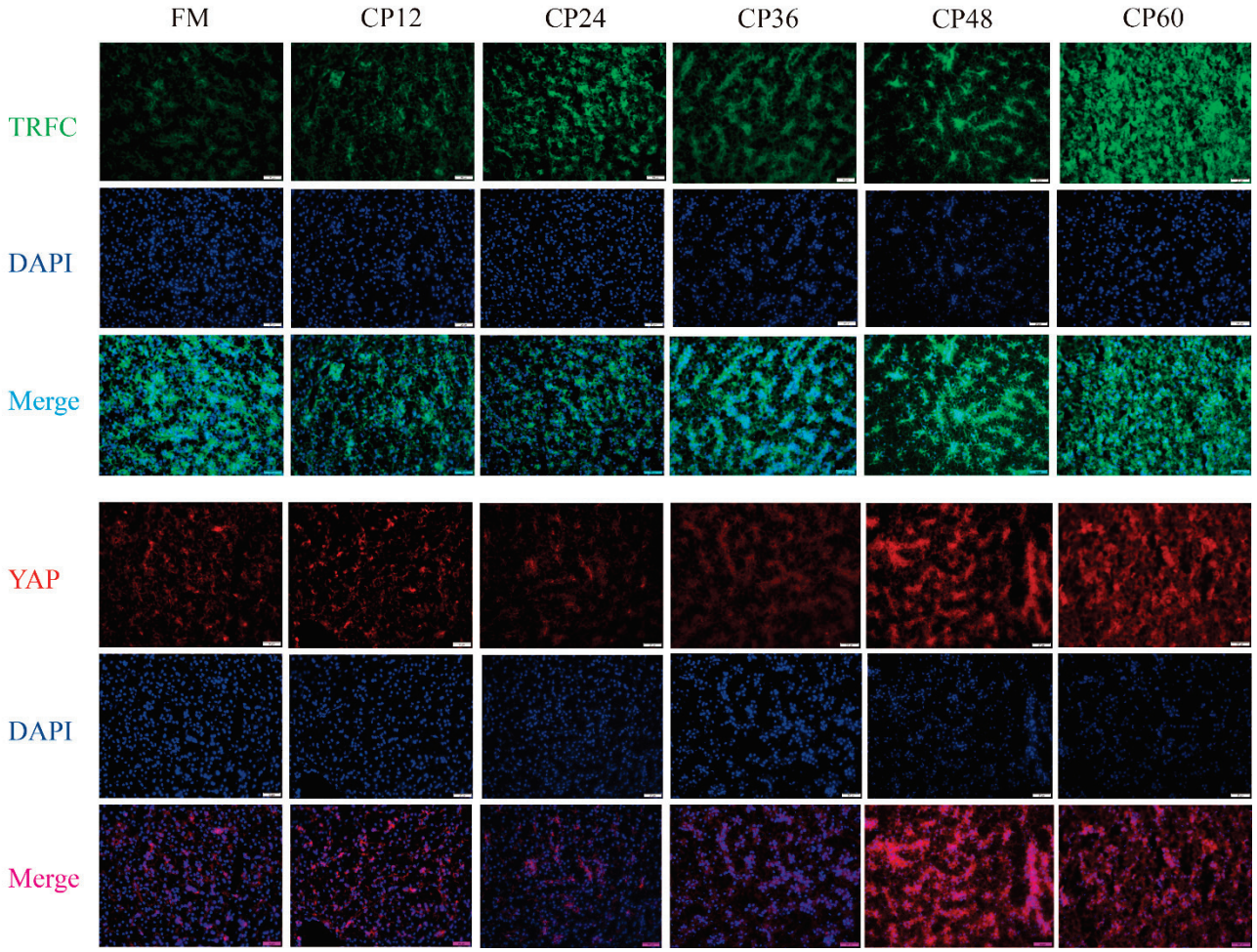


Figure 7. Fluorescence microscopy images of DAPI (Blue), TRFC (Green), and YAP (Red) in the liver of *M. salmoides* fed with different six studied diets. Replacement of fish meal with CP increased hepatocyte expression of TRFC (Green), and nuclear enrichment of YAP protein in the presence of CP48 and CP60 (Scale = 20 μm, n = 9).

3.7. Gossypol and SIRT1 with Molecular Docking

Subsequently, we investigated the mechanism of SIRT1 inhibition by gossypol using molecular docking (Figure 8A,B). The results revealed that the gossypol small molecule fits into the ligand-binding domain pocket of SIRT1, a key regulatory domain for its activity, and forms three hydrogen bonds at ILE 270, Val 266, and ARG 274 rather than non-specific bonds.

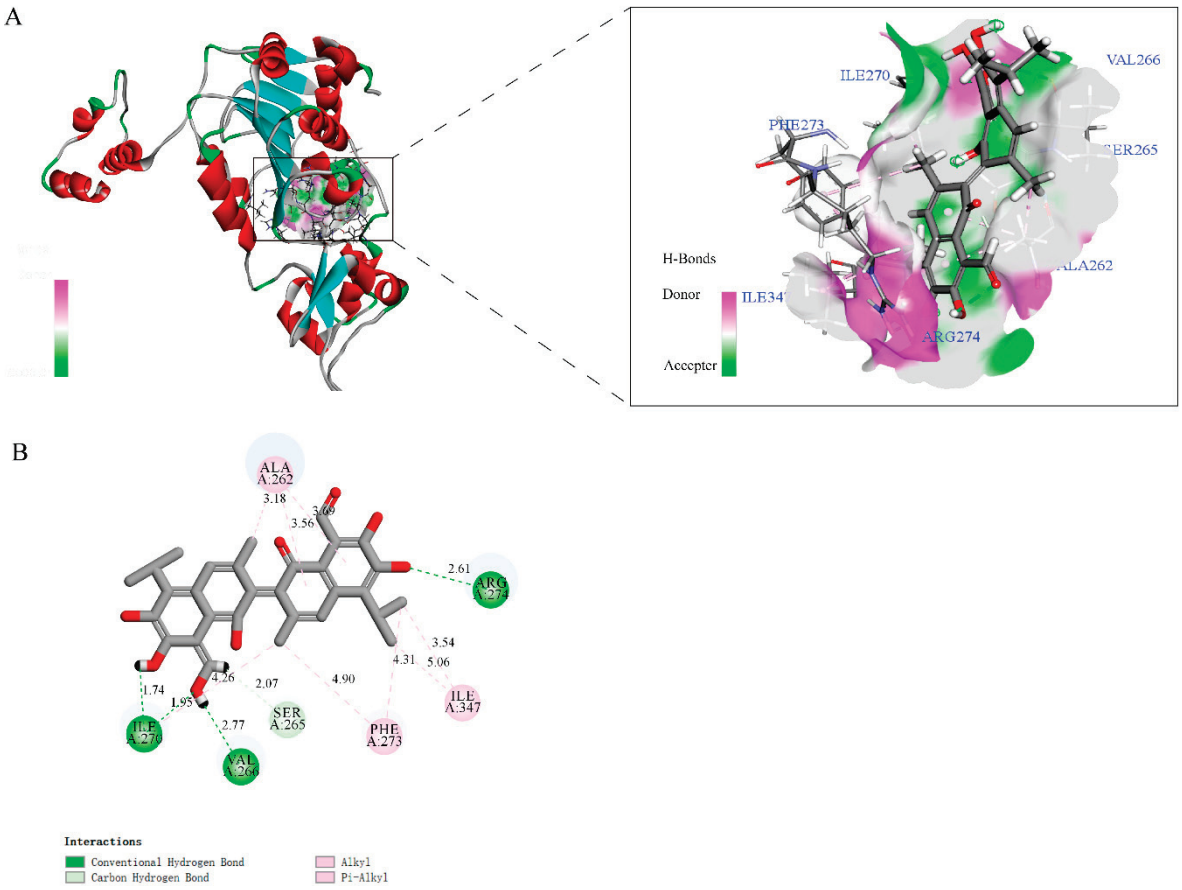


Figure 8. The model of the mechanism of excess CP mediated by ferroptosis following liver damage in M. salmoides. (**A**): The binding mode between micromolecule gossypol and SIRT1 protein, showing interactions between gossypol and key residues. (**B**): A two-dimensional interaction map of gossypol and SIRT1. Excess CP reduced SIRT1 expression to promote the nuclear accumulation of YAP, YAP can directly regulate the TRFC promoter, and promote the expression of TRFC protein, which upregulated the levels of ferroptosis. Cellular ROS content was increased by excess CP-induced ferroptosis, ultimately leading to ferroptotic cell death.

4. Discussion

4.1. Effects of Partial Substitution of FM with CP on Growth Performance Indices of M. salmoides

Studies have indicated that incorporating moderate amounts of vegetable protein into aquatic animal feeds can promote growth, while excessive levels may hinder it by delaying development [25]. The results of this study demonstrated that the final weight, weight gain rate, and specific growth rate of juvenile *M. salmoides* remained unaffected when CP substitution in the diet was below 24%. However, the growth performance of juvenile *M. salmoides* declined when the substitution rate exceeded 24%, with the lowest FBW, PWG, and SGR observed at a 60% substitution rate. Previous studies have explored the substitution of CP for FM in aquatic animal diets. For example, it was observed that replacing 30% of FM with dephenolized CP had no effect on the growth performance of spot prawns, but higher substitution rates significantly reduced their growth [11]. Likewise, large yellow croaker experienced no growth impact with a 9% FM replacement by dephenolized CP [8]. Black seabream exhibited no changes in PWG or SGR when 16% of FM was replaced by fermented CP [25]. However, excessive CP in diets can introduce toxins such as gossypol, which affect growth by inhibiting development. Of the FM replaced with 60% CP decreased FI and FE. The results indicated that CP could reduce the feed efficiency of *M. salmoides*. The reduced growth performance may be partially attributed to decreased feed intake

caused by lower palatability. Free gossypol readily binds with lysine, reducing its activity and making lysine the first limiting amino acid in feed [26,27]. A deficiency in lysine not only diminishes the palatability of the feed but also lowers the efficiency of protein conversion [28]. Adding lysine to plant-based feed can not only replace the high cost of FM but also help reduce phosphorus emissions to the environment, thereby minimizing pollution, as plant protein contains less phosphorus than FM. In addition, factors such as cottonseed detoxification processing technology, feeding methods, growth stages of experimental subjects, and feed palatability also influence FM substitution efficiency [6]. Improving detoxification methods, eliminating anti-nutritional factors, and supplementing essential amino acids are recommended strategies to optimize plant protein utilization.

4.2. Effects of CP Replacement of FM on the Nutrient Deposition of M. salmoides

Protein is the primary energy source for growth and metabolism in fish, especially carnivorous species, which have high dietary protein requirements. The quality of dietary protein is assessed by its absorption and changes in body composition. This study showed no significant effect of CP substitution for FM on crude fat or crude protein content in juvenile *M. salmoides*. However, the moisture content was lowest when FM was replaced with 24% CP in the diet and increased when CP substitution reached 48%. Higher moisture content may result from reduced feed intake due to poor palatability. Similar findings were reported in studies with snapper (*Pagrus major*) [29]. Zhao et al. (2021) observed no significant changes in moisture, ash, crude protein, or crude fat content in anchovy when less than 50% of fishmeal (FM) was replaced with cottonseed protein concentrate [7]. Anderson et al. (2016) reported that replacing 75% of FM with cottonseed meal did not alter moisture, ash, crude protein, or crude fat levels in juvenile black sea bass [30]. In contrast, Alam et al. (2018) found that substituting 75% and 100% of FM with cotton meal significantly increased body fat content in southern flounder (*Paralichthys lethostigma*) [9]. These differences highlight how dietary CP influences nutrient deposition, with variations depending on feed ingredients, substitution levels, species adaptability, and study duration [30]. These results suggest that dietary CP not differ significantly from nutrient deposition.

4.3. Effects of Substituting FM with CP on Hepato-Intestinal Development of M. salmoides

The intestinal tract and liver are essential digestive and immune organs in fish. Their normal development serves as a key indicator of fish health and can directly reflect feed utilization efficiency. In this study, the VSI, HSI, and ISI declined as the proportion of FM replaced by CP in the diet increased. All three ratios significantly decreased when the replacement rate exceeded 24%. Previous research has demonstrated that substituting FM with high levels of plant protein can trigger intestinal inflammatory response, disrupting the structure of intestinal villi and impairing digestion and absorption [31]. Similarly, our study observed that high-level CP substitution (48–60% FM replacement) suppressed growth performance in *M. salmoides*. Sun's findings indicated that as the proportion of fermented CP replacing FM in the diet increased [25], the HSI and VSI of young black sea bass significantly decreased [32]. The reduction in the HSI may be attributed to an uneven distribution of amino acids in the feed, resulting in an imbalance in amino acid catabolism during lipid synthesis [32]. Thus, excessive substitution of CP sources for FM beyond a certain percentage can compromise fish nutritional status and hinder feed utilization.

4.4. Effects of CP Replacement of FM on Liver Morphology, Biochemical Indices, and Inflammation-Related Genes of M. salmoides

This study revealed that when the proportion of CP replacing FM exceeded 24%, the liver of juvenile *M. salmoides* gradually exhibited a lighter, more yellowish, and blunter

appearance. Histological observations revealed hepatocyte enlargement, blurred outlines, disordered hepatic lobule arrangement, infiltration of inflammatory cells, and local necrosis at a 60% replacement ratio. Furthermore, collagen deposition occurred in the liver tissues of the high CP replacement FM group, indicating potential liver fibrosis development. Chronic liver injury of this nature is associated with increased collagen-dominated extracellular matrix synthesis and the activation of hepatic stellate cells into myofibroblasts and fibroblasts. Serum and liver homogenate-based indices effectively reflect changes in liver function. AST primarily transfers the amino group from aspartic acid to α-ketoglutaric acid, forming oxaloacetic acid and glutamic acid. ALT transfers the amino group from alanine to α-ketoglutarate, producing pyruvate and glutamate [33]. Oxaloacetate is crucial in the tricarboxylic acid cycle, providing essential energy for the body [34]. Elevated activities of AST and ALT are indicative of liver damage [35], while AKP serves as a biomarker for biliary stasis and liver fibrosis [36]. In the present experiment, results indicated that when the proportion of CP replacing FM exceeded 24%, the serum TG and TC levels significantly increased. This suggests that the liver lipid content of the fish was increased. Serum AKP activity was highest at the replacement ratio of 36%, indicating potential bile retention in the liver. Transaminase, including ALT and AST, is indicative of liver damage when present in elevated serum levels. Liver AST activity was highest when the replacement ratio was 60%, and ALT activity peaked at the 48% replacement ratio. These findings indicated that excessive substitution of FM with CP can lead to substantial liver damage in fish, with the degree of damage varying according to fish species' tolerance to plant protein products. The research by He et al. revealed that substituting 18% of FM with CP concentrate has been reported to result in liver tissue yellowing and diffuse lipid vacuolation in some hepatocytes of *M. salmoides* [14]. This study not only confirms the negative effects of CP on growth and liver function as reported by He et al., but more importantly elucidates its mechanism of action from perspectives of ferroptosis, signaling pathways, and ultrastructural changes, thereby providing a more comprehensive theoretical basis for the safe utilization of CP in aquatic feeds. Wang et al. found that replacing CP with 27% FM significantly increased liver ALT and AST activity and led to hepatocyte atrophy in juvenile common carp [37]. Collectively, these results suggest that excessive CP substitution for FM induces liver damage, with severity varying depending on the fish species and processing techniques of plant protein products. In fish, cytokines are broadly categorized into pro-inflammatory factors (including IL-1β and TNF-α) and anti-inflammatory factors (e.g., IL-10, TGF-β1), both playing crucial roles in mediating immune responses. Studies have found that CP reduces anti-inflammatory factors and promotes the expression of pro-inflammatory factors, thereby promoting inflammation in *M. salmoides* [38]. In this study, we found that high-level CP could enhance the relative expression of pro-inflammatory factors (IL-1β and TNF-α) and decrease the relative expression of anti-inflammatory factors (IL-10 and TGF-β2) of juvenile *M. salmoides*, agreeing with previous studies, which suggested that high-level CP could decrease the immunity and trigger the inflammation of juvenile *M. salmoides*.

4.5. Excess Substitution of CP for FM Caused Hepatic Fibrosis and Was Associated with Ferroptosis

Liver fibrosis is pathologically defined by excessive deposition of extracellular matrix (ECM) proteins, particularly collagen subtypes, in chronic hepatic injury contexts [39]. With Masson's trichrome staining, a reliable method for highlighting collagen disposition, we found that high-level CP effectively increases collagen fiber accumulation. Hydroxyproline (HYP), a major component of collagen, elevates during liver fibrosis [40,41]. Notably, high-level CP successfully increases serum HYP content. These collective results highlight high-level CP induced hepatic fibrosis of *M. salmoides*. To further investigate the effects of

excessive CP substitution for FM on the liver fibrosis by ferroptosis mediated in juvenile *M. salmoides*. This study used TEM to examine the ultrastructure of hepatocytes. The results demonstrated that when the proportion of CP replacing FM was 60%, there was a significant change in mitochondrial morphology, characterized by mitochondrial atrophy and loss of cristae compared to the FM group. This is a typical morphological feature of cell ferroptosis. In mice, ferroptosis has been linked to liver damage induced by acetaminophen (APAP), lipopolysaccharide (LPS) combined with D-galactose amino, and microplastics (MPs) [42–44]. MMP is a prerequisite for maintaining oxidative phosphorylation of mitochondria to produce ATP, and the stability of MMP is conducive to maintaining the normal physiological function of cells [45,46]. MMP was upregulated in the CP24 group, indicating that it could improve mitochondrial function. However, MMP was downregulated in the CP60 group, indicating that it would lead to abnormal mitochondrial membrane potential and negatively affect mitochondrial function. Ferroptosis is an oxidative stress-related programmed cell death mechanism characterized by iron-dependent lipid peroxide accumulation. This process involves elevated iron ion concentrations, increased ROS, and lipid peroxidation [47]. GPX4 plays a crucial role in mitigating ferroptosis by eliminating lipid peroxides.

In this study, the liver of juvenile *M. salmoides* was examined for Fe^{2+}, ROS, lipid peroxidation product MDA content, and antioxidant factor GSH content in control and test groups. GSH serves as a cofactor of GPX4 and inhibits ferroptosis. The results revealed that in the CP60 group, the accumulation of ROS in the liver tissues of *M. salmoides* was higher than that in the FM and CP24 groups. In the CP48 group, the level of GSH in the liver were significantly reduced. Liver tissue MDA content gradually increased in the CP36 group and reached a maximum in the CP48 group. The study also examined ferroptosis-related gene expression levels and found that hepatic TRF protein expression levels were highest in the CP60 group compared to the FM group. GPX4 mRNA and protein levels were significantly lower in the CP48 and CP60 groups. *Acsl4* and *Ptgs2* mRNA levels were significantly higher in the CP36, CP48, and CP60 groups compared to the control FM group. *Lcpat3* mRNA expression was the highest in the CP48 and CP60 groups.

Excessive substitution of FM with plant protein has been studied to result in elevated levels of oxidative stress ROS in the intestine of *Schizothorax prenanti*, causing damage to the intestinal barrier [48]. Additionally, replacing FM with dephenolized CP has been shown to reduce the antioxidant immune function of the liver in silver perch, leading to elevated ROS levels in the liver [49]. Circulating Fe^{3+} binds to and is transported by TRF. Once it enters the cell via TFRC, it undergoes reduction and is released into the cytoplasmic unstable iron pool (LIP) and the excess iron is stored in ferritin. Iron has the capability to react directly with polyunsaturated fatty acids found in cell membranes and other biological membranes due to its instability and high reactivity as Fe^{2+}. This reaction generates substantial amounts of lipid peroxides through the fenton reaction in conjunction with hydroxyl radicals like H_2O_2 [50]. Consequently, iron overload can induce ferroptosis and exacerbate liver injury. The over-substitution of CP for FM decreases hepatic antioxidant GSH levels and increases ROS accumulation in hepatocytes. ROS, in turn, initiates lipid peroxidation in polyunsaturated fatty acid-rich lipid bilayers, such as cell and mitochondrial membranes. Additionally, excess Fe^{2+} directly catalyzes lipid peroxidation, leading to the production of more lipid peroxides. This destructive feedback loop culminates in ferroptosis and liver damage.

4.6. Replacement of FM by Excess CP Caused Ferroptosis Through SIRT1-AP-TRFC Signaling Pathway

Liver damage in *M. salmoides* due to excessive FM replacement with CP was closely associated with ferroptosis, as evidenced by hepatic iron overload, mitochondrial morpho-

logical alterations, and lipid peroxide accumulation. To investigate potential regulatory signaling pathways, this study considered the involvement of the SIRT1-YAP-TRFC pathway. Previous studies have shown that CP hydrolysates replacing FM can impact hepatic *Sirt1* mRNA expression, affecting the amino acid metabolism of pomfrets. Sirt1 is a prominent member of histone deacetylases, widely involved in oxidative stress, inflammation, cell metabolism, Alzheimer's disease, and cardiovascular diseases [17,51,52]. For instance, SIRT1-mediated deacetylation of transcription factor C/EBP-β inhibits YAP, reducing hypertrophic scarring [53]. Overexpression of Sirt1 can also inhibit the Hippo/YAP signal and reduce periarterial sclerosis [19]. Recent studies have suggested that SIRT1 may regulate downstream transcriptional coactivators, participating in ferroptosis-induced liver injury. Ubiquitin-specific peptidase 22 (USP22) stabilizes SIRT1 protein, reduces P53 acetylation, and upregulates SLC7A11, ultimately inhibiting ferroptosis and myocardial cell damage caused by ischemia-reperfusion [54]. Furthermore, the Merlin–Hippo pathway has been implicated in ferroptosis regulation [55]. Activated YAP promotes ferroptosis in epithelial cancer cells by upregulating ferroptosis-regulatory genes such as ACSL4 and TRFC [21]. O-GlcNAc glycosylation modifies the YAP/TFRC pathway, increasing susceptibility to ferroptosis induced by GSH peroxidase 4 inhibitors (RSL4) [56]. Based on this, we hypothesize that excessive substitution of CP for FM contributes to liver injury associated with ferroptosis by influencing the SIRT1-YAP-TRFC pathway. Our results demonstrated that as the proportion of CP replacing FM increased, Sirt1 and Yap mRNA levels decreased, while Trfc mRNA levels rose. Phosphorylated YAP (p-YAP) protein levels were significantly higher in the CP60 group compared to other groups. SIRT1 protein levels followed a similar pattern to their mRNA levels, reaching their lowest levels in the CP48 and CP60 groups. Additionally, p-YAP protein levels decreased progressively with increasing CP replacement rates, indicating substantial translocation of YAP into the nucleus. YAP protein expression levels in both the nucleus and TRFC increased with higher CP replacement rates, with the CP48 and CP60 groups exhibiting the highest expression of these proteins. This study also observed that SIRT1 deacetylation promotes the nuclear accumulation of YAP, which directly regulates the TRFC promoter. This regulation enhances TRFC protein expression, leading to iron imbalance and contributing to ferroptosis in the liver. Although further research is needed, we hypothesize that the accumulation of gossypol—resulting from CP substitution for FM—may influence SIRT1 expression, thereby contributing to the occurrence of liver ferroptosis. Notably, this study is the first to report on the specific mechanism by which CP substitution regulates SIRT1 expression.

5. Conclusions

In a word, our findings showed that high-level CP replacing FM may suppress growth performance. Meanwhile, high-level CP significantly upregulated the relative expression of pro-inflammatory factors (IL-1β and TNF-α), while suppressing anti-inflammatory mediators (IL-10 and TGF-β2). Higher levels of CP substitution may induce liver ferroptosis by activating the SIRT1-YAP-TRFC pathway, leading to liver damage in *M. salmoides*. Without compromising the growth performance of juvenile *M salmoides*, broken-line regression analysis using SGR as the indicator determined that the optimal replacement level of FM with CP in the diet was 23%.

Supplementary Materials: The following supporting information can be downloaded at: https://www.mdpi.com/article/10.3390/biology14070748/s1, Figure S1: The original Western blot images.

Author Contributions: Q.C. and J.Z.: Writing—original draft, Supervision, Resources, Data curation, Writing—review & editing. X.Z.: Project administration, Writing—original draft. L.R.: Writing—review and editing. H.L.: Supervision, Resources, Funding acquisition. J.J.: Supervision, Resources,

Data curation, Writing—review and editing, Funding acquisition. All authors have read and agreed to the published version of the manuscript.

Funding: This study was financially supported by National Natural Science Foundation of China (31702362), National Key R&D Program of China (32172987 and 2019YFD0900200), and Natural Science Foundation of Sichuan Province (2022NSFSC0057).

Institutional Review Board Statement: All experimental procedures used were conducted with the approval of the Animal Care Advisory Committee of Sichuan Agricultural University, license number DKY-2018202027.

Informed Consent Statement: Not applicable.

Data Availability Statement: The datasets used and analyzed during the current study are available from the corresponding author on reasonable request.

Conflicts of Interest: The authors declare that they have no competing interests.

List of Abbreviations

FM: Fish meal; CP: Cottonseed Protein; IBW: Initial Body Weight; FBW: Final Body Weight; PWG: Percent Weight Gain; SGR: Specific Growth Rate; SR: Survival Rate; FI: Feed Intake; FE: Feed Efficiency; PPV: Protein Production Value; LPV: Lipid Production Value; APV: Ash Production Value; HSI: Hepatosomatic Index; ISI: Intestosomatic Index; RGL: Relative Gut Length; VSI: Viscerosomatic index; AST: Aspartate aminotransferase; ALT: Alanine aminotransferase; AKP: Alkalinephosphatase; HYP: L-Hydroxyproline; ROS: Reactive Oxygen Species; MDA: Malondialdehyde; MMP: mitochondrial membrane potentials; GST: Glutathione-S-Transferase; GSH: Glutathione; Acsl4: acyl-CoA Synthetase long chain family member 4; Gpx4: glutathione peroxidase 4; Lpcat3: lysophosphatidylcholine acyltransferase 3; Ptgs2: prostaglandin endoperoxide synthase 2; Sirt1: sirtuin 1; Trf: transferrin; Trfc: transferrin receptor; Yap: yes associated protein.

References

1. Liu, H.; Dong, X.; Tan, B.; Du, T.; Zhang, S.; Yang, Y.; Chi, S.; Yang, Q.; Liu, H. Effects of fish meal replacement by low-gossypol cottonseed meal on growth performance, digestive enzyme activity, intestine histology and inflammatory gene expression of silver sillago (*Sillago sihama* Forsskal). *Aquacult Nutr.* **2020**, *26*, 1724–1735. [CrossRef]
2. Tacon, A.G.J.; Metian, M. Global overview on the use of fish meal and fish oil in industrially compounded aquafeeds: Trends and future prospects. *Aquaculture* **2008**, *285*, 146–158. [CrossRef]
3. Iii, D.M.G.; Barrows, F.T.; Brown, P.; Dabrowski, K.; Wurtele, E. Expanding the utilization of sustainable plant products in aquafeeds: A review. *Aquac. Res.* **2007**, *38*, 551–579.
4. Cheng, H.N.; He, Z.; Ford, C.; Wyckoff, W.; Wu, Q. A review of cottonseed protein chemistry and non-food applications. *Sustain. Chem.* **2020**, *1*, 256–274. [CrossRef]
5. Khan, M.A.; Wahid, A.; Ahmad, M.; Tahir, M.T.; Ahmed, M.; Ahmad, S.; Hasanuzzaman, M. World cotton production and consumption: An overview. In *Cotton Production and Uses*; Springer: Singapore, 2020.
6. Luo, L.; Xue, M.; Wu, X.; Cai, X.; Cao, H.; Liang, Y. Partial or total replacement of fishmeal by solvent-extracted cottonseed meal in diets for juvenile rainbow trout (*Oncorhynchus mykiss*). *Aquacult Nutr.* **2006**, *12*, 418–424. [CrossRef]
7. Zhao, W.; Liu, Z.; Niu, J. Growth performance, intestinal histomorphology, body composition, hematological and antioxidant parameters of Oncorhynchus mykiss were not detrimentally affected by replacement of fish meal with concentrated dephenolization cottonseed protein. *Aquac. Rep.* **2021**, *19*, 100557. [CrossRef]
8. Chen, S.; Tang, Y.; Zhang, Z.; Zheng, J.; He, Y.; Wang, Z.; Mai, K.; Ai, Q. Replacement of dietary fishmeal protein with degossypolized cottonseed protein on growth performance, nonspecific immune response, antioxidant capacity, and target of rapamycin pathway of juvenile large yellow croaker (*Larimichthys crocea*). *Aquacult Nutr.* **2022**, *2022*, 12. [CrossRef]
9. Alama, M.S.; Watanabea, W.O.; Carrolla, P.; Gabela, J.; Coruma, M.; Seatona, P.; Wedegaertnerb, T.C.; Rathorec, K.S.; Dowdd, M.K. Evaluation of genetically-improved (glandless) and genetically-modi fi ed low-gossypol cottonseed meal as alternative protein sources in the diet of juvenile southern fl ounder *Paralichthys lethostigma* reared in a recirculating aquaculture system. *Aquaculture* **2018**, *489*, 36–45. [CrossRef]

10. He, Y.; Guo, X.; Tan, B.; Dong, X.; Yang, Q.; Liu, H.; Zhang, S.; Chi, S. Replacing fishmeal with cottonseed protein concentrate in feed for pearl gentian groupers (*Epinephelus fuscoguttatus*♀× *E. lanceolatus*♂): Effects on growth and expressions of key genes involved in appetite and hepatic glucose and lipid metabolism. *Aquac. Rep.* **2021**, *20*, 100710. [CrossRef]
11. Jiang, S.; Chen, Z.; Zhou, F.; Yang, Q.; Jiang, S. Study on partial replacement of fish meal with concentrated dephenolized cottonseed protein in feed of *Penaeus monodon*. *Aquac. Res.* **2021**, *52*, 3871–3881. [CrossRef]
12. Rezaei, S.; Mohammadiazarm, H.; Keyvanshokooh, S.; Pasha-Zanoosi, H.; Sharif-Kanani, H. Nutritional nano-selenium inclusion in fishmeal-free plant-based diets enhances stress resistance and post-stress recovery of common carp (*Cyprinus carpio*). *Aquac. Rep.* **2024**, *38*, 102298. [CrossRef]
13. Sharif-Kanani, H.; Keyvanshokooh, S.; Mohammadiazarm, H.; Pasha-Zanoosi, H.; Rezaei, S. Nano-selenium (nano-Se) removes the detrimental impacts of plant-based diets on the production performance and well-being of common carp (*Cyprinus carpio*). *Aquac. Rep.* **2024**, *36*, 102107. [CrossRef]
14. He, G.; Zhang, T.; Zhou, X.; Liu, X.; Sun, H.; Chen, Y.; Tan, B.; Lin, S. Effects of cottonseed protein concentrate on growth performance, hepatic function and intestinal health in juvenile largemouth bass, *Micropterus salmoides*. *Aquac. Rep.* **2022**, *23*, 101052. [CrossRef]
15. Crielaard, B.J.; Lammers, T.; Rivella, S. Targeting iron metabolism in drug discovery and delivery. *Nat. Rev. Drug Discov.* **2017**, *16*, 400–423.
16. Wang, R.; Lv, Y.; Ni, Z.Y.; Feng, W.; Fan, P.; Wang, Y.; Lin, Y.; Chen, X. Intermittent hypoxia exacerbates metabolic dysfunction-associated fatty liver disease by aggravating hepatic copper deficiency-induced ferroptosis. *FASEB J.* **2024**, *38*, e23788. [CrossRef]
17. Chen, X.; Comish, P.B.; Tang, D.; Kang, R. Characteristics and biomarkers of ferroptosis. *Front. Cell Dev. Biol.* **2021**, *9*, 637162. [CrossRef] [PubMed]
18. He, X.; Wu, C.; Cui, Y.; Zhu, H.; Zhao, B. The aldehyde group of gossypol induces mitochondrial apoptosis via ROS-SIRT1-p53-PUMA pathway in male germline stem cell. *Oncotarget* **2017**, *8*, 100128–100140. [CrossRef]
19. Yuan, P.; Hu, Q.; He, X.; Long, Y.; Zhou, X. Laminar flow inhibits the Hippo/YAP pathway via autophagy and SIRT1-mediated deacetylation against atherosclerosis. *Cell Death Dis.* **2020**, *11*, 141. [CrossRef]
20. Wu, Q.J.; Zhang, T.N.; Chen, H.H.; Yu, X.F.; Lv, J.L.; Liu, Y.Y.; Liu, Y.S.; Zheng, G.; Zhao, J.Q.; Wei, Y.F. The sirtuin family in health and disease. *Signal Transduct. Target. Ther.* **2023**, *8*, 146–219.
21. Wu, J.; Minikes, A.M.; Gao, M.; Bian, H.; Jiang, X. Publisher Correction: Intercellular interaction dictates cancer cell ferroptosis via NF2–YAP signalling. *Nature* **2019**, *572*, E20. [CrossRef]
22. Dias, C.T.D.S.; Cyrino, J.E.P.; Dairiki, J.K. Lysine requirements of largemouth bass, *Micropterus salmoides*: A comparison of methods of analysis of dose-response trials data. *J. Appl. Aquac.* **2007**, *19*, 1–27.
23. Zhao, Y.; Yang, C.; Zhu, X.; Feng, L.; Liu, Y.; Jiang, W.; Wu, P.; Huang, X.; Chen, D.; Yang, S.; et al. Dietary methionine hydroxy analogue supplementation benefits on growth, intestinal antioxidant status and microbiota in juvenile largemouth bass *Micropterus salmoides*. *Aquaculture* **2022**, *556*, 738279. [CrossRef]
24. AOAC. *Official Methods of Analysis of AOAC International*, 18th ed.; AOAC International: Arlington, VA, USA, 2005.
25. Yao, X.-H.; Sun, H.; Lou, B.; Wang, X.; Wu, Y.-F. Partial substitution of fish meal with fermented cottonseed meal in juvenile black sea bream (*Acanthopagrus schlegelii*) diets. *Aquaculture* **2015**, *446*, 30–36.
26. Wilson, R.P.; Robinson, E.H.; Poe, W.E. Apparent and true availability of amino acids from common feed ingredients for channel catfish. *J. Nutr.* **1981**, *111*, 923. [CrossRef] [PubMed]
27. Fombad, R.B.; Bryant, M.J. Effects of cottonseed cake-based diets supplemented with blood meal, alone or with lysine, on the growth of pigs. *Trop. Anim. Health Prod.* **2004**, *36*, 385–395. [CrossRef]
28. Jiang, H.B.; Chen, L.Q.; Qin, J.G.; Gao, L.J.; Jiang, X.Q. Partial or complete substitution of fish meal with soybean meal and cottonseed meal in Chinese mitten *crab Eriocheir* sinensis diets. *Aquacult Int.* **2013**, *21*, 617–628. [CrossRef]
29. Dossou, S.; Koshio, S.; Ishikawa, M.; Yokoyama, S.; Dawood, M.A.; El Basuini, M.F.; El-Hais, A.M.; Olivier, A. Effect of partial replacement of fish meal by fermented rapeseed meal on growth, immune response and oxidative condition of red sea bream juvenile, *Pagrus major*. *Aquaculture* **2018**, *490*, 228–235. [CrossRef]
30. Anderson, A.D.; Alam, M.S.; Watanabe, W.O.; Carroll, P.M.; Wedegaertner, T.C.; Dowd, M.K. Full replacement of menhaden fish meal protein by low-gossypol cottonseed flour protein in the diet of juvenile black sea bass *Centropristis striata*. *Aquaculture* **2016**, *464*, 618–628. [CrossRef]
31. Boshra, H.; Li, J.; Sunyer, J.O. Recent advances on the complement system of teleost fish. *Fish. Shellfish. Immun.* **2006**, *20*, 239–262. [CrossRef]
32. Chatzifotis, S.; Panagiotidou, M.; Papaioannou, N.; Pavlidis, M.; Nengas, I.; Mylonas, C.C. Effect of dietary lipid levels on growth, feed utilization, body composition and serum metabolites of meagre (*Argyrosomus regius*) juveniles. *Aquaculture* **2010**, *307*, 65–70. [CrossRef]

33. Zhang, J.; Zhao, N.; Sharawy, Z.; Li, Y.; Ma, J.; Lou, Y. Effects of dietary lipid and protein levels on growth and physiological metabolism of *Pelteobagrus fulvidraco* larvae under recirculating aquaculture system (RAS). *Aquaculture* **2018**, *495*, 458–464. [CrossRef]
34. Arnold, P.K.; Finley, L.W.S. Regulation and function of the mammalian tricarboxylic acid cycle. *J. Biol. Chem.* **2023**, *299*, 102838. [CrossRef] [PubMed]
35. Nyblom, H. High AST/ALT ratio may indicate advanced alcoholic liver disease rather than heavy drinking. *Alcohol. Alcohol.* **2004**, *39*, 336–339. [CrossRef] [PubMed]
36. Nyblom, H.; Björnsson, E.; Simrén, M.; Aldenborg, F.; Almer, S.; Olsson, R. The AST/ALT ratio as an indicator of cirrhosis in patients with PBC. *Liver Int.* **2010**, *26*, 840–845. [CrossRef]
37. Wang, X.F.; Li, X.Q.; Leng, X.J.; Shan, L.L.; Zhao, J.X.; Wang, Y.T. Effects of dietary cottonseed meal level on the growth, hematological indices, liver and gonad histology of juvenile common carp (*Cyprinus carpio*). *Aquaculture* **2014**, *428–429*, 79–87. [CrossRef]
38. Yang, M.; Jiang, D.; Lai, W.; Chen, K.; Xu, S.; Yu, R.; Li, L.; Zhang, L.; Lu, L.; Xu, Y.; et al. Condensed tannin improves growth and alleviates intestinal inflammation of juvenile largemouth bass (*Micropterus salmoides*) fed with high cottonseed protein concentrate diet. *Int. J. Biol. Macromol.* **2024**, *280*, 135874. [CrossRef] [PubMed]
39. Balta, C.; Herman, H.; Boldura, O.M.; Gasca, I.; Rosu, M.; Ardelean, A.; Hermenean, A. Chrysin attenuates liver fibrosis and hepatic stellate cell activation through TGF-β/Smad signaling pathway. *Chem-Biol. Interact.* **2015**, *240*, 94–101. [CrossRef]
40. Bolarin, D.M.; Azinge, E.C. Biochemical markers, extracellular components in liver fibrosis and cirrhosis. *Niger. Q. J. Hosp. Med.* **2007**, *17*, 42–52. [CrossRef]
41. Pihlajaniemi, T.; Myllylä, R.; Kivirikko, K.I. Prolyl 4-hydroxylase and its role in collagen synthesis. *J. Hepatol.* **1991**, *13*, S2–S7. [CrossRef]
42. Mu, Y.; Sun, J.; Li, Z.; Zhang, W.; Liu, Z.; Li, C.; Peng, C.; Cui, G.; Shao, H.; Du, Z. Activation of pyroptosis and ferroptosis is involved in the hepatotoxicity induced by polystyrene microplastics in mice. *Chemosphere* **2022**, *291*, 132944. [CrossRef] [PubMed]
43. Niu, B.; Lei, X.; Xu, Q.; Ju, Y.; Xu, D.; Mao, L.; Li, J.; Zheng, Y.; Sun, N.; Zhang, X.; et al. Protecting mitochondria via inhibiting VDAC1 oligomerization alleviates ferroptosis in acetaminophen-induced acute liver injury. *Cell Biol. Toxicol.* **2022**, *38*, 505–530. [CrossRef] [PubMed]
44. Wang, Y.; Chen, Q.; Shi, C.; Jiao, F.; Gong, Z. Mechanism of glycyrrhizin on ferroptosis during acute liver failure by inhibiting oxidative stress. *Mol. Med. Rep.* **2019**, *20*, 4081–4090. [CrossRef]
45. Chen, S.; Che, S.; Li, S.; Wan, J.; Ruan, Z. High-fat diet exacerbated decabromodiphenyl ether-induced hepatocyte apoptosis via intensifying the transfer of $Ca^{2+}$from endoplasmic reticulum to mitochondria. *Environ. Pollut.* **2022**, *292*, 118297. [CrossRef] [PubMed]
46. Stulczewski, D.; Zgorzynska, E.; Dziedzic, B.; Wieczorek-Szukala, K.; Szafraniec, K.; Walczewska, A. EPA stronger than DHA increases the mitochondrial membrane potential and cardiolipin levels but does not change the ATP level in astrocytes. *Exp. Cell Res.* **2023**, *424*, 113491. [CrossRef] [PubMed]
47. Dixon, S.J.; Lemberg, K.M.; Lamprecht, M.R.; Skouta, R.; Zaitsev, E.M.; Gleason, C.E.; Patel, D.N.; Bauer, A.J.; Cantley, A.M.; Yang, W.S. Ferroptosis: An iron-dependent form of nonapoptotic cell death. *Cell* **2012**, *149*, 1060–1072. [CrossRef]
48. Wei, H.C.; Chen, P.; Liang, X.F.; Yu, H.H.; Wu, X.F.; Han, J.; Luo, L.; Gu, X.; Xue, M. Plant protein diet suppressed immune function by inhibiting spiral valve intestinal mucosal barrier integrity, anti-oxidation, apoptosis, autophagy and proliferation responses in amur sturgeon (*Acipenser schrenckii*). *Fish Shellfish. Immun.* **2019**, *94*, 711–722. [CrossRef] [PubMed]
49. Liu, H.; Zhou, M.; Dong, X.; Tan, B.; Du, T.; Zhang, S.; Yang, Y.; Chi, S.; Yang, Q.; Liu, H. Liver immune parameters, complement pathway, inflammatory factor and TOR genes expression of silver sillago, *Sillago sihama*, fed with diets replacing fish meal with low-gossypol cottonseed meal. *Aquacult Nutr.* **2021**, *27*, 1934–1945. [CrossRef]
50. Tang, D.; Chen, X.; Kang, R.; Kroemer, G. Ferroptosis: Molecular mechanisms and health implications. *Cell Res.* **2020**, *31*, 107–125. [CrossRef]
51. Kilic, U.; Gok, O.; Bacaksiz, A.; Izmirli, M.; Elibol-Can, B.; Uysal, O. SIRT1 gene polymorphisms affect the protein expression in cardiovascular diseases. *PLoS ONE* **2014**, *9*, e90428. [CrossRef] [PubMed]
52. Ren, Z.; He, H.; Zuo, Z.; Xu, Z.; Deng, J. The role of different SIRT1-mediated signaling pathways in toxic injury. *Cell Mol. Biol. Lett.* **2019**, *24*, 36. [CrossRef]
53. Zhang, J.; Li, Y.; Liu, J.; Han, F.; Shi, J.; Wu, G.; Wang, K.; Shen, K.; Zhao, M.; Gao, X.; et al. Adiponectin ameliorates hypertrophic scar by inhibiting Yes-associated protein transcription through SIRT1-mediated deacetylation of C/EBPβ and histone H3. *iScience* **2022**, *25*, 105236. [CrossRef]
54. Ma, S.; Sun, L.; Wu, W.; Wu, J.; Sun, Z.; Ren, J. USP22 protects against myocardial ischemia-reperfusion injury via the SIRT1-p53/SLC7A11-dependent inhibition of ferroptosis-induced cardiomyocyte death. *Front. Physiol.* **2020**, *11*, 551318. [CrossRef] [PubMed]

55. Zhou, X.; Fu, Y.; Liu, W.; Mu, Y.; Zhang, H.; Chen, J.; Liu, P. Ferroptosis in chronic liver diseases: Opportunities and challenges. *Front. Mol. Biosci.* **2022**, *9*, 928321. [CrossRef] [PubMed]
56. Zhu, G.; Murshed, A.; Li, H.; Ma, J.; Pan, Q. O-GlcNAcylation enhances sensitivity to RSL3-induced ferroptosis via the YAP/TFRC pathway in liver cancer. *Cell Death Discov.* **2021**, *7*, 83. [CrossRef] [PubMed]

Disclaimer/Publisher's Note: The statements, opinions and data contained in all publications are solely those of the individual author(s) and contributor(s) and not of MDPI and/or the editor(s). MDPI and/or the editor(s) disclaim responsibility for any injury to people or property resulting from any ideas, methods, instructions or products referred to in the content.

biology

MDPI

Article

Effects of Hypoxia and Reoxygenation on Hypoxia-Responsive Genes, Physiological and Biochemical Indices in Hybrid Catfish (*Pelteobagrus vachelli* ♀× *Leiocassis longirostris* ♂)

Jie Yan [1,†], Faling Zhang [1,†], Fenfei Liang [2], Cheng Zhao [1,3], Shaowu Yin [1,3,*] and Guosong Zhang [2,*]

[1] College of Marine Science and Engineering, Nanjing Normal University, Nanjing 210098, China; yanjie2547@163.com (J.Y.); 18383465626@163.com (F.Z.); zhaochengfish@foxmail.com (C.Z.)
[2] School of Agriculture and Bioengineering, Heze University, Heze 274015, China; fenfeiliang@163.com
[3] Co-Innovation Center for Marine Bio-Industry Technology, Lian Yungang 222005, China
* Correspondence: yinshaowu@163.com (S.Y.); zhangguosong@hezeu.edu.cn (G.Z.)
† These authors contributed equally to this work and should be considered co-first authors.

Simple Summary: This study explored how hybrid catfish respond to low oxygen levels (hypoxia) and subsequent recovery (reoxygenation), a common challenge in aquatic environments due to factors like pollution and climate change. We examined changes in genes and physiological processes in the brain, liver, and muscle tissues of the fish under controlled hypoxia and reoxygenation conditions. We found that low oxygen triggered adaptive responses, such as switching energy production from aerobic to anaerobic pathways in the liver, while the brain reduced anaerobic activity to avoid harmful lactate buildup. Muscle tissue showed the most severe effects, including oxidative stress, mitochondrial damage, and increased cell death. After oxygen levels were restored, the fish recovered, but signs of stress lingered in some tissues. These findings help explain how hybrid catfish tolerate fluctuating oxygen levels, which is crucial for improving aquaculture practices and ensuring fish health in changing environments. The study provides insights that could aid in breeding more resilient fish species, supporting sustainable fisheries and food security.

Abstract: Hypoxia represents a critical environmental stressor in aquaculture, significantly disrupting aquatic organisms' physiological homeostasis and thereby constraining the sustainable development of aquaculture industries. To elucidate the mechanisms underlying hypoxia-induced metabolic regulation in aquatic species, this study employed hybrid yellow catfish (*Pelteobagrus vachelli* ♀× *Leiocassis longirostris* ♂) as a model organism to systematically investigate the multidimensional physiological responses in brain, liver, and muscle tissues under hypoxia (0.7 mg/L) and reoxygenation (7.0 mg/L) conditions. Through qRT-PCR and enzymatic activity analyses, we comprehensively assessed molecular alterations associated with oxygen sensing (HIF-1α gene), respiratory metabolism (PFKL, HK1, PK, CS, and LDHA genes and corresponding enzyme activities), oxidative stress (SOD1, SOD2, GSH-PX, and CAT genes, along with LPO, MDA, PCO, T-SOD, GSH-PX, and CAT levels), apoptosis (Caspase-3, Bax/Bcl-2), inflammatory response (IL-1β, IKKβ), and mitochondrial function (COXIV, PGC-1α, ATP5A1). Key findings demonstrated pronounced HIF-1α activation across all examined tissues. Hepatic tissues exhibited adaptive metabolic reprogramming from aerobic to anaerobic metabolism, whereas cerebral tissues displayed suppressed anaerobic glycolysis during prolonged hypoxia, and muscular tissues manifested concurrent inhibition of both glycolytic and aerobic metabolic pathways. Notably, skeletal muscle exhibited marked oxidative stress accompanied by mitochondrial dysfunction, exacerbated inflammation, and apoptosis activation during hypoxia/reoxygenation cycles. This study delineates tissue-specific adaptive mechanisms

to hypoxia in yellow catfish, providing theoretical foundations for both piscine hypoxia physiology research and aquaculture practices.

Keywords: hybrid catfish; hypoxic stress; reoxygenation; metabolic reprogramming; oxidative stress; mitochondrial function; apoptosis

1. Introduction

Dissolved oxygen (DO) content in aquatic ecosystems is a critical factor for the survival, growth, and development of aquatic organisms [1,2]. However, DO concentration in aquatic ecosystems exhibits greater spatial and temporal variability compared to terrestrial environments due to factors such as global warming, eutrophication, pollution, photosynthesis, temperature, salinity, and seasonal variations [3]. Fish, as aquatic organisms, are highly susceptible to low-oxygen stress, and severe hypoxia can lead to large-scale mortality, resulting in a decline in fishery production. Therefore, hypoxia in aquatic ecosystems has become a significant concern in aquaculture and fishery science research.

Hypoxic conditions can significantly impact various physiological processes in fish, including behavior, growth, development, metabolism, and immune responses, potentially leading to mortality. To cope with dynamic fluctuations in dissolved oxygen (DO) concentrations, fish have evolved sophisticated adaptive mechanisms through long-term evolutionary processes [4,5]. For instance, fish can enhance hypoxia tolerance by regulating the transcription of relevant genes through the hypoxia-inducible factor (HIF) signaling pathway [6]. As a core component of oxygen-sensing proteins, HIF-1α is activated under hypoxic conditions and subsequently modulates the expression of downstream target genes, such as glycolysis-related genes (phosphofructokinase, liver type (*PFKL*), hexokinase 1 (*HK1*), pyruvate kinase (*PK*), lactate dehydrogenase A (*LDHA*)) and the tricarboxylic acid (TCA) cycle key enzyme gene (citrate synthase (CS)), thereby adjusting energy metabolism patterns [7,8]. Studies have demonstrated significant upregulation of HIF-1αA gene expression in the white muscle tissue of *Gymnocypris eckloni* under hypoxic conditions [9]. Similarly, *Hexagrammos otakii* exhibited markedly elevated serum HIF-1α levels following hypoxic stress [10]. Furthermore, fish can shift their respiratory metabolic mode from aerobic to anaerobic respiration to sustain energy supply under oxygen deprivation. For example, *Oncorhynchus mykiss* [11] and *Megalobrama amblycephala* [12] displayed reduced aerobic respiration rates, increased lactate concentrations, and decreased adenosine triphosphate (ATP) production rates under hypoxic conditions. Concurrently, fish enhance their antioxidant capacity to mitigate oxidative damage. Key enzymes in the antioxidant defense system, including superoxide dismutase (SOD), catalase (CAT), and glutathione peroxidase (GSH-PX), scavenge reactive oxygen species (ROS) and minimize oxidative injury [13,14]. Notably, *Larimichthys crocea* [15] showed significantly elevated activities of SOD, CAT, and GSH-PX under hypoxia, with similar antioxidant enzyme activity enhancements observed in *G. przewalskii* [16] and *Micropterus salmoides* [17]. These findings collectively demonstrate that fish achieve adaptive regulation to variable oxygen environments by activating a series of complex biological processes, thereby maintaining homeostasis.

Nevertheless, research on the adaptive mechanisms of hybrid fish to hypoxic environments, particularly the molecular regulatory mechanisms, remains relatively scarce. Significant variations exist in the hypoxic adaptability among different fish species, which may be attributed to their genetic backgrounds and physiological characteristics. For instance, darkbarbel catfish (*Pelteobagrus vachelli*) and longsnout catfish (*Leiocassis longirostris*), two

species with distinct ecological adaptations, may produce hybrid offspring exhibiting enhanced hypoxia tolerance. *P. vachelli* belongs to the order Siluriformes, family Bagridae, and genus *Pelteobagrus*, while *L. longirostris* is classified under the same order and family but within the genus *Leiocassis*. The latter exhibits significantly faster growth rates and larger adult body sizes compared to the former. Interspecific hybridization breeding was conducted using 3-year-old *L. longirostris* as the paternal parent and *P. vachelli* as the maternal parent. The resulting hybrid offspring exhibited heterosis, demonstrating significantly faster growth rates compared to both parental species [18]. This study employs hybrid catfish as the experimental model to systematically investigate the effects of hypoxia stress and reoxygenation on oxygen-sensing proteins, respiratory metabolism, oxidative stress, apoptosis, inflammatory responses, and mitochondrial function in the brain, liver, and muscle tissues. The research aims to elucidate the dynamic changes in hypoxia-responsive genes and physiological–biochemical indicators, as well as to preliminarily clarify the molecular regulatory mechanisms underlying the responses of brain, liver, and muscle tissues to hypoxic stress.

2. Materials and Methods

2.1. Experimental Materials

The experimental 1-year-old hybrid yellow catfish (*Pelteobagrus vachelli* ♀× *Leiocassis longirostris* ♂) were obtained from the Lukou Base of Nanjing Institute of Fisheries Sciences in Jiangsu Province, China (Nanjing, China). The fish had an average body weight of 20 ± 1.1 g and an average body length of 12 ± 0.7 cm. A total of 150 healthy and vigorous individuals were randomly allocated into three recirculating aquaculture glass tanks (equipped with biofiltration systems; dimensions: 1.2 m × 0.85 m × 0.55 m), with 50 fish per tank. The fish were acclimatized for 3 days under controlled conditions: water temperature was maintained at 25 ± 1 °C, dissolved oxygen (DO) at 7.0 mg/L, and pH at 7.5. During acclimation, the fish were fed twice daily (08:00 and 17:00) with formulated feed (Tongwei Yellow Catfish Floating Feed, Chengdu, China). This study was approved by the Nanjing Normal University Animal Ethics Committee (approval no. SYXK [Jiangsu] 2015-0028).

2.2. Hypoxic Stress Treatment

Prior to the formal experiments, preliminary trials were conducted to establish the hypoxia tolerance thresholds of *P. vachelli*, *L. longirostris*, and their hybrid under controlled temperature conditions (25 ± 1 °C). During the procedure, the aeration and water circulation systems in the aquaculture tanks were temporarily suspended, while high-purity nitrogen (99.99%) was introduced via a precision gas flow controller (Aosong Electronics, Guangzhou, China, AS200; regulation accuracy: ±0.05 L/min). The initial nitrogen flow rate was set at 3.0 L/min to rapidly reduce dissolved oxygen (DO) levels below 1.0 mg/L. As DO approached the target concentration (±0.2 mg/L), the flow rate was reduced to 0.8 L/min to prevent abrupt hypoxia-induced stress in the fish. Real-time DO monitoring was performed using an LDO101 (HACH, Singapore, Singapore, HQ1130) probe, with automated data logging at 10 s intervals. A PID feedback control system dynamically adjusted the nitrogen–air mixture ratio to maintain DO fluctuations within ±0.03 mg/L. Threshold breaches triggered automatic compensatory measures: fine-tuning nitrogen flow (±0.1 L/min) or brief air infusion (0.5 L/min). Results demonstrated species-specific surfacing responses: *L. longirostris* surfaced at 0.64 mg/L, *P. vachelli* at 0.61 mg/L, and the hybrid at 0.60 mg/L. Each experiment was replicated three times to ensure data robustness.

Preliminary experiments determined the surfacing point of hybrid yellow catfish to be 0.60 mg/L DO. Accordingly, the hypoxic stress condition was set at 0.7 mg/L DO, en-

suring sustained and stable hypoxic exposure. Experimental groups included a normoxic control (C, 7.0 mg/L DO); hypoxic groups (H2, H4, H6 at 0.7 mg/L DO for 2, 4, and 6 h, respectively); and reoxygenation groups (R2, R4, R6 at 7.0 mg/L DO for 2, 4, and 6 h post-hypoxia). Each group contained three biological replicates (n = 5 fish per replicate). Prior to hypoxia induction, 15 fish (5 from each of 3 tanks at 7.0 mg/L DO) were sampled as controls. Brain, liver, and muscle tissues were collected, rinsed with ice-cold physiological saline (0.8%), and pooled as composite samples (5 fish/sample) in 1.5 mL cryotubes before flash-freezing in liquid nitrogen and storage at −80 °C. Following the termination of aeration and water circulation systems, pure nitrogen gas was immediately infused into the recirculating aquaculture glass tanks to rapidly reduce dissolved oxygen (DO) to 0.7 mg/L within 30 min. The hypoxic exposure period commenced upon reaching the target DO level, which was continuously monitored using an oxygen meter. Precise regulation of nitrogen and air infusion rates maintained the desired DO concentration throughout the experiment. Biological sampling was performed at three hypoxic timepoints (2 h, 4 h, and 6 h), with 15 specimens collected at each interval using identical procedures to the control group. After 6 h of hypoxic exposure, nitrogen infusion was discontinued and the system was restored through activation of water circulation with atmospheric aeration, maintaining DO at 7.0 mg/L during reoxygenation. Subsequent sampling was conducted at 2 h, 4 h, and 6 h reoxygenation intervals (15 specimens per timepoint), adhering to the standardized sampling protocol.

2.3. Temporal Gene Expression Analysis

All brain, liver, and muscle tissue samples were retrieved from −80°C storage and homogenized into powder using liquid nitrogen in pre-chilled mortars. Total RNA was extracted from brain, liver, and muscle tissues using the FastPure RNA Kit (Nanjing Vazyme, China RC101-01, Nanjing, China). Briefly, 10–20 mg of tissue was homogenized in 500 μL Buffer RL, followed by gDNA removal and RNA purification through column filtration. RNA quality was verified by spectrophotometry (OD260/280 ratio 1.8–2.0) and agarose gel electrophoresis. cDNA was synthesized with 1 μg total RNA using the Hifair® III cDNA Synthesis Kit (Hubei Yeasen, Wuhan, China), including gDNA digestion (42 °C, 2 min) and reverse transcription (25 °C for 5 min, 55 °C for 15 min, 85 °C for 5 min). Gene-specific primers (Table 1) were designed with Premier 5.0, and qRT-PCR was performed using SYBR Green Master Mix (Hubei Yeasen, China Yeasen) under standard cycling conditions (95 °C for 5 min; 40 cycles of 95 °C/10 s and 60 °C/30 s). Relative expression was calculated via the $2^{-\Delta\Delta Ct}$ method with β-actin as the reference.

2.4. Enzyme Activity Assay

A precise weight of 0.1 g of tissue was measured and homogenized mechanically in a 1:9 weight-to-volume ratio with 0.9% physiological saline under ice-bath conditions to prepare a 10% homogenate. The homogenate was centrifuged at 4 °C and 2500 r/min for 10 min, and the supernatant was collected for enzyme activity determination. The enzyme activity assay kits used in this experiment, including those for hexokinase (HK), citrate synthase (CS), lactate dehydrogenase (LDH), pyruvate kinase (PK), lipid peroxidase (LPO), malondialdehyde (MDA), protein carbonyl (PCO), total superoxide dismutase (T-SOD), glutathione peroxidase (GSH-PX), and catalase (CAT), were all sourced from Nanjing Jiancheng Bioengineering Institute (Nanjing, China). The specific detection methods followed the instructions provided with the kits (Table S1).

Table 1. Description of the primers used in this study.

Gene	Primer Sequence (5′-3′)	Product Size (bp)	Accession No. Or Publication	Amplification Efficiency
HIF-1α	Forward: CTGGAAAGAGGGCTAAGGTG Reverse: AGTGACGGTCCTGAATAGGG	151	XP_027023235.1	98.26
PFKL	Forward: TTGTGGATACCTGGCAACCA Reverse: AGTCGGTGCTGTATTGTGGA	188	XP_027018682.1	98.81
PK	Forward: GGCTAATGCTGTTCTGGATG Reverse: GGGTCGGTAGAGTAGGCTGT	166	XP_027029118.1	97.74
HK1	Forward: CGAGACTGTGGACGGAGACG Reverse: TTTGCCAGGGTTGAGGGAGA	141	XP_027030735.1	98.12
CS	Forward: GATGGGTGAAGTGGGGAAGA Reverse: GGTGTTGAGCAGGAAGTTGG	154	XP_027016864.1	98.63
LDHA	Forward: ATCTGGACTCTGCTCGGTTC Reverse: CATACAGGCACGCTTGAGTC	112	XP_027028964.1	98.73
SOD1	Forward: GTAATGTGACTGCCGGTTCC Reverse: TGAATCACCATGGTCCTCCC	106	AOQ25512.1	97.72
SOD2	Forward: CCAAAGGTGACGTGACAACA Reverse: AATCACGCTTAATGGCCTCC	153	AOQ25511.1	97.95
GSH-PX	Forward: GAATGGGAAAGACGCTCACC Reverse: GCACACAGGACTCCAGATGA	118	XP_026771571.1	98.25
CAT	Forward: TCCCACACCTTCAAGCTGAT Reverse: GGAGTTGTACAGGTCACGGA	156	XP_027019602.1	98.17
Bcl-2	Forward: CTTGTACCGACCCGACTTTG Reverse: GTCCCCAGTTGATCCCGTC	122	XM_027142465.2	97.88
Bax	Forward: TGGAGATGAACTGGACAGCA Reverse: TGCCCCAGTTAAACTTCCCA	128	XP_027009035.1	97.52
IL-1β	Forward: TTAGGCATAGAGGAGGTAAAAGAC Reverse: TTCACCGACTCGAAGGTGTT	123	XP_027008231.1	97.92
IKKβ	Forward: GCGAGAGATGGAGCAAACTG Reverse: TTCTCTCTCAGCTTGCGGAA	183	XM_047823116.1	98.59
Caspase 3	Forward: AGACCTGGACCCTGGTATTG GAGTAGTAACCTGGTGCTGTAGAA	138	XP_026990614.1	97.64
PGC-1α	Forward: TTGACCACCACAGGCATAGT Reverse: GTCCTCTCTTCTGGTGGCAT	112	XM_027150337.2	98.87
COXIV	Forward: ACTGAATCCGGAGCAGAAGT Reverse: AACAACATTCCAGCGACCAC	165	XM_027177342.2	98.45
ATP5A1	Forward: ACTGATACCGGTGCCATGAA Reverse: ATAAGTGCGTGTTTGCCGTT	137	XM_027133276.2	97.29
β-actin	Forward: CACTGCTGCCTCTTCCTC Reverse: ATCCACATCGCACTTCAT	181	XM_027148463.2	98.62

2.5. Data Processing

Statistical analysis of the data was performed using SPSS 27.0 software. One-way ANOVA and Dunnett *t*-tests were conducted to analyze significant differences between the control group and the hypoxia and reoxygenation groups. A *p*-value of less than 0.05 was considered statistically significant (denoted by *). Experimental data are presented as mean ± SD. Graphs were generated using GraphPad Prism 9 based on the analysis results.

3. Results

3.1. Effects of Hypoxia and Reoxygenation on Oxygen-Sensing Proteins and Respiratory Metabolism-Related Genes in Hybrid Catfish

Under acute hypoxia, the expression of the *HIF-1α* gene in brain tissue exhibited a significant upward trend, peaking at H6 ($p < 0.05$), with a 2.27-fold increase compared to the control group. This elevated expression remained significantly different from the control group at R2 ($p < 0.05$) before gradually returning to baseline levels. The *HK1* gene exhibited a fluctuating expression pattern, peaking at H2 ($p < 0.05$) with a 1.63-fold increase relative to the control group, followed by a decline. Upon reoxygenation, its expression rebounded and remained significantly elevated at R4 ($p < 0.05$) compared to the control. In contrast, the *PFKL*, *PK*, and *CS* genes showed no significant changes under hypoxic conditions ($p > 0.05$). However, the *PFKL* and *PK* genes were significantly upregulated at R2 and R4, respectively ($p < 0.05$), before returning to control levels. Conversely, the *LDHA* gene displayed a downward trend, with significant downregulation observed at H6 ($p < 0.05$), reaching 0.63 times the control level, and gradually returning to baseline levels after reoxygenation (Figure 1).

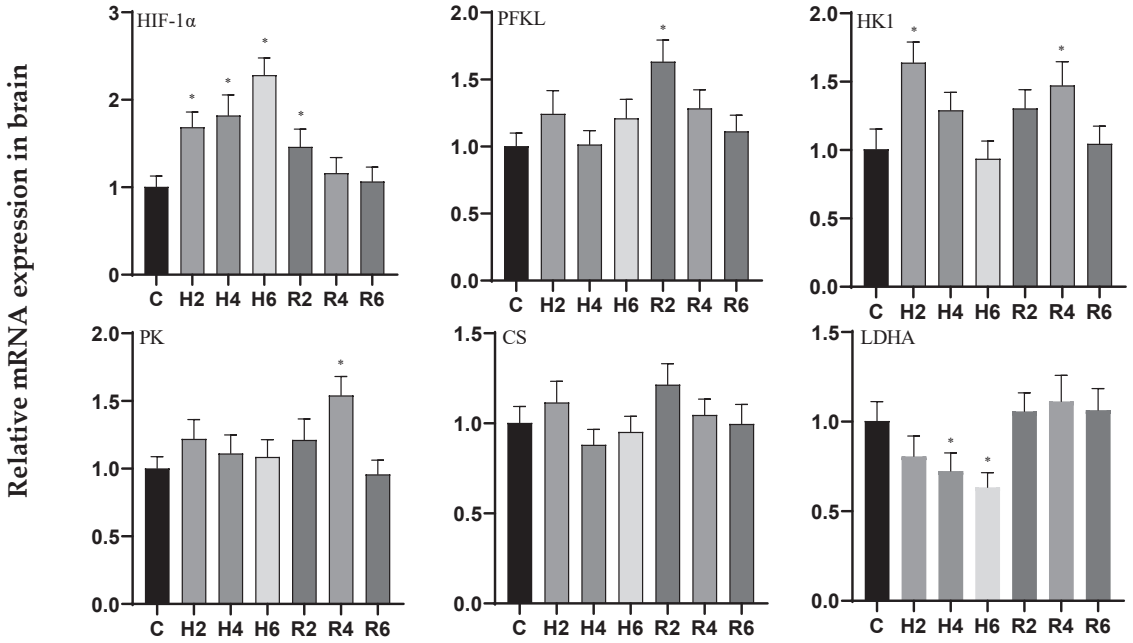


Figure 1. Effects of hypoxia (2 h, 4 h, and 6 h) and reoxygenation (2 h, 4 h, and 6 h) on brain oxygen-sensing protein and respiratory metabolism-related genes of hybrid catfish. Note: * at $p < 0.05$.

In liver tissue under acute hypoxia, the expression of the *HIF-1α* and *PFKL* genes initially increased, peaking at H4 and H2, respectively ($p < 0.05$), with 1.97- and 1.39-fold increases compared to the control group. These levels remained significantly elevated at R4 and R2, respectively ($p < 0.05$), following reoxygenation. The *HK1* and *PK* genes exhibited a fluctuating upward trend, while the *LDHA* gene showed a consistent upward trend, all reaching their peaks at H6 ($p < 0.05$), with 2.74-, 3.31-, and 3.03-fold increases relative to the control group, respectively. These levels remained significantly higher than the control group at R2 ($p < 0.05$) after reoxygenation. In contrast, the *CS* gene showed no significant changes under either hypoxic or reoxygenation conditions (Figure 2).

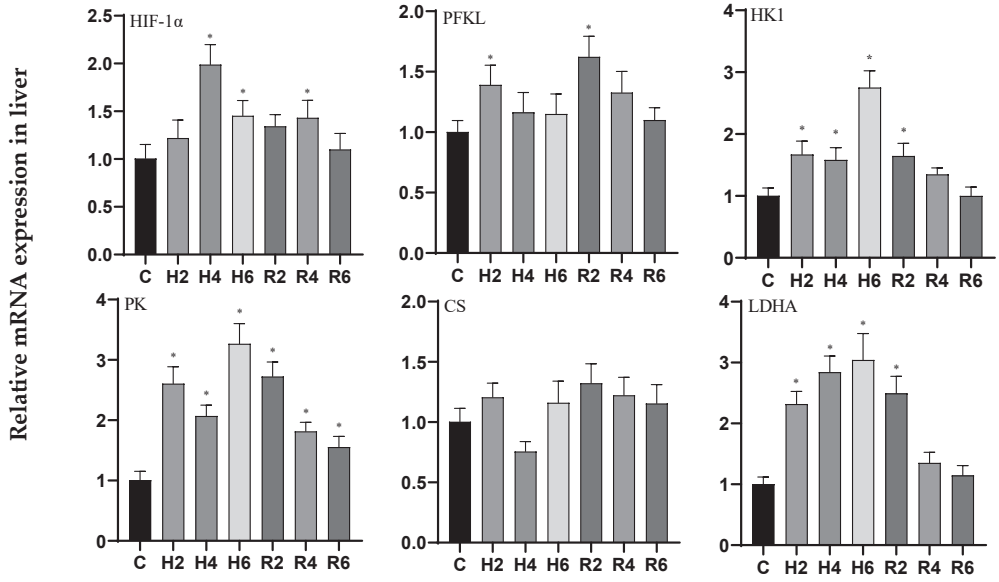


Figure 2. Effects of hypoxia (2 h, 4 h, 6 h) and reoxygenation (2 h, 4 h, 6 h) on liver oxygen-sensing protein and respiratory metabolism-related genes of hybrid catfish. Note: * at $p < 0.05$.

In muscle tissue under acute hypoxia, the expression of the *HIF-1α* and *HK1* genes initially increased, peaking at H4, and then decreased to a minimum at H6 ($p < 0.05$), with 2.58- and 0.50-fold changes relative to the control group, respectively. These levels remained significantly elevated at R2 and R4 ($p < 0.05$) following reoxygenation. The *PFKL* gene exhibited an initial increase followed by a decrease, showing no significant changes compared to the control group. However, it was significantly upregulated at R2 after reoxygenation before returning to baseline levels. Similarly, the *PK* gene initially increased and then decreased, showing no significant changes compared to the control group, but was significantly higher than the control group at R2 ($p < 0.05$) after reoxygenation before returning to baseline levels. In contrast, the *CS* and *LDHA* genes both displayed a downward trend, with significant downregulation observed at H6 ($p < 0.05$), reaching 0.57 and 0.72 times the control levels, respectively. After reoxygenation, the *CS* gene was significantly upregulated compared to the control group ($p < 0.05$), while the *LDHA* gene showed no significant changes (Figure 3).

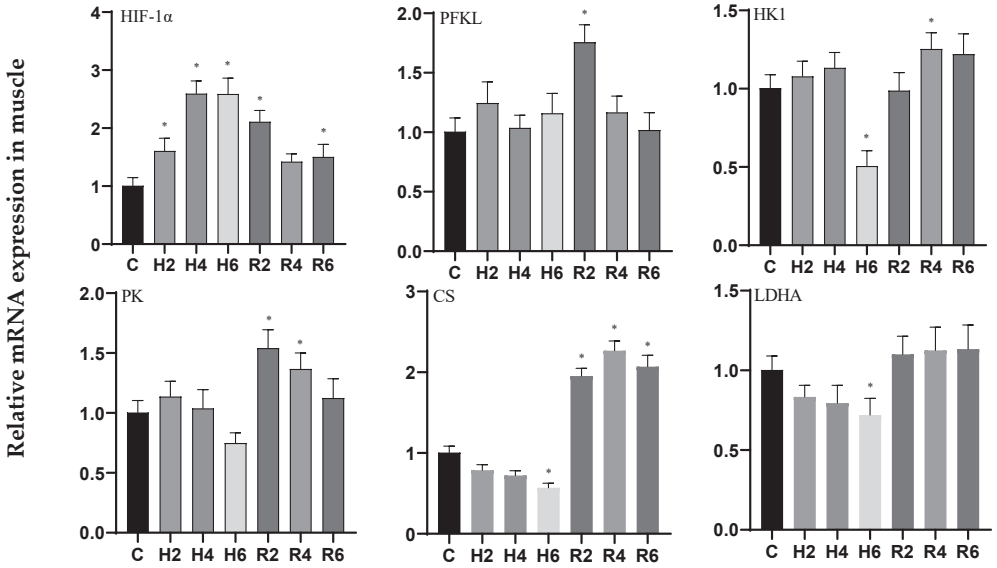


Figure 3. Effects of hypoxia (2 h, 4 h, 6 h) and reoxygenation (2 h, 4 h, 6 h) on muscle oxygen-sensing protein and respiratory metabolism-related genes of hybrid catfish. Note: * at $p < 0.05$.

3.2. Effects of Hypoxia and Reoxygenation on Respiratory Metabolism-Related Enzyme Activities in Hybrid Catfish

Under acute hypoxia, the activity of pyruvate kinase (PK) in brain tissue initially increased, peaking at H2 ($p < 0.05$), reaching 1.45 times the level of the control group, followed by a gradual decline and eventual return to baseline levels after reoxygenation. In contrast, the activities of hexokinase (HK) and lactate dehydrogenase (LDH) exhibited an initial decrease followed by an increase. Although HK activity did not significantly differ from the control group under hypoxic conditions, it peaked at R6 following reoxygenation, demonstrating a significant difference compared to the control group ($p < 0.05$). LDH activity reached its minimum at H6, decreasing to 0.56 times the control level, but no significant difference was observed compared to the control group after reoxygenation. Citrate synthase (CS) activity displayed a downward trend during hypoxia and an upward trend following reoxygenation, with no significant differences observed compared to the control group under either condition (Figure 4).

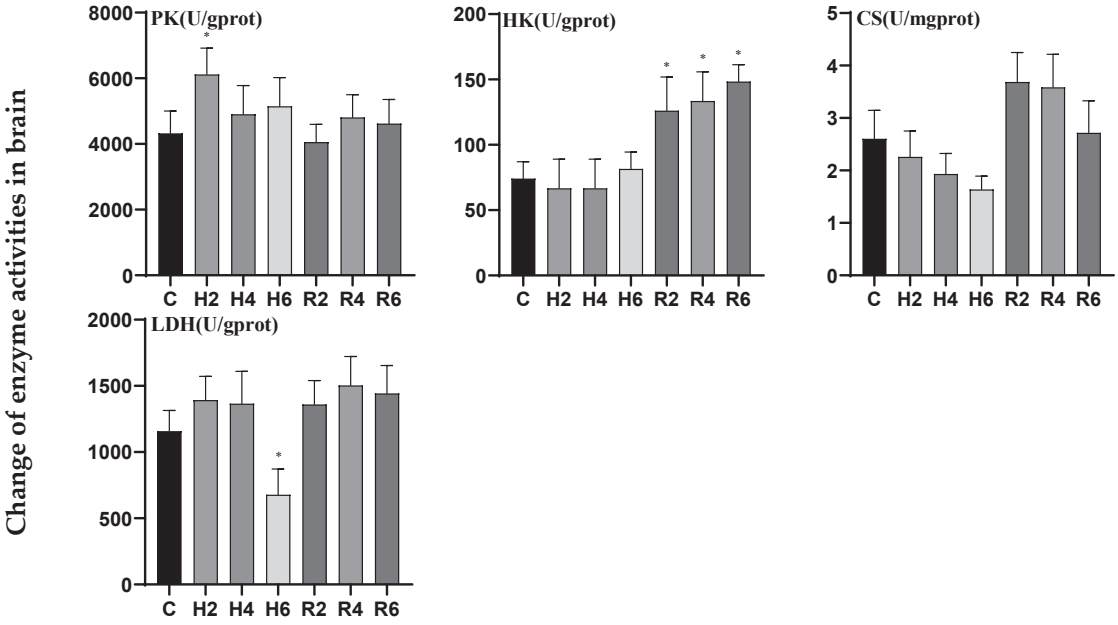


Figure 4. Effects of hypoxia (2 h, 4 h, 6 h) and reoxygenation (2 h, 4 h, 6 h) on brain respiratory metabolism-related enzyme activities of hybrid catfish. Note: * at $p < 0.05$.

In liver tissue under acute hypoxia, the activities of pyruvate kinase (PK) and lactate dehydrogenase (LDH) generally exhibited an upward trend, peaking at H6 ($p < 0.05$), reaching 4.16 and 1.53 times the levels of the control group (C), respectively. Following reoxygenation, PK activity peaked at R4, demonstrating a significant difference compared to the control group ($p < 0.05$), whereas LDH activity showed no significant difference. Hexokinase (HK) activity initially increased, significantly upregulated at H2 ($p < 0.05$), and peaked at H4, reaching 2.76 times the control level (C), before gradually returning to baseline levels after reoxygenation. The citrate synthase (CS) activity exhibited an initial decline followed by a subsequent increase, reaching its minimum value at H4 ($p < 0.05$), which was 0.71-fold of the control group (C). The activity gradually recovered to control levels following reoxygenation (Figure 5).

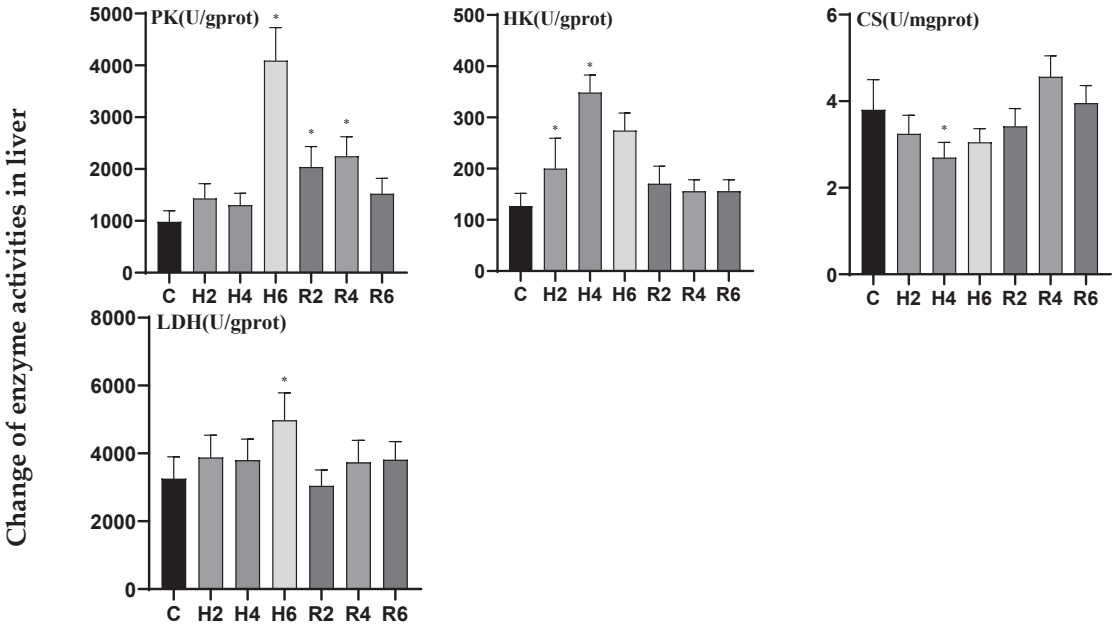


Figure 5. Effects of hypoxia (2 h, 4 h, 6 h) and reoxygenation (2 h, 4 h, 6 h) on liver respiratory metabolism-related enzyme activities of hybrid catfish. Note: * at $p < 0.05$.

In muscle tissue under acute hypoxia, hexokinase (HK) activity initially increased, reaching its minimum at H6 ($p < 0.05$), decreasing to 0.56 times the control level (C), and gradually returned to baseline levels after reoxygenation. Citrate synthase (CS) activity exhibited a downward trend, reaching its minimum at H6, decreasing to 0.60 times the control level (C), and subsequently peaked at R2 after reoxygenation, demonstrating a significant difference compared to the control group ($p < 0.05$). The activities of pyruvate kinase (PK) and lactate dehydrogenase (LDH) exhibited no significant differences compared to the control group under either hypoxic or reoxygenation conditions (Figure 6).

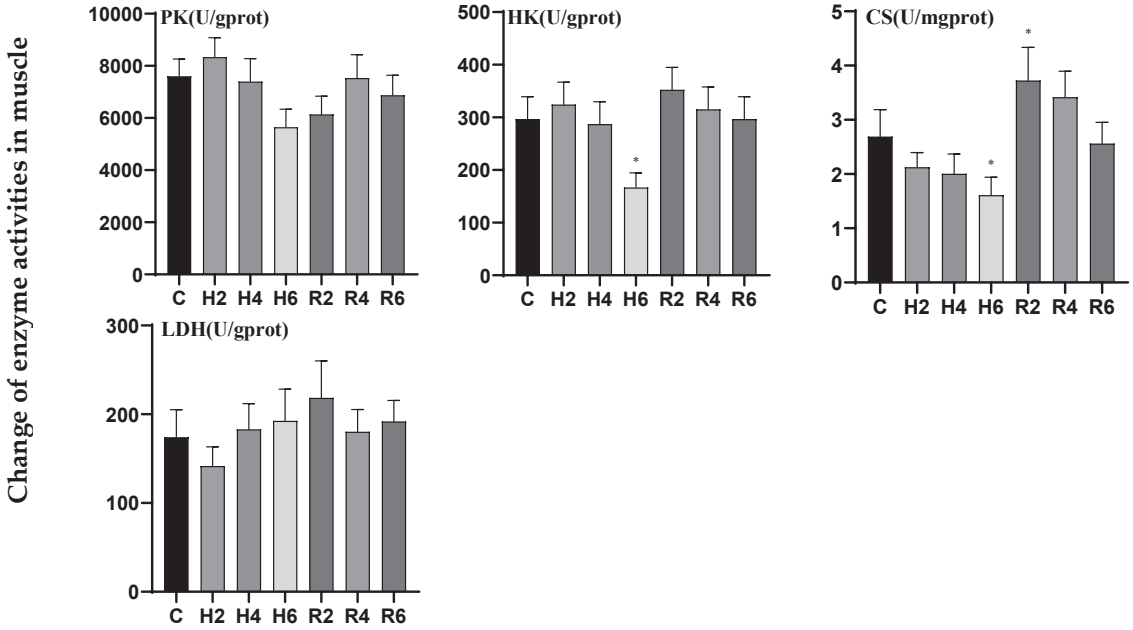


Figure 6. Effects of hypoxia (2 h, 4 h, 6 h) and reoxygenation (2 h, 4 h, 6 h) on muscle respiratory metabolism-related enzyme activities of hybrid catfish. Note: * at $p < 0.05$.

3.3. Effects of Hypoxia and Reoxygenation on Oxidative Stress-Related Genes in Hybrid Catfish

Under acute hypoxia, the expression levels of *SOD1* and *GSH-PX* genes in brain tissue exhibited a biphasic response, showing an initial decrease followed by an increase, with minimum levels observed at H4 ($p < 0.05$), corresponding to 0.51- and 0.69-fold changes relative to the control group (C), respectively. Following reoxygenation, both genes demonstrated peak expression at R4, with statistically significant differences compared to the control group ($p < 0.05$). The expression pattern of the *SOD2* gene displayed a progressive increase, whereas *CAT* gene expression demonstrated a decreasing trend. Both genes attained their maximum expression levels at R2 post-reoxygenation, with values significantly elevated compared to the control group ($p < 0.05$) (Figure 7).

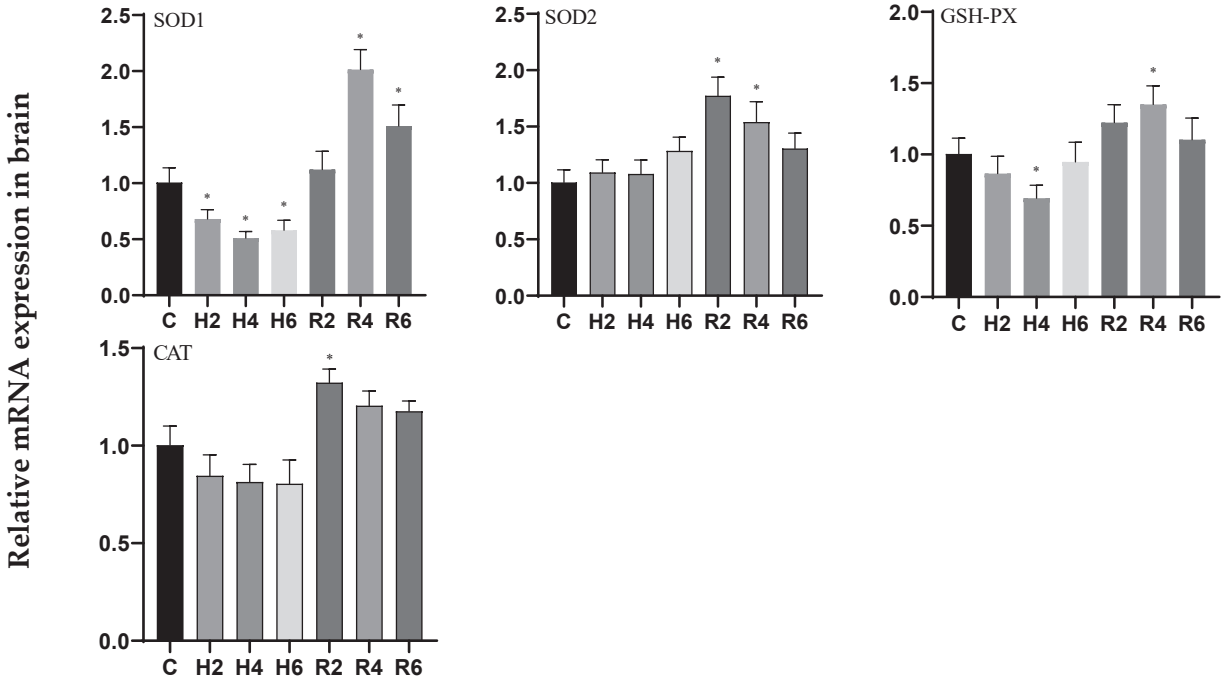


Figure 7. Effects of hypoxia (2 h, 4 h, 6 h) and reoxygenation (2 h, 4 h, 6 h) on oxidative stress-related genes in brain of hybrid catfish. Note: * at $p < 0.05$.

In liver tissue under acute hypoxia, the expression levels of *SOD1* and *CAT* genes showed an increasing trend, reaching peak levels at H6 ($p < 0.05$), with 1.79- and 2.05-fold increases relative to the control group (C), respectively. During the reoxygenation phase, *SOD1* expression remained significantly elevated compared to control levels, while *CAT* expression peaked at R2, showing a significant increase over control values ($p < 0.05$), before gradually returning to baseline levels. The expression profiles of *SOD2* and *GSH-PX* genes exhibited an initial increase followed by a decrease, with maximum levels observed at H4 ($p < 0.05$), corresponding to 2.0- and 1.46-fold changes relative to control levels, respectively. Following reoxygenation, these genes demonstrated peak expression at R2 and R4, respectively, showing statistically significant differences from control values ($p < 0.05$), before gradually returning to baseline levels (Figure 8).

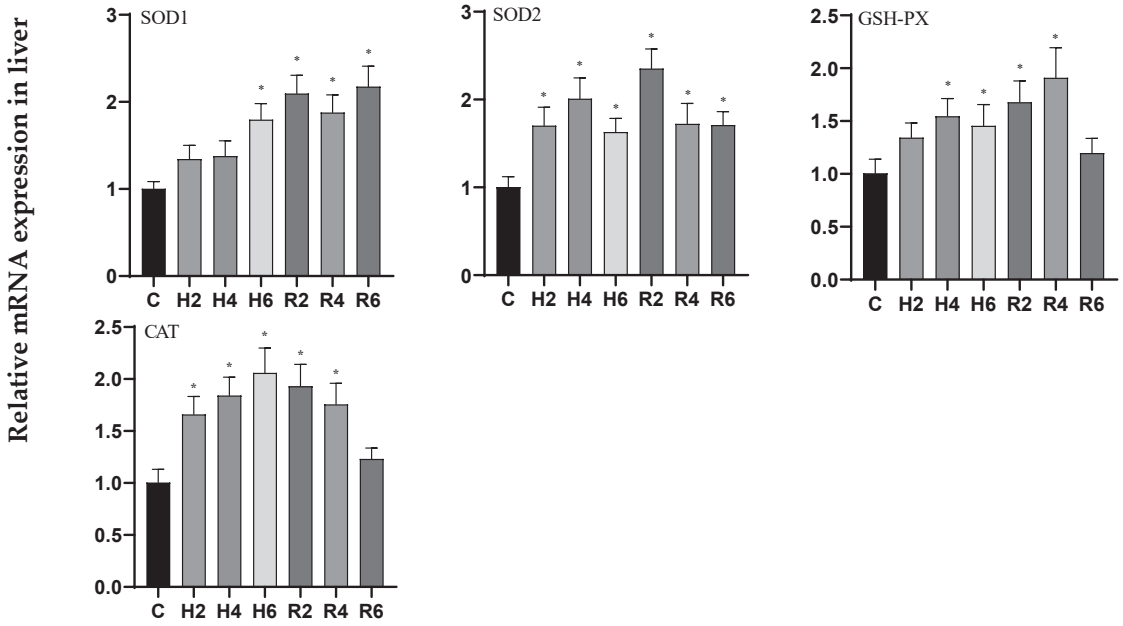


Figure 8. Effects of hypoxia (2 h, 4 h, 6 h) and reoxygenation (2 h, 4 h, 6 h) on oxidative stress-related genes in liver of hybrid catfish. Note: * at $p < 0.05$.

In muscle tissue subjected to acute hypoxia, the expression levels of *SOD1*, *SOD2*, and *CAT* genes displayed an initial increase followed by a decrease, reaching peak levels at H4 ($p < 0.05$), with 2.80-, 2.59-, and 2.32-fold increases relative to control values, respectively. During the reoxygenation phase, *SOD1* expression showed a gradual decline while maintaining significantly higher levels than the control group, whereas *SOD2* and *CAT* expression levels progressively increased, peaking at R6 and showing statistically significant differences from control values ($p < 0.05$). The *GSH-PX* gene expression profile demonstrated a continuous upward trend, reaching maximum levels at H6 ($p < 0.05$), representing a 2.70-fold increase over control values, and remained significantly elevated compared to control levels throughout the reoxygenation period ($p < 0.05$) (Figure 9).

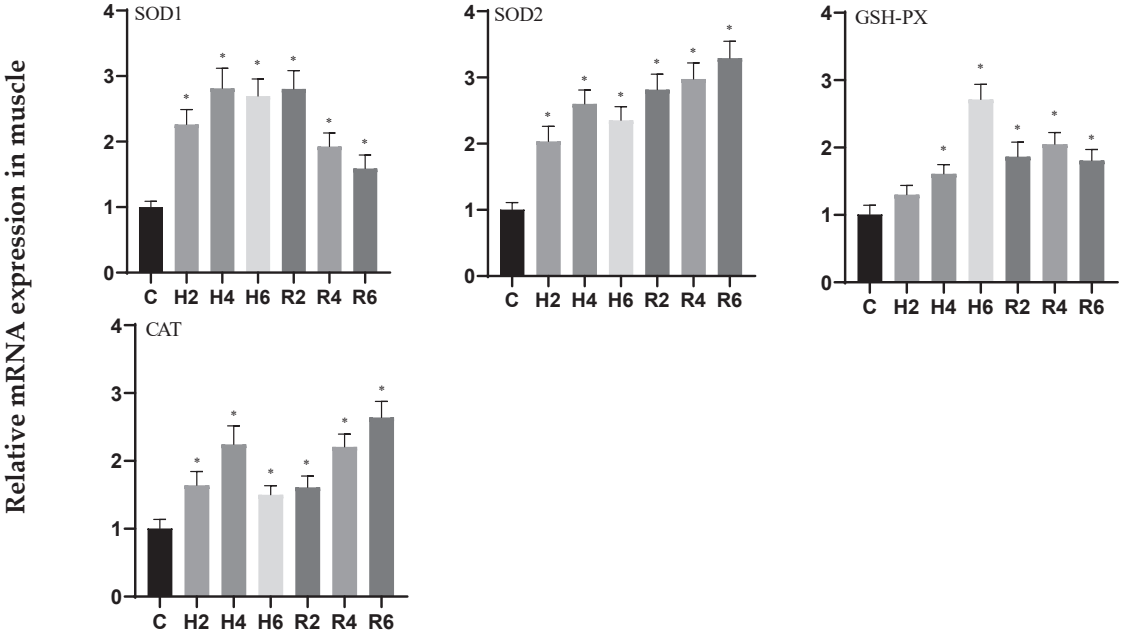


Figure 9. Effects of hypoxia (2 h, 4 h, 6 h) and reoxygenation (2 h, 4 h, 6 h) on oxidative stress-related genes in muscle of hybrid catfish. Note: * at $p < 0.05$.

3.4. Effects of Hypoxia and Reoxygenation on Oxidative Stress Enzyme Activities and Parameters in Hybrid Catfish

Under acute hypoxia, the activities of T-SOD and GSH-PX in brain tissue decreased significantly, reaching their lowest levels at H6 ($p < 0.05$), representing 0.66 and 0.54 times the levels of the control group (C), respectively. After reoxygenation, these activities remained significantly lower than the control group at R2, after which they gradually increased and returned to control levels. The activities of CAT and PCO declined with fluctuations, with only PCO activity significantly reduced at H6 ($p < 0.05$), reaching 0.55 times the control level (C). After reoxygenation, only CAT activity showed a gradual increase, peaking at R6 and demonstrating a significant difference from the control group ($p < 0.05$). The activities of LPO and MDA initially rose and then declined, with only MDA activity significantly reduced at H6 ($p < 0.05$), reaching 0.65 times the control level (C). After reoxygenation, only LPO activity reached its peak at R2, after which it gradually decreased and returned to control levels (Figure 10).

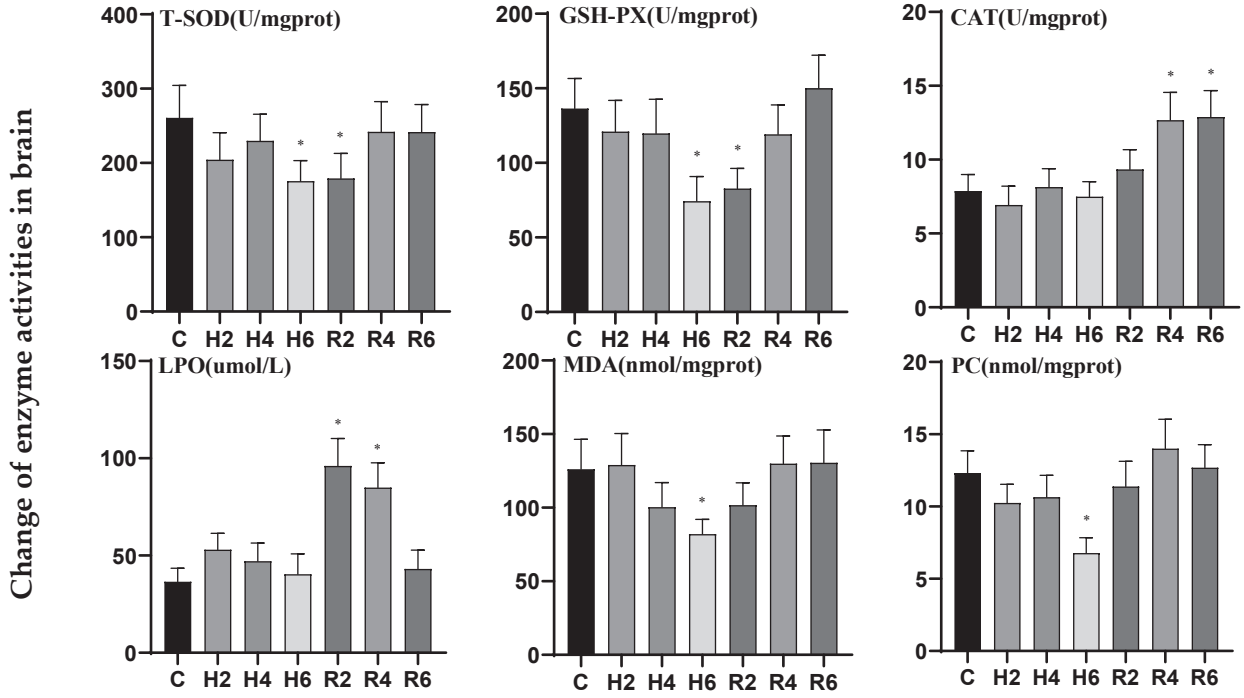


Figure 10. Effects of hypoxia (2 h, 4 h, 6 h) and reoxygenation (2 h, 4 h, 6 h) on brain oxidative kinase activity and parameters of hybrid catfish. Note: * at $p < 0.05$.

In liver tissue under acute hypoxia, the activities of T-SOD, CAT, LPO, and MDA increased significantly, peaking at H6 ($p < 0.05$), reaching 2.05, 1.41, 2.0, and 2.38 times the levels of the control group (C), respectively. After reoxygenation, the activities of T-SOD, CAT, LPO, and MDA reached their peaks at R4, R2, R4, and R6, respectively. While CAT activity gradually returned to control levels, the activities of the other enzymes remained significantly elevated compared to the control group ($p < 0.05$). The activities of GSH-PX and PC exhibited an increasing trend, both reaching their peak values at H6 ($p < 0.05$), which were 2.27-fold and 1.39-fold of the control group (C), respectively. After reoxygenation, GSH-PX activity showed a gradual increase, peaking at R6 and demonstrating a significant difference from the control group ($p < 0.05$), while PCO activity reached its peak at R2, significantly elevated compared to the control group ($p < 0.05$), before gradually declining and returning to control levels (Figure 11).

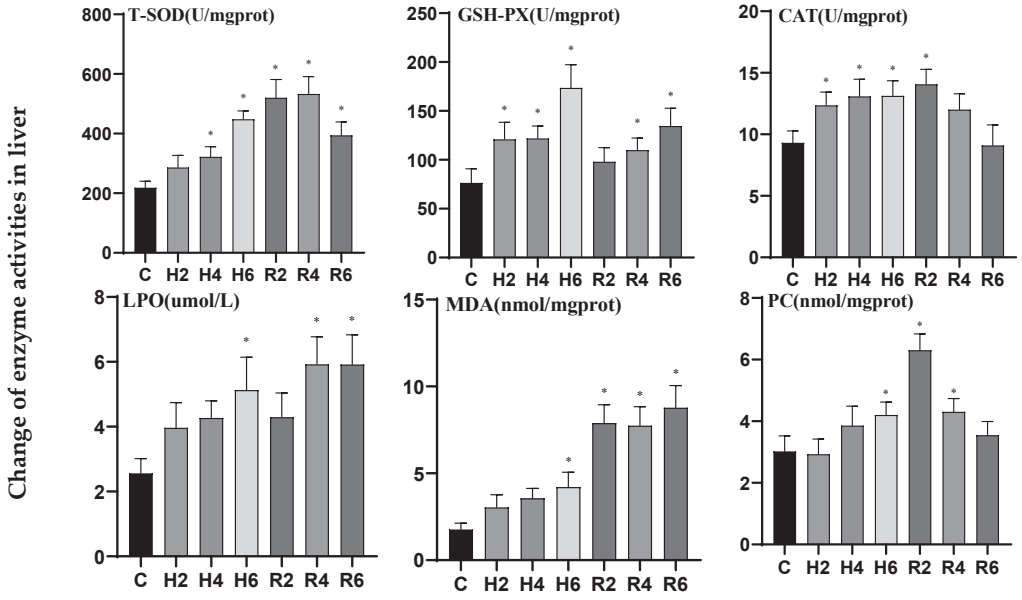


Figure 11. Effects of hypoxia (2 h, 4 h, 6 h) and reoxygenation (2 h, 4 h, 6 h) on liver oxidative kinase activity and parameters of hybrid catfish. Note: * at $p < 0.05$.

In muscle tissue under acute hypoxia, the activities of T-SOD, CAT, LPO, MDA, and PCO increased significantly, peaking at H6 ($p < 0.05$), reaching 2.41, 1.32, 2.03, 3.74, and 3.81 times the levels of the control group (C), respectively. After reoxygenation, the activities of T-SOD, CAT, and MDA reached their peaks at R2, demonstrating significant differences from the control group ($p < 0.05$), before gradually declining and returning to control levels. In contrast, the activities of LPO and PCO remained significantly elevated compared to the control group after reoxygenation ($p < 0.05$). The activity of glutathione peroxidase (GSH-PX) demonstrated a significant upward trend, peaking at H6 ($p < 0.05$) with levels reaching 2.52-fold of the control group (C). Notably, during the reoxygenation phase, GSH-PX activity remained significantly elevated compared to control values ($p < 0.05$) (Figure 12).

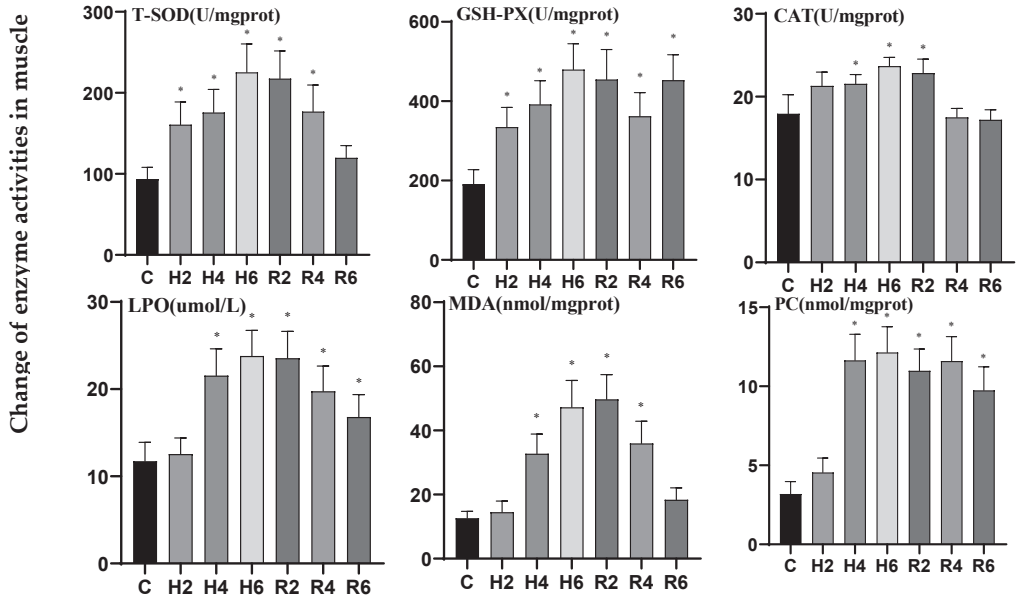


Figure 12. Effects of hypoxia (2 h, 4 h, 6 h) and reoxygenation (2 h, 4 h, 6 h) on muscle oxidative kinase activity and parameters of hybrid catfish. Note: * at $p < 0.05$.

3.5. Effects of Hypoxia and Reoxygenation on Mitochondrial Damage Genes in Hybrid Catfish

During acute hypoxia and subsequent reoxygenation, the expression levels of *PGC-1α*, *COXIV*, and *ATP5A1* genes in brain tissue remained unchanged compared to the control group (Figure 13).

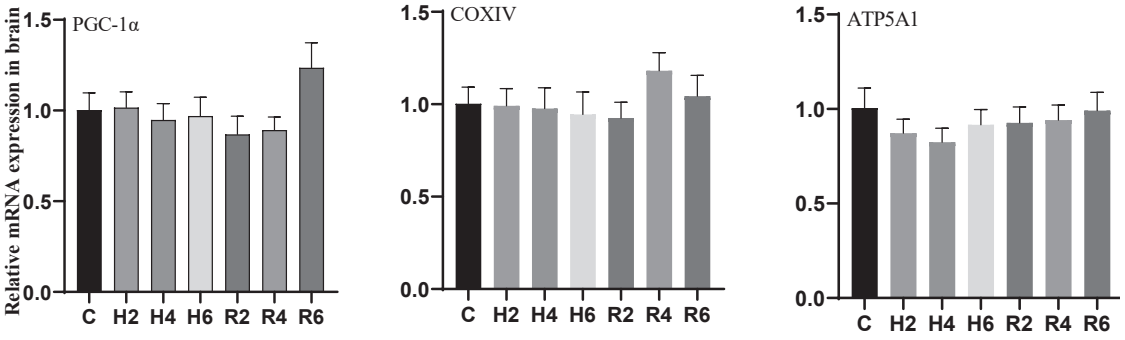


Figure 13. Effects of hypoxia (2 h, 4 h, 6 h) and reoxygenation (2 h, 4 h, 6 h) on brain mitochondrial damage-related genes of hybrid catfish.

Under acute hypoxia, the expression of *PGC-1α* and *COXIV* genes in liver tissue decreased significantly, reaching their minimum values at H6 ($p < 0.05$), which were 0.59 and 0.58 times that of the control group, respectively. After reoxygenation, the expression of *PGC-1α* and *COXIV* genes recovered gradually to control levels, although *COXIV* expression remained significantly lower than the control group at R2 ($p < 0.05$). The *ATP5A1* gene expression initially decreased, reaching its minimum value at H4 ($p < 0.05$), which was 0.58 times that of the control group, and subsequently increased to control levels after reoxygenation (Figure 14).

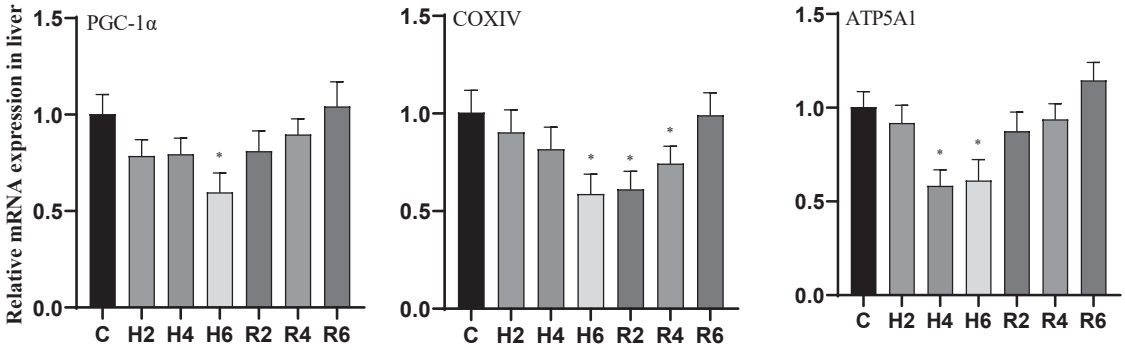


Figure 14. Effects of hypoxia (2 h, 4 h, 6 h) and reoxygenation (2 h, 4 h, 6 h) on liver mitochondrial damage-related genes of hybrid catfish. Note: * at $p < 0.05$.

Under acute hypoxia, the expression of the *PGC-1α* gene in muscle tissue decreased significantly, reaching its minimum value at H6 ($p < 0.05$), which was 0.42 times that of the control group. After reoxygenation, *PGC-1α* expression remained significantly lower than the control group at R2 ($p < 0.05$) but gradually recovered to control levels thereafter. The expression of *COXIV* and *ATP5A1* genes initially decreased, reaching their minimum values at H4 ($p < 0.05$), which were 0.27 and 0.38 times that of the control group (C), respectively. After reoxygenation, their expression remained significantly lower than the control group at R2 ($p < 0.05$) but gradually recovered to control levels (Figure 15).

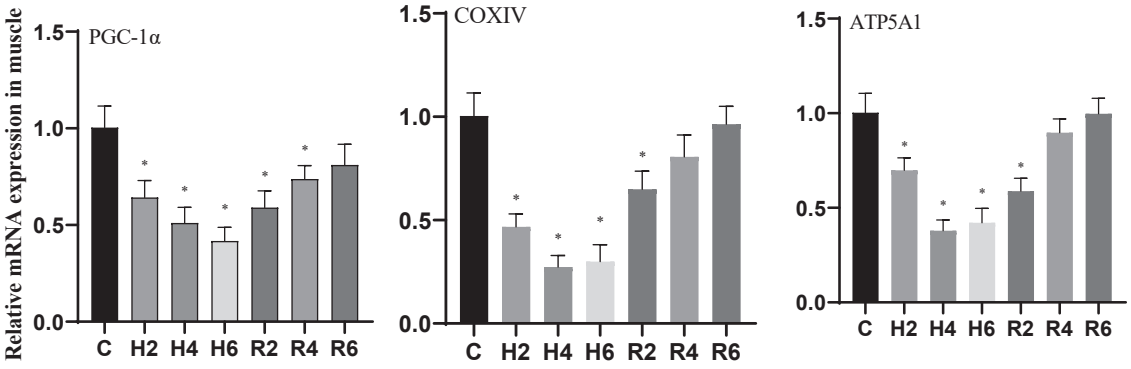


Figure 15. Effects of hypoxia (2 h, 4 h, 6 h) and reoxygenation (2 h, 4 h, 6 h) on muscle mitochondrial damage-related genes of hybrid catfish. Note: * at $p < 0.05$.

3.6. Effects of Hypoxia and Reoxygenation on Inflammation and Apoptosis-Related Genes in Hybrid Catfish

During acute hypoxia and subsequent reoxygenation, no significant differences were observed in the expression levels of *IL-1β*, *IKKβ*, *Caspase 3*, *Bax*, and *Bcl-2* genes in brain tissue when compared to the control group (Figure 16).

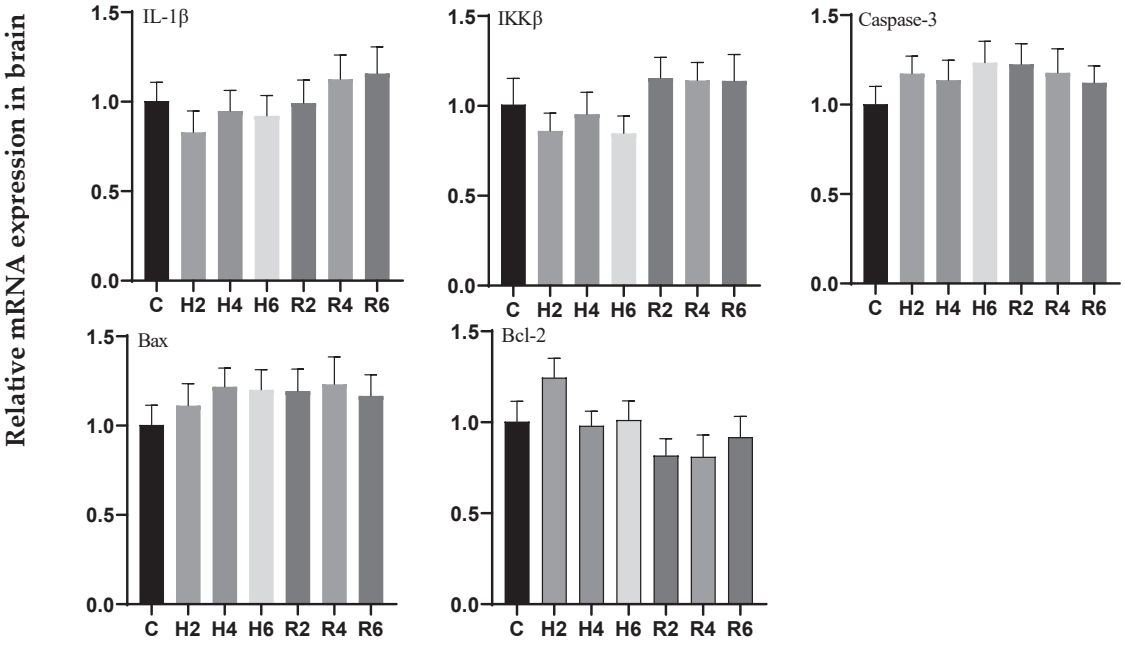


Figure 16. Effects of hypoxia (2 h, 4 h, 6 h) and reoxygenation (2 h, 4 h, 6 h) on apoptosis and inflammation-related genes in brain cells of hybrid catfish.

Under acute hypoxia, the expression levels of *IL-1β*, *IKKβ*, *Caspase 3*, and *Bax* genes in liver tissue significantly increased, reaching their maximum values at H6 ($p < 0.05$), with expression levels 1.95-, 1.96-, 2.00-, and 2.13-fold higher than those of the control group (C), respectively. After reoxygenation, the expression levels of these genes gradually decreased, returning to control levels, although *IL-1β*, *IKKβ*, and Bax remained significantly elevated compared to the control group at R2 ($p < 0.05$). In contrast, the expression of the *Bcl-2* gene significantly decreased, reaching its minimum value at H6 ($p < 0.05$), with expression levels 0.66-fold lower than those of the control group (C), and subsequently increased to control levels following reoxygenation (Figure 17).

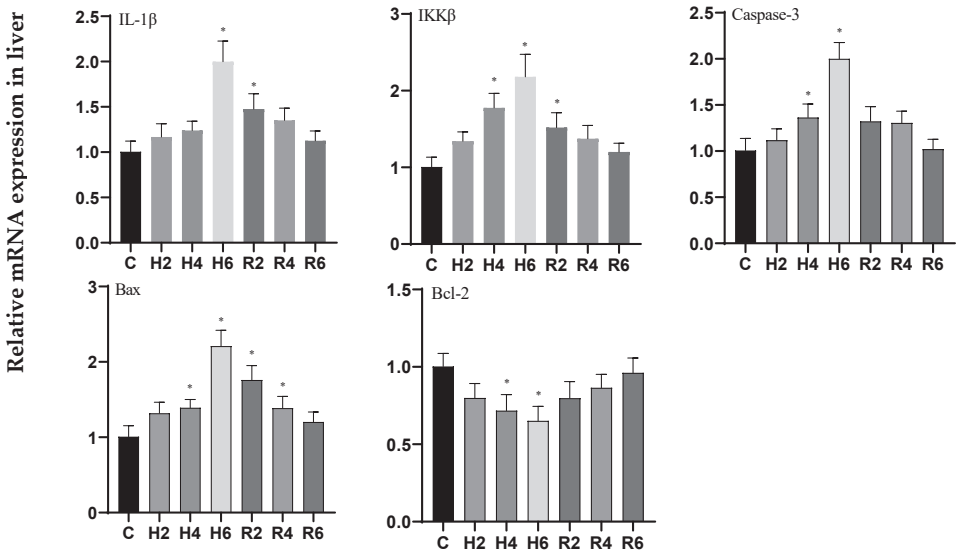


Figure 17. Effects of hypoxia (2 h, 4 h, 6 h) and reoxygenation (2 h, 4 h, 6 h) on apoptosis and inflammation-related genes in liver cells of hybrid catfish. Note: * at $p < 0.05$.

Under acute hypoxia, the expression of *IL-1β* and *IKKβ* genes in muscle tissue initially increased, peaking at H4 ($p < 0.05$), with expression levels 3.26- and 2.84-fold higher than those of the control group (C), respectively, before subsequently decreasing. After reoxygenation, the expression levels of these genes gradually declined, returning to control levels, although *IL-1β* remained significantly elevated compared to the control group at R2 ($p < 0.05$). The expression of the *Caspase 3* gene significantly increased, reaching its maximum value at H6 ($p < 0.05$), with expression levels 2.44-fold higher than those of the control group (C), and subsequently decreased to control levels following reoxygenation. The expression of the *Bax* gene fluctuated but overall increased, peaking at H6 ($p < 0.05$), with expression levels 2.30-fold higher than those of the control group (C), and remained significantly elevated compared to the control group at R2 ($p < 0.05$) before gradually declining to control levels. The expression of the *Bcl-2* gene initially decreased, reaching its minimum value at H4 ($p < 0.05$), with expression levels 0.54-fold lower than those of the control group (C), and subsequently increased to control levels following reoxygenation (Figure 18).

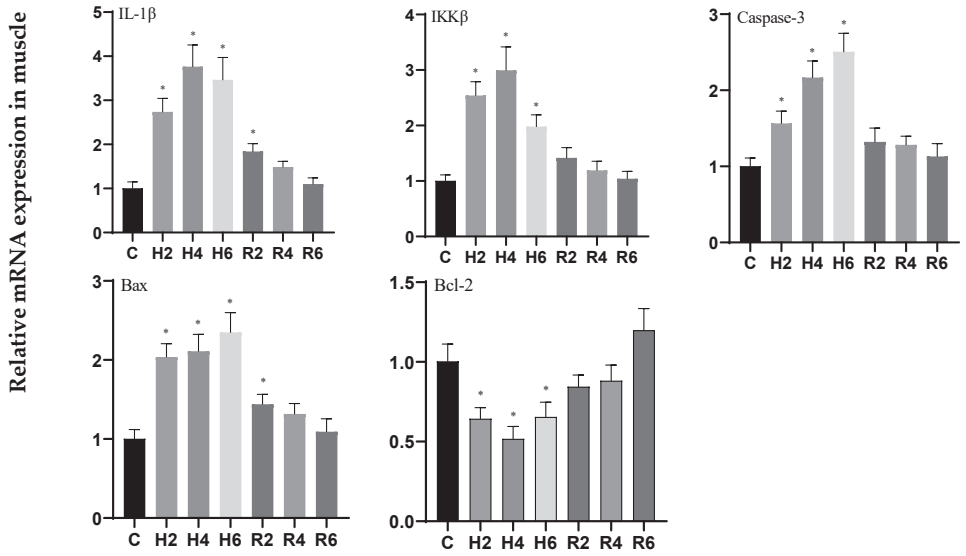


Figure 18. Effects of hypoxia (2 h, 4 h, 6 h) and reoxygenation (2 h, 4 h, 6 h) on apoptosis and inflammation-related genes in muscle cells of hybrid catfish. Note: * at $p < 0.05$.

4. Discussion

4.1. Effects of Hypoxia and Reoxygenation on Oxygen-Sensing Protein HIF-1α and Respiratory Metabolism in Hybrid Catfish

The survival of aquatic organisms is primarily dependent on the stability of their aquatic environment, with fluctuations in dissolved oxygen (DO) levels being of particular significance for fish [19]. To cope with significant changes in DO, fish have evolved a series of complex physiological adaptation mechanisms, among which the activation of the *HIF-1* signaling pathway is of paramount importance [20]. This pathway, mediated by the binding of HIF heterodimers to hypoxia response elements (*HREs*), activates a cascade of genes involved in angiogenesis, glucose and iron transport, glycolysis, and cell cycle regulation, thereby enabling fish to maintain viability under hypoxic conditions [21]. The results of this study indicate that the expression of the *HIF-1α* gene in the brain, liver, and muscle tissues of hybrid catfish was significantly upregulated during hypoxia and subsequently returned to control levels after reoxygenation. These findings are consistent with studies on other fish species, such as *Sebastes schlegelii* [22], *Leiostomus xanthurus* [23], and *Oreochromis niloticus* [24], thereby reinforcing *HIF-1α* as a key oxygen-sensing protein that is significantly activated under hypoxic conditions.

Research demonstrates that the *HIF-1* signaling pathway regulates key genes such as *PFKL, HK1, PK, LDHA*, and *CS*, which are integral to glycolysis, anaerobic respiration, and the tricarboxylic acid (TCA) cycle [25–28]. Under hypoxia, organisms typically adapt by lowering basal metabolic rates and transitioning between aerobic and anaerobic metabolic pathways [29]. Although this adaptation may result in physiological burdens such as lactate accumulation, it is critical for survival [11]. In this study, glycolysis-related (*PFKL*, HK1, PK) and anaerobic respiration-related (*LDHA*) genes and enzyme activities in the liver of hybrid catfish were significantly upregulated under hypoxia and subsequently returned to normal levels after reoxygenation. These results align with findings in *P. fulvidraco* [30], *P. vachelli* [31], and hybrid yellow catfish (*P. fulvidraco* ♀× *P. vachelli* ♂) [32], indicating that liver tissue adapts to hypoxia by enhancing glycolysis and anaerobic respiration to ensure energy supply. Additionally, in the brain tissue, the *HK* gene and PK enzyme activity were significantly upregulated at H2, suggesting the activation of glycolysis during the early stages of hypoxia. Notably, *LDHA* was significantly downregulated at H6, potentially representing a protective mechanism to prevent lactate accumulation. In contrast, some glycolysis-, CS-, and anaerobic respiration-related genes and enzyme activities in muscle tissue exhibited a downward trend, consistent with findings in *P. vachelli* [33,34] and *Trachinotus blochii* [35]. This implies that muscle tissue may experience more severe hypoxia-induced metabolic disturbances compared to other tissues.

4.2. Effects of Hypoxia and Reoxygenation on Oxidative Stress in Hybrid Catfish

Under physiological homeostasis, the generation and clearance of reactive oxygen species (ROS) maintain a delicate dynamic equilibrium [36]. However, exposure to environmental stressors can disrupt this equilibrium, resulting in oxidative stress [37]. Numerous studies have demonstrated that various aquatic organisms, including *Carassius auratus* [38], *Sinonovacula constricta* [39], *Megalobrama amblycephala* [40], and *Neohelice granulata* [41], exhibit significant upregulation of antioxidant enzyme activities under hypoxic conditions, a phenomenon termed "oxidative stress preparation" to mitigate potential oxidative stress during reoxygenation [42]. Similarly, hybrid catfish exhibited analogous alterations in antioxidant enzyme activities under hypoxic conditions. Our findings revealed that antioxidant enzymes (e.g., SOD, CAT, GSH-PX) in hepatic and muscular tissues exhibited significant increases during the initial hypoxic phase (H2–H4), whereas oxidative stress markers

(e.g., LPO, MDA, PCO) demonstrated substantial elevation during H4-H6. These observations suggest that hybrid catfish may possess an anticipatory antioxidant defense mechanism to counteract potential oxidative stress induced by hypoxic conditions [43]. In contrast, both antioxidant enzymes and oxidative stress markers in cerebral tissue remained stable or exhibited minimal declines, maintaining relatively consistent levels. Comparable findings have been documented in *P. glenii* [44] and *P. vachelli* [31], suggesting that cerebral tissue, as a vital organ, may receive preferential oxygen supply during acute hypoxic conditions, thereby minimizing oxidative stress damage [45,46]. Notably, oxidative stress markers in hepatic and muscular tissues demonstrated significant elevation during the advanced hypoxic phase, with muscular tissue displaying higher oxidative stress levels compared to hepatic tissue, indicating more pronounced oxidative damage in muscular tissue.

Reoxygenation has been demonstrated to induce rapid ROS accumulation, resulting in secondary oxidative stress responses. For instance, *Cyprinus carpio var qingtianensis* [47] and *Mugil cephalus* [48] demonstrated significant oxidative stress during reoxygenation. Similarly, the hybrid catfish exhibited ROS accumulation during reoxygenation. The present study revealed that antioxidant enzyme activities and oxidative stress parameters in brain, liver, and muscle tissues were significantly elevated following reoxygenation, suggesting that the antioxidant enzyme system maintains high activity to mitigate reoxygenation-induced oxidative stress.

4.3. Effects of Hypoxia and Reoxygenation on Mitochondrial Damage, Inflammation, and Apoptosis in Hybrid Catfish

Mitochondria, serving as the central organelles for cellular energy metabolism, predominantly depend on oxidative phosphorylation for energy conversion [49]. Numerous studies have demonstrated that hypoxia or ischemia significantly impairs mitochondrial oxidative phosphorylation, resulting in diminished mitochondrial biogenesis and functional impairments [50]. Key regulatory genes including *PGC-1α*, *COXIV*, and *ATP5A1* are intrinsically linked to mitochondrial function, orchestrating mitochondrial biogenesis and maintenance, while their expression profiles serve as reliable biomarkers for mitochondrial dysfunction [51–54]. These genes play pivotal roles in regulating oxidative phosphorylation, thereby directly modulating cellular energy metabolism and maintaining functional homeostasis [55]. Experimental studies conducted on rat models [56,57] and *P. vachelli* [34] have consistently demonstrated that hypoxia significantly downregulates the expression of *PGC-1α*, *COXIV*, and *ATP5A1* genes, highlighting the profound detrimental effects of hypoxia on mitochondrial functionality. In the current investigation, we observed significant downregulation of mitochondrial-related genes (*PGC-1α*, *COXIV*, *ATP5A1*) in the liver and muscle tissues of hybrid catfish under hypoxic conditions, suggesting substantial impairment in mitochondrial respiration and biogenesis processes. However, in brain tissue, these genes maintained stable expression levels, suggesting the presence of robust protective mechanisms and adaptive responses that preserve mitochondrial function under hypoxic stress.

The NF-κB signaling pathway plays a pivotal role in regulating inflammatory signaling transduction and mediating the expression of inflammatory factors [58]. This signaling cascade modulates the transcriptional activation of specific inflammatory factors, including TNF-α and IL-1β, in response to various cellular stress stimuli [59]. In *P. vachelli* [45], hypoxia-induced mitochondrial dysfunction was found to activate the NF-κB signaling pathway, subsequently triggering the release of pro-inflammatory cytokines and initiating apoptotic processes. Our experimental results demonstrated that the expression levels of *IKKβ*, *IL-1β*, *Caspase-3*, and *Bax* genes in muscle tissue were significantly upregulated during the initial phase of hypoxia exposure, showing more pronounced elevation compared to hepatic tissue, indicating that muscle cells might exhibit enhanced susceptibility

to hypoxia-induced apoptosis. Furthermore, the elevated expression of *IKKβ*, a pivotal regulatory component of the NF-κB signaling cascade, was observed in both hepatic and muscular tissues, providing additional evidence for the pathway's essential involvement in hypoxia-mediated cellular stress responses. Notably, the pronounced upregulation of *IKKβ* in muscular tissue suggests a potentially heightened cellular sensitivity to hypoxic conditions. Comparable observations have been documented in *Rachycentron canadum* [60], *L. crocea* [61], and *Epinephelus coioides* [62], where hypoxia-triggered reactive oxygen species (ROS) and peroxide accumulation were shown to activate the NF-κB signaling cascade [63], resulting in the upregulation of inflammatory mediators (*TNF-α*, *IL-1β*) and pro-apoptotic factors (*Caspase-3*, *Bax*), concomitant with downregulation of anti-apoptotic Bcl-2 expression. In the current investigation, we observed significant upregulation of *IL-1β*, *Caspase-3*, and *Bax* gene expression in both hepatic and muscular tissues under hypoxic conditions, accompanied by downregulation of *Bcl-2* expression, which is presumably attributable to excessive ROS generation and subsequent NF-κB pathway activation. Conversely, the expression profiles of these inflammatory and apoptotic markers remained relatively stable in cerebral tissue, in agreement with previous findings in *P. vachelli* [33], implying that neural tissue might possess specialized metabolic adaptations and enhanced antioxidant defense mechanisms to counteract hypoxia-mediated cellular injury.

5. Conclusions

This study systematically investigated the effects of hypoxia–reoxygenation on oxygen-sensing proteins, respiratory metabolism, oxidative stress, mitochondrial function, inflammatory responses, and apoptosis in the brain, liver, and muscle tissues of hybrid catfish. Hypoxia significantly activated HIF-1α expression and induced metabolic reprogramming, with the liver shifting toward anaerobic metabolism, while the brain exhibited suppressed glycolysis and the muscle displayed concurrent inhibition of glycolysis and aerobic respiration. Notably, muscle tissue demonstrated heightened oxidative stress, mitochondrial dysfunction, inflammatory cascades, and apoptosis during hypoxia–reoxygenation. These findings elucidate the multi-tissue adaptive mechanisms in hybrid catfish under oxygen fluctuations. Future research should explore interspecific variations in hypoxia adaptation and genetic strategies to enhance hypoxia tolerance, providing insights for sustainable aquaculture development.

Supplementary Materials: The following supporting information can be downloaded at https://www.mdpi.com/article/10.3390/biology14080915/s1. Table S1: Enzyme activity determination method.

Author Contributions: Conceptualization, J.Y. and F.Z.; methodology, C.Z.; software, J.Y.; validation, F.Z.; formal analysis, J.Y.; investigation, J.Y. and F.Z.; data curation, F.Z.; writing—original draft preparation, J.Y.; writing—review and editing, F.L. and G.Z.; visualization, C.Z.; supervision, S.Y.; project administration, F.L., G.Z. and S.Y.; funding acquisition, G.Z. All authors have read and agreed to the published version of the manuscript.

Funding: This research was funded by the National Natural Science Foundation of China (No. 32402983), Qingchuang science and technology support program of Shandong provincial college (2024KJG006) and the "JBGS" Project of Seed Industry Revitalization in Jiangsu Province (JBGS [2021] 034).

Institutional Review Board Statement: This study was approved by the Nanjing Normal University Animal Ethics Committee (approval no. SYXK [Jiangsu] 2015-0028).

Informed Consent Statement: Not applicable.

Data Availability Statement: The data that support the findings of this study are available in [Mendeley Data] at [https://data.mendeley.com/preview/wn9fp3xfbm?a=597e50bd-e39e-47a3-bb16-ad66f914bda1], accessed on 23 May 2025.

Acknowledgments: We cordially thank the anonymous referees and the editors for their helpful suggestions on the earlier draft of our paper.

Conflicts of Interest: The authors declare no conflict of interest.

References

1. Hammarlund, E.U.; Flashman, E.; Mohlin, S.; Licausi, F. Oxygen-sensing mechanisms across eukaryotic kingdoms and their roles in complex multicellularity. *Science* **2020**, *370*, eaba3512. [CrossRef] [PubMed]
2. Wu, C.-B.; Zheng, G.-D.; Zhao, X.-Y.; Zhou, S.; Zou, S.-M. Hypoxia tolerance in a selectively bred F4 population of blunt snout bream (*Megalobrama amblycephala*) under hypoxic stress. *Aquaculture* **2020**, *518*, 734484. [CrossRef]
3. Jenny, J.P.; Francus, P.; Normandeau, A.; Lapointe, F.; Perga, M.E.; Ojala, A.; Schimmelmann, A.; Zolitschka, B. Global spread of hypoxia in freshwater ecosystems during the last three centuries is caused by rising local human pressure. *Glob. Change Biol.* **2016**, *22*, 1481–1489. [CrossRef] [PubMed]
4. Wang, Z.; Pu, D.; Zheng, J.; Li, P.; Lü, H.; Wei, X.; Li, M.; Li, D.; Gao, L. Hypoxia-induced physiological responses in fish: From organism to tissue to molecular levels. *Ecotoxicol. Environ. Saf.* **2023**, *267*, 115609. [CrossRef] [PubMed]
5. Xie, R.; Guo, H.; Luo, Y.; Huang, W.; Ruan, Z.; Liu, W. New Insights into the Mechanism by Which the Pituitary Gland Copes with Hypoxia Stress Based on a Transcriptomic Analysis of *Megalobrama amblycephala*. *Genes* **2024**, *15*, 987. [CrossRef] [PubMed]
6. Zhu, C.-D.; Wang, Z.-H.; Yan, B. Strategies for hypoxia adaptation in fish species: A review. *J. Comp. Physiol. B* **2013**, *183*, 1005–1013. [CrossRef] [PubMed]
7. Wang, X.-J.; Si, L.-B. Advances on hypoxia inducible factor-1. *Chin. Med. J.* **2013**, *126*, 3567–3571. [CrossRef] [PubMed]
8. Kumar, H.; Choi, D.-K. Hypoxia inducible factor pathway and physiological adaptation: A cell survival pathway? *Mediat. Inflamm.* **2015**, *2015*, 584758. [CrossRef] [PubMed]
9. Wu, R.; Chao, Y.; Zhao, Y.; Chen, Q.; Zheng, Z.; Xia, M.; Qi, D. Molecular evolution and hypoxia-induced expression of Hif-α gene in *Schizothoracinae fishes*. *Acta Lab. Anim. Sci. Sin.* **2019**, *27*, 433–443.
10. Zhan, Y.; Qi, X.; Wu, Y.; Gao, D.; Zhao, L.; Cao, S.; Xue, Z.; Wang, W. Hypoxia-inducible factor-1α as a biomarker for individuals under hypoxia duration and pattern in fat greenling *Hexagrammos otakii*. *Aquac. Rep.* **2024**, *39*, 102459. [CrossRef]
11. Omlin, T.; Weber, J.-M. Hypoxia stimulates lactate disposal in rainbow trout. *J. Exp. Biol.* **2010**, *213*, 3802–3809. [CrossRef] [PubMed]
12. Hoseini, S.M.; Taheri Mirghaed, A.; Pagheh, E.; Hoseinifar, S.H.; Van Doan, H. Anesthesia of rainbow trout with citronellal: Efficacy and biochemical effects. *J. Exp. Zool. Part A Ecol. Integr. Physiol.* **2022**, *337*, 227–237. [CrossRef] [PubMed]
13. Chowdhury, S.; Saikia, S. Oxidative stress in fish: A review. *J. Sci. Res.* **2020**, *12*, 145–160. [CrossRef]
14. Birnie-Gauvin, K.; Costantini, D.; Cooke, S.J.; Willmore, W.G. A comparative and evolutionary approach to oxidative stress in fish: A review. *Fish Fish.* **2017**, *18*, 928–942. [CrossRef]
15. Wang, Q.-F.; Shen, W.-L.; Hou, C.-C.; Liu, C.; Wu, X.-F.; Zhu, J.-Q. Physiological responses and changes in gene expression in the large yellow croaker *Larimichthys crocea* following exposure to hypoxia. *Chemosphere* **2017**, *169*, 418–427. [CrossRef] [PubMed]
16. Chen, F.; Ling, X.; Zhao, Y.; Fu, S. Hypoxia-induced oxidative stress and apoptosis in gills of scaleless carp (*Gymnocypris przewalskii*). *Fish Physiol. Biochem.* **2022**, *48*, 911–924. [CrossRef] [PubMed]
17. Yang, S.; Yan, T.; Wu, H.; Xiao, Q.; Fu, H.; Luo, J.; Zhou, J.; Zhao, L.; Wang, Y.; Yang, S. Acute hypoxic stress: Effect on blood parameters, antioxidant enzymes, and expression of HIF-1alpha and GLUT-1 genes in largemouth bass (*Micropterus salmoides*). *Fish Shellfish Immunol.* **2017**, *67*, 449–458. [CrossRef] [PubMed]
18. Qian, L. *Sex* Determination in Ictalurus punctatus and Genetic Identification of Pelteobagrus Vachelli, Leiocassis Longirostris, and their Hybrids. Master's Thesis, Huazhong Agricultural University, Wuhan, China, 2023.
19. Bulbul Ali, A.; Mishra, A. Effects of dissolved oxygen concentration on freshwater fish: A review. *Int. J. Fish. Aquat. Stud.* **2022**, *10*, 113–127. [CrossRef]
20. Babin, C.H.; Leiva, F.P.; Verberk, W.C.; Rees, B.B. Evolution of key oxygen-sensing genes is associated with hypoxia tolerance in fishes. *Genome Biol. Evol.* **2024**, *16*, evae183. [CrossRef] [PubMed]
21. Corrado, C.; Fontana, S. Hypoxia and HIF signaling: One axis with divergent effects. *Int. J. Mol. Sci.* **2020**, *21*, 5611. [CrossRef] [PubMed]
22. Qin, H.; Zhang, X.; Xie, T.; Gao, Y.; Li, J.; Jia, Y. Hepatic transcriptomic analysis reveals that Hif1α/ldha signal is involved in the regulation of hypoxia stress in black rockfish *Sebastes schlegelii*. *Comp. Biochem. Physiol. Part D Genom. Proteom.* **2023**, *47*, 101098. [CrossRef] [PubMed]
23. Smith, M.J.; Gelsleichter, J.; Smith, K.J. Protein expression of hypoxia-inducible factor 1-alpha (HIF-1α) in spot (*Leiostomus xanthurus*) exposed to constant and diel-cycling hypoxia. *J. Exp. Mar. Biol. Ecol.* **2012**, *424*, 1–4. [CrossRef]
24. Li, M. Study on the Effects of Hypoxic Stress on Glycolipid Metabolism in Nile Tilapia and the Regulatory Role of Salidroside. Master's Thesis, East China Normal University, Shanghai, China, 2018.

25. Lynch, E.M.; Hansen, H.; Salay, L.; Cooper, M.; Timr, S.; Kollman, J.M.; Webb, B.A. Structural basis for allosteric regulation of human phosphofructokinase-1. *bioRxiv* **2024**. [CrossRef] [PubMed]
26. Li, Z.-L.; Ding, L.; Ma, R.-X.; Zhang, Y.; Zhang, Y.-L.; Ni, W.-J.; Tang, T.-T.; Wang, G.-H.; Wang, B.; Lv, L.-L. Activation of HIF-1α C-terminal transactivation domain protects against hypoxia-induced kidney injury through hexokinase 2-mediated mitophagy. *Cell Death Dis.* **2023**, *14*, 339. [CrossRef] [PubMed]
27. Lantushenko, A.; Kohan, A.; Soldatov, A.; Degtyar, I.; Andreeva, A.Y. Expression of pyruvate kinase, malate and octopine dehydrogenase genes in the gills of the Mediterranean mussel *Mytilus galloprovincialis* (Lamarck, 1819) under conditions of hypoxia and reoxygenation. *Biol. Bull.* **2024**, *51*, 1206–1211. [CrossRef]
28. Dong, M.; Tang, R.; Wang, W.; Xu, J.; Liu, J.; Liang, C.; Hua, J.; Meng, Q.; Yu, X.; Zhang, B. Integrated analysis revealed hypoxia signatures and LDHA related to tumor cell dedifferentiation and unfavorable prognosis in pancreatic adenocarcinoma: Hypoxia in PDAC. *Transl. Oncol.* **2023**, *33*, 101692. [CrossRef] [PubMed]
29. Qi, R.; Zhang, X.; Shao, G.; Qi, R.; Zhang, X.; Shao, G. Advances in adaptive mechanisms to oxygen and research on hypoxic preconditioning. *Sci. Technol. Rev.* **2020**, *38*, 86–91.
30. Wang, J.; Wang, M.; Li, B.; Guo, H.; Zhu, X.; Zhang, L. The combined effect of acute hypoxic stress and feeding status on the metabolism of yellow catfish (*Pelteobagrus fulvidraco*). *Aquaculture* **2022**, *560*, 738605. [CrossRef]
31. Zhang, G. Molecular Mechanisms of Hypoxia Stress Response in Pelteobagrus Vachelli. Master's Thesis, Nanjing Normal University, Nanjing, China, 2017.
32. Sun, J.; Han, G.; Liu, Y.; Li, M.; Yuan, Y.; Fan, Q.; Wang, Y.; Yang, H. Comparison of growth performance and hypoxia tolerance between hybrid yellow catfish and common yellow catfish juveniles. *Acta Hydrobiol. Sin.* **2019**, *43*, 1271–1279.
33. Li, J.; Yang, Z.; Yan, J.; Zhang, K.; Ning, X.; Wang, T.; Ji, J.; Zhang, G.; Yin, S.; Zhao, C. Multi-omics analysis revealed the brain dysfunction induced by energy metabolism in *Pelteobagrus vachelli* under hypoxia stress. *Ecotoxicol. Environ. Saf.* **2023**, *254*, 114749. [CrossRef] [PubMed]
34. Li, J.; Zhang, G.; Yin, D.; Li, Y.; Zhang, Y.; Cheng, J.; Zhang, K.; Ji, J.; Wang, T.; Jia, Y. Integrated application of multiomics strategies provides insights into the environmental hypoxia response in *Pelteobagrus vachelli* muscle. *Mol. Cell. Proteom.* **2022**, *21*, 100196. [CrossRef] [PubMed]
35. Sun, J.L.; Liu, Y.F.; Jiang, T.; Li, Y.Q.; Song, F.B.; Wen, X.; Luo, J. Golden pompano (*Trachinotus blochii*) adapts to acute hypoxic stress by altering the preferred mode of energy metabolism. *Aquaculture* **2021**, *542*, 736842. [CrossRef]
36. Lushchak, V.I.; Lushchak, L.P.; Mota, A.A.; Hermes-Lima, M. Oxidative stress and antioxidant defenses in goldfish *Carassius auratus* during anoxia and reoxygenation. *Am. J. Physiol.-Regul. Integr. Comp. Physiol.* **2001**, *280*, R100–R107. [CrossRef] [PubMed]
37. Lushchak, V.I. Adaptive response to oxidative stress: Bacteria, fungi, plants and animals. *Comp. Biochem. Physiol. Part C Toxicol. Pharmacol.* **2011**, *153*, 175–190. [CrossRef] [PubMed]
38. Hermes-Lima, M.; Moreira, D.C.; Rivera-Ingraham, G.A.; Giraud-Billoud, M.; Genaro-Mattos, T.C.; Campos, É.G. Preparation for oxidative stress under hypoxia and metabolic depression: Revisiting the proposal two decades later. *Free Radic. Biol. Med.* **2015**, *89*, 1122–1143. [CrossRef] [PubMed]
39. Liu, T.; Lu, Y.; Sun, M.; Shen, H.; Niu, D. Effects of acute hypoxia and reoxygenation on histological structure, antioxidant response, and apoptosis in razor clam Sinonovacula constricta. *Fish Shellfish Immunol.* **2024**, *145*, 109310. [CrossRef] [PubMed]
40. Shuang, L.; Chen, S.-L.; Ren, C.; Su, X.-L.; Xu, X.-N.; Zheng, G.-D.; Zou, S.-M. Effects of hypoxia and reoxygenation on oxidative stress, histological structure, and apoptosis in a new hypoxia-tolerant variety of blunt snout bream (*Megalobrama amblycephala*). *Comp. Biochem. Physiol. Part A Mol. Integr. Physiol.* **2023**, *278*, 111358. [CrossRef] [PubMed]
41. Geihs, M.A.; Vargas, M.A.; Maciel, F.E.; Vakkuri, O.; Meyer-Rochow, V.B.; Allodi, S.; Nery, L.E.M. Effects of hypoxia and reoxygenation on the antioxidant defense system of the locomotor muscle of the crab *Neohelice granulata* (Decapoda, Varunidae). *J. Comp. Physiol. B* **2016**, *186*, 569–579. [CrossRef] [PubMed]
42. Hermes-Lima, M.; Zenteno-Savın, T. Animal response to drastic changes in oxygen availability and physiological oxidative stress. *Comp. Biochem. Physiol. Part C Toxicol. Pharmacol.* **2002**, *133*, 537–556. [CrossRef] [PubMed]
43. Welker, A.F.; Moreira, D.C.; Campos, É.G.; Hermes-Lima, M. Role of redox metabolism for adaptation of aquatic animals to drastic changes in oxygen availability. *Comp. Biochem. Physiol. Part A Mol. Integr. Physiol.* **2013**, *165*, 384–404. [CrossRef] [PubMed]
44. Lushchak, V.I.; Bagnyukova, T.V. Hypoxia induces oxidative stress in tissues of a goby, the rotan *Perccottus glenii*. *Comp. Biochem. Physiol. Part B Biochem. Mol. Biol.* **2007**, *148*, 390–397. [CrossRef] [PubMed]
45. Li, J.; Li, Y.; Liang, X.; Yang, Z.; Peng, Y.; Zhang, Y.; Ning, X.; Zhang, K.; Ji, J.; Wang, T. Blood redistribution preferentially protects vital organs under hypoxic stress in *Pelteobagrus vachelli*. *Aquat. Toxicol.* **2023**, *258*, 106498. [CrossRef] [PubMed]
46. Chapman, C.L.; Hess, H.W.; Worley, M.L. Heterogeneous redistribution of cerebral oxygen delivery to combined thermal and hypoxic exposure. *J. Physiol.* **2020**, *598*, 443–445. [CrossRef] [PubMed]

47. Qi, M.; Hou, Y.; Liu, T.; Miao, Y.; Zhuang, S.; Qu, X.; Liu, Q. Effects of acute hypoxia stress and reoxygenation recovery on oxidative stress and energy metabolism in juvenile Qingtian paddy fish. *Freshw. Fish* **2020**, *50*, 92–98. [CrossRef]
48. Xiong, X.; Huang, G.; Peng, Y.; Liu, X. Effects of hypoxia stress on growth, energy metabolism, and oxidative stress in juvenile mullet (*Mugil cephalus*). *J. Fish. China* **2016**, *40*, 73–82.
49. Fuhrmann, D.C.; Brüne, B. Mitochondrial composition and function under the control of hypoxia. *Redox Biol.* **2017**, *12*, 208–215. [CrossRef] [PubMed]
50. Cerretelli, P.; Gelfi, C. Energy metabolism in hypoxia: Reinterpreting some features of muscle physiology on molecular grounds. *Eur. J. Appl. Physiol.* **2011**, *111*, 421–432. [CrossRef] [PubMed]
51. Casanova, A.; Wevers, A.; Navarro-Ledesma, S.; Pruimboom, L. Mitochondria: It is all about energy. *Front. Physiol.* **2023**, *14*, 1114231. [CrossRef] [PubMed]
52. McMeekin, L.J.; Fox, S.N.; Boas, S.M.; Cowell, R.M. Dysregulation of PGC-1α-dependent transcriptional programs in neurological and developmental disorders: Therapeutic challenges and opportunities. *Cells* **2021**, *10*, 352. [CrossRef] [PubMed]
53. Tang, J.X.; Thompson, K.; Taylor, R.W.; Oláhová, M. Mitochondrial OXPHOS biogenesis: Co-regulation of protein synthesis, import, and assembly pathways. *Int. J. Mol. Sci.* **2020**, *21*, 3820. [CrossRef] [PubMed]
54. Kim, H.J.; Saikia, J.M.; Monte, K.M.A.; Ha, E.; Romaus-Sanjurjo, D.; Sanchez, J.J.; Moore, A.X.; Hernaiz-Llorens, M.; Chavez-Martinez, C.L.; Agba, C.K. Deep scRNA sequencing reveals a broadly applicable Regeneration Classifier and implicates antioxidant response in corticospinal axon regeneration. *Neuron* **2023**, *111*, 3953–3969.e3955. [CrossRef] [PubMed]
55. Wu, N.; Liu, X. The effect of L-arginine supplementation on mitochondrial biogenesis in skeletal muscle induced by endurance exercise in rats. In Proceedings of the Chinese Physiological Society, Annual Meeting of the Exercise Physiology Committee of Chinese Physiological Society and the Academic Seminar on "Exercise and Health", Guangzhou, China, 8 November 2013; Capital Institute of Physical Education: Beijing, China, 2013; pp. 101–102.
56. Bo, H.; Peng, P.; Qin, Y.; Zhang, Y. Effects of hypoxia combined with exercise on mitochondrial content in rat skeletal muscle. *Chin. J. Pathophysiol.* **2014**, *30*, 1461–1466.
57. Wu, J.; Ju, L.; Weng, X.; Xu, G.; Lin, W. Research progress on the effect of hypoxia stimulation on PGC-1α expression. *Chem. Life* **2016**, *36*, 81–87. [CrossRef]
58. Chen, Y.; Chen, R.; Yuan, R.; Huo, L.; Gao, H.; Zhuo, Y.; Chen, X.; Zhang, C.; Yang, S. Discovery of New Heterocyclic/Benzofuran Hybrids as Potential Anti-Inflammatory Agents: Design, Synthesis, and Evaluation of the Inhibitory Activity of Their Related Inflammatory Factors Based on NF-κB and MAPK Signaling Pathways. *Int. J. Mol. Sci.* **2023**, *24*, 3575. [CrossRef] [PubMed]
59. Ullah, S.; Feng, F.; Zhao, M.; Zhang, J.; Shao, Q. Comparative Effects of Dietary Supplementations with Microencapsulated Sodium Butyrate, Glycerol Monolaurate and Tributyrin on Growth, Immunity, and Gut Health in Black Sea Bream. *Animals* **2025**, *15*, 810. [CrossRef] [PubMed]
60. Wang, W.; Zeng, Z.; Huang, J.; Guo, Z.; Li, H.; Chen, G. Effects of hypoxia stress on growth, serum biochemistry, and non-specific immune indices of juvenile cobia (*Rachycentron canadum*). *Acta Ocean. Sin* **2021**, *43*, 49–58.
61. Mu, Y.; Li, W.; Wu, B.; Chen, J.; Chen, X. Transcriptome analysis reveals new insights into immune response to hypoxia challenge of large yellow croaker (*Larimichthys crocea*). *Fish Shellfish Immunol.* **2020**, *98*, 738–747. [CrossRef] [PubMed]
62. Lai, X.-X.; Zhang, C.-P.; Wu, Y.-X.; Yang, Y.; Zhang, M.-Q.; Qin, W.-J.; Wang, R.-X.; Shu, H. Comparative transcriptome analysis reveals physiological responses in liver tissues of *Epinephelus coioides* under acute hypoxia stress. *Comp. Biochem. Physiol. Part D Genom. Proteom.* **2022**, *43*, 101005. [CrossRef] [PubMed]
63. Takahashi, Y.; Ganster, R.W.; Gambotto, A.; Shao, L.; Kaizu, T.; Wu, T.; Yagnik, G.P.; Nakao, A.; Tsoulfas, G.; Ishikawa, T. Role of NF-κB on liver cold ischemia-reperfusion injury. *Am. J. Physiol.-Gastrointest. Liver Physiol.* **2002**, *283*, G1175–G1184. [CrossRef] [PubMed]

Disclaimer/Publisher's Note: The statements, opinions and data contained in all publications are solely those of the individual author(s) and contributor(s) and not of MDPI and/or the editor(s). MDPI and/or the editor(s) disclaim responsibility for any injury to people or property resulting from any ideas, methods, instructions or products referred to in the content.

biology

MDPI

Article

Effects of Dietary *Rhodotorula mucilaginosa* on Muscle Composition, Serum Biochemical Indicators, Antioxidant Capacity, Lipid Metabolism, and mTOR Signaling Pathway in Red Claw Crayfish (*Cherax quadricanatus*)

Liuqing Meng [1,†], Luoqing Li [1,†], Ziyi Ma [1], Wenyan He [1], Qin Zhang [1], Tong Tong [1], Dapeng Wang [2], Rui Wang [2], Huizan Yang [2], Yongqiang Liu [1,*] and Yin Huang [2,*]

[1] Guangxi Key Laboratory for Polysaccharide Materials and Modifications, School of Marine Sciences and Biotechnology, Guangxi Marine Microbial Resources Industrialization Engineering Technology Research Center, Guangxi Minzu University, 158 University Road, Nanning 530008, China; mengliuqing@stu.gxmzu.edu.cn (L.M.); liluoqing@stu.gxmzu.edu.cn (L.L.); maziyi@stu.gxmzu.edu.cn (Z.M.); hewenyan@stu.gxmzu.edu.cn (W.H.); zhangqin@gxmzu.edu.cn (Q.Z.); tongtong@gxmzu.edu.cn (T.T.)

[2] Guangxi Key Laboratory for Aquatic Genetic Breeding and Healthy Aquaculture, Guangxi Academy of Fishery Sciences, 8 Qingshan Road, Nanning 530021, China; oucwdp@163.com (D.W.); raywongxx@163.com (R.W.); yhzyang@163.com (H.Y.)

* Correspondence: liuyongqiang@gxmzu.edu.cn (Y.L.); hy033130@163.com (Y.H.)

† Liuqing Meng and Luoqing Li contributed equally to this work.

Simple Summary: Red claw crayfish (*Cherax quadricarinatus*) is an important aquatic species whose health and quality depend largely on diet. To assess the benefits of *Rhodotorula mucilaginosa*, we studied its effects on muscle composition, blood parameters, antioxidant capacity, and lipid metabolism. We tested four feed formulations containing 0, 0.1, 1.0, and 10.0 g/kg of the yeast. Results showed that *R. mucilaginosa* improved the crayfish's nutritional profile. Muscle protein, beneficial fatty acids, and essential nutrients such as amino acids and minerals increased. Blood analysis revealed higher levels of immune-boosting and antioxidant substances. The yeast also positively affected lipid metabolism and mTOR pathways. The optimal dose was found to be 1.0 g/kg. These findings support the development of more sustainable and nutritionally enhanced feeds for crayfish farming.

Abstract: This study investigated the effects of dietary supplementation with varying levels (CK: 0.0 g/kg; RL: 0.1 g/kg; RM: 1.0 g/kg; RH: 10.0 g/kg) of *Rhodotorula mucilaginosa* on muscle composition, serum biochemical indicators, antioxidant capacity, lipid metabolism, and the mTOR signaling pathway in red claw crayfish (*Cherax quadricarinatus*). Results showed that, compared to CK, treatment groups had higher muscle crude protein, fat, leucine, histidine, arginine, and essential amino acids ($p < 0.05$), and lower saturated fatty acids ($p < 0.05$). Treatment groups also exhibited increased activities of alkaline phosphatase, acid phosphatase, superoxide dismutase, catalase, glutathione S-transferase, lysozyme, albumin, total protein, and antioxidant capacity ($p < 0.05$), with reduced activities of aspartate aminotransferase, alanine aminotransferase, lactate dehydrogenase, and triglycerides ($p < 0.05$). In the hepatopancreas, treatment groups showed significant downregulation of AMP-activated protein kinase α, β, and γ, and carnitine palmitoyltransferase 1 genes ($p < 0.05$). Conversely, genes involved in lipid anabolism (peroxisome proliferator-activated receptor γ, acetyl-CoA carboxylase, fatty acid synthase, sterol regulatory element-binding protein, protein kinase B, and mammalian target of rapamycin 1 and 2) were upregulated ($p < 0.05$). In conclusion, *R. mucilaginosa* supplementation affects muscle composition, lipid metabolism, and mTOR signaling. The optimal dose is 1.0 g/kg.

Keywords: red claw crayfish; red yeast; lipid metabolism; signal pathway activation; gene expression

1. Introduction

Aquatic animals have a high demand for lipids, and the balance of lipid metabolism is directly related to their growth performance, immunity, and environmental adaptability [1]. As a primary source of energy, lipids play a crucial role in essential biological functions, including the synthesis of hormones, the regulation of the immune system, and signal transmission within cells [2]. They function not only as essential precursors for the synthesis of steroid hormones, which influence growth and reproductive processes, but also play a key role in preserving immune balance by modulating the activity and functionality of immune cells, including macrophages and T lymphocytes [3]. However, environmental stress can lead to disruptions in lipid metabolism, which in turn can cause serious problems such as liver dysfunction, impaired immune responses, and delayed growth and development, as seen in studies on juvenile turbot (*Scophthalmus maximus* L.) exposed to high temperatures [4]. In this complex physiological process, the mTOR signaling pathway, as a core regulatory pathway for cell growth, metabolism, and energy balance, regulates protein synthesis, lipid metabolism, and cell growth by integrating nutritional, energy, and growth factor signals [5]. When nutrient levels are adequate and lipid availability is optimal, the mTOR signaling pathway becomes activated. This activation leads to increased expression of fatty acid synthase genes and improves the activity of fatty acid transport proteins, helping to preserve intracellular lipid homeostasis in support of cell growth and essential physiological processes [6].

The red claw crayfish (*Cherax quadricarinatus*), a species of significant economic value in China, relies heavily on the nutritional quality of its feed for healthy development [7]. Since red claw crayfish cannot synthesize essential fatty acids like EPA and DHA de novo, it must rely on its feed to obtain these fatty acids and meet its physiological needs [8]. This dependency highlights the crucial role of lipid metabolism balance in the growth, molting, and immune regulation of crustaceans [9]. Once lipid metabolism becomes abnormal, crustaceans often face problems such as slow growth and molting failure [10].

At present, research on using probiotics to regulate animal lipid metabolism and improve body health has been attracting increasing attention. Dawood et al. found that adding probiotics *Lactobacillus* spp. to feed can effectively regulate the lipid metabolism of tilapia (*Oreochromis niloticus*) by regulating gut microbiota and host metabolism, which not only reduces liver fat deposition but also optimizes the fatty acid composition, thereby promoting the healthy growth of fish [11]. The study by Wang et al. also showed that adding the probiotic *Lactobacillus casei* to feed can improve the effectiveness of high-density lipoprotein cholesterol, reduce the levels of total cholesterol, triglycerides, and low-density lipoprotein cholesterol in the serum and liver tissues of largemouth bass (*Micropterus salmoides*), promote lipid metabolism, lower the blood lipid of largemouth bass, and help the healthy growth of fish [12].

Probiotics play crucial roles in antioxidant defense and immune regulation systems. During metabolic processes in aquatic organisms, homeostasis is maintained through a dynamic equilibrium between reactive oxygen species (ROS) generation and elimination, wherein the antioxidant enzyme defense system plays a pivotal role in reducing and neutralizing ROS [13]. Disruption of this ROS balance accelerates intracellular lipid peroxide formation, subsequently inducing oxidative damage [14]. Probiotics can mitigate oxidative stress damage to organisms by enhancing antioxidant enzyme activity and scavenging free

radicals, thereby preserving physiological health [15]. Total antioxidant capacity (T-AOC) serves as an indicator of an organism's comprehensive antioxidant capability, encompassing the collective action of all antioxidants (e.g., vitamins, enzymes, polyphenolic compounds), and is utilized to assess overall antioxidant status [16]. Superoxide dismutase (SOD) and catalase (CAT) are essential intracellular antioxidant enzymes that scavenge oxygen free radicals, converting superoxide radicals into non-toxic oxygen molecules and water, to maintain normal physiological functions [17]. Concurrently, probiotic-mediated immunomodulation is critically important, with numerous studies documenting yeast applications in aquaculture, such as evidence demonstrating that yeasts enhance antioxidant capacity and immunity in Pacific white shrimp (*Litopenaeus vannamei*), thereby promoting growth [18].

As an emerging probiotic additive, *Rhodotorula mucilaginosa* has been confirmed to possess multifaceted physiological functions and demonstrates unique advantages in regulating lipid metabolism compared to *Lactobacillus* spp., which primarily function by modulating gut microbiota balance and influencing host metabolic pathways; not only can it provide the organism with abundant nutrients, but it can also remodel energy metabolism and immune homeostasis by regulating the expression of lipid metabolism-related genes [19]. *Rhodotorula mucilaginosa* synthesizes bioactive carotenoids that enhance antioxidant capacity and immune function, critically improving health status and stress resistance in aquatic organisms [20]. Simultaneously, yeast-based probiotics have demonstrated promising application potential in aquaculture; for instance, yeast solid-state fermentation products and yeast cultures can significantly downregulate genes associated with lipid synthesis in the liver of zebrafish (*Danio rerio*), alleviate high-fat-diet-induced hepatic inflammation, and maintain organismal health through the regulation of lipid metabolism [21]. As a member of the yeasts, *Rhodotorula mucilaginosa* is also anticipated to play a positive role in aquaculture. Moreover, additional research demonstrates that Torularhodin—a β-carotenoid analog and bioactive component of *Sporidiobolus paradoxus*—functions as a PPAR-γ ligand; engaging in lipid metabolism via the PPAR signaling pathway; modulating key gene expression to enhance adipocyte differentiation and fatty acid uptake; while concurrently suppressing lipolysis [22]. Although the impact of *Rhodotorula mucilaginosa* on lipid metabolism in red claw crayfish has not been systematically investigated, and its capacity to produce bioactive compounds analogous to other yeasts remains unverified, the established physiological functionalities of this yeast, combined with foundational research on yeast-derived probiotics, substantiate its selection as a feed additive with significant research merit and translational potential.

Based on the above studies, this study selected *R. mucilaginosa* as a feed additive to investigate its effects on muscle composition, hemolymph biochemical indices, lipid metabolism, and the mTOR signaling pathway in red claw crayfish. The experimental results will provide a scientific basis for the development of efficient and environmentally friendly feed additives.

2. Materials and Methods

2.1. Experimental Diets

This research utilized freeze-dried *R. mucilaginosa* powder ($\geq 1 \times 10^{10}$ CFU/g, stored at −20 °C), provided by Guangzhou Xinhaili Biotechnology Co., Ltd. (Zhanjiang, China). The nutritional profile of the powder, on a wet weight basis, included 81.17% water content, 9.27% crude protein, 4.45% crude fat, 4.20% total triglycerides, and 1.30% β-glucan, along with 1.40 mg/kg of β-carotene, 1.00 mg/kg of astaxanthin, and 172.00 mg/kg of vitamin E.

Previous to the experimentation trial, a safety assessment was elaborated following Kang et al.'s protocol [23], utilizing healthy juvenile red claw crayfish (initial body weight

1.10 ± 0.09 g, length 3.08 ± 0.12 cm) purchased from the Nanning Breeding Base of Guangxi Academy of Fishery Sciences (Nanning, China). The red claw crayfish were randomly allocated into six groups (10 individuals/group) and reared in recirculating aquaculture systems under controlled conditions: temperature 26 ± 0.5 °C, ammonia nitrogen < 0.25 ppm, dissolved oxygen 4.7–6.2 mg/L, nitrite 0.01 ppm, nitrate < 10 ppm, pH 7.6 ± 0.2, with a 10 h photoperiod. The tanks measured 60 × 40 × 40 cm with a water flow rate of 2 L/min and a salinity of 0.5%. The treatment groups maintained *R. mucilaginosa* concentrations of 1×10^8 CFU/mL in water, while control groups received no supplementation, with three replicates per group. During the 7-day trial, growth and feeding behavior were monitored daily, with one-third water exchange, bacterial supplementation (treatment groups only), scheduled feeding, and thorough removal of residual feed and feces before/after feeding.

Based on Yang et al.'s findings [24] and safety evaluation data (1×10^8 CFU/mL), four isoproteic (35% CP) and isolipidic experimental diets were formulated with different inclusion levels (Table 1). The preparation protocol involved initially grinding basal feed (Guangdong Hengxing Feed Co., Ltd., Zhanjiang, China) through a 60-mesh sieve (250 μm pore size) to ensure particle uniformity, followed by precise division into four aliquots supplemented with 0 g/kg (Control group, CK), 0.1 g/kg (Low-concentration *R. mucilaginosa* group, RL), 1.0 g/kg (Middle-concentration *R. mucilaginosa* group, RM), and 10.0 g/kg (High-concentration *R. mucilaginosa* group, RH) *R. mucilaginosa* powder, respectively. The components were thoroughly blended for 15 min in a Hobart N50 mixer (Hobart Corporation, Troy, OH, USA) to achieve a consistent mixture. Sterile distilled water, accounting for 40% of the total weight, was then incorporated to create a dough-like consistency, which was subsequently processed into pellets using a Labtech LT-100 pellet mill (Labtech Engineering Co., Ltd., Samut Prakan, Thailand). The pellets, with a uniform diameter ranging from 1.00 to 1.50 mm, were air-dried in an oven (Memmert UN55, Memmert GmbH, Büchenbach, BY, Germany) at a temperature of 30 °C until their moisture level dropped below 10%. The resulting feed was preserved in sealed bags at −20 °C, and new batches were prepared on a weekly basis. To ensure bacterial stability during storage, the viability of live *R. mucilaginosa* in the feed was assessed weekly by plate counting. Detailed nutritional compositions are presented in Table 1.

To ensure the stability of live *R. mucilaginosa* during storage, the viability of the *R. mucilaginosa* in the feed was monitored weekly using standard plate counting throughout the 56-day experimental period [25]. Specifically, 1.0 g feed samples were vortexed with 9.0 mL sterile saline to prepare primary suspensions. Ten-fold serial dilutions were performed to achieve 10^3–10^8 concentration gradients. From each dilution, 0.1 mL aliquots were spread on nutrient agar plates in triplicate. All plates were incubated anaerobically at 35 °C for 48 h. Colony counts were recorded post-incubation using a colony counter. Viable counts were calculated as

$$\text{The number of viale} R.mucilaginosa = \mathrm{B} \times \frac{\mathrm{C}}{10} \times \mathrm{f}$$

In the above formula, B is the total number of plate colonies on nutrient agar medium, C is the number of *R. mucilaginosa* colonies identified from 10 colonies, and f is the dilution multiple.

Table 1. The formulation and composition of the experimental diets for red claw crayfish (g/kg of dried diet).

Ingredients	CK	RL	RM	RH
Fish meal	485.00	485.00	485.00	485.00
Soybean meal	119.30	119.20	118.30	109.30
Sorghum flour	106.50	106.50	106.50	106.50
Wheat flour	139.00	139.00	139.00	139.00
Corn flour	45.00	45.00	45.00	45.00
Soy Lecithin	10.00	10.00	10.00	10.00
Fish oil	15.20	15.20	15.20	15.20
Gelatin	20.00	20.00	20.00	20.00
Calcium carbonate	10.00	10.00	10.00	10.00
Choline chloride	5.00	5.00	5.00	5.00
Mineral premixes [a]	20.00	20.00	20.00	20.00
Vitamin premixes [b]	20.00	20.00	20.00	20.00
Vitamin C	5.00	5.00	5.00	5.00
Proximal composition [c] (% Dry Matter)				
Dry material	92.56	92.56	92.56	92.56
Ash	7.76	7.76	7.76	7.76
Ethereal extract	7.40	7.40	7.40	7.40
Crude protein	35.20	35.20	35.20	35.20
Crude lipid	7.84	7.84	7.84	7.84
Fiber	3.43	3.43	3.43	3.43

Note: All ingredients used in this study were sourced from Guangdong Hengxing Feed Co., Ltd. (Zhanjiang, China)., and are marketed under the brand name "Hengxing". [a] Mineral premixes (mg/kg): KCl, 0.5; $MgSO_4 \cdot 7H_2O$, 0.5; $ZnSO_4 \cdot 7H_2O$, 0.09; $MnCl_2 \cdot 4H_2O$, 0.0234; $CuSO_4 \cdot 5H_2O$, 0.005; KI, 0.005; $CoCl_2 \cdot 2H_2O$, 0.0025; Na_2HPO_4, 2.37. [b] Vitamin premixes (mg/kg): Vitamin B_{12}, 0.02; Vitamin A acetate, 5000 IU; Vitamin D_3, 4000 IU; α-tocopherol acetate, 100 IU; menadione, 5; thiamine HCl, 60; riboflavin, 25; pyridoxine HCl, 50; folic acid, 10; dl-capantothenic acid, 75; nicotinic acid, 5; biotin, 1; inositol, 5. [c] These values are calculated from the formulation and do not represent actual measured values.

Results showed that viable counts remained stable in each treatment group: $0.89 \pm 0.09 \times 10^6$ CFU/g (RL group), $0.97 \pm 0.12 \times 10^7$ CFU/g (RM group), and $0.92 \pm 0.16 \times 10^8$ CFU/g (RH group), with no significant fluctuations observed during storage. No viable *R. mucilaginosa* was detected in the control group (CK group). This confirmed that the viability of *R. mucilaginosa* was maintained under −20 °C storage conditions, ensuring the accuracy of the experimental doses across the treatment groups.

2.2. Experimental Animals and Husbandry Management

Healthy juvenile red claw crayfish, weighing 0.13 ± 0.06 g on average with an average body length of 0.58 ± 0.02 cm, were obtained from the Nanning Breeding Base affiliated with the Guangxi Academy of Fishery Sciences (Nanning, China) for use in this study. Before the start of the experiment, the crayfish were acclimated for a period of 7 days in a recirculating water system within the laboratory environment to ensure they adapted to the experimental conditions and achieved physiological stability. During acclimatization, the crayfish were fed a basal diet daily, and their health status was closely monitored. After acclimatization, healthy juveniles with uniform size, no physical damage, active behavior, and in the intermolt stage were selected for subsequent experiments. All experimental procedures were conducted by the Laboratory Animal Ethics Guidelines of Guangxi Minzu University, Nanning, China (Approval No. GXUN 2023-018).

The formal experiment was carried out in a static rearing system with tanks measuring 1 m × 2 m × 1 m (L × W × H), filled with fresh water to a depth of 70 cm (useful area of 1.4 m^2). Each tank contained sixteen PVC pipes (75 cm in diameter and 40 cm in length) to serve as shelters, offering hiding spots and minimizing stress. Continuous aeration was

provided through oxygen stones, while aquatic plants (*Eichhornia crassipes*) were added to each rearing tank, with four plants per tank, to replicate a natural ecosystem, promoting higher survival rates and improving dissolved oxygen levels. During the experimental period, water conditions were carefully controlled: temperature at 26 ± 0.5 °C, ammonia nitrogen below 0.25 ppm, dissolved oxygen ranging from 4.7 to 6.2 mg/L, nitrite at 0.01 ppm, nitrate under 10 ppm, and pH maintained at 7.6 ± 0.2. Additionally, a 10 h light cycle was implemented to reflect the natural habitat of red claw crayfish.

The experiment consisted of four groups: the CK group (0 g/kg) and three *R. mucilaginosa*-supplemented groups (RL, RM, and RH), with three replicates per group (totaling 12 tanks). Each tank was stocked with 50 juveniles (600 crayfish in total), resulting in a stocking density of 35.71 crayfish/m^3. The rearing period lasted 56 days. Daily observations were conducted to record growth performance and mortality, allowing timely adjustments in husbandry practices. Following established protocols [26], the daily feeding ratio was set at 5% of body weight, divided into two feedings (08:30 and 18:30), with each feeding administered in two rounds (30 min intervals), and adjusted based on actual consumption to ensure sufficient intake, with 50% of the total feeding provided at each feeding time. Every morning after feeding, residual feed and feces were promptly removed, and one-third of the water volume was exchanged to maintain water quality.

2.3. Sample Collection

After the experimental period, all red claw crayfish were fasted for 24 h before sample collection. First, an anticoagulant solution was prepared with glucose (20.5 g/L), sodium citrate (8 g/L), and sodium chloride (4.2 g/L), adjusted to pH 7.5, and then pre-chilled for later use. From each experimental replicate, 12 red claw crayfish were randomly selected, rinsed with sterile physiological saline, and then anesthetized in an ice-water mixture (0 °C) for 10 min to achieve immobilization by freezing. Using a 2.5 mL disposable syringe, 300 μL of pre-chilled anticoagulant was aspirated, and hemolymph was slowly drawn from the ventral sinus at the base of the first abdominal segment. The hemolymph was gently transferred into a 1.5 mL centrifuge tube and centrifuged at 1000× *g* for 10 min at 4 °C. The supernatant was aliquoted into fresh centrifuge tubes and immediately stored at −80 °C for subsequent analysis of hemolymph biochemical indicators and antioxidant enzyme activities (N = 12). After hemolymph collection, the crayfish were transferred to a laminar flow hood for sterile dissection. Abdominal muscle tissue was excised from ten crayfish per group. Muscle samples from five randomly selected crayfish were pooled into a sterile centrifuge tube, flash-frozen in liquid nitrogen, and then stored at −80 °C for subsequent muscle composition analysis (N = 5). Muscle samples from the remaining five crayfish were pooled into another sterile centrifuge tube, flash-frozen in liquid nitrogen, and then stored at −80 °C for subsequent analysis of amino acid and fatty acid composition (N = 5). Simultaneously, hepatopancreas tissue was extracted, weighed using an electronic balance (LICHEN, LC-3000A, Hunan, China), and homogenized in sterile physiological saline at a 1:10 (*w*/*v*) ratio. The homogenate was centrifuged at 1000× *g* for 10 min at 4 °C, and the supernatant was aliquoted into sterile centrifuge tubes before being stored at −80 °C (N = 10).

2.4. Determination of Muscle Composition and Nutritional Components

Abdominal muscle tissue from five crayfish per tank was pooled as test samples for the determination of conventional muscle composition. Following the method of Liu et al. [27], the nutritional composition of red claw crayfish muscle samples was analyzed in strict accordance with the standard methods of the Association of Official Analytical Chemists (AOAC, 2005). Crude lipid content was determined using the Soxhlet extraction method,

with anhydrous ether as the solvent, under continuous extraction at 65 °C for 6–8 h. Crude protein content was measured using the Kjeldahl method, where muscle samples were digested with concentrated sulfuric acid and then subjected to distillation titration in a Kjeldahl nitrogen analyzer (nitrogen-to-protein conversion factor: 6.25). Moisture content was determined by the constant-weight drying method, where samples were dried in a 105 °C oven until a constant weight was achieved (approximately 6–8 h). Ash content was measured using the high-temperature incineration method, where dried samples were incinerated in a muffle furnace (CHY, CHY-M1700, Zhengzhou, Henan, China) at 550 °C for 4–6 h until complete ashing.

Additionally, muscle tissue samples from five crayfish per tank were collected for nutritional composition analysis. Fatty acid composition was determined by extracting lipids with chloroform–methanol (2:1, *v*/*v*), followed by methylation with boron trifluoride-methanol (BF_3-MeOH), and analyzing fatty acid methyl esters (FAMEs) via gas chromatography with flame ionization detection (GC-FID). Total and free fatty acid contents in muscle were quantified according to China National Standard GB 5009.168-2016 (Determination of fatty acids in foods) [28]. Hydrolyzed amino acid profiles (17 analytes) were analyzed using a Hitachi L-8900 amino acid analyzer after acid hydrolysis (6 mol/L HCl, 110 °C, 24 h), following China National Standard GB 5009.124-2016 (Determination of amino acids in foods) [29].

2.5. Determination of Physiological-Biochemical Parameters and Antioxidant Enzyme Activities in Hemolymph

The hemolymph supernatant previously centrifuged and stored at −80 °C was thawed for analysis. According to the method described by Zhang et al. [30], biochemical parameters and antioxidant enzyme activities in the hemolymph of red claw crayfish were measured using the Rayto RT-6100 ELISA analyzer (Shenzhen, China) with reagent kits supplied by Nanjing Jiancheng Bioengineering Institute. Lysozyme (LZM) in hemolymph was measured by turbidimetry, with units of μg/mL. Alkaline phosphatase (AKP) and acid phosphatase (ACP) were measured by microplate enzymatic methods. The unit of AKP was defined as the amount of enzyme that produces 1 mg of phenol per 100 mL hemolymph after 15 min of reaction with substrate at 37 °C (King unit/100 mL). The unit of ACP was defined as the amount of enzyme that produces 1 mg of phenol per 100 mL hemolymph after 30 min of reaction with substrate at 37 °C (King unit/100 mL). Aspartate aminotransferase (AST) and alanine aminotransferase (ALT) were measured by the microplate method, with units of U/L. Lactate dehydrogenase (LDH) was measured by the microplate method, with one unit defined as the production of 1 μmol pyruvate per liter of serum after 15 min of reaction with substrate at 37 °C (U/L). Total protein (TP) was measured by the BCA microplate method (g/L). Albumin (ALB) was measured by the microplate enzymatic method (g/L). Glucose (GLU) was measured by the glucose oxidase method (mmol/L). Triglycerides (TG) were measured by the GPO-PAP enzymatic method (mmol/L). Total cholesterol (T-CHO) was measured by the COD-PAP method (mmol/L). Catalase (CAT) activity was determined by the ammonium molybdate method and expressed in U/mL, where one unit was defined as the amount of enzyme decomposing 1 μmol of H_2O_2 per second in 1 mL of hemolymph supernatant. Superoxide dismutase (SOD) activity was assayed using the WST-1 method, with one unit (U/mL) representing the enzyme quantity required to achieve 50% inhibition in the reaction system. Glutathione S-transferase (GST) and glutathione peroxidase (GPX) activities were measured colorimetrically, both reported in U/mL. One GST unit corresponds to a 1 mol/L decrease in reduced glutathione (GSH) per minute per mL of hemolymph supernatant at 37 °C after deducting non-enzymatic reactions. Similarly, one GPX unit was defined as the enzyme causing a 1 mol/L reduction of GSH in the system per 5 min per 0.1 mL of hemolymph supernatant at 37 °C, corrected for

non-enzymatic activity. Malondialdehyde (MDA) content in hemolymph was quantified by the thiobarbituric acid (TBA) assay and expressed in nmol/mL. Total antioxidant capacity (T-AOC) of hemolymph was evaluated using the ABTS radical cation decolorization assay, with results in mmol/L. Detailed protocols can be accessed at http://www.njjcbio.com/ (accessed on 8 March 2025).

2.6. Determination of Relative Expression Levels of Genes

Following the method of Liu et al. [31], real-time quantitative PCR (RT-qPCR) was used to detect the expression levels of related genes under RNase-free conditions. Specific primers for AMP-activated protein kinase α (*ampkα*), *ampkβ*, *ampkγ*, peroxisome proliferator-activated receptor γ (*pparγ*), adiponectin receptor (*adipor*), carnitine palmitoyltransferase 1 (*cpt1*), sterol regulatory element-binding protein (*srebp*), acetyl-CoA carboxylase (acc), fatty acid synthase (*fas*), protein kinase B (*akt*), mammalian target of rapamycin 1 (*mtor1*), and *mtor2* were designed using Primer Premier 6.0 software based on published gene sequences in GenBank. *β-Actin* was used as the reference gene for normalization, and primers were synthesized by Sangon Biotech (Shanghai, China). The primer sequences are listed in Table 2.

Table 2. Primer sequences for RT-qPCR in red claw crayfish.

Gene	Primer Sequence (5′→3′)	Amplicon Size (bp)	Tm (°C)	Gene Bank
fas [1]	F: TTGACTTCAAAGGTCCCAGC R: GGTTAGTACCTCCCACCACT	126	58	XM_053782425.1
acc [2]	F: GTCAGGAAGTTTGGAGGCAA R: TGAAATGAAAGGCACGGTCA	136	58	XM_053793522.1
cpt1 [3]	F: ACACCTGCCTATTGGTTGGG R: CTCAAGTCTTGGTGGGCTCC	142	60	XM_053797361.1
adipor [4]	F: AACGACAGTGTACGCCTCTG R: TGAGGAAAGGCAGCGTGAAG	155	60	XM_053787771.1
ampkα [5]	F: TTAAGTGGTGACCGAGGAGT R: AAACCTCGCTCATGATGTCC	186	60	XM_053773531.1
ampkβ [6]	F: ATGATGTAGGCTCGCAGAAC R: GCGGCTTGTCCTTATTGTTG	108	58	XM_053796745.1
ampkγ [7]	F: CTGACCCCTTCCTGGAAAAC R: AGGTCATAGGTGTGGTGGAA	97	58	XM_053773266.1
ppar-γ [8]	F: CGGATGGTGGTGGAGGAGTAGG R: CCCAGGAGCCAACGACAACAC	81	63	XM_053785396.1
srebp [9]	F: GTCTTCCTGGTGGGTCTCCTCTAC R: CGACTTCCGCCTCACTCTCAATG	85	63	XM_053788865.1
akt [10]	F: GGAAGCAGCAGCAGCAGTGG R: TGGAAGTTCGGCGGTCAATCATC	136	63	XM_053793380.1
mtor1 [11]	F: GGAGGAGGAGGAAGAAGAGGAAGC R: GCACAACACCAGAGCCACACTC	142	64	XM_053785700.1
mtor2 [12]	F: GTAGCGGCACTGCGGGTTG R: TTGGTGGGAGGTGGCTGGTG	175	64	XM_053771218.1
β-actin [13]	F: ATCACTGCTCTGGCTCCTGCTACC R: CGGACTCGTCGTACTCCTCCTTGG	148	60	XM_053800817.1

Note: F: Forward primer. R: Reverse primer. [1] *fas*: Fatty acid synthetase; [2] *acc*: acetyl-CoA carboxylase; [3] *cpt1*: Carnitine palmitoyltransferase 1; [4] *adiopor*: Adiponectin receptor; [5] *ampkα*: AMP-activated protein kinase α; [6] *ampkβ*: AMP-activated protein kinase β; [7] *ampkγ*: AMP-activated protein kinase γ; [8] *pparγ*: Proliferator-activated receptors γ; [9] *srebp*: Sterol-regulatory element binding proteins; [10] *akt*: Protein kinase B; [11] *mtor1*: Mammalian target of rapamycin 1; [12] *mtor2*: Mammalian target of rapamycin 2; [13] *β-actin*: Non-regulated reference gene.

After thawing the hepatopancreas homogenate supernatant stored at −80 °C, total RNA was extracted using the TaKaRa MiniBEST Universal RNA Extraction Kit (TaKaRa, Beijing, China). RNA concentration (30–1000 ng/μL) and purity (A260/A280 ratio of

1.9–2.1) were measured using a NanoDrop-2000 spectrophotometer, and integrity was verified by 1% agarose TAE gel electrophoresis. RNA was reverse transcribed into cDNA using PrimeScript™ RT Master Mix (Perfect Real Time) (TaKaRa, Beijing, China) according to the manufacturer's instructions. The reaction system (20 μL) consisted of 10 μL 2× Taqman PCR mix, 1 μL each of forward and reverse primers, RNA template, and DEPC-treated ddH_2O. Reaction conditions were 30 °C for 10 min, 42 °C for 15 min, 95 °C for 5 min, and 5 °C for 5 min.

RT-qPCR was performed using TB Green® Premix Ex Taq™ II (Tli RNaseH Plus) (TaKaRa, Beijing, China) on a LongGene Q2000B real-time PCR system. The reaction system contained 2 μL cDNA, 10 μL 2 × TB Green Premix Ex Taq II, 6.4 μL DEPC water, and 0.8 μL each of forward and reverse primers (final concentration 0.4 μM). Reaction conditions were pre-denaturation at 95 °C for 30 s; 40 cycles of PCR amplification (95 °C for 5 s, 60 °C for 20 s); and melting curve analysis (95 °C for 0 s, 65 °C for 15 s, 95 °C for 0 s). Each sample was analyzed in triplicate to minimize experimental error.

2.7. Data Calculation and Statistics Analysis

All experimental data were initially recorded and processed using Microsoft Excel 2019. Statistical analysis was performed using SPSS Statistics 25.0 software. One-way ANOVA was first conducted to determine significant differences among treatment groups. For a more precise comparison between groups, multiple comparisons were performed using the least significant difference (LSD) method. The significance level was set at $p < 0.05$. Statistically significant differences ($p < 0.05$) between groups were indicated by different letters, while non-significant differences ($p > 0.05$) were indicated by the same letters. Results were presented as mean ± standard deviation (Mean ± SD) to show data central tendency and dispersion. GraphPad Prism 8 software was used for the graphical presentation of data. For RT-qPCR data, the relative expression levels of target genes were calculated using the $2^{-\Delta\Delta CT}$ method [32].

3. Results

3.1. Muscle Composition and Nutritional Components

As shown in Table 3, compared to CK, the crude protein content in the muscle of red claw crayfish in the RM group was significantly increased ($p < 0.05$), while no significant differences were observed in the RL, RH, and CK groups ($p > 0.05$).

Table 3. The effects of *Rhodotorula mucilaginosa* in crayfish diets on the muscle composition.

Index	CK	RL	RM	RH	F-Value	*p*-Value
Moisture (%)	80.67 ± 1.79	80.23 ± 1.52	78.03 ± 1.41	79.57 ± 1.27	1.757	0.233
Ash (%)	5.38 ± 0.15	5.41 ± 0.13	5.41 ± 0.08	5.40 ± 0.12	0.040	0.989
Crude protein (%)	9.84 ± 0.23 ^{b}	10.37 ± 0.52 ^{a,b}	11.37 ± 0.55 ^{a}	10.90 ± 0.25 ^{a,b}	7.623	0.010
Crude lipid (%)	1.28 ± 0.03 ^{b}	1.30 ± 0.04 ^{b}	1.41 ± 0.05 ^{a}	1.39 ± 0.03 ^{a}	8.475	0.007

Note: All the data are presented as mean ± SD ($n = 3$). Within the same row, different superscript letters indicate significant differences between the values ($p < 0.05$).

Compared to the CK group, the crude lipid content in the muscle of red claw crayfish in the RM and RH groups was significantly increased ($p < 0.05$), while no significant differences were observed in the RL and CK groups ($p > 0.05$).

No significant differences were observed in the moisture and ash contents in the muscle of red claw crayfish in the treatment groups and the CK group ($p > 0.05$).

The effects of varying levels of *R. mucilaginosa* on the amino acid composition in the muscle of red claw crayfish are presented in Table 4. Among essential amino acids: arginine

(Arg) content in treatment groups was significantly higher than in CK group ($p < 0.05$), wherein the RM and RH groups exhibited significantly elevated arginine (Arg) content compared to the RL group ($p < 0.05$); the RM group displayed the highest leucine content, which was significantly greater than that of CK group ($p < 0.05$), yet demonstrated no statistically significant differences relative to the other two treatment groups; histidine content and total essential amino acid levels in both RM and RH treatment groups were significantly higher than those in CK group ($p < 0.05$), moreover, no significant differences in histidine content were detected between the RL group and all other groups ($p > 0.05$); whereas the total essential amino acid content in the RL group was significantly lower than in both RM and RH groups ($p > 0.05$); but showed no significant difference when compared with CK group ($p > 0.05$).

Table 4. The effects of *Rhodotorula mucilaginosa* in crayfish diets on the amino acid composition of muscle (g/100 g dry matter).

Index	CK	RL	RM	RH	F-Value	*p*-Value
Arginine	10.05 ± 0.07^{c}	10.18 ± 0.04^{b}	10.45 ± 0.12^{a}	10.32 ± 0.04^{a}	17.268	0.001
Histidine	2.3 ± 0.04^{b}	$2.33 \pm 0.03^{a,b}$	2.38 ± 0.03^{a}	2.39 ± 0.04^{a}	5.263	0.027
Isoleucine	3.55 ± 0.05	3.58 ± 0.03	3.67 ± 0.09	3.67 ± 0.07	2.669	0.119
Leucine	6.74 ± 0.07^{b}	$6.78 \pm 0.09^{a,b}$	6.89 ± 0.03^{a}	$6.85 \pm 0.04^{a,b}$	3.138	0.087
Lysine	7.56 ± 0.03	7.59 ± 0.04	7.62 ± 0.06	7.64 ± 0.04	2.121	0.176
Methionine	2.1 ± 0.05	2.14 ± 0.03	2.15 ± 0.02	2.14 ± 0.04	1.270	0.348
Phenylalanine	3.32 ± 0.04	3.29 ± 0.07	3.27 ± 0.07	3.29 ± 0.04	0.517	0.682
Threonine	3.4 ± 0.03	3.4 ± 0.04	3.37 ± 0.06	3.42 ± 0.03	0.793	0.531
Valine	3.91 ± 0.04	3.95 ± 0.03	3.99 ± 0.04	3.97 ± 0.06	1.749	0.234
Total essential amino acids	42.94 ± 0.23^{b}	43.23 ± 0.26^{b}	43.79 ± 0.06^{a}	43.68 ± 0.12^{a}	13.129	0.002
Alanine	4.53 ± 0.06	4.5 ± 0.06	4.52 ± 0.03	4.17 ± 0.52	1.281	0.345
Aspartic acid	9.04 ± 0.08	9.07 ± 0.09	9.08 ± 0.09	9.09 ± 0.09	0.135	0.937
Glutamic acid	14.91 ± 0.09	14.98 ± 0.11	15.09 ± 0.09	15.01 ± 0.09	1.974	0.196
Glycine	3.76 ± 0.09	3.8 ± 0.08	3.74 ± 0.09	3.85 ± 0.08	1.060	0.418
Proline	3.63 ± 0.06	3.65 ± 0.05	3.65 ± 0.07	3.65 ± 0.05	0.103	0.956
Serine	3.65 ± 0.08	3.72 ± 0.05	3.67 ± 0.05	3.71 ± 0.05	1.088	0.408
Tyrosine	3.77 ± 0.05	3.77 ± 0.03	3.78 ± 0.05	3.77 ± 0.05	0.026	0.994
Total non-essential amino acids	43.3 ± 0.31	43.48 ± 0.14	43.53 ± 0.19	43.26 ± 0.56	0.456	0.721
Total amino acids	86.24 ± 0.53	86.72 ± 0.33	87.32 ± 0.25	86.94 ± 0.58	3.078	0.090

Note: All the data are presented as mean ± SD ($n = 3$). Within the same row, different superscript letters indicate significant differences between the values ($p < 0.05$).

Non-essential amino acids and total amino acid content in muscle tissue of treatment groups manifested an increasing tendency relative to the CK group, although no statistically significant differences were observed among the experimental groups ($p > 0.05$).

The effects of *R. mucilaginosa* on the fatty acid composition in crayfish muscle are presented in Table 5. Saturated fatty acid (∑SFAs) content in the muscle tissue of treatment groups was significantly lower than that in the control group ($p < 0.05$). Specifically, the C14:0 content in the RH group was significantly reduced compared to the CK group ($p < 0.05$), yet showed no significant differences relative to either the RL group or the RM group ($p > 0.05$); whereas stearic acid (C18:0) content across all treatment groups was significantly elevated compared to the CK group ($p < 0.05$), with no statistically significant variations observed among the supplementation groups ($p > 0.05$).

Table 5. The effects of *Rhodotorula mucilaginosa* in crayfish diets on muscle fatty acid composition (% of total fatty acids).

Index	CK	RL	RM	RH	F-Value	*p*-Value
C14:0	0.4 ± 0.03 [a]	0.38 ± 0.02 [a,b]	0.36 ± 0.02 [a,b]	0.35 ± 0.03 [b]	2.568	0.127
C16:0	1.55 ± 0.03	1.53 ± 0.03	1.53 ± 0.03	1.53 ± 0.03	0.615	0.624
C17:0	0.39 ± 0.01	0.38 ± 0.01	0.38 ± 0.01	0.38 ± 0.01	0.800	0.528
C18:0	8.75 ± 0.04 [a]	8.7 ± 0.02 [b]	8.68 ± 0.02 [b]	8.66 ± 0.03 [b]	6.927	0.013
∑SFAs [1]	11.1 ± 0.05 [a]	10.99 ± 0.03 [b]	10.95 ± 0.06 [b]	10.93 ± 0.03 [b]	9.088	0.006
C16:1n-7	4.89 ± 0.04 [c]	4.99 ± 0.03 [b]	5.09 ± 0.04 [a]	5.12 ± 0.04 [a]	20.829	<0.001
C18:1n-9	25.55 ± 0.13 [c]	25.99 ± 0.12 [b]	26.48 ± 0.33 [a]	26.75 ± 0.24 [a]	17.251	0.001
∑MUFAs [2]	30.44 ± 0.14 [c]	30.98 ± 0.15 [b]	31.57 ± 0.34 [a]	31.87 ± 0.28 [a]	20.807	<0.001
C20:2n-9	0.88 ± 0.01	0.87 ± 0.01	0.88 ± 0.02	0.88 ± 0.01	0.889	0.487
C18:2n-6	14.4 ± 0.04 [b]	14.47 ± 0.09 [b]	14.61 ± 0.04 [a]	14.6 ± 0.05 [a]	9.125	0.006
C18:3n-6	0.18 ± 0.01	0.18 ± 0.01	0.18 ± 0.01	0.18 ± 0.01	1.222	0.363
C20:3n-6	3.33 ± 0.02	3.33 ± 0.02	3.33 ± 0.02	3.33 ± 0.02	0.111	0.951
C20:4n-6 (ARA [3])	0.81 ± 0.01 [b]	0.81 ± 0.01 [b]	0.85 ± 0.03 [a]	0.86 ± 0.02 [a]	6.838	0.013
C22:4n-6	1.1 ± 0.02	1.09 ± 0.03	1.09 ± 0.04	1.09 ± 0.03	0.190	0.900
∑n-6 PUFAs [4]	19.82 ± 0.04 [b]	19.87 ± 0.09 [b]	20.06 ± 0.03 [a]	20.06 ± 0.03 [a]	17.797	0.001
C18:3n-3	3.82 ± 0.06	3.82 ± 0.04	3.77 ± 0.09	3.71 ± 0.04	1.797	0.226
C20:5n-3 (EPA [5])	13.35 ± 0.29 [b]	13.79 ± 0.81 [b]	15.07 ± 0.28 [a]	15.31 ± 0.19 [a]	12.880	0.002
C22:5n-3	1.24 ± 0.03	1.25 ± 0.02	1.26 ± 0.02	1.26 ± 0.02	0.523	0.679
C22:6n-3 (DHA [6])	3.68 ± 0.05 [c]	3.74 ± 0.03 [b,c]	3.82 ± 0.05 [a,b]	3.84 ± 0.04 [a]	8.350	0.008
∑n-3 PUFAs [7]	22.1 ± 0.37 [b]	22.6 ± 0.86 [b]	23.92 ± 0.14 [a]	24.12 ± 0.19 [a]	12.680	0.002
∑PUFAs [8]	42.8 ± 0.39 [b]	43.34 ± 0.82 [b]	44.86 ± 0.15 [a]	45.06 ± 0.18 [a]	17.018	0.001
∑LC-PUFAs [9]	23.52 ± 0.31 [b]	24 ± 0.82 [b]	25.43 ± 0.21 [a]	25.68 ± 0.17 [a]	16.007	0.001
n-3/n-6	1.11 ± 0.02 [b]	1.14 ± 0.05 [b]	1.19 ± 0.01 [a]	1.2 ± 0.01 [a]	8.611	0.007
DHA+EPA	17.04 ± 0.33 [b]	17.53 ± 0.83 [b]	18.89 ± 0.23 [a]	19.15 ± 0.16 [a]	14.37	0.001
DHA/EPA	0.28 ± 0.01 [a]	0.27 ± 0.01 [a]	0.25 ± 0.01 [b]	0.25 ± 0.01 [b]	6.536	0.015
∑FAI [10]	84.34 ± 0.51 [b]	85.31 ± 0.96 [b]	87.37 ± 0.42 [a]	87.85 ± 0.48 [a]	21.196	<0.001

Note: All the data are presented as mean ± SD (n = 3). Within the same row, different superscript letters indicate significant differences between the values ($p < 0.05$). [1] ∑SFAs: Saturated fatty acids; [2] ∑MUFAs: Monounsaturated fatty acids; [3] ARA: Arachidonic acid; [4] ∑n-6 PUFAs: n-6 Polyunsaturated fatty acids; [5] EPA: Eicosapentaenoic acid; [6] DHA: Docosahexaenoic acid; [7] ∑n-3 PUFAs: n-3 Polyunsaturated fatty acids; [8] ∑PUFAs: Polyunsaturated fatty acids; [9] ∑LC-PUFAs: Long-chain polyunsaturated fatty acids; [10] ∑FAI: Fatty acid index.

Monounsaturated fatty acid (∑MUFAs) levels in the muscle of treatment groups were significantly higher than those in the CK group ($p < 0.05$). Notably, palmitoleic acid (C16:1n-7) and oleic acid (C18:1n-9) content in both RM and RH groups were significantly greater than in both CK and RL groups ($p < 0.05$). Polyunsaturated fatty acid (∑PUFAs), ∑n-6 PUFAs, and ∑n-3 PUFAs contents in the muscle tissue of the RM and RH groups demonstrated significant increases relative to the CK group ($p < 0.05$). Specifically, linoleic acid (C18:2n-6), arachidonic acid (C20:4n-6), and eicosapentaenoic acid (C20:5n-3, EPA) levels in the RM and RH groups were significantly higher than in the RL group ($p < 0.05$); whereas no significant difference in docosahexaenoic acid (C22:6n-3, DHA) content was observed between the RM and RL groups ($p > 0.05$).

Long-chain polyunsaturated fatty acid (∑LC-PUFAs) content, total DHA+EPA content, n-3/n-6 PUFA ratio, and fatty acid index (∑FAI) in RM and RH groups were all significantly elevated compared to the other two groups ($p < 0.05$), while the DHA/EPA ratio was significantly lower than in the other treatment groups ($p < 0.05$).

3.2. Physiological-Biochemical Parameters and Antioxidant Enzyme Activities in Hemolymph

As shown in Table 6, red claw crayfish in all treatment groups exhibited significantly higher AKP and ACP activities than the CK group ($p < 0.05$). In contrast, the activities of AST, ALT, and LDH were significantly reduced in all three treatment groups ($p < 0.05$).

Table 6. The effects of *Rhodotorula mucilaginosa* in crayfish diets on the hemolymph biochemical indices.

Index	CK	RL	RM	RH	F-Value	*p*-Value
AKP 1 (King unit/100 mL)	18.76 ± 0.24 ^{c}	20.46 ± 0.38 ^{b}	22.17 ± 0.11 ^{a}	20.73 ± 0.68 ^{b}	11.481	0.003
ACP 2 (King unit/100 mL)	16.10 ± 0.41 ^{b}	18.11 ± 0.51 ^{a}	18.81 ± 0.29 ^{a}	17.71 ± 0.38 ^{a}	24.115	<0.001
AST 3 (U/L)	2.51 ± 0.14 ^{a}	1.65 ± 0.09 ^{b}	1.16 ± 0.21 ^{b}	1.40 ± 0.13 ^{b}	15.869	0.001
ALT 4 (U/L)	1.65 ± 0.08 ^{a}	1.13 ± 0.07 ^{b}	0.93 ± 0.04 ^{b}	1.05 ± 0.11 ^{b}	16.514	0.001
LZM 5 (μg/mL)	212.12 ± 6.31 ^{c}	224.24 ± 6.43 ^{c}	282.83 ± 2.67 ^{a}	262.63 ± 2.67 ^{b}	46.203	<0.001
LDH 6 (U/L)	1476.92 ± 106.59 ^{a}	1219.38 ± 63.96 ^{b}	1015.38 ± 53.29 ^{b}	1083.08 ± 67.69 ^{b}	7.275	0.011
TP 7 (g/L)	44.00 ± 0.66 ^{c}	48.85 ± 0.82 ^{b}	51.48 ± 0.35 ^{a}	48.46 ± 0.60 ^{b}	72.653	<0.001
ALB 8 (g/L)	18.83 ± 0.11 ^{c}	19.46 ± 0.11 ^{c}	22.74 ± 0.59 ^{a}	21.47 ± 0.46 ^{b}	22.41	<0.001
GLU 9 (mmol/L)	5.46 ± 0.02 ^{a}	5.11 ± 0.11 ^{a}	4.55 ± 0.17 ^{b}	5.13 ± 0.03 ^{a}	13.193	0.002
TG 10 (mmol/L)	6.07 ± 0.04 ^{a}	5.9 ± 0.02 ^{b,c}	5.69 ± 0.11 ^{c}	5.94 ± 0.04 ^{b}	19.006	0.001
T-CHO 11 (mmol/L)	10.14 ± 0.22	10.21 ± 0.17	9.75 ± 0.24	10.25 ± 0.37	2.552	0.129

Note: All the data are presented as mean ± SD (n = 3). Within the same row, different superscript letters indicate significant differences between the values ($p < 0.05$). [1] AKP: Alkaline phosphatase; [2] ACP: Acid phosphatase; [3] AST: Glutamic-oxalacetic transaminase; [4] ALT: Glutamic-pyruvic transaminase; [5] LZM: Lysozyme; [6] LDH: Lactate dehydrogenase; [7] TP: Total protein; [8] ALB: Albumin; [9] GLU: Glucose; [10] TG: Triglyceride; [11] T-CHO: Total cholesterol.

LZM activity was significantly elevated in the RM and RH treatment groups ($p < 0.05$), whereas no significant difference was observed between the RL and control groups ($p > 0.05$). TP content in the hemolymph was significantly increased in all treatment groups ($p < 0.05$), while ALB content was significantly enhanced only in the RM and RH treatment groups ($p < 0.05$).

Regarding energy metabolism, GLU content significantly decreased only in the RM group ($p < 0.05$), and TG levels were significantly lower in all treatment groups compared to the CK group ($p < 0.05$). T-CHO content, however, showed no significant difference among any groups ($p > 0.05$).

The effects of *R. mucilaginosa* on antioxidant enzyme activities in crayfish hemolymph are shown in Table 7. *R. mucilaginosa* supplementation groups enhanced SOD, CAT, GPX, and GST activities as well as T-AOC, while reducing MDA content in hemolymph. Specifically, SOD, CAT, and GST activities, along with T-AOC in treatment groups, were significantly elevated compared to the CK group ($p < 0.05$), with no significant variations observed among supplementation groups ($p > 0.05$).

Table 7. The effects of *Rhodotorula mucilaginosa* in crayfish diets on the activity of antioxidant enzymes in the hemolymph.

Index	CK	RL	RM	RH	F-Value	*p*-Value
SOD [1] (U/mL)	106.98 ± 4.88 ^{b}	127.21 ± 2.09 ^{a}	126.05 ± 2.97 ^{a}	119.3 ± 1.63 ^{a}	8.685	0.007
CAT [2] (U/mL)	2.95 ± 0.12 ^{c}	3.46 ± 0.08 ^{b}	4.02 ± 0.03 ^{a}	3.57 ± 0.15 ^{b}	30.044	<0.001
GST [3] (U/mL)	15.09 ± 0.98 ^{c}	20.35 ± 0.93 ^{b}	27.37 ± 0.91 ^{a}	22.98 ± 0.93 ^{b}	30.044	<0.001
GPX [4] (U/mL)	360.63 ± 11.01 ^{b}	401.68 ± 6.83 ^{a}	416.84 ± 4.77 ^{a}	365.68 ± 14.8 ^{b}	7.334	0.011
MDA [5] (nmol/mL)	1.83 ± 0.07 ^{a}	1.32 ± 0.07 ^{b,c}	1.22 ± 0.12 ^{c}	1.6 ± 0.09 ^{a,b}	9.261	0.006
T-AOC [6] (mmol/L)	0.64 ± 0.03 ^{c}	0.67 ± 0.01 ^{b}	0.71 ± 0.01 ^{a}	0.67 ± 0.04 ^{b}	108.453	<0.001

Note: All the data are presented as mean ± SD (n = 3). Within the same row, different superscript letters indicate significant differences between the values ($p < 0.05$). [1] SOD: Superoxide dismutase; [2] CAT: Catalase; [3] GST: Glutathione S-transferase; [4] GPX: Glutathione peroxidase; [5] MDA: Malondialdehyde; [6] T-AOC: Total antioxidant capacity.

Furthermore, relative to the CK group, only the RL and RM treatment groups demonstrated significantly enhanced GPX activity and markedly reduced MDA content ($p < 0.05$), whereas no significant differences in GPX activity or MDA content were detected in the RH group ($p > 0.05$).

3.3. Lipid Metabolism and mTOR Signaling Pathway

Compared to the CK group, the relative expression levels of *adipor*, *ampkα*, *ampkβ*, and *ampkγ* genes in the hepatopancreas of red claw crayfish in the RL, RM, and RH groups significantly decreased ($p < 0.05$). Compared to the CK group, the relative expression level of *the cpt1* gene in the hepatopancreas of red claw crayfish in the RM and RH groups significantly decreased ($p < 0.05$), while no significant differences were observed in the RL group and CK group ($p > 0.05$), as shown in Figure 1.

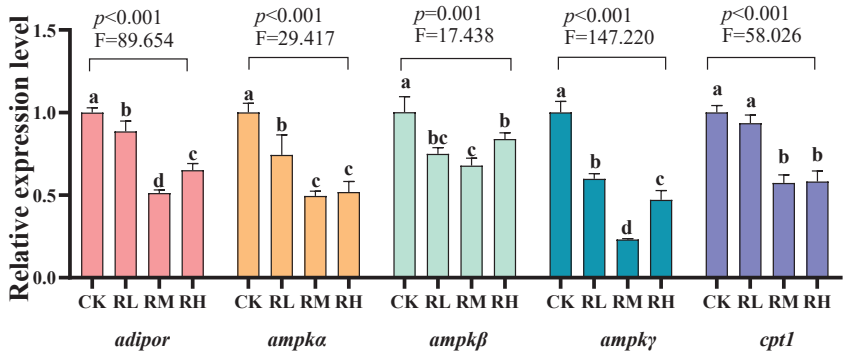


Figure 1. Effects of *Rhodotorula mucilaginosa* on the relative expression levels of adiponectin receptor (*adiopor*), AMP-activated protein kinase α (*ampkα*), AMP-activated protein kinase β (*ampk*β), AMP-activated protein kinase γ (*ampk*γ), and carnitine palmitoyltransferase 1 (*cpt1*) genes in the hepatopancreas of red claw crayfish. All the data are presented as mean ± SD ($n = 3$). Within the same figure, different superscript letters indicate significant differences between the values ($p < 0.05$).

Compared to the CK group, the relative expression levels of *fas* and *pparγ* genes in the hepatopancreas of red claw crayfish in the RL, RM, and RH groups significantly increased ($p < 0.05$). The relative expression level of the *acc* gene in the hepatopancreas of red claw crayfish in the RL and RM groups significantly increased ($p < 0.05$). The relative expression level of the *srebp* gene in the hepatopancreas of red claw crayfish in the RM and RH groups significantly increased ($p < 0.05$), as shown in Figure 2.

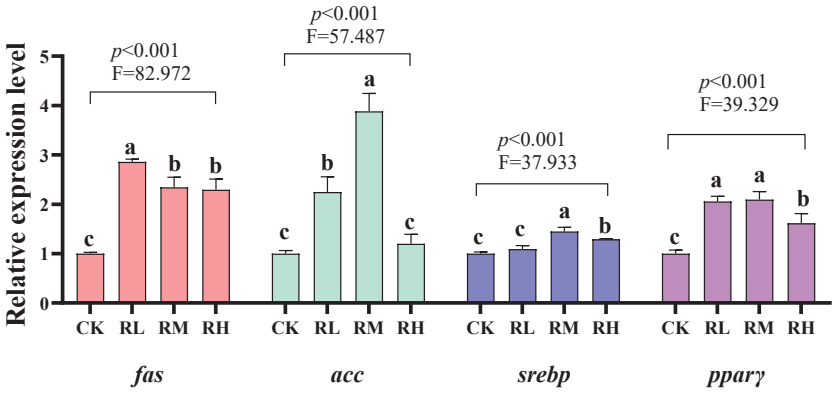


Figure 2. Effects of *Rhodotorula mucilaginosa* on the relative expression levels of fatty acid synthetase (*fas*), acetyl-CoA carboxylase (*acc*), sterol-regulatory element binding proteins (*srebp*), and proliferator-activated receptors γ (*pparγ*) genes in the hepatopancreas of red claw crayfish. All the data are presented as mean ± SD ($n = 3$). Within the same figure, different superscript letters indicate significant differences between the values ($p < 0.05$).

Compared to the CK group, the relative expression levels of the *akt*, *mtor1*, and *mtor2* genes in the hepatopancreas of red claw crayfish in the RM and RH groups significantly increased ($p < 0.05$), while no significant differences were observed in the RL and CK groups ($p > 0.05$), as shown in Figure 3.

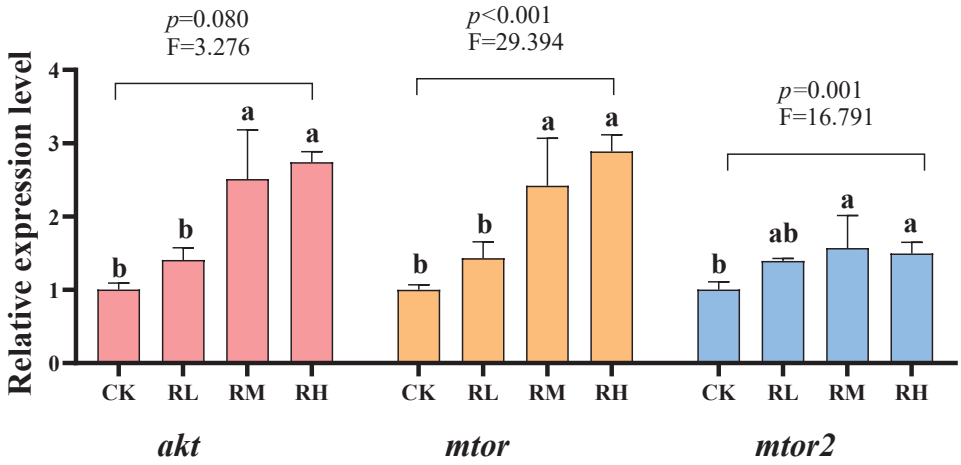


Figure 3. Effects of *Rhodotorula mucilaginosa* on the relative expression levels of protein kinase B (*akt*), mammalian target of rapamycin (*mtor*), and mammalian target of rapamycin 2 (*mtor2*) genes in the hepatopancreas of red claw crayfish. All the data are presented as mean ± SD ($n = 3$). Within the same figure, different superscript letters indicate significant differences between the values ($p < 0.05$).

4. Discussion

4.1. The Effect of Rhodotorula Mucilaginosa on the Muscle Composition and Nutritional Quality in Red Claw Crayfish

Variations in feed composition exert significant influences on the nutritional profile of shrimp meat, which consequently mirrors the metabolic status and growth potential of crustaceans [33]. The nutritional composition of muscle tissue, such as crude protein, crude fat, ash, and moisture content, serves as an important biological indicator for assessing the growth performance and health status of shrimp, as these components are influenced by dietary composition and other environmental factors [34]. The current experimental findings reveal that incorporating varying concentrations of *R. mucilaginosa* into the diet significantly influences the muscle composition of red claw crayfish. Notably, the RM group displayed markedly higher levels of crude protein and lipids in the muscle tissue when compared to the untreated CK group. This suggests that *R. mucilaginosa* can enhance the nutritional value of crayfish. The potential mechanism behind this effect may be attributed to the nutrient-rich composition of *R. mucilaginosa*, which supplies key metabolic precursors, such as amino acids and fatty acids, that activate the mTOR signaling pathway, subsequently promoting increased protein and lipid synthesis [35]. Furthermore, functioning as a probiotic, *R. mucilaginosa* modulates enteroendocrine system functionality to enhance nutrient absorption efficiency, ultimately augmenting protein and lipid retention capacity [27]. Parallel findings documented that probiotic supplementation significantly increased crude protein and ash content in the muscle of Pacific white shrimp (*Litopenaeus vannamei*) [36]. Chen et al. observed that a 1% dietary inclusion of marine red yeast (*Rhodotorula* spp.) elevated crude protein levels in tilapia [37]. Furthermore, this study observed no significant increase in crude muscle protein content in the RH group, a phenomenon potentially attributable to the dose-dependent effects of probiotics. Specifically, the excessively high dose of *R. mucilaginosa* may trigger sustained hyperactivation of immune responses, thereby elevating metabolic burden. This process diverts substantial energy and protein resources—originally

allocated for growth—toward immune processes; ultimately reducing energy partitioning for protein synthesis and resulting in the absence of significant crude protein elevation [38].

The types and composition of amino acids are crucial for the growth and development of aquatic organisms, wherein the variety and proportional composition of essential amino acids constitute a core indicator determining the nutritional value of proteins, while the amino acid content in aquatic products serves as a key parameter directly reflecting their nutritional quality [39]. Protein content directly influences muscle growth and nutritional value in crustaceans, and the crux lies in the fact that proteins consist of diverse amino acids, among which the content of essential amino acids (EAAs) represents a vital metric for assessing muscle nutritional value [40]. Results from this study demonstrate that dietary supplementation with *R. mucilaginosa* significantly enhances the content of essential amino acids (arginine, histidine, and leucine) in the muscle of red claw crayfish. Arginine (Arg), as a critical precursor for protein synthesis, not only participates in polyamine biosynthesis, hormonal secretion regulation, and immune function enhancement, but also exerts significant effects on animal growth and cardiovascular health through nitric oxide (NO) generation [41]. Histidine, an essential alkaline amino acid for crustaceans, promotes DNA and protein synthesis by participating in one-carbon metabolism; its imidazole side chain renders it a direct precursor of carnosine and histamine, playing pivotal roles in maintaining homeostasis, regulating muscle pH and osmolality, scavenging reactive oxygen species, and modulating immune functions [42]. Leucine, a key branched-chain amino acid, promotes protein synthesis by activating the mTOR pathway while regulating energy metabolism and glucose homeostasis; it is indispensable for normal growth and reproduction in fish, particularly in stimulating protein synthesis within muscle tissue [43]. Recent research by Xiao et al. [44] revealed that total essential amino acid (TEAA) content in the muscle of greasyback shrimp (*Metapenaeus ensis*) increases with escalating dietary protein levels. Their study indicated that under high-protein feeding regimes, surplus essential amino acids are channeled into catabolism for energy production, whereas low-protein diets induce amino acid deficiencies that subsequently inhibit protein synthesis in shrimp muscle, thereby reducing muscle protein content. In the present experiment, we observed increased essential amino acid content concomitant with elevated crude protein levels in red claw crayfish muscle. Consequently, we posit that this phenomenon may be attributed to the abundant protein constituents in *R. mucilaginosa*, which fulfill the high-protein dietary requirements of red claw crayfish. This suggests that *R. mucilaginosa* not only facilitates the accumulation of essential amino acids but also optimizes the nutritional profile of shrimp muscle by enhancing protein provision. Analogously, Seenivasan et al. [45] reported that *Bacillus subtilis* supplementation elevates arginine, histidine, and leucine content in the muscle of freshwater prawn (*Macrobrachium rosenbergii*).

Fatty acid content and composition in muscle tissue critically determine the nutritional value of aquatic organisms and profoundly influence their flavor profile [40]. Muscle fatty acids are categorized into saturated fatty acids (SFAs) and unsaturated fatty acids (UFAs). In crustaceans, specific fatty acid compositions not only impact their intrinsic health and growth but also determine the quality of their muscle tissues. Research has demonstrated that optimizing feed formulations to reduce saturated fatty acid (SFA) content and increase unsaturated fatty acid (UFA) levels in muscles exerts a proven positive effect on enhancing both the nutritional physiological status and muscle quality of crustaceans themselves [46]. In this experiment, decreased SFA content concomitant with elevated UFA levels in crayfish muscle indicates that *R. mucilaginosa* supplementation enhances muscle quality by modulating fatty acid composition. Studies confirm that MUFAs play vital roles in regulating lipid metabolism, reducing LDL oxidation susceptibility, protecting vascular endothelial function, and attenuating blood hypercoagulability, thereby mitigating cardiovascular

disease risks, including coronary heart disease [47]. This study revealed that *R. mucilaginosa* significantly increased palmitoleic acid (C16:1n-7), oleic acid (C18:1n9c), and total MUFA content in crayfish muscle, consistent with alterations in lipid metabolism-related genes, demonstrating its capacity to modulate lipid metabolism via MUFA enrichment. PUFAs markedly enhance aroma and reflect muscle juiciness, with EPA and DHA serving as critical n-3 fatty acids that are key indicators of lipid nutritional value [48]. EPA must be obtained from dietary sources, while DHA is essential for brain development [49]. Higher n-3/n-6 ratios, particularly those rich in EPA and DHA, confer benefits for inflammation control and cardiovascular disease prevention [46]. Additionally, ARA exerts positive effects on growth promotion, immune function enhancement, and antioxidant capacity improvement [50]. This investigation found significantly elevated levels of PUFAs, n-3 PUFAs, linoleic acid (C18:2n6c), ARA (C20:4n6), n-6 PUFAs, EPA (C20:5n3), DHA (C22:6n3), long-chain PUFAs (LC-PUFAs), DHA+EPA, n-3/n-6 ratio, and fatty acid index (FAI) in crayfish muscle, whereas the DHA/EPA ratio was significantly reduced. These findings indicate that *R. mucilaginosa* enhances muscle quality, elevates nutritional value, and boosts immune competence in crayfish. The significantly elevated unsaturated fatty acid (UFA) content observed in crayfish muscle in this study may be attributed to the inherent UFA-rich properties of dietary-supplemented *Rhodotorula mucilaginosa*, which functions as an exogenous UFA source that undergoes digestive absorption and deposition in muscle tissue [51]. Results from Rasool et al. [52] and Mang et al. [53] were consistent with the present experimental outcomes.

4.2. The Effect of Rhodotorula Mucilaginosa on the Hemolymph Biochemical Indices and Antioxidant Enzyme Activities in Red Claw Crayfish

As an important body fluid in aquatic animals, the biochemical indices of hemolymph can reflect the health, immune, and metabolic status of the organism [54]. In this experiment, the addition of *R. mucilaginosa* significantly increased the activities of AKP, ACP, and LZM in the hemolymph of red claw crayfish, indicating that it can promote the synthesis of metabolic immune enzymes in crayfish and enhance disease resistance and immunity. This may be related to the presence of β-glucan in *R. mucilaginosa* cells, which binds to high-density lipoproteins and activates the prophenoloxidase system, thereby enhancing the activity of immune-related enzymes [55]. Similar results have been reported in Pacific white shrimp [35].

AST and ALT are key indicators reflecting liver function, and an increase in their activities often suggests hepatopancreas damage or metabolic disorders [53]. In this experiment, *R. mucilaginosa* significantly reduced the activities of ALT and AST, indicating that it can alleviate stress in crayfish and maintain stable metabolic function. This may be attributed to the prebiotic components in yeast activating the Toll-like receptor pathway and enhancing the phagocytic activity of hemocytes to improve hepatopancreas health [56]. A similar effect has been demonstrated in Pacific white shrimp with the use of *Bacillus* T23 [57].

LDH, a key enzyme in glycolysis, exhibits increased activity during organismal stress or tissue damage [58], while blood glucose levels reflect the state of energy metabolism [59]. This experiment showed that *R. mucilaginosa* significantly reduced LDH activity and blood glucose levels in the hemolymph of red claw crayfish. It is speculated that this may be due to astaxanthin in yeast activating the AMPK signaling pathway to regulate glycolysis, consume energy, and produce ATP through glucose metabolism [60].

TP and ALB levels can be used to evaluate the immune status of aquatic animals [61]. In this study, the *R. mucilaginosa* groups exhibited higher TP and ALB levels compared to the CK group, which may be related to the astaxanthin and mannan oligosaccharides in yeast increasing metabolic rates and accelerating protein synthesis [27]. TG is an important energy source for the organism, and fluctuations in T-CHO levels can reflect lipid metabolism

in the liver [62]. In this experiment, *R. mucilaginosa* significantly reduced TG levels but had no significant effect on T-CHO, indicating its beneficial role in metabolic activities. This may be attributed to the nutrient-rich composition of *R. mucilaginosa* enhancing lipase activity and improving lipid metabolism [63]. These findings are consistent with the results reported by Liu et al., where the addition of *R. mucilaginosa* to tilapia feed led to increased serum TP and ALB levels and decreased GLU, TG, and T-CHO levels [27].

This study observed significantly enhanced SOD and CAT activities along with elevated T-AOC in crayfish hemolymph, indicating that *R. mucilaginosa* strengthens antioxidant capacity, mitigates oxidative stress, and preserves physiological integrity—effects we attribute primarily to yeast-derived carotenoids; particularly β-carotene and astaxanthin [38]. Carotenoids function as potent antioxidants that effectively scavenge oxygen radicals, attenuate cellular oxidative damage, and modulate SOD/CAT activities [64], consistent with findings reported by Kieliszek et al. [65]. GPX eliminates hydrogen peroxide and other peroxides to protect cells from oxidative injury, while GST facilitates ROS clearance through concerted action with GPX in hydrogen peroxide detoxification [66]. Significantly increased GPX and GST activities observed herein may result from astaxanthin in red yeast maintaining cellular redox homeostasis and reducing ROS levels, thereby indirectly potentiating these enzymatic activities [67]. MDA, as a lipid peroxidation end-product, quantitatively reflects cellular oxidative damage [68]. Our results demonstrated significantly reduced MDA content in the hepatopancreas of *R. mucilaginosa*-supplemented red claw crayfish. This reduction likely stems from β-glucans and mannans in the yeast cell wall forming complexes with Fe^{2+}, inhibiting hydroxyl radical (·OH) generation, consequently disrupting lipid peroxidation chain reactions, and decreasing MDA production [69]. Analogous results were reported by Sriphuttha et al. [70], where *Rhodotorula paludigena* enhanced antioxidant and immune capacities in Pacific white shrimp (*Litopenaeus vannamei*). Similarly, Wang et al. documented that selenium yeast supplementation boosts antioxidant capability in Chinese mitten crab (*Eriocheir sinensis*) [71].

4.3. Effects of Rhodotorula Mucilaginosa on Lipid Metabolism and mTOR Signaling Pathway in Red Claw Crayfish

Lipid metabolism, serving as a fundamental physiological process governing the synthesis, degradation, and transport of fatty acids, triglycerides, and related compounds, plays a pivotal role in the growth, development, and health maintenance of aquatic species [72]. This study revealed that *R. mucilaginosa* supplementation downregulated the expression of key fatty acid β-oxidation genes (including *ampkα*, *ampkβ*, *ampkγ*, *adipor*, and *cpt1*) in the hepatopancreas of crayfish, suggesting its potential regulatory effects on energy sensing and signal transduction pathways. AMP-activated protein kinase (AMPK), functioning as an energy-sensing kinase, becomes activated under low ATP conditions to restore energy homeostasis by enhancing fatty acid oxidation while suppressing lipid synthesis. The *adipor* potentiates fatty acid uptake and oxidation by transducing adiponectin signals to activate AMPK and its downstream pathways [73]. Carnitine palmitoyl transferase 1 (CPT1), the rate-limiting enzyme for mitochondrial fatty acid β-oxidation, exhibits reduced activity when downregulated, thereby impeding the transport of fatty acyl-CoA into mitochondria and attenuating oxidative processes [74]. The observed gene downregulation may stem from dual mechanisms: primarily, the protein-, polysaccharide-, and carotenoid-rich composition of *R. mucilaginosa* [35] could elevate cellular ATP levels, diminishing AMPK pathway activation and consequently suppressing *ampkα*, *ampkβ*, *ampkγ*, and *cpt1* expression. Alternatively, *R. mucilaginosa* might disrupt adiponectin-receptor binding or AMPK signaling cascades, inhibiting fatty acid oxidation-related signal transmission via *adipor* downregulation [75]. Notably, AMPK in crustaceans operates as a master energy sensor, with its activity and gene expression dynamically responding to environmental fluctuations

to modulate energy demands [76]. Thus, *R. mucilaginosa*-induced transcriptional alterations likely reflect an adaptive metabolic reprogramming under energy-replete conditions—curtailing fatty acid oxidation to minimize energy expenditure while augmenting lipid storage to accommodate nutritional shifts.

The study also demonstrated that dietary *R. mucilaginosa* significantly upregulated hepatopancreatic expression of *fas*, *acc*, *srebp*, and *pparγ*, indicating its capacity to stimulate lipogenesis via modulation of core fatty acid synthesis genes. Acetyl-CoA carboxylase (ACC), the rate-limiting enzyme in fatty acid biosynthesis, catalyzes malonyl-CoA formation [77]. Fatty acid synthase (FAS) mediates long-chain fatty acid elongation [78]. Sterol regulatory element-binding proteins (SREBPs), encoded by *srebp*, bind promoter regions of *fas* and *acc* to activate their transcription and coordinate lipid biosynthesis [79]. Peroxisome proliferator-activated receptor gamma (PPARγ), a central regulator of adipogenesis, enhances lipid deposition by transactivating lipogenic enzyme genes [80]. Mechanistically, AMPK pathway activation suppresses *srebp* transcription and ACC enzymatic activity to potentiate fatty acid oxidation while inhibiting synthesis [81]. In this study, *R. mucilaginosa*-mediated AMPK inhibition (via *ampkα/β/γ* downregulation) presumably alleviated AMPKs suppression of *srebp*, enabling its upregulated expression and subsequent initiation of *fas/acc* transcriptional programs. Moreover, bioactive constituents in *R. mucilaginosa* (e.g., carotenoids and polysaccharides) may directly engage PPARγ signaling, activating *pparγ* expression to synergize with SREBP in orchestrating a lipogenic transcriptional network that collectively drives fatty acid synthesis and lipid accumulation [82]. These coordinated gene expression shifts reveal *R. mucilaginosa*'s dual-modulatory mechanism, which simultaneously suppresses fatty acid oxidation pathways while activating lipogenic routes, thereby remodeling crayfish lipid metabolism and ultimately enhancing lipid storage capacity.

Previous studies established the mTOR pathway as a central hub for cellular growth, metabolism, and energy homeostasis, wherein mTOR complex 1 (mTORC1) and mTORC2 integrate nutrient, energy, and growth factor signals to coordinately regulate protein synthesis and lipid metabolism [5]. Specifically, mTORC1 promotes protein biosynthesis via phosphorylation of downstream effectors (e.g., S6K1 and 4E-BP1) while modulating lipid metabolism through transcriptional regulators like sterol regulatory element-binding proteins (SREBPs). mTORC2 participates in cytoskeletal reorganization and metabolic regulation [83]. AKT, a critical upstream mTOR regulator, phosphorylates and inhibits tuberous sclerosis complex 2 (TSC2), thereby relieving its suppression on the small GTPase Rheb to activate mTORC1 [84]. Dietary *R. mucilaginosa*, abundant in proteins and polysaccharides, likely elevates phosphorylated AKT levels via PI3K/AKT pathway activation, subsequently triggering Rheb-mediated mTORC1 stimulation through this mechanism. Activated mTOR signaling enhances ribosomal biogenesis and translation initiation via S6K1 and 4E-BP1 phosphorylation to potentiate protein synthesis. Concurrently, it upregulates SREBP transcriptional activity and downstream *fas*/*acc* expression, synergizing with PPARγ signaling to collectively drive fatty acid biosynthesis and lipid deposition [6]. This mechanism aligns precisely with our observations of upregulated lipogenic genes (*fas*, *acc*, *srebp*, and *pparγ*) and increased muscle crude fat content. *R. mucilaginosa* optimizes nutrient partitioning by leveraging mTOR-mediated dual effects on protein anabolism and lipogenesis, thereby modulating growth and lipid metabolism.

5. Conclusions

In conclusion, supplementing the diet with *R. mucilaginosa* has a notable impact on the muscle composition of red claw crayfish, influencing both amino acid and fatty acid profiles, as well as affecting hemolymph biochemical parameters and antioxidant enzyme activities. The supplementation suppresses genes associated with lipid breakdown, enhances those

related to lipid synthesis, and modulates key metabolic signaling pathways by inhibiting AMPK while activating mTOR. Based on the findings of this research, the recommended minimum inclusion level of *R. mucilaginosa* is 1.0 g per kg of diet.

Author Contributions: Conceptualization, L.M. and Y.L.; Methodology, L.M., L.L., Z.M., W.H., Q.Z., T.T., D.W., R.W., H.Y., Y.L. and Y.H.; Investigation, L.M., L.L., Z.M., W.H., Q.Z., T.T., D.W., R.W., H.Y., Y.L. and Y.H.; Validation and visualization, L.M., L.L., Z.M., W.H., Q.Z., T.T., D.W., R.W., H.Y., Y.L. and Y.H.; Data curation, L.M. and Y.L.; Writing original draft preparation, L.M.; Writing-review and editing, Y.L.; Supervision, Y.L. and Y.H.; Funding acquisition, Y.L. and Y.H.; Formal analysis, Y.L. and Y.H.; Project administration, Y.L. and Y.H. All authors have read and agreed to the published version of the manuscript.

Funding: This study was supported by the Guangxi Science and Technology Base and Talent Special Project (GuikeAD24010034) and the Scientific Research Fund for the Introduction of Excellent Talents in Guangxi University for Nationalities (2018KJQD14).

Institutional Review Board Statement: The experimental design in this study was approved by the Biomedical Ethics Committee of Guangxi Minzu University, Nanning, China (Approval No. GXMZU-2023–018 and May 16, 2023 of approval), and no human participants were involved in this research.

Informed Consent Statement: Not applicable.

Data Availability Statement: The original contributions presented in the study are included in the article, and further inquiries can be directed to the corresponding author(s).

Conflicts of Interest: The authors declare that they have no known competing financial interests or personal relationships that could have appeared to influence the work reported in this paper.

References

1. Wu, S.; Pan, M.; Zan, Z.; Jakovlić, I.; Zhao, W.; Zou, H.; Ringø, E.; Wang, G. Regulation of Lipid Metabolism by Gut Microbiota in Aquatic Animals. *Rev. Aquac.* **2024**, *16*, 34–46. [CrossRef]
2. Calder, P.C. Functional Roles of Fatty Acids and Their Effects on Human Health. *J. Parenter. Enter. Nutr.* **2015**, *39*, 18S–32S. [CrossRef]
3. Hubler, J.M.; Kennedy, J.A. Role of Lipids in the Metabolism and Activation of Immune Cells. *J. Nutr. Biochem.* **2016**, *34*, 1–7. [CrossRef]
4. Zhang, W.; Dan, Z.; Zheng, J.; Du, J.; Liu, Y.; Zhao, Z.; Gong, Y.; Mai, K.; Ai, Q. Optimal Dietary Lipid Levels Alleviated Adverse Effects of High Temperature on Growth, Lipid Metabolism, Antioxidant and Immune Responses in Juvenile Turbot (*Scophthalmus maximus* L.). *Comp. Biochem. Physiol. Part B Biochem. Mol. Biol.* **2024**, *272*, 110962. [CrossRef]
5. Saxton, R.A.; Sabatini, D.M. mTOR Signaling in Growth, Metabolism, and Disease. *Cell* **2017**, *168*, 960–976. [CrossRef]
6. Xu, J.; Yao, X.; Li, X.; Xie, S.; Chi, S.; Zhang, S.; Cao, J.; Tan, B. Farnesoid X Receptor Regulates PI3K/AKT/mTOR Signaling Pathway, Lipid Metabolism, and Immune Response in Hybrid Grouper. *Fish Physiol. Biochem.* **2022**, *48*, 1521–1538. [CrossRef]
7. Chen, C.; Xu, C.; Yang, X.; Qian, D.; Gu, Z.; Jia, Y.; Li, E. Growth, Antioxidant Capacity, Intestine Histology and Lipid Metabolism of Juvenile Red Claw Crayfish, *Cherax quadricarinatus*, Fed Different Lipid Sources. *Aquac. Nutr.* **2021**, *27*, 261–273. [CrossRef]
8. Saoud, I.P.; Garza De Yta, A.; Ghanawi, J. A review of nutritional biology and dietary requirements of redclaw crayfish *Cherax quadricarinatus* (von M artens 1868). *Aquac. Nutr.* **2012**, *18*, 349–368. [CrossRef]
9. Kumar, V.; Sinha, A.K.; Romano, N.; Allen, M.K.; Bowman, A.B.; Thompson, R.K.; Tidwell, H.J. Metabolism and Nutritive Role of Cholesterol in the Growth, Gonadal Development, and Reproduction of Crustaceans. *Rev. Fish. Sci. Aquac.* **2018**, *26*, 254–273. [CrossRef]
10. Yuan, Y.; Jin, M.; Fang, F.; Tocher, R.D.; Betancor, B.M.; Jiao, L.; Hong, Y.; Zhou, Q. New Insight into the Molting and Growth in Crustaceans: Regulation of Energy Homeostasis Through the Lipid Nutrition. *Front. Mar. Sci.* **2022**, *9*, 914590. [CrossRef]
11. Dawood, O.A.M.; Magouz, I.F.; Salem, I.F.M.; Elbialy, I.Z.; Abdel-Daim, A.H. Synergetic Effects of *Lactobacillus plantarum* and β-Glucan on Digestive Enzyme Activity, Intestinal Morphology, Growth, Fatty Acid, and Glucose-Related Gene Expression of Genetically Improved Farmed Tilapia. *Probiotics Antimicrob. Proteins* **2020**, *12*, 389–399. [CrossRef]
12. Wang, J.; Zhu, Z.; Tian, S.; Fu, H.; Leng, X.; Chen, L. Dietary *Lactobacillus Casei* K17 Improves Lipid Metabolism, Antioxidant Response, and Fillet Quality of *Micropterus salmoides*. *Animals* **2021**, *11*, 2564. [CrossRef]

13. Alexander, C.T.; Han, X.F.; Arslan, Z.; Tchounwou, B.P. Toxicity of As in *Crassostrea virginica* (Gmelin, 1791) from the Northern Gulf of Mexico at the Presence of Zn and Its Antioxidant Defense Mechanisms. *Ecotoxicol. Environ. Saf.* **2019**, *172*, 514–522. [CrossRef] [PubMed]
14. Xiao, Y.; Zhang, Y.; Xu, W.; Chen, D.; Li, B.; Cheng, Y.; Guo, X.; Dong, W.; Shu, M. The Effects of Salinities Stress on Histopathological Changes, Serum Biochemical Index, Non-Specific Immune and Transcriptome Analysis in Red Swamp Crayfish *Procambarus clarkii*. *Sci. Total Environ.* **2022**, *840*, 156502. [CrossRef]
15. Hoseinifar, S.H.; Yousefi, S.; Van Doan, H.; Ashouri, G.; Gioacchini, G.; Maradonna, F.; Carnevali, O. Oxidative stress and antioxidant defense in fish: The implications of probiotic, prebiotic, and synbiotics. *Rev. Fish. Sci. Aquac.* **2020**, *29*, 198–217. [CrossRef]
16. Ye, Y.; Huang, J.; Li, S.; Li, Y.; Zhao, Y. Effects of Dietary Melatonin on Antioxidant Capacity, Immune Defense, and Intestinal Microbiota in Red Swamp Crayfish (*Procambarus clarkii*). *Mar. Biotechnol.* **2024**, *26*, 623–638. [CrossRef] [PubMed]
17. Han, M.; Gao, T.; Liu, G.; Zhu, C.; Zhang, T.; Sun, M.; Li, J.; Ji, F.; Si, Q.; Jiang, Q. The Effect of a Polystyrene Nanoplastic on the Intestinal Microbes and Oxidative Stress Defense of the Freshwater Crayfish, *Procambarus clarkii*. *Sci. Total Environ.* **2022**, *833*, 155722. [CrossRef]
18. Zheng, L.; Xie, S.; Zhuang, Z.; Liu, Y.; Tian, L.; Niu, J. Effects of yeast and yeast extract on growth performance, antioxidant ability and intestinal microbiota of juvenile Pacific white shrimp (*Litopenaeus vannamei*). *Aquaculture* **2021**, *530*, 735941. [CrossRef]
19. Liu, Y.; Huang, E.; Li, X.; Xie, Y.; Tong, T.; Wang, J.; Zhang, Q. Effects of Dietary Marine Red Yeast Supplementation on Growth Performance, Antioxidant, Immunity, Lipid Metabolism and mTOR Signaling Pathway in Juvenile Tilapia (*Oreochromis niloticus*). *Aquac. Rep.* **2024**, *37*, 102196. [CrossRef]
20. Mosqueda-Martínez, E.; Chiquete-Félix, N.; Castañeda-Tamez, P.; Ricardez-García, C.; Gutiérrez-Aguilar, M.; Uribe-Carvajal1, S.; Mendez-Romero, O. In *Rhodotorula mucilaginosa*, Active Oxidative Metabolism Increases Carotenoids to Inactivate Excess Reactive Oxygen Species. *Front. Fungal Biol.* **2024**, *5*, 1378590. [CrossRef] [PubMed]
21. Li, J.; Xia, D.; Jing, X.; Zhao, Y.; Hao, Q.; Zhang, Q.; Xie, M.; Yang, Y.; Ran, C.; Xu, Q.; et al. Addition of Solid-State Fermentation Product of Yeast Ameliorated the Effects of High-Fat Diet on Hepatic Lipid Metabolism, Epidermal Mucus, Intestine and Liver Health, and Gut Microbiota of Zebrafish. *Aquac. Rep.* **2023**, *30*, 101589. [CrossRef]
22. Li, X.; Cheng, Y.; Li, J.; Liu, C.; Qian, H.; Zhang, G. Torularhodin Alleviates Hepatic Dyslipidemia and Inflammations in High-Fat Diet-Induced Obese Mice via PPARα Signaling Pathway. *Molecules* **2022**, *27*, 6398. [CrossRef]
23. Kang, M.; Su, X.; Yun, L.; Shen, Y.; Feng, J.; Yang, G.; Meng, X.; Zhang, J.; Chang, X. Evaluation of Probiotic Characteristics and Whole Genome Analysis of *Bacillus velezensis* R-71003 Isolated from the Intestine of Common Carp (*Cyprinus carpio* L.) for Its Use as a Probiotic in Aquaculture. *Aquac. Rep.* **2022**, *25*, 101254. [CrossRef]
24. Yang, S.; Wu, Z.; Jian, J.; Zhang, X. Effect of Marine Red Yeast *Rhodosporidium Paludigenum* on Growth and Antioxidant Competence of *Litopenaeus vannamei*. *Aquaculture* **2010**, *309*, 62–65. [CrossRef]
25. Zhang, Q.; Meng, L.; Li, J.; Li, L.; Zeng, Q.; Wang, R.; Wang, D.; Tong, T.; Liu, Y.; Yang, H. Effects of *Rhodotorula mucilaginosa* on Growth, Antioxidant, and Immune Function, and Toll/Imd and JAK-STAT Signaling Pathways in Red Claw Crayfish (*Cherax quadricanatus*). *Aquac. Nutr.* **2025**, *2025*, 4904293. [CrossRef]
26. Ren, X.; Liu, X.; Zhu, X.; Xiong, L.; Bai, X. Trained Immunity Can Improve the Disease Resistance of Red Swamp Crayfish (*Procambarus clarkii*). *Fish Shellfish Immunol.* **2023**, *132*, 108468. [CrossRef]
27. Liu, Y.; Huang, E.; Li, X.; Xie, Y.; Meng, L.; Liu, D.; Tong, T.; Wang, J.; Zhang, Q. Serum Biochemistry, Fatty Acids, Lipid Metabolism, Antioxidants, and Inflammation Response Were Significantly Affected by Feeding Different Marine Red Yeast Supplementation in Juvenile Tilapia (GIFT Strain, *Oreochromis niloticus*). *Front. Mar. Sci.* **2024**, *11*, 1426848. [CrossRef]
28. *GB 5009.168-2016*; National Food Safety Standard—Determination of Fatty Acids in Foods. National Health and Family Planning Commission. State Food and Drug Administration: Beijing, China, 2016.
29. *GB 5009.124-2016*; National Food Safety Standard—Determination of Amino Ccids in Foods. National Health and Family Planning Commission. State Food and Drug Administration: Beijing, China, 2016.
30. Zhang, Q.; Xie, Y.; Tang, J.; Meng, L.; Huang, E.; Liu, D.; Tong, T.; Liu, Y.; Guo, Z. Effects of Dietary Chitosan on Growth Performance, Serum Biochemical Indices, Antioxidant Capacity, and Immune Response of Juvenile Tilapia (*Oreochromis niloticus*) under Cadmium Stress. *Animals* **2024**, *14*, 2259. [CrossRef] [PubMed]
31. Liu, Y.; Huang, E.; Xie, Y.; Meng, L.; Liu, D.; Zhang, Z.; Zhou, J.; Zhang, Q.; Tong, T. The Effect of Dietary Lipid Supplementation on the Serum Biochemistry, Antioxidant Responses, Initial Immunity, and mTOR Pathway of Juvenile Tilapia (*Oreochromis niloticus*). *Fishes* **2023**, *8*, 535. [CrossRef]
32. Guo, M.; Meng, L.; Li, F.; Liu, Y.; Zhang, Z.; Zhang, Q.; Kong, W. Effects of Dietary Bacillus Pumilus on the Growth, Intestinal Health, Lipid Metabolism, and mTOR Signaling Pathway of Juvenile Coho Salmon (*Oncorhynchus kisutch*). *Water Biol. Secur.* **2025**, *4*, 100313. [CrossRef]
33. Ayiku, S.; Shen, J.; Tan, B.; Dong, X.; Liu, H. Effects of Dietary Yeast Culture on Shrimp Growth, Immune Response, Intestinal Health and Disease Resistance against *Vibrio harveyi*. *Fish Shellfish Immunol.* **2020**, *102*, 286–295. [CrossRef]

34. Abdelsamad, M.E.A.; Said, M.E.R.; Assas, M.; Gaafar, Y.A.; Hamouda, H.A.; Mahdy, A. Effects of Dietary Supplementation with *Bacillus velezensis* on the Growth Performance, Body Composition, Antioxidant, Immune-Related Gene Expression, and Histology of Pacific White Shrimp, *Litopenaeus vannamei*. *BMC Vet. Res.* **2024**, *20*, 368. [CrossRef]
35. Wang, B.; Liu, Y.; Luo, K.; Zhang, S.; Wei, C.; Wang, L.; Qiu, Y.; Tian, X. 'Biotic' Potential of the Red Yeast *Rhodotorula mucilaginosa Strain* JM-01 on the Growth, Shell Pigmentation, and Immune Defense Attributes of the Shrimp, *Penaeus vannamei*. *Aquaculture* **2023**, *572*, 739543. [CrossRef]
36. Eissa, H.E.; Dowidar, A.H.; Al-Hoshani, N.; Baazaoui, N.; Alshammari, M.N.; Bahshwan, A.M.S.; Kari, A.Z.; Ibrahim, S.; Munir, B.M.; AL-Farga, A.; et al. Dietary Supplementation with Fermented Prebiotics and Probiotics Can Increase Growth, Immunity, and Histological Alterations in Pacific Whiteleg Shrimp (*Litopenaeus vannamei*) Challenged with *Vibrio parahaemolyticus*. *Aquac. Int.* **2024**, *33*, 62. [CrossRef]
37. Chen, X.; Zhao, W.; Xie, S.; Xie, J.; Zhang, Z.; Tian, L.; Liu, Y.; Niu, J. Effects of Dietary Hydrolyzed Yeast (*Rhodotorula mucilaginosa*) on Growth Performance, Immune Response, Antioxidant Capacity and Histomorphology of Juvenile Nile Tilapia (*Oreochromis niloticus*). *Fish Shellfish Immunol.* **2019**, *90*, 30–39. [CrossRef]
38. Zhang, Q.; Meng, L.; Lu, H.; Li, L.; Zeng, Q.; Wang, D.; Wang, R.; Tong, T.; Liu, Y.; Yang, H. Dietary Supplementation with *Rhodotorula mucilaginosa* Enhances Resistance to *Aeromonas veronii* Infection in Red Claw Crayfish (*Cherax quadricarinatus*). *Animals* **2025**, *15*, 1912. [CrossRef] [PubMed]
39. Huang, Y.; Gao, P.; Yu, D.; Sun, Z.; Yang, X.; Lai, Q.; Chi, H. A Comparative Analysis on the Biochemical Composition and Nutrition Evaluation of Crayfish (*Procambarus clarkii*) Cultivated in Saline-Alkali and Fresh Water. *Foods* **2025**, *14*, 1997. [CrossRef]
40. Yang, Z.; Jiang, Q.; Zhang, W.; Xia, S.; Tian, H.; Liu, F.; Yang, W.; Yu, Y.; Wu, Y.; Zhu, Y.; et al. Comparison of Morphometric Parameters, Nutritional Composition, and Textural Properties of Seven Crustaceans Species. *Fishes* **2024**, *9*, 141. [CrossRef]
41. Qi, C.; Wang, X.; Han, F.; Jia, Y.; Lin, Z.; Wang, C.; Lu, J.; Yang, L.; Wang, X.; Li, E.; et al. Arginine Supplementation Improves Growth, Antioxidant Capacity, Immunity and Disease Resistance of Juvenile Chinese Mitten Crab, *Eriocheir sinensis*. *Fish Shellfish Immunol.* **2019**, *93*, 463–473. [CrossRef] [PubMed]
42. Brosnan, E.M.; Brosnan, T.J. Histidine Metabolism and Function. *J. Nutr.* **2020**, *150*, 2570S–2575S. [CrossRef]
43. Wei, Z.; Zhuang, Y.; Liu, X.; Zou, D.; Mai, K.; Sun, Z.; Ye, C. Leucine Promotes Protein Synthesis of Juvenile White Shrimp *Litopenaeus vannamei* through TOR Signaling Pathway. *Aquaculture* **2023**, *564*, 739060. [CrossRef]
44. Xiao, F.; Wang, J.; Liu, H.; Zhuang, M.; Wen, X.; Zhao, H.; Wu, K. Effects of Dietary Protein Levels on Growth, Digestive Enzyme Activity, Antioxidant Capacity, and Gene Expression Related to Muscle Growth and Protein Synthesis of Juvenile Greasyback Shrimp (*Metapenaeus ensis*). *Animals* **2023**, *13*, 3886. [CrossRef]
45. Seenivasan, C.; Radhakrishnan, S.; Muralisankar, T.; Saravana Bhavan, P. Effects of Probiotics on Survival, Growth and Digestive Enzymes Activities in Freshwater Prawn *Macrobrachium rosenbergii* (De Man 1879). *Proc. Zool. Soc.* **2016**, *69*, 52–60. [CrossRef]
46. Li, M.; Lv, W.; Zhao, Y.; Huang, W.; Yuan, Q.; Yang, H.; Wang, A.; Zhou, W.; Li, M. Effects of Substituting *Tenebrio Molitor* and *Elodea Nuttallii* as Feed on Growth, Flesh Quality and Intestinal Microbiota of Red Swamp Crayfish (*Procambarus clarkii*). *Foods* **2024**, *13*, 2292. [CrossRef]
47. Jiang, W.; Wu, P.; Tang, R.; Liu, Y.; Kuang, S.; Jiang, J.; Tang, L.; Tang, W.; Zhang, Y.; Zhou, X.; et al. Nutritive Values, Flavor Amino Acids, Healthcare Fatty Acids and Flesh Quality Improved by Manganese Referring to up-Regulating the Antioxidant Capacity and Signaling Molecules TOR and Nrf2 in the Muscle of Fish. *Food Res. Int.* **2016**, *89*, 670–678. [CrossRef]
48. Zhu, T.; Yang, R.; Xiao, R.; Ni, W.; Liu, L.; Zhao, J.; Ye, Z. Effect of Swimming Training on the Flesh Quality in Chinese Perch (*Siniperca chuatsi*) and Its Relationship with Muscle Metabolism. *Aquaculture* **2023**, *577*, 739926. [CrossRef]
49. Sun, Y.; Shan, X.; Li, D.; Liu, X.; Han, Z.; Qin, J.; Guan, B.; Tan, L.; Zheng, J.; Wei, M.; et al. Analysis of the Differences in Muscle Nutrition among Individuals of Different Sexes in Redclaw Crayfish, *Cherax quadricarinatus*. *Metabolites* **2023**, *13*, 190. [CrossRef]
50. Rombenso, N.A.; Trushenski, T.J.; Jirsa, D.; Drawbridge, M. Docosahexaenoic Acid (DHA) and Arachidonic Acid (ARA) Are Essential to Meet LC-PUFA Requirements of Juvenile California Yellowtail (*Seriola dorsalis*). *Aquaculture* **2016**, *463*, 123–134. [CrossRef]
51. Gupta, A.; Vongsvivut, J.; Barrow, C.J.; Puri, M. Molecular identification of marine yeast and its spectroscopic analysis establishes unsaturated fatty acid accumulation. *J. Biosci. Bioeng.* **2012**, *114*, 411–417. [CrossRef]
52. Zare, R.; Abedian Kenari, A.; Yazdani Sadati, M. Influence of Dietary Acetic Acid, Protexin (Probiotic), and Their Combination on Growth Performance, Intestinal Microbiota, Digestive Enzymes, Immunological Parameters, and Fatty Acids Composition in Siberian Sturgeon (*Acipenser baerii*, Brandt, 1869). *Aquac. Int.* **2021**, *29*, 891–910. [CrossRef]
53. Mang, Q.; Gao, J.; Li, Q.; Sun, Y.; Xu, G.; Xu, P. Probiotics Enhance *Coilia Nasus* Growth Performance and Nutritional Value by Regulating Glucolipid Metabolism via the Gut–Liver Axis. *Int. J. Mol. Sci.* **2024**, *25*, 12196. [CrossRef]
54. Hassaan, S.M.; Nssar, M.K.; Mohammady, Y.E.; Amin, A.; Tayel, I.S.; El-Haroun, R.E. Nano-Zeolite Efficiency to Mitigate the Aflatoxin B1 (AFB1) Toxicity: Effects on Growth, Digestive Enzymes, Antioxidant, DNA Damage and Bioaccumulation of AFB1 Residues in Nile Tilapia (*Oreochromis niloticus*). *Aquaculture* **2020**, *523*, 735123. [CrossRef]

55. Xu, T.; Wang, J.; Xu, H.; Wang, Z.; Liu, Y.; Bai, H.; Zhang, Y.; Kong, Y.; Liu, Y.; Ding, Z. Dietary β-1,3-Glucan Promotes Growth Performance and Enhances Non-Specific Immunity by Modulating Pattern Recognition Receptors in Juvenile Oriental River Prawn (*Macrobrachium nipponense*). *Fishes* **2024**, *9*, 379. [CrossRef]
56. Machuca, C.; Méndez-Martínez, Y.; Reyes-Becerril, M.; Angulo, C. Yeast β-Glucans as Fish Immunomodulators: A Review. *Animals* **2022**, *12*, 2154. [CrossRef] [PubMed]
57. Yang, H.; Du, D.; Zhang, Q.; Teame, T.; Wang, A.; Hao, Q.; Liu, S.; Ding, Q.; Yao, Y.; Yang, Y.; et al. Dietary *Bacillus velezensis* T23 Fermented Products Supplementation Improves Growth, Hepatopancreas and Intestine Health of *Litopenaeus vannamei*. *Fish Shellfish Immunol.* **2024**, *149*, 109595. [CrossRef] [PubMed]
58. Sundh, H.; Finne-Fridell, F.; Ellis, T.; Taranger, L.G.; Niklasson, L.; Pettersen, F.E.; Wergeland, I.H.; Sundell, K. Reduced Water Quality Associated with Higher Stocking Density Disturbs the Intestinal Barrier Functions of Atlantic Salmon (*Salmo salar* L.). *Aquaculture* **2019**, *512*, 734356. [CrossRef]
59. Safaeian, S.; Gholamhosseini, A.; Heidari, F.; Kordestani, H.; Nazifi, S. Biochemical and Total Hemocyte Count Profiles of Long-Clawed Crayfish (*Astacus leptodactylus*) as a Reference Interval in Southern Iran. *Comp. Clin. Pathol.* **2020**, *29*, 361–368. [CrossRef]
60. Li, Y.; Ye, Y.; Li, W.; Liu, X.; Zhao, Y.; Jiang, Q.; Che, X. Effects of Salinity Stress on Histological Changes, Glucose Metabolism Index and Transcriptomic Profile in Freshwater Shrimp, *Macrobrachium nipponense*. *Animals* **2023**, *13*, 2884. [CrossRef]
61. Chen, S.; Guo, Y.; Espe, M.; Yang, F.; Fang, W.; Wan, M.; Niu, J.; Liu, Y.; Tian, L. Growth Performance, Haematological Parameters, Antioxidant Status and Salinity Stress Tolerance of Juvenile Pacific White Shrimp (*Litopenaeus vannamei*) Fed Different Levels of Dietary *Myo*-Inositol. *Aquac. Nutr.* **2018**, *24*, 1527–1539. [CrossRef]
62. Hackl, T.M.; Fürnsinn, C.; Schuh, M.C.; Krssak, M.; Carli, F.; Guerra, S.; Freudenthaler, A.; Baumgartner-Parzer, S.; Helbich, H.T.; Luger, A.; et al. Brain Leptin Reduces Liver Lipids by Increasing Hepatic Triglyceride Secretion and Lowering Lipogenesis. *Nat. Commun.* **2019**, *10*, 2717. [CrossRef]
63. Castillo, S.; Rosales, M.; Pohlenz, C.; Gatlin, D.M. Effects of Organic Acids on Growth Performance and Digestive Enzyme Activities of Juvenile Red Drum *Sciaenops ocellatus*. *Aquaculture* **2014**, *433*, 6–12. [CrossRef]
64. Wade, M.N.; Gabaudan, J.; Glencross, D.B. A Review of Carotenoid Utilisation and Function in Crustacean Aquaculture. *Rev. Aquac.* **2017**, *9*, 141–156. [CrossRef]
65. Kieliszek, M.; Kot, M.A.; Kolotylo, V. Bioaccumulation of Selenium and Production of Carotenoids by the Yeast *Rhodotorula mucilaginosa*. *Biocatal. Agric. Biotechnol.* **2023**, *53*, 102903. [CrossRef]
66. Ighodaro, M.O.; Akinloye, A.O. First Line Defence Antioxidants-Superoxide Dismutase (SOD), Catalase (CAT) and Glutathione Peroxidase (GPX): Their Fundamental Role in the Entire Antioxidant Defence Grid. *Alex. J. Med.* **2018**, *54*, 287–293. [CrossRef]
67. Jiang, G.; Yang, Z.; Wang, Y.; Yao, M.; Chen, Y.; Xiao, W.; Yuan, Y. Enhanced Astaxanthin Production in Yeast via Combined Mutagenesis and Evolution. *Biochem. Eng. J.* **2020**, *156*, 107519. [CrossRef]
68. Liang, X.; Zhang, J.; Guo, F.; Wei, L.; Zhou, Q. Oxidative Stress and Inflammatory Responses in the Liver of Swamp Eel (*Monopterus albus*) Exposed to Carbon Tetrachloride. *Aquaculture* **2018**, *496*, 232–238. [CrossRef]
69. Tang, Q.; Huang, G.; Zhao, F.; Zhou, L.; Huang, S.; Li, H. The Antioxidant Activities of Six (1 → 3)-β- d -Glucan Derivatives Prepared from Yeast Cell Wall. *Int. J. Biol. Macromol.* **2017**, *98*, 216–221. [CrossRef]
70. Sriphuttha, C.; Limkul, S.; Pongsetkul, J.; Phiwthong, T.; Massu, A.; Sumniangyen, N.; Boontawan, P.; Ketudat-Cairns, M.; Boontawan, A.; Boonchuen, P. Effect of Fed Dietary Yeast (*Rhodotorula paludigena* CM33) on Shrimp Growth, Gene Expression, Intestinal Microbial, Disease Resistance, and Meat Composition of *Litopenaeus vannamei*. *Dev. Comp. Immunol.* **2023**, *147*, 104896. [CrossRef]
71. Wang, X.; Shen, Z.; Wang, C.; Li, E.; Qin, J.G.; Chen, L. Dietary Supplementation of Selenium Yeast Enhances the Antioxidant Capacity and Immune Response of Juvenile *Eriocheir sinensis* under Nitrite Stress. *Fish Shellfish Immunol.* **2019**, *87*, 22–31. [CrossRef] [PubMed]
72. Yoon, S.D.; Kim, H.D.; Kim, H.J.; Sakakura, Y.; Hagiwara, A.; Park, G.H.; Lee, C.M.; Lee, S.J. Interactions between Lipid Metabolism and the Microbiome in Aquatic Organisms: A Review. *Mar. Pollut. Bull.* **2024**, *207*, 116858. [CrossRef] [PubMed]
73. Kim, R.A.; Alam, J.M.; Yoon, T.; Lee, R.S.; Park, H.; Kim, N.D.; An, H.D.; Lee, B.J.; Lee, I.C.; Kim, W.H. Molecular Characterization of an Adiponectin Receptor Homolog in the White Leg Shrimp, *Litopenaeus vannamei*. *PeerJ* **2016**, *4*, e2221. [CrossRef]
74. Sun, P.; Jin, M.; Jiao, L.; Monroig, Ó.; Navarro, C.J.; Tocher, R.D.; Betancor, B.M.; Wang, X.; Yuan, Y.; Zhou, Q. Effects of Dietary Lipid Level on Growth, Fatty Acid Profiles, Antioxidant Capacity and Expression of Genes Involved in Lipid Metabolism in Juvenile Swimming Crab, *Portunus trituberculatus*. *Br. J. Nutr.* **2020**, *123*, 149–160. [CrossRef] [PubMed]
75. Hardie, G.D.; Ross, A.F.; Hawley, A.S. AMPK: A Nutrient and Energy Sensor That Maintains Energy Homeostasis. *Nat. Rev. Mol. Cell Biol.* **2012**, *13*, 251–262. [CrossRef] [PubMed]
76. Jin, M.; Luo, J.; Zhu, T.; Fang, F.; Xie, S.; Lu, J.; Betancor, B.M.; Tocher, R.D.; Zhou, Q. Examination of Role of the AMP-Activated Protein Kinase (Ampk) Signaling Pathway during Low Salinity Adaptation in the Mud Crab, *Scylla paramamosain*, with Reference to Glucolipid Metabolism. *Aquaculture* **2024**, *593*, 741329. [CrossRef]

77. Zhong, W.; Chen, C.; Tan, S.; He, X.; Wang, S.; Tocher, D.R.; Lin, F.; Sun, Z.; Wen, X.; Li, Y.; et al. Identification of a Novel Crustacean Vascular Endothelial Growth Factor B-like in the Mud Crab *Scylla paramamosain*, and Examination of Its Role in Lipid Accumulation. *Aquaculture* **2023**, *575*, 739793. [CrossRef]
78. Zuo, H.; Gao, J.; Yuan, J.; Deng, H.; Yang, L.; Weng, S.; He, J.; Xu, X. Fatty Acid Synthase Plays a Positive Role in Shrimp Immune Responses against *Vibrio parahaemolyticus* Infection. *Fish Shellfish Immunol.* **2017**, *60*, 282–288. [CrossRef]
79. Zhao, Y.; Li, H.; Zhang, Y.; Li, L.; Fang, R.; Li, Y.; Liu, Q.; Zhang, W.; Qiu, L.; Liu, F.; et al. Oncoprotein HBXIP Modulates Abnormal Lipid Metabolism and Growth of Breast Cancer Cells by Activating the LXRs/SREBP-1c/FAS Signaling Cascade. *Cancer Res.* **2016**, *76*, 4696–4707. [CrossRef]
80. Li, Q.; Zheng, Y.; Sun, Y.; Xu, G. Resveratrol Attenuated Fatty Acid Synthesis through MAPK-PPAR Pathway in Red Tilapia. *Comp. Biochem. Physiol. Part C Toxicol. Pharmacol.* **2023**, *268*, 109598. [CrossRef] [PubMed]
81. Li, J.; Liang, X.-F.; Alam, S.M.; Luo, H.; Zhang, Y.; Peng, B.; Xiao, Q.; Zhang, Z.; Liu, L.; He, S. Adaptation of AMPK-mTOR-Signal Pathways and Lipid Metabolism in Response to Low- and High-Level Rapeseed Meal Diet in Chinese Perch (*Siniperca chuatsi*). *J. Comp. Physiol. B* **2021**, *191*, 881–894. [CrossRef]
82. Zhao, T.; Ma, A.; Huang, Z.; Liu, Z.; Sun, Z.; Wang, X.; Xu, R. Structural and Functional Characterization of Turbot *Ppar*γ: Activation during High Temperature and Regulation of Lipid Metabolism. *J. Therm. Biol.* **2022**, *108*, 103279. [CrossRef] [PubMed]
83. Yang, H.; Rudge, G.D.; Koos, D.J.; Vaidialingam, B.; Yang, H.J.; Pavletich, P.N. mTOR Kinase Structure, Mechanism and Regulation by the Rapamycin-Binding Domain. *Nature* **2013**, *497*, 217–223. [CrossRef] [PubMed]
84. Abuhagr, M.A.; MacLea, S.K.; Chang, S.E.; Mykles, L.D. Mechanistic Target of Rapamycin (mTOR) Signaling Genes in Decapod Crustaceans: Cloning and Tissue Expression of mTOR, Akt, Rheb, and P70 S6 Kinase in the Green Crab, *Carcinus Maenas*, and Blackback Land Crab, *Gecarcinus lateralis*. *Comp. Biochem. Physiol. Part A Mol. Integr. Physiol.* **2014**, *168*, 25–39. [CrossRef] [PubMed]

Disclaimer/Publisher's Note: The statements, opinions and data contained in all publications are solely those of the individual author(s) and contributor(s) and not of MDPI and/or the editor(s). MDPI and/or the editor(s) disclaim responsibility for any injury to people or property resulting from any ideas, methods, instructions or products referred to in the content.

biology

MDPI

Article

Metabolic Adaptation to Following Temperature Acclimation in Fish on the Yun-Gui Plateau

Wei Dao [1,2,3], Jing Long [1,2,3], Yanhui Yin [1,2], Anli Wu [1,2], Yuanchao Chen [1,2], Haitao Gao [4], Xiaofu Pan [1,2], Junxing Yang [1,2], Xiaoai Wang [1,2,*] and Yuanwei Zhang [1,2,*]

1 State Key Laboratory of Genetic Evolution & Animal Models, Kunming Institute of Zoology, Chinese Academy of Sciences, Kunming 650201, China; daowei01@163.com (W.D.); longjing995@163.com (J.L.); yinyanhui603@163.com (Y.Y.); wuanli@mail.kiz.ac.cn (A.W.); 15187602713@163.com (Y.C.); xiaofupan@163.com (X.P.); yangjx@mail.kiz.ac.cn (J.Y.)
2 Yunnan Key Laboratory of Plateau Fish Breeding, Kunming Institute of Zoology, Chinese Academy of Sciences, Kunming 650201, China
3 University of Chinese Academy of Sciences, Beijing 100049, China
4 Yunnan Institute of Fishery Sciences Research, Kunming 650111, China; ynkhtt@126.com
* Correspondence: xueaiw@126.com (X.W.); zhangyuanwei@mail.kiz.ac.cn (Y.Z.)

Simple Summary: The study depicted the metabolic responses of plateau fish to temperature changes. Plateau fish exhibit higher metabolic sensitivity, with more pronounced changes in metabolic rates as temperature increases, coupled with limited organ size plasticity, making them potentially more vulnerable to climate warming. Additionally, these fish demonstrate higher metabolic rates and larger heart, red muscle, and liver masses. The trade-off between high metabolic rates and organ size may represent an adaptive strategy to high-altitude environments. This research fills a knowledge gap regarding the metabolic characteristics of fish on the Yun-Gui Plateau.

Abstract: Temperature is crucial for fish physiology, as metabolism and related physiological processes are directly influenced by thermal energy. Against the backdrop of global warming, climate-induced variations in water temperature increasingly constrain fish physiology. Consequently, understanding the effects of temperature on fish metabolism is vital for predicting how global warming might impact various fish species. Plateau fish, predominantly cold-water species, exhibit greater sensitivity to temperature fluctuations. However, research on the effects of temperature on plateau fish is currently limited. Consequently, this study employed low-altitude *H. nobilis* as a reference while *D. macrophthalmus* and *A. grahami* were selected from the Yun–Gui Plateau. Following 15 days of temperature acclimation at 10, 15, 20, 25, and 30 °C, organ mass, the resting metabolic rate, and mitochondrial function were measured. The results indicated that high-altitude fish exhibit heightened metabolic sensitivity, demonstrating more pronounced increases or decreases in metabolic rates as temperature increases, along with limited plasticity in organ size. This may render high-altitude fish more vulnerable to the impacts of climate warming. Furthermore, physiological differences between altitudes and species were observed, primarily characterized by higher metabolic rates across all measured temperatures in plateau species. Additionally, plateau fish presented greater masses of heart, red muscle, and liver but smaller masses of brain and kidney. We propose that the trade-off between elevated metabolic rates and organ size may represent an adaptive strategy for fish inhabiting high-altitude environments, involving specific ecological costs and benefits. These findings not only address the knowledge gap regarding the metabolic characteristics of fish on the Yun–Gui Plateau but also provide theoretical and experimental foundations for the conservation of high-altitude fish populations.

Keywords: metabolic rate; temperature; high altitude; adaptation strategies

1. Introduction

In the context of global warming, increasing attention has been given to understanding organismal responses to ongoing climate change, with considerable research focused on examining variations in thermal tolerance and acclimation both within and among species [1]. The metabolic rate is frequently one of the earliest traits to respond to climate change and is considered a key ecological parameter [2,3]. Among ectotherms, temperature is one of the most critical and extensively studied factors influencing metabolic rates [4]. Generally, the metabolic rate increases with temperature; however, this increase is bounded by a thermal limit, beyond which the metabolic rate decreases with increasing temperature [5–8]. Consequently, the metabolic rate reflects evolutionary optimization within species, making understanding metabolic patterns crucial to contemporary ecological theory [4,9]. Metabolism also varies among species according to latitude, altitude, and climate zone [10]. For example, the metabolic cold adaptation (MCA) hypothesis suggests that organisms from cold environments (high latitudes or altitudes) exhibit higher metabolic rates than those from warmer regions when measured at identical temperatures [4]. This phenomenon may serve as a mechanism to sustain physiological function under cold conditions [11,12]. Additionally, the climate variability (CVH) hypothesis posits that species from stable environments tend to have narrower temperature ranges, facilitating evolutionary specialization [13,14] and consequently exhibiting lower physiological plasticity [15,16]. Conversely, species from more variable habitats demonstrate broader thermal tolerance and greater thermal plasticity, allowing rapid adaptation to highly variable climates [3,16,17]. Such species also maintain relatively lower metabolic rates over wider temperature ranges to minimize energy expenditure [13]. Therefore, assessing how metabolic rates respond to temperature fluctuations is crucial for evaluating the vulnerability of species to climate change.

Fish represent a significant group of aquatic vertebrates and display extensive diversity across altitudes and climatic zones. Their growth [18], reproduction [19,20], and metabolism [21–23] are strongly influenced by temperature. The metabolic rate, which represents kinetic energy expenditure at the cellular level, is a fundamental requirement for fish growth and survival and is especially susceptible to temperature changes. Organisms can adaptively modulate their metabolic responses to temperature through phenotypic plasticity or genetic evolution [24,25]. Phenotypic plasticity may involve alterations at the organ, individual, or cellular/subcellular level. In particular, the metabolic rate can be modified by adjusting the organ size (e.g., liver, brain, and heart) and mitochondrial function [26–28]. Mitochondria act as cellular energy 'powerhouses', providing approximately 90% of ATP through oxidative phosphorylation (OXPHOS), thus underpinning nearly all animal activities [8,29,30]. For example, acute warming initially triggers an increase in OXPHOS, enabling tissues to meet increased metabolic demands and sustain ATP production [7]. However, mitochondrial capacity becomes compromised (plateauing or declining) near a fish's upper thermal limit [6–8]. Currently, water temperature shifts driven by climate change increasingly constrain the physiological functions of fish [31]. Plateau fish, predominantly cold-water species, have garnered significant attention because of their increased sensitivity to climate change. The Yun–Gui Plateau is located in the low-latitude transitional region east of the Qinghai–Tibet Plateau and is one of China's four major plateaus [32]. Through natural evolution and historical development, this region has gradually produced numerous highly specialized endemic cold-water fish species [33,34].

However, previous research on fish from the Yun–Gui Plateau has focused predominantly on conservation and systematic evolution, whereas studies on fish from other plateau regions have also concentrated on conservation [35–37] and genetic foundations [38,39]. These genetic studies indicate that adaptation to high altitudes involves genetic modifications related to energy metabolism, yet evidence for phenotypic plasticity adjustments in plateau fishes remains limited. Consequently, it is imperative to investigate metabolic adaptations in plateau fishes at the organ, individual, and mitochondrial levels following temperature changes.

To elucidate the metabolic responses of plateau fishes to temperature fluctuations and characterize their metabolism, we employed low-altitude *Hypophthalmichthys nobilis* as a reference species. We then conducted comparative analyses of the metabolic responses to temperature changes in two plateau species, *Distoecodon macrophthalmus* and *Anabarilius grahami*. *H. nobilis* is widely distributed at low altitudes (average altitude < 500 m), primarily in subtropical and temperate zones (e.g., the Yangtze River, Pearl River, and their affiliated lakes in central and southern China), with a natural habitat temperature range of 4–34 °C [40]. *D. macrophthalmus* and *A. grahami* are cold-water species endemic to lakes on the Yun-Gui Plateau. Both species are economically important and have long adapted to low-temperature environments; thus, they are considered narrow-temperature-range species. *D. macrophthalmus* exclusively inhabits Chenghai Lake, Yunnan (altitude: 1503 m), with a natural habitat temperature range of 9–28 °C [41,42]. *A. grahami* exclusively inhabits Fuxian Lake, Yunnan (altitude: 1721 m), with a natural habitat temperature range of 12–23 °C (Figure 1) [41,43]. All three species belong to the family Xenocyprididae (Cypriniformes) [44] and are omnivorous, primarily feeding on plankton. In this study, individuals of each species were subjected to temperature treatments (10, 15, 20, 25, and 30 °C) for 15 days, after which organ sizes, resting metabolic rates, and mitochondrial respiration rates were measured. By analyzing variations in organ size, the resting metabolic rate (RMR), and mitochondrial function across these three fish species, we obtained valuable insights into the metabolic characteristics of plateau fishes. Our findings may provide novel perspectives for elucidating the physiological adaptation mechanisms of fish inhabiting high-altitude environments [45,46].

2. Materials and Methods

All experimental fish (juvenile *H. nobilis*, *D. macrophthalmus*, and *A. grahami*) were obtained from the Endangered Fish Conservation Center (EFCC) of the Kunming Institute of Zoology (KIZ), Chinese Academy of Sciences, Kunming, Yunnan, China.

2.1. Thermal Acclimation

Before the experiments, the fish were acclimated for two weeks in a recirculating-water tank system. During acclimation, the water temperature was maintained at 20 ± 0.5 °C, and the dissolved oxygen (DO) concentration was maintained above 5 mg/L. Commercial feed (composed of crude protein 36.0%, crude fat 6.0%, crude fiber 6.0%, crude ash 12.0%, calcium 0.5–1.5%, total phosphorus 0.9%, sodium chloride 0.3–1.6%, lysine 2.2%, and moisture 12.5%) was provided daily to satiate between 17:00 and 18:00. Approximately one-third of the water volume was replaced daily to prevent ammonia nitrogen accumulation. The photoperiod was set to 12 h light and 12 h dark.

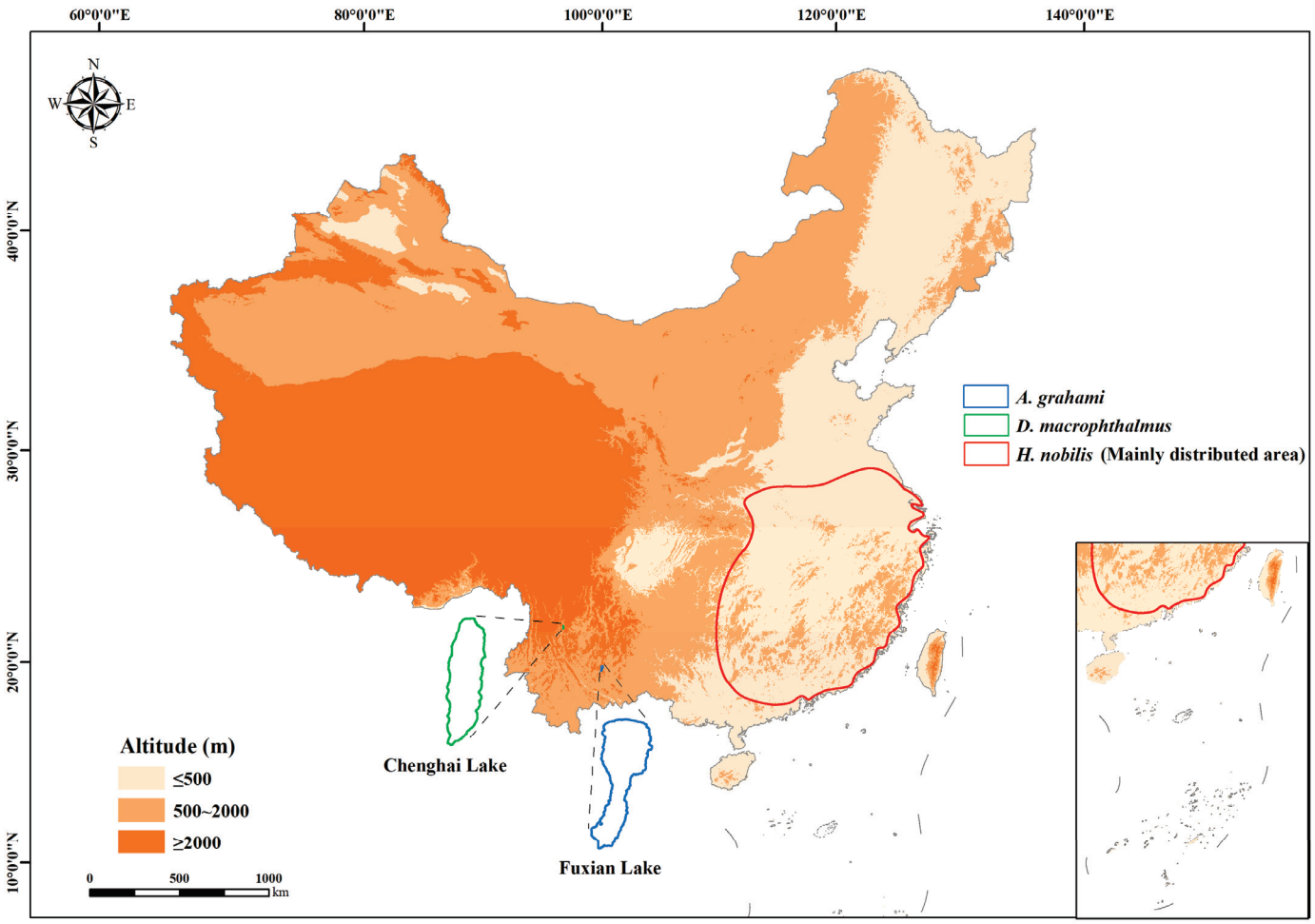


Figure 1. Distribution areas of *H. nobilis*, *D. macrophthalmus*, and *A. grahami*.

After body weight (BW) and standard body length (SL) were measured, the fish of each species were randomly assigned to warm or cold acclimation treatments. BW content was similar among the *H. nobilis* (BW: 21.33 ± 4.74 g, SL: 9.66 ± 1.26 cm), *D. macrophthalmus* (BW: 23.84 ± 6.83 g, SL: 10.93 ± 0.86 cm), and *A. grahami* (BW: 20.58 ± 2.93 g, SL: 12.16 ± 0.66 cm) treatments. Each treatment group was gradually adjusted to the experimental temperature (10 °C, 15 °C, 25 °C, and 30 °C) at a rate of 1 °C per day and then maintained for 15 days. After acclimation, the RMR, organ size, and mitochondrial respiration rate (liver, brain, heart, kidney, and red muscle) were measured. During temperature acclimation, the fish were fed, the water quality was maintained, and the photoperiod remained consistent with the adaptive acclimation phase. The fish were fasted for 48 h before the measurements were taken to ensure complete evacuation of the gastrointestinal contents [47].

2.2. Resting Metabolic Rate Measurement

After acclimation, the RMR of each fish was determined via a flow-through respirometer (laboratory self-designed) at five temperatures (10, 15, 20, 25, and 30 °C), and the measurement method followed Yan et al. [47] and Fu et al. [48]. The fish were then individually placed in the respirometer chamber and allowed to acclimate for approximately 12 h before the experiment. The next day, oxygen consumption was measured ten times at 1 h intervals, and the means were used as the RMRs. Each respirometry chamber housed one fish, with one additional chamber left empty as a blank control. The water temperature was controlled within ±0.5 °C. The water flow rates were adjusted before the measurements were taken to ensure that the DO concentrations in the chambers remained above

70% saturation to avoid hypoxic stress. This adjustment maintained a DO difference of 1.0–2.0 mg L^{-1} between the experimental and blank control groups.

2.3. Organ Size Determination

After the RMR measurements were completed at all temperatures, three fish from each treatment of each species were sacrificed and dissected for organ size determination. The fresh livers, brains, hearts, kidneys, and red muscles were removed, and the samples were weighed (0.0001 g) immediately. Then, the mitochondria of fresh tissues were extracted following published methods for measuring mitochondrial respiration and citrate synthase (CS) activity [47,49]. The organ index for the livers, hearts, brains, kidneys, and red muscles was calculated via the following formula: Organ Index (%) = (organ mass/body mass) × 100%.

2.4. Mitochondrial Isolation

After the fish were euthanized, heart, liver, kidney, brain, and red muscle tissues were immediately collected and weighed. Hearts, brains, and kidneys, as well as approximately 0.1–0.2 g each of liver and red muscle tissue, were collected. The tissue samples were coarsely chopped with scissors, suspended in 1.5 mL of isolation buffer A (250 mM sucrose, 10 mM TES, 1 mM EDTA, 0.4% BSA, pH 7.4), and homogenized via a glass–Teflon homogenizer. The homogenates were centrifuged at 12,100× g for 10 min to remove lipid droplets. The pellet, containing cell debris, nuclei, and mitochondria, was resuspended in 1 mL of ice-cold isolation buffer B (250 mM sucrose, 10 mM TES, 1 mM EGTA, 0.4% BSA, pH 7.4) and centrifuged again at 980× g for 10 min to remove nuclei and cellular debris. The supernatants were transferred to fresh tubes and centrifuged at 8800× g for 10 min. The mitochondrial pellets were resuspended (1:1, w/v) in ice-cold isolation buffer C (100 mM KCl, 20 mM TES, and 1 mM EGTA, pH 7.4). All procedures were conducted on ice.

Mitochondrial respiration levels in various tissues were measured at 10, 15, 20, 25 and 30 °C using a temperature-controlled Clark electrode system (Hansatech Instruments, Pentney, UK). A 100-µL mitochondrial suspension was added to the assay medium (1.25 mM succinate, 1.25 mM pyruvate, 1.25 mM glutamate, 0.75 mM malate, 50 mM Tris-base, 1 mM EDTA, 15 mM KH_2PO_4, 5 mM $MgCl_2 \cdot 6H_2O$, 250 mM sucrose, pH 7.4) to reach a final volume of 2 mL. The maximal OXPHOS rate (state III respiration) was measured after adding ADP to a final concentration of 0.25 mM.

The mitochondrial protein content was determined via the Folin phenol method, with bovine serum albumin used as a standard. The mitochondrial respiration rates were calculated as nmol O_2 min^{-1} mg^{-1} mitochondrial protein. The respiratory control ratio (RCR) was calculated as the ratio of state III respiration to state IV or state II respiration to determine the coupling rates.

2.5. CS Activity Measurement

After the fish were euthanized, heart, liver, kidney, brain, and red muscle tissues were immediately collected, weighed, immersed in liquid nitrogen, and stored at −80 °C. CS activity was measured via a Fish Citrate Synthase (CS) ELISA Kit (Beijing Jinzhiyan Biotechnology Co., Ltd., Beijing, China). The specific method and steps for enzyme extraction followed the kit instructions. The absorbance (OD value) was measured at 450 nm via a microplate reader at 20 °C, and the enzyme activity was calculated according to the provided formula. Protein concentrations in homogenates were measured using bovine serum albumin as a standard. Enzyme activities are expressed as U mg^{-1} protein. CS is a critical enzyme in aerobic respiration, and previous studies have shown a strong correlation between CS activity and mitochondrial content in tissues. Therefore, this study used

tissue CS activity as an indicator of the mitochondrial content instead of the mitochondrial protein content [50].

2.6. Temperature Quotient Calculations (Q_{10})

The Q_{10} value is an indicator of metabolic sensitivity to temperature changes. We calculated the thermal sensitivity (Q_{10}) of metabolic rates and mitochondrial respiration rates as follows:

$$Q_{10} = \left(\frac{M_2}{M_1}\right)^{\left(\frac{10}{T_2 - T_1}\right)}$$

where M_2 is the biological rate (e.g., state III respiration) at temperature T_2 (e.g., 20 °C) and where M_1 is the rate at temperature T_1 (e.g., 25 °C). Typically, the Q_{10} values range between 2 and 3, indicating that the reaction rate doubles or triples with a 10 °C temperature change [45,51,52].

2.7. Statistical Analysis

All the data were analyzed via SPSS 27.0 (SPSS Inc., Chicago, IL, USA). Before analysis, normality and homogeneity of variance were tested. One-way ANOVA followed by post hoc Tukey's tests was used to analyze the mitochondrial respiration rates, mitochondrial protein content, and CS activity among the tissues of the three species. Two-way ANOVA was used to assess potential interactions between experimental variables (temperature, species, and tissue) and mitochondrial respiration or the mitochondrial content (Table A1). Three-way ANOVA was applied to evaluate the effects of temperature, tissue, and species on mitochondrial respiration rates and mitochondrial content (Table A2). All values are presented as the means ± standard errors (SEs). $p < 0.05$ was considered statistically significant.

3. Results

3.1. Organ Sizes

The brain, heart, kidney, and red muscle indices did not differ significantly between treatments in any species (Table A1). However, the liver index in *H. nobilis* was approximately 1.2-fold greater under cold treatments (10 and 15 °C) than under warm treatments (25 and 30 °C), whereas the liver indices did not differ between the treatments in *D. macrophthalmus* and *A. grahami* (Figure 2). Organ indices differed significantly among the five tissues across species. The heart and red muscle indices of *D. macrophthalmus* and *A. grahami* were greater than those of *H. nobilis*, whereas the brain and kidney indices showed the opposite pattern. The liver index of *H. nobilis* was greater than that of *D. macrophthalmus* and *A. grahami* at 10 and 15 °C but lower at 20–30 °C (Figure 2).

3.2. Resting Metabolic Rate (RMR)

For all three species, the RMR increased with temperature (10–30 °C) (Figure 3A). The RMRs were different between the temperature treatments in *D. macrophthalmus* and *A. grahami* but not between the 10 °C and 15 °C treatments in *H. nobilis*. At all the acclimation temperatures, *A. grahami* had the highest RMR, followed by *D. macrophthalmus*, with *H. nobilis* having the lowest (Figure 3A).

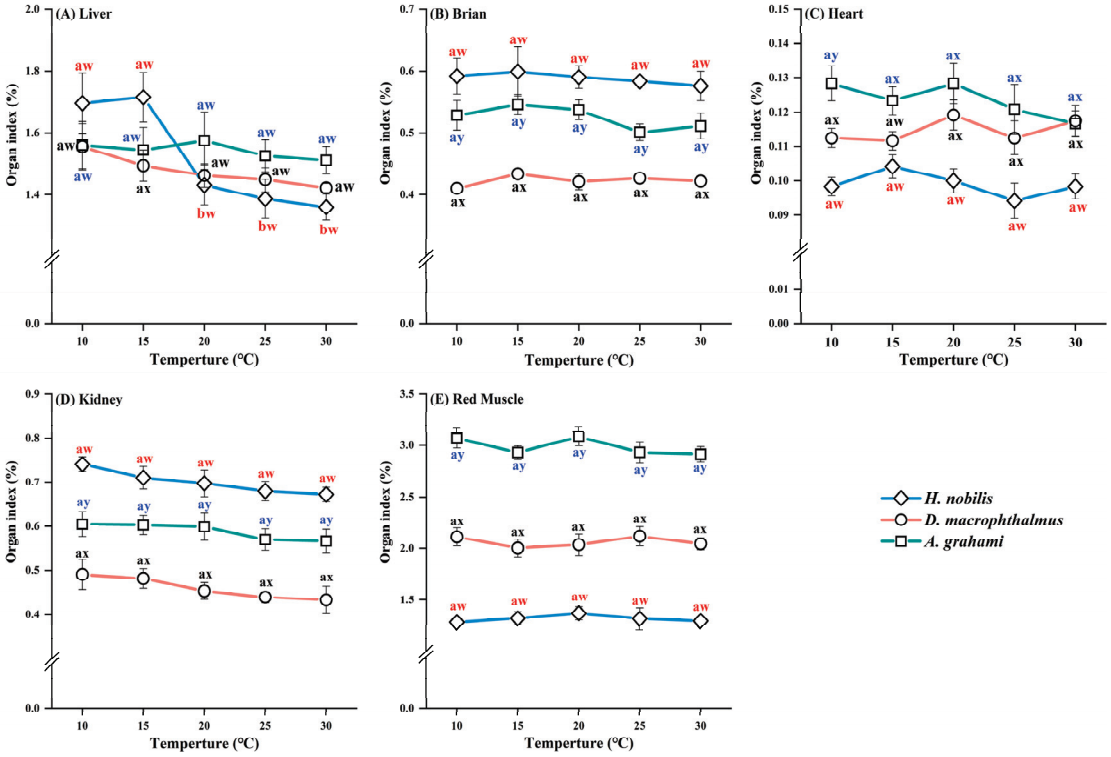


Figure 2. Organ indices of *H. nobilis*, *D. macrophthalmus*, and *A. grahami* tissues. The data are expressed as the means ± SEs, $n = 12$; a and b indicate significant differences between temperatures ($p < 0.05$); w, x, and y indicate significant differences between species ($p < 0.05$).

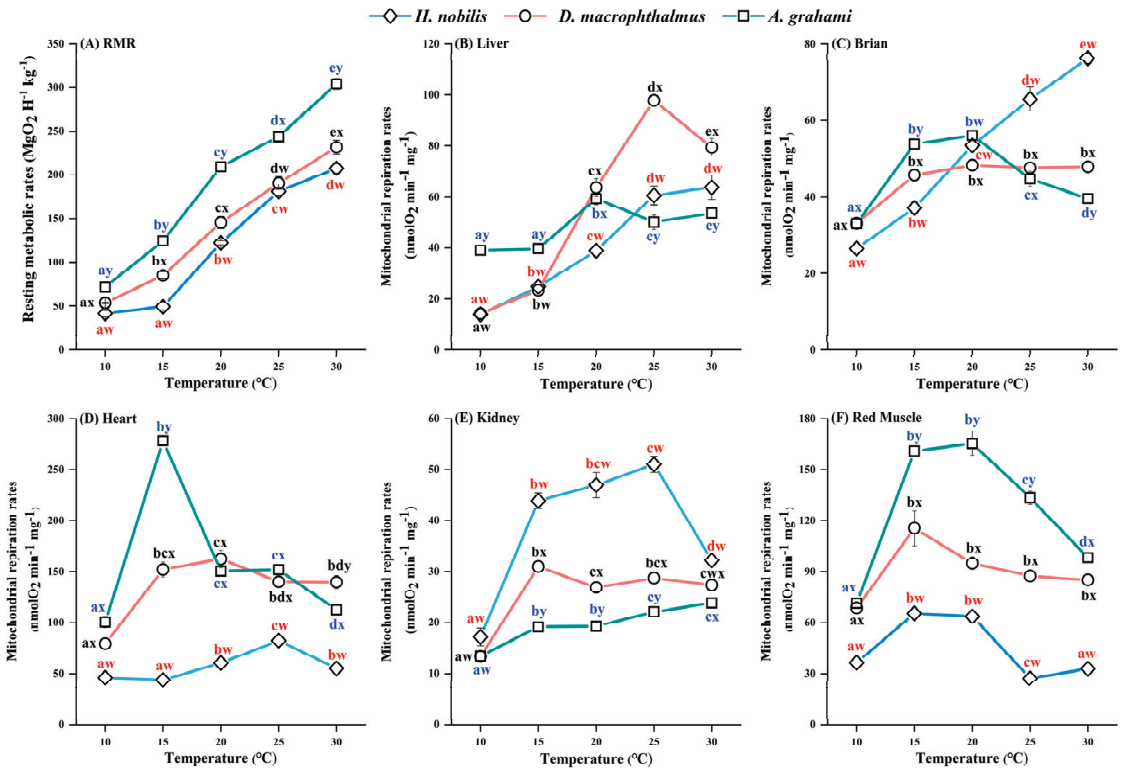


Figure 3. Effects of temperature on the RMRs and mitochondrial respiration rates of *H. nobilis*, *D. macrophthalmus*, and *A. grahami*. (**A**): the resting metabolic rates, $n = 6$; (**B**–**F**): the mitochondrial respiration rates in the tissues, $n = 4$. The data are presented as the means ± SEs; a–e indicate significant differences between temperatures ($p < 0.05$); w–y indicate significant differences between species ($p < 0.05$).

3.3. Mitochondrial Respiration Rates and the RCR

In all the species, the mitochondrial respiration rates of all the tissues initially increased but subsequently decreased with increasing temperature, but the temperature at which peak respiration occurred varied among the species and tissues (Figure 3B–F). In *H. nobilis*, the liver and brain mitochondria increased consistently with temperature, whereas the heart and kidney rates peaked at 25 °C, decreased at 30 °C, and the red muscle rates plateaued at 15 °C. In *D. macrophthalmus*, liver mitochondria peaked at 25 °C and then declined at 30 °C, whereas other tissues plateaued or peaked at 15 °C. In *A. grahami*, liver mitochondria peaked at 20 °C and then declined at 25 °C, with other tissues plateauing or peaking at 15 °C. Among the species, heart tissue presented the highest mitochondrial respiration rates, followed by red muscle, brain, and liver, with the kidney showing the lowest rates (Figure 3B–F). At all temperatures, the mitochondrial respiration rates of heart and red muscle tissues from *D. macrophthalmus* and *A. grahami* were significantly greater than those of *H. nobilis* (Figure 3D,F), whereas kidney mitochondria presented the opposite pattern (Figure 3E). Under cold treatments (10 and 15 °C), liver and brain mitochondrial respiration rates were higher in *D. macrophthalmus* and *A. grahami* than in *H. nobilis* (Figure 3B,C). However, under warm conditions (25 and 30 °C), brain mitochondrial respiration was higher in *H. nobilis* (Figure 3C).

Temperature significantly affected the RCR values (Table A1). The RCR values for most tissues of the three species were greater than 3 at most temperatures, first increasing but then decreasing as the temperature increased (Figure 3B–F). In *H. nobilis*, the kidney RCR was only 1.96 at 10 °C, and red muscle had lower RCR values (1.32–2.51) across temperatures (Table 1). Notably, at 30 °C, the RCR values of most tissues in the three species were low (<3) (Table 1), indicating a reduced coupling rates of mitochondrial respiration at relatively high temperatures.

Table 1. RCR values of mitochondria isolated from five tissues of *H. nobilis*, *D. macrophthalmus*, and *A. grahami* in the presence of different temperatures.

Tissue	Species	Temperature (°C)				
		10	**15**	**20**	**25**	**30**
Liver	*H. nobilis*	4.83 ± 0.09^{ax}	6.32 ± 0.23^{bw}	5.25 ± 0.34^{aw}	4.94 ± 0.42^{aw}	3.31 ± 0.12^{cw}
	D. macrophthalmus	4.19 ± 0.11^{aw}	5.81 ± 0.33^{bw}	7.07 ± 0.31^{cx}	5.23 ± 0.36^{bdw}	4.96 ± 0.17^{adx}
	A. grahami	9.40 ± 0.16^{ax}	7.69 ± 0.46^{bx}	7.36 ± 0.37^{bx}	3.69 ± 0.27^{cx}	3.64 ± 0.21^{cw}
Brian	*H. nobilis*	5.30 ± 0.31^{aw}	4.26 ± 0.34^{aw}	6.01 ± 0.15^{acw}	4.42 ± 0.37^{bdw}	4.61 ± 0.10^{adw}
	D. macrophthalmus	5.66 ± 0.42^{aw}	4.80 ± 0.19^{bw}	5.11 ± 0.35^{bw}	4.04 ± 0.01^{bw}	2.69 ± 0.09^{cx}
	A. grahami	5.57 ± 0.19^{aw}	5.13 ± 0.38^{aw}	5.11 ± 0.18^{aw}	3.34 ± 0.13^{bx}	2.63 ± 0.09^{cx}
Heart	*H. nobilis*	3.85 ± 0.29^{aw}	7.02 ± 0.70^{bw}	6.66 ± 0.30^{bcw}	5.27 ± 0.60^{cw}	4.35 ± 0.21^{aw}
	D. macrophthalmus	4.72 ± 0.11^{ax}	5.37 ± 0.00^{abx}	5.97 ± 0.43^{bw}	3.53 ± 0.21^{cx}	3.65 ± 0.17^{cw}
	A. grahami	3.14 ± 0.17^{ay}	5.43 ± 0.31^{bx}	4.47 ± 0.21^{cx}	3.16 ± 0.31^{ax}	2.03 ± 0.10^{dx}
Kidney	*H. nobilis*	1.96 ± 0.18^{aw}	5.55 ± 0.33^{bw}	4.16 ± 0.08^{cw}	4.52 ± 0.11^{cw}	2.29 ± 0.10^{aw}
	D. macrophthalmus	5.19 ± 0.39^{ax}	5.49 ± 0.42^{aw}	5.03 ± 0.22^{bx}	4.74 ± 0.30^{bw}	2.06 ± 0.19^{cw}
	A. grahami	3.09 ± 0.14^{aw}	4.55 ± 0.15^{bw}	1.94 ± 0.34^{cy}	1.83 ± 0.24^{cx}	1.62 ± 0.08^{cw}
Red muscle	*H. nobilis*	2.51 ± 0.20^{aw}	2.12 ± 0.18^{aw}	1.59 ± 0.11^{bw}	1.32 ± 0.08^{bw}	1.38 ± 0.08^{bw}
	D. macrophthalmus	5.26 ± 0.08^{ax}	3.33 ± 0.36^{bx}	1.59 ± 0.10^{cw}	2.16 ± 0.09^{dew}	1.80 ± 0.10^{cew}
	A. grahami	4.36 ± 0.13^{ax}	3.68 ± 0.26^{by}	3.22 ± 0.17^{bcx}	3.78 ± 0.20^{bdy}	3.86 ± 0.13^{dx}

Note: The date were expressed as mean ± SEs, $n = 4$; a–e: different superscripts in the same line indicate significant differences between different temperature of the same species ($p < 0.05$); w–y: different superscripts in the same column indicate significant differences among different species in the same tissue ($p < 0.05$).

3.4. Mitochondrial Protein Content and CS Activity

Under each temperature treatment, the mitochondrial protein content did not differ significantly among the three species (Tables A1 and A2). The heart mitochondrial protein content was significantly lower than that in other tissues but not different from that in other tissues (Figure 4).

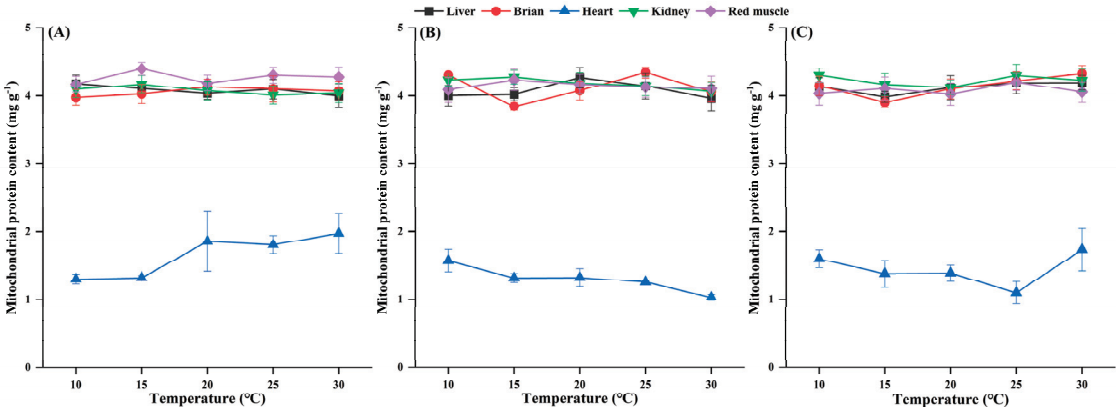


Figure 4. Effects of temperature on the mitochondrial protein content in the tissues of *H. nobilis* (**A**), *D. macrophthalmus* (**B**), and *A. grahami* (**C**). The data are expressed as the means ± SEs, $n = 4$.

Significant differences in CS activity were observed among species across the temperature treatments (Tables A1 and A2). Among all the tissues, *H. nobilis* had the highest CS activity, followed by *A. grahami*, with *D. macrophthalmus* exhibiting the lowest activity. CS activity in *D. macrophthalmus* was the lowest. The CS activity of *D. macrophthalmus* was significantly lower than that of the other two species, whereas the differences between *H. nobilis* and *A. grahami* were not significant (Figure 5).

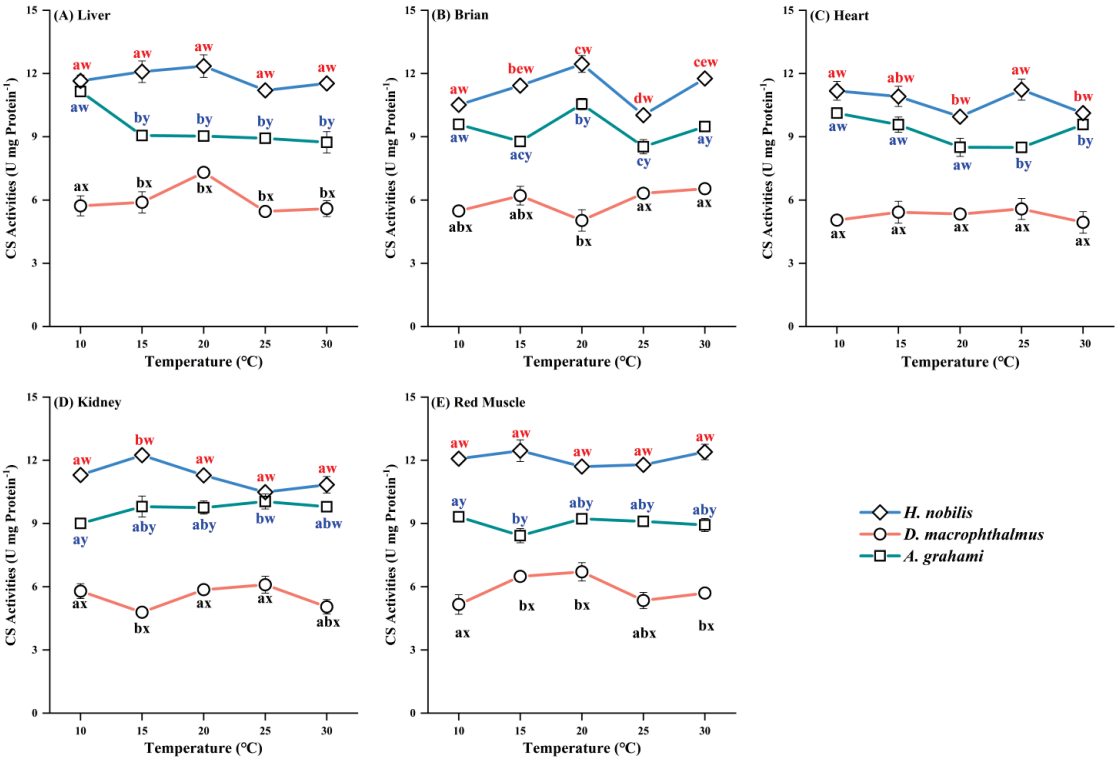


Figure 5. Effects of temperature on CS activity in the tissues of *H. nobilis*, *D. macrophthalmus*, and *A. grahami*. The data are expressed as the means ± SEs, $n = 3$; a–e indicate significant differences between temperatures ($p < 0.05$); w–y indicate significant differences between species ($p < 0.05$).

3.5. Thermal Sensitivity (Q_{10})

The three species presented considerable variability in terms of their Q_{10} values across the experimental temperature range (Table 2). The Q_{10} values indicated greater thermal sensitivity at lower temperatures (10–15 °C and 15–20 °C) and decreased at higher temperatures (20–25 °C and 25–30 °C) (Figure 4). Overall, high-altitude species presented greater thermal sensitivity in terms of metabolic rates at both lower (10–15 °C) and higher (25–30 °C) temperatures than did low-altitude species.

Table 2. Q_{10} values for RMRs and mitochondrial respiration rates in *H. nobilis*, *D. macrophthalmus*, and *A. grahami* for each temperature range after short-term temperature adaptation.

Parameter		Species	Temperature Ranges			
			10–15 °C	15–20 °C	20–25 °C	25–30 °C
Resting metabolic rates		*H. nobilis*	1.28 ± 0.08	5.28 ± 0.22	2.66 ± 0.18	1.31 ± 0.02
		D. macrophthalmus	2.52 ± 0.14	2.93 ± 0.13	1.74 ± 0.13	1.48 ± 0.03
		A. grahami	3.14 ± 0.30	2.84 ± 0.09	1.36 ± 0.03	1.56 ± 0.02
Mitochondrial respiration rates	Liver	*H. nobilis*	3.17 ± 0.28	2.52 ± 0.18	2.43 ± 0.13	1.11 ± 0.06
		D. macrophthalmus	2.74 ± 0.18	7.47 ± 0.57	2.40 ± 0.19	0.66 ± 0.04
		A. grahami	1.04 ± 0.05	2.24 ± 0.14	0.71 ± 0.03	1.17 ± 0.11
	Brian	*H. nobilis*	1.97 ± 0.09	2.09 ± 0.11	1.51 ± 0.12	1.37 ± 0.09
		D. macrophthalmus	1.91 ± 0.06	1.12 ± 0.04	0.97 ± 0.03	1.01 ± 0.04
		A. grahami	2.65 ± 0.06	1.09 ± 0.05	0.64 ± 0.03	0.79 ± 0.06
	Heart	*H. nobilis*	0.95 ± 0.13	1.89 ± 0.11	1.87 ± 0.07	0.45 ± 0.03
		D. macrophthalmus	3.70 ± 0.32	1.14 ± 0.05	0.75 ± 0.05	1.00 ± 0.03
		A. grahami	7.80 ± 0.66	0.29 ± 0.01	1.02 ± 0.02	0.55 ± 0.03
	Kidney	*H. nobilis*	6.84 ± 0.82	1.15 ± 0.07	1.20 ± 0.08	0.40 ± 0.01
		D. macrophthalmus	5.44 ± 0.36	0.75 ± 0.02	1.15 ± 0.04	0.92 ± 0.04
		A. grahami	2.03 ± 0.04	1.01 ± 0.02	1.31 ± 0.05	1.17 ± 0.07
	Red muscle	*H. nobilis*	3.23 ± 0.10	0.95 ± 0.04	0.18 ± 0.01	1.45 ± 0.06
		D. macrophthalmus	2.88 ± 0.46	0.70 ± 0.09	0.85 ± 0.04	0.95 ± 0.03
		A. grahami	5.08 ± 0.12	1.06 ± 0.09	0.65 ± 0.03	0.54 ± 0.01

Note: These values represent the magnitude of increase in a rate with a 10 °C increase in temperature, such that a value of two represents a doubling of the rate per 10 °C increase, values of one represent thermal independence, and values of 0.5 represent a halving of the rate per 10 °C increase, n = 4–6.

4. Discussion

4.1. Comparison of Metabolic Rates

Temperature is a crucial factor influencing the metabolic requirements of fish. Typically, metabolic rates initially increase with increasing temperature, reach a peak, and subsequently decline [13]. In this study, the resting metabolic rates (RMRs) of all three species increased with temperature (Figure 3A), whereas the mitochondrial respiration rates in the tissues first increased but then decreased (Figure 3B–F). In general, mitochondrial metabolic capacity is regulated by alterations in mitochondrial abundance and/or oxidative capacity [48]. CS activity, which reflects flux rates in the tricarboxylic acid cycle and is often used as a proxy for mitochondrial density, shows a pattern inconsistent with mitochondrial respiration rates [53]. Specifically, CS activity remained relatively stable across acclimation conditions when acute temperatures matched acclimation temperatures, suggesting enzyme quantity and/or quality adjustments [53]. The adjustment of mitochondrial respiration rates to changing temperatures is likely primarily mediated by modifications in mitochondrial oxidative capacity. Extensive research has demonstrated that temperature significantly influences metabolic rates in ectotherms. We observed that the Q_{10} values for all three species presented marked metabolic stress responses at relatively

low temperatures, which decreased with increasing temperature, which was consistent with observations in other taxa [54]. Beyond 30 °C, respiratory rates decline (Q_{10} < 1.0), indicating impaired mitochondrial function [54]. Although temperatures exceeding 30 °C were not investigated in this study, metabolic efficiencies across all species contributed to declining Q_{10} values with increasing temperature, resulting in lower Q_{10} values at higher temperatures (Table 2). The RCR serves as a sensitive indicator of mitochondrial functional status [55]. Low RCR values indicate impaired mitochondrial ATP synthesis and dysfunction, whereas high RCR values reflect robust cellular activity and enhanced metabolism [56,57]. The RCR values exhibited a pattern similar to that of Q_{10}, decreasing at higher temperatures (30 °C) (Table 1). These findings suggest that 30 °C may exceed the optimal physiological temperature range for these species. We also noted that this influence varies among species. Notably, high-altitude fish (*D. macrophthalmus* and *A. grahami*) exhibited steeper ascending and descending metabolic phases overall (Figure 3). This divergence likely reflects not only acute or passive temperature responses but also differences in thermophysiology, with high-altitude fish exhibiting greater metabolic thermosensitivity.

With respect to metabolic rates, our findings align with the MCA hypothesis. Specifically, high-altitude fish (*D. macrophthalmus* and *A. grahami*) presented greater metabolic rates than did low-altitude species (*H. nobilis*) across all measured temperatures (Figure 3). Such elevated metabolic rates may confer significant advantages for ectotherms, enabling faster food processing and providing organisms with enhanced cellular capacity to respond rapidly to environmental challenges [9,58]. At the mitochondrial level, we also observed greater energy allocation in the cardiac and red muscle tissues of high-altitude species, potentially reflecting an adaptation to prolonged low temperatures and resource scarcity in high-altitude environments [59,60]. The high metabolic capacity of cardiac and red muscle tissues enables plateau fish to consume oxygen more effectively, maintain blood flow, and satisfy the energy demands associated with extended food foraging periods [61]. Moreover, the elevated metabolic rates of plateau fish do not result from increased mitochondrial content but is instead achieved through comparatively fewer mitochondria, suggesting an efficient, resource-conserving strategy.

4.2. Changes in Organs

Organ size is among the most significant intrinsic factors influencing metabolic scaling [62]. Among various organs, the liver, and heart contribute most substantially to the whole-organism metabolic rate [6,27]. During thermal or seasonal acclimation, some fish species undergo adjustments in the relative mass of certain organ tissues to meet the energy metabolic demands under different temperature environments [63,64]. In this study, under cold acclimation (10 °C and 15 °C), the liver of *H. nobilis* was approximately 1.2 times larger than that under warm acclimation, indicating that cold compensation of the liver in *H. nobilis* may be achieved at the whole organ rather than at the tissue level [65]. From an ecological perspective, many physiological challenges posed by temperature fluctuations may be partially counterbalanced by adjustments in organ size [66]. In contrast, the brain, heart, kidney, and red muscle of *H. nobilis*, as well as organ sizes in high-altitude fish (*D. macrophthalmus* and *A. grahami*), showed no response to temperature acclimation, remaining relatively constant across all acclimation temperatures (Figure 2). The precise mechanisms remain unknown, though one hypothesis is that the short acclimation period limited the phenotypic plasticity of these organs. Similarly, the lack of change in liver size in plateau fish may stem from restricted plasticity, which partially supports CVH. However, owing to their limited plasticity, these organs may experience stronger selective pressures, thus promoting rapid adaptive evolution [67–69] and enabling unique local adaptations. We observed that high-altitude species (*D. macrophthalmus* and *A. grahami*) presented higher

organ indices for the heart, red muscle, and liver than *H. nobilis* did (Figure 2A,C,E). The greater heart mass observed in plateau fish likely enhances blood circulation and transport capacity, serving as the "powerhouse" of the circulatory system [61], and may also improve resistance to extreme cold conditions [70] liver, the primary energy storage organ in fish [70], plays a crucial role in environmental adaptation. Additionally, red muscle continuously generates ATP through efficient aerobic metabolism (OXPHOS), thus supporting prolonged swimming activity [63]. Conversely, we found that the organ indices of the brain and kidney were lower in plateau fish (Figure 2). This finding likely arises from resource allocation constraints at high altitudes, where metabolic processes among organs may interact: some organs enlarge, whereas others shrink to maintain energy balance and ensure sustained growth [71]. This strategy may effectively conserve energy, allowing high-altitude species to maintain normal physiological functions.

4.3. Contribution of Mitochondria to Physiological Thermal Limits

Mitochondria provide cellular energy through OXPHOS and are essential for aerobic metabolism and maintaining the organismal energy balance. Consequently, temperature-induced impairments in mitochondrial function may critically affect thermal tolerance in animals [5,6]. Mitochondria have been proposed as key determinants of whole-organism thermal limits [72]. Moreover, mitochondrial physiological adjustments associated with thermal acclimation may lead to dysfunction during acute temperature changes, potentially resulting in shifts in thermal limits [5]. As temperature increases, mitochondrial oxygen consumption initially increases; however, beyond optimal physiological temperatures, oxygen consumption either plateaus or decreases, impairing ATP production [6,72,73]. Numerous studies suggest that high-temperature-induced declines in mitochondrial function significantly determine physiological thermal limits in many ectotherms [72]. Consistent with previous findings, the mitochondrial respiration rates in this study initially increased with increasing temperature but stabilized or declined at relatively high temperatures (Figure 3B–F), and the RCR values exhibited a similar trend (Figure 4). This finding suggests reduced coupling rates in mitochondrial OXPHOS, indicating that temperatures may exceed optimal physiological thresholds. Interestingly, among the five tissues examined, the heart was the first to show reduced mitochondrial function (Figure 3C), suggesting that the heart may be the earliest organ to fail under thermal stress. Numerous studies have also identified the heart as particularly vulnerable to heat stress, which restricts energy provision and consumption when fish exceed their optimal thermal limits [26,72,74–77]. Thus, we speculate that the temperature at which heart mitochondrial respiration peaks may represent a species' optimal physiological temperature. In this study, the maximum heart respiration rates occurred at 25 °C (*H. nobilis*), 20 °C (*D. macrophthalmus*), and 15 °C (*A. grahami*), which aligns with their previously documented optimal growth temperatures [40–43,78]. The mitochondrial energy transduction efficiency of the electron transfer and phosphorylation system is often employed as an indicator of mitochondrial function and dysfunction [78]. While our investigation centered on the oxidative phosphorylation (OXPHOS) process, it did not include the electron transfer process itself. Additionally, other critical aspects—such as reactive oxygen species (ROS) production and the antioxidant defense system, mitochondrial membrane integrity (fluidity), permeability, and stability—have been strongly linked to animal thermal tolerance [72,73,79]. These aspects warrant further investigation in future research.

5. Conclusions

Currently, research on the metabolic responses and characteristics of plateau fishes during temperature acclimation is limited and remains unclear. This study revealed that

the basal metabolic rates of all three species increased with increasing temperature, whereas the mitochondrial respiration rates across tissues initially increased but subsequently decreased. Under all the acclimation conditions, the CS activity remained relatively constant across the three species, indicating that changes in the mitochondrial respiration rate were independent of the mitochondrial content. In contrast, plateau fish species (*D. macrophthalmus* and *A. grahami*) presented greater temperature sensitivity and lower plasticity, suggesting increased vulnerability to climate warming. Furthermore, we observed increased metabolic rates in both *D. macrophthalmus* and *A. grahami* across all acclimation temperatures, supporting the MCA and CVH hypotheses. At the organ level, the liver, heart, and red muscle presented increased organ indices, whereas the brain and kidney presented decreased indices. This adaptive strategy involving elevated metabolic rates and adjustments in organ size may confer advantages for plateau fish in maintaining energy balance, with significant implications for survival. Nevertheless, this study has several limitations. First, this study focused on short-term thermal acclimation. While our results demonstrate significant physiological plasticity, long-term adaptation involves genetic changes. Future studies should thus employ long-term designs to fully assess the adaptive potential of these fish to challenges like climate change, and to determine if the observed responses are heritable and contribute to evolutionary fitness. Second, our investigation centered on mitochondrial oxidative phosphorylation but omitted other critical aspects like reactive oxygen species (ROS) production or membrane potential. Measuring these parameters in future work is essential. Elucidating these dynamics remains a key future goal, which will provide a more holistic view of mitochondrial physiology and deepen insights into the evolutionary and developmental dimensions of thermal adaptation in fish.

Author Contributions: Conceived and designed the study: W.D., Y.Z., J.Y., and X.W.; collected the data: W.D., J.L., Y.Y., A.W., Y.C., H.G., and X.P.; performed the analysis: W.D., and J.L.; wrote the manuscript: W.D., and Y.Z.; flow-type breath analyzer designed by J.L. All authors contributed critically to the drafts, revisions, and gave final approval for publication. All authors have read and agreed to the published version of the manuscript.

Funding: This study was funded by the Program of Yunnan Provincial Science and Technology Department (Nos. 202303AC100011, 202301AT070305, 202105AD160026, 202305AM340026) and Youth program of Yunnan Talent Support Plan (No. XDYC-QNRC-2023-0542).

Institutional Review Board Statement: All research protocols and treatments of the experimental fish were reviewed and approved by the Institutional Review Board of the Kunming Institute of Zoology (KIZ), Chinese Academy of Sciences (CAS), China (approval ID: IACUC-PA-2022-07-049).

Informed Consent Statement: Not applicable.

Data Availability Statement: The raw data supporting the conclusions of this article will be made available by the authors on request.

Conflicts of Interest: The authors declare no conflicts of interest.

Abbreviations

ADP	Adenosine diphosphate
ATP	Adenosine triphosphate
CVH	Climate variability hypothesis
MCA	Metabolic cold adaptation hypothesis
OXPHOS	Oxidative phosphorylation
RMR	Resting metabolic rate
CS	Citrate synthase activity
RCR	Respiratory control ratio

Appendix A

Table A1. Summary of two-way ANOVA results for metabolic parameters in *H. nobilis*, *D. macrophthalmus*, and *A. grahami*.

Species	Parameter	Factors/Interaction		
		Temperature	Tissue	Temperature * Tissue
H. nobilis	RMR	$F_{4, 25} = 350.081$, $p < 0.001$	—	—
	Mitochondrial protein content	$F_{4, 95} = 0.008$, $p = 1.00$	$F_{4, 95} = 243.549$, $p < 0.001$	$F_{16, 75} = 0.275$, $p = 0.997$
	CS activity	$F_{4, 70} = 3.772$, $p < 0.05$	$F_{4, 70} = 7.378$, $p < 0.001$	$F_{14, 52} = 2.332$, $p < 0.05$
	Mitochondrial respiration rates	$F_{4, 95} = 11.673$, $p < 0.001$	$F_{4, 95} = 4.411$, $p < 0.05$	$F_{16, 75} = 48.221$, $p < 0.001$
	RCR	$F_{4, 95} = 3.426$, $p < 0.05$	$F_{4, 95} = 36.648$, $p < 0.001$	$F_{16, 75} = 9.992$, $p < 0.05$
	Organ index	$F_{4, 295} = 0.291$, $p = 0.884$	$F_{4, 295} = 663.610$, $p < 0.001$	$F_{16, 275} = 2.402$, $p < 0.05$
D. macrophthalmus	RMR	$F_{4, 25} = 150.766$, $p < 0.001$	—	—
	Mitochondrial protein content	$F_{4, 95} = 0.046$, $p = 0.996$	$F_{4, 95} = 438.312$, $p < 0.001$	$F_{16, 75} = 0.861$, $p = 0.614$
	CS activity	$F_{4, 70} = 1.144$, $p = 0.343$	$F_{4, 70} = 2.313$, $p = 0.066$	$F_{14, 52} = 1.540$, $p = 0.130$
	Mitochondrial respiration rates	$F_{4, 95} = 2.807$, $p < 0.05$	$F_{4, 95} = 73.712$, $p < 0.001$	$F_{16, 75} = 24.034$, $p < 0.001$
	RCR	$F_{4, 95} = 8.544$, $p < 0.001$	$F_{4, 795} = 13.060$, $p < 0.001$	$F_{16, 75} = 15.418$, $p < 0.05$
	Organ index	$F_{4, 295} = 0.802$, $p = 0.525$	$F_{4, 295} = 900.219$, $p < 0.001$	$F_{16,275} = 13.553$, $p < 0.001$
A. grahami	RMR	$F_{4, 25} = 295.432$, $p < 0.001$	—	—
	Mitochondrial protein content	$F_{4, 95} = 0.062$, $p = 0.993$	$F_{4, 95} = 319.933$, $p < 0.001$	$F_{16,75} = 0.325$, $p = 0.993$
	CS activity	$F_{4, 70} = 2.364$, $p = 0.061$	$F_{4, 70} = 1.521$, $p = 0.205$	$F_{14, 52} = 5.040$, $p < 0.001$
	Mitochondrial respiration rates	$F_{4, 95} = 2.750$, $p < 0.05$	$F_{4, 95} = 60.670$, $p < 0.001$	$F_{16, 75} = 167.354$, $p < 0.001$
	RCR	$F_{4, 95} = 9.503$, $p < 0.001$	$F_{4, 95} = 17.926$, $p < 0.001$	$F_{16, 75} = 23.893$, $p < 0.05$
	Organ index	$F_{4, 295} = 0.682$, $p = 0.605$	$F_{4, 295} = 1259.665$, $p < 0.001$	$F_{16, 275} = 10.746$, $p < 0.001$

Table A2. Summary of three-way ANOVA results for metabolic parameters.

Parameter	Factors/Interaction			
	Species	Species * Temperature	Species * Tissue	Species * Temperature * Tissue
RMR	$F_{2, 75} = 240.611$, $p < 0.05$	$F_{8, 75} = 7.916$, $p < 0.05$	—	—
Mitochondrial protein content	$F_{2, 297} = 0.029$, $p = 0.971$	$F_{8, 255} = 0.805$, $p = 0.805$	$F_{8, 255} = 1.269$, $p = 0.260$	$F_{32, 255} = 0.343$, $p = 1.00$
CS activity	$F_{2, 222} = 893.394$, $p < 0.001$	$F_{8, 156} = 3.130$, $p < 0.05$	$F_{8, 156} = 4.354$, $p < 0.001$	$F_{28, 156} = 2.904$, $p < 0.001$
Mitochondrial respiration rates	$F_{2, 297} = 13.586$, $p < 0.001$	$F_{8, 255} = 76.907$, $p < 0.001$	$F_{8, 255} = 455.965$, $p < 0.001$	$F_{32, 255} = 53.852$, $p < 0.001$
RCR	$F_{2, 297} = 0.425$, $p = 0.654$	$F_{8, 255} = 17.233$, $p < 0.05$	$F_{8, 255} = 59.754$, $p < 0.05$	$F_{32, 255} = 11.859$, $p < 0.05$
Organ index	$F_{2, 897} = 8.164$, $p < 0.001$	$F_{8, 825} = 21.540$, $p < 0.0001$	$F_{8, 825} = 268.301$, $p < 0.001$	$F_{32, 825} = 12.667$, $p < 0.001$

References

1. Verberk, W.C.E.P.; Hoefnagel, K.N.; Peralta-Marave, I.; Floury, M.; Rezende, E.L. Long-term forecast of thermal mortality with climate warming in riverine amphipods. *Glob. Change Biol.* **2023**, *29*, 5033–5043. [CrossRef] [PubMed]
2. Brandl, S.J.; Lefcheck, J.S.; Bates, A.E.; Rasher, D.B.; Norin, T. Can metabolic traits explain animal community assembly and functioning? *Biol. Rev.* **2022**, *98*, 1–18. [CrossRef] [PubMed]

3. Shokri, M.; Cozzoli, F.; Vignes, F.; Bertoli, M.; Pizzul, E.; Basset, A. Metabolic rate and climate change across latitudes: Evidence of mass-dependent responses in aquatic amphipods. *J. Exp. Biol.* **2022**, *225*, jeb244842. [CrossRef] [PubMed]
4. Schaefer, J.; Walters, A. Metabolic cold adaptation and developmental plasticity in metabolic rates among species in the *Fundulus notatus* species complex. *Funct. Ecol.* **2010**, *2024*, 1087–1094. [CrossRef]
5. Chung, D.J.; Schulte, P.M. Mechanisms and costs of mitochondrial thermal acclimation in a eurythermal killifish (*Fundulus heteroclitus*). *J. Exp. Biol.* **2015**, *218*, 1621–1631. [CrossRef]
6. Michaelsen, J.; Fago, A.; Bundgaard, A. High temperature impairs mitochondrial function in rainbow trout cardiac mitochondria. *J. Exp. Biol.* **2021**, *224*, jeb242382. [CrossRef]
7. Gerber, L.; Clow, K.A.; Gamperl, A.K. Acclimation to warm temperatures has important implications for mitochondrial function in Atlantic salmon (*Salmo salar*). *J. Exp. Biol.* **2021**, *224*, jeb236257. [CrossRef]
8. Willis, J.R.; Hickey, A.J.R.; Devaux, J.B.L. Thermally tolerant intertidal triplefin fish (Tripterygiidae) sustain ATP dynamics better than subtidal species under acute heat stress. *Sci. Rep.* **2021**, *11*, 11074. [CrossRef]
9. Clarke, A. Fraser KPP. Why does metabolism scale with temperature? *Funct. Ecol.* **2004**, *18*, 243–251. [CrossRef]
10. Nati, J.J.H.; Svendsen, M.B.S.; Marras, S.; Killen, S.S.; Steffensen, J.F.; McKenzie, D.J.; Domenici, P. Intraspecific variation in thermal tolerance differs between tropical and temperate fishes. *Sci. Rep.* **2021**, *11*, 21272. [CrossRef]
11. da Silva, C.R.B.; Beaman, J.E.; Tuiwawa, M.; Stevens, M.I.; Schwarz, M.P.; Gloag, R.; Kellermann, V.; Alton, L.A. Temperature and precipitation explain variation in metabolic rate but not frequency of gas exchange in Fijian bees. *J. Exp. Biol.* **2025**, *228*, jeb249948. [CrossRef]
12. White, C.R.; Alton, L.A.; Frappell, P.B. Metabolic cold adaptation in fishes occurs at the level of whole animal; mitochondria and enzyme. *Proc. Biol. Sci.* **2012**, *279*, 1740–1747. [CrossRef]
13. Shah, A.A.; Woods, H.A.; Havird, J.C.; Encalada, A.C.; Flecker, A.S.; Funk, W.C.; Guayasamin, J.M.; Kondratieff, B.C.; Poff, N.L.; Thomas, S.A.; et al. Temperature dependence of metabolic rate in tropical and temperate aquatic insects, Support for the Climate Variability Hypothesis in mayflies but not stoneflies. *Glob. Change Biol.* **2021**, *27*, 297–311. [CrossRef]
14. Sun, B.J.; Williams, C.M.; Li, T.; Speakman, J.R.; Jin, Z.G.; Lu, H.L.; Luo, L.G.; Du, W.G. Higher metabolic plasticity in temperate compared to tropical lizards suggests increased resilience to climate change. *Ecol. Monogr.* **2022**, *92*, e1512. [CrossRef]
15. Dillon, M.E.; Wang, G.; Huey, R.B. Global metabolic impacts of recent climate warming. *Nature* **2010**, *467*, 704–706. [CrossRef]
16. Sunday, J.; Bennett, J.M.; Calosi, P.; Clusella-Trullas, S.; Gravel, S.; Hargreaves, A.L.; Leiva, F.P.; Verberk, W.C.E.P.; Olalla-Tárraga, M.Á.; Morales-Castilla, I. Thermal tolerance patterns across latitude and elevation. *Philos. Trans. R. Soc. Lond. B Biol. Sci.* **2019**, *374*, 20190036. [CrossRef]
17. Peralta-Maraver, I.; Rezende, E.L. Heat tolerance in ectotherms scales predictably with body size. *Nat. Clim. Change* **2021**, *11*, 58–63. [CrossRef]
18. Lindmark, M.; Ohlberger, J.; Gårdmark, A. Optimum growth temperature declines with body size within fish species. *Glob. Change Biol.* **2022**, *28*, 2259–2271. [CrossRef] [PubMed]
19. Koenigbauer, S.T.; Cubbage, M.L.; Warren, L.D.; Tellier, J.M.; Selz, O.M.; Sass, G.G.; Höök, T.O. Fish reproductive phenology shifts with increasing temperature and year. *Biol. Lett.* **2025**, *21*, 20240240. [CrossRef]
20. Wootton, H.F.; Morrongiello, J.R.; Schmitt, T.; Audzijonyte, A. Smaller adult fish size in warmer water is not explained by elevated metabolism. *Ecol. Lett.* **2022**, *25*, 1177–1188. [CrossRef] [PubMed]
21. Gillooly, J.F.; Brown, J.H.; West, G.B.; Savage, V.M.; Charnov, E.L. Effects of size and temperature on metabolic rate. *Science* **2001**, *293*, 2248–2251. [CrossRef]
22. von Herbing, I.H.; Pan, T.C.F. Metabolic energetics of developing fish from different thermal habitats exposed to chronic and acute temperature stressors. *Integr. Comp. Biol.* **2025**, *18*, icaf129. [CrossRef] [PubMed]
23. Watanabe, Y.Y.; Payne, N.L. Thermal sensitivity of metabolic rate mirrors biogeographic differences between teleosts and elasmobranchs. *Nat. Commun.* **2023**, *14*, 2054. [CrossRef]
24. Benavente, J.N.; Fryxell, D.C.; Kinnison, M.T.; Palkovacs, E.P.; Simon, K.S. Plasticity and evolution shape the scaling of metabolism and excretion along a geothermal temperature gradient. *Funct. Ecol.* **2022**, *36*, 1303–1314. [CrossRef]
25. Kefford, B.J.; Ghalambor, C.K.; Dewenter, B.; Poff, N.L.; Hughes, J.; Reich, J.; Thompson, R. Acute; diel; and annual temperature variability and the thermal biology of ectotherms. *Glob. Change Biol.* **2022**, *28*, 6872–6888. [CrossRef] [PubMed]
26. Dawson, N.J.; Magierecka, A.; McLennan, D.; Millet, C.; Czyzewski, J.; Metcalfe, N.B. Mitochondrial efficiency impacts nocturnal sheltering in juvenile salmon (*Salmo salar*), affecting the trade-off between foraging and predation risk. *Proc. Biol. Sci.* **2024**, *291*, 20241788. [CrossRef]
27. Luo, Y.P.; Wang, W.; Zhang, Y.R.; Huang, Q.D. Effect of body size on organ-specific mitochondrial respiration rate of the largemouth bronze gudgeon. *Fish Physiol. Biochem.* **2013**, *39*, 513–521. [CrossRef] [PubMed]

28. Watson, J.; Souques, C.; Dechaume-Moncharmont, F.X.; Roussel, D.; Le Guyader, J.; Lassus, R.; Guillard, L.; Clair, A.; Averty, L.; Bastianini, C.; et al. A multi-scaling approach showing a transient metabolic mismatch in a freshwater fish (*Zingel asper*) during an acute heat stress. *J. Exp. Biol.* **2025**, *228*, jeb250202. [CrossRef]
29. Morla, J.; Salin, K.; Lassus, R.; Favre-Marinet, J.; Sentis, A.; Daufresne, M. Multigenerational exposure to temperature influences mitochondrial oxygen fluxes in the Medaka fish (*Oryzias latipes*). *Acta Physiol.* **2024**, *240*, e14194. [CrossRef]
30. Ryu, K.W.; Fung, T.S.; Baker, D.C.; Favre-Marinet, J.; Sentis, A.; Daufresne, M. Cellular ATP demand creates metabolically distinct subpopulations of mitochondria. *Nature* **2024**, *635*, 746–754. [CrossRef]
31. Dahlke, F.T.; Wohlrab, S.; Butzin, M.; Pörtner, H.O. Thermal bottlenecks in the life cycle define climate vulnerability of fish. *Science* **2020**, *369*, 65–70. [CrossRef]
32. Chen, S.Y.; Wang, J.X. Progress in research on tectonic uplift in Yunnan-Guizhou plateau. *Yunnan Geogr. Environ. Res.* **2017**, *29*, 23–29, 40.
33. Ding, C.; Jiang, X.; Xie, Z.; Brosse, S. Seventy-five years of biodiversity decline of fish assemblages in Chinese isolated plateau lakes, Widespread introductions and extirpations of narrow endemics lead to regional loss of dissimilarity. *Divers. Distrib.* **2017**, *23*, 171–184. [CrossRef]
34. Shi, L.; Xiang, T.; Dong, X.H.; Xu, C.; Wang, H.; Jeppesen, E.; Xie, P. Homogenization of fish assemblages in an endemic biodiversity hot spot: Evidence from 70-year data from the Yun-Gui Plateau, China. *Freshw. Biol.* **2024**, *69*, 1537–1552. [CrossRef]
35. Hof, A.R.; Allen, A.M. An uncertain future for the endemic Galliformes of the Caucasus. *Sci. Total Environ.* **2019**, *651*, 725–735. [CrossRef]
36. Pastorino, P.; Elia, A.C.; Mossotto, C.; Gabetti, A.; Maganza, A.; Renzi, M.; Pizzul, E.; Faggio, C.; Prearo, M.; Barceló, D. Potential ecotoxicological effects of global change on organisms inhabiting high-mountain lakes in the Alps. *Sci. Total Environ.* **2025**, *975*, 179180. [CrossRef]
37. Zhao, G.L.; Tian, S.M.; Chen, R.X.; Cao, Y.T.; Zhang, Y.; Han, B. Effect of global climate change on the sustainability of cold-water fish habitat in the alpine region: A case study on the *Gymnocypris eckloni* in the source region of the Yellow River. *J. Environ. Manag.* **2024**, *367*, 121926. [CrossRef] [PubMed]
38. Chen, Y.Y.; Wu, X.Y.; Li, P.C.; Liu, Y.; Song, M.J.; Li, F.Y.; Ou, J.; Lai, J.S. Integrated metabolomic and transcriptomic responses to heat stress in a high-altitude fish; *Triplophysa siluroides*. *Fish Shellfish Immunol.* **2023**, *142*, 109118. [CrossRef]
39. Zhu, T.B.; Li, X.M.; Wu, X.B.; Yang, D.G. Temperature Acclimation Alters the Thermal Tolerance and Intestinal Heat Stress Response in a Tibetan Fish *Oxygymnocypris stewarti*. *Front. Microbiol.* **2022**, *13*, 898145. [CrossRef]
40. Li, X.Z.; Fang, F. On the geographical distribution of the four kinds of pond-cultured carps in china. *Acta Zool. Sin.* **1990**, *36*, 244–250.
41. Duan, H.M. The Impact of Anthropogenic Activities on Lake Surface Water Temperature Changes a Case Study of Lakes in the Yunnan-Guizhou Plateau. Master's Thesis, Yunnan Normal University, Yunnan, China, 2023.
42. Hu, W.Y.; Ji, H.; Pan, H.X. A preliminarystudy of water quality and saliniza in Chenghai Lake. *J. Lake Sci.* **1992**, *4*, 60–66.
43. Yang, J.X.; Chen, Y.R. *The Biology and Resource Utilization of the Fishes of Fuxian Lake, Yunnan*; Yunnan Science and Technology Press Kunming: Yunnan, China, 1995; pp. 36–42.
44. Chen, F.; Xue, G.; Wang, Y.K.; Zhang, H.C.; Clift, P.D.; Xing, Y.W.; He, J.; Albert, J.S.; Chen, J.; Xie, P. Evolution of the Yangtze River and its biodiversity. *Innovation* **2023**, *4*, 100417. [CrossRef]
45. Schmidt, E.; Milles, H.; Kennedy, L.; Donelson, J. Interspecies differences in lactate dehydrogenase and citrate synthase activity among damselfish and cardinalfish. *J. Therm. Biol.* **2025**, *129*, 104089. [CrossRef]
46. Zhang, X.J.; Men, S.K.; Tang, X.L.; Storey, K.B.; Niu, Y.; Chen, Q. Comparative metabolomics analysis reveals high-altitude adaptations in a toad-headed viviparous lizard, *Phrynocephalus vlangalii*. *Front. Zool.* **2023**, *20*, 35. [CrossRef]
47. Yan, Y.L.; Xie, X.J.; Yuan, L.Q. Effects of temperature on oxygen consumption rate in metabolism of mitochondria isolated from liver of the southern catfish; *Silurus meridionalis* Chen. *Acta Hydrobiol. Sin.* **2008**, *32*, 237–243. [CrossRef]
48. Fu, S.J.; Zeng, L.Q.; Li, X.M.; Pang, X.; Cao, Z.D.; Peng, J.L.; Wang, Y.X. Effect of meal size on excess post-exercise oxygen consumption in fishes with different locomotive and digestive performance. *J. Comp. Physiol. B.* **2009**, *179*, 509–517. [CrossRef]
49. Long, J.; Xia, Y.; Qiu, H.; Xie, X.J.; Yan, Y.L. Respiratory substrate preferences in mitochondria isolated from different tissues of three fish species. *Fish Physiol. Biochem.* **2022**, *48*, 1555–1567. [CrossRef]
50. Benard, G.; Faustin, B.; Passerieux, E.; Galinier, A.; Rocher, C.; Bellance, N.; Delage, J.P.; Casteilla, L.; Letellier, T.; Rossignol, R. Physiological diversity of mitochondrial oxidative phosphorylation. *Am. J. Physiol. Cell Physiol.* **2006**, *291*, C1172–C1182. [CrossRef]
51. Borowiec, B.G.; Robichaud, K.B.; Craig, P.M. Interactive effects of elevated temperature and venlafaxine on mitochondrial respiration and enzymatic capacity in Nile tilapia (*Oreochromis niloticus*). *Environ. Toxicol. Chem.* **2025**, *44*, 737–750. [CrossRef]

52. Newell, R.C.; Walkey, M. Oxidative activity of mammalian liver mitochondria as a function of temperature. *Nature* **1966**, *212*, 428–429. [CrossRef] [PubMed]
53. Hoffschröer, N.; Laspoumaderes, C.; Zeis, B.; Tremblay, N. Mitochondrial metabolism and respiration adjustments following temperature acclimation in *Daphnia magna*. *J. Therm. Biol.* **2024**, *119*, 103761. [CrossRef] [PubMed]
54. Kake-Guena, S.A.; Touisse, K.; Warren, B.E.; Scott, K.Y.; Dufresne, F.; Blier, P.U.; Lemieux, H. Temperature-related differences in mitochondrial function among clones of the cladoceran *Daphnia pulex*. *J. Therm. Biol.* **2017**, *69*, 23–31. [CrossRef]
55. Guderley, H.; Pierre, J.S.; Couture, P.; Hulbert, A.J. Plasticity of the properties of mitochondria from rainbow trout red muscle with seasonal acclimatization. *Fish Physiol. Biochem.* **1997**, *16*, 531–541. [CrossRef]
56. Müller, M.E.; Vikstrom, S.; König, M.; Schlichting, R.; Zarfl, C.; Zwiener, C.; Escher, B.I. Mitochondrial Toxicity of Selected Micropollutants; Their Mixtures; and Surface Water Samples Measured by the Oxygen Consumption Rate in Cells. *Environ. Toxicol. Chem.* **2019**, *38*, 1000–1011. [CrossRef]
57. Thomas, L.W.; Ashcroft, M. Exploring the molecular interface between hypoxia-inducible factor signalling and mitochondria. *Cell Mol. Life Sci.* **2019**, *76*, 1759–1777. [CrossRef]
58. Mirón-Gatón, J.M.; Velasco, J.; Pallarés, S.; García-Meseguer, A.J.; Millán, A.; Bilton, D.T. Testing metabolic cold adaptation and the climatic variability hypothesis in two latitudinally distant populations of a supratidal water beetle. *J. Therm. Biol.* **2024**, *123*, 103934. [CrossRef]
59. Grady, J.M.; Maitner, B.S.; Winter, A.S.; Kaschner, K.; Tittensor, D.P.; Record, S.; Smith, F.A.; Wilson, A.M.; Dell, A.I.; Zarnetske, P.L.; et al. Metabolic asymmetry and the global diversity of marine predators. *Science* **2019**, *363*, eaat4220. [CrossRef]
60. Kordas, R.L.; Pawar, S.; Kontopoulos, D.G.; Woodward, G.; O'Gorman, E.J. Metabolic plasticity can amplify ecosystem responses to global warming. *Nat. Commun.* **2022**, *13*, 2161. [CrossRef]
61. Padilla, P.; Courant, J.; Herrel, A. Allocation trade-offs impact organ size and muscle architecture in an invasive population of *Xenopus laevis* in Western France. *J. Anat.* **2019**, *235*, 1057–1064. [CrossRef] [PubMed]
62. Hochachka, P.W.; Darveau, C.A.; Andrews, R.D.; Suarez, R.K. Allometric cascade: A model for resolving body mass effects on metabolism. *Comp. Biochem. Physiol. A Mol. Integr. Physiol.* **2003**, *134*, 675–691. [CrossRef] [PubMed]
63. Johnston, I.A.; Guderley, H.; Franklin, C.E.; Crockford, T.; Kamunde, C. Are mitochondria subject to evolutionary temperature adaptation? *J. Exp. Biol.* **1994**, *195*, 293–306. [CrossRef] [PubMed]
64. Pörtner, H.O. Physiological basis of temperature-dependent biogeography: Trade-offs in muscle design and performance in polar ectotherms. *J. Exp. Biol.* **2002**, *205*, 2217–2230. [CrossRef] [PubMed]
65. Hardewig, I.; van Dijk, P.L.; Moyes, C.D.; Pörtner, H.O. Temperature-dependent expression of cytochrome-c oxidase in Antarctic and temperate fish. *Am. J. Physiol.* **1999**, *277*, R508–R516. [CrossRef]
66. Zak, M.A.; Regish, A.M.; McCormick, S.D.; Manzon, R.G. Exogenous thyroid hormones regulate the activity of citrate synthase and cytochrome c oxidase in warm- but not cold-acclimated lake whitefish (*Coregonus clupeaformis*). *Gen. Comp. Endocrinol.* **2017**, *247*, 215–222. [CrossRef]
67. Hoffmann, A.A.; Sgrò, C.M. Climate change and evolutionary adaptation. *Nature* **2011**, *470*, 479–485. [CrossRef]
68. Catullo, R.A.; Llewelyn, J.; Phillips, B.L.; Moritz, C.C. The Potential for Rapid Evolution under Anthropogenic Climate Change. *Curr. Biol.* **2019**, *29*, R996–R1007. [CrossRef] [PubMed]
69. Zhang, S.D.; Yang, C.H.; Li, B.; Zhang, Z.T.; Su, J.P.; Lin, G.H. Study on the Correlation between Visceral Organs of Plateau Zokor (*Myospalax baileyi*) and Altitude. *Sichuan J. Zool.* **2015**, *34*, 574–578.
70. Johnston, I.A.; Dunn, J. Temperature acclimation and metabolism in ectotherms with particular reference to teleost fish. *Symp. Soc. Exp. Biol.* **1987**, *41*, 67–93.
71. Agrawal, A.A. A scale-dependent framework for trade-offs; syndromes; and specialization in organismal biology. *Ecology* **2020**, *101*, e02924. [CrossRef]
72. Iftikar, F.I.; Hickey, A.J. Do mitochondria limit hot fish hearts? Understanding the role of mitochondrial function with heat stress in *Notolabrus celidotus*. *PLoS ONE* **2013**, *8*, e64120. [CrossRef]
73. Onukwufor, J.O.; Kamunde, C. Interactive effects of temperature; cadmium; and hypoxia on rainbow trout (*Oncorhynchus mykiss*) liver mitochondrial bioenergetics. *Ecotoxicol. Environ. Saf.* **2025**, *289*, 117450. [CrossRef]
74. Anttila, K.; Casselman, M.T.; Schulte, P.M.; Farrell, A.P. Optimum temperature in juvenile salmonids: Connecting subcellular indicators to tissue function and whole-organism thermal optimum. *Physiol. Biochem. Zool.* **2013**, *86*, 245–256. [CrossRef]
75. Chouinard-Boisvert, S.; Ghinter, L.; St-Pierre, A.; Mortz, M.; Desrosiers, V.; Dufresne, F.; Tardif, J.C.; Huard, J.; Sirois, P.; Fortin, S.; et al. Mitochondrial functions and fatty acid profiles in fish heart, an insight into physiological limitations linked to thermal tolerance and age. *J. Exp. Biol.* **2024**, *227*, jeb247502. [CrossRef] [PubMed]
76. Gilbert, M.J.H.; Hardison, E.A.; Farrell, A.P.; Eliason, E.J.; Anttila, K. Measuring maximum heart rate to study cardiac thermal performance and heat tolerance in fishes. *J. Exp. Biol.* **2024**, *227*, jeb247928. [CrossRef] [PubMed]

77. She, P.L.; Gao, B.J.; Li, D.L.; Wu, C.; Zhu, X.J.; He, Y.; Mo, F.; Qi, Y.; Jin, D.Q.; Chen, Y.W.; et al. The transcriptional repressor HEY2 regulates mitochondrial oxidative respiration to maintain cardiac homeostasis. *Nat. Commun.* **2025**, *16*, 232. [CrossRef] [PubMed]
78. Martinez, E.; Hendricks, E.; Menze, M.A.; Torres, J.J. Physiological performance of warm-adapted marine ectotherms: Thermal limits of mitochondrial energy transduction efficiency. *Comp. Biochem. Physiol. A Mol. Integr. Physiol.* **2016**, *191*, 216–225. [CrossRef]
79. Lei, H.; Chen, F.; Huang, D.M. Ecological Effect of Water Temperature and Impact of Reservoir Water Temperature Variation on Fish. *Environ. Impact Assess.* **2017**, *39*, 36–44. [CrossRef]

Disclaimer/Publisher's Note: The statements, opinions and data contained in all publications are solely those of the individual author(s) and contributor(s) and not of MDPI and/or the editor(s). MDPI and/or the editor(s) disclaim responsibility for any injury to people or property resulting from any ideas, methods, instructions or products referred to in the content.

biology

MDPI

Article

Integrated Oxygen Consumption Rate, Energy Metabolism, and Transcriptome Analysis Reveal the Heat Sensitivity of Wild Amur Grayling (*Thymallus grubii*) Under Acute Warming

Cunhua Zhai [1,2,†], Ziyang Wang [1,2,†], Luye Bai [2,3] and Bo Ma [1,2,3,4,5,*]

[1] College of Life Science and Technology, Harbin Normal University, Harbin 150025, China
[2] Heilongjiang River Fishery Research Institute, Chinese Academy of Fishery Sciences, Harbin 150070, China
[3] College of Fisheries and Life Science, Dalian Ocean University, Dalian 116023, China
[4] Research Station for Wild Scientific Observation on Fishery Resources and Ecological Environment Protection, Jiamusi, Ministry of Agriculture and Rural Affairs, Jiamusi 154000, China
[5] Scientific Observation Station of Fisheries Resource and Environment in Heilongjiang River Basin, Ministry of Agriculture, Harbin 150070, China
* Correspondence: hsymabo@163.com
† These authors contributed equally to this work.

Simple Summary: Global warming is heating up cold mountain rivers. We wanted to know how much heat the Amur grayling, a cold-water fish, can take before its body starts to fail. Fish were placed in tanks with the same water speed but six temperatures from 9 °C to 24 °C. We tracked their breathing rate, hemoglobin, energy stores, and liver activity. Breathing quickened up to 15 °C then dropped, showing the fish were stressed. Hemoglobin rose to 18 °C but fell sharply above that. Sugar and starch stored in the liver first increased then plummeted, while lactic acid (a fatigue signal) built up. At 15 °C the fish still used sugar and protein for fuel, but at 21 °C they had to switch to fat breakdown, a sign of emergency metabolism. These changes point to a critical comfort zone between 12 °C and 15 °C. Keeping river temperatures below this range through shade, flow protection, and reduced heat inputs will help wild Amur grayling survive hotter summers.

Abstract: Cold-water fish, particularly stenothermal species, are increasingly affected by rising temperatures driven by global warming. To explore the hepatic metabolism mode of Amur grayling under warming, *Thymallus grubii* was selected as the experimental model. Here, we measured the oxygen consumption rate (MO_2), energy metabolism enzymes, and transcription profiling in *Thymallus grubii* that was exposed to increased temperatures (9, 12, 15, 18, 21, and 24 °C) with the same flow velocity (34 cm/s). In this study, MO_2 initially increased and then decreased with rising temperature, with peak sensitivity between 12 and 15 °C (Q_{10} = 5.30). Hemoglobin increased significantly at 12–18 °C but decreased in the 18–24 °C group ($p < 0.05$). Additionally, hepatic glycogen content (the amount of stored sugar in the liver, which serves as an energy reserve) also first increased and then decreased markedly ($p < 0.05$). Lactic acid in plasma and muscle contents increased, but creatine phosphate and glucose levels significantly decreased ($p < 0.05$). The result of transcriptome analysis showed that individuals in the 15 °C group could supply energy through glucose and amino acid metabolism. In contrast, individuals under 21 °C exposure could mainly supply energy through the lipid metabolism pathway. Our study underscores the vulnerability of Amur grayling to environmental temperature and identifies the instantaneous metabolic limit range, providing numerical limits (e.g., maximum river temperature) that managers can use to protect wild populations.

Keywords: *Thymallus grubii*; warming; oxygen consumption rate; transcriptome

1. Introduction

Acute warming is one of the most significant environmental challenges that wild fish may encounter [1]. Because fish are poikilothermic, water temperature governs their physiology and life-cycle events, making them dependent on natural cycles of flow and temperature for successful reproduction and survival [2]. Currently, water temperature effects on cold-water fish constitute a major research area due to the catastrophic mortality that occurs when temperatures exceed their thermal tolerance [3]. Evidence has confirmed that temperature change affects the survival, reproduction, growth performance, and physiological parameters of cold-water fish. For example, the existence, nutrition, and development of Atlantic salmon (*Salmo salar*) are diminished after exposure to high water temperatures (>25 °C) [4], while exposure to high temperature stress (>21 °C) evokes immune responses and histopathological damage in rainbow trout (*Oncorhynchus mykiss*) [5]. The adverse impacts on the antioxidant systems and the histopathology were observed when tsinling lenok trout (*Brachymystax lenok tsinlingensis*) were exposed to heat stress (>24 °C) [6]. While water temperature plays a crucial role in the survival and distribution of stenothermal species, there is a scarcity of research on the stress response to temperature in the grayling species.

When fish suffer from acute temperature changes, fish species adjust a series of physiological reactions to build an adaptation to current survival conditions [7]. Among them, the most direct response is energy metabolism mode alteration. Metabolic rate, measured as oxygen consumption rate (MO_2), is widely used to determine physiological responses to an energy-demanding process [8]. Brett [9] studied the swimming capacity and oxygen consumption rate of sockeye salmon at five different temperatures and different flow velocities, and the results showed that the activity and metabolism of sockeye salmon were obviously limited by oxygen supply above 15 °C. In addition, the MO_2 of bat rays (*Myliobatis californica*) was particularly temperature-sensitive between 14 °C and 20 °C [10]. Therefore, exploring the relationship between respiratory rate and various environmental factors will help us to further understand the physiological and metabolic patterns and energy requirements of fish.

In poikilothermic animals, the control mechanisms of metabolism processes are attributed to enzymatic regulation [11]. Energy metabolism is considered the most important factor that helps adaptation to changing environmental conditions. Under stress conditions, fish species affect the glycometabolism process by regulating the enzyme's activities [12]. The glycolysis pathway provides energy essential for life activity [13]. Under the aerobic condition, pyruvate enters into the mitochondria and then undergoes the oxidative phosphorylation process. Glycolysis starts with hexokinase (HK) phosphorylating glucose to glucose-6-phosphate (G6P). Subsequently, pyruvate kinase (PK) phosphorylates ADP into ATP to meet the requirement for energy supplement. Succinate dehydrogenase (SDH) couples oxidative phosphorylation with electron transport to involve the process of aerobic metabolism, thereby producing sufficient energy for physiological responses [14]. In vertebrates, the reduction of pyruvate to lactate is catalyzed by lactate dehydrogenase (LDH), an indicator of anaerobic glycolytic capacity [15]. In addition, glucose, lactate, and glycogen contents could also reflect the stress conditions [16]. Therefore, studying energy-related metabolite contents has always been a direct response for the physiological processes of fish.

In natural environments, the preferred temperatures of grayling vary seasonally across different life-history stages, requiring specific thermal windows to optimize growth,

reproduction, and the survival of eggs and larvae [17,18]. During summer, the optimal temperature range for European grayling is 12.0–15.7 °C [19], whereas in winter it survives under ice at temperatures close to 0 °C [20]. Spawning occurs in early spring at low temperatures, with successful reproduction requiring 7.8–11.5 °C [21]. The physiological requirements of grayling are tightly coupled to temperature throughout their life history, exhibiting highly specific physiological thermal limits that are lower than those of other cold-water salmonids such as brown trout (*Salmo trutta*), Atlantic salmon (*Salmo salar*), and brook charr (*Salvelinus fontinalis*) [22]. This elevated heat sensitivity indicates that prolonged exposure to temperatures exceeding their physiological tolerance could be detrimental.

Amur grayling (*Thymallus grubii*) is endemic to the Amur River system of China and Russia. Within China, it occurs exclusively in the upper mountain reaches of the Amur, Nenjiang, and Songhua rivers and is a cold-water freshwater fish species with high nutrition value. Wild resources live in mountain streams, accompanied by high-velocity waters and lower water temperatures. The adult grayling prefers water velocities between 20 and 45 cm/s [23]. The temperature range allowing survival of the grayling species is extremely narrow (8–18 °C) [18]. It has been listed in the "China Red Data Book of Endangered Animals" [24] due to Amur grayling being easily affected by external environmental changes and human activities [25]. Now, field surveys at summertime (August) have documented that Amur grayling actively abandoned habitats where water temperatures exceeded 20 °C and relocated to adjacent cooler refuges whenever these were accessible. Despite the concerning trends in water temperatures, there is a paucity of knowledge regarding the physiological response of Amur grayling. Therefore, the factor of most concern affecting the distribution and survival of grayling in the future is the increases in water temperatures where they reside [26,27]. In order to more accurately reflect the effect of temperature change for the fish, the combined effect of water temperature and flow velocity should be considered to implement a more realistic simulation of its environment [28]. Therefore, we have taken the Amur grayling as an example to investigate the metabolism response mode to warming in grayling while monitoring velocities.

Based on the above, the objectives of the present study were to (1) explore the effect of fixed flow velocity (the suitable flow velocity for *Thymallus grubii*) on metabolite levels and oxygen consumption rate (MO_2) of *Thymallus grubii* under different water temperature scenarios (9, 12, 15, 18, 21, and 24 °C) and (2) investigate the possible mechanism of MO_2 change in adult *Thymallus grubii* under key high-temperature points (9, 15, and 21 °C) according to the results of MO_2, providing initial insights into the physiological regulatory mechanisms employed by *Thymallus grubii* to cope with warming. Our study will clarify the adaptation feature to acute warming in *Thymallus grubii* and pave a path for future advancements in the habitat restoration of cold-water fish.

2. Material and Methods

2.1. Experimental Animal Preparation and Breeding

Animal care laws and guidelines (Directive 2010(63)EU) were followed for all treatment procedures and were submitted by the Laboratory Animal Ethics Committee of the Research Institute of Fisheries of the Heilongjiang River (No. 20231028-001). We confirm that the study is reported in accordance with ARRIVE guidelines.

All experimental fish were collected by our team using angling and cast nets in the Huma river from the upper Amur River (Figure 1a) in China in autumn and then transported to the indoor culture facility (Harbin, China). All fish were habituated for 3 d prior to the formal experiment in a temperature-controlled recirculating water tank (80.5 cm × 48 cm × 39 cm) to remove transport stress and maintain wild habits [29]. Fish

were not fed during this period. The tap water was aired for 5 h and changed on a daily basis, the temperature of the water was maintained at about 9 °C, and the pH value was in the range of 6.8 ± 0.12. In addition, dissolved oxygen (DO) was controlled at 8.2 ± 0.3 mg/L and the light cycle was set to 12 h light/12 h dark. In this study, the water quality was analyzed using a Water Quality Meter (Thermo, 4-Star, Waltham, MA, USA).

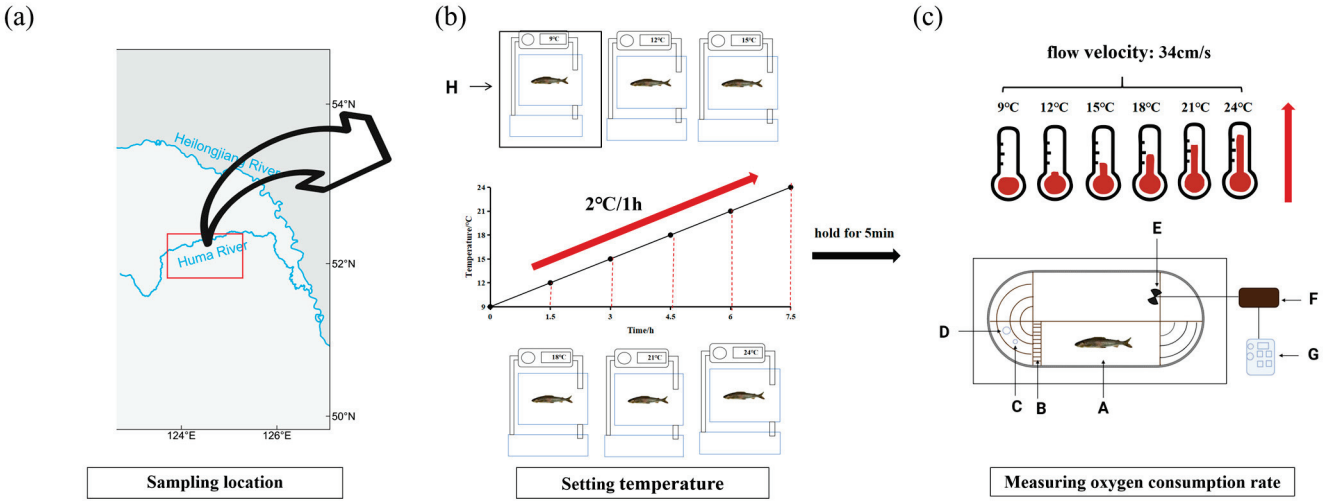


Figure 1. Sampling flow chart of Amur grayling during warming. (**a**) Sampling location, (**b**) thermal equilibration, (**c**) schematic diagram of the flume-type swimming respirometer. (A) Fish swimming area, (B) rectifier, (C) dissolved oxygen (DO) probe, (D) temperature sensor, (E) propeller, (F) propeller motor, (G) frequency changer, (H) temperature-controlled recirculating water tank.

2.2. Experimental Facility Overview

Fish were tested in a 10 L (40 cm × 10 cm × 10 cm) rectangular swim chamber of the Loligo system (Loligo system SY28060, Viborg, Denmark) recirculating swim channel. An automatic water temperature controller was used to control the water temperature during the experiment. A multiparameter probe (HACH HQ30d, Loveland, CO, USA) was used to monitor DO. Subsequently, the data were transmitted to the Witroxview program (Loligo System, Viborg, Denmark). The relationship between flow velocity in the experimental tank measured by tachometer and frequency adjusted by the controller was shown in Figure S1.

2.3. Experiment Designs

Sixty healthy fish were chosen and indiscriminately allocated to six tanks (ten fish per tank) for the MO_2 measurement assay for Amur grayling with similar body lengths (16.98 ± 0.34 cm). Zhai et al. [30] have shown that the optimal flow velocity for Amur grayling with body lengths of 16.98 ± 0.34 cm is determined to be 34 cm/s. Because 9 °C is the ideal temperature for sustaining the healthy metabolic activity of Amur grayling in autumn, 9 °C was used as the initial temperature of Amur grayling. Subsequently, the water temperature in one of the tanks remained unchanged at 9 °C, which was defined as the control group, and the water in the others were increased in temperature at a rate of 2 °C/1 h until the target temperature (12, 15, 18, 21, and 24 °C) was reached (Figure 1b). Eight fish were randomly selected from each temperature group after 5 min and were transferred to a 10 L rectangular swim chamber (Loligo system) containing the target temperature (9, 12, 15, 18, 21, and 24 °C) maintained by the automatic water temperature controller (Figure 1c). Then, eight fish were kept at target temperature for 40 min with the same flow velocity (34 cm/s) until oxygen consumption data were collected. Oxygen concentration was maintained above 90% saturation (>8.6 mg O_2 L^{-1}) throughout the acclimation and

experimentation period. Temperature and oxygen saturation were measured continuously (1 s response time) using calibrated oxygen and temperature electrodes. The fish had enough time to adjust to the tank's new environment to avoid stress, which was controlled remotely by a computer with cameras and free of human interference. Six fish were chosen randomly from each temperature group and immediately anesthetized using 0.02% Methane Sulfonate-222 (MS-222; Sigma, St. Louis, MO, USA). After adequate anesthesia, fish were weighed immediately (Table 1), while the blood, liver, and tail muscle tissues were immediately collected. In the following studies, the serum, liver, and tail muscle tissues of each group were obtained to determine blood glucose, glycogen, lactic acid, and creatine phosphate contents. Under the ice bath, extraction solution was added to the second portion of liver tissue to homogenate for SDH, PK, HK, LDH activities, and liver glycogen determinations. The third portion of liver tissue was placed in liquid nitrogen and then stored at −80 °C for quantitative real-time PCR and transcriptome analyses.

Table 1. The size of target fish for the experiment.

Water Temperature	9 °C	12 °C	15 °C	18 °C	21 °C	24 °C
age/year	3^+	3^+	3^+	3^+	3^+	3^+
sample size	8	8	8	8	8	8
wet weight/g	50.43 ± 5.21 [a]	55.84 ± 7.98 [a]	54.39 ± 7.41 [a]	54.67 ± 7.85 [a]	53.93 ± 3.30 [a]	54.92 ± 4.96 [a]
body length/cm	16.98 ± 0.47 [a]	17.00 ± 0.47 [a]	16.91 ± 0.30 [a]	17.03 ± 0.44 [a]	17.16 ± 0.38 [a]	17.13 ± 0.30 [a]

Note: Different lowercase letters represent significant differences ($p < 0.05$) between groups. Data are presented as mean ± SD (n = 8). 3^+: 3–4 years old.

MO_2 was calculated using the equation

$$MO_2 = V \times (d(DO)/dt)/M \quad (1)$$

where V is the volume of the respirometer (L), M represents the mass value of the subjected fish, and d(DO)/dt means the regression equation slope (mg O_2/min). DO was recorded every 1 s.

At the end of each 40 min measurement period, the chamber was flushed with fish-free and temperature-matched water, and the dissolved oxygen was recorded for 5 min. This background MO_2 value (always <1% of fish MO_2) was subtracted from the preceding fish recording.

The thermal coefficient (Q_{10}), which represents the sensitivity of an organism to temperature variations, was estimated for Amur grayling at different temperatures. Q_{10} was calculated as

$$Q_{10} = (K2/K1)^{10/(T2-T1)}$$

where K1 and K2 are the oxygen consumption at temperatures T1 and T2, respectively.

2.4. Determination of the Enzyme Activity of Glucose Metabolism, the Content of Substances of Energy Metabolism, and Hemoglobin Concentration Analysis

Hepatic SDH, PK, HK, LDH activities, and the content of glycogen, lactic acid, and creatine phosphate were measured utilizing kits purchased from Shanghai Jianglai Industrial. Blood glucose was measured using chemistry analyzers (AU5800, Beckman Coulter, Brea, CA, USA). Muscle and liver samples were homogenized and fixed with cold extraction solution at a ratio of 1:9 (*w*:*v*). After it was centrifuged at 14,000 rpm for 10 min at 4 °C, the fresh homogenate was collected into sterile tubes. The absorbance microplate reader (SpectraMax Plus 384, Molecular Devices, San Jose, CA, USA) was used to determine optical density values at 600 nm (SDH), 340 nm (PK), 340 nm (HK), 450 nm (LDH), 450 nm (lactic acid), 510 nm (glycogen), and 520 nm (creatine phosphate), respectively. Hemoglobin con-

centrations (HGB g/L) were determined through measurement by the Auto Hematology Analyzer (BC-2800Vet, Mindray, Shenzhen, China).

2.5. Project for the Construction of cDNA Libraries and Transcriptome Sequencing

The 80 mg fresh liver tissue samples were collected using sterile scissors and forceps. Total RNA samples were extracted using standard TRIzol reagent (Invitrogen, Waltham, MA, USA) according to the manufacturer's protocol. The NanoDrop ND-1000 spectrophotometer (Thermo Fisher Scientific, Wilmington, DE, USA) was used to evaluate the quality (purity, concentration, and integrity) of the RNA. RNA integrity was detected using 1% agarose gel electrophoresis. The qualified samples were used to build sequencing libraries. mRNA was enriched using oligo (dT) beads and digested into short segments using buffer. Then, DNA polymerase I, RNase H, dNTP, and buffer were used to synthesize first-strand cDNA. Following purification and end repair, cDNA fragments were sequenced based on the Illumina HiSeq^{TM}2500 platform (Allwegene Tech Co., Ltd., Beijing, China).

2.6. Quality Control, De Novo Assembly, and Annotation

Raw data were filtered by removing the reads of adapters, containing > 10% unknown bases (N), and low-quality reads containing > 50% low-quality (Q-value $\leq$ 20) bases. The clean data were de novo assembled using Trinity v2.4 software. The assembled unigenes were aligned by using the Blastx program of the BLAST package (v.2.15.0) to obtain comprehensive gene function information based on a public database, including Nr (NCBI non-redundant protein sequences) and an evolutionary genealogy of genes: Non-supervised Orthologous Groups (eggNOGs), Protein family (Pfam), Swiss-Prot (a manually annotated and reviewed protein sequence database), and Kyoto Encyclopaedia of Genes and Genomes (KEGG) and Gene Ontology (GO).

2.7. Differentially Expressed Gene (DEG) Identification

Raw reads for each sample were assembled with reference genomes using StringTie (v3.0.2) and then fragment per kilobase of transcript per million (FPKM) values were calculated to analyze the relative gene expression amount. To compare the DEGs among different temperature treatments, six samples from 9 °C, 15 °C, and 21 °C conditions were used for transcriptome analysis. Clean data were analyzed using DESeq2 to identify the DEGs between the 9 °C group and 15 °C group and between the 9 °C group and 21 °C group. Q values < 0.005 and $|\log2(\text{fold change})| \geq 1$ were regarded as the threshold for DEG filtration.

2.8. Quantitative Real-Time PCR (qRT-PCR) Verification

To validate the accuracy of sequencing data, typical DEGs in comparison (9 °C vs. 15 °C and 9 °C vs. 21 °C) were selected for qRT-PCR verification (Table S1). Primer pairs were designed based on Primer premier 6.0 software and synthesized by Sangon Co., ltd., Shanghai, China. The β-actin gene was selected as the internal reference gene. The first strand cDNA was synthesized using Prime Script^{TM} RT reagent kit with DNA Eraser (TaKaRa, Shiga, Japan). The reaction mixture contained 5 μL 2 × TB Green Premix Ex Taq II (Tli RNaseH Plus), 0.4 μL of each forward and reverse primer, 3 μL sterile distilled H_2O (dH_2O), 1 μL template cDNA, and 0.2 μL 50 × ROX Reference Dye II (Roche, Basel, Switzerland). qRT-qPCR was performed in the ABI 7500 real-time PCR instrument (Thermo Fisher Scientific). Detailed cycle parameters were set at 95 °C for 180 s, 40 cycles of 95 °C for 5 s, 60 °C for 15 s, and 72 °C for 30 s. The $2^{-\Delta\Delta CT}$ method was used to calculate relative gene expression levels.

2.9. Statistical Analysis

The statistic processing procedure was implemented based on IBM SPSS Statistics 23.0 software and experiment data was shown as the mean ± standard deviation (SD). The normality and variance homogeneity of the data were assessed through the Kolmogorov–Smirnov and Levene tests, respectively. Subsequently, one-way ANOVA was utilized to determine the significance of differences. $p < 0.05$ was regarded as the significance threshold. Plots were visualized using GraphPad Software (Version 8.4.3, USA). The unary linear regression equation model was utilized to analyze the relationship between water temperature and MO_2. For the visualization process of transcriptome analysis results, standard bioinformatics script was run in the R package (R 4.4.2) and the process obtained technological support from the professional cloud platform provided by the third-party company (Allwegene Tech Co., Ltd., Beijing, China).

3. Results

3.1. Oxygen Consumption Rates at Different Temperatures

MO_2 was calculated using equation (1). MO_2 increased initially and then decreased with increasing water temperature (Figure 2). There was a statistical difference between the 12 °C group and 15 °C group, and between the 18 °C group and 21 °C group ($p < 0.05$). Q_{10} was highest between 12 and 15 °C (Q_{10} = 5.30) (Table 2). MO_2 increased significantly at 12–15 °C (Q_{10} = 5.30), then decreased at 18–21 °C (Q_{10} = 0.05). Environmental temperatures of 15 °C and 21 °C were an important node to explore the pattern of change in the respiratory metabolism of *Thymallus grubii* at high temperatures. This provided a basis for selecting 15 °C and 21 °C as the test group of transcriptome analysis.

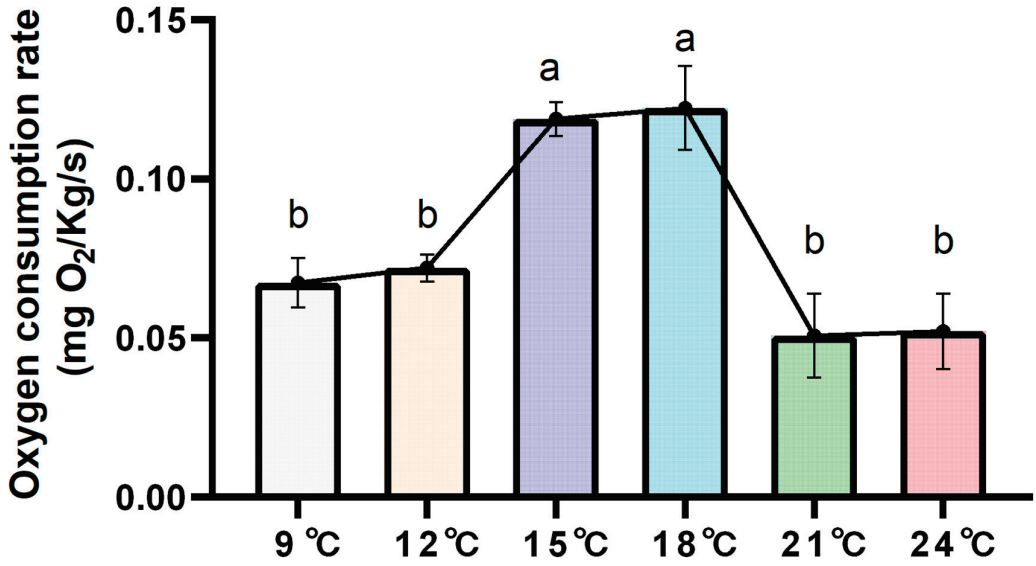


Figure 2. The relationship between oxygen consumption rate (MO_2) and water temperature (T) (n = 8). Different lowercase letters represent significant differences ($p < 0.05$) between groups (mean ± SD).

Table 2. Temperature coefficient Q_{10} values of respiration of Amur grayling at different temperatures.

Temperature/°C	Temperature Coefficient Q_{10}
9–12	1.25
12–15	5.30
15–18	1.10
18–21	0.05
21–24	1.09

3.2. Effects of Temperature Changes on Physiological Indexes of Amur Grayling

LDH activity significantly increased in the liver of the Amur grayling at 9–15 °C, then decreased with the increase in water temperature ($p < 0.05$) (Figure 3a). HK activity gradually increased then decreased with the increase in temperature, but there was no obvious difference observed between the 9 and 12 °C group and between the 18 and 24 °C group ($p > 0.05$) (Figure 3b). Conversely, SDH activity gradually decreased with the increase in temperature, but no significant difference was observed between 9 °C and 12 °C ($p > 0.05$) (Figure 3c). PK activity was significantly elevated ($p < 0.05$) from 9 to 15 °C and then markedly decreased ($p < 0.05$) under the 18–24 °C condition (Figure 3d).

Hepatic glycogen content rose markedly at 9–12 °C but decreased markedly at 15–24 °C ($p < 0.05$). Similarly, the glycogen contents of muscle rose significantly at 9–15 °C but decreased considerably in the 18-24 °C group ($p < 0.05$) (Figure 3e,f). With increasing temperature, muscle creatine phosphate was not significant at 9–18 °C ($p > 0.05$) but then significantly decreased at 21–24 °C (Figure 3g). Blood glucose levels declined gradually with the increase in experimental temperature, but the difference was not significantly obvious between 15 and 18 °C and between 21 and 24 °C ($p > 0.05$) (Figure 3h). Conversely, plasma and muscle lactate levels rose as temperature increased ($p < 0.05$), but the difference was not obvious between 15 and 18 °C and between 21 and 24 °C ($p > 0.05$) (Figure 3i,j).

In order to further explore the reasons for the decrease in MO_2, the HGB of Amur grayling was measured (Table 3). The HGB increased significantly at 12–18 °C but decreased considerably in the 18–24 °C group ($p < 0.05$).

Table 3. Effects of warming on hemoglobin concentrations (HGB) of Amur grayling.

Water Temperature	9 °C	12 °C	15 °C	18 °C	21 °C	24 °C
HGB (g/L)	96.07 ± 6.84 ^{c}	102.62 ± 10.43 ^{c}	117 ± 9.12 ^{b}	127.78 ± 3.49 ^{a}	37.9 ± 6.14 ^{d}	42.29 ± 9.52 ^{d}

Note: Different lowercase letters represent significant differences ($p < 0.05$) between groups. Data are presented as mean ± SD (n = 3).

3.3. Changes in Transcriptome Profile Induced by Temperature Stress

A total of 37.73 Gb clean reads were generated in this project (Table S2). They showed that 72403, 53508, 46471, 37509, 51687, and 50335 unigenes were mapped to Nr, eggNOG, Swiss-Prot, Pfam, Gene Ontology (GO), and KEGG databases, respectively (Table S3). Principle component analysis (PCA) demonstrated marked discrepancy among different groups (Figure 4a). A total of 6251 DEGs (3263 up-regulation and 2988 down-regulation) and 80647 DEGs (33678 up-regulation and 46969 down-regulation) were found in C15 (15 °C) vs. Con (9 °C) and C21 (21 °C) vs. Con (9 °C), respectively (Figure 4b,c). According to GO analysis, unigenes in both 15 °C vs. 9 °C and 21 °C vs. 9 °C were assigned to the three GO domains (biological process, cellular component, and molecular function; Figure 4d,e), with cellular and metabolic processes constituting the dominant biological process categories. The main GO terms in cellular components were membrane and cell part. In the molecular function, binding and catalytic activity were the most enriched GO terms. KEGG enrichment analysis showed that all unigenes were assigned to 92 functional types, such as "Amino acid metabolism", "Energy metabolism", "Lipid metabolism", and "Immune system" (Figure 4f–i).

3.4. GO Enrichment and KEGG Pathway Analysis for DEGs

DEGs between the 9 °C and 15 °C groups were enriched in the GO term biological process, cellular component, and molecular function categories, and the top 20 GO terms are shown in Figure 5a. In the liver of *Thymallus grubii*, the most representative DEGs annotated to biological process were protein localization to endoplasmic reticulum; the most dominant GO term mapped to cellular component was membrane; in molecular function, the most

primary GO term was nutrient reservoir activity. GO enrichment analysis (Figure 5b) revealed that DEGs (21 °C vs. 9 °C) were largely enriched into regulation of biological process, cellular components, and molecular function. Among the enrichment, biological process was mainly the RNA metabolic process and RNA processing; the main category of cellular component and molecular function was mitochondrial protein-containing complex and RNA binding, respectively.

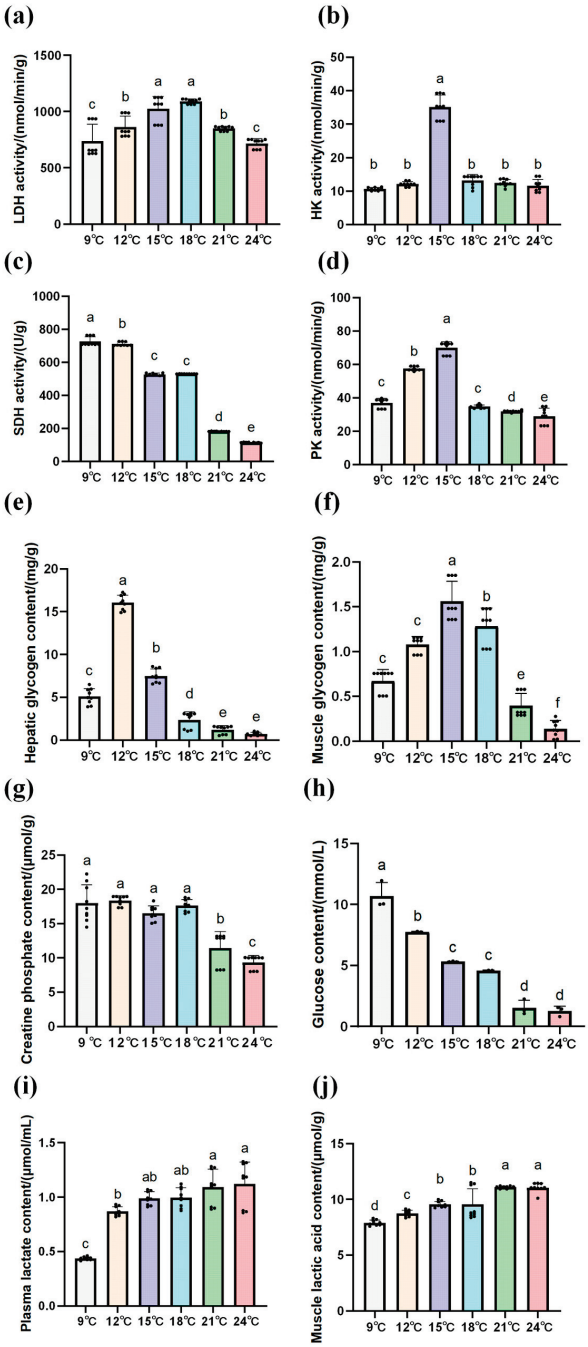


Figure 3. Effects of carbohydrate metabolism on enzyme activities and contents of biochemical substances in liver tissues under warming (n = 3). (**a**) LDH activity. (**b**) HK activity. (**c**) SDH activity. (**d**) PK activity. (**e**) The content of liver glycogen. (**f**) The content of muscle glycogen. (**g**) The content of creatine phosphate. (**h**) The content of blood glucose. (**i**) The content of plasma lactic acid. (**j**) The content of muscle lactic acid. Different lowercase letters represent significant differences ($p < 0.05$) among different temperature groups (mean ± SD). A one-way ANOVA test was used to identify the statistical significance.

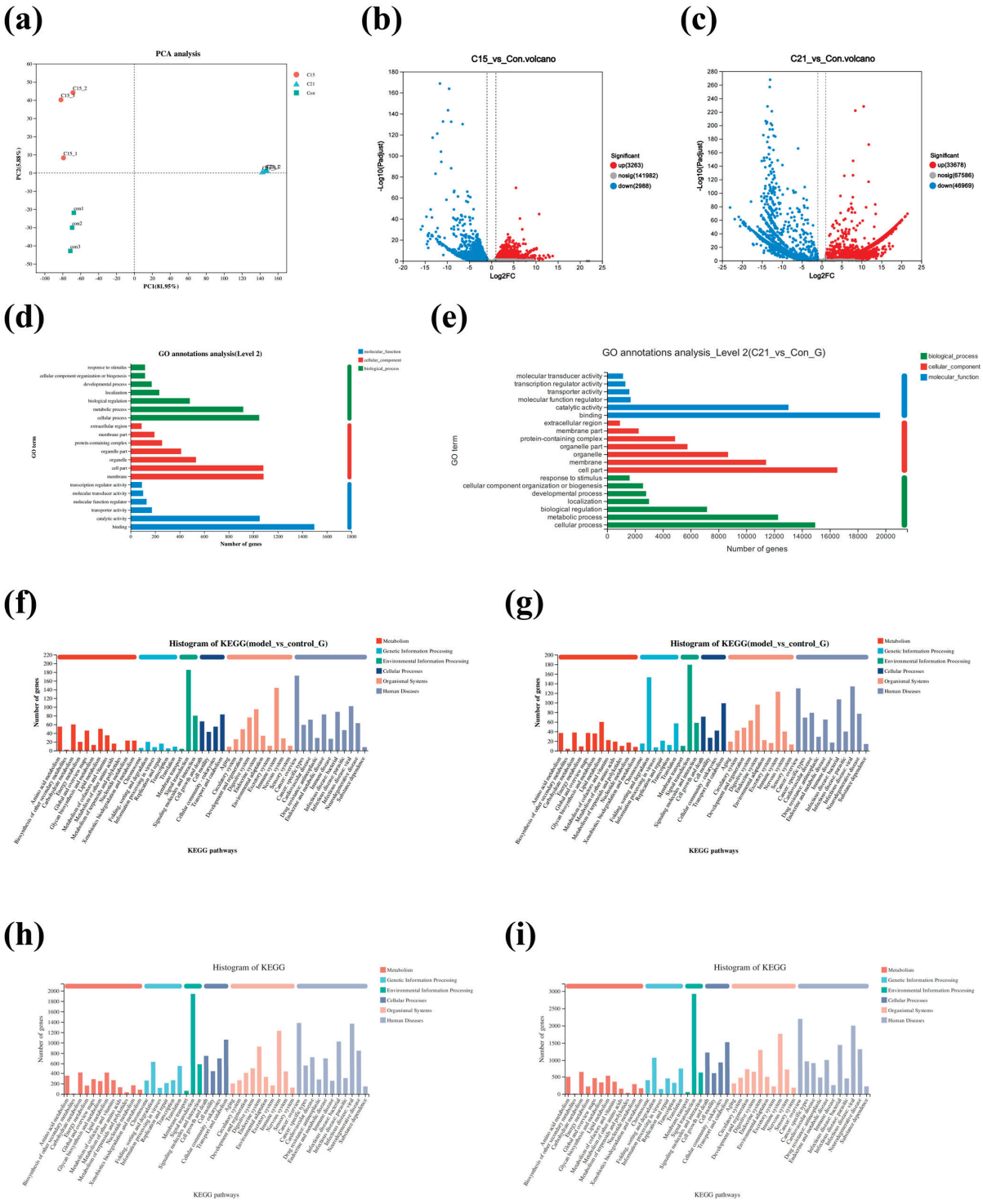


Figure 4. Non-reference genome-based transcriptome analysis for liver under warming (n = 3). (**a**) Principal component analysis (PCA) scatter diagram. The 9, 15, and 21 °C groups were represented by green squares, orange circles and blue triangles, respectively. (**b**) Volcano map of the distribution trends of differentially expressed genes (DEGs) between 15 and 9 °C. Each dot represents one gene. Blue and red dots represent DEGs. Gray dots represent non-differentially expressed genes. (**c**) Volcano map of the distribution trends of differentially expressed genes (DEGs) between 21 and 9 °C. (**d**) Bar chart showing the significantly enriched GO terms in 15 °C vs. 9 °C. (**e**) Bar chart showing the significantly enriched GO terms in 21 °C vs. 9 °C. The results for 15 vs. 9 °C and 21 °C vs. 9 °C are divided into three main categories: cellular components, biological process, and molecular. The X-axis at the bottom indicates the number of unigenes. The Y-axis indicates the subcategories. (**f**,**g**) Bar chart of enriched KEGG pathways of up-regulated and down-regulated genes of 15 °C vs. 9 °C. (**h**,**i**) Bar chart of enriched KEGG pathways of up-regulated and down-regulated genes of 21 °C vs. 9 °C. Con: control group (9 °C); C15: 15 °C group; C21: 21 °C group.

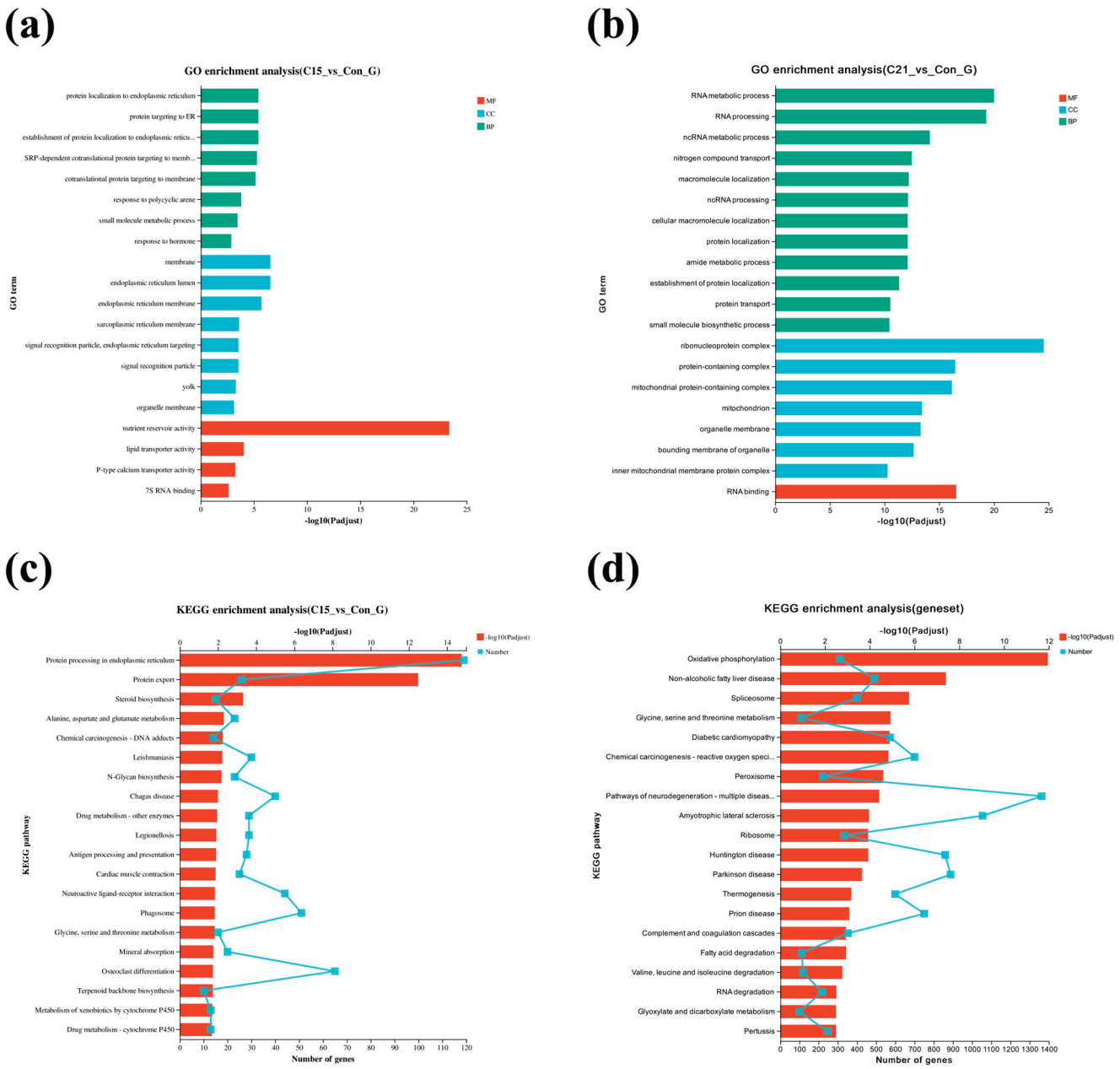


Figure 5. Enrichment analysis of gene GO term and KEGG pathway for DEGs under warming. (**a**,**b**) Bar chart of the top 20 significantly enriched DEGs of the two comparison groups in Amur grayling. The two comparison groups include 15 °C vs. 9 °C and 21 °C vs. 9 °C. The different colors in the GO chart represent the enriched categories with −log10(Padjust) as the standard. (**c**,**d**) KEGG enrichment of the two DEG comparison groups in Amur grayling. The two comparison groups include 15 °C vs. 9 °C and 21 °C vs. 9 °C. The red bar in the KEGG chart represents the enriched categories with -log10(Padjust) as the standard. The polylines represent the number of genes enriched into different categories. Con: control group (9 °C); C15: 15 °C group; C21: 21 °C group. KEGG pathway: © Kanehisa Laboratories; reproduced with permission. Individual pathway IDs are listed in Supplementary Table S5. establishment of protein localization to endoplasmic reticu. . .: establishment of protein localization to endoplasmic reticulum; SRP-dependent cotranslational protein targeting to memb. . .: SRP-dependent cotranslational protein targeting to membrane; Chemical carcinogenesis-reactive oxygen speci. . .: Chemical carcinogenesis-reactive oxygen species; Pathways of neurodegeneration-multiple diseas. . .: Pathways of neurodegeneration-multiple diseases.

The KEGG pathway analysis showed that protein processing in the endoplasmic reticulum, protein export, and steroid biosynthesis were enriched mainly in the 15 °C

vs. 9 °C comparison (Figure 5c). Oxidative phosphorylation, non-alcoholic liver disease, and spliceosomes were enriched mainly in the 21 °C vs. 9 °C comparison (Figure 5d). The fatty-acid degradation pathway was predominant in 21 °C vs. 9 °C. In addition, the pathways linked to protein processing or amino acid metabolism, such as glycine, serine, and threonine metabolism, N-glycan biosynthesis, and valine, leucine, and isoleucine degradation were included in both pairwise comparisons. KEGG enrichment analysis also identified glycolysis/gluconeogenesis, citrate cycle (TCA cycle), and apoptosis to be significantly enriched. Specifically, glycolysis/gluconeogenesis (*hk*)-, citrate cycle (TCA cycle) (*sdh, idh, aco*)-, fatty-acid biosynthesis (*fasn*)-, and fatty-acid degradation (*hadh, hadha*)-related genes were identified (Table S4). Combined transcriptomic and physiological evidence indicates that warming affected the oxygen transport and energy metabolism in the liver and muscle tissue (Figure 6).

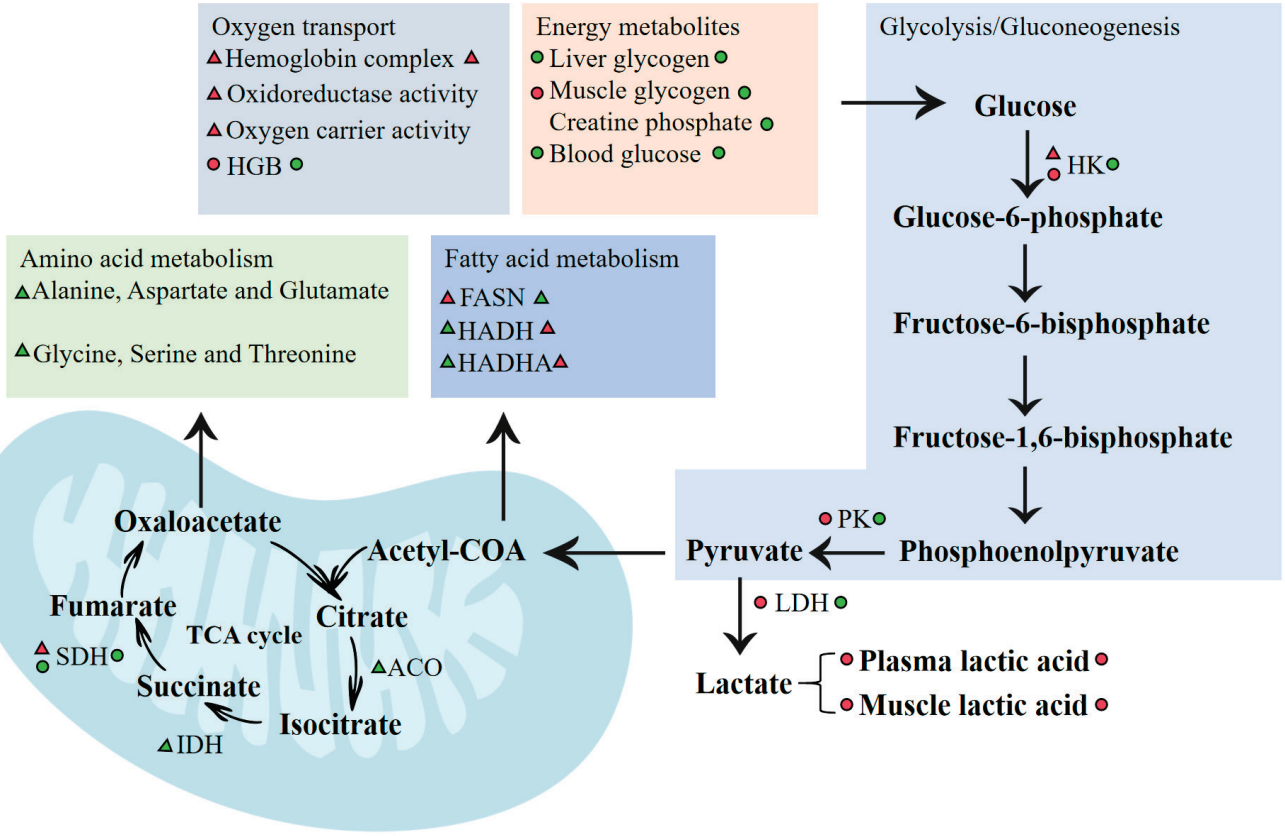


Figure 6. Schematic overview of the alteration in physiological parameters and transcriptome in the 15 and 21 °C groups of Amur grayling. Green and red represent up-regulation and down-regulation, respectively. Triangles represent DEGs. Circles represent physiological parameters. The shape on the left and right represent 15 and 21 °C, respectively. HGB: Hemoglobin concentrations; FASN: Fatty-acid synthase, animal type; HADH: 3-hydroxyacyl-CoA dehydrogenase; HADHA: Enoyl-CoA hydratase/long-chain 3-hydroxyacyl-CoA dehydrogenase; HK: Hexokinase; PK: Pyruvate kinase; LDH: Lactate dehydrogenase; ACO: Aconitate hydratase; IDH: Isocitrate dehydrogenase; SDH: Succinate dehydrogenase.

3.5. Validation of RNA-Seq Profiles

To verify the credibility of the transcriptome sequencing results, nine DEGs were randomly chosen (Figure S2). It has been shown that the trends of the changes in these candidate genes are in agreement with the results provided by the transcriptome project.

4. Discussion

Temperature change is a critical challenge for fish survival. It can influence the metabolism mode, including overall metabolic rate and oxygen consumption, and reduce nutrient digestion and absorption efficiency [31,32].

Oxygen consumption directly affects efficient energy usage and reflects overall physiological function under stress conditions [33]. It was found that MO_2 in rainbow trout (*Oncorhynchus mykiss*) increased with rising environmental temperature [34]. Between 9 and 15 °C, MO_2 in *Thymallus grubii* rose significantly with temperature, reflecting the exponential increase in metabolic demand for growth and reproduction [35]. The inflection point at 15 and 18 °C—where MO_2 reached its maximum—thus marks the upper limit of the species' optimal metabolic window. Further warming to 21 °C led to a decline in MO_2, accompanied by a parallel drop in liver glycogen and muscle creatine phosphate content. This suggests that depleted energy reserves constrain metabolic scope.

In addition, the most pronounced changes in energy metabolism enzyme activities occurred between 12 and 15 °C, indicating that this range is vital for the acclimation process of *Thymallus grubii* to acute warming. In addition, genes associated with the hemoglobin complex (GO: 0005833), oxidoreductase activity (GO:0016491), and oxygen carrier activity (GO:0005344) were up-regulated after exposure at 15 °C, which is in accordance with the results of landscape transcriptomic analysis in wild brook trout (*Salvelinus fontinalis*) under heat stress [36]. Because warmer water holds less dissolved oxygen and requires higher respiration rates to maintain activity levels, genes (*hbad*, *hbb1*, *hba*, *hba4*, *hbb*, *hbb2*, and *kdm6a*) involved in oxygen transport and the content of HGB increased at 15 °C, which is the critical metabolic window of Amur grayling. Other studies have reported increased HGB and oxygen carrier activity in salmonids acclimated to high temperatures [37]. Nevertheless, there are also studies that found HGB content can decrease following shorter periods of acute temperature stress more similar to the heat stress in this study [38,39]. It was observed that only the hemoglobin complex (GO: 0005833) enriched in the 21 °C and HGB decreased above 21 °C, which reduced respiratory efficiency for Amur grayling. The result of this study is consistent with recent wild environment-based thermal tolerances [36]. It is evident that experimental methods which incorporated flow rate into temperature provide an effective experimental model for field testing. We coupled a Loligo swim-tunnel respirometer with an automatic temperature-control unit so that water temperature could be raised at 2 °C/h while flow velocity was held constant at 34 cm/s (Figure 1). This simultaneous control of both thermal and hydraulic variables mimicked the acute warming and steady current velocity conditions of the Amur grayling experience in mountain rivers. Because MO_2, enzyme activities, and gene expression were recorded in real time, the setup provides a field-realistic, high-throughput model that could be deployed directly in river-side mobile laboratories for heat sensitivity testing of other stenothermal species.

PK and HK are key regulators of energy balance [40]. In *Thymallus grubii*, hepatic HK and PK activities peaked at 15 °C and then declined sharply above 18 °C, mirroring the temperature-dependent switch from aerobic to anaerobic metabolism. Reduced glucose availability under warming further suppressed HK activity, whereas PK remained elevated between 12 and 15 °C to accelerate glycolysis and replenish ATP for stress responses. These kinetics parallel observations in blue tilapia under acute warming [41]. Additionally, although HK did not reach statistical significance, its activity rose modestly from 9 to 15 °C and declined thereafter, mirroring the significant PK peak observed at the same temperatures. This parallel behavior supports the notion that HK and PK remained elevated between 12 and 15 °C to accelerate glycolysis and replenish ATP for stress responses and down-regulated once the critical metabolic window (>15 °C) was exceeded. LDH content and activity increased progressively from 12 to 18 °C, consistent with a compensatory shift

towards anaerobic glycolysis as hemoglobin–oxygen affinity decreased [42]. Conversely, SDH activity declined continuously beyond 18 °C, confirming suppressed aerobic respiration. Blood glucose decreased steadily from 12 to 24 °C, indicating rapid utilization to fuel stress-induced metabolic demands. Liver and muscle glycogen peaked at 12–15 °C and then declined, demonstrating that acute warming first promotes glycogen deposition and subsequently accelerates glycogenolysis to maintain glucose supply. Comparable glycogen depletion has been reported in Chinese bream exposed to rising temperatures [43]. Between 9 and 15 °C, elevated aerobic efficiency provided ample energy, promoting the conversion of blood glucose into glycogen in the liver and muscles, with concurrent up-regulation of glycogen synthase, leading to glycogen accumulation and a simultaneous fall in blood glucose. When temperatures exceeded the critical thermal threshold of Amur grayling (15 °C), aerobic metabolism was suppressed (MO_2 inflection), energy availability became limited, and rapid glycogenolysis mobilized hepatic and muscular glycogen to glucose, which was then channeled through enhanced glycolysis to meet urgent energy demands, perpetuating the decline in blood glucose. Transcriptomic analysis revealed that DEGs involved in the TCA cycle were down-regulated at 15 °C, suggesting that warming inhibits mitochondrial oxidative metabolism and redirects carbon flux towards glycolysis. Collectively, these data establish 15 °C as the upper boundary of the optimal thermal range for *Thymallus grubii* and highlight the pivotal role of rapid energy redistribution in coping with warming.

In order to physiologically compensate for environmental stressors, fish need to utilize energy substrates [44]. In the present study, transcriptomic analysis revealed that fatty-acid degradation, fatty-acid metabolism, and fatty-acid biosynthesis pathways were significantly enriched in the 15 °C and 21 °C groups. Fish can therefore fine-tune lipid metabolism to maintain homeostasis under warming. FASN, a multi-functional enzyme, catalyzes fatty-acid biosynthesis, whereas HADH and HADHA are key genes involved in fatty-acid degradation [45]. In this study, the expression level of *fasn* increased in the 15 °C group, whereas those of *hadh* and *hadha* decreased. As temperature increased, the opposite trend was observed in the 21 °C group. The results suggest that 21 °C inhibited the lipid synthesis pathway and facilitated the fatty-acid degradation, presumably to meet the elevated energy demand by regulating lipid metabolism in response to high temperature stress. Above all, fatty-acid metabolism in fish may play an important role in adaptation to environmental temperature stress [46]. Meanwhile, *Thymallus grubii* significantly regulated amino acid, lipid, and glucose metabolism pathways to defend against physiological perturbations caused by acute warming.

In fish, temperature affects protein synthesis, and a clear relationship exists between the optimal temperature range for survival and modifications in protein metabolism [47]. In the present study, transcriptomic analyses revealed that the expression levels of *nef*, *calr*, and *erp27* were down-regulated within the endoplasmic reticulum protein-processing pathway. Similar reductions were observed for genes involved in protein export, including those encoding the protein transport proteins *sec61α* and *sec61β*, the signal peptidase complex subunits *spcs1* and *spcs2*, and the signal recognition particle subunits *srp14* and *srp68*. Comparable patterns have been reported across a range of fish species [48]. Compared with the 9 °C group, the 15 °C group exhibited markedly reduced hepatic concentrations of alanine, aspartate, glutamate, glycine, serine, and threonine, results that align with observations in grass carp (*Ctenopharyngodon idellus*) [49]. Exposure to a high temperature of 15 °C decreased amino acid synthesis efficiency, thereby inhibiting protein synthesis in *Thymallus grubii*. Because the TCA cycle is fueled by amino acids such as aspartate, alanine, glutamate, serine, glycine, and threonine, the reduced availability of these substrates is a major reason for the observed down-regulation of the TCA cycle in the 15 °C group. Previous studies have shown that elevated temperatures increase hepatic ammonia con-

centrations as a consequence of accelerated protein and amino acid catabolism, a process that can damage liver tissue and compromise fish health [50,51]. Glutamate is the principal form of deamination in fish. In contrast to the decline in other amino acids, glutamate levels were elevated in the present study. These findings diverge from those reported for steelhead trout (*Oncorhynchus mykiss*) and Atlantic salmon (*Salmo salar*) [52,53], possibly owing to species-specific thermal stress thresholds.

In natural environments, grayling exhibit stage-specific temperature preferences throughout their life history. For European grayling (*Thymallus thymallus*), the preferred summer temperature ranges from 12.0 to 15.7 °C [19], whereas Arctic grayling (*Thymallus arcticus*) thrive at 6–12 °C during the same season [54]. In the present study, the optimal physiological thermal limit for Amur grayling did not exceed 15 °C, a threshold that closely matches the upper thermal limits documented for other Thymallus species in nature. These findings demonstrate a tight coupling between physiological requirements and temperature across the examined life-history stages, a conclusion further corroborated by our laboratory investigations into the underlying physiological response mechanisms of grayling.

As water temperature increases, cold-water populations retreat to higher, cooler thermal refuges; however, such refuges are limited in extent and therefore reduce the amount of suitable habitat [55]. Studies have shown that warming within or beyond the temperature preference and tolerance ranges of bull trout (*Salvelinus confluentus*) and brook trout (*Salvelinus fontinalis*) results in the loss of thermally suitable natal habitat [56,57]. Consequently, it is hypothesized that Amur grayling will seek cooler habitats once the water temperature exceeds 15 °C, provided that such refuges are accessible. In addition, elevated temperatures can shift the timing of grayling spawning either earlier or later, disrupting synchrony with food resources and thereby reducing the survival of embryos, larvae, and fry, which ultimately contributes to population decline [17,58]. Hauer et al. [21] documented that grayling spawning occurs within 7.8–11.5 °C. It can therefore be reasonably deduced that reproduction may be impaired when the water temperature exceeds 15 °C, thereby accelerating the risk of population extinction.

5. Conclusions

Our study provided comprehensive overviews for the detailed effect of change in warming on energy metabolism mode in *Thymallus grubii* based on transcriptome technology. Our results indicate that warming contributed to changes in transcriptome profiles, as well as a series of metabolism imbalance responses mediated by enzymatic reaction, which may be appropriate for assessing the health status of Amur grayling in natural environments to deal with temperature changes. Meanwhile, *Thymallus grubii* may be able to maintain physiological homeostasis under high thermal challenge through activation of the gluconeogenesis process and regulation of lipid/amino acid metabolic pathways. Our study provided basic information for exploring the molecular mechanism of warming on cold water fish. Our results suggest that acute exposure of adult Amur grayling to temperatures above approximately 15 °C during active swimming induces substantial physiological stress, which supports existing concerns about summer warming in their habitats. However, chronic exposure (days to weeks) and early life stages (eggs, larvae, and juveniles) were not examined, and longer-term effects on growth, reproduction, and lifetime fitness remain unknown. We therefore recommend that 15 °C be used only as an acute warming threshold for river management until chronic and ontogenetic thermal limits are established through prolonged warming experiments and field validation. Further work is vital to study how to increase Amur grayling population resilience via restoring natural discharge regimes and limiting future temperature increases [23,59].

Supplementary Materials: The following supporting information can be downloaded at: https://www.mdpi.com/article/10.3390/biology14121718/s1, Figure S1. Relationship between flow velocity in the experimental tank measured by tachometer and frequency adjusted by the controller. Table S1. The primer sequence of qRT-PCR. Table S2. Quality control of the RNA-seq data obtained from different samples. Table S3. Statistical of database annotation. Table S4. The detailed description of DEGs and KEGG pathway associated with energy metabolism. Table S5. Individual pathway IDs of KEGG pathway in Figure 5. Figure S2. qRT-PCR validation for the RNA-seq results (n = 3).

Author Contributions: C.Z. and B.M., Conceptualization; C.Z. and Z.W., Methodology; C.Z. and Z.W., Software; C.Z. and L.B., Validation; B.M., Resources; C.Z. and Z.W., Data curation; C.Z., Writing—original draft; B.M., Writing-review and editing; B.M., Supervision; B.M., Funding acquisition. All authors have read and agreed to the published version of the manuscript.

Funding: The study was supported by the Agricultural Finance Special Project of the Ministry of Agriculture and Rural Affairs, "Normalization Monitoring of Fisheries Resources and Environment in Key Waters of Northeast China" and Central Public-interest Scientific Institution Basal Research Fund (NO. 2023TD07).

Institutional Review Board Statement: The study was approved by the Laboratory Animal Ethics Committee of the Research Institute of Fisheries of the Heilongjiang River (No. 20231028-001).

Informed Consent Statement: Not applicable.

Data Availability Statement: The datasets presented in this study can be found in online repositories. The names of the repository/repositories and accession number(s) can be found below: https://www.ncbi.nlm.nih.gov/bioproject/PRJNA1369758, accessed on 27 November 2025.

Acknowledgments: We thank all anonymous reviewers for their constructive comments on our manuscript. We would thank Allwegene Tech for their sincere assistance during transcriptome analysis.

Conflicts of Interest: The authors declare no conflict of interest.

References

1. Pörtner, H.O.; Peck, M.A. Climate change effects on fishes and fisheries: Towards a cause-and-effect understanding. *J. Fish Biol.* **2010**, *77*, 1745–1779. [CrossRef]
2. Morales-Marín, L.A.; Rokaya, P.; Sanyal, P.R.; Sereda, J.; Lindenschmidt, K.E. Changes in stream flow and water temperature affect fish habitat in the Athabasca River basin in the context of climate change. *Ecol. Model.* **2019**, *407*, 108718. [CrossRef]
3. Ge, G.; Long, Y.; Shi, L.; Ren, J.; Yan, J.; Li, C.; Li, Q.; Cui, Z. Transcriptomic profiling revealed key signaling pathways for cold tolerance and acclimation of two carp species. *BMC Genom.* **2020**, *21*, 539. [CrossRef]
4. Elliott, J.M.; Elliott, J. Temperature requirements of Atlantic salmon *Salmo salar*, brown trout *Salmo trutta* and Arctic charr *Salvelinus alpinus*: Predicting the effects of climate change. *J. Fish Biol.* **2010**, *77*, 1793–1817. [CrossRef]
5. Zhao, C.; Wang, J.; Ren, W.; Zheng, S.; Ren, Y. Histological, immune, and intestine microbiota responses of the intestine of rainbow trout (*Oncorhynchus mykiss*) to high temperature stress. *Aquaculture* **2024**, *582*, 740465. [CrossRef]
6. Ma, F.; Ma, B.; Zhang, B.; He, Y.; Wang, Y. Disturbance of oxidation/antioxidant status and histopathological damage in tsinling lenok trout under acute thermal stress. *Trop. Anim. Health Prod.* **2023**, *55*, 287. [CrossRef] [PubMed]
7. Di Prisco, G.; Verde, C. Predicting the impacts of climate change on the evolutionary adaptations of polar fish. In *Life in Extreme Environments*; Springer: Dordrecht, The Netherlands, 2006; pp. 385–397.
8. Lefevre, S.; Mckenzie, D.J.; Nilsson, G.E. Models projecting the fate of fish populations under climate change need to be based on valid physiological mechanisms. *Glob. Change Biol.* **2017**, *23*, 34493459. [CrossRef] [PubMed]
9. Brett, J.R. The respiratory metabolism and swimming performance of young sockeye salmon. *J. Fish. Res. BOARD Can.* **1964**, *21*, 1183–1226. [CrossRef]
10. Matern, S.A.; Cech, J.J.; Hopkins, T.E. Diel movements of bat rays, *Myliobatis californica*, in Tomales Bay, California: Evidence for behavioral thermoregulation? *Environ. Biol. Fishes* **2000**, *58*, 173–182. [CrossRef]
11. Vodianitskyi, O.; Potrokhov, O.; Zinkovskyi, O.; Khudiiash, Y.; Prychepa, M. Effects of increasing water temperature and decreasing water oxygen concentration on enzyme activity in developing carp embryos (*Cyprinus carpio*). *Fish. Aquat. Life* **2021**, *29*, 35–44. [CrossRef]

12. Leung, L.; Woo, N. Influence of dietary carbohydrate level on endocrine status and hepatic carbohydrate metabolism in the marine fish Sparus sarba. *Fish Physiol. Biochem.* **2012**, *38*, 543–554. [CrossRef]
13. Zhang, C.Q.; Ding, D.; Wang, B.; Wang, Y.; Li, N.; Li, R.; Yan, Y.; He, J. Effect of potato glycoside alkaloids on energy metabolism of *Fusarium solani*. *J. Fungi* **2023**, *9*, 777. [CrossRef]
14. Akila, P.; Asaikumar, L.; Vennila, L. Chlorogenic acid ameliorates isoproterenol-induced myocardial injury in rats by stabilizing mitochondrial and lysosomal enzymes. *Biomed. Pharmacother.* **2017**, *85*, 582–591. [CrossRef]
15. Granchi, C.; Bertini, S.; Macchia, M.; Minutolo, F. Inhibitors of lactate dehydrogenase isoforms and their therapeutic potentials. *Curr. Med. Chem.* **2010**, *17*, 672–697. [CrossRef] [PubMed]
16. Zikos, A.; Seale, A.; Lerner, D.; Grau, E.; Korsmeyer, K. Effects of salinity on metabolic rate and branchial expression of genes involved in ion transport and metabolism in Mozambique tilapia (*Oreochromis mossambicus*). *Comp. Biochem. Physiol. A Mol. Integr. Physiol.* **2014**, *178*, 121–131. [CrossRef] [PubMed]
17. Wedekind, C.; Kueng, C. Shift of spawning season and effects of climate warming on developmental stages of a grayling (*Salmonidae*). *Conserv. Biol.* **2010**, *24*, 1418–1423. [CrossRef] [PubMed]
18. Carrillo-Longoria, J.A.; Gaylord, G.; Andrews, L.; Powell, M. Effect of temperature on growth, survival, and chronic stress responses of Arctic Grayling juveniles. *Trans. Am. Fish. Soc.* **2024**, *153*, 3–22. [CrossRef]
19. Nykänen, M.; Huusko, A.; Mäki-Petäys, A. Seasonal changes in the habitat use and movements of adult European grayling in a large subarctic river. *J. Fish Biol.* **2001**, *58*, 506–519. [CrossRef]
20. Bass, A.L.; Haugen, T.O.; Vøllestad, L.A. Distribution and movement of European grayling in a subarctic lake revealed by acoustic telemetry. *Ecol. Freshw. Fish* **2014**, *23*, 149–160. [CrossRef]
21. Hauer, C.; Unfer, G. Spawning activity of European grayling (*Thymallus thymallus*) driven by interdaily water temperature variations: Case study Gr. *Mühl River/Austria. River Res. Appl.* **2021**, *37*, 900–906. [CrossRef]
22. Jonsson, B.; Jonsson, N. A review of the likely effects of climate change on anadromous Atlantic salmon Salmo salar and brown trout Salmo trutta, with particular reference to water temperature and flow. *J. Fish Biol.* **2009**, *75*, 2381–2447. [CrossRef]
23. Vehanen, T.; Huusko, A.; Yrjänä, T.; Lahti, M.; Mäki-Petäys, A. Habitat preference by grayling (*Thymallus thymallus*) in an artificially modified, hydropeaking riverbed: A contribution to understand the effectiveness of habitat enhancement measures. *J. Appl. Ichthyol.* **2003**, *19*, 15–20. [CrossRef]
24. Wang, S.; Zheng, G.; Wang, Q. *China Red Data Book of Endangered Animals*; Science Press: Beijing, China, 1998; pp. 204–206.
25. Liu, L.; Luo, Y.; Liang, X.; Ma, B.; Song, D. Occurrence of Amur grayling (*Thymallus grubii grubii* Dybowski, 1869) in the Amur River. *J. Appl. Ichthyol.* **2013**, *29*, 666–667. [CrossRef]
26. Yue, Q.; Yu, G.; Miao, Y.; Zhou, Y. Analysis of Meteorological Element Variation Characteristics in the Heilongjiang (Amur) River Basin. *Water* **2024**, *16*, 521. [CrossRef]
27. Yu, L.L.; Xia, Z.Q.; Li, J.K.; Cai, T. Climate change characteristics of Amur River. *Water Sci. Eng.* **2013**, *6*, 131–144.
28. Wenger, S.J.; Isaak, D.J.; Luce, C.H.; Neville, H.M.; Fausch, K.D.; Dunham, J.B.; Dauwalter, D.C.; Young, M.K.; Elsner, M.M.; Rieman, B.E.; et al. Flow regime, temperature, and biotic interactions drive differential declines of trout species under climate change. *Proc. Natl. Acad. Sci. USA* **2011**, *108*, 14175–14180. [CrossRef]
29. Cai, L.; Chen, J.H.; Johnson, D.; Tu, Z.Y.; Huang, Y.P. Effect of body length on swimming capability and vertical slot fishway design. *Glob. Ecol. Conserv.* **2020**, *22*, e00990. [CrossRef]
30. Zhai, C.; Li, Y.; Zhu, G.; Peng, W.; E, Q.; Zhang, Y.; Ma, B. The Effects of Water Flow Speed on Swimming Capacity and Energy Metabolism in Adult Amur Grayling (*Thymallus grubii*). *Fishes* **2024**, *9*, 272. [CrossRef]
31. Bagnyukova, T.; Lushchak, O.; Storey, K.; Lushchak, V. Oxidative stress and antioxidant defense responses by goldfish tissues to acute change of temperature from 3 to 23 °C. *J. Therm. Biol.* **2007**, *32*, 227–234. [CrossRef]
32. Qian, B.; Xue, L. Liver transcriptome sequencing and de novo annotation of the large yellow croaker (*Larimichthy crocea*) under heat and cold stress. *Mar. Geonomics* **2015**, *25*, 95–102. [CrossRef]
33. Cano, J.; Nicieza, A. Temperature, metabolic rate, and constraints on locomotor performance in ectotherm vertebrates. *Funct. Ecol.* **2006**, *20*, 464–470. [CrossRef]
34. Christensen, E.; Svendsen, M.; Steffensen, J. The combined effect of body size and temperature on oxygen consumption rates and the size-dependency of preferred temperature in European perch Perca fluviatilis. *J. Fish. Biol.* **2020**, *97*, 794–803. [CrossRef]
35. Crocker, C.E.; Cech, J.J. Effects of environmental hypoxia on oxygen consumption rate and swimming activity in juvenile white sturgeon, *Acipenser transmontanus*, in relation to temperature and life intervals. *Environ. Biol. Fishes* **1997**, *50*, 383–389. [CrossRef]
36. Waraniak, J.; Batchelor, S.; Wagner, T.; Keagy, J. Landscape transcriptomic analysis detects thermal stress responses and potential adaptive variation in wild brook trout (*Salvelinus fontinalis*) during successive heatwaves. *Sci. Total Environ.* **2025**, *969*, 178960. [CrossRef]

37. Lahnsteiner, F. Hematological adaptations in diploid and triploid *Salvelinus fontinalis* and diploid *Oncorhynchus mykiss* (Salmonidei, Teleostei) in response to long-term exposure to elevated temperature. *J. Therm. Biol.* **2022**, *106*, 103256. [CrossRef]
38. Roh, H.J.; Kim, A.; Kim, N.; Lee, Y.; Kim, D.H. Multi-omics analysis provides novel insight into immuno-physiological pathways and development of thermal resistance in rainbow trout exposed to acute thermal stress. *Int. J. Mol. Sci.* **2020**, *21*, 9198. [CrossRef]
39. Kang, Y.; Liu, Z.; Shi, H.; Wang, J.; Huang, J.; Li, Y.; Li, J.; Wang, Y. Label-free quantification of protein expression in the rainbow trout (*Oncorhynchus mykiss*) in response to short-term exposure to heat stress. *Comp. Biochem. Physiol. Part D Genom. Proteom.* **2019**, *30*, 158–168. [CrossRef]
40. Guillen, A.C.; Borges, M.E.; Herrerias, T.; Kandalski, P.K.; Marins, E.d.A.; Viana, D.; de Souza, M.R.D.P.; Daloski, L.O.D.C.; Donatti, L. Effect of gradual temperature increase on the carbohydrate energy metabolism responses of the Antarctic fish *Notothenia rossii*. *Mar. Environ. Res.* **2019**, *150*, 104779. [CrossRef]
41. Younis, E. Variation in metabolic enzymatic activity in white muscle and liver of blue tilapia, *Oreochromis aureus*, in response to long-term thermal acclimatization. *Chin. J. Ocean. Limnol.* **2015**, *33*, 696–704. [CrossRef]
42. Edmunds, R.; Van-Herwerden, L.; Smith-Keune, C.; Jerry, D. Comparative characterization of a temperature responsive gene (lactate dehydrogenase-B, ldh-b) in two congeneric tropical fish, *Lates calcarifer* and *Lates niloticus*. *Int. J. Biol. Sci.* **2009**, *5*, 558–569. [CrossRef]
43. He, W.; Cao, Z.; Fu, S. Effect of temperature on hypoxia tolerance and underlying biochemical mechanism in two juvenile cyprinids with different hypoxia sensitivity. *Comp. Biochem. Physiol. A* **2014**, *187*, 232–241. [CrossRef]
44. Costas, B.; Conceição, L.E.; Aragão, C.; Martos, J.A.; Ruiz-Jarabo, I.; Mancera, J.M.; Afonso, A. Physiological responses of Senegalese sole (*Solea senegalensis* Kaup, 1858) after stress challenge: Effects on non-specific immune parameters, plasma free amino acids and energy metabolism. *Aquaculture* **2011**, *316*, 68–76. [CrossRef]
45. Ye, B.; Li, J.; Xu, L.; Liu, H.; Yang, M. Metabolomic Effects of the Dietary Inclusion of *Hermetia illucens* Larva Meal in Tilapia. *Metabolites* **2022**, *12*, 286. [CrossRef]
46. Zhao, H.; Ke, H.; Zhang, L.; Zhao, Z.; Lai, J.; Zhou, J.; Huang, Z.; Li, H.; Du, J.; Li, Q. Integrated analysis about the effects of heat stress on physiological responses and energy metabolism in *Gymnocypris chilianensis*. *Sci. Total Environ.* **2022**, *806*, 151252. [CrossRef]
47. McCarthy, I.D. The effect of temperature on protein metabolism in fish: The possible consequences for wild Atlantic salmon (*Salmo salar* L.) stocks in Europe as a result of global warming. In *Global Warming: Implications for Freshwater and Marine Fish*; Cambridge University Press: Cambridge, UK, 1996; pp. 51–77.
48. Dettleff, P.; Zuloaga, R.; Fuentes, M.; Gonzalez, P.; Aedo, J.; Estrada, J.M.; Molina, A.; Valdés, J.A. High-temperature stress effect on the red cusk-eel (*geypterus chilensis*) liver: Transcriptional modulation and oxidative stress damage. *Biology* **2022**, *11*, 990. [CrossRef]
49. Huang, D.; Ren, M.; Liang, H.; Ge, X.; Xu, H.; Wu, L. Transcriptome analysis of the effect of high-temperature on nutrient metabolism in juvenile grass carp (*Ctenopharyngodon idellus*). *Gene* **2022**, *809*, 146035. [CrossRef]
50. Currie, S.; Bagatto, B.B.; DeMille, M.D.; Learner, A.L.; LeBlanc, D.L.; Marks, C.M.; Ong, K.O.; Parker, J.P.; Templeman, N.T.; Tufts, B.L.T.; et al. Metabolism, nitrogen excretion, and heat shock proteins in the central mudminnow (*Umbra limi*), a facultative air-breathing fish living in a variable environment. *Can. J. Zool.* **2010**, *88*, 43–58. [CrossRef]
51. Eom, J.; Wood, C. Brain and gills as internal and external ammonia sensing organs for ventilatory control in rainbow trout, *Oncorhynchus mykiss*. *Compar. Biochem. Physiol. Part A Mol. Integrat. Physiol.* **2021**, *254*, 110896. [CrossRef]
52. Kullgren, A.; Jutfelt, F.; Fontanillas, R.; Sundell, K.; Samuelsson, L.; Wiklander, K.; Kling, P.; Koppe, W.; Larsson, D.G.J.; Björnsson, B.T.; et al. The impact of temperature on the metabolome and endocrine metabolic signals in Atlantic salmon (*Salmo salar*). *Comp. Biochem. Physiol. A Mol. Integr. Physiol.* **2013**, *164*, 44–53. [CrossRef]
53. Viant, M.R.; Werner, I.; Rosenblum, E.S.; Gantner, A.S.; Tjeerdema, R.S.; Johnson, M.L. Correlation between heat-shock protein induction and reduced metabolic condition in juvenile steelhead trout (*Oncorhynchus mykiss*) chronically exposed to elevated temperature. *Fish Physiol. Biochem.* **2003**, *29*, 159–171. [CrossRef]
54. McPherson, M.D.; Lewis, J.B.; Cott, P.A.; Baker, L.F.; Mochnacz, N.J.; Swanson, H.K.; Poesch, M.S. Habitat use by fluvial Arctic grayling (*Thymallus arcticus*) across life stages in northern mountain streams. *Environ. Biol. Fishes* **2023**, *106*, 1001–1020. [CrossRef]
55. Eby, L.A.; Helmy, O.; Holsinger, L.M.; Young, M.K. Evidence of climate-induced range contractions in bull trout *Salvelinus confluentus* in a Rocky Mountain watershed, USA. *PLoS ONE* **2014**, *9*, e98812. [CrossRef]
56. Rieman, B.E.; Isaak, D.; Adams, S.; Horan, D.; Nagel, D.; Luce, C.; Myers, D. Anticipated climate warming effects on bull trout habitats and populations across the interior Columbia River basin. *Trans. Am. Fish. Soc.* **2007**, *136*, 1552–1565. [CrossRef]
57. Rahel, F.J.; Keleher, C.J.; Anderson, J.L. Potential habitat loss and population fragmentation for cold water fish in the North Platte River drainage of the Rocky Mountains: Response to climate warming. *Limnol. Oceanogr.* **1996**, *41*, 1116–1123. [CrossRef]

58. Warren, D.R.; Robinson, J.M.; Josephson, D.C.; Sheldon, D.R.; Kraft, C.E. Elevated summer temperatures delay spawning and reduce redd construction for resident brook trout (*Salvelinus fontinalis*). *Glob. Change Biol.* **2012**, *18*, 1804–1811. [CrossRef]
59. Ruiz-Navarro, A.; Gillingham, P.K.; Britton, J.R. Predicting shifts in the climate space of freshwater fishes in Great Britain due to climate change. *Biol. Conserv.* **2016**, *203*, 33–42. [CrossRef]

Disclaimer/Publisher's Note: The statements, opinions and data contained in all publications are solely those of the individual author(s) and contributor(s) and not of MDPI and/or the editor(s). MDPI and/or the editor(s) disclaim responsibility for any injury to people or property resulting from any ideas, methods, instructions or products referred to in the content.

MDPI AG
Grosspeteranlage 5
4052 Basel
Switzerland
Tel.: +41 61 683 77 34

Biology Editorial Office
E-mail: biology@mdpi.com
www.mdpi.com/journal/biology



Disclaimer/Publisher's Note: The title and front matter of this reprint are at the discretion of the Guest Editor. The publisher is not responsible for their content or any associated concerns. The statements, opinions and data contained in all individual articles are solely those of the individual Editor and contributors and not of MDPI. MDPI disclaims responsibility for any injury to people or property resulting from any ideas, methods, instructions or products referred to in the content.





Academic Open
Access Publishing

mdpi.com

ISBN 978-3-7258-9144-3